

Frontiers
in
Artificial
Intelligence
and
Applications

FUZZY SYSTEMS AND DATA MINING VII

Proceedings of FSDM 2021

Edited by
Antonio J. Tallón-Ballesteros



IOS Press

FUZZY SYSTEMS AND DATA MINING VII

Fuzzy systems and data mining are indispensable aspects of the computer systems and algorithms on which the world has come to depend.

This book presents papers from FSDM 2021, the 7th International Conference on Fuzzy Systems and Data Mining. The conference, originally due to take place in Seoul, South Korea, was held online on 26-29 October 2021, due to ongoing restrictions connected with the COVID-19 pandemic. The annual FSDM conference provides a platform for knowledge exchange between international experts, researchers, academics and delegates from industry. This year, the committee received 266 submissions, and this book contains 52 papers, including keynotes and invited presentations, oral and poster contributions. The papers cover four main areas: 1) fuzzy theory, algorithms and systems – including topics like stability; 2) fuzzy applications – which are widely used and cover various types of processing as well as hardware and architecture for big data and time series; 3) the interdisciplinary field of fuzzy logic and data mining; and 4) data mining itself. The topic most frequently addressed this year is fuzzy systems.

The book offers an overview of research and developments in fuzzy logic and data mining, and will be of interest to all those working in the field of data science.



ISBN 978-1-64368-214-3 (print)
ISBN 978-1-64368-215-0 (online)
ISSN 0922-6389 (print)
ISSN 1879-8314 (online)

FUZZY SYSTEMS AND DATA MINING VII

Frontiers in Artificial Intelligence and Applications

The book series Frontiers in Artificial Intelligence and Applications (FAIA) covers all aspects of theoretical and applied Artificial Intelligence research in the form of monographs, selected doctoral dissertations, handbooks and proceedings volumes. The FAIA series contains several sub-series, including ‘Information Modelling and Knowledge Bases’ and ‘Knowledge-Based Intelligent Engineering Systems’. It also includes the biennial European Conference on Artificial Intelligence (ECAI) proceedings volumes, and other EurAI (European Association for Artificial Intelligence, formerly ECCAI) sponsored publications. The series has become a highly visible platform for the publication and dissemination of original research in this field. Volumes are selected for inclusion by an international editorial board of well-known scholars in the field of AI. All contributions to the volumes in the series have been peer reviewed.

The FAIA series is indexed in ACM Digital Library; DBLP; EI Compendex; Google Scholar; Scopus; Web of Science: Conference Proceedings Citation Index – Science (CPCI-S) and Book Citation Index – Science (BKCI-S); Zentralblatt MATH.

Series Editors:

Joost Breuker, Nicola Guarino, Pascal Hitzler, Joost N. Kok, Jiming Liu,
Ramon López de Mántaras, Riichiro Mizoguchi, Mark Musen, Sankar K. Pal,
Ning Zhong

Volume 340

Recently published in this series

- Vol. 339. M. Villaret, T. Alsinet, C. Fernández and A. Valls (Eds.), Artificial Intelligence Research and Development – Proceedings of the 23rd International Conference of the Catalan Association for Artificial Intelligence
- Vol. 338. C. Frasson, K. Kabassi and A. Voulodimos (Eds.), Novelties in Intelligent Digital Systems – Proceedings of the 1st International Conference (NIDS 2021), Athens, Greece, September 30 – October 1, 2021
- Vol. 337. H. Fujita and H. Perez-Meana (Eds.), New Trends in Intelligent Software Methodologies, Tools and Techniques – Proceedings of the 20th International Conference on New Trends in Intelligent Software Methodologies, Tools and Techniques (SoMeT_21)
- Vol. 336. A. Biere, M. Heule, H. van Maaren and T. Walsh (Eds.), Handbook of Satisfiability – Second Edition
- Vol. 335. M. Nørskov, J. Seibt and O.S. Quick (Eds.), Culturally Sustainable Social Robotics – Proceedings of Robophilosophy 2020 – August 18–21, 2020, Aarhus University and online

ISSN 0922-6389 (print)
ISSN 1879-8314 (online)

Fuzzy Systems and Data Mining VII

Proceedings of FSDM 2021

Edited by

Antonio J. Tallón-Ballesteros

University of Huelva, Spain



IOS Press

Amsterdam Berlin Washington, DC

© 2021 The authors and IOS Press.

This book is published online with Open Access and distributed under the terms of the Creative Commons Attribution Non-Commercial License 4.0 (CC BY-NC 4.0).

ISBN 978-1-64368-214-3 (print)

ISBN 978-1-64368-215-0 (online)

Library of Congress Control Number: 2021948308

doi: 10.3233/FAIA340

Publisher

IOS Press BV

Nieuwe Hemweg 6B

1013 BG Amsterdam

Netherlands

fax: +31 20 687 0019

e-mail: order@iospress.nl

For book sales in the USA and Canada:

IOS Press, Inc.

6751 Tepper Drive

Clifton, VA 20124

USA

Tel.: +1 703 830 6300

Fax: +1 703 830 2300

sales@iospress.com

LEGAL NOTICE

The publisher is not responsible for the use which might be made of the following information.

PRINTED IN THE NETHERLANDS

Preface

Fuzzy Systems and Data Mining (FSDM) is a yearly well-established international conference dealing with four main groups of topics: a) fuzzy theory, algorithm and system, b) fuzzy application, c) interdisciplinary field of fuzzy logic and data mining and d) data mining. Following the great success of previous FSDM editions, which started in 2015, FSDM 2021 has become the seventh edition in the FSDM series, to be held in Seoul (South Korea) initially, and finally as an online conference, in a forum for experts, researchers, academics and industry people to introduce the last advances in the field of Fuzzy Sets and Data Mining. The most frequent topic this year is Fuzzy Systems.

This volume contains the papers accepted and presented at the 7th International Conference on Fuzzy Systems and Data Mining (FSDM 2021), held online on 26–29 October 2021, due to the pandemic. All papers were carefully reviewed by program committee members and took into account the breadth and depth of the research topics that fall into FSDM scopes. From 266 submissions, the 52 most promising and relevant contributions were included in this volume, which presents original ideas or results of general significance supported by clear reasoning and compelling evidence, and methods.

The conference program of FSDM 2021 includes keynote and invited presentations, oral and poster contributions. This event brought together more than 100 qualified and high-level researchers and experts from over 20 countries, including 6 keynote speakers, which created a good platform for researchers and engineers worldwide to enjoy academic communication.

I would like to thank all the keynote and invited speakers, authors and anonymous reviewers for putting their effort in preparing a contribution for the conference. We are also very grateful to the people, especially the program committee members and reviewers, who devoted time to assessing the papers. It is an honour to continue with the publication of these proceedings in the prestigious series *Frontiers in Artificial Intelligence and Applications (FAIA)* published by IOS Press. Our particular thanks also go to Joost Breuker, Nicola Guarino, Pascal Hitzler, Joost N. Kok, Jiming Liu, Ramon Lopez de Mantaras, Riichiro Mizoguchi, Mark Musen, Sankar K. Pal, Ning Zhong, who are the FAIA series editors, for supporting this conference.

Last but not least, I hope you enjoyed your online stay and first virtual contact with Seoul city, which may be followed with a face-to-face conference in Seoul in the future if the situation of the global pandemic of COVID-19 is brought under control.

Antonio J. Tallón-Ballesteros
University of Huelva, Spain

This page intentionally left blank

Contents

Preface	v
<i>Antonio J. Tallón-Ballesteros</i>	
How Artificial Intelligence May Impact Your Job	1
<i>Gianluca P.M. Virgilio and Manuel Ernesto Paz López</i>	
Rényi Differential Privacy Protection Algorithm for SVD Recommendation Model	8
<i>Shaoquan Chen, Jianping Cai and Lan Sun</i>	
A Deep Neural Network Model for the Prediction of Major Adverse Cardiovascular Event Occurrences in Patients with non-ST-Elevation Myocardial Infarction	23
<i>Huilin Zheng, Syed Waseem Abbas Sherazi, Sang Hyeok Son and Jong Yun Lee</i>	
Do Reviews Influence Real Estate Marketing: The Experience Combing with Natural Language Processing	30
<i>Ting Wu, Guang Yu, Tong Li, Dan Shang and Wuwu Yan</i>	
Ranking of Trapezoidal Bipolar Fuzzy Numbers Based on a New Improved Score Function	41
<i>Jeevaraj S</i>	
Interpretable Dual-Feature Recommender System Using Reviews	54
<i>Jing Sheng Lei, Chen Si Cong Zhu, Sheng Ying Yang, Guan Mian Liang, Cong Hu and Wei Song</i>	
Facial Expression Recognition and Image Description Generation in Vietnamese	63
<i>Khang Nhut Lam, Kim-Ngoc Thi Nguyen, Loc Huu Nguy and Jugal Kalita</i>	
Hierarchical Digital Control System Performance	70
<i>Larkin Eugene Vasilevich, Akimenko Tatiana Alekseevna and Grishin Konstantin Anatolievich</i>	
Generalized-Multiquadric Radial Basis Function Neural Networks (RBFNs) with Variable Shape Parameters for Function Recovery	77
<i>Sayan Kaennakham, Pichapop Paewpolsong, Natdanai Sriapai and Sunisa Tavaen</i>	
A Bolt Defect Recognition Algorithm Based on Attention Model	86
<i>Zhijun Lin, Yingjie Liang and Qineng Jiang</i>	
Edge Analytics for Bearing Fault Diagnosis Based on Convolution Neural Network	94
<i>Valentin Perminov, Vladislav Ermakov and Dmitry Korzun</i>	
Modeling of Ship Micro-Grid Based on Wind and Solar Power Generation Technology	104
<i>Lanyong Zhang and Ziming Yuan</i>	

Is the TikTok Hype Real? A Contextual Analysis of the #FordWatchMe Challenge <i>Markus Rach</i>	115
Design and Implementation of International Trade Virtual Experiment Platform <i>Meilin Yin, Chuting Liang and Ning Luo</i>	122
Personalized Information Recommendation for Chinese Paper Cutting Culture Heritage <i>Weibo Huang, Bairu Xie and Xiaoyue Liao</i>	130
Multi-Granularity and Internal-External Correlation Residual Model for Chinese Sentence Semantic Matching <i>Lan Zhang and Hongmei Chen</i>	140
Mass Ratio Variance Majority Undersampling and Minority Oversampling Technique for Class Imbalance <i>Piboon Polvimoltham and Krung Sinapiromsaran</i>	152
Hierarchical Structure in Fuzzy Multi-Information Granular Computing Model <i>Weijie Liu and Qinghai Wang</i>	162
Support Vector Machine Technique as Classifier of Impaired Body Fat Percentage <i>Alexandra La Cruz, Erika Severeyn, Mónica Huerta and Sara Wong</i>	175
Uncertainty Measure of Pythagorean Fuzzy Sets <i>Xiaozhuan Gao, Lipeng Pan and Yong Deng</i>	183
Open Access Digital Thesaurus on Ethnic Groups in the Mekong River Basin <i>Wirapong Chansanam, Kanyarat Kwiecien, Marut Buranarach and Kulthida Tuamsuk</i>	190
Semantic Repeatability Screening Mechanism of Intelligent Learning Platform Based on Bi-LSTM <i>Jianghui Liu, Bairu Xie and Yuqing Shi</i>	200
Short Note on “Nonlinear Optimization Problem Subjected to Fuzzy Relational Equations Defined by Dubois-Prade Family of t-Norms” <i>Xiaoling Liu, Khizar Hayat and Xiaopeng Yang</i>	210
A New Group Fuzzy-Delphi Analytic Hierarchy Process Method with Its Application in Enterprise Intellectual Property Financing Decision Analysis <i>Bo Feng, Zhipeng Hui and Junwen Feng</i>	220
Category of $\mathbf{CFR}(Y)^C$ and Weak Topos <i>Shao-Jun Yang and Xinyi Huang</i>	226
Control Design for One Class of Uncertain Metzler-Takagi-Sugeno Time-Delay Systems <i>Dušan Krokavec and Anna Filasová</i>	236
A Deep Learning Approach to Recognize Human Activity Using Inertial Sensors and Motion Capture Systems <i>M. Jaén-Vargas, K. Reyes Leiva, F. Fernandes, S.B. Gonçalves, M. Tavares Silva, D.S. Lopes and J. Serrano Olmedo</i>	250

Tracking Control Design for Positive T-S Fuzzy Systems Under H_∞ Performance <i>Lining Fu, Fucui Liu, Aiwen Meng, H.K. Lam and Jilong Xu</i>	257
An Aspect of Bilevel Indefinite Quadratic Transportation Problem Under Intuitionistic Fuzzy Environment <i>Ritu Arora, Aakanksha Singh and Shalini Arora</i>	264
A Secure Image Authentication Scheme with Tamper Localization and Recovery <i>Neena Raj N.R. and Shreelekshmi R.</i>	277
Securing Mobile Adhoc Networks from Black-Hole Attacks <i>Fahmina Taranum and Khaleel Ur Rahman Khan</i>	285
Performance Evaluation of Radar Range-Bearing Centroid Processing Using Time Series Analysis <i>Nguyen Van Loi, Tran Quoc Tuan, Tran Trung Kien, Tran Van Truong and Tran Vu Hop</i>	296
The Prime Ideals of QMV*-algebras <i>Yingying Jiang and Wenjuan Chen</i>	305
A Novel Method for Mining Fuzzy Co-Location Patterns <i>Jinyu Guo and Lizhen Wang</i>	314
An Optimization of Several Distance Function on Fuzzy Subtractive Clustering <i>Sugiyarto Surono, Annisa Eka Haryati and Joko Eliyanto</i>	329
Optimization Model of Unmanned Aerial Vehicle Distribution Path with Integrated Loading and Unloading <i>Lei Wu, Ming Wei and Xiang Chen</i>	339
Responses of Climate Indicators to Droughts in SF Bay Area <i>Patrick Li and Gang Li</i>	348
Social Media User Profiling Based on Genre Extraction <i>Konstantin Belousov and Ivan Labutin</i>	356
Ontology-Driven Data Mining Platform for Fuzzy Classification of Mental Maps <i>Konstantin Ryabinin, Konstantin Belousov and Roman Chumakov</i>	363
R-Calculus for Post Three-Valued Description Logic <i>Cungen Cao, Lanxi Hu and Yuefei Sui</i>	371
Creation of a Digital Passport for an Electronic Product and Generation of Design Solutions Based on It <i>Julia V. Donetskaya</i>	379
Feature Back-Tracking with Sparse Deep Belief Networks <i>Chen Qiao, Jijia Li, Xuewu Zhang, Cheng Zhang, Wenfeng Jing and Danglin Yang</i>	386
Multi-Step Low-Rank Decomposition of Large PageRank Matrices <i>Zhao-Li Shen and Bruno Carpentieri</i>	397
A Novel Possibilistic Variance of Trapezoidal Intuitionistic Fuzzy Number <i>Qiansheng Zhang</i>	405

Knowledge Map Reasoning Technology Based on Complex Network <i>Xiang Dai and Yongchao Wei</i>	412
Semantic Supervised Training for General Artificial Cognitive Agents <i>Roman V. Dushkin and Vladimir Y. Stepankov</i>	422
A Theorem About the Existence of Minimax Rules for Statistical Decision Problems with Trapezoidal Fuzzy Losses <i>Alexey S. Shvedov</i>	431
Chinese Text Event Detection Technology Based on Improved Neural Network <i>Ying Cui and Yongchao Wei</i>	436
An Optimized Clustering Algorithm for Contour Data <i>Yucheng Chu and Lizhen Wang</i>	443
The Employment Senson System of College Students <i>MinChuan Huang, I Ping Chen, ShuYing Chung and AiGuo Wang</i>	454
Real Time Warning Model of Transmission Tower Tilt Based on Multi-Sensor Data <i>Xie Hu, Huikun Pei, Bingcai Liu, Chen Wang and Changjin Hao</i>	460
A New Indeterminacy Decision Making Approach Considering Partial Environmental State Knowledge <i>Bo Feng, Zhipeng Hui and Junwen Feng</i>	469
Subject Index	477
Author Index	481

How Artificial Intelligence May Impact Your Job

Gianluca P. M. VIRGILIO^{a,1} and Manuel Ernesto PAZ LÓPEZ^b
^aUniversidad Católica Sedes Sapientiae, Nueva Cajamarca, Peru
^bUniversidad Nacional de Tumbes, Tumbes, Peru

Abstract. Recent developments of Artificial Intelligence, Machine Learning and Big Data technologies are posing a threat to white-collar workers and managers alike. Whereas until a few years ago only manual jobs were at risk of replacement, nowadays there is no guarantee that intellectual jobs will remain in human's hands for long. Hopes that new technologies will generate more new jobs than those lost are vanishing. The new challenge faced by human workers is made up of entities that display more intelligence, whether real or just simulated, than them. We, as humans, need to invent new strategies to survive in a job market that seems ready, in one or two generations, to get rid of us. This paper identifies the main issues around intelligence and provides hints about what intelligence imitation/simulation cannot do that human intelligence can. It also discusses aspects of creativity, allegedly a human-only skill that looks like the most promising area in which human development may progress, reducing risk of silicon replacement.

Keywords. Artificial Intelligence, Big Data, Machine Learning, unemployment

1. Introduction

The more and more ubiquitous presence of Artificial Intelligence (AI) in business processes is going to impact firms at all levels. The origins of the Fourth Industrial Revolution date back to the 1960s with introduction of mechanical robots in the automotive manufacturing industry to replace blue collar workers in unsafe and unhealthy tasks. Since then, progression towards the unmanned workplace has been abrupt and irregular. However, recent advances in the AI arena seem to have paved the way to the future.

The famous Turing Test defines AI as a machine behavior that an independent evaluator would be unable to distinguish from a human one [1]. Many years have passed since the original formulation of the Turing Test and the problem seems to have turned around [2]. Currently it is up to humans to simulate AI behavior if they want to safeguard their jobs against silicon competitors. Not only can blue collar workers now be replaced, but even physicians, engineers, teachers, and managers are not guaranteed to keep their job against AI carrying out similar tasks with better performance.

Several categories of low-skill workers are now at risk to lose their job to AI. Hopes they will re-train into AI scientists to find another job are thin; once fired, they are likely to face life-long unemployment. It may be argued that this is the price to pay to progress

¹ Corresponding Author: Gianluca P. M. VIRGILIO, FCEC, Universidad Católica Sedes Sapientiae, Nueva Cajamarca, Rioja, San Martín, Peru. ORCID: 0000-0002-1616-0557. E-mail: consultgv@gmail.com.

and it is true that their children who studied engineering or business management may fill the newly-created positions (the ‘digital divide’). Yet, because of ever-improving AI capabilities, they may follow their parents’ destiny in one decade or two. Technology is progressing (at worst) linearly whereas human capabilities are improving (at best) asymptotically. The AI bar keeps moving upward and mankind may not keep pace.

In the last few decades, managers and other highly skilled professionals have been at the forefront of industrial automation, only to find themselves on the brink of being ousted by the Artificial Intelligence Revolution, where the intelligence to be replaced is theirs. It is no longer enough to label a job as ‘intellectual’ or ‘cognitive’ to make it immune from the risk of falling prey to AI.

2. Artificial Activities

2.1. AI in manufacturing

The First Industrial Revolution began with the deployment of mechanical looms in textile factories. Since then, automation in the clothing industry has progressed a long way. Yang et al. [3] argue as today AI-based systems make decisions on production, marketing, choice of fabrics, colors, shapes. The proposed solutions adhere most to customer’s preferences, selected on the basis of advanced statistical techniques and Big Data, by retrieving information from a huge number of fashion magazines.

More in general, in the manufacturing industry, AI has proved able to identify the production processes that need improvement. Then, it collects data, executes analyses, identifies causes of poor performance, provides measures for improvement and carries it out [4]. On the supply side, Thomassey and Zeng [5] describe a digital platform consisting of two modules: the first one allows to make decisions about selecting suppliers using multi-criteria techniques while the second one uses a genetic algorithm for optimizing cost and lead time. Finally, Nanda Kumar and Panneerselvam [6] propose an AI-based solution for optimizing the outbound logistic process.

2.2. AI and MOOCs

Massive Open Online Courses, Knowledge Management, and Computer-Assisted Learning are terms that have taken on the meaning of flexibility and ease of learning for students [7] and unemployment for teachers, educational programmers and school managers. According to the World Economic Forum report, the day of human teachers being largely replaced by AI is not far away: World Economic Forum [8] includes university and higher education teachers among the most likely redundant jobs in the next future.

2.3. AI in Medicine

In medicine, Arslan et al. [9] report of high performance, AI-assisted investigation methods that made early diagnosis of prostate cancer achievable. Additionally, with the aid of AI-driven deep learning, Big Data and statistical techniques it was possible to successfully identify the most appropriate therapeutic intervention for gastroenterological patients [10] or patients with Alzheimer’s disease [11]. In spine

surgery, Buza and Gum [12] present a case of robotic-assisted surgery in which screw size, length and orientation are delegated to robotic technology in order to ensure a minimally invasive approach. In these and many other cases AI has at some extent been replacing physicians' work; more pervasive replacement is expected in the next decade [13].

2.4. AI and speech content

A common criticism to Artificial Intelligence applications concerns its lack of content-comprehension, a core topic in managerial jobs. Gröndahl et al. [14] addressed this issue by detecting hate speech on social networks. They used node-representation learning techniques as anti-fraudster tool in order to identify opinion frauds, groups of fake accounts and search engine poisoning [15]. AI has also been used to combat adversarial perturbations and malicious data manipulation through Big Data and machine learning techniques [16].

2.5. AI in Human Resources Management

Klüver and Klüver [17] simulate the behavior of a human brain by implementing input and output neurons, activation functions, learning rules and variable weight values to make decisions about Human Resources (HR) Management and Models of Procedure for planning and performing industrial processes. As long as firms keep employing human workers, human behavior will remain a parameter to be closely monitored within organizations, with motivation being as usual at the forefront of search for performance. Technology-based communication is spreading all over and lack of face-to-face relationships is a serious concern for HR managers. Pratt and Cakula [18] highlight the potential AI has in increasing effectiveness of communications and enhancing motivation, moving one step forward to replacing humans in this area as well.

2.6. AI in decision-making

Research is progressing fast in machine-simulation of brain thinking processes by mimicking its internal structure (made of synapses and neurons) via Neural Networks and Deep Learning. This way AI has been used to take charge of decision making tasks by accessing huge databases, making use of sophisticated statistical tools and selecting the solutions most likely to succeed. Intelligence no longer seems to be a human-only capability [19]. An enthusiastic prediction, which actually conceals a gloomy future for managers, states "time will come when the management of the organisation will be entrusted in the hands of the AI system thus automating the entire decision-making process. Decisions will be taken at the speed of light [...]. Managers will be relieved from the day-to-day micro-management" [20, pp.xii-xiii]. Until they will, of course, be relieved from macro-management tasks too. In the meantime, skeptical managers will be shown all details of the AI-based decision-making process through Explainable AI (XAI), where the internal reasoning mechanism of intelligent systems will be kindly presented in a way suitable for even humans to understand [21].

3. Intelligent Activities

Historically, all industrial revolutions of the past resulted in a net increment of higher paid and more intellectually stimulating jobs. Yet, for the first time in history, mankind faces a competitor. AI displays, or can simulate, more intelligence than us. This leads to a complex question, about the essence of intelligence itself, and whether mere imitation would suffice to replace it. The issue is paramount to the future of human employment since HR managers will hire the entity that demonstrates the best performance, whether flesh-and-blood or silicon. No matter if business goals will be reached via sophisticated human reasoning or brute computing power. As we have seen over the last fifty years, unintelligent tasks can be easily replaced by robots. With support of AI technology managerial tasks can be replaced as well. The ‘mythical’ Zero-Defect (ZD) target, dream and goal of a bevy of production managers, can now be achieved by their silicon counterparts: Psarommatis and Kiritsis [22] propose a methodology to assess and select the best-fitting approach between product-based and process-based ZD manufacturing. Humans definitely need to mark the difference of their contribution to business results compared to what AI can, or can’t, do, if they are to safeguard their jobs.

3.1. *Making use of intelligence*

Although this may sound disappointing, we have to admit that most activities humans execute do not actually involve ‘intelligence’, according to how we are used to defining it [23]. In most of our daily activities, like walking, washing hands, eating, waiting for the bus, drinking a glass of water, and so on, the actual amount of intelligence we make use of, is small. In all these, and many other cases, our brain reacts to external inputs according to standard protocols: applying intelligence not required. A simple demonstration comes from everyday life. We all, as students or parents, have heard teachers complaining about pupils ‘not committing enough’. It means that just applying standard protocols to studying would hardly get a pass. More commitment is required, more dedication, more effort. In a word: more intelligence. Most of the times, average pupils (in their teachers’ opinion) do not seem to make enough use of their brain. The same reasoning applies to adults. Most of the times we do not commit enough.

3.2. *Making use of enough intelligence*

Occasionally, for example when studying hard and in several other cases, humans do get involved in less mundane activities than those listed above. In such cases, we use a higher amount of intelligence, yet hardly the amount required to demonstrate our (supposed) superiority to machines. A typical example of an activity that no animal could carry out, and that therefore we consider ‘intelligent’, is driving a car. Unfortunately, also in this case we are actually behaving rather mechanically, displaying no more intelligence than an AI-driven car does: we receive inputs from our visual system (the human sensors) and apply a set of standard rules. We tend to apply the same approach to decisions at work. With the exception of facing an unfamiliar problem, like studying a new topic, or a brand new situation, we have been trained to apply solutions learned from books or from previous experience. Yet, this is also the approach AI would apply.

By suitably increasing knowledge bases, logical relations between information, and learning from previous attempts in a trial-and-error process, AI and Big Data can mimic (and improve) the human learning mechanism. This is the essence of Machine Learning:

doing exactly what human children do very easily in early years of their existence with lots of time and application by their instructors. Machines can accomplish this much quicker, at lower cost and to better results.

4. Countermeasures

Manager and executives are now facing the problem of retaining their job against silicon competitors that are less prone to errors, act faster, cost less and are more suitable to expand their capabilities. The only reasonable solution is looking for activities that computers, algorithms and AI will never be able to replicate – and extract jobs out of them. In the last few decades, though technology has progressed dramatically, improvements in performing innovative tasks did not match advancements in repetitive or mechanical routines.

4.1. *Non-replaceable activities*

Generation of new ideas, philosophy, negotiation, debates in court, and commercial activity are tasks we do not use computers for. These are activities that need to be invented every time anew. Novel problems require novel solutions; ideas can spring from general principles but must be specific for the problem on the table. Similarly, interacting with humans on the other side, like a judge, a reader, a political or commercial counterpart, cannot be copied-and-pasted from previous experience as is: it requires innovation. Machines can simulate intelligence but they still lack what is known as ‘emotional intelligence’, the ability to empathize with others. So far AI has not proved able to identify the subtlety of an argument to convince a jury of its own view or a customer about her need to purchase a good or service. Additionally, fact interpretation heavily depends on human sensitivity, and as such it seems unsuitable to machines. Not every aspect of our life seems suitable for automations.

4.2. *Human uniqueness*

The trend seems now clear: whatever can be automated will be. This assigns significant importance to what makes us as humans unique: application of curiosity, humor, empathy, creativity, wisdom, figures of speech, and metaphors [24] among many other human features. Algorithms are not able to simulate or adopt any of the above. Interpretation of the content of a book is another activity that seems for-human-only since it needs a complex mix of knowledge and capability to understand the inexplicit [25]. The nuances required by a human being to understand how to correctly interpret events are by far too ethereal for fitting a, no matter how large, database table.

Despite their huge improvements, computers did not prove able so far to produce something that was not, one way or another, already written in their hardware, software, or stored knowledge. Algorithms never displayed the capability of intuition quantum leap. A stimulating point is algorithm’s capability to write another algorithm whose logic is not already included in the former. Creating a solution model from scratch is a basic skill that even beginner programmers can display, but hard to achieve by AI. The reason being that in order to write anything, software or poetry, a certain degree of creativity, or innovation, or intuition is required, and thus far it is not completely clear even to psychologists what such concepts really mean [23].

Interpretation of meanings is much more complex and beyond the grasping of any chip, algorithm or database. AI cannot interpret the meaning of books and even short documents. The subtle details of legal language may be hard to grasp by outsiders, let alone Artificial Intelligence. Nevertheless, legal and formal language is used for writing important documents: international agreements and commercial contracts.

4.3. AI conferences vs. Employment conferences

Inventing ways in which humans can retain their jobs in an AI-led world should be the main focus of white collar workers, managers and executives. That should be the real hot topic of academic and business conferences. At the contrary, the more news about scientific conferences we hear and more academic papers we read, and the more we realize that they deal with new successes achieved and old hurdles left behind.

A (non-exhaustive) internet search about AI-related conferences in 2019-2021 (up to August) and those programmed in September-December 2021 and in 2022 reveals 81 congresses subdivided as follows: 23 on generic AI, 12 on Computer Vision, 11 on Computer Speech, 9 on Machine Learning, 6 on Big Data, 5 each on Knowledge Management, Robotics and Multimedia, 3 on (AI-related) Health Care and 2 on Neural Networks. On the other side, just 7 conferences (less than 8%) over the same period were found when using the 'Employment' keyword, 2 of which dealt with employment law (which sounds suspiciously akin to researching new ways for firing human workers in order to make room for intelligent computers!).

To the best of my knowledge this trivial comparison has never been carried out before and although both searches can certainly be improved and extended, it is unlikely that the ratio between the two types of congress will change significantly. A complete change of paradigm is long overdue. We only have our brain to compete in this contest; let's make use of it!

5. Conclusion

Impressive technological advancements achieved thanks to AI means humans will have to adapt, once more in Mankind's history, to the newly generated environment, not differently to what happened during the First Industrial Revolution in the XVIII century. Because of the different characteristics of the current industrial revolution, the skills required to remain attractive in the newly generated work environment will be very different from the ones needed so far. It will be the goal of the human race to learn them in a short timeframe. A newly designed course of study will hardly provide the required answer; a much wider effort is called for by academia, business practitioners, politicians, trade unions, and the whole community of white collar workers, including managers and executives. Several unresolved issues are piling up: without a thorough comprehension of what intelligence is, what its unique features are and what can we do to exploit this gift to the maximum, the race for sustainable human employment in the future cannot be won. We need to provide answers to what computers can and will be able to do in the future in order to find alternative applications for humans to carry out – and to earn their living from. The risk in twenty years' time is having eight billion people struggling to get the relatively few jobs available as lawyers, psychologists or salespeople and other jobs requiring soft skills: a very serious discussion on this vital topic is now called for.

White collar workers, managers and executives will have to be at the forefront of this debate: their future is at stake.

References

- [1] Turing A. Computing machinery and intelligence. *Mind*, 49:433–460
- [2] Hall O. Passing the Turing Test. *Graziadio Business Review* 21(2)
- [3] Yang T, Feng J, Chen J, Dong C, Shi Y, Tao R. A Clothing Recommendation System Based on Expert Knowledge. In: Wong W. (ed.) *Artificial Intelligence on Fashion and Textiles. AIFT 2018*, Hong Kong
- [4] Yang B, He Y, Yin H. Data Analysis and Production Process Control. In: Dolgui A, Bernard A, Lemoine D, von Cieminski G, Romero D. (eds) *Advances in Production Management Systems. APMS 2021*. Nantes, France. Springer. Cham, Switzerland
- [5] Thomassey S, Zeng X. FBD_Bmodel Digital Platform: A Web-Based Application for Demand Driven Fashion Supply Chain. In: Dolgui A, Bernard A, Lemoine D, von Cieminski G, Romero D. (eds) *Advances in Production Management Systems. APMS 2021 Nantes, France Springer*. Cham, Switzerland
- [6] Nanda Kumar S, Panneerselvam R. A Genetic Algorithm-based Artificial Intelligence Solution for Optimizing E-Commerce Logistics Vehicle Routing. In: Suguna SK, Dhivya M, Paiva S. *Artificial Intelligence (AI) Recent Trends and Applications*. CRC Press. Boca Raton, FL
- [7] Botticelli M, Gasparetti F, Sciarone F, Temperini M. Deep Learning to Monitor Massive Open Online Courses Dynamics. In: De la Prieta F, Gennari R, Temperini M, Di Mascio T, Vittorini P, Kubincova Z, Popescu E, Rua Carneiro D, Lancia L, Addone A (eds). *Methodologies and Intelligent Systems for Technology Enhanced Learning, 11th Conference*. Springer. Cham, Switzerland
- [8] World Economic Forum. *The Future of Jobs Report 2020*. www.weforum.org
- [9] Arslan M, Arslan D, Haznedar B. Training ANFIS Systems With Genetic Algorithm For Diagnosis Of Prostate Cancer. *Technological Applied Sciences*. 13(4):301-309.
- [10] Ruffle JK, Farmer AD, Aziz Q. Artificial Intelligence-Assisted Gastroenterology—Promises and Pitfalls. *The American Journal of Gastroenterology*. October 2018.
- [11] Tang H, Yao E, Tan G, Guo X. A Fast and Accurate 3D Fine-Tuning Convolutional Neural Network for Alzheimer’s Disease Diagnosis. In: Zhou Z, Yang Q, Gao Y, Zheng Y (eds.). *Artificial Intelligence. ICAI 2018*; Jinan, China
- [12] Buza J, Gum J. Cortical Screw Fixation. In: Wang MY, Steele III WJ, Urakov T. *Advanced Robotic Spine Surgery*. CRC Press. Boca Raton, FL
- [13] Davenport T, Kirby J. *Only Humans Need Apply*. Harper Collins, New York
- [14] Gröndahl T, Pajola L, Juuti M, Conti M, Asokan N. All You Need is “Love”: Evading Hate Speech Detection. *AISeC’18*. Toronto, Canada.
- [15] Xu C, Feng Z, Chen Y, Wang M, Wei T. FeatNet: Large-scale Fraud Device Detection by Network Representation Learning with Rich Features. *AISeC’18*. Toronto, Canada
- [16] Rieck K. Family Reunion: Adversarial Machine Learning meets Digital Watermarking. In: *Multimedia Privacy and Security 2018 (invited keynote)*. Toronto, Canada. <https://doi.org/10.1145/3267357.3267366>
- [17] Klüver C., Klüver J. Decision Support in Everyday Business Using Self-enforcing Networks. In: Dingli A, Haddod F, Klüver C. (eds.) *Artificial Intelligence in Industry 4.0*. Springer. Cham, Switzerland
- [18] Pratt M, Cakula S. Motivation in a Business Company Using Technology-Based Communication. In *Artificial Intelligence in Industry 4.0*. Springer. Cham, Switzerland
- [19] Finlay R, Takeda H. Reflections on Decision-Making and Artificial Intelligence. In: Braunschweig B, Ghallab M. *Reflections on Artificial Intelligence for Humanity*. Springer. Cham, Switzerland
- [20] Dingli A, Haddod F, Klüver C. *Artificial Intelligence in Industry 4.0*. Springer. Cham, Switzerland
- [21] Mallia N, Dingli A, Haddod F. MIRAI: A Modifiable, Interpretable, and Rational AI Decision Support System. In: Dingli A, Haddod F, Klüver C. (eds.) *Artificial Intelligence in Industry 4.0*. Springer. Cham, Switzerland
- [22] Psarommatis F, Kiritsis D. Comparison Between Product and Process Oriented Zero-Defect Manufacturing (ZDM) Approaches. In: Dolgui A, Bernard A, Lemoine D, von Cieminski G, Romero D. (eds) *Advances in Production Management Systems - Artificial Intelligence for Sustainable and Resilient Production Systems. APMS 2021*. Nantes, France. Springer. Cham, Switzerland
- [23] Purves D. *Why Brains Don’t Compute*. Springer. Cham, Switzerland
- [24] Egan Y, Chesley J. Leadership in a Smart Machine Age Lessons on Becoming More Human from the Mind-Brain Revolution. *Graziadio Business Review* 21(2)
- [25] Smith G. *The AI Delusion*. Oxford University Press. New York

Rényi Differential Privacy Protection Algorithm for SVD Recommendation Model

Shaoquan CHEN^a, Jianping CAI^a and Lan SUN^{a,1}

^aCollege of Computer and Data Science, Fuzhou University, Fuzhou 350108, China

Abstract. With the widely use of recommendation systems in various mobile applications, privacy leakage has been a longstanding threat, for which many researchers have come up with a great number of methods that achieve the protective effect to a certain extent. However, the protection scope of these methods is limited, especially in the protection of original data. To address this issue, we propose a data perturbation based Rényi differential privacy algorithm to protect the SVD recommendation model. This paper uses the data perturbation method to perturb the original training dataset in the data preprocessing stage, then leverages the perturbed data to train the SVD model, and the unperturbed data is used as a test set to verify the accuracy of the model. Compared with the objective perturbation, gradient perturbation, and output perturbation, the data perturbation can protect a broader range and realize the corresponding functions of the other three perturbed methods by using the post-processing property of differential privacy. Experimental results show that the proposed method can effectively protect user privacy, improve the effectiveness of data, and generate better recommendation results without seriously affecting the accuracy of the model.

Keywords. Rényi differential privacy, data perturbation, SVD recommendation model, recommendation system, differential privacy

1. Introduction

In recent years, with the rapid development of Internet technology and the advent of the era of big data, a large amount of data will be generated every day. The recommendation system uses a large amount of user data to mine the consumption needs of potential users and recommend the items they need. In the fierce market competition environment, whether to use the recommendation algorithm to accurately grasp the needs of users and provide them with good services and then obtain more potential customers has become a major challenge for enterprises.

As an important and popular recommendation strategy, collaborative filtering [1] technology predicts the evaluation of various commodities by collecting a large number of users' evaluation data and then provides personalized recommendation services to users according to the predicted score. Compared with other recommendation strate-

¹Corresponding Author: Lan Sun, College of Computer and Data Science, Fuzhou University, Fuzhou 350108, China; E-mail: lsun@fzu.edu.cn.

gies, collaborative filtering technology can achieve more accurate recommendations by using only a small amount of user evaluation data. It is relatively simple to realize, and there is no need to understand the correlation between items. It can not only generate relatively novel recommendation results, but also recommend more complex items to users. Therefore, this technology is also widely used by well-known enterprises such as Amazon.

However, when collecting a large number of user evaluation data, we will face a bigger problem: leaking the sensitive personal information of potential customers. Because some evaluation data will contain users' privacy preferences, we will inevitably leak some sensitive data when using user evaluation data for the recommendation. In a real scene, not only the original dataset may leak some personal information, but also some parameters may indirectly leak user-sensitive data in the training process. How to effectively deal with the effectiveness of the model and data protection has become a research hotspot in recent years.

In recent years, a great number of researchers have proposed many methods for privacy protection, such as k-anonymity [2], t-closeness [3], l-diversity [4] and so on. However, these methods have some limitations in background knowledge and attack assumptions, and can't provide sufficient privacy guarantee. Moreover, there is a lack of effective and strict proof to explain their privacy protection level.

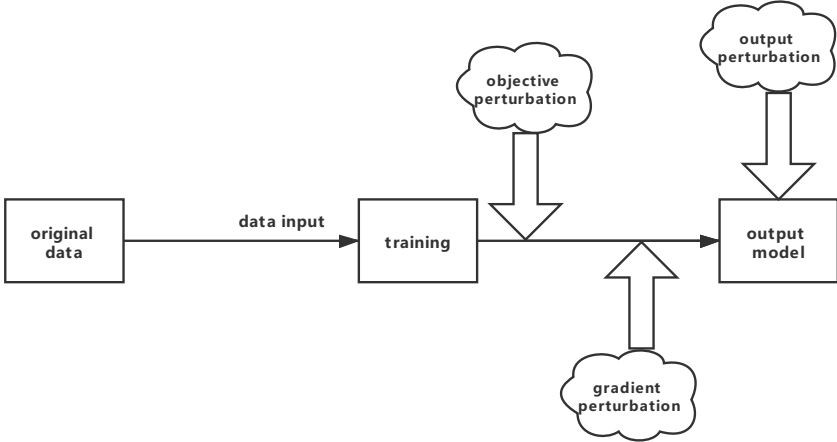
In 2006, Dwork et al. [5] proposed a differential privacy mechanism, which has attracted extensive attention. In recent years, this mechanism has been widely used in many fields for privacy protection. The mechanism fully considers the availability of data and the privacy and security of users. By adding random noise to perturb the published data, whether a single record is in the dataset has little impact on the calculation results. The commonly used perturbation methods mainly include objective perturbation, gradient perturbation, and output perturbation.

McSherry et al. [6] combined differential privacy with a recommendation system to realize corresponding privacy protection. They mainly started with the item covariance matrix and randomly added noise to the item covariance matrix to perturb the recommendation results. Hua et al. [7] mainly started from the perspective of objective perturbation and added random noise to the objective function to realize the corresponding privacy protection. Xian Zhengzheng et al. [8] proposed SVD ++ privacy protection recommendation models based on gradient perturbation, objective perturbation, and output perturbation. Yan Shen et al. [9] proposed a collaborative filtering method for differential privacy protection with social awareness. Zheng Jian et al. [10] used differential privacy and added random noise to a matrix decomposition recommendation model based on fusion label similarity, which still has high recommendation accuracy under the condition of ensuring user privacy. Friedman A et al. [11] proposed a method of using differential privacy in each step of matrix decomposition, Wang et al. [12] proposed a privacy protection model with objective perturbation by adding differential privacy noise to the bias matrix decomposition recommendation model. Kamalika Chaudhuri et al. [13] proposed differential privacy based on the exponential mechanism to add random noise to the PCA process, then the processed matrix is applied to the SVD model to realize the corresponding privacy protection.

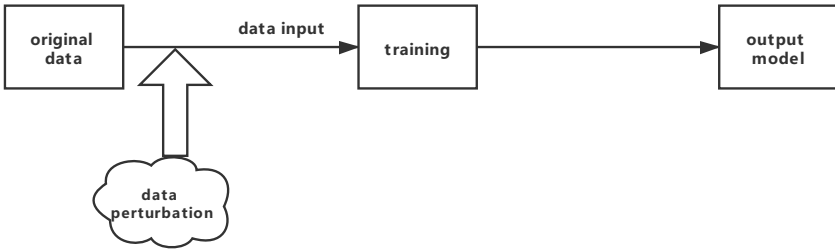
However, these privacy protection methods described above are based on three technologies: objective perturbation, output perturbation, and gradient perturbation to protect

the data. They do not protect the original data, and the original data is also likely to be attacked by attackers, so it is also very important to protect the original dataset.

To solve the above problems, this paper uses the data perturbation [14] method proposed in recent years, which makes the final model achieve (ϵ, δ) -differential privacy by adding random noise to the original training dataset. The difference between the data perturbation method used in this paper and the three perturbation methods mentioned earlier is shown in Figure 1.



(a) three common perturbed methods



(b) data perturbation

Figure 1. different perturbation methods

From Figure 1, we can see that the data perturbation method that we use can protect the final model with the help of the post-processing property of differential privacy.

Considering privacy protection and the final recommendation effect of the model, this paper adopts the SVD model based on the optimization algorithm of block coordinate descent and proposes a collaborative filtering algorithm based on data perturbation Rényi differential privacy protection, called data perturbation based Rényi differential privacy (DBRDP). The main contributions of this paper are as follows:

- In the process of data preprocessing, we add random Gaussian noise to the original training dataset and use the perturbed training dataset to train the SVD model so that the final model not only obtains the corresponding privacy protection but also has high model accuracy.

- We propose the DBRDP algorithm to protect the privacy of the BCDSVD model. In the process of data preprocessing, the original dataset is protected by adding the random Gaussian noise processed by Rényi differential privacy. Because of the post-processing property of differential privacy, the characteristic matrix is also protected, and the final model can be protected and still have high recommendation accuracy.
- We use the real datasets filmtrust, movielens100K and movielens1M in the experiment. The results show that the DBRDP algorithm has a better recommendation effect under the same privacy budget.

The rest of this paper is organized as follows: Section 2 introduces the relevant background knowledge, Section 3 introduces the process of the DBRDP algorithm, Section 4 shows the relevant experimental results and analyzes the experimental results, Section 5 concludes the work of the full text.

2. Background

In this section, we will introduce some related concepts of the BCDSVD model, differential privacy definition, and some related contents of Rényi differential privacy(RDP).

2.1. Block Coordinate Descent

Block coordinate descent (BCD) [15] algorithm is a method to optimize the subset of variables at the same time and decomposes the original problem into multiple subproblems. The core idea of this method is to divide the variables x to be optimized into p blocks, which are recorded as follows: $x = [x_1, x_2, \dots, x_p]$. In each iteration, the original problem optimizes the i th block, and the other blocks remain unchanged, then the optimization expression of each subblock is:

$$x_i^{t+1} \in \arg \min_{x_i} f(x_1^{t+1}, x_2^{t+1}, \dots, x_{i-1}^{t+1}, x_i^t, \dots, x_p^t) \quad (1)$$

The pseudocode of the block coordinate descent algorithm is shown in algorithm 1:

Algorithm 1 Block Coordinate Descent Method

```

1: Initialize  $x^0 \leftarrow [x_1^0, x_2^0, \dots, x_p^0]$ ,  $t \leftarrow 0$ ;
2: while stopping criteria have not been satisfied do
3:   for each  $i \in \{1, 2, \dots, p\}$  do
4:      $x_i^{t+1} \leftarrow \arg \min_{x_i} f(x_1^{t+1}, x_2^{t+1}, \dots, x_{i-1}^{t+1}, x_i^t, \dots, x_p^t)$ ;
5:   end for
6:    $t \leftarrow t + 1$ ;
7: end while
8: return  $x^t$ ;

```

Compared with other optimization algorithms, the BCD algorithm has the advantages of fast speed, simple implementation, and strong stability. It will also be affected

by some properties of the objective function, such as the fast convergence that BCD can achieve $O(1/k)$ when the objective function is block strong convex. Because of its low iterative cost, the block coordinate descent method is also widely used in large-scale numerical optimization.

2.2. BCDSVD Recommendation Model

SVD recommendation model obtains the user characteristic matrix $U \in \mathbb{R}^{d \times n}$ and the corresponding item characteristic matrix $M \in \mathbb{R}^{d \times m}$ by singular value decomposition of the user scoring matrix $S \in \mathbb{R}^{n \times m}$, and calculates the corresponding predicted score matrix $P \in \mathbb{R}^{n \times m}$. SVD model is a common model in collaborative filtering recommendation algorithm. n represents the number of users, m represents the number of scoring items, d represents the dimension of a feature vector. Based on the SVD model, Paterek A [16] improves the model, and introduces the concept of bias vector $\mathbf{0}$ to learn the preference factors of users and items, and puts forward the BiasSVD model to further improve the recommendation accuracy of the model. The expression of the BiasSVD model is:

$$P = U^T M + b_n \mathbf{1}_m^T + \mathbf{1}_n b_m^T + c \quad (2)$$

In Eq.(2), $b_n \in \mathbb{R}^{n \times 1}$ represents the user bias vector, $b_m \in \mathbb{R}^{m \times 1}$ represents the item bias vector, c represents the mean value of all scoring records, and $\mathbf{1}$ represents a column vectors with all value of 1.

Compared with the traditional SVD recommendation model, BCDSVD [17] recommendation model uses the optimization algorithm of block coordinate descent in the solution process and solves the problems of capacity matrix inversion and sparse matrix solution. It has also been further improved in terms of speed and model accuracy, which is better than the traditional SVD model. BCDSVD model also has good expansibility. It can be used to solve the SVD recommendation model with implicit feedback. The high efficiency and good expansibility of the BCDSVD model make it have good usability and research value.

2.3. Differential Privacy

This subsection mainly introduces some differential privacy mathematical formulas and some common basic concepts and definitions.

There is only one data difference between two datasets $D, D' \in \mathcal{D}^n$. We call such dataset sibling dataset. Based on sibling dataset, some common differential privacy concepts are defined as follows:

Definition 1 ((ϵ, δ) - Differential Privacy) [5]. A random function $M : \mathcal{D}^n \rightarrow \mathcal{R}^m$ satisfies (ϵ, δ) - differential privacy if the following conditions satisfy:

$$\Pr[M(D) \in S] \leq e^\epsilon \Pr[M(D') \in S] + \delta \quad (3)$$

In Eq. (3), $S \in \text{range}(M)$. ϵ is the privacy budget, and its value range is $\epsilon \geq 0$. The smaller the value of the privacy budget, the higher the degree of protection. The value range of δ is $0 \leq \delta \leq 1$, and when δ is 0, it is called pure differential privacy, and when $\delta > 0$, it is called approximate differential privacy.

Definition 2 (Gaussian Mechanism) [18]. Given the function $f : D^m \rightarrow R$, for any $D \in D^m$, the definition of Gaussian mechanism G is:

$$G(f(D)) = f(D) + v \tag{4}$$

In Eq. (4), v follows the Gaussian distribution $N(0, \sigma^2 I)$ with mean value of 0 and variance $\sigma \geq \frac{\sqrt{2 \log(1.25/\delta)} \Delta_2 f}{\epsilon}$, where f is L_2 - sensitivity is defined as

$$\Delta_2 f \triangleq \max_{D, D'} \|f(D) - f(D')\|_2 \tag{5}$$

Definition 3 (Rényi Divergence) [19]. For the two probability distributions P and Q which are defined on R , when $\alpha > 1$, the definition of Rényi divergence is as follows:

$$D_\alpha(P \parallel Q) \triangleq \frac{1}{\alpha - 1} \log E_{x \sim Q} \left(\frac{P(x)}{Q(x)} \right)^\alpha \tag{6}$$

In Eq. (6), $P(x)$ and $Q(x)$ are the density at x . The relationship between Rényi divergence and differential privacy can obtain directly when $\alpha = \infty$. A random mechanism M satisfies ϵ -differential privacy if and only if it is distributed between two adjacent input datasets D and D' , and satisfies Eq. (7):

$$D_\infty(M(D) \parallel M(D')) \leq \epsilon \tag{7}$$

Definition 4 ((α, ϵ) - RDP) [19]. Given parameters $\alpha > 1$, privacy budget $\epsilon \geq 0$. If a random mechanism $M : D \rightarrow R$ satisfies Eq.(8) for any sibling dataset:

$$D_\alpha(M(D) \parallel M(D')) \leq \epsilon \tag{8}$$

we call the random mechanism satisfied (α, ϵ) - RDP. RDP is a relaxation of the concept of differential privacy. Using Rényi divergence to measure the difference between two sibling datasets can provide stronger privacy protection than (ϵ, δ) - differential privacy.

Definition 5 (RDP to (ϵ, δ) -Differential Privacy) [19]. Given a function M which satisfies (α, ϵ) - RDP, it will also satisfy $(\epsilon(\delta), \delta)$ - differential privacy, where

$$\epsilon(\delta) \geq \epsilon + \frac{\log(\frac{1}{\delta})}{\alpha - 1} \tag{9}$$

3. Algorithm

In this section, before introducing our DBRDP algorithm, we first introduce the data perturbation based Gaussian noise(DBGDP) and then propose an improved algorithm DBRDP for the data perturbation based Gaussian noise algorithm.

3.1. Data Perturbation Based Gaussian Noise

In this paper, when we mention the data perturbation, we will turn $z = (x, y)$ into $z' = (x + noise, y)$, which *noise* represents the random noise that we add, z represents the original data, and z' represents the perturbed data. In the process of algorithm processing, we mainly add random noise to the original training dataset at the data preprocessing stage, the random noise follows the Gaussian distribution $N(0, \sigma^2 I)$, where the mean value is 0, and the variance is $\sigma = \frac{d+1}{n\epsilon} \sqrt{2 \log \left(\frac{d^2+d}{82\sqrt{2\pi}} \right) + \frac{1}{\sqrt{\epsilon n}}}$ [13], where d represents the dimension of query data, n represents the amount of query data, and ϵ represents the privacy budget. Then we apply the perturbed data to the training process of the BCDSVD recommendation model. Due to the post-processing property of differential privacy, it is not difficult to see that when using the processed perturbed data to process the block data by the BCD method, block data will also be protected. Moreover, when applying BCD to the SVD recommendation model, the output of the final model is also protected.

Compared with objective perturbation, gradient perturbation, and output perturbation, data perturbation has a broader protection range. It can even be said that the data perturbation can indirectly realize the output perturbation, objective perturbation, and gradient perturbation because of the post-processing property of differential privacy. In subsequent processing, it will also have varying degrees of impact on the other three corresponding perturbations. Moreover, it can protect data input, which can better prevent the attack of attackers. The pseudocode of data perturbation based Gaussian noise (DBGDP) algorithm is shown in algorithm 2.

Algorithm 2 Data Perturbation Based Gaussian Noise(DBGDP)

- 1: **Inputs:** Dataset D , privacy budget ϵ , privacy bias δ , variance σ ;
 - 2: **Output:** perturbed dataset $D_{privacy}$;
 - 3: for all data instances $z_i (i \in \{1, 2, \dots, n\})$, transform them to $z' = z_i + b$
 $b \sim N(0, \sigma^2 I)$;
 - 4: $D_{privacy} = \{z'\}$;
 - 5: **return** $D_{privacy}$;
-

In this paper, we use the perturbed training dataset obtained by algorithm 2 to train the BCDSVD recommendation model. We assume that the predicted score matrix \mathbf{P} is a function of characteristic parameter λ (column vector). For this problem, the loss function we use is the mean square error. We use the minimization function of the loss function $E(\lambda)$ [17] to solve the subsequent problem. The expression is:

$$E(\lambda) = \frac{1}{2} \text{trace} \left((\mathbf{J} * (\mathbf{V} - \mathbf{P}))^T (\mathbf{J} * (\mathbf{V} - \mathbf{P})) \right) + \text{reg}(\lambda) \quad (10)$$

In Eq. (10), \mathbf{J} is the matrix to mark whether the user has scored the corresponding items, $*$ represents the Hadamard product operator, $\text{reg}(\lambda)$ is a regularization function, which can be expressed as $\text{reg}(\lambda) = \frac{1}{2} \lambda^T \text{diag}(\kappa) \lambda$, κ is the vector composed of various characteristic parameters, and the corresponding gradient of the regularization function is $\text{diag}(\kappa) \lambda$. Following this, we can get the gradient expression of the loss function $E(\lambda)$ [17]:

$$\frac{\partial E(\lambda)}{\partial \lambda} = \sum_{i,j} (e_i^T (\mathbf{J} * (\mathbf{P} - \mathbf{V})) e_j \times \frac{\partial (e_i^T \mathbf{P} e_j)}{\partial \lambda}) + \frac{\partial \text{reg}(\lambda)}{\partial \lambda} \quad (11)$$

In Eq. (11), e_i represents the basic column vector in which the i th element is 1 and the other elements are 0. Eq. (11) transforms the gradient solution of the loss function $E(\lambda)$ into the gradient solution of each predicted score.

Based on the related concepts and the input perturbed dataset, we can solve the corresponding gradients of the user characteristic matrix \mathbf{U} and item characteristic matrix \mathbf{M} under the BCDSVD model. Due to the post-processing property of differential privacy, the corresponding gradient perturbation will also be generated when using the perturbed data to solve the corresponding gradient. Therefore, the gradient expression corresponding to the user characteristic matrix is:

$$\frac{\partial E(\mathbf{U})}{\partial \mathbf{U}} = \mathbf{M}(\mathbf{J} * (\mathbf{P} - \mathbf{V}))^T + k_u \mathbf{U} + v \quad (12)$$

The item characteristic matrix is:

$$\frac{\partial E(\mathbf{M})}{\partial \mathbf{M}} = \mathbf{U}(\mathbf{J} * (\mathbf{P} - \mathbf{V}))^T + k_q \mathbf{M} + v \quad (13)$$

v is the noise added indirectly in the gradient processing process due to the use of the perturbed original dataset to train the model. There is no noise added to the gradient again. The random noise v follows the distribution of $v \sim N(0, \sigma^2 \mathbf{I})$. It is difficult to directly use Eqs. (12) and (13) to solve the user characteristic matrix and item characteristic matrix. Therefore, in the process of solving the model, we adopt the block idea to divide the original characteristic matrix by column. The subblocks S can express as:

$$\mathbf{S} = \mathbf{V} - b_u \mathbf{1}_q^T - \mathbf{1}_u b_q^T - c \quad (14)$$

After block processing, the corresponding gradient solution formula can transform into:

$$\frac{\partial E(\mathbf{u}_i)}{\partial \mathbf{u}_i} = (\mathbf{M} \text{diag}(\mathbf{e}_i^T \mathbf{J}) \mathbf{Q}^T + k_u \mathbf{I}) \mathbf{u}_i - \mathbf{Q}(\mathbf{J} * \mathbf{W})^T \mathbf{e}_i + v \quad (15)$$

$$\frac{\partial E(\mathbf{m}_i)}{\partial \mathbf{m}_i} = (\mathbf{U} \text{diag}(\mathbf{J} \mathbf{e}_i) \mathbf{U}^T + k_q \mathbf{I}) \mathbf{m}_i - \mathbf{U}(\mathbf{J} * \mathbf{V})^T \mathbf{e}_i + v \quad (16)$$

In addition, the gradient value after block processing is $\mathbf{0}$. After transposition, the general expression of user feature subblock \mathbf{u}_i is:

$$\mathbf{u}_i = (\mathbf{M} \text{diag}(\mathbf{e}_i^T \mathbf{J}) \mathbf{Q}^T + k_u \mathbf{I})^{-1} \mathbf{Q}(\mathbf{J} * \mathbf{W})^T \mathbf{e}_i - (\mathbf{M} \text{diag}(\mathbf{e}_i^T \mathbf{J}) \mathbf{Q}^T + k_u \mathbf{I})^{-1} v \quad (17)$$

The item feature subblock \mathbf{m}_i is:

$$\mathbf{m}_i = (\mathbf{U} \text{diag}(\mathbf{J}\mathbf{e}_i)\mathbf{U}^T + k_q \mathbf{I})^{-1} \mathbf{U}(\mathbf{J} * \mathbf{V})^T \mathbf{e}_i - (\mathbf{U} \text{diag}(\mathbf{J}\mathbf{e}_i)\mathbf{U}^T + k_q \mathbf{I})^{-1} \mathbf{v} \quad (18)$$

Based on Eqs. (17) and (18), we can get the final user feature matrix $\mathbf{U} = [\mathbf{u}_1, \mathbf{u}_2, \dots, \mathbf{u}_u]$ and item feature matrix $\mathbf{M} = [\mathbf{m}_1, \mathbf{m}_2, \dots, \mathbf{m}_q]$.

3.2. Data Perturbation Based Rényi Differential Privacy

When the privacy budget is small, the effect of some datasets in training the DBGDP-BCDSVD model is not very good, and the running efficiency is also worse than that of the non-noisy BCDSVD model. In recent years, Rényi differential privacy(RDP) proposed by Mironov I has been gradually applied. Under the same privacy budget, by using RDP, we can get better results than the general differential privacy. Therefore, this subsection uses Rényi differential privacy to control the random noise added to the original training dataset. With the help of the relationship between Rényi differential privacy and (ϵ, δ) -differential privacy, under the same privacy budget ϵ , using the relationship between (α, ϵ) -RDP and (ϵ, δ) -differential privacy, and inequality $\epsilon(\delta) \geq \epsilon + \frac{\log(\frac{1}{\delta})}{\alpha-1}$. Under the premise of ensuring (ϵ, δ) -differential privacy, our model can get better performance. Under the same privacy protection, the method of random perturbation using Rényi differential privacy can improve the performance of our BCDSVD recommendation model and obtain a better recommendation effect. The specific flow chart of DBRDP-BCDSVD is shown in Figure 2.

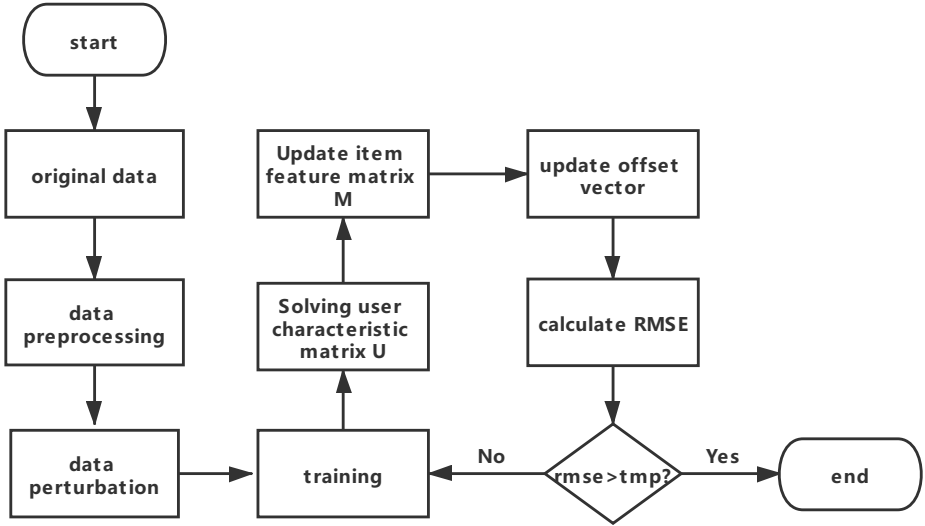


Figure 2. the flow chart of DBRDP-BCDSVD.

To prevent the algorithm from iterating continuously and affecting the efficiency, we set the iteration termination condition in the process of model training: when the model evaluation index $rmse$ meets $rmse > tmp$, we terminate the algorithm, where tmp is the difference between the RMSE value of the previous round of training and a pre-set error threshold. The pseudocode of data perturbation based Rényi Differential Privacy(DBRDP) algorithm is shown in algorithm 3.

Algorithm 3 Data Perturbation Based Rényi Differential Privacy(DBRDP)

-
- 1: **Inputs:** Dataset D , privacy budget ϵ , privacy bias δ , variance σ , Rényi parameter α ;
 - 2: **Output:** perturbed dataset $D_{privacy}$;
 - 3: for all data instances $z_i (i \in \{1, 2, \dots, n\})$, transform them to $z' = z_i + b$;
 $b \sim N(0, \sigma^2 I)$;
 - 4: $D_{privacy} = \{z'\}$;
 - 5: **return** $D_{privacy}$;
-

When perturbed the original training dataset, it is not difficult to see that it is satisfied (α, ϵ) - RDP in the process of perturbation. Due to the post-processing property of differential privacy, when the BCDSVD model is trained with the perturbed dataset, the model will also be protected. After privacy processing is performed on the most original training dataset, we do not need to perform output perturbation, objective perturbation, and gradient perturbation on the model in the process of model training iterations. Due to using the perturbed training dataset, the user characteristic matrix will also be protected. The protected user characteristic matrix will also be used for subsequent model parameter updating, such as item characteristic matrix and offset vector. After privacy processing of the original dataset, other important data, such as user characteristic matrix and item characteristic matrix, will also be protected. Therefore, using the perturbed training dataset to train the BCDSVD model, its overall training process will be satisfied (α, ϵ) - RDP.

4. Experimental Results And Analysis

This section mainly implements the two algorithms proposed in Section 3 and analyzes the corresponding experimental results.

4.1. Experimental Datasets

This paper mainly adopts the movie scoring datasets filmtrust, movielens100K, and movielens1M, which are commonly used in the recommendation system. The size of filmtrust is [35494,3], the size of movielens100K is [100000,3], and the size of movielens1M is [1000209,3]. The dimension (i.e. the number of columns) of these three datasets is 3, and the third column of data is the user's rating data of items. Filmtrust is the data captured from the whole filmtrust website in 2011. Movielens is the data collected and rated by GroupLens research on its film website.

4.2. Some Main Parameters in Experiment

The main parameters that we use in the experiment are shown in Table 1.

Table 1. Experimental Parameters

<i>Variable</i>	<i>Description</i>	<i>Default Value</i>
ϵ	Privacy Budget	-
δ	Privacy Bias	1e-5
d	Dataset Dimension	3
n	Dataset Size	-
α	Rényi Parameter	1000

The default value of these parameters is set by relevant reference or by the structure of the dataset used in this experiment.

4.3. Evaluation

The recommendation system often takes some errors as performance evaluation index, such as RMSE, MSE, MAE, etc. In the process of the experiment, we use the root mean square error (RMSE) as the corresponding evaluation index, and its expression is:

$$RMSE = \sqrt{\frac{1}{n} \sum_{i=1}^n (y_i - \hat{y}_i)^2} \quad (19)$$

Where n is the total number of samples, y_i is the real value of the i th sample, and \hat{y}_i is the predicted value of the i th sample. The evaluation standard of root mean square error (RMSE) is: the smaller the value of root mean square error, the better performance of the system.

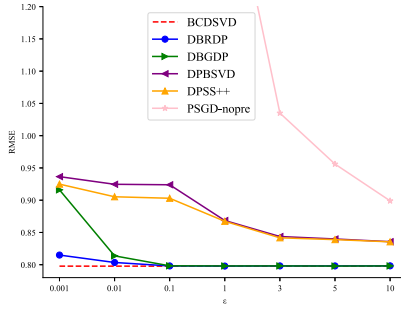
4.4. Experimental Results And Analysis

This paper takes the BCDSVD algorithm without privacy protection as the benchmark, the SVD algorithm PSGD based on gradient perturbation PSGD-nopre proposed by Berlioz A et al, and the DPBSVD algorithm based on gradient perturbation proposed by Paterek A, and the DPSS ++ algorithm based on gradient perturbation proposed by Xian Zhengzheng et al are compared with the data perturbation based Gaussian noise(DBGDP) and the data perturbation based Rényi differential privacy(DBRDP) proposed in this paper. In the process of comparative experiment, we conduct 10 experiments on a privacy budget value and calculate the average value of the 10 experiments as the evaluation index to compare the advantages and disadvantages of various algorithms. To facilitate viewing, we summarize all the experiments in Table 2.

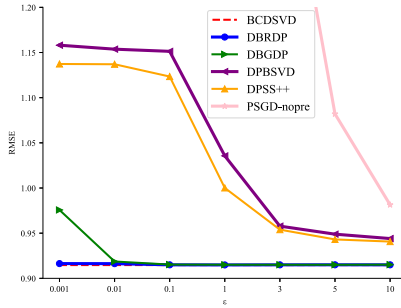
Table 2. Experimental Algorithms

Algorithms	Description
BCDSVD	Non-privacy protection
PSGD-nopre	SVD algorithm based on gradient perturbation, without preprocessing
DPSS ++	SVD ++ algorithm based on gradient perturbation
DPBSVD	BiasSVD algorithm based on gradient perturbation
DBGDP	BCDSVD algorithm based on data perturbation, and adds Gaussian random noise
DBRDP	BCDSVD algorithm based on data perturbation, and satisfies (α, ϵ) - RDP

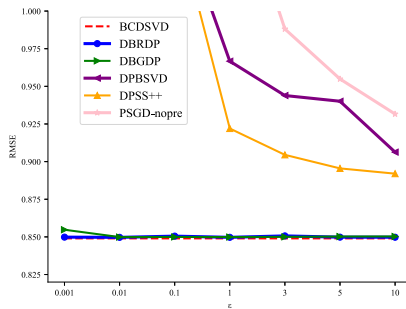
The algorithms listed in Table 2 are trained with filmtrust, movielens100K and movielens1M. We take root mean square error (RMSE) as the experimental evaluation index of various algorithms. The experimental results are shown in Figure 3.



(a) filmtrust



(b) movielens100K



(c) movielens1M

Figure 3. The RMSE of different datasets

From Figure 3, we can see that under different datasets, with the value of privacy budget ϵ increasing, the RMSE of different algorithms will roughly show a downward trend. Because the larger ϵ is, the smaller the random noise adds. Besides, the corre-

sponding degree of protection will also decrease, and the recommendation effect of the algorithm will be better.

From Figure 3, we can also see that different models will also have a certain impact on the evaluation indicators. For example, the effect of DPSS ++ is better than DPBSVD. This is because the SVD ++ recommendation model used by DPSS ++ has better performance and higher accuracy than the BiasSVD model used by DPBSVD. The reason is that the SVD ++ model increases the performance of implicit feedback. In this way, the accuracy of the model will be improved to a certain extent and the recommendation performance will be better. From Figure 3, we can see that the algorithms proposed in this paper have a better recommendation effect than several comparison algorithms, and with the increase of privacy budget, The changing trend of RMSE is also relatively stable and the convergence speed is relatively fast. Compared with the comparative experiment, the recommendation effect of the DBRDP algorithm in the three datasets is better and has been improved to some extent, and is closer to the benchmark experiment in this paper than other comparative experiments.

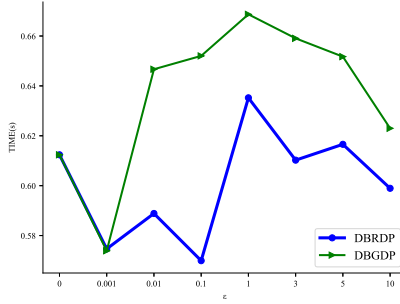
Figure 3 shows that the algorithms proposed in this paper can provide privacy protection for the model on different privacy budgets, and the evaluation index RMSE is smaller than the previously mentioned methods under the same privacy budget, which can provide privacy protection for the model and maintain the recommendation performance of the model.

In addition, to verify whether the proposed method will affect the performance of BCDSVD, this paper also compares the running time of DBGDP-BCDSVD, DBRDP-BCDSVD, and non-noisy BCDSVD models(where $\epsilon = 0$) to verify whether different privacy budgets will affect the performance of the BCDSVD model. We still repeat the experiment 10 times under the same privacy budget and take the average time of these 10 experiments as the measurement index for comparison. The experimental results are shown in Figure 4.

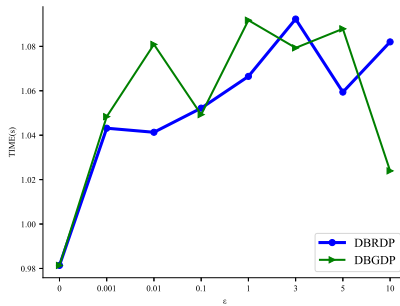
Figure 4 shows that although the algorithm of adding privacy has a certain impact on the running performance of the BCDSVD model under different privacy budgets, it is within an acceptable range. Although in some datasets, the running time of the method proposed in this paper is larger and more unstable than the non-noisy method, the recommended performance of the algorithm proposed in this paper is better, and it can quickly converge to the situation without noise. Therefore, we believe that on the premise of not seriously affecting the recommendation effect of the model, the running speed of the model will be affected and fluctuate under different privacy budgets, but we think such fluctuations are acceptable.

5. Conclusion

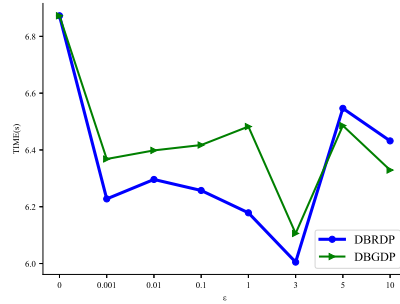
We design two algorithms by using the BCDSVD recommendation model and related differential privacy technology. The first one is data perturbation based Gaussian noise(DBGDP), and the other is data perturbation based Rényi differential privacy(DBRDP). Through corresponding theoretical and experimental analysis, we can conclude that the method proposed in this paper can better protect the model without seriously affecting the model recommendation effect, and can quickly converge to the non-noisy recommendation model. It can not only provide a better recommendation ef-



(a) filmtrust



(b) movielens100K



(c) movielens1M

Figure 4. The running time of different datasets

fect, but also provide privacy protection for the model. The usability and practicability of the model are better.

The main research work in the future is whether we can use the relevant technology of data perturbation to add dynamically allocated random noise to the dataset and apply it to model training without seriously affecting the performance of the model, and obtain better privacy protection.

References

- [1] Shi Y, Larson M, Hanjalic A. Collaborative filtering beyond the user-item matrix: A survey of the state of the art and future challenges[J]. *ACM Computing Surveys (CSUR)*, 2014, 47(1): 1-45.
- [2] Sweeney L. k-anonymity: A model for protecting privacy[J]. *International Journal of Uncertainty, Fuzziness and Knowledge-Based Systems*, 2002, 10(05): 557-570.
- [3] Li N, Li T, Venkatasubramanian S. t-closeness: Privacy beyond k-anonymity and l-diversity. 2007 IEEE 23rd International Conference on Data Engineering. IEEE, 2007: 106-115.
- [4] Machanavajjhala A, Kifer D, Gehrke J, et al. l-diversity: Privacy beyond k-anonymity[J]. *ACM Transactions on Knowledge Discovery from Data (TKDD)*, 2007, 1(1): 3-es.
- [5] Dwork C. Differential Privacy. *International Colloquium on Automata, Languages and Programming*. Springer, Berlin, Heidelberg, 2006: 1-12.
- [6] McSherry F, Mironov I. Differentially private recommender systems: Building privacy into the netflix prize contenders. *Proceedings of the 15th ACM SIGKDD international conference on Knowledge discovery and data mining*. 2009: 627-636.
- [7] Hua J, Xia C, Zhong S. Differentially private matrix factorization. *International Conference on Artificial Intelligence*. 2015: 1763-1770.
- [8] Xian Zhengzheng et al. Collaborative filtering via SVD ++ with differential privacy. *Control and Decision*. 2019.
- [9] Yan Shen et al. DynaEgo: Privacy-reserving collaborative filtering recommender system based on social-Aware differential privacy. *Proc of the Int Conf on Information and Communications Security*. Berlin: Springer, 2016: 347-357.
- [10] Zheng et al. Differential privacy matrix factorization recommendation algorithm fusing tag similarity. *Application Research of Computers*. 2020.
- [11] Friedman A, Berkovsky S, Kaafar M A. A differential privacy framework for matrix factorization recommender systems[J]. *User Modeling and User-Adapted Interaction*, 2016, 26(5): 1-34.
- [12] Wang J, Wang A. An Improved Collaborative Filtering Recommendation Algorithm Based on Differential Privacy. 2020 IEEE 11th International Conference on Software Engineering and Service Science (ICSESS). IEEE, 2020: 310-315.
- [13] K. Chaudhuri, A. Sarwate, and K. Sinha. Near-optimal differentially private principal components. In *Advances in Neural Information Processing Systems*, pages 989-997, 2012.
- [14] Kang et al. "Differentially Private ERM Based on Data Perturbation" . (2020). <https://arxiv.org/abs/2002.08578>.
- [15] Xu Y, Yin W. A block coordinate descent method for regularized multiconvex optimization with applications to nonnegative tensor factorization and completion. *SIAM J Imag Sci*, 2013, 6: 1758-1789
- [16] Paterek A. Improving regularized singular value decomposition for collaborative filtering. *Proceedings of KDD cup and workshop*. 2007, 2007: 5-8.
- [17] Cai et al. Efficient solution of the SVD recommendation model with implicit feedback. *SciSinInform*, 2020, 50: 1544-1558.
- [18] Martin Abadi, Andy Chu, Ian Goodfellow, H Brendan McMahan, Ilya Mironov, Kunal Talwar, and Li Zhang. Deep learning with differential privacy. In *Proceedings of the 2016 ACM SIGSAC Conference on Computer and Communications Security*. 308-318.
- [19] Mironov I. Rényi Differential Privacy. 2017 IEEE 30th Computer Security Foundations Symposium (CSF). IEEE, 2017.

A Deep Neural Network Model for the Prediction of Major Adverse Cardiovascular Event Occurrences in Patients with non-ST-Elevation Myocardial Infarction

Huilin ZHENG^a, Syed Waseem Abbas SHERAZI^a, Sang Hyeok SON^a, and Jong Yun LEE^{a,1}

^a*Department of Computer Science, Chungbuk National University, Cheongju, Chungbuk 28644, South Korea*

Abstract. Cardiovascular disease (CVD) is one of the major causes of death all over the world and the mortality rate is higher than other causes. Hence, we propose a novel deep neural network (DNN)-based prediction model for the major adverse cardiovascular event (MACE) occurrences in patients with non-ST-Elevation myocardial infarction (NSTEMI) to improve the prediction accuracy of CVD. The research contents are described as follows. First, for the experiment, we use the Korean Acute Myocardial Infarction Registry (KAMIR-NIH) dataset with 2 years follow-ups and then preprocess the extracted data, such as processing the missing values, solving the imbalance problem, and applying the normalization method to scale all the datasets in the same range for the experiment. Then we design a DNN-based prognosis model for the occurrences of MACE in NSTEMI patients. Finally, we evaluate the proposed model's performance and compare it with several applied machine learning algorithms, such as logistic regression, K-Nearest Neighbors, decision tree, and support vector machine. The result shows that the performance of our proposed method outperformed other machine learning-based prediction models.

Keywords. Cardiovascular disease, major adverse cardiovascular event, deep learning, NSTEMI, imbalanced data

1. Introduction

Cardiovascular disease (CVD) has been one of the major problems for all human beings and is considered the highest cause of mortality globally. There was an approximated 17.9 million death from CVD and accounted for 31% of all worldwide deaths in 2016 [1]. In addition, the CVD death is also severe in South Korea [2]. The treatment of the patients who suffering the CVD is expensive in hospitals. Therefore, the prediction of CVD at the early step is necessary for all people, especially for the aged, since the CVD burden will rise a lot with population aging [3]. Traditional prediction of the CVD has concentrated on regression-based models like Global Registry of Acute Coronary Events

¹ Corresponding Author: Jong Yun Lee, Department of Computer Science, Chungbuk National University, Cheongju, Chungbuk 28644, South Korea; E-mail: jonyun@chungbuk.ac.kr.

(GRACE) [4], Framingham risk scores [5], Thrombolysis in Myocardial Infarction (TIMI) [6], etc. Even though those regression-based models are commonly accepted tools for CVD, they were developed long since and cannot address the complex interactions between the risk factors [7, 8, 9].

Recently, various machine learning (ML) techniques have been developed for the prediction of CVD, which can reveal the complex interactions between different risk factors and also improve the accuracy of the prognosis model [7-10]. A ML-based prognosis model for the 1-year mortality was applied in Korean acute coronary syndrome patients using several ML algorithms such as generalized linear model (GLM), gradient boosting machine, etc., which showed that the ML-based prediction models enhanced the performances than the traditional regression-based GRACE model [7]. In addition, a paper used ML-based methods such as GLM, decision tree models, and Bayes models to predict the mortality of in-hospital for Chinese patients with ST-Elevation myocardial infarction (STEMI), which achieved higher prognosis performance than the previous in-hospital mortality prognosis STEMI models [10]. On the other hand, as a set of ML methods, the deep learning (DL) techniques also have shown strong abilities in many domains recently because of the increase of computational power [11]. In a paper, the authors developed a DL-based AI algorithm to predict the mortality of acute heart failure patients [12]. Another paper also generated a DL-based prognosis model of the occurrences of major adverse cardiovascular event (MACE) during the 1, 6, and 12-month follow-ups after discharge in patients with acute myocardial infarction using a deep neural network (DNN), where the result showed that the DL-based prediction model was superior to the GRACE model [13]. Nevertheless, most of the previous studies, which have used the conventional regression or ML-based models with limited risk factors, could not predict CVD accurately.

Hence, we propose a novel AI-based prognosis model using the DNN to get more accurate performance for the prognosis of MACE occurrences in patients with non-ST-Elevation myocardial infarction (NSTEMI). The research contents are shown as follows. Firstly, we extract the experimental NSTEMI patients' data from the raw KAMIR-NIH dataset and preprocess it by dealing with the missing values, solving the imbalance problem, and using the normalization approach to scale all the experimental data in the same range for the experiment. Secondly, we develop our DNN-based prognosis model for the MACE occurrences in NSTEMI patients. Finally, we evaluate and compare the performance of the proposed model with several popular machine learning algorithms, such as logistic regression (LR), K-Nearest Neighbors (KNN), decision tree (DT), and support vector machine (SVM).

2. Materials and Methods

The overall experimental framework of this paper mainly includes three parts, which is shown in Figure 1. The first part is the data extraction and preprocessing of the raw KAMIR-NIH dataset, which extracts and preprocesses the dataset for the experiment. The second part is the model generation, where we design the proposed DNN-based model and apply the other ML-based prognosis models for the occurrences of MACE in NSTEMI patients. The final part is the performance evaluation, where the performances of the proposed DNN-based and other ML-based prognosis models are evaluated and compared by several useful performance measures.

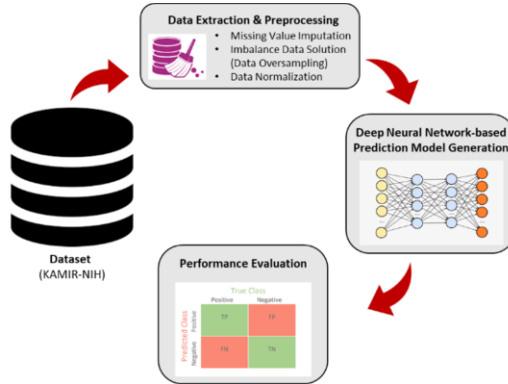


Figure 1. The overall experimental framework.

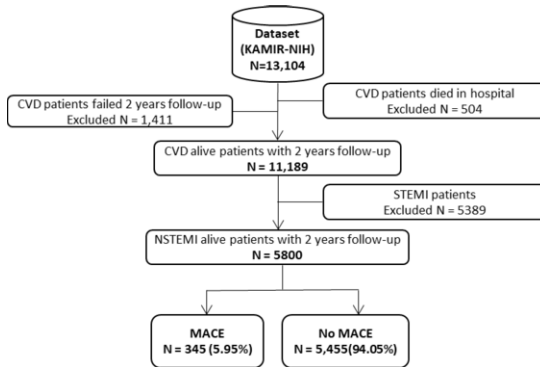


Figure 2. The process of data extraction.

2.1. Data source and preprocessing

The KAMIR-NIH dataset is used for the experiment in this paper. It is the first nationwide, multi-center registry with CVD patients in South Korea [14]. The dataset extraction process for getting the experimental dataset is shown in Figure 2, which includes 5,800 NSTEMI alive patients with 2 years follow-ups. The extracted variables include total 60 numerical and nominal features, where the nominal features are gender, previous chest pain, chest pain, electrocardiogram (ECG) use at admission, Killip class, dyspnea, ST-change on ECG, previous angina pectoris, previous myocardial infarction (MI), previous cerebrovascular disease, previous heart failure, diabetes mellitus, hypertension, dyslipidemia, family history of early age ischemic heart disease, family history of heart disease, history of smoking, symptoms of MI, pre-TIMI flow of target vessel, post-TIMI flow of target vessel, percutaneous coronary intervention (PCI), MI ECG change, use of coronary angiogram (CAG), result of CAG, use of thrombolysis, outcome of thrombolysis, initial diagnosis of STEMI & NSTEMI, final diagnosis of STEMI & NSTEMI, coronary artery bypass grafting (CABG), use of ECG in hospital, discharge type of patient, MACE, and the numerical features comprise age, diastolic blood pressure (DBP), Systolic Blood Pressure (SBP), height, weight, heart rate, abdominal circumference, white blood cells (WBC), WBC lymphocyte, WBC neutrophil, platelet, hemoglobin, creatinine, glucose, total cholesterol, maximum creatine kinase MB,

maximum creatine kinase peak, TnI, low-density lipoprotein cholesterol, high-density lipoprotein cholesterol, hsCRP, HbA1c, BNP, NTproBNP, triglyceride, discharge heart rate, discharge DBP, discharge SBP. The target variable MACE is defined as myocardial infarction (MI), CABG, non-cardiac death, cardiac death, and re-percutaneous coronary intervention (re-PCI), whereas other events are considered as No_MACE. Nevertheless, there are numerous missing values in the extracted data. Therefore, we impute those missing values with zero in this paper to solve the missing values. In addition, the data imbalanced problem is obvious in our experimental data, where the ratio of the No_MACE and MACE is 15.8:1. Many different techniques were implemented to deal with the data imbalance issue, such as data sampling, cost-sensitive techniques, etc. [15]. This paper use one of the data sampling methods to overcome the imbalance issue for the experimental data, which is called borderline synthetic minority oversampling (Borderline-SMOTE1) [16]. It is an extension of the Synthetic Minority Oversampling Technique (SMOTE) technique [17], which can only produce synthetic minority cases to oversample the minority group along the decision boundary between the two classes [16]. After that, we apply the MinMaxScaler to normalize the training dataset into range 0 to 1, and then use it to transform the test dataset for improving the prediction accuracy. The mathematical equation of the MinMaxScaler is shown in Eq. (1) [18].

$$x_{scaled} = \frac{x - x_{min}}{x_{max} - x_{min}} \quad (1)$$

2.2. Proposed method

A DNN is an artificial neural network with manifold hidden layers between the input and output layers [19]. In this paper, a DNN-based prognosis model was proposed which is presented in Figure 3. The proposed DNN-based prediction model includes two hidden layers. To get optimal performance, the neurons of each hidden layer are tuned by the grid search method because the grid search is simple to implement and parallelization is trivial [20], where there are 100 optimal neurons in each hidden layer. In modern artificial neural networks, the activation function is an important feature that decides whether a neuron should be activated or not. Many different types of typical activation functions like tanh, sigmoid, rectified linear unit (ReLU), etc. were introduced [21]. In this paper, the ReLU activation function is used by reason of its efficiency. It outputs the input directly if it is a positive value or simply replaces the input with zero if it is a negative value [21]. In addition, the Adam optimizer is used to update network weights iterative which is an extension to stochastic gradient descent-based optimizer and computationally efficient [22]. And during the model training, the dropout layer [23] (dropout rate=0.2) and early stopping [24] methods are used to reduce overfitting and improve the generation of DNN.

We have compared the designed DNN-based prediction model with four popular ML-based prognosis models for MACE occurrences, such as LR [25], KNN [26], DT [27], and SVM [28], where the LR algorithm uses a sigmoid function to map the predicted values to probabilities within the range of [0,1] and then assign examples to a discrete set of classes; KNN algorithm captures the idea of similarity and put the new case into the category that is most similar to the available categories; DT algorithm learns simple decision rules using the tree representation to solve the classification or regression problems; SVM algorithm creates a hyperplane that can segregate a higher dimensional space into classes. The default parameters of the four ML algorithms in the scikit-learn

package are used to create the compared models, where the *max_iter* parameters of LR and SVM are set to 20,000 for the solvers to converge.

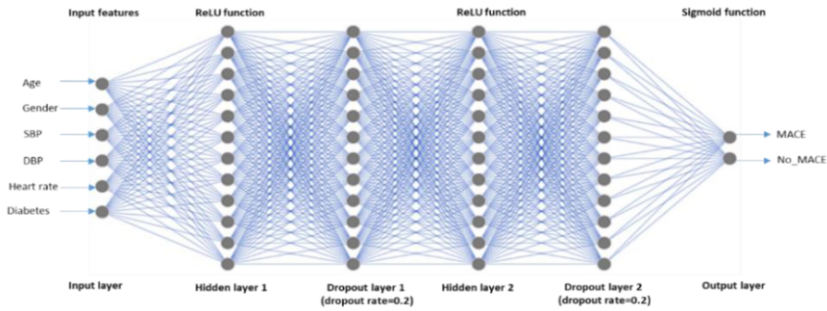


Figure 3. Proposed deep neural network-based prediction model for MACE occurrences.

2.3. Performance measures

For the evaluation of our prediction model, we split our dataset as 70% training and 30% test dataset, where the training dataset is applied to create the proposed prognosis model for the occurrences of MACE in NSTEMI patients, and the test dataset is utilized to evaluate the performance of the proposed prediction model. The performance is evaluated by the precision, recall, F1-score, accuracy, and the area under the ROC curve (AUC) for the applied prediction models.

3. Results and Discussion

In the experiment, we proposed a DNN-based model for the prognosis of MACE occurrences in patients with NSTEMI. The performance of the proposed prediction model was compared with four popular ML-based prognosis models such as LR, KNN, DT, and SVM. The results of the performance comparison for the proposed and compared prognosis models are shown in Table 1, where the best results are presented in bold. The Receiver Operating Characteristic (ROC) curves of the proposed and compared prediction models are shown in Figure 4.

The result shows that the performance of the proposed prognosis model outperformed other statistic-based, instance-based, and tree-based prediction models with the highest accuracy, precision, F1-score, and AUC scores as 0.9594, 0.9487, 0.9611, and 0.9589, respectively, however, the KNN-based prediction model got the best recall as 0.9864. In addition, in the four compared prediction models, the DT and KNN-based prediction models got higher performance with more than 91% accuracy than the LR and SVM-based models.

Table 1. Results of the performance comparison of the proposed and compared prediction models.

	LR	SVM	KNN	DT	Proposed Model
Accuracy	0.7372	0.7372	0.9132	0.9248	0.9594
Precision	0.7576	0.7612	0.8646	0.9197	0.9487
Recall	0.7217	0.7152	0.9864	0.9361	0.9739
F1-score	0.7392	0.7375	0.9215	0.9278	0.9611
AUC	0.7378	0.738	0.9108	0.9245	0.9589

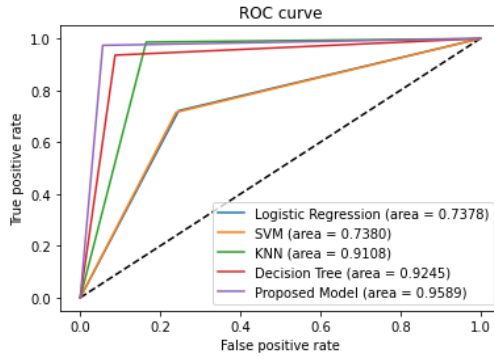


Figure 4. Receiver Operating Characteristic (ROC) curves of the proposed and compared prediction models.

4. Conclusion

In this paper, a DNN-based model was proposed for the prediction of MACE occurrences in NSTEMI patients using the KAMIR-NIH dataset with 2 years follow-ups. The performance of the designed DNN-based prognosis model was evaluated and compared with the other four ML-based models, which showed that the proposed DNN-based prognosis model achieved the greatest performance around 96% accuracy to the prognosis of MACE occurrences in patients with NSTEMI. Consequently, the DL method showed more accurate prediction results for MACE occurrences in NSTEMI patients.

However, there are several limitations to this paper. First, the result of this paper is difficult to apply to other populations since we experimented on the Korean dataset. Second, we only applied one type of data sampling technique to oversample the minority class without comparing with other popular methods to solve the data imbalance problem.

Acknowledgments

This work was supported in part by the Korea Institute for Advancement of Technology (KIAT) Grant through the Korean Government by the Ministry of Trade, Industry and Energy (MOTIE) under Grant N0002429, in part by the Basic Science Research Program through the National Research Foundation of Korea (NRF) by the Ministry of Education under Grant 2017R1D1A1A02018718, and in part by the Ministry of Science and ICT (MSIT), South Korea, through the Grand Information Technology Research Center Support Program supervised by the Institute for Information and Communications Technology Planning and Evaluation (IITP) under Grant IITP-2021-2020-0-01462.

References

- [1] World Health Organization, Cardiovascular diseases (CVDs). Available from: [https://www.who.int/news-room/fact-sheets/detail/cardiovascular-diseases-\(cvds\)](https://www.who.int/news-room/fact-sheets/detail/cardiovascular-diseases-(cvds)) [Accessed 06 Sept 2021]
- [2] Shin HY, Lee JY, Song J, Lee S, Lee J, Lim B, ... Huh S. Cause-of-death statistics in the Republic of Korea, 2014. *Journal of the Korean Medical Association*. 2016;59(3):221-232.

- [3] Roth GA, Mensah GA, Johnson CO, Addolorato G, Ammirati E, Baddour LM, ... Fuster V. Global Burden of Cardiovascular Diseases Writing Group. Global burden of cardiovascular diseases and risk factors, 1990–2019: update from the GBD 2019 paper. *Journal of the American College of Cardiology*. 2020;76(25):2982-3021.
- [4] Fox KA, Dabbous OH, Goldberg RJ, Pieper KS, Eagle KA, Van de Werf F, ... Granger CB. Prediction of risk of death and myocardial infarction in the six months after presentation with acute coronary syndrome: prospective multinational observational paper (GRACE). *bmj*. 2006;333(7578):1091.
- [5] Wilson PW, D'Agostino RB, Levy D, Belanger AM, Silbershatz H, Kannel WB. Prediction of coronary heart disease using risk factor categories. *Circulation*. 1998;97(18), 1837-1847.
- [6] Antman EM, Cohen M, Bernink PJ, McCabe CH, Horacek T, Papuchis G, ... Braunwald E. The TIMI risk score for unstable angina/non-ST elevation MI: a method for prognostication and therapeutic decision making. *Jama*. 2000;284(7):835-842.
- [7] Sherazi SWA, Jeong YJ, Jae MH, Bae JW, Lee JY. A machine learning-based 1-year mortality prediction model after hospital discharge for clinical patients with acute coronary syndrome. *Health informatics journal*. 2020;26(2):1289-1304.
- [8] Patel B, Sengupta P. Machine learning for predicting cardiac events: what does the future hold?. *Expert review of cardiovascular therapy*. 2020;18(2):77-84.
- [9] Zheng H, Sherazi SWA, Lee JY. A Stacking Ensemble Prediction Model for the Occurrences of Major Adverse Cardiovascular Events in Patients With Acute Coronary Syndrome on Imbalanced Data. *IEEE Access*. 2021;9:113692-113704.
- [10] Li X, Liu H, Yang J, Xie G, Xu M, Yang Y. Using machine learning models to predict in-hospital mortality for ST-elevation myocardial infarction patients. In *MEDINFO 2017: Precision Healthcare through Informatics*. IOS Press, 2017;476-480.
- [11] Bizopoulos P, Koutsouris D. Deep learning in cardiology. *IEEE reviews in biomedical engineering*. 2018;12:168-193.
- [12] Kwon JM, Kim KH, Jeon KH, Lee SE, Lee HY, Cho HJ, ... Oh BH. Artificial intelligence algorithm for predicting mortality of patients with acute heart failure. *PloS one*. 2019;14(7):e0219302.
- [13] Kim YJ, Saqlian M, Lee JY. Deep learning-based prediction model of occurrences of major adverse cardiac events during 1-year follow-up after hospital discharge in patients with AMI using knowledge mining. *Personal and Ubiquitous Computing*. 2019;1-9.
- [14] Korea Acute Myocardial Infarction Registry. Available from: <http://kamir5.kamir.or.kr> [Accessed 06 Sept 2021]
- [15] Ali A, Shamsuddin SM, Ralescu AL. Classification with class imbalance problem. *Int. J. Advance Soft Compu. Appl*. 2013;5(3).
- [16] Han H, Wang WY, Mao BH. Borderline-SMOTE: a new over-sampling method in imbalanced data sets learning. In *International conference on intelligent computing*. Hefei, China, 2005;878–887. Springer, Berlin, Heidelberg.
- [17] Chawla NV, Bowyer KW, Hall LO, Kegelmeyer WP. SMOTE: synthetic minority over-sampling technique. *Journal of artificial intelligence research*. 2002;16:321-357.
- [18] Bisong E. Introduction to Scikit-learn. In *Building Machine Learning and Deep Learning Models on Google Cloud Platform*. Apress, Berkeley, CA; 2019. 215-229.
- [19] Sze V, Chen YH, Yang TJ, Emer JS. Efficient processing of deep neural networks: A tutorial and survey. *Proceedings of the IEEE*. 2017;105(12):2295-2329.
- [20] Bergstra J, Bengio Y. Random search for hyper-parameter optimization. *Journal of machine learning research*. 2012;13(2):281-305.
- [21] Sharma S, Sharma S. Activation functions in neural networks. *Towards Data Science*. 2017;6(12):310-316.
- [22] Kingma DP, Ba J. Adam: A method for stochastic optimization. *arXiv preprint arXiv:1412.6980*. 2014;1-15.
- [23] Srivastava N, Hinton G, Krizhevsky A, Sutskever I, Salakhutdinov R. Dropout: a simple way to prevent neural networks from overfitting. *The journal of machine learning research*. 2014;15(1):1929-1958.
- [24] Prechelt L. Early stopping-but when?. In *Neural Networks: Tricks of the trade*. 1998;55-69. Springer, Berlin, Heidelberg.
- [25] Bagley SC, White H, Golomb BA. Logistic regression in the medical literature: Standards for use and reporting, with particular attention to one medical domain. *Journal of clinical epidemiology*, 2001;54(10):979-985.
- [26] Cover T, Hart P. Nearest neighbor pattern classification. *IEEE transactions on information theory*. 1967;13(1):21-27.
- [27] Breiman L, Friedman JH, Olshen RA, Stone CJ. *Classification and Regression Trees*. Routledge, 1984.
- [28] Hearst MA, Dumais ST, Osman E, Platt J, Scholkopf B. Support vector machines. *IEEE Intell. Syst. Appl*. 2008;13(4):18–28.

Do Reviews Influence Real Estate Marketing: The Experience Combing with Natural Language Processing

Ting WU^a, Guang YU^{a,1}, Tong LI^a, Dan SHANG^b and Wuwu YAN^c

^a*School of Management, Harbin Institute of Technology, P.R.China*

^b*Heilongjiang Eldath Educational Information Consulting Co., Ltd, P.R.China*

^c*Pang An property & casualty insurance company of China. LTD, P.R.China*

Abstract. In the Internet era, since online user reviews play an important role in various fields, various industries including real estate industry attach great importance to that. However, according to the existing literatures, there is no clear conclusion that whether online user reviews have an impact on real estate marketing. In order to figure out this problem, this paper will combine traditional real estate theories and machine learning technology to mine data on Chinese real estate online user reviews. We use natural language processing technology and panel data regression analysis method to explore whether the emotional tendency of online user reviews have an impact on the price of second-hand housing in real estate companies, and research more deeply about its impact on marketing of real estate companies. Our research provides a reference for real estate companies to make effective marketing strategies.

Keywords. Estate marketing, Reviews, Sentiment analysis, Word2vec, Natural Language Processing

1. Introduction

In the Internet era, online user reviews play a pivotal role in product marketing. Especially for enterprises, online user reviews can not only influence on the judgment of customers but also change their desire of purchasing. At the same time, they greatly influence on corporate brand image and provide companies with opportunities for better business activities. Therefore, online user reviews are widely valued by companies.

There are many existing researches on online user reviews in recent years. In the field of marketing, online user reviews can boost sales of fashion shopping, electronics and video games [1; 2], and help companies identify consumer needs and adjust marketing strategies to increase their competitiveness [3; 4]. In addition, digital marketing strategies affect both the quantity and value of online reviews and indirectly impact on hotel performance [5]. Online user reviews can also help customers make reasonable shopping decisions and reduce the risk of shopping [6]. On the electronic word-of-mouth, researching online user reviews can help companies identify potential electronic word-of-mouth customers to improve product sales [7]. On the other hand,

¹ Corresponding author, Guang YU, School of Management, Harbin Institute of Technology, 92 Xidazhi Street, Nangang District, Harbin, P.R.China; E-mail: yug@hit.edu.cn.

reveal the mechanism that affects companies' reputation and provide references for companies to change their marketing strategies[8; 9]. In forecasting and recommendation system, Tingting Song, Siering M, Bakhshi S and others[10-12] have shown that online user reviews can assist to improve the performance of the movie box, airline and catering industry's forecasting and recommendation systems. These studies have fully demonstrated that user reviews play different roles in various fields.

Due to this, online user reviews are also valued by real estate marketers. In order to promote real estate marketing by that, major real estate companies set up homepages, community forums or user reviews windows on different platforms (as shown in Figure 1.), and spend human labour and material resources to maintain and control them. However, there are few related literatures available about whether online user reviews affect real estate sales. Therefore, there is great uncertainty for real estate marketing strategies by online user reviews.

In order to solve the above problems, this paper intends to analyze the impact of online user reviews on real estate marketing. We add other online user reviews factors based on traditional real estate marketing theory[13-15]. The research data are from three Real estate related websites. By web crawler technology, we collect and figure out sales data, online user evaluation data and reviews about 12 real estate companies in around 10 months. And then we start our research by combining with natural language processing technology and panel data regression analysis method.

The research uses natural language processing technology to calculate the text data. Initially, through web crawler technology, relevant data is accessed online. Based on PyCharm development environment, the structure of the unstructured raw data obtained by web crawler is set up. And real estate companies' related data and user reviews data are extracted and stored in a table format. Secondly, we use Python language for data preprocessing, which include data cleaning, using the jieba lexicon to perform word segmentation processing on online Chinese text-data user reviews, then the user reviews dataset is formed. Thirdly, based on the skip-gram model from word2vec, a word vector calculation tool launched by Google in 2013[16; 17], the user reviews dataset is vectorized and the user review dictionary is constructed.

Finally, based on GitHub open source of Random Forest algorithm[18; 19], which uses the decision tree to vote together to determine the advantages of classification results, we analyze online user reviews data of sentiment orientation, and obtain the quantitative representation of user reviews data.

The research combines with real estate marketing theory[13-15] and panel data regression analysis method. First of all, we establish a regression model about the impact of online user reviews on real estate sales. We define the explained variables and the explanatory variables based on real estate marketing theory. Next, performing unit root test and cointegration test ensure the stability of the variables and avoid the occurrence of pseudo-regression. Finally, by using the individual fixed-effects model for analysis, this research establishes the models, which are the models for analysis in terms of both two explained variables, according to adding user reviews or not.

The purpose of this research is to reveal the relationship between online user reviews and real estate marketing.

The structure of this paper is as follows: the second part describes the methodology, including data collection and preprocessing, user reviews sentiment analysis and exploratory analysis; the third part shows the results of exploratory analysis; and the fourth part summarizes the research briefly.



Figure 1. Online user reviews windows

2. Methodology

Real estate marketing is mainly product-oriented because it has the characteristics of fixedness, single-piece, large amount of value and high unit price. For example, real estate marketing based on 4P theory mainly focuses on product, price, place and promotion[15]. With the changes in the marketing environment, real estate marketing also considers the needs of consumers. But real estate prices which include second-hand housing prices are still an important factor in marketing. The factors affecting real estate prices are mainly divided into three parts, that are general factors, regional factors and individual factors. Among them, the general factors mainly include economic factors, social factors, administrative factors, and so on; regional factors mainly include the prosperity of business services, traffic convenience, urban facilities, environmental conditions, etc.; and individual factors mainly include land and buildings. Among the above three parts of factors, regional factors are more concerned by consumers, so the impact on the price of housing, especially the price of second-hand housing is more obvious.

Based on the above theory, this paper selects second-hand housing as the explained variables for considering that the new housing price is relatively stable, and the second-hand housing price fluctuation range is large. Specifically, that are the difference between the price of second-hand housing and the price of the district, and the difference between the price of second-hand housing and the price of real estate. In addition, when setting explanatory variables, this paper considers the regional factors of housing prices, and adds the impact of consumer reviews, which would help to explore the relationship between user reviews and real estate marketing. Specifically, the explanatory variables include the online user evaluation dimension and online user reviews, that are price, district, transportation, support, environment and online reviews.

2.1. Data collection and preprocessing

2.1.1. Data collection

The data in this paper comes from Chongqing Online Real Estate, National Real Estate Market Data Center and Fangtianxia platform. Chongqing Online Real Estate has official real estate authority data. National Real Estate Market Data Center has a real estate

market database covering the whole China. Fangtianxia platform is the leading professional network platform for real estate industry and provides services such as owners' forums and community websites for all real estate projects.

Web crawler is used to collect online user related information, user evaluation data and user review data of real estates from January 1, 2018 to October 31, 2018 from the above network platforms, which includes real estate name, reviews time, user ratings of various factors (including price, district, transportation, support and environment) and user reviews. And then collect second-hand housing prices from real estates from Chongqing online real estate. A total of 12 real estates and 973 data were collected.

2.1.2. Data preprocessing

Data preprocessing flowchart is shown in Figure 2.

First of all, as the original data obtained by web crawler is unstructured data, which contains irrelevant information for the research, the information related to the research needs to be extracted from the original data and stored for the form data available. Based on Pycharm development environment, we use Python programming language to extract real estates' name, user name, user reviews time, user evaluation data (including price, district, transportation, support and environment), user reviews and real estate second-hand housing prices from the original data. After being extracted, these data are saved as a tabular form.

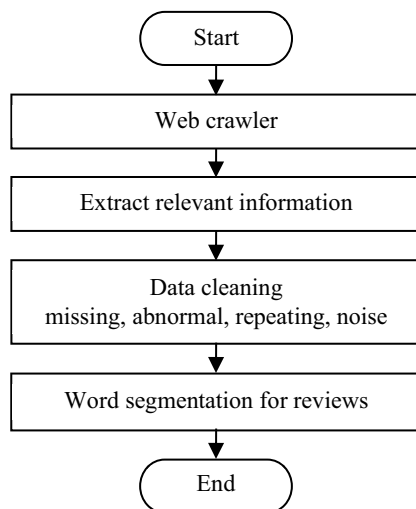


Figure 2. Data preprocessing flowchart

Next, we clean the data in tabular form by using python programming language, which includes missing values, outliers, duplicate values, and noise data. The first step is to delete or fill the missing values and the outliers; the next is to combine the repeated values by sorting and data similarity calculation; and the last step is to use the regression method to smooth the noise data. After cleaning, there are 263 data for 6 real estate companies available.

At the end of data processing, the text of user reviews is processed by using jieba lexicon of the GitHub open-source community, which is a third-party library of Chinese word segmentation with excellent performance, and uses a Chinese vocabulary to determine the probability of association between Chinese characters.

Through jieba lexicon, Chinese characters with high probability would form a phrase and build up the result of word segmentation[20]. Jieba lexicon participle supports three modes of word segmentation, namely precise mode, full mode and search engine mode. In precise mode, text can be accurately separated and there are no redundant words, in which it is suitable for text analysis; while in full mode, all possible words in the text can be scanned with excellent computing performance, but there is redundant and it cannot solve the ambiguity problem. Based on precise mode, search engine mode split the long words again to improve the recall rate, which is suitable for search engine segmentation. According to the characteristics of each mode and the applicable scenarios, our research selects precise mode for user reviews segmentation processing and obtains a list of user reviews data.

2.2. Comment sentiment analysis

2.2.1. Comment data dictionary construction based on word2vec

Before conducting sentiment analysis of the reviews data, the reviews text needs to be converted into vectors by using skip-gram model in word2vec. Word2vec is a natural language processing tool launched by Google in 2013, and skip-gram model is an effective method to learn high-quality distributed word vector representation[16; 17], which is able to capture a large number of precise syntactic and semantic word relationships. The specific equation is expressed as follows: for a given set of training words, w_1, w_2, \dots, w_T , the purpose of skip-gram model is to maximize the average log probability, which is shown in Eq. (1).

$$\frac{1}{T} \sum_{t=1}^T \sum_{-c < j \leq c, j \neq 0} \log p(w_{t+j} | w_t) \quad (1)$$

Where c is the size of the training context. While the larger c is, the larger the training set, which means higher training accuracy. And $p(w_{t+j} | w_t)$ is defined by a softmax function shown in Eq. (2).

$$p(w_o | w_I) = \frac{\exp(v'_{w_o} v_{w_I})}{\sum_{w=I}^W \exp(v'_{w} v_{w_I})} \quad (2)$$

Where v_w and v'_w respectively represents the input and output vector representations of, and W is the number of words in the vocabulary.

Due to the high computational complexity of $\nabla \log p(w_o | w_I)$, it is really inefficient to train the model directly using the basic skip-gram formulation. Therefore, word2vec also provides two efficient training methods (including negative sampling and hierarchical softmax) to improve training speed and quality of skip-gram model. By using the computationally efficient skip-gram model here, high quality word and phrase representations would be learned in this section. In order to prepare for subsequent sentiment analysis of reviews, this section uses word2vec from GitHub b's open source to perform a vector representation for reviews dataset.

2.2.2. Sentiment analysis

In this section, Random Forest algorithm is used to classify the sentimental tendency of user reviews data. Random Forest algorithm is a supervised learning algorithm based on Bagging integration that is built by the based learning device of decision tree, and further introduces random attribute selection in the decision tree training process[18; 19]. Different from traditional decision tree which selects an optimal attribute in the attribute set of the current node when selecting the partition attribute, Random Forest algorithm selects the randomly selected feature to construct the optimal segmentation, that is, Random Forest algorithm only considers the random subset used to segment the nodes, and then selects an optimal attribute from this subset for partitioning. The schematic diagram of Random Forest algorithm structure is shown in Figure 3.

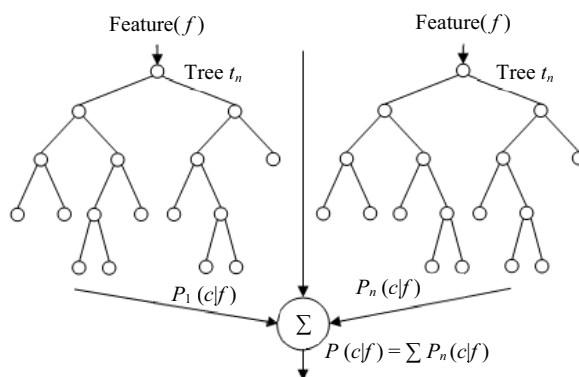


Figure 3. Schematic diagram of Random Forest structure

Random Forest consist of multiple CART (Classification and Regression Trees) and each decision tree is independent of each other. When a sample is input, each decision tree will get a result. The final result will be voted, and the one with the most votes will be the output result. Random forest has two random sampling processes, namely row and column sampling:

- (1) In row sampling, the number of random sampling samples is the same as the number of input samples, and sampling with replacement is used. In this way, the input samples of each tree are not all samples, which can prevent the occurrence of over-fitting.
- (2) Column sampling is randomly sampled without replacement according to a certain proportion. Assuming that there are M features and the number of samples is m , where $m \ll M$, the ratio can be \sqrt{M} , $1/2 * \sqrt{M}$ or $2 * \sqrt{M}$.

The decision tree is built from the sampled data. A certain node of the decision tree either cannot continue to split, or all its samples point to one category. Row sampling and column sampling together ensure randomness. When the number of layers is low, even without pruning, over-fitting will not occur.

The training process of Random Forest is as follows:

- (1) Given training set S , test set T and feature dimension F . Determine the parameters, that is, the number of CARTs used t , the depth d of each tree, the number of features f used by each node, and the termination conditions (including the minimum number of samples on the node s , and the minimum information gain on the node m).

For the i - t tree, $i=1-t$,

- (2) From S , there is a training set $S(i)$ with the same size as S , randomly selected as the sample of the root node, and training is started from the root node.
- (3) If the termination condition is reached on the current node, set the current node as a leaf node.
 - 1) If it is a classification problem, the predicted output of the leaf node is the largest type $c(j)$ in the current node sample set, and the probability p is the proportion of $c(j)$ in the current sample set.
 - 2) If it is a regression problem, the prediction output is the average value of each sample value of the current node sample set. Then continue to train other nodes.

If the current node does not meet the termination condition, f -dimensional features are randomly selected from the F -dimensional features without replacement. Use this f -dimensional feature to find the one-dimensional feature k with the best classification effect and its threshold th . The samples with the k -th dimension of the sample on the current node less than th are divided into the left node, and the rest are divided into the right node. Continue to train other nodes.

- (4) Repeat (2) and (3) until all nodes are trained or marked as leaf nodes.
- (5) Repeat (2), (3), (4) until all CARTs have been trained.

The prediction process of random forest is as follows:

For the $1-t$ tree, $i=1-t$,

- (1) Starting from the root node of the current tree, judge whether to enter the left node ($<th$) or the right node ($\geq th$) according to the threshold th of the current node, until reaching a certain leaf node, and output the predicted value.
- (2) Repeat (1) until all t trees have output predicted values.
 - 1) For a classification problem, the result is the class with the largest sum of predicted probabilities in all trees, that is, the p of each $c(j)$ is accumulated.
 - 2) For a regression problem, the result is the average of the outputs of all trees.

This process produces a wide range of versatility and enables better performance models. Random Forest algorithm exhibit powerful performance in many real-world tasks because of the advantages of simple, easy to implement, lower computational cost and good generalization performance. We classify user reviews data through Random Forest algorithm from GitHub's open source. The labels of sentiment analysis were independently annotated by three researchers, and finally they were collated with each other. Data that cannot be agreed upon will be eliminated, so we can guarantee the accuracy of the proofreading data. We use the labeled data as training data, put it into the model for training, and make predictions on the unlabeled data. In the end, we used the 10-fold cross-validation to valid, and the accuracy of Random Forest algorithm is 63.7, so we finish scoring the emotional tendencies of user reviews data. The accuracy of the prediction result is the problem, and finally the error is introduced into the regression model. Through analysis, it is found that the correct examples of predictions have sentence sentiment consistency and sentiment clarity, while wrong examples are manifested as emotional inconsistencies, such as inconsistent evaluations of different aspects in a sentence, or even large differences.

2.3. Exploratory analysis

Further, we use panel data regression analysis to research the impact of online user reviews on real estate sales [21-23]. We define two explained variables as the difference between the price of second-hand housing and the price of the district, and the difference between the price of second-hand housing and the price of real estate. And the explanatory variables are the evaluation dimension and online reviews of the online user for the real estate that includes price, district, transportation, support, environment and online reviews.

Before starting panel data regression analysis, the unit root test and the cointegration test are needed to ensure the stability of the variables, avoid the occurrence of pseudo-regression and ensure the validity of the subsequent analysis results. The unit root test results of panel data regression analysis show that the variables are stable in all cases and are single-order in the same order. Since the purpose of the cointegration test is to investigate whether a linear combination of a set of non-stationary sequences has a cointegration relationship, it's unnecessary to perform the cointegration test on each variable.

This research will use individual fixed-effect models to analyze. There're four models to research the impact of online user reviews on real estate sales. For two explained variables (the difference between the price of second-hand housing and the price of the district, and the difference between the price of second-hand housing and the price of real estate), considering whether the factor of user reviews is taken into account, we establish regression models as Eqs. (3) and (4):

$$PD_1 = \alpha_{01} + \alpha_{11}COM_1 + \alpha_{21}PRI_1 + \alpha_{31}DIS_1 + \alpha_{41}TRA_1 + \alpha_{51}SUP_1 + \alpha_{61}ENV_1 + \varepsilon_1 \quad (3)$$

$$PD_2 = \alpha_{02} + \alpha_{12}COM_2 + \alpha_{22}PRI_2 + \alpha_{32}DIS_2 + \alpha_{42}TRA_2 + \alpha_{52}SUP_2 + \alpha_{62}ENV_2 + \varepsilon_2 \quad (4)$$

Where PD_1 is the difference between the price of second-hand housing and the price of the district, PD_2 is the price of second-hand housing and difference between real estate prices, and COM , PRI , DIS , TRA , SUP , and ENV respectively represents user reviews, user evaluation about price, district, transportation, support and environment.

3. Results

For the difference between the price of second-hand housing and the price of the district, Model 1 is a model in which user reviews isn't taken into account while Model 2 is; and for the difference between the price of second-hand housing and the price of real estate, Model 3 is a model in which user reviews isn't taken into account while Model 4 is.

Table. 1 shows the results of panel data regression analysis. Among them, the units of PDI and $PD2$ are *RMB* yuan, and the other variables are scores (1-5 points). The coefficient of regression analysis is determined by R-squared in panel analysis. Tabel.1 shows that the R^2 of each model is greater than 70%, indicating that each model has a good fitting effect on the sample data. This shows the effectiveness of the model.

Table 1. Results of panel data regression analysis

	Model 1 (PD ₁ , no COM)	Model 2 (PD ₁ , contained COM)	Model 3 (PD ₂ , no COM)	Model 4 (PD ₂ , contained COM)
COM	-	281.4906 (0.124410)	-	-1094.152 (-0.345290)
PRI	-5017.377*** (-3.431980)	-4962.971*** (-3.215353)	-7937.725*** (-3.871720)	-8149.199*** (-3.769799)
DIS	4217.333** (2.359367)	4148.147** (2.190837)	7462.432*** (2.976994)	7731.358*** (2.915602)
TRA	127.6533 (0.104681)	88.05184 (0.069054)	493.6364 (0.288657)	647.5670 (0.362620)
SUP	-1048.875 (-0.717813)	-1086.942 (-0.719430)	-324.6592 (-0.158436)	-176.6957 (-0.083507)
ENV	-815.5719 (-0.523779)	-800.0388 (-0.505857)	234.4921 (0.107388)	174.1153 (0.078609)
R-squared	0.868042	0.868094	0.703902	0.704804
Adjusted R-squared	0.805362	0.800450	0.563255	0.553422
F-statistic	13.84875	12.83327	5.004758	4.655790

Note: ** indicates that the 0.05 level is significant; *** indicates that the 0.01 level is significant; the value in parentheses is the estimated T statistic; '-' indicates that the corresponding explanatory variable is not included in the model.

Explanatory variable of user's evaluation of price (*PRI*) is significant for the difference between the price of second-hand housing and the price of the district (*PD*₁), and the difference between the price of second-hand housing and the price of real estate (*PD*₂) at the 0.01 level. It shows that the impact of *PRI* on *PD*₁ and *PD*₂ is very significant and shows a negative correlation. When *PRI* decreases, *PD*₁ and *PD*₂ will increase tremendously. Explanatory variable of user's evaluation of district (*DIS*) is significant for the difference between the price of second-hand housing and the price of the district (*PD*₁) at the 0.05 level, while it's significant for the difference between the price of second-hand housing and the price of real estate (*PD*₂) at the 0.01 level. It shows that *DIS* has a significant impact on *PD*₁ and *PD*₂, and shows a positive correlation. That is, the larger the *DIS*, the larger the *PD*₁ and *PD*₂. But other explanatory variables, including online reviews (*COM*), online user's evaluation of transportation (*TRA*), support (*SUP*) and environment (*ENV*) aren't significant for both *PD*₁ and *PD*₂. That means *COM*, *TRA*, *SUP* and *ENV* have no effect on *PD*₁ and *PD*₂.

The results show that the emotional tendency of user reviews does not constitute an influencing factor of the difference between the price of second-hand housing and the price of the district (*PD*₁) and the price of second-hand housing and the price of real estate (*PD*₂).

4. Conclusion

Online user reviews have an increasing impact on various fields, especially in the field of marketing, which not only affect companies' reputation and marketing strategies, improve corporate recommendation and predicts system performance, but also help customers make consumption decisions and reduce consumption risks. In view of their huge influence, real estate marketers have been paying increasing attention to online user reviews and spending human labour and material resources to maintain and control them. However, according to the existing literatures, there is no clear conclusion that whether online user reviews affect real estate sales. And it brings great uncertainty to formulate real estate marketing strategies. Therefore, this paper explains the relationship between online user reviews and real estate sales, and provides a reference for real estate companies to make effective marketing strategies.

This research combines traditional real estate theories with natural language processing technology. We take online user reviews into account and analyze the impact of online user reviews on real estate marketing. The research firstly collects online user reviews data of real estate companies by using natural language processing technology, and then conducts sentiment analysis of online user reviews based on word2vec and Random Forest algorithm. Secondly, we adopt panel data regression analysis method to analyze the relationship between the emotional tendency of online user reviews and second-hand housing prices.

The results show that the emotional tendency of online user reviews does not affect the price of second-hand housing. It means online user reviews have no impact on the real estate marketing. Therefore, the real estate companies' marketing strategies based on online user reviews are worthless. Real estate companies can adjust marketing strategies based on the results of the research to improve marketing effectiveness.

When online user reviews are taken into account during analyzing real estate marketing strategies, traditional real estate marketing theory is improved. And that provides new theoretical ideas for subsequent research. At the same time, we find that natural language processing technology and real estate marketing strategy analysis can be combined. The research methods of real estate marketing strategy are enriched by using natural language processing technology to mine potential marketing influence factors.

While we use word2vec and Random Forest algorithm to conduct sentiment analysis of online reviews, there are two models, BERT and ERNIE, launched some time ago. BERT was launched by Google in 2018, and it achieved the best results than other models in different natural language processing tasks. And ERNIE, Baidu's NLP pre-training model, was released in 2019, and surpassed BERT in several Chinese tasks. Future research can expand the research dataset, and use BERT and ERNIE for sentiment analysis to explore the impact of online reviews on marketing. That is predicted to enrich the analysis methods of marketing strategies.

References

- [1] Kawaf, F, Istanbuluoglu, D. Online fashion shopping paradox: The role of customer reviews and facebook marketing[J]. *Journal of Retailing and Consumer Services*, 2019, 48: 144-153.
- [2] Cui, G, Lui, H.-K, Guo, X. The effect of online consumer reviews on new product sales[J]. *International Journal of Electronic Commerce*, 2012, 17(1): 39-58.

- [3] Timoshenko. A, Hauser. J. R. Identifying customer needs from user-generated content[J]. *Marketing Science*, 2019, 38(1): 1-20.
- [4] Cezar. A, gütt. H. Analyzing conversion rates in online hotel booking: The role of customer reviews, recommendations and rank order in search listings[J]. *International Journal of Contemporary Hospitality Management*, 2016, 28(2): 286-304.
- [5] De Pelsmacker. P, Van Tilburg. S, Holthof. C. Digital marketing strategies, online reviews and hotel performance[J]. *International Journal of Hospitality Management*, 2018, 72: 47-55.
- [6] Hong. H, Xu. D, Wang. G. A, Fan. W. Understanding the determinants of online review helpfulness: A meta-analytic investigation[J]. *Decision Support Systems*, 2017, 102: 1-11.
- [7] Zhao. P, Wu. J, Hua. Z, Fang. S. Finding ewom customers from customer reviews[J]. *Industrial Management & Data Systems*, 2019, 119(1): 129-147.
- [8] Zhang. Z, Ye. Q, Law. R, Li. Y. The impact of e-word-of-mouth on the online popularity of restaurants: A comparison of consumer reviews and editor reviews[J]. *International Journal of Hospitality Management*, 2010, 29(4): 694-700.
- [9] Park. S, Nicolau. J. L. Asymmetric effects of online consumer reviews[J]. *Annals of Tourism Research*, 2015, 50: 67-83.
- [10] Song. T, Huang. J, Tan. Y, Yu. Y. Using user-and marketer-generated content for box office revenue prediction: Differences between microblogging and third-party platforms[J]. *Information Systems Research*, 2019.
- [11] Siering. M, Deokar. A. V, Janze. C. Disentangling consumer recommendations: Explaining and predicting airline recommendations based on online reviews[J]. *Decision Support Systems*, 2018, 107: 52-63.
- [12] Bakhshi. S, Kanuparth. P, Gilbert. E. Demographics, weather and online reviews: A study of restaurant recommendations[C]. *Proceedings of the 23rd international conference on World wide web*, 2014: 443-454.
- [13] Wu. Z. H, Liu. C. B, Jin. H. Y. The analysis of the main influence factors of real estate price in shenzhen[M]. 2006: 1534-1538.
- [14] Wu. J, Deng. Y, Liu. H. House price index construction in the nascent housing market: The case of china[J]. *The Journal of Real Estate Finance and Economics*, 2014, 48(3): 522-545.
- [15] Chen. J, Han. W. The research on the marketing strategies theory and empirical based on the product value[C]. *2009 International Symposium on Marketing Management (ISMM 2009)-Marketing Innovations and Economic Development*, 2009: 286-290.
- [16] Mikolov. T, Sutskever. I, Chen. K, Corrado. G. S, Dean. J. Distributed representations of words and phrases and their compositionality[C]. *Advances in neural information processing systems*, 2013: 3111-3119.
- [17] Mikolov. T, Chen. K, Corrado. G, Dean. J. Efficient estimation of word representations in vector space[J]. *arXiv preprint arXiv:1301.3781*, 2013.
- [18] Breiman. L. Random forests[J]. *Machine learning*, 2001, 45(1): 5-32.
- [19] Svetnik. V, Liaw. A, Tong. C, Culberson. J. C, Sheridan. R. P, Feuston. B. P. Random forest: A classification and regression tool for compound classification and qsar modeling[J]. *Journal of chemical information and computer sciences*, 2003, 43(6): 1947-1958.
- [20] Sun. J. 'Jieba'chinese word segmentation tool. 2012.
- [21] Hsiao. C. *Analysis of panel data*[M]. Cambridge university press, 2014.
- [22] Canay. I. A. A simple approach to quantile regression for panel data[J]. *The Econometrics Journal*, 2011, 14(3): 368-386.
- [23] Choi. I. Unit root tests for panel data[J]. *Journal of international money and Finance*, 2001, 20(2): 249-272.

Ranking of Trapezoidal Bipolar Fuzzy Numbers Based on a New Improved Score Function

Jeevaraj S^{a,1}

^a*Atal Bihari Vajpayee Indian Institute of Information Technology and Management
Gwalior, Madhya Pradesh, India-474015*

Abstract. Bipolar fuzzy numbers plays a vital role in any Decision-making problem modelled under a bipolar fuzzy environment. In 2018, Akram and Arshad [1] introduced a new ranking function on the class of Trapezoidal Bipolar fuzzy numbers based on the area of the left and right membership function of a TrBFN, and they have discriminated any two TrBFNs by using it. The ranking principle introduced by Akram and Arshad [1] works better only when two bipolar fuzzy numbers have different rankings. We describe that the ranking function does not work with counterexamples when two or more bipolar fuzzy numbers have the same rankings. In this paper, we improve the ranking principle introduced in [1] by introducing a new Improved Score function. Firstly, we discuss the drawbacks and limitations of the ranking function introduced by Akram and Arshad [1]. Secondly, we introduce a new ranking function and study its properties. Thirdly, we introduce a new ranking principle by combining Akram and Arshad's [1] ranking function and the proposed ranking function. Finally, we show the efficiency of the proposed ranking principle in comparing arbitrary TrBFNs.

Keywords. Trapezoidal Bipolar fuzzy number, Ranking, Triangular Bipolar fuzzy number, Improved score function

1. Introduction

Fuzzy numbers play a major in solving problems involving imprecise numerical quantity. Further, it has been generalized to various forms such as intuitionistic fuzzy numbers, Pythagorean fuzzy numbers, Fermatean fuzzy numbers, Bipolar fuzzy numbers, etc. Various ranking procedures are available on the different classes of fuzzy and intuitionistic fuzzy numbers [1,2,3,5,6,7,8,9,10,11]. Bipolar fuzzy numbers are very much valuable for modelling problems with imprecise and incomplete information. Especially, Trapezoidal (Triangular) Bipolar Fuzzy numbers (TrBFN) are widely used in the literature [1,4,12,13] for uncertainty modelling, and sometimes it performs better than the trapezoidal fuzzy numbers and trapezoidal intuitionistic fuzzy numbers. Ranking of Trapezoidal Bipolar fuzzy numbers plays a vital role in any Decision-making problem mod-

¹Corresponding Author: Assistant Professor in Mathematics, Atal Bihari Vajpayee Indian Institute of Information Technology and Management Gwalior, Madhya Pradesh, India-474015; E-mail:jeevaraj@iiitm.ac.in

elled under a bipolar fuzzy environment. Reza et al. [11] discussed the idea of duality in Linear programming problems. Rayappan and Mohana discuss the applications of spherical fuzzy sets in solving the MCDM problem. Akram and Arshad [1] has derived a new ranking principle for ordering any two Trapezoidal (Triangular) Bipolar Fuzzy Numbers (TrBFN), and they have compared any two Trapezoidal (Triangular) Bipolar Fuzzy Numbers by using the same ranking principle. They have also developed a group decision-making method based on trapezoidal bipolar fuzzy TOPSIS. Using the formula (3.3) and formula (3.4) on page number 574 (of Akram and Arshad [1]), they have shown that they can compare any two Trapezoidal (Triangular) Bipolar Fuzzy Numbers utilizing proposed ranking function R_{f1}, R_{f2} . However, their method does not compare any two arbitrary TrBFNs effectively. Highly motivated by the work of Akram and Arshad [1], firstly, we introduce a new improved score function on the class of TrBFNs and study its properties. Then, we present a new ranking principle by combining Akram and Arshad's [1] ranking function and the proposed ranking function. Finally, we show the efficiency of the proposed ranking principle in comparing arbitrary TrBFNs.

2. Preliminaries

Here we give some of the basic definitions defined on the class of TrBFNs.

Definition 2.1. Akram and Arshad [1].

A Bipolar Fuzzy Number (BFN) $A = \langle I, K \rangle = \langle [t_1, t_2, t_3, t_4], [k_1, k_2, k_3, k_4] \rangle$ is a Trapezoidal Bipolar Fuzzy Number (TrBFN), denoted by $\langle (t_1, t_2, t_3, t_4), (k_1, k_2, k_3, k_4) \rangle$, if its satisfaction degree λ_I and dissatisfaction degree λ_K are given as:

$$\lambda_I = \begin{cases} \frac{x-t_1}{t_2-t_1} & \text{if } x \in [t_1, t_2] \\ 1 & \text{if } x \in [t_2, t_3] \\ \frac{t_4-x}{t_4-t_3} & \text{if } x \in [t_3, t_4] \\ 0 & \text{Otherwise} \end{cases} \text{ and } \lambda_K = \begin{cases} \frac{k_1-x}{k_2-k_1} & \text{if } x \in [k_1, k_2] \\ -1 & \text{if } x \in [t_2, t_3] \\ \frac{x-k_4}{k_4-k_3} & \text{if } x \in [k_3, k_4] \\ 0 & \text{Otherwise} \end{cases}$$

Note: Here, $t_1 \leq t_2 \leq t_3 \leq t_4$ and $k_1 \leq k_2 \leq k_3 \leq k_4$.

Definition 2.2. Akram and Arshad [1].

A BFN, $A = \langle I, K \rangle = \langle [t_1, t_2, t_3, t_4], [k_1, k_2, k_3, k_4] \rangle$ is a Triangular Bipolar Fuzzy Number (TBFN), denoted by $\langle (t_1, t_2, t_3), (k_1, k_2, k_3) \rangle$, if its satisfaction degree λ_I and dissatisfaction degree λ_K are given as:

$$\lambda_I = \begin{cases} \frac{x-t_1}{t_2-t_1} & \text{if } x \in [t_1, t_2] \\ \frac{t_3-x}{t_3-t_2} & \text{if } x \in [t_2, t_3] \\ 0 & \text{Otherwise} \end{cases} \text{ and } \lambda_K = \begin{cases} \frac{k_1-x}{k_2-k_1} & \text{if } x \in [k_1, k_2] \\ \frac{x-k_3}{k_3-k_2} & \text{if } x \in [k_2, k_3] \\ 0 & \text{Otherwise} \end{cases}$$

Note: Here, $t_1 \leq t_2 \leq t_3$ and $k_1 \leq k_2 \leq k_3$.

Definition 2.3. Akram and Arshad [1].

Ranking Function R_{f1} for TrBFN

Let $A = \langle I, K \rangle = \langle (t_1, t_2, t_3, t_4), (k_1, k_2, k_3, k_4) \rangle$ be the TrBFN. Then by using Definition 2.1, they have derived the ranking function R_{f1} of TrBFN as $R_{f1}(A) = (m(I) + \sigma(I) - (m(K) + \sigma(K)))$, where the means $(m(I), m(K))$ are defined as $m(I) = \frac{t_1+t_2+t_3+t_4}{4}$, $m(K) = \frac{k_1+k_2+k_3+k_4}{4}$ and the areas $(\sigma(I), \sigma(K))$ are defined as $\sigma(I) =$

$$\frac{-t_1-t_2+t_3+t_4}{2} \text{ and } \sigma(K) = \frac{-k_1-k_2+k_3+k_4}{2}.$$

$$\text{Therefore, } R_{f1}(A) = \frac{(-t_1-t_2+3t_3+3t_4)-(-k_1-k_2+3k_3+3k_4)}{4} = \frac{-t_1-t_2+3t_3+3t_4+k_1+k_2-3k_3-3k_4}{4}.$$

If $\sigma(I), \sigma(K) \geq 1$, then the ranking function R_{f2} for TrBFNs can also be defined as,

$$R_{f2}(A) = m(I)\sigma(I) - m(K)\sigma(K) = \frac{(t_1+t_2+t_3+t_4)(-t_1-t_2+t_3+t_4)}{8} - \frac{(k_1+k_2+k_3+k_4)(-k_1-k_2+k_3+k_4)}{8}$$

Definition 2.4. Akram and Arshad [1].

Ranking Function R_{f1} for TBFN

Let $A = \langle I, K \rangle = \langle (t_1, t_2, t_3), (k_1, k_2, k_3) \rangle$ be the TBFN. Then by using Definition 2.2, they have derived the ranking function R_{f1} of TBFN as $R_f(A) = (m(I) + \sigma(I) - (m(K) + \sigma(K)))$, where the means $(m(I), m(K))$ are defined as $m(I) = \frac{t_1+t_2+t_3}{3}$, $m(K) = \frac{k_1+k_2+k_3}{3}$ and the areas $(\sigma(I), \sigma(K))$ are defined as $\sigma(I) = \frac{t_3-t_1}{2}$, $\sigma(K) = \frac{k_3-k_1}{2}$.

$$\text{Therefore, } R_{f1}(A) = \frac{(-t_1+2t_2+5t_3)-(-k_1+2k_2+5k_3)}{6} = \frac{-t_1+2t_2+5t_3+k_1-2k_2-5k_3}{6}.$$

If $\sigma(I), \sigma(K) \geq 1$, then the ranking function R_{f2} for TBFNs can also be defined as,

$$R_{f2}(A) = m(I)\sigma(I) - m(K)\sigma(K) = \frac{(t_1+t_2+t_3)(t_3-t_1)}{6} - \frac{(k_1+k_2+k_3)(k_3-k_1)}{6}$$

Definition 2.5. Ranking of Bipolar Fuzzy Numbers. Akram and Arshad [1].

Let $H = \{h_1, h_2, h_3, \dots, h_n\}$ be the set of BFNs then for any distinct $h_i, h_j \in H$, the ranking function R_{f1} from H to real line \mathfrak{R} is mapping satisfying the following characteristics,

- If $R_{f1}(h_i) < R_{f1}(h_j)$, then $h_i < h_j$,
- If $R_{f1}(h_i) = R_{f1}(h_j)$, then $h_i = h_j$,
- If $R_{f1}(h_i) > R_{f1}(h_j)$, then $h_i > h_j$,

The ranking function for a BFN $h_i = \langle I_i, K_i \rangle = \langle (t_{i1}, t_{i2}, t_{i3}, t_{i4}), (k_{i1}, k_{i2}, k_{i3}, k_{i4}) \rangle$ as, $R_{f1}(h_i) = [m(I_i) + \sigma(I_i)] - [m(K_i) + \sigma(K_i)]$, $k = 1, 2, 3, 4$. Where $m(I_i)$ and $m(K_i)$ denote the mean of I_i and the mean of K_i respectively, $\sigma(I_i)$ represents the area of I_i and $\sigma(K_i)$ represents the area of K_i .

If $\sigma(I_i), \sigma(K_i) \geq 1$ for each i , then the ranking function R_{f2} for TrBFNs can also be defined as,

$$R_{f2}(h_i) = m(I_i)\sigma(I_i) - m(K_i)\sigma(K_i)$$

3. Limitations of the Ranking Functions R_{f1}, R_{f2} in ranking Trapezoidal Bipolar Fuzzy Numbers

In this section, we discuss some limitations of Akram and Arshad's [1] ranking function in comparing different Trapezoidal Bipolar Fuzzy Numbers using numerical examples.

Definition 3.1. Let $A = \langle I_1, K_1 \rangle = \langle (t_{11}, t_{12}, t_{13}, t_{14}), (k_{11}, k_{12}, k_{13}, k_{14}) \rangle$ and $B = \langle I_2, K_2 \rangle = \langle (t_{21}, t_{22}, t_{23}, t_{24}), (k_{21}, k_{22}, k_{23}, k_{24}) \rangle$ be any two TrBFN. Using Definition 2.3, we can rewrite the Akram and Arshad's [1] ranking principle (Definition 2.5) that utilizes R_{f1} and R_{f2} in the following way,

1. If $\frac{-t_{11}-t_{12}+3t_{13}+3t_{14}+k_{11}+k_{12}-3k_{13}-3k_{14}}{4} < \frac{-t_{21}-t_{22}+3t_{23}+3t_{24}+k_{21}+k_{22}-3k_{23}-3k_{24}}{4}$, then $A < B$.
2. If $\frac{-t_{11}-t_{12}+3t_{13}+3t_{14}+k_{11}+k_{12}-3k_{13}-3k_{14}}{4} = \frac{-t_{21}-t_{22}+3t_{23}+3t_{24}+k_{21}+k_{22}-3k_{23}-3k_{24}}{4}$, then $A = B$.
3. If $\frac{-t_{11}-t_{12}+3t_{13}+3t_{14}+k_{11}+k_{12}-3k_{13}-3k_{14}}{4} > \frac{-t_{21}-t_{22}+3t_{23}+3t_{24}+k_{21}+k_{22}-3k_{23}-3k_{24}}{4}$, then $A > B$.
4. If $\sigma(I_i), \sigma(K_i) \geq 1$, for each i , then the ranking function R_{f2} for TrBFNs can also be defined as,

$$\frac{(t_{11}+t_{12}+t_{13}+t_{14})(-t_{11}-t_{12}+t_{13}+t_{14})-(k_{11}+k_{12}+k_{13}+k_{14})(-k_{11}-k_{12}+k_{13}+k_{14})}{8}$$

The limitations of Akram and Arshad’s [1] Ranking function can be seen from the following Examples.

Example 3.1. Let $A = \langle I_1, K_1 \rangle = \langle (10, 20, 30, 40), (10, 20, 30, 40) \rangle$,
 $B = \langle I_2, K_2 \rangle = \langle (90, 120, 150, 180), (90, 120, 150, 180) \rangle$,
 $C = \langle I_3, K_3 \rangle = \langle (0, 0, 1, 1), (0, 0, 1, 1) \rangle$,
 $D = \langle I_4, K_4 \rangle = \langle (20, 30, 40, 50), (20, 30, 40, 50) \rangle$,
 $E = \langle I_5, K_5 \rangle = \langle (30, 50, 70, 90), (30, 50, 70, 90) \rangle$ be five different TrBFNs and their pictorial representation is given in Figure 1.

If we apply Akram and Arshad’s [1] ranking function R_f to the above five differ-

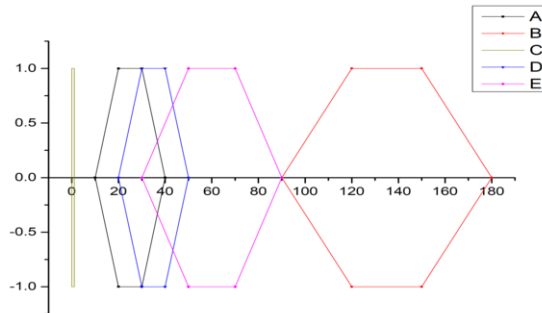


Figure 1. Pictorial representation of Example 3.1

ent TrBFNs, then we get $R_{f1}(A) = R_{f1}(B) = R_{f1}(C) = R_{f1}(D) = R_{f1}(E) = 0$ and $R_{f2}(A) = R_{f2}(B) = R_{f2}(C) = R_{f2}(D) = R_{f2}(E) = 0$ which implies that (from Definition 3.1) $A = B = C = D = E$. But from Figure 1, it is very clear that all the given TrBFNs are different in nature and which does not favor the human intuition.

Example 3.2. Let $A = \langle I_1, K_1 \rangle = \langle (0.10, 0.20, 0.30, 0.40), (0.50, 0.60, 0.70, 0.80) \rangle$,
 $B = \langle I_2, K_2 \rangle = \langle (0.3, 0.4, 0.5, 0.6), (0.7, 0.8, 0.9, 1) \rangle$, be two different TrBFNs and their pictorial representation is given in Figure 2.

If we apply Akram and Arshad’s [1] ranking function R_f to the above two different TrBFNs, then we get $R_{f1}(A) = R_{f1}(B) = -0.4$ which implies that (from Definition 3.1) $A = B$. This is an anti-intuitive case of Akram and Arshad’s [1] ranking function.

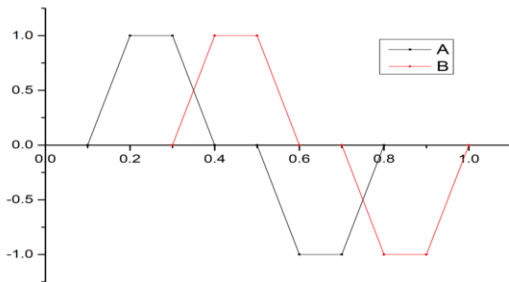


Figure 2. Pictorial representation of Example 3.2

Example 3.3. Let $A = \langle I_1, K_1 \rangle = \langle (2, 4, 6, 8), (4, 5, 6, 7) \rangle$,
 $B = \langle I_2, K_2 \rangle = \langle (4, 6, 8, 10), (6, 7, 8, 9) \rangle$,
 $C = \langle I_3, K_3 \rangle = \langle (82, 84, 86, 88), (84, 85, 86, 87) \rangle$, be three different TrBFNs and their pictorial representation is given in Figure 3.

If we apply Akram and Arshad's [1] ranking function R_f to the above three differ-

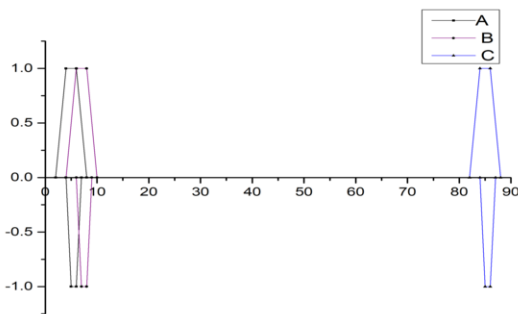


Figure 3. Pictorial representation of Example 3.3

ent TrBFNs, then we get $R_{f1}(A) = R_{f1}(B) = R_{f1}(C) = 1.5 \Rightarrow A = B = C$. Suppose if we consider the fourth formula (in Definition 3.1) then we get $R_{f2}(A) = 9, R_{f2}(B) = 13, R_{f2}(C) = 169$ (Since $\sigma(I_1), \sigma(I_2), \sigma(I_3), \sigma(K_1), \sigma(K_2), \sigma(K_3) > 1$) which implies that $A < B < C$. i.e., If we consider the second score function R_{f2} (once after the first score function R_{f1} fails), then we can rank the arbitrary TrBFNs effectively.

Example 3.4. Let $A = \langle I_1, K_1 \rangle = \langle (5, 20, 30, 40), (25, 35, 45, 60) \rangle$,
 $B = \langle I_2, K_2 \rangle = \langle (10, 15, 25, 45), (30, 30, 40, 65) \rangle$,
 $C = \langle I_3, K_3 \rangle = \langle (0, 25, 25, 45), (30, 30, 35, 70) \rangle$,
 $D = \langle I_4, K_4 \rangle = \langle (12, 13, 13, 57), (15, 45, 50, 55) \rangle$,
 $E = \langle I_5, K_5 \rangle = \langle (2, 23, 27, 43), (27, 33, 43, 62) \rangle$ be five different TrBFNs and their pictorial representation is given in Figure 4.

If we apply Akram and Arshad's [1] ranking function R_f to the above five different TrBFNs, then we get $R_{f1}(A) = R_{f1}(B) = R_{f1}(C) = R_{f1}(D) = R_{f1}(E) = -17.5$ which implies that (from Definition 3.1) $A = B = C$. Suppose if we consider the fourth formula (in

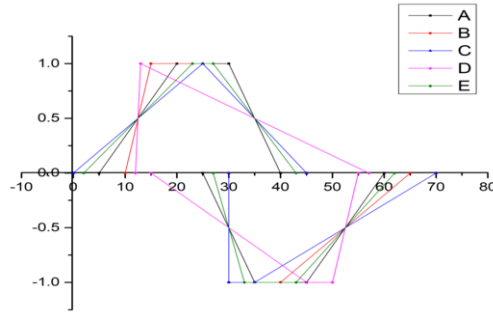


Figure 4. Pictorial representation of Example 3.4

Definition 3.1), then we get $R_{f_2}(A) = R_{f_2}(B) = R_{f_2}(C) = R_{f_2}(D) = R_{f_2}(E) = -393.75$ (Since $\sigma(I_i), \sigma(K_i) > 1$, for $i = 1$ to 5) which implies that $A = B = C = D = E$. i.e., In both the cases, ranking is same and it is anti-intuitive.

Example 3.5. Let $A = \langle I_1, K_1 \rangle = \langle (5, 70, 90, 110), (70, 80, 110, 140) \rangle$,
 $B = \langle I_2, K_2 \rangle = \langle (10, 65, 70, 130), (60, 90, 120, 130) \rangle$,
 $C = \langle I_3, K_3 \rangle = \langle (20, 55, 75, 125), (40, 110, 115, 135) \rangle$, be three different TrBFNs and their pictorial representation is given in Figure 5.

If we apply Akram and Arshad's [1] ranking function R_f to the above five different

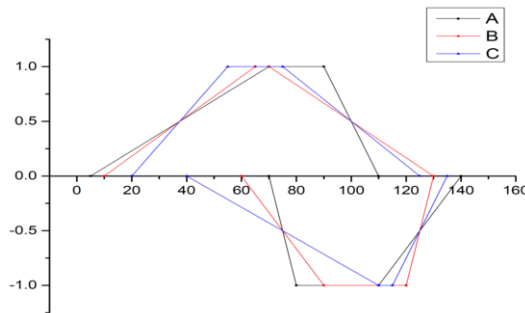


Figure 5. Pictorial representation of Example 3.5

TrBFNs, then we get $R_{f_1}(A) = R_{f_1}(B) = R_{f_1}(C) = -18.75$ which implies that (from Definition 3.1) $A = B = C$. Suppose if we consider the fourth formula (in Definition 3.1), then we get $R_{f_2}(A) = R_{f_2}(B) = R_{f_2}(C) = -703.125$ (Since $\sigma(I_i), \sigma(K_i) > 1$, for $i = 1$ to 3) which implies that $A = B = C$. i.e., In both the cases, ranking is same and it is anti-intuitive.

3.1. Limitations of Ranking functions R_{f_1}, R_{f_2} of Triangular Bipolar Fuzzy Numbers

In this subsection, we discuss the various drawbacks of Akram and Arshad's [1] ranking function in comparing different Triangular Bipolar Fuzzy Numbers using numerical examples.

Definition 3.2. Let $A = \langle I_1, K_1 \rangle = \langle (t_{11}, t_{12}, t_{13}), (k_{11}, k_{12}, k_{13}) \rangle$ and $B = \langle I_2, K_2 \rangle = \langle (t_{21}, t_{22}, t_{23}), (k_{21}, k_{22}, k_{23}) \rangle$ be any two TrBFN. Using Definition 2.4, we can rewrite the Akram and Arshad's [1] ranking principle (Definition 2.5) in the following way,

1. If $\frac{-t_{11}+2t_{12}+5t_{13}+k_{11}-2k_{12}-5k_{13}}{6} < \frac{-t_{21}+2t_{22}+5t_{23}+k_{21}-2k_{22}-5k_{23}}{6}$, then $A < B$.
2. If $\frac{-t_{11}+2t_{12}+5t_{13}+k_{11}-2k_{12}-5k_{13}}{6} = \frac{-t_{21}+2t_{22}+5t_{23}+k_{21}-2k_{22}-5k_{23}}{6}$, then $A = B$.
3. If $\frac{-t_{11}+2t_{12}+5t_{13}+k_{11}-2k_{12}-5k_{13}}{6} > \frac{-t_{21}+2t_{22}+5t_{23}+k_{21}-2k_{22}-5k_{23}}{6}$, then $A > B$.
4. If $\sigma(I_i), \sigma(K_i) \geq 1$, for each i , then the ranking function R_{f2} for TBFNs can also be defined as,

$$\frac{(t_{11}+t_{12}+t_{13})(t_{13}-t_{11})-(k_{11}+k_{12}+k_{13})(k_{13}-k_{11})}{6}$$

Akram and Arshad [1] have introduced the ranking method without investigating its Mathematical Properties. Ranking principle of TBFN defined in [1] is not true for any two TBFNs which can be seen by using the following examples,

Example 3.6. Let $A = \langle I_1, K_1 \rangle = \langle (3, 4.2, 4.8), (4.2, 5.1, 6) \rangle$,
 $B = \langle I_2, K_2 \rangle = \langle (3.6, 4.8, 4.92), (4.8, 5.7, 6.12) \rangle$,
 $C = \langle I_3, K_3 \rangle = \langle (4.8, 5.1, 5.16), (6, 6, 6.36) \rangle$, be three different TBFNs and their pictorial representation is given in Figure 6.

If we apply Akram and Arshad's [1] ranking function R_f to the above 3 different

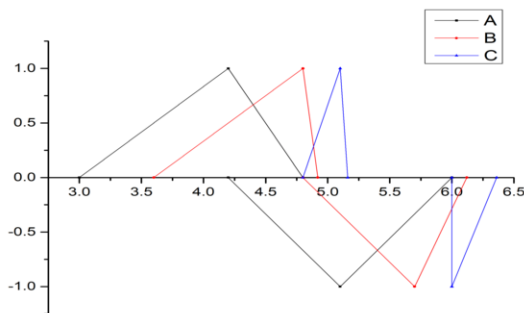


Figure 6. Pictorial representation of Example 3.6

TBFNs, then we get $R_{f1}(A) = R_{f1}(B) = R_{f1}(C) = -1.1$, $R_{f2}(A) = -0.99, R_{f2}(B) = -0.726, R_{f2}(C) = -0.198$ which implies that (from Definition 3.2) $A < B < C$. i.e., If we consider the second score function R_{f2} (once after the first score function R_{f1} fails), then we can rank the arbitrary TBFNs effectively.

Example 3.7. Let $A = \langle I_1, K_1 \rangle = \langle (30, 50, 60), (30, 50, 60) \rangle$, $B = \langle I_2, K_2 \rangle = \langle (40, 60, 70), (40, 60, 70) \rangle$, $C = \langle I_3, K_3 \rangle = \langle (10, 20, 30), (10, 20, 30) \rangle$, $D = \langle I_4, K_4 \rangle = \langle (1, 2, 3), (1, 2, 3) \rangle$, $E = \langle I_5, K_5 \rangle = \langle (50, 70, 90), (50, 70, 90) \rangle$, $F = \langle I_6, K_6 \rangle = \langle (20, 50, 70), (20, 50, 70) \rangle$ be six different TBFNs and their pictorial representation is given in Figure 7.

If we apply Akram and Arshad's [1] ranking function R_f to the above five different

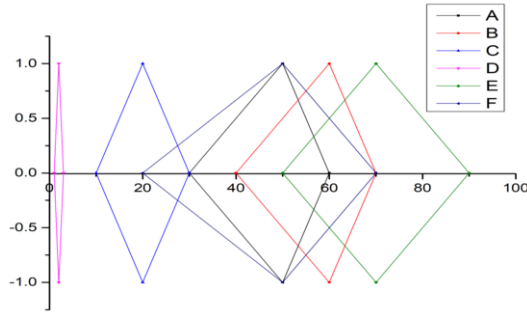


Figure 7. Pictorial representation of Example 3.7

TBFNs, then we get $R_{f1}(A) = R_{f1}(B) = R_{f1}(C) = R_{f1}(D) = R_{f1}(E) = R_{f1}(F) = 0$ which implies that (from Definition 3.2) $A = B = C = D = E = F$. Suppose if we consider the fourth formula (in Definition 3.2), then we get $R_{f2}(A) = R_{f2}(B) = R_{f2}(C) = R_{f2}(D) = R_{f2}(E) = R_{f2}(F) = 0$ (Since $\sigma(I_i), \sigma(K_i) > 1$, for $i = 1$ to 6) which implies that $A = B = C = D = E = F$. i.e., In both the cases, ranking is same and it does not favor the human intuition.

3.2. Limitations of R_f

In this subsection, we discuss some limitations of the score functions R_{f1} and R_{f2} in a Mathematical way.

1. Let $A_1 = \langle I_1, K_1 \rangle = \langle (t_{11}, t_{12}, t_{13}, t_{14}), (t_{11}, t_{12}, t_{13}, t_{14}) \rangle, A_2 = \langle I_2, K_2 \rangle = \langle (t_{21}, t_{22}, t_{23}, t_{12}), (t_{21}, t_{22}, t_{23}, t_{24}) \rangle$ any two TrBFNs. Then $R_{f1}(A_1) = R_{f1}(A_2) = 0$ and $R_{f2}(A_1) = R_{f2}(A_2) = 0$. (Example 3.1 represents the numerical illustration of this Theoretical (Mathematical) drawback 1)
2. Let $A_1 = \langle I_1, K_1 \rangle = \langle (t_{11}, t_{12}, t_{13}, t_{14}), (k_{11}, k_{12}, k_{13}, k_{14}) \rangle, A_2 = \langle I_2, K_2 \rangle = \langle (t_{11} + \varepsilon, t_{12} + \varepsilon, t_{13} + \varepsilon, t_{14} + \varepsilon), (k_{11} + \varepsilon, k_{12} + \varepsilon, k_{13} + \varepsilon, k_{14} + \varepsilon) \rangle$ any two TrBFNs and $\varepsilon \leq t_{11}, k_{11}$. Then $R_{f1}(A_1) = R_{f1}(A_2)$. (Example 3.2, Example 3.3 represent the numerical illustration of this Theoretical (Mathematical) drawback)
3. Let $A_1 = \langle I_1, K_1 \rangle = \langle (t_{11}, t_{12}, t_{13}, t_{14}), (k_{11}, k_{12}, k_{13}, k_{14}) \rangle, A_2 = \langle I_2, K_2 \rangle = \langle (t_{11} - \varepsilon_1, t_{12} + \varepsilon_2, t_{13} - \varepsilon_1, t_{14} + \varepsilon_2), (k_{11} + \varepsilon_1, k_{12} - \varepsilon_2, k_{13} + \varepsilon_1, k_{14} - \varepsilon_2) \rangle$ any two TrBFNs and $\varepsilon_1 \leq t_{11}, \varepsilon_2 \leq k_{12}$ and $\varepsilon_1 \leq \varepsilon_2$. Then $R_{f1}(A_1) = R_{f1}(A_2)$.
4. Let $A_1 = \langle I_1, K_1 \rangle = \langle (t_{11}, t_{12}, t_{13}, t_{14}), (k_{11}, k_{12}, k_{13}, k_{14}) \rangle, A_2 = \langle I_2, K_2 \rangle = \langle (t_{11} - \varepsilon, t_{12} + \varepsilon, t_{13} - \varepsilon, t_{14} + \varepsilon), (k_{11} + \varepsilon, k_{12} - \varepsilon, k_{13} + \varepsilon, k_{14} - \varepsilon) \rangle$ any two TrBFNs and $\varepsilon \leq t_{11}, k_{11}$. Then $R_{f1}(A_1) = R_{f1}(A_2)$ and $R_{f2}(A_1) = R_{f2}(A_2)$.
5. Let $A_1 = \langle I_1, K_1 \rangle = \langle (t_{11}, t_{12}, t_{13}, t_{14}), (k_{11}, k_{12}, k_{13}, k_{14}) \rangle, A_2 = \langle I_2, K_2 \rangle = \langle (t_{11} - \varepsilon, t_{12} + \varepsilon, t_{13} + \varepsilon, t_{14} - \varepsilon), (k_{11} - \varepsilon, k_{12} + \varepsilon, k_{13} + \varepsilon, k_{14} - \varepsilon) \rangle$ any two TrBFNs and $\varepsilon \leq t_{11}, k_{11}$. Then $R_{f1}(A_1) = R_{f1}(A_2)$ and $R_{f2}(A_1) = R_{f2}(A_2)$.

Note: Here, all the values of ε_i have been chosen without violating the conditions of TrBFNs (TBFNs). Numerical illustration of these theoretical drawbacks 3, 4, and 5 are given in the example 3.4, example 3.5, example 3.6 and example 3.7.

From the limitations of Akram and Arshad’s [1] score functions, we can conclude that the score functions R_{f1} and R_{f2} are not sufficient for ranking any two TrBFNs (TBFNs). In order to improve the ranking principle, we define a new score function in the following section.

4. New Score function R_{f3}

In this section, first, we define a new score function on the class of TrBFNs (TBFNs) that can overcome the drawbacks of Akram and Arshad’s ranking functions. Then we study some properties of the proposed score function, and finally, we discuss the efficiency of a score function in ranking TrBFNs that are not ranked by using R_{f1} and R_{f2} . From the previous limitations, we can conclude that if the mean and area of both the membership and non-membership functions of any two TrBFNs are equal, then they are ranked equal. In order to distinguish any two TrBFNs with same mean and area, here we made a small change in the score function R_f and defined a new score function R_{f3} on the class of Trapezoidal Bipolar Fuzzy Numbers as follows.

Definition 4.1. *Ranking Function R_{3f} for TrBFN*

Let $A = \langle I, K \rangle = \langle (t_1, t_2, t_3, t_4), (k_1, k_2, k_3, k_4) \rangle$ be any TrBFN. Then the new score function

$$R_{f3} \text{ of TrBFN is defined as } R_{3f}(A) = \frac{(m(I) + \frac{-t_1 - t_2 + t_3 + t_4}{2})t_4 + (m(K) + \frac{-k_1 - k_2 + k_3 + k_4}{2})k_4}{1 + m(I) + m(K)},$$

where $m(I) = \frac{t_1 + t_2 + t_3 + t_4}{4}$ and $m(K) = \frac{k_1 + k_2 + k_3 + k_4}{4}$.

$$\text{Therefore, } R_{f3}(A) = \frac{(-t_1 - t_2 + 3t_3 + 3t_4)t_4 + (-k_1 - k_2 + 3k_3 + 3k_4)k_4}{4 + t_1 + t_2 + t_3 + t_4 + k_1 + k_2 + k_3 + k_4}.$$

Definition 4.2. *Ranking Principle on the class of TrBFN (TBFN):*

Let $A = \{A_1, A_2, \dots, A_n\}$ be the set of TrBFNs (TBFNs) then for any distinct $A_i, A_j \in A$, the ranking functions $R_{fi}, i = 1, 2, 3$ from A to real line \mathfrak{R} is a mapping satisfying the following characteristics,

- If $R_{f1}(A_i) < R_{f1}(A_j)$, then $A_i < A_j$
- If $R_{f1}(A_i) > R_{f1}(A_j)$, then $A_i > A_j$ or
- If $R_{f1}(A_i) = R_{f1}(A_j)$, then
 - * If $R_{f2}(A_i) < R_{f2}(A_j)$, then $A_i < A_j$
 - * If $R_{f2}(A_i) > R_{f2}(A_j)$, then $A_i > A_j$ or
 - * If $R_{f1}(A_i) = R_{f1}(A_j)$, $R_{f2}(A_i) = R_{f2}(A_j)$, then
 - * If $R_{f3}(A_i) < R_{f3}(A_j)$, then $A_i < A_j$
 - * If $R_{f3}(A_i) > R_{f3}(A_j)$, then $A_i > A_j$ or
 - * If $R_{f1}(A_i) = R_{f1}(A_j)$, $R_{f2}(A_i) = R_{f2}(A_j)$ and $R_{f3}(A_i) = R_{f3}(A_j)$, then $A_i \approx A_j$.

4.1. Properties of R_{f1}, R_{f2}, R_{f3} and their comparison

In this subsection, we see the properties of different ranking functions R_{f1}, R_{f2}, R_{f3} .

1. **The function R_f maps the set of TrBFNs (which are Symmetric about X-axis) to 0**

Let $A = \{A_i | A_i = \langle I_i, K_i \rangle = \langle (t_{i1}, t_{i2}, t_{i3}, t_{i4}), (t_{i1}, t_{i2}, t_{i3}, t_{i4}) \rangle\}$ the set of TrBFNs. Then $R_{f1}(A_i) = 0$ and $R_{f2}(A_i) = 0$. This property is true for any TrBFN. But R_{f3} is not mapping the set of TrBFNs (TrBFNs) (that are symmetric about X-axis) to zero.

2. Let $A_1 = \langle I_1, K_1 \rangle = \langle (t_1, t_2, t_3), (k_1, k_2, k_3) \rangle$ be any Triangular Bipolar fuzzy number (TrBFN).

$$\begin{aligned} \text{Then } R_{f3}(A) &= \frac{(m(I) + \frac{t_3 - t_1}{2})t_3 + (m(K) + \frac{k_3 - k_1}{2})k_3}{1 + m(I) + m(K)} \\ &= \frac{(\frac{t_1 + t_2 + t_3}{3} + \frac{t_3 - t_1}{2})t_3 + (\frac{k_1 + k_2 + k_3}{3} + \frac{k_3 - k_1}{2})k_3}{1 + \frac{t_1 + t_2 + t_3}{3} + \frac{k_1 + k_2 + k_3}{3}} = \frac{(\frac{-t_1 + 2t_2 + 5t_3}{6})t_3 + (\frac{-k_1 + 2k_2 + 5k_3}{6})k_3}{\frac{(3+t_1+t_2+t_3+k_1+k_2+k_3)}{3}} \\ &= \frac{(-t_1 + 2t_2 + 5t_3)t_3 + (-k_1 + 2k_2 + 5k_3)k_3}{2(3+t_1+t_2+t_3+k_1+k_2+k_3)}. \end{aligned}$$

3. **Ranking function R_{f1} is Translation Invariant:**

Let $A_1 = \langle I_1, K_1 \rangle = \langle (t_{11}, t_{12}, t_{13}, t_{14}), (k_{11}, k_{12}, k_{13}, k_{14}) \rangle$, $A_2 = \langle I_2, K_2 \rangle = \langle (t_{11} + \varepsilon, t_{12} + \varepsilon, t_{13} + \varepsilon, t_{14} + \varepsilon), (k_{11} + \varepsilon, k_{12} + \varepsilon, k_{13} + \varepsilon, k_{14} + \varepsilon) \rangle$ any two TrBFNs. Then $R_{f1}(A_1) = R_{f1}(A_2)$.

i.e., $R_f(A + \varepsilon) = R_f(A), \forall \varepsilon \geq 0$. This property holds for the set of TrBFNs too. R_{f2} and R_{f3} are not Translation Invariant.

4. Let $A_1 = \langle I_1, K_1 \rangle = \langle [t_1, t_2], [k_1, k_2] \rangle$ be any interval-valued Bipolar fuzzy number (IVBFN). Then $R_{f1}(A) = t_2 - k_2$, $R_{f2}(A) = \frac{t_2^2 - t_1^2 - k_2^2 + k_1^2}{4}$ and $R_{f3}(A) = \frac{2(t_2^2 + k_2^2)}{2 + t_1 + t_2 + k_1 + k_2}$.

Observation: For the interval-valued BFNs,

- The score function R_{f1} represents the length between the supremum of membership function and supremum of the non-membership function. R_{f1} does not consider the other two legs t_1, k_1 in the score function which is a limitation for the score function R_{f1} . But the score function R_{f2} overcomes this limitation.
 - The score function R_{f2} has the drawback that, if $t_1 = k_1, t_2 = k_2$, then $R_{f2}(A) = 0$. However, this drawback has been overcome by R_{f3} . In this way, a sequential ordering in the Definition 4.2 performs better.
5. • For any $A_1 = \langle I_1, K_1 \rangle = \langle (t_{11}, t_{12}, t_{13}, t_{14}), (k_{11}, k_{12}, k_{13}, k_{14}) \rangle$ TrBFN (where all $t_{1k}, k_{1k} \in [0, 1], k = 1, 2, 3, 4$), $R_{f1}(A) \in [-\frac{3}{2}, \frac{3}{2}]$.
- If $A = \langle (0, 0, 0, 0), (0, 0, 1, 1) \rangle$, then $R_{f1}(A) = -\frac{3}{2}$.
 - If $A = \langle (0, 0, 1, 1), (0, 0, 0, 0) \rangle$, then $R_{f1}(A) = \frac{3}{2}$.

Definition 4.3. Let $\zeta = \{A_i | A_i = \langle (t_{i1}, t_{i2}, t_{i3}, t_{i4}), (k_{i1}, k_{i2}, k_{i3}, k_{i4}) \rangle\}$ be the subset of the set of TrBFNs. Then the subset relation \subseteq is defined as, $A_1 \subseteq A_2$, if $t_{11} \geq t_{21}, t_{12} \geq t_{22}, t_{13} \leq t_{23}, t_{14} \leq t_{24}$ and $k_{11} \leq k_{21}, k_{12} \leq k_{22}, k_{13} \geq k_{23}, k_{14} \geq k_{24}$.

From the above properties and the limitations, we can conclude that Arshad and Akram's ranking principle alone cannot discriminate any two TrBFNs (TrBFNs). That is, Akram and Arshad's [1] ranking principle does not define Total ordering on the entire class of TrBFNs (TrBFNs). However, Akram and Arshad's [1] ranking function (R_f) can define Total ordering in the subset ζ which can be proved using the following theorem.

Theorem 4.1. Let $A_1, A_2 \in \zeta$. If $A_1 \subseteq A_2$, then $R_{fi}(A_1) \leq R_{fi}(A_2)$.

Proof: Case 1: If $A_1 \subseteq A_2$, then $R_{f1}(A_1) \leq R_{f1}(A_2)$

We assume that $A_1, A_2 \in \zeta$ and $A_1 \subseteq A_2$ which imply that

$$t_{11} \geq t_{21}, t_{12} \geq t_{22}, t_{13} \leq t_{23}, t_{14} \leq t_{24} \text{ and } k_{11} \leq k_{21}, k_{12} \leq k_{22}, k_{13} \geq k_{23}, k_{14} \geq k_{24} \quad (1)$$

Therefore from equation 1, we get

$$t_{11} + t_{12} \geq t_{21} + t_{22}, t_{13} + t_{14} \leq t_{23} + t_{24}, \quad (2)$$

and

$$k_{11} + k_{12} \leq k_{21} + k_{22}, k_{13} + k_{14} \geq k_{23} + k_{24} \quad (3)$$

By using Equation 2 and Equation 3, we get

$$-t_{11} - t_{12} + 3t_{13} + 3t_{14} \leq -t_{21} - t_{22} + 3t_{23} + 3t_{24} \quad (4)$$

and

$$k_{11} + k_{12} - 3k_{13} - 3k_{14} \leq k_{21} + k_{22} - 3k_{23} - 3k_{24} \quad (5)$$

By adding Equation 4 and Equation 5, we get

$$-t_{11} - t_{12} + 3t_{13} + 3t_{14} + k_{11} + k_{12} - 3k_{13} - 3k_{14} \leq -t_{21} - t_{22} + 3t_{23} + 3t_{24} + k_{21} + k_{22} - 3k_{23} - 3k_{24} \quad (6)$$

Dividing both the sides of Equation 6 by 4, we get $R_{f1}(A) \leq R_{f1}(B)$ (See Definition 2.3). Hence the proof.

Note: Proofs of other cases are similar to case 1 and hence they are omitted.

The ranking principle given in Definition 4.2 is an updated version of the ranking principle given by Akram and Arshad's [1] (Definition 2.3, 3.1). Adding a new score function R_{f3} to the ranking principle in Definition 2.3 gives a better ranking scenario which can be seen from the following Table 1.

Table 1. Efficiency of the proposed ranking function

Examples	Akram and Arshad Ranking Principle	Proposed Ranking Principle
Let $A = \langle I_1, K_1 \rangle = \langle (10, 20, 30, 40), (10, 20, 30, 40) \rangle$, $B = \langle I_2, K_2 \rangle = \langle (90, 120, 150, 180), (90, 120, 150, 180) \rangle$, $C = \langle I_3, K_3 \rangle = \langle (0, 0, 1, 1), (0, 0, 1, 1) \rangle$, $D = \langle I_4, K_4 \rangle = \langle (20, 30, 40, 50), (20, 30, 40, 50) \rangle$, $E = \langle I_5, K_5 \rangle = \langle (30, 50, 70, 90), (30, 50, 70, 90) \rangle$ be five different TrBFNs.	$R_{f1}(A) = R_{f1}(B) = R_{f1}(C) = R_{f1}(D) = R_{f1}(E) = 0$, and $R_{f2}(A) = R_{f2}(B) = R_{f2}(C) = R_{f2}(D) = R_{f2}(E) = 0$ $\Rightarrow A = B = C = D = E$.	$R_{f1}(A) = R_{f1}(B) = R_{f1}(C) = R_{f1}(D) = R_{f1}(E) = 0$ $R_{f2}(A) = R_{f2}(B) = R_{f2}(C) = R_{f2}(D) = R_{f2}(E) = 0$ $R_{f3}(A) = 17.64, R_{f3}(B) = 64.76, R_{f3}(C) = 0.375,$ $R_{f3}(D) = 19.36, R_{f3}(E) = 37.19.$ $\Rightarrow C < A < D < E < B$.
Let $A = \langle I_1, K_1 \rangle = \langle (0.1, 0.2, 0.3, 0.4), (0.5, 0.6, 0.7, 0.8) \rangle$, $B = \langle I_2, K_2 \rangle = \langle (0.3, 0.4, 0.5, 0.6), (0.7, 0.8, 0.9, 1) \rangle$ be two different TrBFNs.	$R_{f1}(A) = R_{f1}(B) = -0.4$, and $R_{f2}(A) = R_{f2}(B) = -0.08 \Rightarrow A = B$.	$R_{f1}(A) = R_{f1}(B) = -0.4, R_{f2}(A) = R_{f2}(B) = -0.4,$ and $R_{f3}(A) = 0.113 < R_{f3}(B) = 0.156 \Rightarrow A < B$.
Let $A = \langle I_1, K_1 \rangle = \langle (5, 20, 30, 40), (25, 35, 45, 60) \rangle$, $B = \langle I_2, K_2 \rangle = \langle (10, 15, 25, 45), (30, 30, 40, 65) \rangle$, $C = \langle I_3, K_3 \rangle = \langle (0, 25, 25, 45), (30, 30, 35, 70) \rangle$, $D = \langle I_4, K_4 \rangle = \langle (12, 13, 13, 57), (15, 45, 50, 55) \rangle$, $E = \langle I_5, K_5 \rangle = \langle (2, 23, 27, 43), (27, 33, 43, 62) \rangle$ be five different TrBFNs.	$R_{f1}(A) = R_{f1}(B) = R_{f1}(C) = R_{f1}(D) = R_{f1}(E) = -17.5$, $R_{f2}(A) = R_{f2}(B) = R_{f2}(C) = R_{f2}(D) = R_{f2}(E) = -393.75$ $\Rightarrow A = B = C = D = E$.	$R_{f1}(A) = R_{f1}(B) = R_{f1}(C) = R_{f1}(D) = R_{f1}(E) = -17.5,$ $R_{f2}(A) = R_{f2}(B) = R_{f2}(C) = R_{f2}(D) = R_{f2}(E) = -393.75,$ and $R_{f3}(A) = 21.49, R_{f3}(B) = 23.57, R_{f3}(C) = 24.78,$ $R_{f3}(D) = 23.26, R_{f3}(E) = 22.50.$ $Rightarrow A < E < D < B < C$.
Let $A = \langle I_1, K_1 \rangle = \langle (5, 70, 90, 110), (70, 80, 110, 140) \rangle$, $B = \langle I_2, K_2 \rangle = \langle (10, 65, 70, 130), (60, 90, 120, 130) \rangle$, $C = \langle I_3, K_3 \rangle = \langle (20, 55, 75, 125), (40, 110, 115, 135) \rangle$, be three different TrBFNs.	$R_{f1}(A) = R_{f1}(B) = R_{f1}(C) = -18.75$, $R_{f2}(A) = R_{f2}(B) = R_{f2}(C) = -703.125$, $\Rightarrow A = B = C$.	$R_{f1}(A) = R_{f1}(B) = R_{f1}(C) = -18.75,$ $R_{f2}(A) = R_{f2}(B) = R_{f2}(C) = -703.125,$ and $R_{f3}(A) = 52.19 < R_{f3}(B) = 53.84 < R_{f3}(C) = 53.98 \Rightarrow A < B < C$
Let $A = \langle I_1, K_1 \rangle = \langle (30, 50, 60), (30, 50, 60) \rangle$, $B = \langle I_2, K_2 \rangle = \langle (40, 60, 70), (40, 60, 70) \rangle$, $C = \langle I_3, K_3 \rangle = \langle (10, 20, 30), (10, 20, 30) \rangle$, $D = \langle I_4, K_4 \rangle = \langle (1, 2, 3), (1, 2, 3) \rangle$, $E = \langle I_5, K_5 \rangle = \langle (50, 70, 90), (50, 70, 90) \rangle$, $F = \langle I_6, K_6 \rangle = \langle (20, 50, 70), (20, 50, 70) \rangle$ be six different TrBFNs.	$R_{f1}(A) = R_{f1}(B) = R_{f1}(C) = R_{f1}(D) = R_{f1}(E) = R_{f1}(F) = 0$, $R_{f2}(A) = R_{f2}(B) = R_{f2}(C) = R_{f2}(D) = R_{f2}(E) = R_{f2}(F) = 0$ and $R_{f3}(A) = 78.44, R_{f3}(B) = 87.75, R_{f3}(C) = 43.90,$ $R_{f3}(D) = 3.6, R_{f3}(E) = 114.89, R_{f3}(F) = 106.36.$ $\Rightarrow D < C < A < B < F < E$.	$R_{f1}(A) = R_{f1}(B) = R_{f1}(C) = R_{f1}(D) = R_{f1}(E) = R_{f1}(F) = 0$, $R_{f2}(A) = R_{f2}(B) = R_{f2}(C) = R_{f2}(D) = R_{f2}(E) = R_{f2}(F) = 0$ and $R_{f3}(A) = 78.44, R_{f3}(B) = 87.75, R_{f3}(C) = 43.90,$ $R_{f3}(D) = 3.6, R_{f3}(E) = 114.89, R_{f3}(F) = 106.36.$ $\Rightarrow D < C < A < B < F < E$.

5. Conclusion

In this paper, the shortcomings of a new ranking function introduced by Akram and Arshad [1] were discussed using various cases. Further, We proposed a new ranking function and studied its properties. Finally, we introduced a new ranking principle by combining Akram and Arshad's [1] ranking function and the proposed ranking function and also the efficiency of the proposed ranking principle in comparing arbitrary TrBFNs discussed. The proposed ranking principle can give better results for the decision-making problems under Bipolar fuzzy environment, which would be studied in future.

References

- [1] Akram, Muhammad and Arshad, Maham, (2019). A Novel Trapezoidal Bipolar Fuzzy TOPSIS Method for Group Decision-Making. *Group Decision and Negotiation*, 28, 565-584.
- [2] Atanassov, K. T. (1986). Intuitionistic fuzzy sets. *Fuzzy Sets and Systems*, 20, 87-96.
- [3] Atanassov, K. T., & Gargov, G, (1989). Interval-valued intuitionistic fuzzy sets. *Fuzzy Sets and Systems*, 31(3), 343-349.
- [4] Akram, M., Shumaiza and M. Arshad, (2020). Bipolar fuzzy TOPSIS and bipolar fuzzy ELECTRE-I methods to diagnosis. *Computational and Applied Mathematics*, 39, 1-21.
- [5] Nayagam, VLG., Dhanasekaran, P., Jeevaraj, S. (2016). A complete ranking of incomplete trapezoidal information. *Journal of Intelligent & Fuzzy Systems* 30 (6), 3209-3225.
- [6] Dhanasekaran, P., Jeevaraj, S., Nayagam, VLG. (2018). A complete ranking of trapezoidal fuzzy numbers and its applications to multi-criteria decision making. *Neural Computing and Applications*, 30 (11), 3303-3315.
- [7] Jeevaraj S (2021). Ordering of interval-valued Fermatean fuzzy sets and its applications. *Expert Systems with Applications* 185, 115613.
- [8] Przemyslaw Grzegorzewski, Olgierd Hryniewicz, Maciej Romaniuk, (2020). Flexible resampling for fuzzy data. *International Journal of Applied Mathematics and Computer Science*, 30 (2), 281-297.
- [9] Reza Ghanbari, Khatere Ghorbani-Moghadam, Nezam Mahdavi-Amiri, (2018). A Direct Method to Compare Bipolar LR-Fuzzy Numbers. *Advances in Fuzzy Systems*, 1-8, 2018
- [10] Rayappan Princy, Krishnaswamy Mohana, (2019). Spherical Bipolar Fuzzy Sets and Its Application in Multi Criteria Decision Making Problem. *Journal of New Theory*, 32, 58-70.
- [11] Reza Ghanbari, Khatere Ghorbani-Moghadam, Nezam Mahdavi-Amiri, (2019). Duality in Bipolar Fuzzy Number Linear Programming Problem. *Fuzzy Information and Engineering*, 172-185.
- [12] Shumaiza, Akram, M., Ahmad N. Al-Kenani, Alcantud, J.C.R. (2019). Group Decision Making Based on the VIKOR Method with Trapezoidal Bipolar Fuzzy Information, *Symmetry*, 11(10), 1313.
- [13] Shumaiza, Akram, M. and Ahmad N. Al-Kenani, (2019). Multiple-Attribute Decision Making ELECTRE II Method under Bipolar Fuzzy Model, *Algorithms*, 12(11), 226.

Interpretable Dual-Feature Recommender System Using Reviews¹

Jing Sheng LEI^a, Chen Si Cong ZHU^a, Sheng Ying YANG^{a,2}, Guan Mian LIANG^b,
Cong HU^a and Wei SONG^a

^a*Department of School of Information and Electronic Engineering, Zhejiang University of Science and Technology, Hangzhou, PR China*

^b*Cancer Hospital of the University of Chinese Academy of Science, Hangzhou, PR China*

Abstract. Reviews have been commonly used to alleviate the sparsity problem in recommender systems, which has significantly improved the recommender performance. The review-based recommender systems can extract users features and items from review texts. The existing models such as D-Attn and NARRE employ convolutional neural networks and a coarse-grained attention mechanism to code reviews that have been embedded using the static word embedding, ignoring the long distance text information and lacks interpretability. To overcome these problems, this paper proposes the DNRDR (Dual-feature Neural Recommender with Dual-attention using Reviews) model, which can extract dual features of review text and can also enhance the interpretability using the word-level and review-level attention mechanisms. The proposed model is verified by experiments and compared with the state-of-the-art models. Besides, the dual-level attention mechanism can be visualized to improve interpretability.

Keywords. Neural networks, recommender systems, review text, multiple features

1. Introduction

As an effective method to alleviate information sparsity in the e-commerce field, recommender systems enable consumers to find their interested information. Collaborative filtering technology that can find out users' preferences and accordingly predicts products that users may like using the mining of users' historical behavior has been the most widely used recommendation algorithm currently [1, 2, 3, 4, 5, 6]. However, it is difficult to produce reliable recommendations for users with few ratings [7]. In addition, contextual information cannot be clearly reflected in the rating matrix. These problems can be solved using textual reviews [8]. Specifically, users will explain the reason for his rating directly, and then, based on the review text, the corresponding recommendation is given. The existing review-based recommender systems have been using neural networks to ex-

¹This work is supported by Natural Science Foundation of China (No. 61672337, 61972357), Zhejiang Key R&D Program (No. 2019C03135), Basic Public Welfare Research Project of Zhejiang (LGF19F020003).

²Corresponding author: Shengying Yang, Department of School of Information and Electronic Engineering, Zhejiang University of Science and Technology, Hangzhou, 310023, PR China; E-mail: syyang@zust.edu.cn.

tract features, achieving good recommendation results [7, 9, 10]. It should be mentioned that although CNNs(Convolutional Neural Networks) have the ability of local semantic feature extraction, the fixed length of convolution kernels limits the extraction performance of the word order and contextual connection, which could easily result in an understanding deviation of review texts. Furthermore, although CNNs have been proven to be effective in decreasing prediction error, learned filters in a convolutional layer provide little help in interpreting the features of users or items. Attention mechanisms have been proposed to enhance interpretability since attention scores can quantify the importance of words or reviews.

To overcome those problems, in this study, a dual-feature processing module consisting of a CNN and a bidirectional Long Short-Term Memory (LSTM) [11] network is proposed to reduce information loss. In the proposed module, a CNN is used to extract short-distance features from textual reviews and supplemented with long-distance features obtained by an LSTM. Besides, every comment is modeled by a dual-dimension attention mechanism to improve the interpretability and to judge the importance of reviews and words. In addition, a dynamic word vector BERT(Bidirectional Encoder Representations from Transformers) [12] is exploited, and the word vector is calculated according to the context.

The contributions of this paper can be summarized as follows:

1. A neural network model DNRDR, which uses word vectors embedded with BERT as input and a dual-feature processing module to extract short- and long-distance features of users or items review texts, is proposed.
2. Interpretable attention mechanisms, i.e., the word-level attention mechanism used to differentiate the importance of every word and the review-level attention mechanism used to judge the usefulness of every review, which can enhance both interpretability and visualization of a recommender, are introduced.
3. Comparative experiments on four benchmark datasets from Amazon are conducted, and the experimental results have shown that the proposed DNRDR outperforms the baseline recommendation methods. In addition, the proposed text processing module has been proven to be effective in other review-based models, and the interpretability and visualization benefits from the proposed dual-dimension attention mechanism have also been demonstrated.

2. Related Work

There are two research branches closely related to the subject studied in this work. One includes the review-based recommender systems proposed in recent years, and another includes methods for extracting review features.

2.1. Review-based recommender systems in recent years

The Matrix Factorization (MF) [2] that simulates a user's explicit feedback, such as a score, by mapping users and items to a potential space has attained great attention in recent years [2, 4, 5, 13], but it is strongly influenced by sparsity. This limitation can be overcome by introducing review-based models [7, 9, 14, 15, 16], where reviews are mapped to the hidden space so that the neural networks can effectively extract advanced

features. However, most recommenders combine all reviews of users (items) into one long document that is used as an input. Although this approach lowers the prediction error, it neglects differences between reviews. For instance, users comments can refer to a variety of goods, so it would be absurd to predict a score of a movie based on reviews of electronic products. In the 2018 World Wide Web Conference, the NARRE [10] used a review-level attention mechanism to determine the usefulness of every review and further improved the prediction accuracy.

2.2. Review features extraction

The core of the review-based recommender systems is feature extraction from review texts. Many text-processing methods based on deep learning technology have been proposed recently, and good performances have been achieved. The TextCNN [17] conveys word embeddings into a one-dimensional convolution layer, obtaining sentences of a fixed length by pooling operation. In [18], it has been proved that CNNs can extract local features but not long-distance features. Compared to the CNNs, RNNs adopt a linear sequence structure to collect input information from the front to the back continuously, which could easily cause a severe gradient disappearance or gradient explosion [11]. In order to solve this problem, in the proposed model, an LSTM is introduced, adding intermediate state information, so as to alleviate the gradient disappearance problem. With respect to the word embedding, the Transformer [19] was proposed in 2017 by Google in the in the research article about the machine translation task. It abandons the traditional neural network architectures and completely relies on the attention mechanism. The BERT [12] model based on the Transformer can effectively extract context information and thus provides significant progress in the field of natural language processing [20, 21, 22, 23].

3. OUR PROPOSED MODEL

3.1. Structure of DNRDR

This section presents the proposed DNRDR model. As shown in Fig 1, our proposed model consists of two similar networks connected in parallel. Since the network structure of the item part is the same as that of the user part, this section focuses on the left part of the network that processes user input data.

The DNRDR input is a group of reviews, including j user reviews of d words $\{R_{u1}, R_{u2}, \dots, R_{un}\}$, which are then mapped by BERT [12] to a comment matrix $W_{u,r} \in \mathbb{R}^{j \times d \times n}$ where n refers to the word vector dimension. The BERT mapping is performed on each item review to obtain an item comment matrix $W_{i,r} \in \mathbb{R}^{j' \times d \times n}$, where j' refers to the review number of each item.

In the proposed model, the word-level attention module is first used to learn the most informative words. Assume $w_{w-level} \in \mathbb{R}^{1 \times n}$ is a weight matrix of the input word vector; then, the weighting scores for a word are computed as follows:

$$S_i = \text{softmax}(W_a \times \sigma(w_{w-level} \times W_{u,r_i})), i \in [1, j] \quad (1)$$

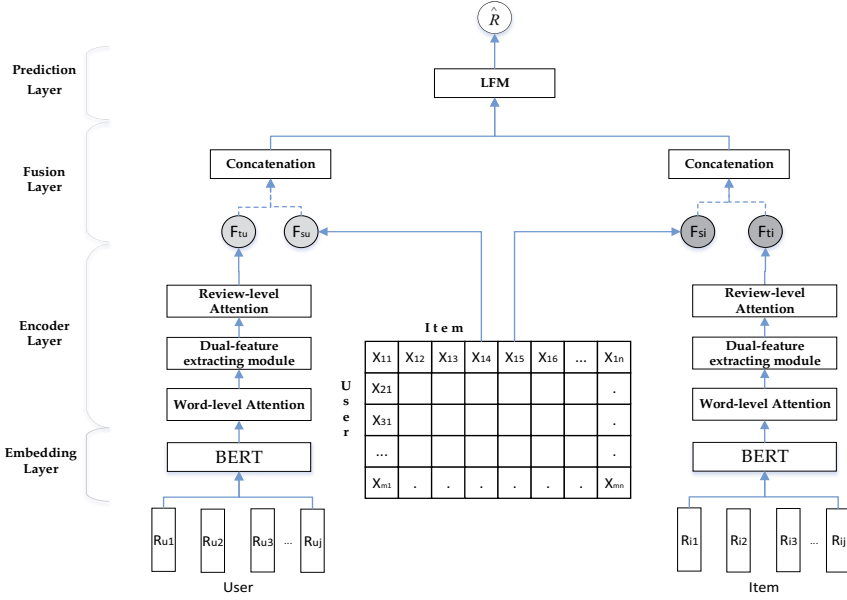


Figure 1. The structure of Dual-feature Neural Recommender with Dual-attention using Reviews is divided into User part(Left), Rating Matrix(Middle) and Item part(Right) from a horizontal perspective. From a longitudinal perspective, the model consists of Embedding Layer, Encoder Layer, Fusion Layer and Prediction Layer.

where $W_a \in \mathbb{R}^{1 \times t}$ are the attention parameters and t is the hyperparameter of the attention dimension. σ represents the tanh function for the activation function. $S_i \in \mathbb{R}^{1 \times d}$ are the attention scores for each word. Then let $O_{ui} = S_i \times W_{u,r_i}, i \in [1, j]$ be the weighted word vectors.

The encoder layer is the core of DNRDR, consisting of two parallel networks that extract the long and short distance features of the review texts, respectively. The long-distance review features for a word h_{ui} are obtained through a two-way LSTM. Then, the $2l$ -dimensional features of the d words are used to obtain the hidden state of the LSTM network $h_{u,L} \in \mathbb{R}^{d \times 2dl}$:

$$h_{u,L} = h_{u1} \oplus h_{u2} \oplus \dots \oplus h_{ui}, i \in [1, j] \tag{2}$$

Then a fully connected layer is used to prepare the long- and short-distance features for merging by setting them to the same dimension. The short-distance reviews features are obtained by a convolutional layer composed of m neurons where each neuron is associated with a convolution kernel as follows::

$$o_i = ReLU(O_{u,i} * K_i + b_i) \tag{3}$$

where b_i is the paranoid term, and $*$ represents the convolution operation.

Suppose $\{o_1, o_2, \dots, o_{d-t+1}\}$ are the features obtained by (5), the final feature of the convolution kernel can be calculated using the maximum pooling [24] operation so the short-distance review features $Review_C$ are merged with the features obtained by m

neurons. Then the long- and short-distance features of the user's reviews are combined to obtain the user's text features $Review_{tu} \in \mathbb{R}^{1 \times 2m}$.

The review-level attention mechanism [25] is utilized to judge which reviews are the most useful. The attention score vector describes the usefulness of reviews, and it is used to weigh each of the comments as follows:

$$\alpha_L = softmax(\tanh(w_{r-level} \times Review_{tu}^T)) \quad (4)$$

where $\alpha_L \in \mathbb{R}^{1 \times j}$, $w_{r-level} \in \mathbb{R}^{1 \times 2j}$ are the parameters. The attention score vector describes the usefulness of the reviews, and it is used to weight each of the comments $F_{tu} \in \mathbb{R}^{1 \times j}$ as follows:

$$F_{tu} = \alpha_L \times Review_{tu} \quad (5)$$

Similarly, the weighted features F_{ti} of an item's review texts can be obtained. Then the proposed model uses LFM [2] which is an algorithm based on matrix factorization technology, to extract the hidden factors of users F_{su} and items F_{si} in the rating matrix.

In the fusion layer, user review features and user rating features are concatenated to a unified vector F_U and the item features F_I can be gained in the same way. Then the prediction layer predicts the users rating for item by using the dot product to map user and item features to the same space as follows:

$$\hat{R}_{u,i} = \omega \times (F_U \otimes F_I) + b_u + b_i + \mu \quad (6)$$

where μ is the fully connected layer parameter.

3.2. Model Learning

$$L = \sum_{u,i \in \Gamma} (\hat{r}_{u,i} - r_{u,i})^2 \quad (7)$$

Γ represents the user-item datasets, $\hat{r}_{u,i}$ is the predicted score of user u for product i , and $r_{u,i}$ is the true rating in the training set. In order to minimize the loss function, the Adam (Adaptive Moment Estimation) [26] estimator is used as an optimizer. In order to prevent overfitting, the dropout [27] is used to solve this problem, whose main idea is to randomly discard some neurons during the training process.

4. EXPERIMENTAL VERIFICATION

4.1. Datasets

In the experiments, four public datasets from the Amazon 5-core [28] review datasets were used including Digital_Music (DM), Movies_and_TV (MT), Kindle_Store (KS), Toys_and_Games (TG). Every user and item in these sets contains at least five reviews. The smallest dataset is TG, which contains 167,597 samples; thus, they all have enough samples to build and verify the model, i.e., they contain enough semantic information to guide modeling the neural networks.

Table 1. Prediction Performance of different models

	NMF	LFM	SVD++	HFT	DeepCoNN	D-Attn	NARRE	DNRDR
Digital_Music	1.228	0.851	0.837	0.849	0.828	0.819	0.816	0.796*
Movies_and_TV	1.415	1.281	1.273	1.211	1.019	1.048	0.998	0.981*
Kindle_Store	0.995	0.623	0.616	0.622	0.614	0.611	0.606	0.593*
Toys_and_Games	1.429	0.869	0.856	0.852	0.849	0.840	0.835	0.827*

4.2. Baselines

We compare our model with the state-of-the-art recommendation models including the NMF [4], LFM [2], SVD++ [5], HFT [29], DeepCoNN [9], D-Attn [7] and NARRE [10]. The NMF, LFM, and SVD++ models utilized only the rating matrix in the model training phase, while the DeepCoNN and D-Attn models used only the reviews; the NARRE used the review texts and incorporated the information on ratings.

4.3. Data Preprocessing

Particularly, the preprocessing task included converting all characters to lowercase, detecting and correcting spelling errors, deleting punctuation marks, stop words and numbers. The stop word frequency was set to 0.7. To prevent the long tail effect, the length and number of reviews covering 80% of users (items) were used in the experiment; every user (item) retained 12 comments, and every comment retained 200 words. The overall dataset were randomly divided into training set (80%), validation set (10%) and test set (10%), and the reviews in the test and validation set were removed.

5. RESULTS ANALYSIS

5.1. Prediction Performance

We use the mean square error (MSE) as the evaluation index of model performance. The prediction performance of our model and the comparison models are shown in Table 1, where it can be seen that the proposed model outperformed all the baseline models on all datasets, which proved the effectiveness of the proposed model. It can be concluded that, compared with the traditional NMF, LFM, SVD++, and HFT models, the DeepCoNN, D-Attn, and NARRE models and the proposed model that used the deep learning methods performed better, demonstrating that the neural networks could extract user preferences and item features contained in the review texts. Among the models considering reviews, the prediction errors of the HFT, DeepCoNN, and D-Attn models were larger than those of the NARRE model and the proposed model. This was expected since the HFT, DeepCoNN, and D-Attn model integrated all review texts into one document for further processing, ignoring differences between the reviews. Besides, they did not consider the rating matrix, so part of the information was lost.

5.2. Attention Mechanism Visualization

To demonstrate the word- and review-level attention mechanisms, the words with a high word-level attention score are highlighted in Table 2; the words with the highest scores

Table 2. Visualization of the attention mechanisms

$\alpha_L = 0.221$	A classically-styled and introverted album. The Memory of Trees is a masterpiece of subtlety . Many of the songs have an endearing shyness to them - soft piano and a lovely , quiet voice. For certain , The Memory Of Trees is melodic, romantic and sensuous .
$\alpha_L = 0.096$	I got this album on vinyl when it came out in the 70s. A lot of people didn't know about this cd when it came out. This was and still is a great buy. The singing is priceless .This is a must album with such iconic hits . Seems like they never get old.

are colored in gray, the middle ones in light gray, and the lowest ones are not colored. A group of reviews for an item were randomly selected. The review-level attention scores that indicate the importance of the review are presented on the left side in Table 2.

The results showed that the two attention mechanisms greatly improved model interpretability. In terms of the word-level attention, the trivial pronoun words were neglected by the model and words rich in the features of users or items were considered. For instance, in Table 2, the conjunction "and" in "For certain, The Memory Of Trees is melodic, romantic and sensuous." is not colored, which indicates the model considered it unimportant. On the contrary, "melodic", "romantic" and "sensuous" that describe the characteristics of the music are marked. With respect to the review-level attention mechanism, the scoring α_L of the first review was higher than those of the other mechanisms, which proves the effectiveness of the proposed attention mechanisms because it is easy to find that the first review contains more instructive information about the item. In contrast, only general opinions and irrelevant information can be obtained from the second review.

6. CONCLUSIONS

This paper proposes a deep learning model DNRDR based on the rating matrix and review texts, which can learn long- and short-distance features of review texts. The proposed model can visualize the learned features by the word-level attention mechanism and can improve the interpretability of recommender systems by the review-level attention mechanism. The proposed model is verified by experiments and compared with a few state-of-the-art models. The experimental results show that the proposed method can reduce the error of prediction scores. Additional experiments are conducted to demonstrate that the proposed DNRDR can deal with the cold start problem more effectively than the related models by fusing the comment text with the ratings rather than using the rating matrix alone, hence could achieve better recommendation results on e-commerce websites.

References

- [1] Silvana Aciar, Debbie Zhang, Simeon Simoff, and John Debenham. Informed recommender: Basing recommendations on consumer product reviews. *IEEE intelligent systems*, 22(3):p.39–47, 2007.
- [2] Y. Koren, R. Bell, and C. Volinsky. Matrix factorization techniques for recommender systems. *Computer*, 42(8):30–37, 2009.

- [3] Mihajlo Grbovic, Vladan Radosavljevic, Nemanja Djuric, Narayan Bhamidipati, Jaikit Savla, Varun Bhagwan, and Doug Sharp. E-commerce in your inbox: Product recommendations at scale. *Proceedings of the 21th ACM SIGKDD international conference on knowledge discovery and data mining*, pages 1809–1818, 2015.
- [4] Daniel D. Lee and H. Sebastian Seung. Algorithms for non-negative matrix factorization. In *Proceedings of the Advances in neural information processing systems, Vancouver, Canada*, pages 556–562, 2001.
- [5] Yehuda Koren. Factorization meets the neighborhood: A multifaceted collaborative filtering model. In *Proceedings of the 14th ACM SIGKDD International Conference on Knowledge Discovery and Data Mining, Las Vegas, Nevada, USA*, pages 24–27, 2008.
- [6] Soroush Ojagh, Mohammad Reza Malek, Sara Saeedi, and Steve Liang. A location-based orientation-aware recommender system using iot smart devices and social networks. *Future Generation Computer Systems*, 108:97–118, 2020.
- [7] Sungyong Seo, Jing Huang, Hao Yang, and Yan Liu. Interpretable convolutional neural networks with dual local and global attention for review rating prediction. In *Proceedings of the eleventh ACM conference on recommender systems*, pages 297–305, 2017.
- [8] Huibing Zhang, Hao Zhong, Weihua Bai, and Fang Pan. Cross-platform rating prediction method based on review topic. *Future Generation Computer Systems*, 101:236–245, 2019.
- [9] Lei Zheng, Vahid Noroozi, and Philip S Yu. Joint deep modeling of users and items using reviews for recommendation. In *Proceedings of the Tenth ACM International Conference on Web Search and Data Mining*, pages 425–434, 2017.
- [10] Chong Chen, Min Zhang, Yiqun Liu, and Shaoping Ma. Neural attentional rating regression with review-level explanations. In *Proceedings of the 2018 World Wide Web Conference*, pages 1583–1592, 2018.
- [11] Sepp Hochreiter and Jürgen Schmidhuber. Long short-term memory. In *Neural computation*, volume 9, pages 1735–1780. MIT Press, 1997.
- [12] Jacob Devlin, Ming-Wei Chang, Kenton Lee, and Kristina Toutanova. Bert: Pre-training of deep bidirectional transformers for language understanding. *arXiv preprint arXiv:1810.04805*, 2018.
- [13] Xiaoyuan Su and Taghi M Khoshgoftaar. A survey of collaborative filtering techniques. *Advances in artificial intelligence*, 2009, 2009.
- [14] Donghyun Kim, Chanyoung Park, Jinoh Oh, Sungyoung Lee, and Hwanjo Yu. Convolutional matrix factorization for document context-aware recommendation. In *Proceedings of the 10th ACM conference on recommender systems*, pages 233–240, 2016.
- [15] Jin Yao Chin, Kaiqi Zhao, Shafiq Joty, and Gao Cong. Anr: Aspect-based neural recommender. In *Proceedings of the 27th ACM International Conference on Information and Knowledge Management*, pages 147–156, 2018.
- [16] Libing Wu, Cong Quan, Chenliang Li, Qian Wang, Bolong Zheng, and Xiangyang Luo. A context-aware user-item representation learning for item recommendation. *ACM Transactions on Information Systems (TOIS)*, 37(2):1–29, 2019.
- [17] Yoon Kim. Convolutional neural networks for sentence classification. *arXiv preprint arXiv:1408.5882*, 2014.
- [18] Gongbo Tang, Mathias Müller, Annette Rios, and Rico Sennrich. Why self-attention? a targeted evaluation of neural machine translation architectures. In *arXiv preprint arXiv:1808.08946*, 2018.
- [19] Ashish Vaswani, Noam Shazeer, Niki Parmar, Jakob Uszkoreit, Llion Jones, Aidan N Gomez, Łukasz Kaiser, and Illia Polosukhin. Attention is all you need. In *Advances in neural information processing systems*, pages 5998–6008, 2017.
- [20] Jianquan Li, Xiaokang Liu, Honghong Zhao, Ruifeng Xu, Min Yang, and Yaohong Jin. Bert-emd: Many-to-many layer mapping for bert compression with earth mover’s distance. *arXiv preprint arXiv:2010.06133*, 2020.
- [21] Canwen Xu, Wangchunshu Zhou, Tao Ge, Furu Wei, and Ming Zhou. Bert-of-theseus: Compressing bert by progressive module replacing. *arXiv preprint arXiv:2002.02925*, 2020.
- [22] Xiaoqi Jiao, Yichun Yin, Lifeng Shang, Xin Jiang, Xiao Chen, Linlin Li, Fang Wang, and Qun Liu. Tinybert: Distilling bert for natural language understanding. *arXiv preprint arXiv:1909.10351*, 2019.
- [23] Xing Wu, Shangwen Lv, Liangjun Zang, Jizhong Han, and Songlin Hu. Conditional bert contextual augmentation. In *International Conference on Computational Science*, pages 84–95. Springer, 2019.
- [24] Ronan Collobert, Jason Weston, Léon Bottou, Michael Karlen, Koray Kavukcuoglu, and Pavel Kuksa. Natural language processing (almost) from scratch. *Journal of Machine Learning Research*, 12(1):2493–2537, 2011.
- [25] Kamal Al-Sabahi, Zhang Zuping, and Mohammed Nadher. A hierarchical structured self-attentive model for extractive document summarization (hssas). *IEEE Access*, PP(99):1–1, 2018.

- [26] Diederik P Kingma and Jimmy Ba. Adam: A method for stochastic optimization. *arXiv preprint arXiv:1412.6980*, 2014.
- [27] Nitish Srivastava, Geoffrey Hinton, Alex Krizhevsky, Ilya Sutskever, and Ruslan Salakhutdinov. Dropout: A simple way to prevent neural networks from overfitting. *Journal of Machine Learning Research*, 15(1):1929–1958, 2014.
- [28] Ruining He and Julian McAuley. Ups and downs: Modeling the visual evolution of fashion trends with one-class collaborative filtering. In *proceedings of the 25th international conference on world wide web*, pages 507–517, 2016.
- [29] Julian McAuley and Jure Leskovec. Hidden factors and hidden topics: understanding rating dimensions with review text. In *Proceedings of the 7th ACM conference on Recommender systems*, pages 165–172, 2013.

Facial Expression Recognition and Image Description Generation in Vietnamese

Khang Nhut LAM ^{a,1}, Kim-Ngoc Thi NGUYEN ^a, Loc Huu NGUY ^a,
and Jugal KALITA ^b

^aCan Tho University, Can Tho, Vietnam

^bUniversity of Colorado, Colorado Springs, USA

Abstract. This paper discusses a facial expression recognition model and a description generation model to build descriptive sentences for images and facial expressions of people in images. Our study shows that YOLOv5 achieves better results than a traditional CNN for all emotions on the KDEF dataset. In particular, the accuracies of the CNN and YOLOv5 models for emotion recognition are 0.853 and 0.938, respectively. A model for generating descriptions for images based on a merged architecture is proposed using VGG16 with the descriptions encoded over an LSTM model. YOLOv5 is also used to recognize dominant colors of objects in the images and correct the color words in the descriptions generated if it is necessary. If the description contains words referring to a person, we recognize the emotion of the person in the image. Finally, we combine the results of all models to create sentences that describe the visual content and the human emotions in the images. Experimental results on the Flickr8k dataset in Vietnamese achieve BLEU-1, BLEU-2, BLEU-3, BLEU-4 scores of 0.628; 0.425; 0.280; and 0.174, respectively.

Keywords. facial expression recognition, image description, CNN, YOLOv5, VGG16, LSTM.

1. Introduction

Facial expression recognition (FER) and image description generation (IDG) are important tasks in image understanding, connecting computer vision with natural language processing. Image content can be partially described through objects and their locations. Huang et al. [1] classify approaches for FER into 2 groups, including conventional FER and deep learning based approaches. Given an input image, the conventional FER approach consists of several steps: pre-processing the image to reduce noise (e.g., Gaussian Filter [2], Bilateral Filter [3]), detecting face and facial components, extracting features (e.g., Local Directional Pattern [4], Histogram of Oriented Gradients [5]), and classifying emotions (e.g., Support Vector Machine [6], Naïve Bayes classifier [7]). Li and Deng [8] report that deep FER consists of several steps including face alignment detectors (e.g., Viola-Jones [9], face alignment 3000fps [10]), data augmentation (e.g., rotation, skew, scaling), face normalization, feature learning, and emotion classification. Several deep neural network models have been used to learn image features such as Convolutional Neural Network (CNN) [11, 12], the hybrid Convolution - RNN [13], and Generative Ad-

¹Corresponding Author: Khang Nhut Lam, Can Tho University, Campus II, 3/2 Street, Can Tho City, Vietnam; E-mail: lnkhang@ctu.edu.vn.

versarial Network [14]. Human facial expressions are usually classified into 7 categories [15]: afraid, angry, disgusted, happy, neutral, sad, and surprised.

Publishing efforts on IDG may be grouped into 3 categories [16,17]: (i) Models rely on computer vision techniques to identify objects in the input image and extract their features [18,19]. Features extracted are fed to a Natural Language Generation (NLG) [20] sub-system. Then, the steps to build a description for the image follow the NLG architecture. (ii) Models are based on a retrieval system, where the image descriptor is retrieved from the training dataset. Most of these systems use neural models to extract image features and linguistic information [21,22]. (iii) A system relies on the generation architecture to generate new descriptions. First, neural models are used to extract features of images (e.g., VGGNet [23], Faster R-CNN [24], ResNet [25], and Inception-V3 [26]), then neural models are used to generate new descriptions [27,28]. For the last category, there are 2 architectures to generate images captions: inject and merge architectures [29]. In the inject architecture, the vectors of image features and words are combined and fed into a neural model for generating image captions; whereas in the merge architecture, the image feature vectors are merged with the final state of the neural model in a multimodal layer. The experiments show that the merge architecture outperforms the inject architecture.

The more information provided in the descriptive sentences, the image caption model is better. For example, the image caption “A boy with a happy face in a red shirt is playing on grass” is more detailed and vivid than the image caption “A boy is playing on the grass”. We have not seen image captioning with emotion recognition. This paper aims to explore the methods for FER and IDG. If the sentence describing the image contains words or phrases referring to a human, the system will identify the facial expression and add this emotion to the image description. In other words, the description sentence describes the content in the image and the facial emotion of the person.

2. Proposed Approach

We first discuss the datasets used and methods to pre-process datasets. Then, we present approaches to recognize human facial expressions and generate descriptions of images.

2.1. Datasets Pre-processing

The KDEF [15], Flickr8k [30], and Flickr30k[31] datasets are used to train the models to recognize the human facial expressions and to generate the image descriptions, respectively. The KDEF dataset comprises 4,900 images of 70 individuals displaying 7 emotional expressions, each of which is viewed from 5 different angles. The dataset is divided by 70%, 20%, and 10% for training, validation, and test sets, respectively. The Flickr8k and Flickr30k datasets consist of 8,092 images and 31,783 images, respectively, each of which has 5 description sentences. Each dataset is divided into 2 parts: 1,000 images for testing, the rest of the images for training.

The description sentences in the Flickr8k dataset are in English. We translate this dataset to Vietnamese using a pre-trained Transformer model². The Transformer translation model was trained on the dataset using 600,000 sentences extracted from TED³. Then, we pre-process the description sentences by converting sentences to lowercases, removing special characters and punctuation marks. The Underthesea⁴ toolkit is used

²<https://github.com/pbcquoc/transformer>

³<https://www.ted.com/>

⁴<https://pypi.org/project/underthesea/>

to segment words in the description sentences. The dictionary created consists of 4,028 words. Image descriptions are embedded in terms of vectors based on the position of words in the dictionary.

2.2. CNN-based and YOLOv5-based FER Models

The CNN model [32] has 3 types of layers, including convolution, pooling, and fully connected layers. The convolution layer extracts feature maps from input images by using filters to perform convolution operations. Then, the features extracted are applied non-linear transfer functions such as ReLU, sigmoid, tanh, and softmax. The pooling layer reduces the dimensionality of the output of the previous layer by performing a pooling operation such as max pooling, average pooling, and sum pooling. Finally, the fully connected layer or dense layer is a normal flat feed-forward neural network layer using a nonlinear activation function to obtain the probability of each class. In this paper, we use a classic feed-forward CNN to detect facial expressions. The OpenCV library is used to detect and crop human faces in each image, and then convert face images to grayscale. The grayscale images are fed to the CNN model using ReLU activation function, average pooling operation for training FER.

A traditional CNN does not detect and label objects well in real-time. YOLO [33] is state-of-the-art in real-time detecting objects. YOLOv3 can predict the bounding box and process the image simultaneously, so it is less time-consuming. The accuracies of using YOLOv3 for facial expression recognition on JAFFE, RaFD, and CK+ are 98.12%, 97.01%, and 99.72% [34], respectively. Currently, the newest version YOLOv5 comprises 3 main components: Cross Stage Partial Network [35] (CSP) backbone (including CSPRestNext50 and CSPDarknet) for feature extraction, PA-NET [36] neck for feature aggregation, and Head with YOLO layer for predicting boxes and labels. In our FER experiment, we use YOLOv5 provided by Ultralytics⁵.

2.3. Image Description Generation Model

We use the merge architecture to construct descriptions for images [29,37] with the VGG16 model for extracting image features and the LSTM model for constructing image caption, as presented in Figure 1. In our implementation, we use the library toolkits supported by TensorFlow.

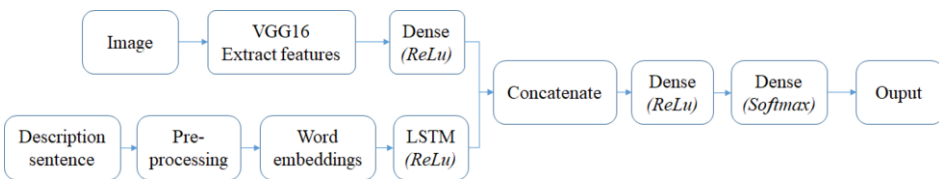


Figure 1. The image description generation model [29,37]

The VGG16 model extracts image feature vectors of size 4,096, which then are fed into a dense layer using the ReLU activation function. Description sentences are pre-processed, segmented, padded, and embedded into vectors. The word embeddings are fed to the LSTM using ReLU function. The outputs of the dense neural network and the LSTM have a similar size of 256 and then are concatenated and passed through a Dense layer using ReLU function with an output space of 256 and the next Dense layer using the softmax activation function with an output space of the dictionary size of 4,028.

⁵<https://ultralytics.com/yolov5>

If there is a personal noun in the caption generated, we simply pass the human image into the FER model and add the result of the model to the description generated. A list of person nouns is constructed manually including {đứa trẻ (kid), người đàn ông (man, male), cậu bé (boy), thanh niên (adolescent), trẻ em (baby), cô bé (girl), người phụ nữ (woman, female, lady), chàng trai (boy), ông già (old man), bà già (old woman), em bé (baby), bé gái (girl)}.

During the experiment, we noticed that sometimes the model did not perform correctly in determining the color of the object in the image. To solve the problem of color recognition (CR), from the built-in descriptive sentence, if the sentence contains color words, we determine the name of the object that needs color recognition. We use the YOLOv5 model to locate the object, crop the object, and save it as a new image for color recognition. An object usually has more than one color, we extract the dominant color of the object following the instructions of Ercolanelli⁶. When cropping an object out of an image, the object is usually in the center of the image, so the colors in the four corners of the image are usually the background colors. Therefore, pixels close to the color of the four corners of the image are considered the background color and excluded from the image. Then, a clustering algorithm, the K-means algorithm, is used to group similar pixels. The most dominant color of the object is considered the color of that object. Finally, the K Nearest Neighbors algorithm is used to convert the object color to words in human language by finding the nearest neighbor color in a large dictionary of colors taken from the XKCD color survey. The color after identification is replaced with the color of the previous description. Figure 2 shows an example of generating an image description.

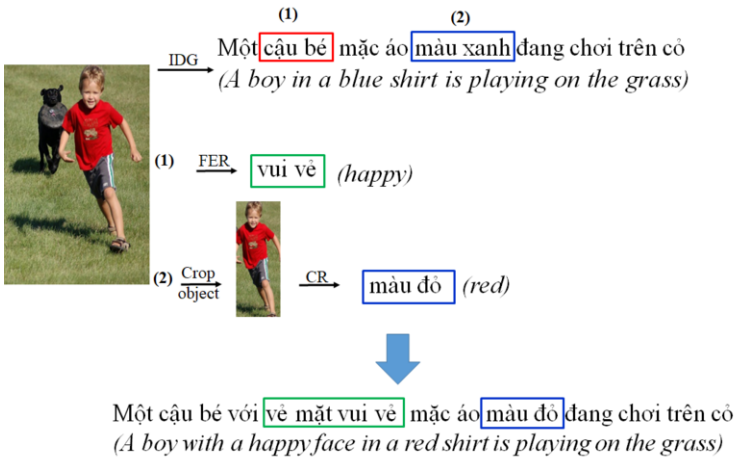


Figure 2. Example of generating an image description

3. Experimental Results

We build the modes in the Google Colab environment with 12GB RAM with GPU. The FER test set has 490 images with 78 afraid (meaning “sợ hãi”), 83 angry (meaning “giận dữ”), 71 disgusted (meaning “ghê tởm”), 65 happy (meaning “vui vẻ”), 66 neutral (meaning “trung lập”), 64 sad (meaning “buồn bã”), and 63 surprised (meaning “ngạc nhiên”) emotions. The results of the FER models are presented in Table 1.

⁶<https://github.com/algolia/color-extractor>

Table 1. Recall, precision and F1-score of the FER models

Facial emotions	Recall		Precision		F1-score	
	CNN	YOLOv5	CNN	YOLOv5	CNN	YOLOv5
Afraid	0.705	0.897	0.785	0.921	0.742	0.908
Angry	0.795	0.939	0.942	0.975	0.862	0.956
Disgusted	0.859	0.901	0.813	0.941	0.835	0.920
Happy	0.953	0.969	0.968	0.984	0.960	0.976
Neutral	0.954	0.984	0.851	0.984	0.899	0.984
Sad	0.812	0.937	0.776	0.845	0.793	0.888
Surprised	0.920	0.952	0.828	0.923	0.871	0.937

The accuracies of the CNN and YOLOv5 models are 0.853 and 0.938, respectively. YOLOv5 recognizes human facial emotions better and faster than CNN in all emotions. The happy emotion can be recognized very well; whereas, the afraid emotion might be mis-recognized as the surprise emotion by both two emotion recognition models. Next, we evaluate the method for generating image descriptions in Vietnamese. Table 2 presents the BLEU-scores of the image description generation model (the so-called IDG) and the image description generation model with facial expression recognition (the so-called IDG with FER). Interestingly, the results show that the Flickr30k dataset, including more images and captions than the Flickr8k dataset, does not help achieve better BLEU scores. Some examples of the image descriptions are shown in Table 3.

Table 2. BLEU-scores of the image description generation models

Dataset	Model	BLEU-1	BLEU-2	BLEU-3	BLEU-4
Flickr8k	IDG	0.629	0.426	0.281	0.175
	IDG with FER	0.628	0.425	0.280	0.174
Flickr30k	IDG	0.616	0.396	0.242	0.136
	IDG with FER	0.615	0.396	0.241	0.135




4. Conclusion

We experiment with CNN and YOLOv5 to recognize facial expressions on the KDEF dataset. The image description generation model integrated with the emotion recognition model and color recognition model achieves acceptable BLEU scores on the Flickr8k dataset. The description sentences generated by the current model can describe one person in an image. For future work, we will study approaches that might describe many people and their emotions in the image. Currently, we are performing experiments using Inception-V3 and YOLOv5 to extract image features instead of the VGG16 model, and training the models on different datasets. Besides, the Transformer model [38] or BERT model [39] will be used to generate description sentences. In addition, we need to improve the quality of the training dataset by improving the translation model.

References

- [1] Huang Y, Chen F, Lv S, Wang X. Facial expression recognition: A survey. *Symmetry*. 2019 Oct; 11(10):1189.
- [2] Deng G, Cahill LW. An adaptive Gaussian filter for noise reduction and edge detection. In *IEEE Conference Record Nuclear Science Symposium and Medical Imaging Conference*; 1993. p. 1615-1619.

Table 3. Examples of the image descriptions

Image	Image description	Image description with correction
	Một người đàn ông đang đi xe đạp trên một con đường (meaning “A man is riding a bicycle on a road”).	None
	Một con chó đen và trắng đang chạy qua một cánh đồng (meaning “A black and white dog is running through a field”).	Một con chó nâu đang chạy qua một cánh đồng (meaning “A brown dog is running through a field”).
	Một cậu bé đang chơi trong hồ bơi (meaning “A boy is playing in the pool”).	Một cậu bé với vẻ mặt vui vẻ đang chơi trong hồ bơi (meaning “A boy with a happy facial expression is playing in the pool”).

- [3] Zhang M. Bilateral filter in image processing. Master’s Thesis, Louisiana State University, Baton Rouge, LA; 2009.
- [4] Jabid T, Kabir MH, Chae O. Facial expression recognition using local directional pattern (LDP). In IEEE International Conference on Image Processing; 2010. p. 1605-1608.
- [5] Dalal N, Triggs B. Histograms of oriented gradients for human detection. In 2005 IEEE Computer Society Conference on Computer Vision and Pattern Recognition (CVPR’05); 2005; Vol. 1, p. 886-893.
- [6] Eng SK, Ali H, Cheah AY, Chong YF. Facial expression recognition in JAFFE and KDEF Datasets using histogram of oriented gradients and support vector machine. In IOP Conference series: materials science and engineering; IOP Publishing; 2019; Vol. 705, No. 1. p. 012031.
- [7] Mao Q, Rao Q, Yu Y, Dong M. Hierarchical Bayesian theme models for multipose facial expression recognition. IEEE Transactions on Multimedia. 2016; 19(4). p.861-873.
- [8] Li S, Deng W. Deep facial expression recognition: A survey. IEEE Transactions on Affective Computing. 2020.
- [9] Viola, P., Jones, M.: Rapid object detection using a boosted cascade of simple features. In Proceedings of the IEEE Computer Society Conference on Computer Vision and Pattern Recognition; 2001; Vol. 1.
- [10] Ren S, Cao X, Wei Y, Sun J. Face alignment at 3000 fps via regressing local binary features. In Proceedings of the IEEE Conference on Computer Vision and Pattern Recognition; 2014. p. 1685-1692.
- [11] Walecki R, Rudovic O, Pavlovic V, Schuller B, Pantic M. Deep structured learning for facial expression intensity estimation. Image Vis. Comput. 259; 2017. p.143-154.
- [12] Pranav E, Kamal S, Chandran CS, Supriya M.H. Facial emotion recognition using Deep Convolutional Neural Network. In Proceedings of the 6th International Conference on Advanced Computing and Communication Systems (ICACCS); 2020. p. 317-320.
- [13] Jain N, Kumar S, Kumar A, Shamsolmoali P, Zareapoor M. Hybrid deep neural networks for face emotion recognition. Pattern Recognition Letters; 2018; 115. p.101-106.
- [14] Yang H, Zhu K, Huang D, Li H, Wang Y, Chen L. Intensity enhancement via GAN for multimodal face expression recognition. Neurocomputing; 2021; 454. p.124-134.
- [15] Lundqvist D, Flykt A, Öhman A. The Karolinska directed emotional faces (KDEF). CD ROM from Department of Clinical Neuroscience, Psychology section, Karolinska Institutet; 1998; 91(630).
- [16] Bernardi R, Cakici R, Elliott D, Erdem A, Erdem E, Ikizler-Cinbis N, Keller F, Muscat A, Plank B. Automatic description generation from images: A survey of models, datasets, and evaluation measures. Journal of Artificial Intelligence Research. 2016; 55. p.409-442.

- [17] Hossain MZ, Sohel F, Shiratuddin MF, Laga H. A comprehensive survey of deep learning for image captioning. *ACM Computing Surveys (CSUR)*. 2019; 51(6). p.1-36.
- [18] Kulkarni G, Premraj V, Ordonez V, Dhar S, Li S, Choi Y, Berg AC, Berg TL. Babytalk: Understanding and generating simple image descriptions. *IEEE Transactions on Pattern Analysis and Machine Intelligence*; 2016; 35(12). p. 2891-2903.
- [19] Elliott D, Keller F. Image description using visual dependency representations. In *Proceedings of the Conference on Empirical Methods in Natural Language Processing*; 2013. p. 1292-1302.
- [20] Reiter E, Dale R. Building applied natural language generation systems. *Natural Language Engineering*. 1997; 3(1). p.57-87.
- [21] Socher R, Karpathy A, Le QV, Manning CD, Ng AY. Grounded compositional semantics for finding and describing images with sentences. *Transactions of the Association for Computational Linguistics*. 2014; 2. p.207-218.
- [22] Sur C. Gaussian smoothen semantic features (GSSF)—exploring the linguistic aspects of visual captioning in Indian languages (Bengali) using MSCOCO framework. *arXiv preprint arXiv:2002.06701*. 2020.
- [23] Simonyan K, Zisserman A. Very deep convolutional networks for large-scale image recognition. *arXiv preprint arXiv:1409.1556*. 2014.
- [24] Ren S, He K, Girshick R, Sun J. Faster R-CNN: Towards real-time object detection with region proposal networks. *Advances in Neural Information Processing Systems*. 2015; 28. p.91-99.
- [25] He K, Zhang X, Ren S, Sun J. Deep residual learning for image recognition. In *Proceedings of the IEEE conference on computer vision and pattern recognition*; 2016. p. 770-778.
- [26] Szegedy C, Vanhoucke V, Ioffe S, Shlens J, Wojna Z. Rethinking the inception architecture for computer vision. In *Proceedings of the IEEE Conference on Computer Vision and Pattern Recognition*; 2016. p. 2818-2826.
- [27] Aneja J, Deshpande A, Schwing AG. Convolutional image captioning. In *Proceedings of the IEEE Conference on Computer Vision and Pattern Recognition*; 2018. p. 5561-5570.
- [28] Guo L, Liu J, Zhu X, Yao P, Lu S, Lu H. Normalized and geometry-aware self-attention network for image captioning. In *Proceedings of the IEEE/CVF Conference on Computer Vision and Pattern Recognition*; 2020. p. 10327-10336.
- [29] Tanti M, Gatt A, Camilleri KP. What is the role of recurrent neural networks (RNNs) in an image caption generator? *arXiv preprint arXiv:1708.02043*. 2017
- [30] Hodosh M, Young P, Hockenmaier J. Framing image description as a ranking task: Data, models and evaluation metrics. *Journal of Artificial Intelligence Research*. 2013; 47. p.853-899.
- [31] Young P, Lai A, Hodosh M, Hockenmaier J. From image descriptions to visual denotations: New similarity metrics for semantic inference over event descriptions. *Transactions of the Association for Computational Linguistics*. 2014; 2. p.67-78.
- [32] LeCun Y, Bottou L, Bengio Y, Haffner P. Gradient-based learning applied to document recognition. In *Proceedings of the IEEE*; 1998; 86(11). p.2278-2324.
- [33] Redmon J, Divvala S, Girshick R, Farhadi A. You only look once: Unified, real-time object detection. In *Proceedings of the IEEE Conference on Computer Vision and Pattern Recognition*; 2016. p. 779-788.
- [34] Luh GC, Wu HB, Yong YT, Lai YJ, Chen YH. Facial expression based emotion recognition employing YOLOv3 deep neural networks. In *2019 International Conference on Machine Learning and Cybernetics (ICMLC)*; 2019. p. 1-7.
- [35] Wang CY, Liao HYM, Wu YH, Chen PY, Hsieh JW, Yeh IH. CSPNet: A new backbone that can enhance learning capability of CNN. In *Proceedings of the IEEE/CVF Conference on Computer Vision and Pattern Recognition Workshops*; 2020. p. 390-391.
- [36] Wang K, Liew JH, Zou Y, Zhou D, Feng J. Panet: Few-shot image semantic segmentation with prototype alignment. In *Proceedings of the IEEE/CVF International Conference on Computer Vision*; 2019. p. 9197-9206.
- [37] Sharma G, Kalena P, Malde N, Nair A, Parkar S. Visual image caption generator using deep learning. In *Proceeding of the 2nd International Conference on Advances in Science & Technology (ICAST)*; 2019.
- [38] Wolf T, Chaumond J, Debut L, Sanh V, Delangue C, Moi A, Cistac P, Funtowicz M, Davison J, Shleifer S, Louf R. Transformers: State-of-the-art natural language processing. In *Proceedings of the Conference on Empirical Methods in Natural Language Processing: System Demonstrations*; 2020. p. 38-45.
- [39] Devlin J, Chang MW, Lee K, Toutanova K. Bert: Pre-training of deep bidirectional transformers for language understanding. *arXiv preprint arXiv:1810.04805*. 2018

Hierarchical Digital Control System Performance

Larkin Eugene VASILEVICH^{a,1}, Akimenko Tatiana ALEKSEEVNA^a, Grishin Konstantin ANATOLIEVICH^a

^aTula State University, Russia

Abstract. A hierarchical multiprocessor system designed to control complex production facilities is investigated. It is shown that distributed computing in such systems is performed at the strategic, tactical and functional-logical levels. Since the control process unfolds in real physical time, in which both digital controllers and a control computer operate, when developing software for such systems, the problem of estimating the time complexity of control algorithms arises. A matrix equation is obtained that describes a closed multi-loop control system, in which data asymmetry and pure delays are taken into account. It is shown that time delays worsen the characteristics of transient processes during the transition of an object to a steady state of operation. A method for soft estimation of time complexity is developed, based on the sequential simplification of the semi-Markov process, represented by the algorithm, with recalculation of its time characteristics at each step. It is shown that the method allows one to estimate both data distortions and delays in the feedback loops.

Keywords. Von Neumann controller, multiprocessing, hierarchical level, semi-Markov process, time interval, recursive procedure

1. Introduction

The complexity of the tasks performed implies the complexity of the structure of the technical means and the digital control system, which is expediently divided into hierarchical levels; strategic, tactical and functional-logical, each of which solves its own range of tasks [1-4]. At the top, strategic, hierarchical level, the tasks of deep production planning are solved, therefore, artificial intelligence or computer methods are used to make decisions at this level. In accordance with the plan, a sequence of tasks is formed, which are fed to the tactical level computer. A middle-level computer, having received a plan from a strategic computer, divides the general problem into tasks that go to the functional-logical level, where feedbacks are closed in fact through the actuators, the controlled object and sensors. If the computer division into strategic and tactical levels can be carried out virtually (depending on the complexity of the planning algorithm), then the division into tactical and functional-logical levels, as a rule, is hardware. This is determined by the properties of von Neumann controllers, which interpret control algorithms sequentially, operator by operator, which unfolds in real physical time [5]. Thus, the digital controller, in addition to the algorithmic

¹ Corresponding Author, Larkin Eugene Vasilevich, Tula State University, Russia; E-mail: elarkin@mail.ru.

implementation of the control law, contributes to delays in the control process, which, in turn, affects the quality characteristics of the control system as a whole [6 - 9]. In addition to the control loop, the scheduling problem only exacerbates the problem of time delays, degrades performance and can lead to a loss of system stability. To simulate time delays, one can use the apparatus of the semi-Markov process [10 - 14], since each control algorithm processes random data generated at the outputs of the sensors and includes decision-making operators at branch points, therefore, when interpreting the operator, the operation execution intervals are random.

2. Configuration of the hierarchical multiprocessor control system

Structure of hierarchical multiprocessor control system is shown on the figure. 1 [4].

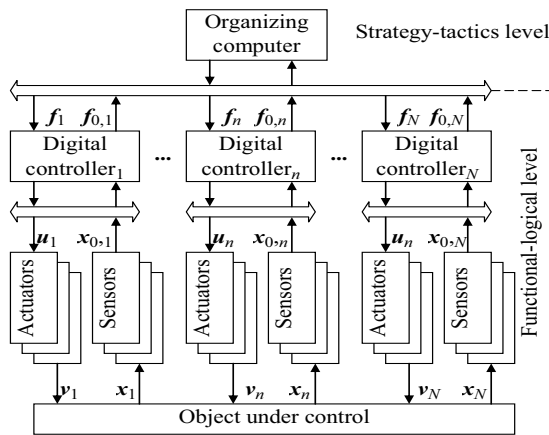


Figure. 1. Flowchart of hierarchical multiprocessor control system

On the flowchart strategy-tactics level is performed by organizing computer, whose destination is generating global aim of industry control system functioning, to dividing global problem onto local tasks and managing by controllers while solving assigned tasks. Every of N digital controllers, forming the functional-logical level, is included into $k(n)$, $1 \leq n \leq N$ control loops, every of which, in turn, includes actuator, which provides proper action on a production installation, part of common technological process and sensor, which measures production process state. Object under control, actuated by control vectors $\mathbf{v}_n(t) = [v_{1(n)}(t), \dots, v_{k(n)}(t), \dots, v_{K(n)}(t)]^\theta$, where θ is matrix transpose sign, t is the time, which, in turn, is transformed from vector $\mathbf{u}_n(t) = [u_{1(n)}(t), \dots, u_{k(n)}(t), \dots, u_{K(n)}(t)]^\theta$, calculated by the n -th controller, is characterized with state vector $\mathbf{x}_n(t) = [x_{1(n)}(t), \dots, x_{k(n)}(t), \dots, x_{K(n)}(t)]^\theta$, whose elements values are measured by sensors, which transform $\mathbf{x}_n(t)$ to feedback vector $\mathbf{x}_{0,n}(t) = [x_{0,n,1(n)}(t), \dots, x_{0,n,k(n)}(t), \dots, x_{0,n,K(n)}(t)]^\theta$. The reference signal vector $\mathbf{f}_n(t) = [f_{1(n)}(t), \dots, f_{k(n)}(t), \dots, f_{K(n)}(t)]^\theta$ is transmitted to n -th controller from

organizing computer. Organizing computer generates quests on the functional-logical level controllers by means of polling procedure, so algorithm, generated quests, is the cyclic one. Algorithms, realized in controllers, also are cyclic, they generate quests both to peripherals (sensors/actuators), and to organizing computer.

3. Estimation of time intervals between transactions

Performance of hierarchical multiprocessor control system highly depends of time intervals between transactions generated by the Von Neumann computer, for estimation of which model of polling procedure, unfolding in time, should be worked out [14 - 16]. Data in digital controller are processed according algorithms, which may be described

as the $(N+1)$ -parallel semi-Markov process

$$\tilde{\mu} = \{\mu_0(t), \mu_1(t), \dots, \mu_n(t), \dots, \mu_N(t)\}, \quad (1)$$

where $\mu_0(t)$ describes organizing computer operation; $\mu_n(t)$ describes operation of n -th, $1 \leq n \leq N$, controller;

$$\mu_n = \{A_n, \mathbf{h}_n(t)\}; \quad (2)$$

$A_n = \{a_{1(n)}, \dots, a_{j(n)}, \dots, a_{J(n)}\}$ are states of semi-Markov process $\mu_n(t)$, which simulate algorithm's operators; $\mathbf{h}_n(t) = \mathbf{g}_n(t) \otimes \mathbf{p}_n = [h_{j(n),l(n)}]$ is the $J(n) \times J(n)$ semi-Markov matrix; $\mathbf{g}_n(t) = [g_{j(n),l(n)}(t)]$ is the $J(n) \times J(n)$ matrix of pure time densities; $\mathbf{p}_n = [p_{j(n),l(n)}]$ is the $J(n) \times J(n)$ stochastic matrix.

With use methods, described in [15 - 17] on the semi-Markov process time delays between transactions may be obtained. Time delays are laid down at the stage of soft design, so, when simulation of the system it is necessary to forecast performance of the system, when at the digital controller such-and-such algorithm is realized with such-and-such time delays between transactions.

Let us consider n -th part of industrial object under managing of n -th digital controller. For simplification of analytical simulation it as more conveniently use instead description signal vectors $\mathbf{v}_n(t)$, $\mathbf{u}_n(t)$, $\mathbf{x}_n(t)$, $\mathbf{x}_{0,n}(t)$, $\mathbf{f}_n(t)$ their Laplace transforms are used, such as:

$$\begin{aligned} \mathbf{V}_n(s) &= L[\mathbf{v}_n(t)], \quad \mathbf{U}_n(s) = L[\mathbf{u}_n(t)], \quad \mathbf{X}_n(s) = L[\mathbf{x}_n(t)], \\ X_{0,n}(s) &= L[\mathbf{x}_{0,n}(t)], \quad \mathbf{F}_n(s) = L[\mathbf{f}_n(t)], \end{aligned} \quad (3)$$

where $L[\dots]$ is the direct Laplace transform operation, s is the Laplace variable (differentiation operator) [18 - 20].

Input of vectors $\mathbf{F}_n(s)$ and $\mathbf{X}_{n,0}(s)$ elements and output of vector $\mathbf{U}_n(s)$ elements are executed in sequence, so in Von Neumann controller there are time intervals between transactions. Delays can be considered as abstract ones, without link with any time co-ordinate system. On the controller/object-under-control interface data are inputted/outputted with delays, nominated as follows:

$F_{n,k}(s)$ is inputted with the lag $\tau_{n,f,k}$, $1 \leq k \leq K$;

$X_{n,0,k}(s)$ is inputted with the lag $\tau_{n,0,k}$, $1 \leq k \leq K$;

$U_k(s)$ is outputted with the lag $\tau_{n,u,k}$, $1 \leq k \leq K$.

Such approach permits to express operation of the linear system through transfer function apparatus. Fully closed loops system is described with matrix equation [2, 3]

$$\mathbf{X}_n(s) = \mathbf{N}_{n,u}(s) \cdot \mathbf{\Phi}_n(s) \cdot [\mathbf{E} + \tilde{\mathbf{\Phi}}_n(s)]^{-1} \cdot \mathbf{N}_{n,f}(s) \cdot \mathbf{\Phi}_{n,f,c}(s) \cdot \mathbf{F}_n(s), \quad (4)$$

in which $\mathbf{N}_{n,u}(s)$ and $\mathbf{N}_{n,f}(s)$ are $K(n) \times K(n)$ diagonal matrices, describing data skews when transmitting data from digital controller to actuator and from reference signal vector to actuator; $\mathbf{\Phi}_n(s)$ is the matrix of transfer functions, describing n -th part of object under control; \mathbf{E} is the $K(n) \times K(n)$ unit diagonal matrix; $\mathbf{\Phi}_{n,0,c}(s)$ and $\mathbf{\Phi}_{n,f,c}(s)$ are $K(n) \times K(n)$ matrices of transfer functions, describing data processing by digital controller soft; $\tilde{\mathbf{\Phi}}_n(s)$ is the $K(n) \times K(n)$ matrix of transfer functions, describing n -th part of object under control with data lags caused by sequential interpretation of control algorithm operators by Von Neumann type controller.

Matrices, describing delays in the system are as follows [18 - 20]:

$$\mathbf{N}_{n,f}(s) = \begin{pmatrix} \exp(-\tau_{n,f,1}s) & \dots & 0 & \dots & 0 \\ 0 & \dots & \exp(-\tau_{n,f,k}s) & \dots & 0 \\ & & \dots & & \\ 0 & \dots & 0 & \dots & \exp(-\tau_{n,f,K}s) \end{pmatrix}; \quad (5)$$

$$\mathbf{N}_{n,0}(s) = \begin{pmatrix} \exp(-\tau_{n,0,1}s) & \dots & 0 & \dots & 0 \\ 0 & \dots & \exp(-\tau_{n,0,k}s) & \dots & 0 \\ & & \dots & & \\ 0 & \dots & 0 & \dots & \exp(-\tau_{n,0,K}s) \end{pmatrix}; \quad (6)$$

$$\mathbf{N}_{n,u}(s) = \begin{pmatrix} \exp(-\tau_{n,u,1}s) & \dots & 0 & \dots & 0 \\ 0 & \dots & \exp(-\tau_{n,u,k}s) & \dots & 0 \\ & & \dots & & \\ 0 & \dots & 0 & \dots & \exp(-\tau_{n,u,K}s) \end{pmatrix}. \quad (7)$$

where $\tau_{n,f,k}$ is the lag of appearance of k -th digital data $f_{k(n)}(t)$ relative to its continual counterparts; $\tau_{n,0,k}$ is the lag of appearance of k -th digital data $x_{0,n,k(n)}(t)$ relative to its continual counterparts; $\tau_{n,u,k}$ is the lag of appearance of k -th analogue data $u_{k(n)}(t)$ relative to its digital counterparts.

Matrix $\tilde{\mathbf{\Phi}}_n(s)$ describes object under control from interface controller/actuator till interface feedback/controller and is as follows:

$$\tilde{\mathbf{\Phi}}_n(s) = \mathbf{N}_{n,u}(s) \cdot \mathbf{\Phi}_{n,a}(s) \cdot \mathbf{\Phi}_n(s) \cdot \mathbf{\Phi}_{n,0}(s) \cdot \mathbf{N}_{n,0}(s), \quad (8)$$

where $\Phi_{n,a}(s) = [\Phi_{n,a,k(n),l(n)}(s)]$ and $\Phi_{n,0,k(n),l(n)}(s) = [\Phi_{n,a,k(n),l(n)}(s)]$ are $K(n) \times K(n)$ diagonal matrices, describing actuators and sensors correspondingly, elements of which are as follows:

$$\Phi_{n,a,k(n),l(n)}(s) = \begin{cases} \Phi_{n,a,k(n)}(s), & \text{when } k(n) = l(n); \\ 0, & \text{when } k(n) \neq l(n). \end{cases} \quad (9)$$

$$\Phi_{n,0,k(n),l(n)}(s) = \begin{cases} \Phi_{n,0,k(n)}(s), & \text{when } k(n) = l(n); \\ 0, & \text{when } k(n) \neq l(n). \end{cases} \quad (10)$$

As it follows from (4) complex exponent, characterizing delays are available both at the numerator, and at the denominator of closed loop transfer function. Those exponents, which are situated at numerator, born data skew at the control system, and insignificantly affect on the result of control on the functional-logical level, but may substantially affect on the performance of the Strategy-tactics level of the system. Those exponents, which are situated at denominator of closed loop transfer function directly influence at the quality characteristics of control, such as transient time, overshooting, and stability.

As for a simulation of strategy-tactics level, approach to modeling highly depends on the on the problems, solving by organizing computer. If it fully controls the operation of object through digital controllers, to simulation of it method, described above may be applied. If its function is the supervision of the process, then theory of relay-races may be used for it simulation [21].

4. Example

As an example, control of object with cross links, shown on the fig. 2, was considered. Feedback signals in the system are generated with inertia-less sensors, which measures state vector $\mathbf{X}(s) = [X_1(s), X_2(s)]^{\theta}$. In the system proportional unit feedback is realized, namely $\mathbf{U}(s) = \mathbf{F}(s) - \mathbf{X}(s)$.

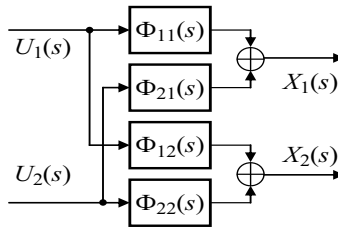


Figure 2. Object under control

Transfer functions, defining object under control dynamics, are as follows:

$$\Phi_{11}(s) = \Phi_{22}(s) = \frac{5}{0,02s^2 + 0,3s + 1}; \quad \Phi_{12}(s) = \Phi_{21}(s) = \frac{1}{0,15s + 1}.$$

System responses on standard control action $\mathbf{F}(s) = [L[1 \cdot 1(t), 0,5 \cdot 1(t)]]^{\theta}$, where $1(t)$ is the Heaviside function, are shown on the figure 3:

Figure 3 a displays plots, when controller is the analogue one, and there are no delays at all, the closed loop system is stable, its overshooting does not exceed 15%, the regulation time is less than 1 s.;

Figure 3 b displays plots, when dispatching is carried out by organizing computer, delays of signals are equal to 0,01 s, delays of signals are equal to 0,015 s, data skew is absent. In this case overshooting increases till 25%, regulation time increases till 2 s., and it is necessary to complicate control algorithm to return to parameters, shown on the figure. 3 a.

Figure 3 c displays plots, when delays are similar with delays on the figure. 3 b, but at the sacrifice of data skew, being equal to 0,01 s, on the plot of x_2 drawdown emerging. That is additional destabilizing factor, which should be avoided with the control algorithm.

Figure 3 d displays plots, when control algorithm is realized on a single controller. In this case delays increase till 0,015 and 0,02 s, respectively, and system is on the border of stability.

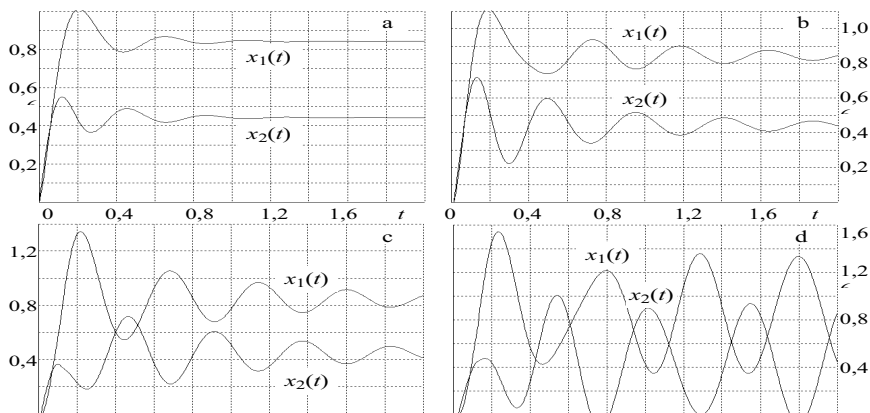


Figure 3. Reaction of the system on the Heaviside function

5. Conclusion

As a result, a simple engineering method for estimating temporal characteristics is proposed. It is shown, that system hierarchical configuration permits to unload controllers from dispatching functions. It also reduces control loop latency and improves system performance. Using by designers the formula of closed loop system transfer function and the simplified method of time intervals estimation permit to forecast system properties on the configuration system working out stage. From this it follows that the time for preliminary debugging of the system will be reduced.

Further investigations in the domain may be directed to working out the model of interaction between organizing computer and controllers in time domain and methods. Second direction of investigation development is forming a genetic algorithm, which ensures guaranteed predetermined hierarchical digital control system performance. The reported study was funded by RFBR, project number 19-38-90066.

References

- [1] Malin Löfving M., Säfssten K.; Winroth M. Manufacturing strategy formulation, leadership style and organizational culture in small and medium-sized enterprises. *IJMTM*. 2016. Vol. 30. No. 5. Pp. 306 - 325.
- [2] Landau I.D., Zito G. *Digital Control Systems, Design, Identification and Implementation*. Springer, 2006. 484 p.
- [3] Åström J., Wittenmark B. *Computer Controlled Systems: Theory and Design*. Tsinghua University Press. Prentice Hall, 2002. 557 p..
- [4] Kostenetskii P.S., Sokolinsky L.B. Simulation of Hierarchical Multiprocessor Database Systems // *Programming and Computer Software/ 2013/* Vol. 39, No. 1, Pp. 10 - 24.
- [5] Arnold K. A. Timing analysis in embedded systems // *In Embedded hardware* by J. Ganssler, K. Arnold et al. MA. 01803 USA. Elsevier Inc. 2008. Pp. 239 - 272.
- [6] Zhang X.M., Min W.U., Yong H.E., Delay dependent robust control for linear systems with multiple time-varying delays and uncertainties // *Control & Decision*, 2004. Vol. 19. N. 5. Pp. 496 – 500,
- [7] Wu M., He Y., She J.H., Liu G.P. Delay-dependent criteria for robust stability of time-varying delay systems // *Automatica*, 2004. Vol. 40, N. 8. Pp. 1435 – 1439.
- [8] Li D., Chen G. Impulses-induced p-exponential input-to-state stability for a class of stochastic delayed partial differential equations // *International Journal of Control*. 2019. Vol.: 92, N.: 8, Pp. 1805 - 1814.
- [9] Sanz R., García P., Albertos P., Fridman E. Robust predictive extended state observer for a class of nonlinear systems with time-varying input delay // *International Journal of Control*. 2020. Vol. 93. N. 2. Pp. 217 - 225.
- [10] Bielecki T.R., Jakubowski J., Niewęglowski M. Conditional Markov chains: Properties, construction and structured dependence // *Stochastic Processes and their Applications*. V. 127, N. 4. 2017. Pp. 1125–1170.
- [11] Ching W.K., Huang X., Ng M.K., Siu T.K. *Markov Chains: Models, Algorithms and Applications / International Series in Operations Research & Management Science*. V. 189. Springer Science + Business Media NY, 2013. 241 p.
- [12] Howard R. A. *Dynamic Probabilistic Systems*. Vol. 1: Markov Models. Vol. II: Semi-Markov and Decision Processes. Courier Corporation, 2012.
- [13] Janssen J., Manca R. *Applied Semi-Markov processes*. Springer US, 2006. 310 p.
- [14] Balsamo S., Harrison P.G., Marin A. Methodological construction of product-form stochastic Petri nets for performance evaluation // *Journal of Systems and Software*. Elsevier Inc. 2012. Vol. 85. № 7. Pp. 1520 – 1539.
- [15] Larkin E.V., Ivutin A.N. Estimation of Latency in Embedded Real-Time Systems // 3-rd Mediterranean Conference on Embedded Computing (MECO-2014). 2014. June 15-19. Budva, Montenegro, 2014. - Pp. 236 - 239.
- [16] Larkin E.V. Bogomolov A.V.; Privalov, A.N. A Method for Estimating the Time Intervals between Transactions in Speech-Compression Algorithms // *Automatic Documentation and Mathematical Linguistics*. 2017. Vol: 51. Iss. 5. Pp.: 214 - 219.
- [17] Larkin, E., Ivutin, A., Esikov, D. Recursive Approach for Evaluation of Time Intervals between Transactions in Polling Procedure // 8th International Conference on Computer and Automation Engineering (ICCAE 2016). Australia, Melbourne. MATEC Web of Conferences, 56 (2016) 01004.
- [18] Pavlov A.V. About the equality of the transform of Laplace to the transform of Fourier // *Issues of Analysis*. 2016. Vol.5(23). N.4(76). Pp. 21 - 30.
- [19] Li J., Farquharson C.G., Hu X. Three effective inverse Laplace transform algorithms for computing time -domain electromagnetic responses // *Geophysics*. 2015. Vol. 81. N. 2. Pp. E75 - E90.
- [20] Pospíšil M. Representation of solutions of delayed difference equations with linear parts given by pairwise permutable matrices via Z-transform // *Applied mathematics and computation*. 2017. V. 294. Pp. 180 - 194.
- [21] Larkin, E.V., Privalov, A.N. The discrete analysis of relay-races. *International Journal of Industrial and Systems Engineering*, 2020, 35(1), Pp. 28-56

Generalized-Multiquadric Radial Basis Function Neural Networks (RBFNs) with Variable Shape Parameters for Function Recovery

Sayan Kaennakham^{a,1}, Pichapop Paewpolsong^a, Natdanai Sriapai^a and Sunisa Tavaen^a

^a*School of Mathematics, Institute of Science, Suranaree University of Technology, Nakhon Ratchasima, Thailand*

Abstract. After being introduced to approximate two-dimensional geographical surfaces in 1971, the multivariate radial basis functions (RBFs) have been receiving a great amount of attention from scientists and engineers. In 1987 the idea was extended into the construction of neural networks corresponding to the beginning of the era of artificial intelligence, forming what is now called ‘Radial Basis Function Neural Networks (RBFNs)’. Ever since, RBFNs have been developed and applied to a wide variety of problems; approximation, interpolation, classification, prediction, in nowadays science, engineering, and medicine. This also includes numerically solving partial differential equations (PDEs), another essential branch of RBFNs under the name of the ‘Meshfree/Meshless’ method. Amongst many, the so-called ‘Multiquadric (MQ)’ is known as one of the mostly-used forms of RBFs and yet only a couple of its versions have been extensively studied. This study aims to extend the idea toward more general forms of MQ. At the same time, the key factor playing a very crucial role for MQ called ‘shape parameter’ (where selecting a reliable one remains an open problem until now) is also under investigation. The scheme was applied to tackle the problem of function recovery as well as an approximation of its derivatives using six forms of MQ with two choices of the variable shape parameter. The numerical results obtained in this study shall provide useful information on selecting both a suitable form of MQ and a reliable choice of MQ-shape for further applications in general.

Keywords. Generalized-Multiquadric, Radial Basis Function Neural Networks (RBFNs), Variable Shape Parameters, Function Recovery

1. Introduction

Radial Basis Functions (RBFs), φ , are commonly found as multivariate functions whose values are dependent only on the distance from the origin. This means that $\varphi(\mathbf{x}) = \varphi(r) \in \mathbb{R}$ with $\mathbf{x} \in \mathbb{R}^n$ and $r \in \mathbb{R}$, or, in other words, on the distance from a point of a given set $\{\mathbf{x}_j\}$, and $\varphi(\mathbf{x} - \mathbf{x}_j) = \varphi(r_j) \in \mathbb{R}$. Here, r_j is the Euclidean distance. As illustrated in Figure 1, RBF networks (RBFNs) broadly consist of three layers; 1) *Input*

¹ Corresponding Author, Sayan Kaennakham, School of Mathematics, Institute of Science, Suranaree University of Technology, Nakhon Ratchasima, Thailand; E-mail: sayan_kk@g.sut.ac.th.

layer – This layer is for independent variables to be imported with their corresponding values. 2) Hidden layer – This is where all the imported data is subjected to the constraints of each neuron. 3) Output later – This layer summaries in a linear combination manner the semi-output variables with their associated weights (w_1, w_2, \dots, w_m) obtained from the previous layer.

The very first problem of interpolation in multidimensional space that was approached by the concept of RBFNs is that documented by Powel [1]. This kind of problem requires as many centres as data points making it challenging for convectional interpolation schemes. With the capability of generating any non-linear mappings between stimulus and response, RBFNs have been developed and applied in a wide range of applications from machine learning to solving partial differential equations (PDE) [2]. Until nowadays, it can be summarized in general that researches on RBFNs are grouped into three branches [3]: i) kernels formation and development, ii) learning mechanism or weight optimization and judgments, and iii) the areas of application, of which the detail shall be provided below.

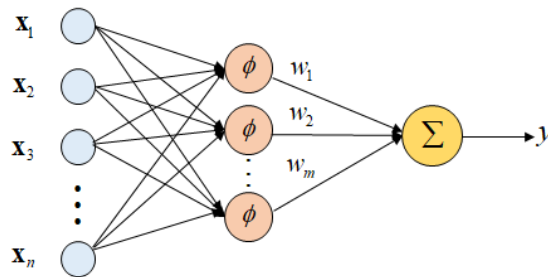


Figure 1. Typical structure of RBFNs.

Some successful applications are the approximation of function in 1-D and 2-D using polynomial with RBFNs [4], the solution to regulator equations based on a class of RBFNs [5], the use of DE- RBFNs for classifying weblog dataset [6], the use of RBFNs optimization for support vector machine classifiers [7], the application of Hermite collocation scheme for coupled PDEs [8], and the application of the modified MQ-RBFNs [9].

In all aspects of the application of RBFNs mentioned so far, searching for a suitable and reliable choice of a shape parameter, embedded in most RBF forms, still remains a great challenge. In this work, we numerically investigate the effectiveness of two recently proposed choices in a variable manner of the parameter as well as focus on a wider range of versions of multiquadric basis function, called ‘generalized MQ’. One and two-dimensional problems are tackled; both the functions themselves and their derivatives. This work is organised as follows. Section 2 provides a short mathematical derivation of the RBFNs before the detail of generalized MQ is provided in section 3 with the two versions of variable shape. Section 4 then demonstrates the main results of the experiment before all the crucial findings are listed in section 5.

2. Function Approximation by RBFNs

It starts with considering the interpolation of a multivariate function $f : \Omega \rightarrow \mathbb{R}$, where $\Omega \subset \mathbb{R}^n$, from a set of sample values $\{f(\mathbf{x}_j)\}_{j=1}^N$ on a discrete set $X = \{\mathbf{x}_j\}_{j=1}^N \subset \Omega$ (later referred to as ‘centres’). These multivariate functions can well be reproduced if appropriate linear combinations of univariate interpolation functions with the Euclidean norm $\|\cdot\|_2$ are used. This process can be carried out using translates $\Phi(\mathbf{x} - \mathbf{x}_j)$ of a continuous real-valued function Φ defined on \mathbb{R} , and by letting Φ be radially symmetric; i.e.,

$$\Phi(\mathbf{x}) := \varphi(\|\mathbf{x}\|_2) \tag{1}$$

with a continuous function φ on \mathbb{R}_0^+ . In general science and engineering literature, φ is often called a radial basis function with centres $\{\mathbf{x}_j\}_{j=1}^N$ and Φ is the associated kernel.

Interpolants F to f can be constructed as.

$$F(\mathbf{x}) = \sum_{j=1}^N a_j \varphi(\|\mathbf{x} - \mathbf{x}_j\|_2) \tag{2}$$

with real coefficients, $\{a_j\}_{j=1}^N$ which can be determined by the following interpolating condition.

$$F(\mathbf{x}_i) = f(\mathbf{x}_i), \tag{3}$$

for all $i = 1, 2, \dots, N$. and it leads to the following form.

$$f(\mathbf{x}_i) = F(\mathbf{x}_i) = \sum_{j=1}^N a_j \varphi(\|\mathbf{x}_i - \mathbf{x}_j\|_2), \quad 1 \leq i \leq N, \tag{4}$$

Hence, what comes next is a system of linear equations with $\{a_j\}_{j=1}^N$ being the unknowns, expressed as follows.

$$\boldsymbol{\varphi} \boldsymbol{\alpha} = \mathbf{f} \tag{5}$$

where $\boldsymbol{\varphi} = [\varphi_{ij}]_{N \times N}$, $\boldsymbol{\alpha} = [a_1, \dots, a_N]^T$, and $\mathbf{f} = [f(\mathbf{x}_1), \dots, f(\mathbf{x}_N)]^T$. The existence of the above system depends highly on the choice of RBF being used (will be more discussed later). Once the coefficient matrix is obtained, the solution calculation process

can then proceed as follows. For unknown locations $\hat{X} = \{\hat{\mathbf{x}}_j\}_{j=1}^{\hat{N}} \subset \Omega$ and $X \cap \hat{X} = \emptyset$, the approximate values of the corresponding function $\hat{f}(\hat{\mathbf{x}}_j)$ can be carried out using the expression below.

$$\hat{f}(\hat{\mathbf{x}}_j) \approx F(\hat{\mathbf{x}}_j) = \sum_{i=1}^N a_i \varphi(\|\hat{\mathbf{x}}_j - \mathbf{x}_i\|_2, \varepsilon) \tag{6}$$

for all $j = 1, 2, \dots, \hat{N}$. Note that the shape parameter ε is added to the equation above to emphasize the objective of this work which deals with the effect of this crucial parameter when the popular multiquadric RBF is utilized.

This similar assumption of approximation using RBFNs can be extended to the approximation of the n -order of function's derivative, provided that the basis function is also n -order differentiable. It is done via the following relation.

$$\frac{\partial^{(n)}}{\partial x_k} [\hat{f}(\hat{\mathbf{x}}_j)] \approx \frac{\partial^{(n)}}{\partial x_k} [F(\hat{\mathbf{x}}_j)] = \sum_{i=1}^N a_i \frac{\partial^{(n)}}{\partial x_k} \varphi(\|\hat{\mathbf{x}}_j - \mathbf{x}_i\|_2, \varepsilon) \tag{7}$$

The next section provides all components used and addressed in this investigation before some demonstrating 1D and 2D numerical tests are carried out in section 4.

3. Generalized MQ and It's Shape Choices

The main focus of this work is on one of the popular form of basis function known as 'multiquadric (MQ)' in its generalized form defined as follows.

$$\varphi_j(x, y) = (\varepsilon^2 + r_j^2)^\beta = (\varepsilon^2 + (x - x_j)^2 + (y - y_j)^2)^\beta \tag{8}$$

where $\beta = \dots, -3/2, -1/2, 1/2, 3/2, \dots$. These values give direct effect on the singularity of the interpolation matrix and, unavoidably, the effectiveness of the methods' performance. Different values yield different shape curves depicted in Figure 2 (a).

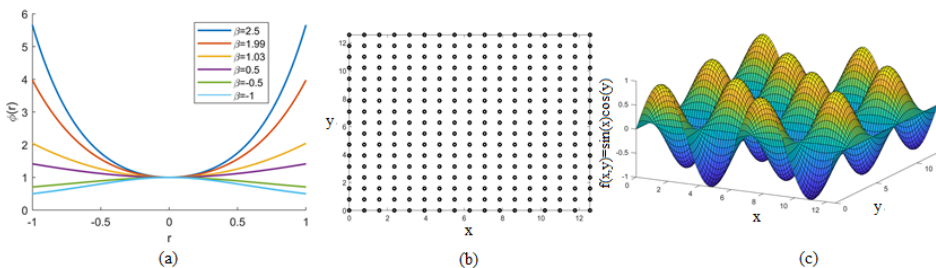


Figure 2. (a) Generalized MQ with six values of β 's, (b) distribution of centres, and (c) two-dimensional test function.

One crucial factor affecting the method’s performance is the shape parameter. Choices available in literature can be categorized into three forms; constant/fixed, variable, and iterative-based. This work focuses on two nonlinear-variable shape strategies (illustrated in Figures 3(a)-3(b)).

- Strategy-1 (**Stg-1**): by Nojavan et.al. (2017) [10], defined as.

$$\varepsilon_j = (c_{\min} + (c_{\max} - c_{\min}) \exp(-j))^{-1} \tag{9}$$

- Strategy-2 (**Stg-2**): by Xiang et.al. (2012) [11], defined as.

$$\varepsilon_j = c_{\min} + (c_{\max} - c_{\min}) \sin(j) \tag{10}$$

with $j = 1, 2, \dots, N$. Apart from these chosen forms of shape selection strategies, those nicely documented in [12] and [13] are also highly recommended for interested readers.

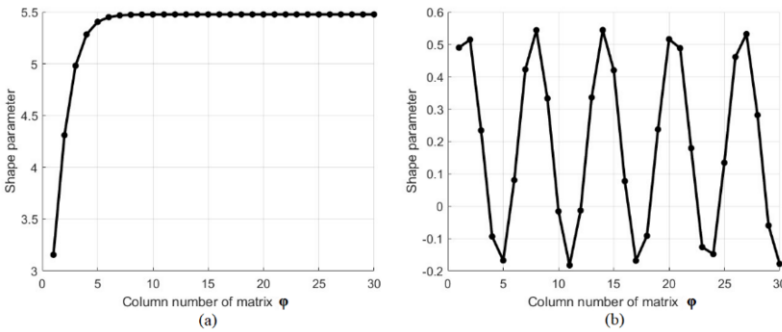


Figure 3. Multiquadrics’ shape determining strategies; (a) **Stg-1**, and (b) **Stg-2** both using $c_{\min} = 1/\sqrt{N}$, $c_{\max} = 3/\sqrt{N}$, and $N = 30$.

4. Numerical Experiments and Results

Results obtained from each case are evaluated using the mean absolute error norms defined as follows.

$$Mean\ Absolute\ Error = \frac{1}{\hat{N}} \left(\sum_{i=1}^{\hat{N}} |u_i^{exact}(x, y) - u_i^{approx.}(x, y)| \right) \tag{11}$$

To cover all subcases involved, a great number of simulations were performed on a machine with Windows 10 (64bit), Intel Corei7-11800H CPU (2.30GHz ,26MB L3 4.60

GHz), 32 GB DDR4 3200MHz. Two main cases are under investigation and presented here.

4.1. One-Dimensional Case

The first case deals with the approximation of a function in one dimension expressed below.

$$f(x) = e^{x^3} + \cos(2x) \quad (12)$$

To compare the overall accuracy, those shape values stated in the work of Maggie [14] were also tested. The total of 25 nodes uniformly distributed over a $-1 \leq x \leq 1$ domain was considered where the function's values at 17 equally-spaced nodes were numerically approximated. The results were obtained from all six forms of MQ with two variable shapes (*Stg-1* and *Stg-2*) together with fixed values are presented in Table 1. It can be shown in the table that all cases performed reasonably well with not much of a significant difference. One interesting finding worth mentioning is that those values obtained by using a fixed value were found the best ones. This might be attributed to the fact that Maggie [14] had actually performed a tremendous amount of experiments to find the best value of shape before utilizing that value for the actual experiment.

Table 1. Mean absolute errors measured for approximation of the function and its derivative for all forms of generalized MQ when using different variable shape forms (compared with a fixed form from literature).

Type	Shape	$\beta=2.50$	$\beta=1.99$	$\beta=1.03$	$\beta=0.50$	$\beta=-0.50$	$\beta=-1.00$
$f(x)$	<i>Stg-1</i>	28.70E-05	12.00E-04	71.60E-05	27.00E-04	11.66E-05	40.57E-05
	<i>Stg-2</i>	61.07E-07	15.18E-06	42.77E-06	48.52E-06	42.48E-05	16.00E-04
	Maggie [14]	16.00E-04	16.00E-04	59.44E-05	89.55E-06	74.68E-07	54.15E-07
$f'(x)$	<i>Stg-1</i>	22.00E-04	70.00E-04	35.00E-04	81.00E-04	12.00E-04	30.00E-04
	<i>Stg-2</i>	29.36E-05	71.61E-05	20.00E-04	23.00E-04	17.80E-03	66.00E-03
	Maggie [14]	33.00E-04	86.00E-04	20.00E-04	21.20E-05	10.05E-05	91.73E-06

4.2. Two-Dimensional Case

A more complex problem is now visited and a two-dimensional function is addressed, defined as follows.

$$f(x, y) = \cos(y) \cdot \sin(x) \quad (13)$$

This is defined on a $[0, 4\pi] \times [0, 4\pi]$ domain where the corresponding centres distribution is depicted in Figure 2(b), and its surface is being visualized in Figure 2(c). To focus on the two main variable shape strategies, the ones from the literature are omitted here. Five densities of centres were tested for each strategy to observe the overall

behavior of the variable when dealing with larger sizes of datasets. The set of 17×17 equally-spaced is used for the target locations for approximation. As depicted in Figures 4-5-6, all three forms; the function itself, its x -direction derivative, and its y -direction derivative, reveal the same trends of accuracy. Those functions' approximation produced by shape strategy 1 (or *Stg-1*) is found to be highly sensitive to the increase in centres (N) while *Stg-2* is not. This could be attributed to the fact that *Stg-1* is in an exponential curve where it can easily be affected by the pre-judged values of C_{\min} and C_{\max} , whose values depend on N . The best accuracy is found for *Stg-1* when $\beta = -0.50$ and $N = 225$ are used where the comparatively worst results are revealed when $\beta = 2.50$ and $N = 625$ are used, see Figures 4(a), 5(a), and 6(a). The opposite scenario is found in the use of *Stg-2* where $\beta = 2.50$ is clearly seen to outperform the rest for all three targeted function forms, see Figures 4(b), 5(b), and 6(b). As can be anticipated, *Stg-2* produces better solutions, for all values of β 's, when more supporting centres are involved, indicating the benefits one can achieve when deploying the strategy for larger datasets. It can also be seen from these same figures that the fastest reduction in error is obtained from $\beta = 2.50$ whereas the slowest one is from $\beta = -1.00$.

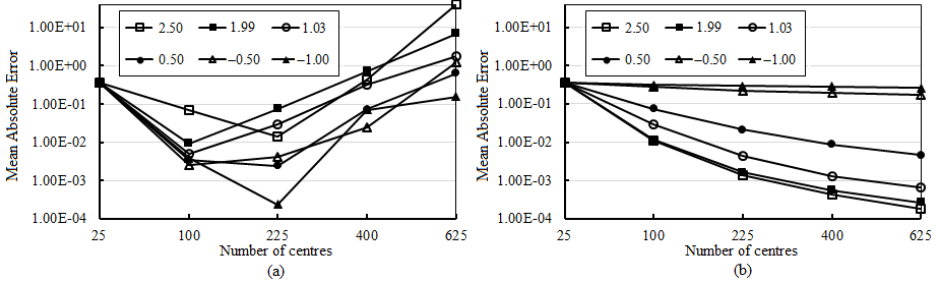


Figure 4. Mean absolute errors measured at different numbers of centres for approximation of $f(x, y)$; (a) using *Stg-1*, and (b) using *Stg-2*.

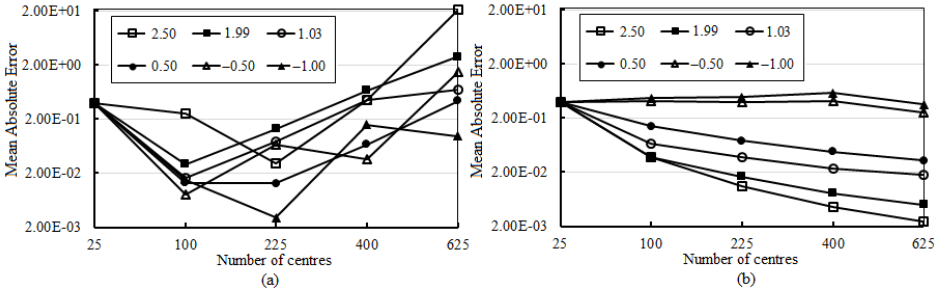


Figure 5. Mean absolute errors measured at different numbers of centres for approximation of df / dx ; (a) using *Stg-1*, and (b) using *Stg-2*.

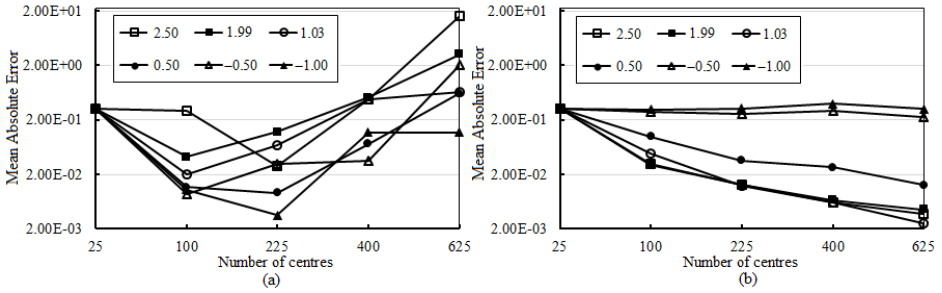


Figure 6. Mean absolute errors measured at different numbers of centres for approximation of $\partial f / \partial y$; (a) using *Stg-1*, and (b) using *Stg-2*.

5. Conclusions

Emerging as an alternative numerical tool for approximating and recovering functions and their derivatives, multiquadric radial basis function neural networks (MQ-RBFNs) are under investigation in this work. Six generalized forms of MQ were numerically applied using two popular choices of shape parameters. It was found that the exponential variable shape (*Stg-1*) is highly sensitive to the number of centres for all forms of MQ used. On the other hand, the trigonometric variable shape (*Stg-2*) provides a monotone of reduction in errors with the increase of centres indicating a more reliable aspect for larger datasets. With the effectiveness in approximating derivatives of a function being also under the study, *Stg-2* is seen promising with a great level of accuracy when the form $(\varepsilon^2 + r^2)^{5/2}$ of MQ is used. This could well have a great effect in the era of solving partial differential equations which shall remain one of our future investigations.

References

- [1] Powell MJD. Radial basis functions for multivariable interpolation: A Review. In: Mason JC, Cox MG, editors. Algorithms for the Approximation. Oxford: Clarendon Press; 1987. p. 143-67.
- [2] Park J, Sandberg IW. Universal approximation using radial basis function networks. Neural Comput. 1991 June;3(2):246-57.
- [3] Beatson RK, Cherrie JB, Mouat CT. Fast fitting of radial basis functions: Methods based on preconditioned GMRES iteration. Advances in Math Comp. 1999 Nov;11(2):253-70. Available from: DOI:10.1023/A:1018932227617.
- [4] Bellil W, Amar CB, Alimi AM. Comparison between beta wavelets neural networks, RBF neural networks and polynomial approximation for 1D, 2D functions approximation. Trans. Eng. Comp. Tech. 2008. Available from: DOI:10.5281/zenodo.1056514.
- [5] Zhou G, Wang C, Su W. Nonlinear output regulation based on RBF neural network approximation. Proceeding of the 2005 International Conference on Control and Automation; 2005 June 26-29; Budapest, Hungary. IEEE; 2005. p. 679-84. Available from: DOI:10.1109/ICCA.2005.1528210.
- [6] Dash CSK, Behera AK, Pandia MK, Dehuri S. Neural networks training based on differential evolution in radial basis function networks for classification of web logs. Proceeding of the International Conference on Distributed Computing and Internet Technology; 2013; Berlin, Heidelberg. Springer; 2013. p. 183-94. Available from: DOI:10.1007/978-3-642-36071-8_14.

- [7] Thurnhofer-Hemsi K, López-Rubio E, Molina-Cabello MA, Najarian K. Radial basis function kernel optimization for support vector machine classifiers. [arXiv:2007.08233](https://arxiv.org/abs/2007.08233)[Preprint]. 2020[cited 2020 Jul 16]. Available from: <https://arxiv.org/abs/2007.08233>.
- [8] Chuathong N, Kaennakham S. Numerical solution to coupled Burgers' equations by gaussian-based hermite collocation scheme. *J. Appl. Math.* 2018 Sep;2018:1-18. Available from: DOI:10.1155/2018/3416860.
- [9] Kaennakham S, Chanthawara K. Numerical solution to nonlinear transient coupled-PDE by the modified multiquadric meshfree method. *Rom. J. Phys.* 2021 Feb;66(108):1-14.
- [10] Nojavan H, Abbasbandy S, Allahviranloo T. Variable shape parameter strategy in local radial basis functions collocation method for solving the 2D nonlinear coupled Burgers' equations. *Mathematics.* 2017 Jul;5(3):1-21. Available from: DOI:10.3390/math5030038.
- [11] Xiang S, Wang K, Ai Y, Sha Y, Shi H. Trigonometric variable shape parameter and exponent strategy for generalized multiquadric radial basis function approximation. *Appl. Math. Model.* 2012 May;36(5):1931-8.
- [12] Cheng AHD, Multiquadric and its shape parameter-A numerical investigation of error estimate, condition number, and round-off error by arbitrary precision computation, *Eng. Anal. with Boundary Elements.* 2012; 36(2): 220-239. Available from: DOI: 10.1016/j.enganabound.2011.07.008.
- [13] Chen W, Hong Y, Lin J, The sample solution approach for determination of the optimal shape parameter in the Multiquadric function of the Kansa method, *Computers and Mathematics with Applications.* 2018; 75(8): 2942-2954. Available from: DOI:10.1016/j.camwa.2018.01.023.
- [14] Chenoweth ME, Sarra SA. A numerical study of generalized multiquadric radial basis function interpolation. *SIURO.* 2009;2(2):58-70. Available from: DOI:10.1137/09S01040X.

A Bolt Defect Recognition Algorithm Based on Attention Model

Zhijun LIN¹, Yingjie LIANG and Qineng JIANG

Jiangmen Power Supply Bureau of Guangdong Power Grid Co., LTD
Jiangmen, China

Abstract. As the largest number of fasteners on power distribution network, bolts are the cornerstone of ensuring the safety and reliability of power system. However, pin losing, nut losing, nut loosening, and rusting can cause damage to power system and even cause terrible accidents. In order to solve the problem that the large number of bolt defects causes traditional manual identification to be difficult and inefficient, this paper proposes a bolt defect identification algorithm based on attention models. The method in this paper improves the traditional deep residual network ResNet network, adds a channel attention mechanism to obtain key channel features, and uses random flipping, translation and other data augment methods to expand the bolt defect dataset. The experimental results show that compared with the traditional model, the improved model can more accurately identify different types of bolt defect images, and the mAP on the testing set reaches 85.9%, which verifies the feasibility and reliability of the ATT-ResNet50 model in bolt defect recognition. The method proposed in this paper has high recognition accuracy, realizes the intelligent recognition of common bolt defects.

Keywords. Attention Mechanism, Deep Residual Network, Data Augment, Bolt Defect Recognition

1. Introduction

As the most basic fastener of power distribution network, bolts produce an essential effect on the deployment of power grids. Affected by a variety of external factors such as the environment, the connecting bolts of the components are caused to produce defects, which in turn will affect the safe connection between the various components of the power distribution network, and cause safety risks to the power system [1,2]. Pin losing, nut losing, nut loosening and rusting are the four most common types of defects in bolts. These defects may cause loose connection of power system components, which not only increases the loss of power system, but also presents the safety hazards of components falling even terrible grid accident [3].

In recent years, for the sake of raising the inspection efficiency of power distribution network, drone inspection technology has been widely used. Regarding the external defects of power grid equipment, drones with data acquisition devices can quickly obtain a large number of pictures and then corresponding defects will be found

¹ Corresponding Author, Zhijun LIN, Jiangmen Power Supply Bureau of Guangdong Power Grid Co., LTD Jiangmen China; E-mail: 7648625@qq.com. The authors would like to thank the anonymous reviewers for their comments on this paper. This research was supported by the science and technology project of China Southern Power Grid Company Limited under Grant No. GDKJXM20198068 (030700KK52190190)

manually. In this process, faced with a large amount of image data, even if it is annotated by professionals with rich experience, its efficiency is very low. For this reason, it has great significance to study an accurate and effective defect recognition technique for common bolt defects.

Traditional power component and defect recognition methods mainly focus on the design of manual features. For example, after image preprocessing with the help of image enhancement and denoising methods, Harr features, moment invariants, color space and other features are combined with support vector machines, level combined with Adaboost and other algorithms to realize the identification of anti-vibration hammers, insulators and other electrical components and corresponding defects [4,5]. In addition to requiring a wealth of professional knowledge support, such methods often only work for a specific category and have poor scalability. Nowadays, deep learning technology has made long-term development, it has been widely employed in all aspects of life. In the meantime, the recognition algorithm based on deep convolutional neural networks has also solved a lot of defect recognition problems and achieved many results [6]. However, its research on the identification of bolt defects is relatively insufficient. The paper [7] uses the traditional object detection algorithm to detect the bolts of the transmission line, by constructing the transmission line inspection image dataset, extracting the HOG features of the bolts, using the SVM classifier to classify, realizes the identification of the bolts in the inspection image, but this method only simple identification of the bolt target is carried out, for the more important bolt defect identification work, further in-depth analysis and research are lacking. In reference to the problem of sample imbalance, the paper [8] introduced auxiliary data and proposed a RetinaNet-based method for identifying missing and loosening bolts of power system, which achieved better performance results, but the types of bolt defects were relatively single.

In view of the problems above, this paper adds an attention module to the ResNet so as to weight different channels more effectively and obtain more key feature channels. At the same time, considering that it is short of training sample of bolt defect dataset which will cause a risk of residual network overfitting. This paper uses a data augment strategy to expand the training dataset, and sets up experiments to discuss the impact of increased data on the accuracy of defects. The results show that adding an appropriate amount of data can notably promote the recognition accuracy of the model.

2. Deep Convolutional Neural Network Model and Attention Mechanism

2.1 Deep Convolutional Neural Network

In the 2012 ILSVRC image classification competition, KRIZHEVSKY et al. proposed AlexNet [9], a classic deep convolutional neural network model. Compared with the shallow convolutional neural network model, AlexNet obtains a significant improvement in performance, and the deep network model has a greater advantage than the shallow network model. The VGG16 [10] network and GoogleNet [11] network constantly refresh the accuracy of the ILSVRC competition. From LeNet [12], AlexNet to VGG16 and GoogleNet, the number of layers of convolutional neural networks is constantly increasing. With the deepening of the number of network layers, the amount of data and the amount of computing are also increasing sharply. The mathematical expression of the convolution module is shown in Equation (1):

$$\begin{cases} y = \text{conv}(x, w) = (y(1), y(2), \dots, y(n - m + 1)) \in R^{n-m+1} \\ y(t) = \sum_{i=1}^m x(t + i - 1)w(i) \end{cases} \quad (1)$$

Among them, x is the input, w is the size of the convolution kernel and $w \in R^{s \times k}$, $x \in R^{n \times m}$, $t=1, 2, \dots, n-m+1$. The outstanding contribution of convolution lies in that it can cut down unnecessary weight connections, introduce sparse or partial links, and the weight sharing strategy brought about greatly reduces the amount of parameters, relatively increases the amount of data, so as to avoid overfitting [13]. What's more, owing to the translation invariance of the convolution, the characteristics learned possess topological robustness and symmetry.

2.2 ResNet Network

As one of the classic models in the field of deep learning, ResNet [14] has surpassed VGG in image classification problems and has become the basic feature extraction network in most visual fields. ResNet introduces the residual element, which makes it not only compress the parameters, but also add a direct channel in the network to further improve the ability of feature learning [15]. Different from the early network, its features such as fewer parameters, deep layers and excellent classification and recognition effects make it still one of the more classic and useful networks so far. The residual module of the network model based on the SE module is shown in Figure 1.

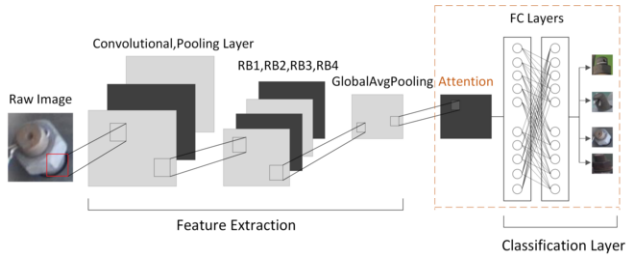


Figure 1 The framework of deep residual network for bolt defect recognition based on attention mechanism

2.3 Attention Mechanism

There are two major kinds of common attention mechanisms, one kind is spatial attention, such as spatial transformer network, the other is channel attention, for instance BAM [16] and SE module (Squeeze-and-Excitation Networks) [17]. In general, the key task of channel attention is to explore discriminative feature. As one of the classic channel attention, SE module is able to transform the response of the channel feature by finding the correlation between different channels [18]. Compared with the traditional neural network, this method cuts down the number of calculation to a great extent. The key purpose of spatial attention is to learn detailed features as much as possible. The STN (spatial transformer network) explicitly allows spatial operations on data and allows data to be processed to enhance the geometric invariance of the model. Besides, it is able to be inserted into any existing convolutional model and only a few modifications are required.

The advantage of attention mechanism is that it is able to distribute different weights to distinct parts of the input so as to help the network obtain as much key information as possible. What is more, it doesn't need additional calculations. Generally speaking, we can divide attention into hard attention and soft attention. Among them, soft attention tends to focus on spaces as well as channels. There are some difference between hard attention and soft attention, for example hard attention focuses more on stochastic prediction and tends to emphasizes the dynamic variations of the model. Consequently, it is hard to apply end-to-end ways to train hard attention and the most commonly used method is reinforcement learning.

In this study, for the sake of obtaining as many discriminant features as possible, we apply the channel attention mechanism. Among them, the SE module is a classic channel attention method. It finds the relationship between channels to freely Adapt to change the channel characteristic response. Compare with the traditional neural network, the core idea of SE module lies in learning the feature weight according to loss through the network, so as to train the model in a way that the weight of effective feature map is large when the weight of ineffective feature map is small, so as to reach better results. Although the process of embedding SE module into some original classification networks inevitably brings a small amount of parameters and computation, it is acceptable.

By means of modeling the interdependencies among the feature channels, SE module is able to ameliorate the representation of the network [19]. Furthermore, Se module can be divided into three parts: squeeze, excitation, and relabeling [20]. First, perform squeeze operation on the feature map calculated by convolution to get the global feature of each channel, then perform extraction operation on the global feature to get the relationship and weight of each channel, and finally use the channel weight to multiply the original image so that the final feature distribution of the feature map is obtained. The schematic diagram of the SE block is shown in Figure 2.

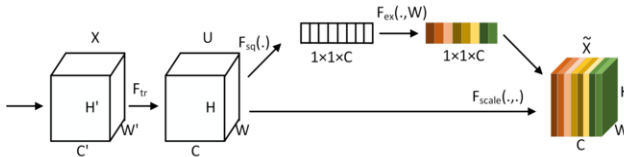


Figure 2 The schematic diagram of the SE block

During squeeze operation, global average pooling is adapted to average all information on a channel to obtain the global features on the channel, which solves the problem of small receptive fields in the CNN network. The calculation method is shown in Equation (2):

$$z_c = F_{sq}(u_c) = \frac{1}{W \times H} \sum_{i=1}^W \sum_{j=1}^H u_c(i, j) \tag{2}$$

Among them, $u_c(i,j)$ represents a pixel in the image, W and H represent the width and height of the image respectively. Moreover, squeeze operation sums all the pixel values and takes the average value.

Excitation operation requires the relationship of information in each channel, which represents as Equation (3). It takes two fully connected bottleneck structure, among them, $W_1 \in R^{\frac{C}{r} \times C}$, $W_2 \in R^{\frac{C}{r} \times C}$, r is a hyperparameter, σ and δ are two activation

functions. After calculation, the image features compressed by Equation (3) can be extracted.

$$s = F_{ex}(z, W) = \sigma(g(z, W)) = \sigma(W_2 \delta(W_1, z)) \quad (3)$$

Finally, use the learned weight parameters to multiply each channel feature calculated by the original convolutional network to calculate the output of SENet, as shown in Equation (4):

$$x_c = F_{scale}(u_c, s) = s_c \cdot u_c \quad (4)$$

Among them, u_c represents the feature image of each channel calculated by the formula and s_c represents the weight of the channel, which is multiplied to obtain the fused image information.

2.4 Application of attention mechanism in the model

The attention mechanism can improve the network's ability to extract regions of interest, and it can also improve the accuracy of network recognition. This paper proposes to add an attention module to the ResNet classic network, and to improve the model parameters, and finally form a network structure suitable for bolt defect recognition task ATT-ResNet50. The core of ResNet50 based on the attention mechanism is the attention layer framed by the dashed line inside the model. The network with the attention module has more powerful feature extraction capabilities. In the meantime, the depth advantage of the ResNet network layer makes the effect more significant [21].

3. Experimental results and analysis

3.1 Dataset

This paper uses the bolt defect dataset to evaluate the proposed model. The bolt defect pictures are all intercepted from samples taken by drone line inspections. After data cleaning and careful data selection, the data set that can be used in this experiment is sorted out. There are four types of data samples, a total of 2000, and the training set and testing set are divided according to the ratio of 7:3. Among them, there are 500 pictures of pin losing, nut losing, nut loosening and rusting respectively. These four kinds of pictures are put respectively in distinct folders and labeled 0-3. The experimental dataset without data augment is shown in Figure 3.



Figure 3 Bolt defect dataset

3.2 Experimental details

The experiment in this paper is implemented using the PyTorch framework, and a single NVIDIA Geforce GTX Titan X GPU is used to train and test the method in this paper. First, build the AlexNet, VGG and ResNet networks, and then load the pre-trained AlexNet, VGG and ResNet50 model weight files, freeze the feature extraction layer, and remove the global average pooling layer and FC layer of the original network. The channel attention module layer is embedded in the model to make the features obtain different weights, and then a new global average pooling layer and FC layer are added to facilitate subsequent model training [22]. Before training, the learning rate is set to 0.001, the dropout rate is set to 0.5. Moreover, we apply SGD [23] algorithm to update the parameters of model.

3.3 Influence and analysis of attention mechanism on experimental results

For the sake of fully validating the performance of the improved model method proposed in this study, the bolt defect dataset is respectively carried out on AlexNet, VGG, ResNet and the above-mentioned network with the attention mechanism to perform identification experiments, and the results are recorded in table 1, which shows the precision comparison between the network models. As we can see from the table, compared to AlexNet and VGG16, ResNet50 is the most effective basic network, and it can achieve a mAP of 82.2% on the bolt defect dataset. After introducing attention mechanism, the recognition effects of these three models have achieved obvious results, and the improvement is the most obvious on the ResNet50 model, not only the mAP is maximized, but the AP of each category is higher, which proves that adding channel attention can effectively ameliorate the recognition effect of the model on the bolt defect dataset.

Table 1 Comparison of bolt defect recognition on different models

models	0	1	2	3	mAP
AlexNet	76.3	76.7	74.4	80.5	77.0
ATT-AlexNet	77.1	76.1	74.8	81.0	77.3
VGG16	78.3	77.9	76.0	81.7	78.5
ATT-VGG16	80.5	79.2	76.7	82.3	79.7
ResNet50	82.6	83.0	78.4	84.8	82.2
ATT-ResNet50	84.4	85.3	80.3	85.5	83.9

Table 2 The relationship between AP and the number of training set

Number of training set	0	1	2	3	mAP
1*1400	84.4	85.3	80.3	85.5	83.9
2*1400	85.6	86.6	81.7	86.5	85.1
3*1400	85.9	87.1	82.3	87.1	85.6
4*1400	86.2	87.3	82.2	87.8	85.9
5*1400	85.4	86.6	81.5	86.4	85.0
6*1400	84.2	85.0	79.8	85.2	83.6

3.4 Quantitative experiments and analysis of data augment

In order to analyze the influence of data augment on the test results, under the original parameter settings, for the ATT-ResNet50 model, different multiples of data samples are added to the original bolt defect dataset for model training, and the same batch of testing set is used to perform model testing. The model is tested and the results

obtained are shown in the table below. From the results in Table 2, it can be seen that after adding different multiples of training data, the model can learn more features during the training process, and there is a significant improvement on mAP from 83.9% to 85.9%. Therefore, when the number of training samples is insufficient to support deep learning defect recognition, the generalization ability of the model can be improved by adding the number of training samples. Furthermore, if the number of training samples reaches four times the original training samples, the mAP reaches the maximum value of 85.9%. However, if the number of training samples is further increased, when the number of training samples reaches five times or more, the mAP will drop sharply.

4. Conclusion and Future Work

Considering that traditional manual identification of common bolt defects on power fittings is consuming with long time as well as labor, and misdetection often occurs, this paper puts forward a bolt defect identification algorithm based on attention model. By improving the traditional deep residual network ResNet50 and adding a channel attention mechanism to obtain key channel features, the effective improvement of defect recognition rate has been realized, which provides a theoretical basis for intelligent defect recognition in the future. In addition, considering that there are fewer samples of bolt defects in reality and the high cost of collection, this paper uses data augment to assist the training of the model, and uses experiments to verify that an appropriate raise of training samples is conducive to improve the generalization ability.

In the future, we would like to expand the current bolt defect data samples and types, and take more effective ways to further improve the model.

References

- [1] Janos Toth, and Adelana Gilpin-Jackson. (2010). Smart view for a smart grid : Unmanned Aerial Vehicles for transmission lines. Applied Robotics for the Power Industry (CARPI), 2010 1st International Conference on IEEE.
- [2] Van Nhan Nguyen, Robert Jenssen, and Davide Roverso. (2018). Automatic autonomous vision-based power line inspection: A review of current status and the potential role of deep learning. International Journal of Electrical Power & Energy Systems 99. JUL. (pp. 107-120).
- [3] Chuang Deng, Shengwei Wang, Zhi Huang and Zhongfu Tan. (2014). Unmanned aerial vehicles for power line inspection: a cooperative way in platforms and communications. Journal of Communications. (pp. 687-692).
- [4] Xian Tao, Dapeng Zhang, Zihao Wang, Xilong Liu, Hongyan Zhang, De Xu. (2018). Detection of power line insulator defects using aerial images analyzed with convolutional neural networks[J]. IEEE Transactions on Systems, Man, and Cybernetics: Systems, 2018, 50(4): 1486-1498.
- [5] Changfu Xu, Bin Bo, Yang Liu, Fengbo Tao. (2018). Detection method of insulator based on single shot multibox detector[C]//Journal of Physics: Conference Series. IOP Publishing, 2018, 1069(1): 012183.
- [6] Xiongwei Wu, Doyen Sahoo and Steven C.H.Hoi. Recent advances in deep learning for object detection[J]. Neurocomputing, 2020, 396: 39-64.
- [7] Min Feng, Wang Luo, Lei Yu, Pei Zhang, Xiaolong Hao, Qiang Fan, Qiwei Peng, Tianbing Zhang and Lingling Cao. (2018). A bolt detection method for pictures captured from an unmanned aerial vehicle in power transmission line inspection[J]. Journal of Electric Power Science and Technology, 2018, 33(4): 135-140.

- [8] Kai Wang, Jian Wang, Gang Liu, Wenqing Zhou and Zhuoyang He. (2019). RetinaNet algorithm based on auxiliary data for intelligent identification on pin defects[J]. *Guangdong Electric Power*, 2019, 32(9): 41-48
- [9] Alex Krizhevsky, I Sutskever and G Hinton. (2012). ImageNet classification with deep convolutional neural networks[C]//NIPS, 2012.
- [10] Karen Simonyan and Andrew Zisserman. (2015). Very deep convolutional networks for large-scale image recognition[J]. *arXiv Preprint*, 2015: arXiv: 1409. 1556.
- [11] Christian Szegedy, Wei Liu, Yangqing Jia and Pierre Sermanet. (2015). Going deeper with convolutions[C]// *Proceedings of the 2015 IEEE Conference on Computer Vision and Pattern Recognition*. Washington, DC: IEEE Computer Society, 2015: 1–8.
- [12] SooBum Kim, JiHoon Lee, SeungYeon You, SungWook Kim and SungChun Kim. (2006). Power-aware Pat Selection Scheme for AOMDV[J]. *Brain Korea21 Project I*, 2006.
- [13] Bin Cheng. (2019). High resolution image classification of urban areas based on convolution neural network[C]//2019 4th International Conference on Mechanical, Control and Computer Engineering (ICMCCE). IEEE, 2019: 417-4174.
- [14] Kaiming He, Xiangyu Zhang, Shaoqing Ren and Jian Sun. (2016). Deep residual learning for image recognition[C]//2016 IEEE Conference on Computer Vision and Pattern Recognition(CVPR), June 27-39, Las Vegas, NV, USA, New York: IEEE, 2016: 770-778
- [15] Xiaoxu Li, Jijie Wu, Dongliang Chang, Weifeng Huang, Zhanyu Ma, Jie Cao. (2019). Mixed Attention Mechanism for Small-Sample Fine-grained Image Classification[C]//2019 Asia-Pacific Signal and Information Processing Association Annual Summit and Conference (APSIPA ASC), 2019: 80-85.
- [16] Jongchan Park, Sanghyun Woo, Joon-Young Lee, In So Kweon. (2018). Bam: Bottleneck attention module[J]. *arXiv preprint arXiv:1807.06514*, 2018.
- [17] Jie Hu, Li Shen, Gang Sun and Samuel Albanie. (2018). Squeeze-and-excitation networks[C]// *Proceedings of the IEEE Conference on Computer Vision and Pattern Recognition*, 2018: 7132-7141.
- [18] Zhen Chen, Maoyong Cao, Peng Ji and Fengying Ma. (2021). Research on Crop Disease Classification Algorithm Based on Mixed Attention Mechanism[C]//*Journal of Physics: Conference Series*. IOP Publishing, 2021, 1961(1): 012048.
- [19] Qiang Chen, Li Liu, Rui Han, Jiaying Qian, Donglian Qi. (2019). Image identification method on high speed railway contact network based on YOLO v3 and SENet[C]//2019 Chinese Control Conference (CCC). IEEE, 2019: 8772-8777.
- [20] Guihui Shi, Jiezhong Huang, Junhua Zhang, Guoqin Tan, Gaoli Sang. (2021). Combined Channel and Spatial Attention for YOLOv5 during Target Detection[C]//2021 IEEE 2nd International Conference on Pattern Recognition and Machine Learning (PRML). IEEE, 2021: 78-85.
- [21] Xianghan Wang, Jie Jiang, Yanming Guo, Yingying Gao, Jun Lei, Lai Kang, Yingmei Wei. (2019). FACPM: Crop Hand Area with Attention[C]//2019 5th International Conference on Big Data and Information Analytics (BigDIA). IEEE, 2019: 139-143.
- [22] Matthew D. Zeiler. (2012). Adadelata: an adaptive learning rate method[J]. *arXiv preprint arXiv:1212.5701*, 2012.
- [23] Bottou L. (2010). Large-scale machine learning with stochastic gradient descent[M]//*Proceedings of COMPSTAT'2010*. Physica-Verlag HD, 2010: 177-186.

Edge Analytics for Bearing Fault Diagnosis Based on Convolution Neural Network

Valentin PERMINOV^a and Vladislav ERMAKOV^a and Dmitry KORZUN^{a,1}

^a *Petrozavodsk State University, Russia*

Abstract. Advanced technologies of Sensorics and Internet of Things (IoT) enable real-time data analytics based on multiple sensors covering the target industrial production system and its manufacturing processes. The rolling bearings fault diagnosis is one of the most urgent problems and can be solved by using convolution neural networks and edge artificial intelligence (edge AI) devices. The limitations of the hardware platform must be taken into account to achieve maximum performance. In this paper, we analyze efficient CNN architecture for bearings fault diagnosis that is able to process data in real-time on edge AI devices. We observe that the accuracy of the proposed CNN is unsatisfactory for practical use, and better accuracy is possible with increasing the number of bearings in the training dataset.

Keywords. Fault diagnosis, convolutional neural network, edge computing, vibration diagnostics, bearing fault diagnosis, edge AI

Introduction

Continuous condition monitoring of industrial equipment enables early detection of malfunctions of machinery and its units, thus increasing the efficiency of staff scheduling, reducing costs, and preventing accidents. In this work, we extend our previous study on applying neural network data analysis to diagnose industrial rotary machinery failures using edge artificial intelligence (edge AI) devices [1]. We focus on the rolling bearings fault diagnosis, as an important practical problem. Up to 40% of rotary machinery failures caused by bearings faults [2]. There are many studies aimed to the problem of bearings fault diagnosis and a number of datasets have been collected for training and evaluating machine learning and deep learning models [3].

In order to increase the autonomy of the monitoring system and reduce the data traffic, it is preferable to analyze the data near the place of its acquisition in accordance with the edge computing paradigm. When building an industrial monitoring system, placing high-performance servers near the monitored equipment is usually difficult due to severe operating conditions, such as a wide range of temperatures, dust, and vibration. In such conditions, it is preferable to use compact, low-power devices.

¹Corresponding Author: Dmitry Korzun, Petrozavodsk State University, Lenin Ave. 33, Petrozavodsk, Republic of Karelia, 185910, Russia; E-mail: dkorzun@cs.karelia.ru.

The balance between the computational complexity of the applied data processing methods and the performance of the used devices should provide real-time analysis, since equipment malfunctions must be detected immediately. Recently, among edge computing devices, the neural network accelerators – edge artificial intelligence (edge AI) devices – have been developed, optimized for intelligent data processing with neural networks usage [4]. At the same time, there has been great progress in the use of neural networks for rolling bearings fault diagnosis [3]. In this paper, we combine these two research directions to assess the practical applicability of existing solutions. Our contribution is the following.

- We propose a CNN architecture that addresses the hardware limitations of the edge AI device and ensures efficient use of hardware resources.
- We evaluate the proposed CNN accuracy in accordance with a protocol close to the conditions of a real industrial monitoring system deployment.
- We evaluate the performance of the proposed CNN on the low-capacity edge AI device and show that can perform real-time sensory data analysis in industrial monitoring tasks.

The rest of the paper is organized as follows. Section 1 considers existing approaches to rotating machinery fault diagnosis and edge neural network computing applications. Section 2 describes our solution to the bearing fault diagnosis using the edge AI device, as well as introduces the dataset and data preprocessing technique. Section 3 shows the results of our experiments. Finally, Section 4 summarizes this study.

1. Related work

1.1. Condition monitoring and bearing fault diagnosis

Bearing defects can be diagnosed using frequency spectral analysis, based on bearings characteristic fault frequencies, which are related to the defect type, bearing geometry and operating mode through a well-defined mechanical model. However, this method requires human expert to make a decision. Machine learning (ML) and deep learning (DL) techniques have been explored to automate bearing diagnostics and enable continuous condition monitoring (CM). The ML includes such methods as artificial neural networks (ANN), principal component analysis (PCA), k-nearest neighbors (k-NN), support vector machines (SVM) and others [2]. These methods perform classification task based on a set of features that describe the original data, such as mean, standard deviation, root mean square, kurtosis, crest factor, etc., calculated from the raw signal, spectrum, envelope spectrum or their intervals. The set of these features is determined by the researcher and affects the accuracy of the resulting method. Therefore, a lot of human effort and proficient domain knowledge are required.

Several DL methods have been developed, such as convolutional neural network (CNN), auto-encoder (AE), deep belief network (DBN), recurrent neural network (RNN), generative adversarial network (GAN). Applying the DL methods to bearing diagnostics has been investigated in [2]. The benefit is end-to-end learning, eliminating the need for manual feature engineering and selection. The CNN shows the state-of-the-art performance in many data classification problems and is therefore of particular interest among researchers involved in solving the problem of bearing diagnostics [3].

The input data of the CNN could be the raw vibration signal, spectrum, spectrogram, envelope spectrum, wavelet scaleogram. The advantage of using a raw vibration signal as input data for a CNN is that there is no need for data preprocessing by other methods, which is especially important when using neural network accelerators, since preprocessing methods may not be supported by such accelerators. Consequently, it becomes necessary to use additional hardware accelerators (for example, FFT), or perform preprocessing on the CPU, which can increase the total processing time, compared to the processing performed entirely on the neural network accelerator. The hardware used can also limit the choice of neural network architectures. In order to enable hardware acceleration for applied in our research hardware, we use 2D CNN (see Section 2).

The use of 2D CNN for raw vibration signal bearing diagnostics has been explored in papers [5,6,7]. Wen et al. [5] apply LeNet consists of four convolution + pooling layers and two fully connected layers to classify bearings fault type by raw vibration signal fitted row-by-row in 64x64 matrix. The obtained model achieves accuracy of 99.79% on Case Western Reserve University (CWRU) dataset. Guo et al. [6] applied a similar approach, differing in that they split the tasks of fault type classification and fault size estimation among separate CNNs. One CNN was used to classify the fault type and other three separate CNNs to estimate the fault size for each type of fault. They demonstrate 97.9% accuracy in fault type classification in tenfold cross validation.

Liu et al. [7] have proposed a dislocated time series convolutional neural network (DTS-CNN), which features the transformation of 1D raw signal into the 2D matrix by row-by-row placing 1D raw signal into the rows of the matrix in such a way that each row shifts relative to the previous one. Wherein the offset step increases with each row. This approach aims to allow CNN to extract periodic fault information between non-adjacent signals. The authors demonstrated up to 6.7% improvement in DTS-CNN accuracy over CNN in the induction motor fault diagnosis task.

Pandhare et al. [8] evaluate the performance of CNN with a 2D input formed from a 1D raw vibration signal. The sizes of the convolution kernels and poolings are one along the first dimension. That is, they cover only one row. Thus, such CNN is equivalent to a 1D CNN that processes a one-dimensional signal by one-dimensional kernels. Cross-validation on Paderborn University dataset was done by splitting the training and test datasets by bearing instances, so CNN performance was evaluated on bearings that were not present in the training dataset. The authors demonstrate that the average accuracy of CNN with raw vibration signal input is superior to other considered alternatives, but does not exceed 61.86%, which is an unsatisfactory result for practical use.

Researches [5,6,7,8] demonstrate that CNN with raw vibration input outperforms machine learning methods based on hand-crafted features. However, in the context of the vibration diagnostics for the edge computing conditions, the mentioned works have the following disadvantages. First, the CNN accuracy evaluation methodology in papers [5,6,7] does not match the actual model performance that would be expected during deployment. The accuracy is evaluated on the same bearings, which was used in training. While when deploying the model to production, CNN will have to determine the condition of the bearing, which was absent in the training dataset. Second, the CNN models proposed in works [5,6,7] do not allow full utilization of hardware acceleration on the edge AI device, since they include an unsupported kernel and pooling sizes.

1.2. Edge neural network computing

The data processing near the place of its acquisition, by the edge computing paradigm, can provide reduced latency and traffic and increased privacy and autonomy. With increased interest in artificial intelligence and its applications, edge AI devices have evolved to accelerate the inference of neural networks.

A comprehensive study of the performance of edge AI devices was carried out in [4]. The authors note that the inference time on neural network accelerators is not directly related to the number of operations, in contrast to the inference on the Central Processing Unit (CPU). It is shown that, in some cases, state-of-the-art lightweight neural networks are computed more slowly than more computationally complex but conformed with the target hardware platform ones. The authors emphasize the need to develop an individual neural network architecture for each accelerator, taking into account the features of the target hardware platform and using such sets of operations, layers, and their parameters that ensure the most efficient utilization of hardware resources.

There are a number of works using edge AI devices for various practical applications, such as face mask detection [9], resilient image compression for IoT cameras [10], mineral granulometric analysis [11], conveyor belt longitudinal rip detection [12]. Most of the work focuses on the problems of image analysis. In this article, we explore the applicability of edge AI devices for analyzing time-domain signals from sensors, specifically, for analyzing vibration signals in order to identify bearing faults.

2. Experimental setup

2.1. Edge neural network computing device

We use the Kendryte K210 system-on-chip as an edge neural network computing device. This system-on-chip has a dual-core CPU, interfaces for connecting sensors and data transmission modules, and a hardware accelerator unit for CNN inference, suiting well for edge AI applications. We simulate the data of vibration sensor by transmitting signal fragments from the dataset via Universal Asynchronous Receiver-Transmitter (UART).

The hardware platform imposes the following restrictions on neural networks used. Only CNN could be hardware accelerated, and its size should not exceed 5 MB. According to the nncase neural network compiler documentation, which is used to deploy CNN to the Kendryte K210, only a sequence of convolution, batch normalization, activation, and pooling operations could be hardware accelerated. The following restrictions are imposed on the parameters of these operations to be accelerated:

- 2D convolution or 2D depthwise convolution;
- kernel size 1x1 or 3x3;
- stride 1 or 2;
- channels number from 1 to 1024;
- input feature map size up to 320x240;
- output feature map size no less than 4x4;
- same symmetric zero padding;
- pooling size 2x2, 4x4, or without pooling;
- pooling type: max or average.

Also, fully connected (dense) layers could be accelerated through conversion to convolution operation. However, such a conversion requires tensor transpose and padding operations that are performed on the CPU and add data transfer operations between the CPU and the hardware accelerator.

We use Kendryte K210 standalone SDK to program Kendryte K210, nncase neural network compiler to deploy CNN to the Kendryte K210 with hardware acceleration and kflash utility for firmware uploading. We measure CNN inference time through the system clock. To profile inference time layer-by-layer we compile firmware with the pre-processor directive `NNCASE_DEBUG` set to 1, which enables the layer execution time to be output to the debug serial port. The CNN inference time measurement and inference profiling were performed separately, using different firmware compilations, since printing the layer execution time to the serial port slows down inference.

Our experiments show the hardware acceleration on Kendryte K210.

- The difference in inference time with kernels 3×3 and 1×1 is less than 5%.
- The layer (as a set of operations convolution+activation+pooling) inference time does not depend on stride, activation function type, pooling size and type.

Considering limitations and features mentioned above, we develop a CNN for rotating machinery fault diagnosis, described in the next section.

2.2. CNN for condition monitoring

In our previous work [1], we used 1D CNN and showed that it was able to run on Kendryte K210. However, the hardware acceleration was not utilized, and all computations were performed on the CPU. Based on this, the measured neural network execution time was approximately 1.66 times larger than the size of the input signal frame. In this paper, we take into account the constraints, which have to be met and solved to enable hardware acceleration (see Section 2.1). Thus, we focus on the 2D CNN.

The input data is the raw vibration signal placed in a 2D tensor (Section 2.3). The convolution of this data with a 2D kernel (for example, 3×3 kernel) could be thought of as a kind of atrous (dilated) 1D convolution. The atrous convolution application to bearing fault diagnosis was studied in [13]. This type of convolution enables filters field of view enlarging without increasing the number of parameters or the amount of computation.

We have chosen the sequence of convolution, batch normalization, activation, and pooling operations as the main building blocks of our CNN and will refer to them as “KPUConv2D” layer. The same denotation is used by nncase neural network compiler in internal representation of computational graph. This choice is justified by the fact that in the used hardware platform, this sequence of operations is an elementary hardware-accelerated operation. The proposed CNN consists of a sequence of KPUConv2D layers followed by a global average pooling layer and a fully connected (dense) layer with a softmax activation function. The detailed description of the architecture of the proposed CNN is shown in Table 3. For all convolutions, we used kernel size of 3×3 and stride 1×1 . These values of kernel size and stride have been selected because they are expected to provide the largest number of degrees of freedom of a neural network while slightly affect the inference time compared with other allowed ones (see Section 2.1). The padding type of convolution was set to “same” to comply with restrictions of used hardware. The Keras with TensorFlow backend is used to implement and train CNN. Deploying CNN on Kendryte K210 was done using the nncase compiler.

Table 1. Categorization of dataset.

<i>Fold No.</i>	<i>Healthy (Class 1)</i>	<i>Outer ring damage (Class 2)</i>	<i>Inner ring damage (Class 3)</i>
1	K001	KA04	KI04
2	K002	KA15	KI14
3	K003	KA16	KI16
4	K004	KA22	KI18
5	K005	KA30	KI21

2.3. Condition monitoring dataset

The Paderborn University Bearing Dataset is used [14] to evaluate the performance of proposed method. The dataset includes 32 bearings, 12 of which have artificial damages and 14 have natural damages caused by accelerated lifetime tests. The rest are the baseline without damages. There are 80 vibration signal fragments for each bearing with duration of 4 s sampled at 64 kHz and acquired in different operating conditions.

We split the dataset into three parts: train, validation, and test datasets. We select different bearings for the test and training datasets based on the fact that when deploying a real monitoring system, bearings are monitored that were not in the training dataset. We evaluate the model in a cross-validation manner, choosing one fold for test and the other four folds for train and validation, as shown in Table 1. The files from train and validation folds were randomly split in the following proportion: 80% as train and 20% as validation dataset. Hence, the validation dataset is similar to the ones that are used in works [7,5] and shows whether the CNN is able to classify the same bearings on which it was trained. The test dataset is the same as in works [8,15] and shows do the CNN can classify new bearings. Thus test dataset shows the applicability of the model in production, where CNN is intended to classify new bearings, which was absent in the training dataset. Further, we will denote a particular combination of train, validation, and test data by the fold number used for the test dataset.

We normalize raw vibration signal from the original dataset to mean and standard deviation. To match 1D raw vibration signal with 2D CNN input, we apply the method suggested in [5]: 1D raw vibration signal is fitted into a 2D array line by line. In production, this transformation would not require any additional operations with data since the raw data from the sensor could accumulate in a memory buffer in the required layout and then be ready to be passed to the 2D CNN input. Since in the Paderborn University Bearing Dataset each file contains a signal fragment with a duration of 4 seconds, but CNN input length is smaller, at each training step, a random frame is selected from a random file from the dataset. At each training epoch, 7680 training, 1920 validation, and 2400 test samples are generated.

3. Results and Discussion

3.1. Rolling bearing fault classification

The neural network was trained for 100 epochs. Each epoch included 7680 training, 1920 validation, and 2400 test unique samples, generated as described in section 2.3. We use

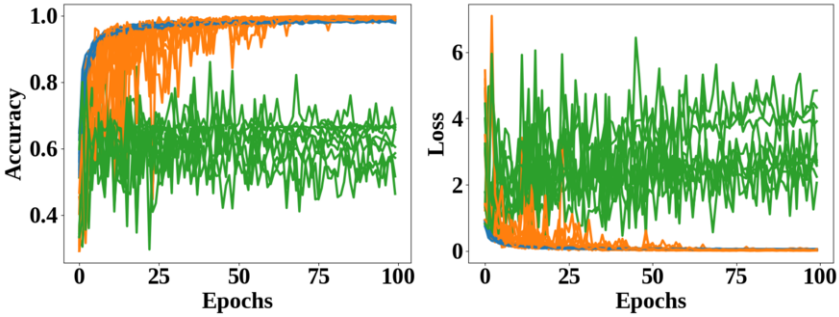


Figure 1. The accuracy (left) and loss (right) curves: training (blue), validation (orange), and test (green).

Adam optimizer with batch size of 32, initial learning rate of 0.001, and exponential learning rate decay after ten epochs with exponent 0.01. The training was performed ten times for each fold to test the stability of the training process. The obtained learning curves of CNN accuracy and loss for fold 1 are shown in Figure 1. The CNN accuracy across all five folds is summarized in Table 2. The accuracy mean and standard deviation were calculated across all trials for each fold and across all folds and trials.

The large fluctuations of accuracy and loss on the validation dataset and even larger on the test dataset are observed. These fluctuations are observed both within an individual training trial and between trials. While the fluctuations on the validation dataset decrease with each epoch as the learning rate decreases and therefore could be caused by the stochastic nature of the training process, the fluctuations on the test dataset are most likely to be related to the characteristics of the test data. The fluctuations on the test dataset within an individual training trial indicate the unrepresentativeness of the test dataset. The fluctuations on the test dataset between trials were caused by random weights initialization at the beginning of each trial and the stochastic nature of the training process. These fluctuations indicate that loss reaches different local minima, and CNN learned to extract different features, which have varying degrees of generalization. This, in turn, indicates the unrepresentativeness of the training dataset.

Table 2 shows that CNN reaches high accuracy on the validation dataset. However, classification accuracy on test dataset is low. Similar results were observed in [8,15], where cross-validation by bearing instance had been used with Paderborn university dataset. The test accuracy drop is most likely due to the unrepresentativeness of the training dataset. The modes of naturally occurring defects would be very diverse. Hence, the training dataset should contain many samples of different damaged bearings to ensure that the CNN can learn to extract the most representative features. The folds 3 and 4 stand out among the others and achieve accuracy of 81.93% and 80.32%, respectively. This indicates that with these combinations of training and test data, the neural network

Table 2. CNN accuracy

Type	Fold 1	Fold 2	Fold 3	Fold 4	Fold 5	Average
Val. mean	99.27	99.31	99.08	98.01	99.67	99.07
Val. std	0.39	0.36	0.36	0.64	0.16	0.38
Test mean	60.70	28.57	81.93	80.32	37.83	57.87
Test std	6.93	5.73	4.64	7.99	4.92	6.04

is able to learn to extract features that describe well those bearings on which the neural network was tested. With an increase in the number of bearings in the training dataset, the accuracy of the CNN will increase and reach a level suitable in practice.

3.2. CNN performance evaluation on edge device

The CNN had been deployed to the Kendryte K210 edge AI device to evaluate its performance. After CNN compilation to KModel format by nncase compiler, the CNN consumes 17 580 bytes of storage and 81 920 bytes of working memory. The measured CNN inference time was 7987 us with a standard deviation of 3 us. Taking into account that the input size of CNN is 128x128 and the sampling frequency of the input signal is 64 kHz, one input sample covers a 256 ms time slice, which is more than 30 times larger than CNN inference time. This enables vibration signal processing and fault diagnosis in real-time with a large margin. However, additional computation resources would be used to acquire the vibration signal, normalize it and handle the result of processing.

Comparing the results with obtained earlier [1], the number of FLOPS increases from 3.3 MFLOPS to 5.6 MFLOPS, while inference time decrease from 212 to 8 ms and the ratio of the incoming data flow intensity to the time of its processing becomes 50 times greater. The performance gain is due to the use of the hardware acceleration of convolution. We profile CNN inference time layer-by-layer (see Table 3). The operation names are taken from the nncase interpreter. The KPUConv2D layer includes a sequence of convolution, batch normalization, activation, and pooling layers.

The KPUConv2D operation is hardware accelerated and therefore consumes less than 10% of the total inference time, despite the fact that it includes more than 99% of the computations. Half of the inference time is spent loading data into the hardware acceleration unit. Unloading data from the hardware acceleration unit also takes additional time, which is included in the last KPUConv2D operation. The quantization and dequantization operations are necessary because the hardware acceleration unit operates with numbers in the uint8 format, while the information at the input and output of the neural network is represented by float32 numbers. These operations take about 30% of the total inference time. The total inference time summed up from the layer-by-layer profile is about 3 ms less than the measured neural network interpreter invocation time. Apparently, this time is spent on auxiliary operations, such as data copying between buffers, DMA and interrupts setting up. This implies that for small neural networks, auxiliary operations take up most of the inference time, and the number of convolution operations does not increase the inference time that much as when executing on the CPU.

The KPUConv2D operation on the hardware accelerator of Kendryte K210 is performed in unsigned integers to increase performance. The quantization of weights and activations can lead to problems with the inference accuracy of the neural network. The test data of one fold were processed on the Kendryte K210 by obtained CNN to assess the accuracy after deployment. Results showed a slight decrease in accuracy of about 1%. However, this degradation of accuracy is negligible compared to misclassification on the test dataset, which is observed even at the stage of training the CNN.

Table 3. CNN architecture and time profiling

<i>Layer</i>	<i>Output Shape</i>	<i>Parameters</i>		<i>Operation</i>	<i>Time, us</i>
Input	(128, 128, 1)			Quantize	1397
				KPUUpload	2598
KPUConv2D	(64, 64, 2)	Filters, Pooling	2, 2x2	KPUConv2D	25
KPUConv2D	(64, 64, 2)	Filters, Pooling	2, –	KPUConv2D	19
KPUConv2D	(64, 64, 2)	Filters, Pooling	2, –	KPUConv2D	18
KPUConv2D	(64, 64, 2)	Filters, Pooling	2, –	KPUConv2D	18
KPUConv2D	(64, 64, 2)	Filters, Pooling	2, –	KPUConv2D	18
KPUConv2D	(32, 32, 4)	Filters, Pooling	4, 2x2	KPUConv2D	21
KPUConv2D	(32, 32, 4)	Filters, Pooling	4, –	KPUConv2D	18
KPUConv2D	(32, 32, 4)	Filters, Pooling	4, –	KPUConv2D	19
KPUConv2D	(32, 32, 4)	Filters, Pooling	4, –	KPUConv2D	18
KPUConv2D	(16, 16, 8)	Filters, Pooling	8, 2x2	KPUConv2D	21
KPUConv2D	(16, 16, 8)	Filters, Pooling	8, –	KPUConv2D	19
KPUConv2D	(16, 16, 8)	Filters, Pooling	8, –	KPUConv2D	20
KPUConv2D	(8, 8, 16)	Filters, Pooling	16, 2x2	KPUConv2D	23
KPUConv2D	(8, 8, 16)	Filters, Pooling	16, –	KPUConv2D	191
Average Pooling Layer	(1, 1, 16)			Dequantize	50
				Reduce	547
Dropout	(16)	Dropout rate	30%		
Dense	(3)	Activation	Softmax	MatMul	14
				Reduce	12
				Binary	17
				Quantize	10
				TableLookup1D	10
				Dequantize	9
				Reduce	11
				Binary	15
				Total	5138

4. Conclusion

This paper considered opportunities of the edge analytics for fault diagnostics in industrial rotary machinery based on CNN methods. We propose a CNN architecture that addresses the hardware features of the edge AI device and ensures efficient use of hardware resources. We show that low-capacity edge AI devices are able to perform real-time CNN-based sensor data analysis in industrial monitoring tasks. We evaluated the proposed CNN accuracy in environment close to real industrial monitoring. Basically, we observed the unsatisfactory accuracy of CNN for practical use. The suggested option for better accuracy is increasing the number of faulty and healthy bearings in the training dataset. Therefore, with the development of Industrial Internet and Big Data larger datasets should be collected for particular machinery equipment.

Acknowledgements

This work is implemented in Petrozavodsk State University (PetrSU) with financial support by the Ministry of Science and Higher Education of Russia within Agreement no. 075-15-2021-1007 on the topic “Software and hardware methods of sensorics and machine perception for robotic systems with autonomous movement”. In part of data computing infrastructure, this study was performed using the Unique Scientific Unit (UNU)—Multicomponent software and hardware system for automated collection, storage, markup of research and clinical biomedical data, their unification and analysis based on Data Center with Artificial Intelligence technologies (UNU for support of medical decision-making) (reg. number: 2075518).

References

- [1] V. Perminov, V. Ermakov, and D. Korzun, “Fault diagnosis for industrial rotary machinery based on edge computing and neural networking,” in *UBICOMM 2020: The Fourteenth International Conference on Mobile Ubiquitous Computing, Systems, Services and Technologies*, 2020, pp. 1–6.
- [2] S. Zhang, S. Zhang, B. Wang, and T. G. Habetler, “Deep learning algorithms for bearing fault diagnostics—a comprehensive review,” *IEEE Access*, vol. 8, pp. 29 857–29 881, 2020.
- [3] J. Jiao, M. Zhao, J. Lin, and K. Liang, “A comprehensive review on convolutional neural network in machine fault diagnosis,” *Neurocomputing*, vol. 417, pp. 36–63, 2020.
- [4] X. Tang, S. Han, L. L. Zhang, T. Cao, and Y. Liu, “To bridge neural network design and real-world performance: A behaviour study for neural networks,” *Proceedings of Machine Learning and Systems*, vol. 3, 2021.
- [5] L. Wen, X. Li, L. Gao, and Y. Zhang, “A new convolutional neural network-based data-driven fault diagnosis method,” *IEEE Transactions on Industrial Electronics*, vol. 65, no. 7, pp. 5990–5998, 2017.
- [6] X. Guo, L. Chen, and C. Shen, “Hierarchical adaptive deep convolution neural network and its application to bearing fault diagnosis,” *Measurement*, vol. 93, pp. 490–502, 2016.
- [7] R. Liu, G. Meng, B. Yang, C. Sun, and X. Chen, “Dislocated time series convolutional neural architecture: An intelligent fault diagnosis approach for electric machine,” *IEEE Transactions on Industrial Informatics*, vol. 13, no. 3, pp. 1310–1320, 2016.
- [8] V. Pandhare, J. Singh, and J. Lee, “Convolutional neural network based rolling-element bearing fault diagnosis for naturally occurring and progressing defects using time-frequency domain features,” in *2019 Prognostics and System Health Management Conference (PHM-Paris)*. IEEE, 2019, pp. 320–326.
- [9] E. Torres-Sánchez, J. Alastruey-Benedé, and E. Torres-Moreno, “Developing an ai iot application with open software on a risc-v soc,” in *2020 XXXV Conference on Design of Circuits and Integrated Systems (DCIS)*. IEEE, 2020, pp. 1–6.
- [10] P. Hu, J. Im, Z. Asgar, and S. Katti, “Starfish: resilient image compression for aiot cameras,” in *Proceedings of the 18th Conference on Embedded Networked Sensor Systems*, 2020, pp. 395–408.
- [11] N. F. d. C. Meira, M. C. Silva, R. A. Oliveira, A. Souza, T. D’Angelo, and C. B. Vieira, “Edge deep learning applied to granulometric analysis on quasi-particles from the hybrid pelletized sinter (hps) process,” in *23rd International Conference on Enterprise Information Systems*, 2021.
- [12] E. Klippel, R. A. R. Oliveira, D. Maslov, A. G. C. Bianchi, S. E. D. Silva, and C. T. B. Garrocho, “Conveyor belt longitudinal rip detection implementation with edge ai,” 2021.
- [13] Y. Chen, G. Peng, C. Xie, W. Zhang, C. Li, and S. Liu, “Acidin: Bridging the gap between artificial and real bearing damages for bearing fault diagnosis,” *Neurocomputing*, vol. 294, pp. 61–71, 2018.
- [14] C. Lessmeier, J. K. Kimotho, D. Zimmer, and W. Sextro, “Condition monitoring of bearing damage in electromechanical drive systems by using motor current signals of electric motors: A benchmark data set for data-driven classification,” in *Proceedings of the European conference of the prognostics and health management society*, 2016, pp. 05–08.
- [15] V. Perminov and D. Korzun, “On applying convolutional neural network to bearing fault detection,” in *Conference of Open Innovations Association, FRUCT*, no. 29. FRUCT Oy, 2021, pp. 475–480.

Modeling of Ship Micro-Grid Based on Wind and Solar Power Generation Technology

Lanyong Zhang^{a,1} and Ziming Yuan^a

^aCollege of Intelligent Science and Engineering, Harbin Engineering University, Harbin 150000, China

Abstract. Under the influence of environmental issues and energy crises, wind and solar power generation technologies have developed rapidly. Compared with terrestrial micro-grid, this technology has relatively few applications on ships. Aiming at the problems of low energy utilization rate of ship micro-grid, imperfect control strategy, and single simulation situation, this paper uses the construction method of terrestrial micro-grid to build a detailed ship micro-grid model based on wind and solar power generation technology on the MATLAB/simulink simulation platform, and uses hill climbing search Method and disturbance observation method to control wind and photovoltaic power generation system. In the simulation process, several situations of wind speed, light intensity, and load sudden changes during the operation of the micro-grid were simulated. The simulation results show that the micro-grid model can track the maximum power point in real time, and the wind energy utilization rate is increased to 0.48, and the bus voltage and current are equal. The actual operation requirements are met, and the correctness and effectiveness of the simulation model and control strategy are verified, which is helpful to the in-depth study of the construction of the ship micro-grid model.

Keywords. Maximum power tracking, ship microgrid, solar power, wind power

1. Introduction

With the continuous development of the marine economy, the number of inland rivers and marine vessels has continued to increase, and the prevention and control of shipping pollution from ships has become a focal issue. The International Maritime Organization (IMO) pointed out in a relevant survey in 2018 that the global carbon emissions from ships accounted for 3.3% of the year. If it cannot be controlled in time, it is expected that its share will increase to 18% in 2050. Therefore, as the main carrier of marine transportation, in order to save fuel costs, reduce fossil energy consumption and carbon emissions, the development and utilization of new energy is of great significance of the development of future ship power[1].

At present, the application of clean energy as wind and solar power generation technology on board the ship by researchers more and more attention. Reference [2] used PSCAD/EMTDC simulation environment to establish simulation models on wind power

¹ Corresponding author, Lanyong Zhang, College of Intelligent Science and Engineering, Harbin Engineering University, Harbin 150000, China; Email: zlyalf@sina.com.

generation, photovoltaic systems, and energy storage systems based on the operating characteristics of the micro-grid, and studies how the micro-grid can be made normal through a control strategy under changes in wind speed and light intensity run. Reference [3] designed a marine micro-grid monitoring system and PLC control program based on wind-solar complementary technology with reference to the terrestrial micro-grid system, which improved the reliability of the ship's micro-grid operation and monitoring. Reference [4] established a single-phase micro-grid system modeled based on the DC bus, using this model and control strategy to simulate the transition state and power flowed direction during micro-grid mode switching, verifying the feasibility and effectiveness of the model. Reference [5] built a machine-side system simulation modeled based on dual closed-loop PI controlled. Through simulation and analysis, it is proved that the dual closed-loop PI control strategy is feasible to achieve maximum power tracking down different wind speeds, and the wind energy utilization rated reaches 0.438. Reference [6] used MATLAB/Simulink software to build a photovoltaic cell model, a simplified fuel cell model, and a diesel generator model and other micro power models for simulation analysis. The model can better simulated the actual operating conditions.

Most of the above-mentioned documents adopt simplified models without realizing maximum power tracking, and the control strategy is not perfect, the energy utilization rate is not high enough, and the simulation situation is relatively simple. Aiming at these problems, first analyze and derive the mathematical model of each power generation unit, and then in the MATLAB / Simulink in detail the establishment of a wind photovoltaic systems and grid-side simulation models, and design appropriate control strategies to achieve maximum power tracking. Constructed a complete simulation model. Based on this, a simulation study was carried out on the situation of wind speed, light intensity and loads changes. The simulation results showed the correctness of the built micro-grid simulation model and the effectiveness of the control strategy.

2. Wind turbine model and control

2.1. Mathematical model of wind power generation

- Mathematical model of wind turbine

Permanent magnet direct-drive wind turbine. The basic principle is to convert wind energy into mechanical rotational energy, the core member is a wind turbine, when the wind blowing blades driven at a constant speed wind turbine rotates, the air moving energy conversion. The mechanical energy for the rotation of the wind wheel drives the permanent magnet generator to emit current. The process of converting wind energy into wind turbine power output is a complex aerodynamic process. The mechanical power captured by wind turbines P_m can be expressed as[7] :

$$P_m = \frac{1}{2} \rho S V_0^3 C_p(\beta, \lambda) \quad (1)$$

Where, ρ is the air density; S is the area of the sweeping wind wheel; V_0 is the input wind speed; $C_p(\beta, \lambda)$ is the wind energy utilization coefficient; λ is the tip speed ratio; β is the blade pitch angle number. In the case of a given wind speed, the wind power captured by the wind turbine mainly depends on the wind energy utilization coefficient $C_p(\beta, \lambda)$. According to the research of Heier et al., the classic C_p calculation formula is:

$$C_p(\beta, \lambda) = 0.5176 \left(\frac{116}{\lambda^*} - 0.4\beta - 5 \right) e^{-\frac{21}{\lambda^*}} + 0.0068\lambda \quad (2)$$

$$\frac{1}{\lambda^*} = \frac{1}{\lambda + 0.08\beta} - \frac{0.035}{\beta^3 + 1}; \quad \lambda = \frac{\omega_T R}{V_0}$$

According to Betz theory, C_p the theoretical maximum value is 0.593, that is, the maximum kinetic energy obtained by the wind wheel in an ideal state accounts for 59.3% of the air kinetic energy on the wind wheel area, and the maximum value of the wind energy utilization coefficient of the actual three-blade wind turbine can reach 0.48 about. According to different β, λ values, the $C_p(\beta, \lambda)$ curve calculated by the formula is shown in Fig.1.

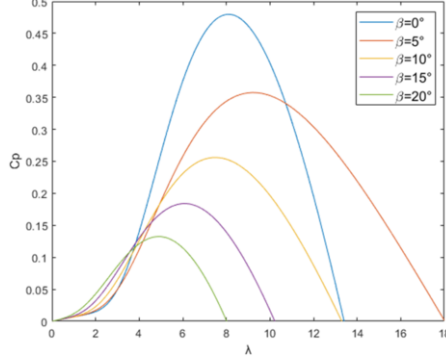


Figure 1. Wind energy utilization curve

- Mathematical model of Permanent Magnet Synchronous Generator(PMSG)

Permanent magnet synchronous generator after coordinate transformation, the time-varying inductance can be eliminated, and a mathematical model of the synchronous generator with clear physical meaning can be obtained.

1) The stator voltage equation is:

$$\begin{cases} u_{sd} = R_s i_{sd} + L_d \dot{i}_{sd} - \omega_r L_q i_{sq} \\ u_{sq} = R_s i_{sq} + L_d \dot{i}_{sq} + \omega_r L_d i_{sd} + \omega_r \Psi_r \end{cases} \quad (3)$$

Where, $u_{sd}, u_{sq}, i_{sd}, i_{sq}, \Psi_r$ respectively the generator stator voltage, current, and rotor permanent magnet flux linkage, R_s is torque; ω_r is the generator rotational speed; L_q and L_d the generator dq-axis inductance.

2) Torque and motion equation are:

$$\begin{cases} T_e = \frac{3}{2} n_p i_{sq} \left((L_q - L_d) i_{sd} + \Psi_r \right) \\ T_e - T_m = \frac{J}{N_p} \frac{d\omega_T}{dt} \end{cases} \quad (4)$$

Where, T_e is the electromagnetic torque; T_m is the mechanical torque; J is the moment of inertia of the generator rotor; N_p is the number of pole pairs; ω_T is the blade speed. The above two sets of equations constitute a complete mathematical model of PMSG.

2.2. Wind power generation control strategy

- Maximum power point tracking control

It can be seen from Fig.1 that when the pitch angle β is fixed, C_p is only related to λ , and there is only one C_p that maximizes λ , which is called the best tip speed ratio λ_{opt} . At this time, the corresponding optimal speed is ω_{opt} , and the corresponding wind energy utilization coefficient is recorded as C_{pmax} . Therefore, ω_T should be changed with the change of wind speed to ensure that the tip speed ratio is always the best tip speed ratio. Therefore, the maximum power tracking control of wind turbines means that under different input wind speeds, by controlling the speed of the wind turbine, C_p is always kept at the maximum value.

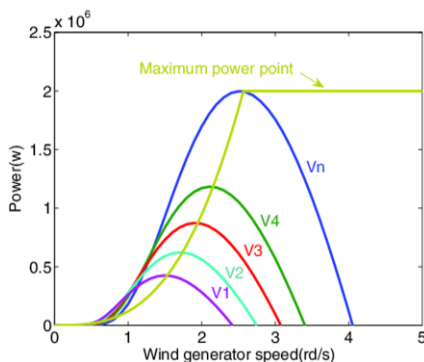


Figure 2. maximum power-optima speed curve

Fig.2 is the curve of the maximum power and the optimal speed of the wind turbine under different wind speeds. Connecting the vertices of the curves in Fig.2 can get an optimal power and speed curve, as shown by the thick green solid line in the figure. Each maximum power point P_{max} on the curve corresponds to an optimal rotation speed ω_{opt} under the current wind speed.

- Principle of MPPT based on hill climbing search method

Compared with the best blade tip speed ratio method and the power signal feedback method, the hill-climbing search method[8] does not require any device for measuring wind speed and does not need to know the exact power characteristics of the wind turbine. The requirements for the power characteristics of wind turbines are relatively low, and the control process is basically realized by software programming; it is independent of the design parameters of the wind turbine and can track the maximum power point autonomously. Impose rotation speed disturbance to cause a change in output power. If the change is greater than zero, when the system becomes stable, continue to add the same sign as the previous disturbance, until the output power change starts to be less than zero before changing the next time The sign of the disturbance. Through the process of gradual optimization, the operating point of the wind turbine will approach the maximum power point. However, the time constant of this method is relatively large, and it takes a long time to realize the maximum power tracking.

3. Photovoltaic power generation system model and control

3.1. Mathematical model of photovoltaic power generation

The equivalent circuit diagram of the photovoltaic cell is shown in Fig.3.

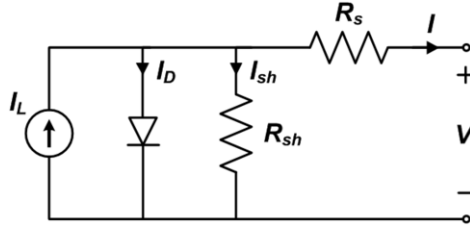


Figure 3. Photovoltaic cell equivalent circuit

The constant current source I_L in the figure can be regarded as a constant current source that generates current in a photovoltaic cell, and in parallel with it is a forward-biased diode. The leakage current through the diode is denoted as I_D , which is called dark current; in practical applications, it can be considered that the parallel resistance $R_{sh} = \infty$; the value of the series equivalent resistance R_s is generally between $7.7 \sim 15.3 \text{ m}\Omega$, which can be ignored in the calculation; the output voltage V is and the output current I is affected by changes in the ambient temperature and photovoltaic intensity Influence, equations[9] (5)~(10) represent the I - V characteristic equation.

$$I = I_{SC} \left(1 - A \left(\frac{U-D}{e^{BU_{oc}} - 1} \right) \right) + C \quad (5)$$

$$A = \left(1 - \frac{I_m}{I_{SC}} \right) e^{-\frac{U_m}{BU_{oc}}} \quad (6)$$

$$B = \frac{\frac{U_m}{U_{oc}} - 1}{\ln\left(1 - \frac{I_m}{I_{SC}}\right)} \quad (7)$$

$$C = \frac{\alpha R}{R_{ref}} E + \left(\frac{R}{R_{ref}} - 1 \right) I_{SC} \quad (8)$$

$$D = -\beta E - R_s C \quad (9)$$

$$E = T_m - T_{ref} \quad (10)$$

Where, α, β respectively the reference radiation current and voltage temperature coefficient; $I_{SC} \approx I_L$ is the short-circuit current; U_{oc} is the open circuit voltage; U is the corresponding photovoltaic array voltage; R_{ref} is the reference radiation intensity, 1 kw/m^2 ; T_{ref} is the reference ambient temperature 25°C ; I_m, U_m is the current and voltage at the corresponding maximum power point.

The output power of the photovoltaic array is:

$$P = IU = \left(I_{SC} \left(1 - A \left(\frac{U-D}{e^{BU_{oc}} - 1} \right) \right) + C \right) U \quad (11)$$

According to formulas (5)~(11), I - U characteristic curve and P - U characteristic curve under any ambient temperature and light radiation can be obtained, as shown in Fig.4 and Fig.5.

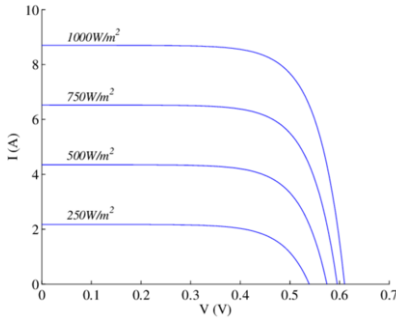


Figure 4. I-V characteristic curve

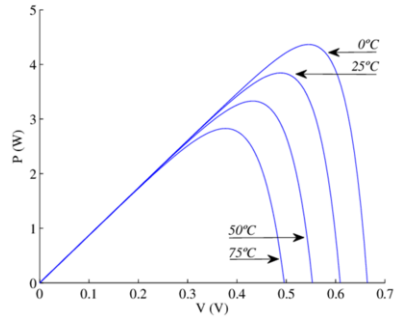


Figure 5. P-V characteristic curve

3.2. Photovoltaic power generation control strategy

It can be seen from the output power curve of the photovoltaic cell in Fig.5 that when the temperature is constant, There is a unique U_m that makes P reach the maximum power point. Therefore, the maximum power output can be controlled by controlling the output voltage U_m of the photovoltaic cell, the principle is to detect the maximum power point of the photovoltaic array under different light intensity and ambient temperature, compare and optimize through the MPPT algorithm, and determine the working voltage corresponding to the maximum power point under this working condition, so that the photovoltaic array is intelligent under different working conditions Maximum output power.

Due to the simple structure of the disturbance observation method[10], there are fewer parameters to be measured, and it is easy to implement in the system, so this paper adopts the disturbance observation method as the photovoltaic array MPPT control strategy. Its algorithm flow chart is shown as in Fig.6

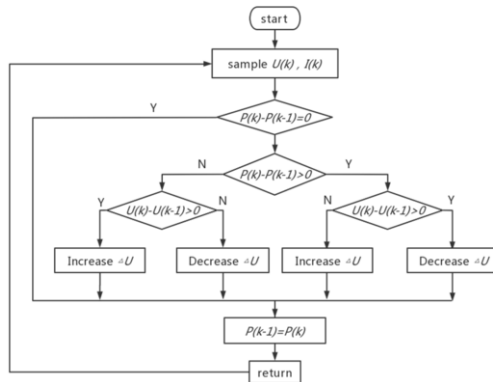


Figure 6. Process of disturbance observation method

The specific method is: First change the output voltage ΔU of a certain amount of photovoltaic cells, and then implement sampling the output voltage $U(k)$ and current $I(k)$ of the photovoltaic cells, calculate the output power $P(k)$ and compare it with the previous output power $P(k - 1)$; if it is less than $P(k - 1)$, it means this time This variable of voltage makes the output power decrease, then the control direction needs to be changed; if it is greater than $P(k - 1)$, the original increase or decrease direction is

maintained, so that the output power can be changed in the direction of increase in the constant repeated disturbance, observation and In comparison, the photovoltaic cell can reach the maximum power point and achieve the maximum power output.

4. Simulation verification

4.1. Partial simulation analysis of wind power generation

As shown in Fig.7, according to the mathematical models and wind turbine control strategies shown, a wind power generation system simulation model based on the hill-climbing search method to achieve maximum power point tracking is built in Simulink. The wind power generation part is composed of wind speed transmission module, PMSG, rectifier and MPPT module. The wind speed drive simulates the input wind speed, realizes the maximum wind machinery power tracking through the MPPT module based on the hill climbing search method, feeds back the speed to the generator, outputs the load torque to drive the generator, and the output power controls the generator DC side rectifier to realize the generator speed control.

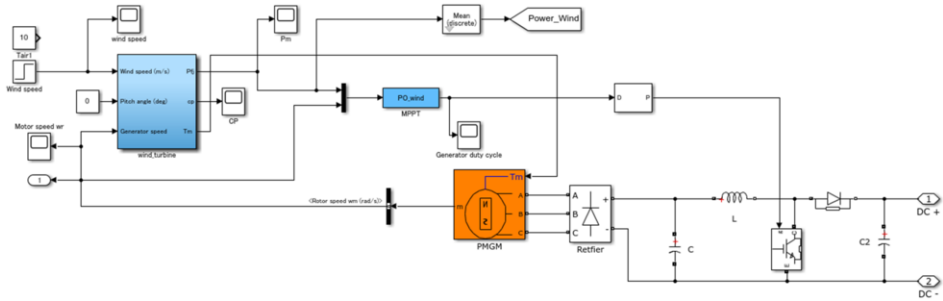


Figure 7. Wind power generation part

In the simulation process, the simulation time is set to 4 seconds, the initial wind speed is set to 8m/s, and the wind speed changes from 8m/s to 12m/s at 1s. Fig.8 shows the simulation results of wind output power. It can be seen from the figure that when the simulated wind turbine is just started, the power will fluctuate in a small range due to unstable wind speed, but it is still within the controllable range. When the wind speed changes suddenly, the output power is quickly changed and the output power is kept stable at 18kW. Fig.9 is a graph of the simulation results of the wind energy utilization coefficient curve. It can be seen that the maximum wind energy utilization coefficient can reach about 0.48, with rapid dynamic response and stable maintenance.

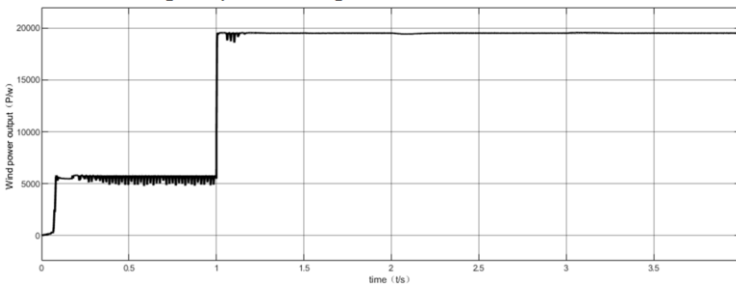


Figure 8. Wind power output

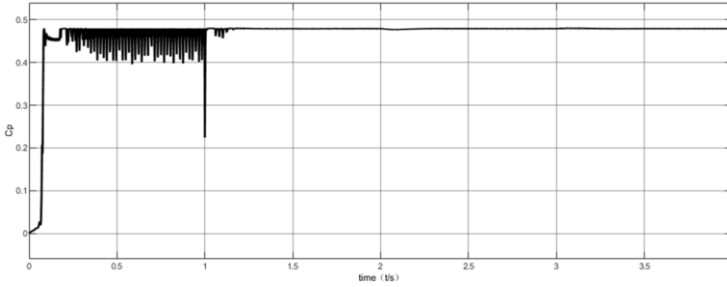


Figure 9. Wind energy utilization coefficient curve

4.2. Partial simulation analysis of photovoltaic power generation

As shown in Fig.10, based on the mathematical model and photovoltaic power generation control strategy shown, a photovoltaic power generation system simulation model based on the disturbance observation method to achieve maximum power point tracking is built. The photovoltaic power generation part mainly consists of photovoltaic cell modules, MPPT modules, voltage stabilizing and filtering circuits. The input variable S is the solar radiation intensity, T is the ambient temperature, and the maximum power is tracked in real time through the MPPT module based on the disturbance observation method.

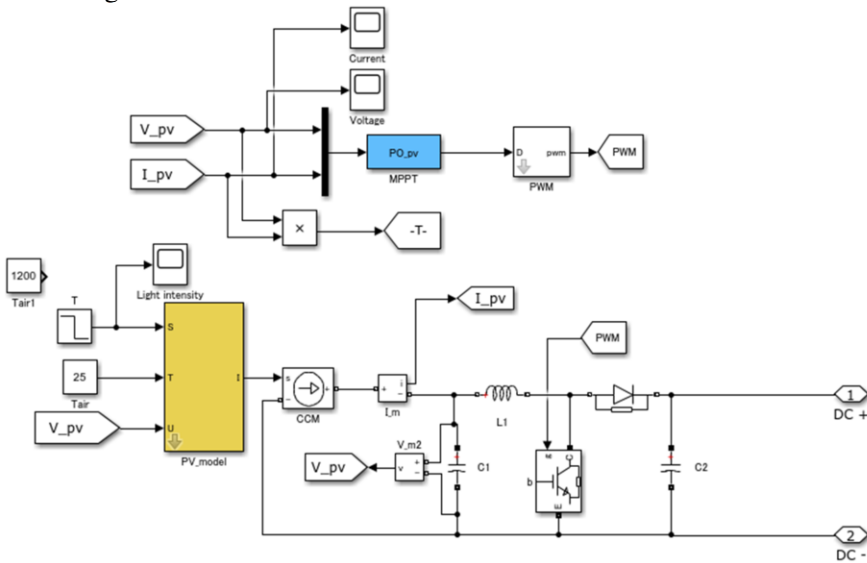


Figure 10. Photovoltaic power generation part

Set the simulation time to 4 seconds, the ambient temperature to 25°C, the initial light radiation intensity is set to 1200W/m², and the sudden change to 1000W/m² at 1.5s. Fig.11 shows the simulation results of the photovoltaic output power. Due to the light radiation intensity The power dropped from 3.76kW to 3kW at 1.5s, and the output power quickly returned to stability.

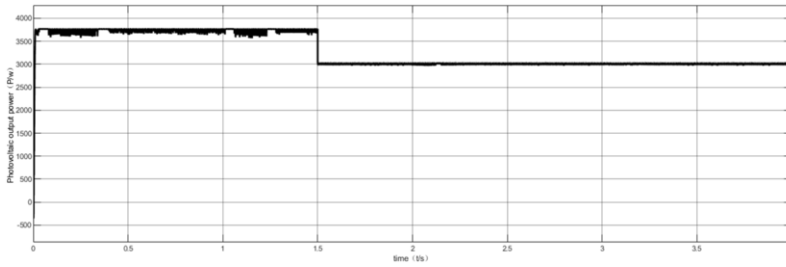


Figure 11. Photovoltaic output power

4.3. Simulation analysis on the grid-connected side

As shown in Fig.12, the grid-connected side simulation model is built, which is composed of inverter modules, power measurement circuits and load cells. The inverter adopts double-loop cascade control with current, which can effectively stabilize the bus voltage and realize the stable operation of the system. The simulation sets the initial load power to 5kW. At 2s, the load power changes from 5kW to 8kW, and then changes back to 5kW at 3s. The bus voltage, current and power fluctuations are detected.

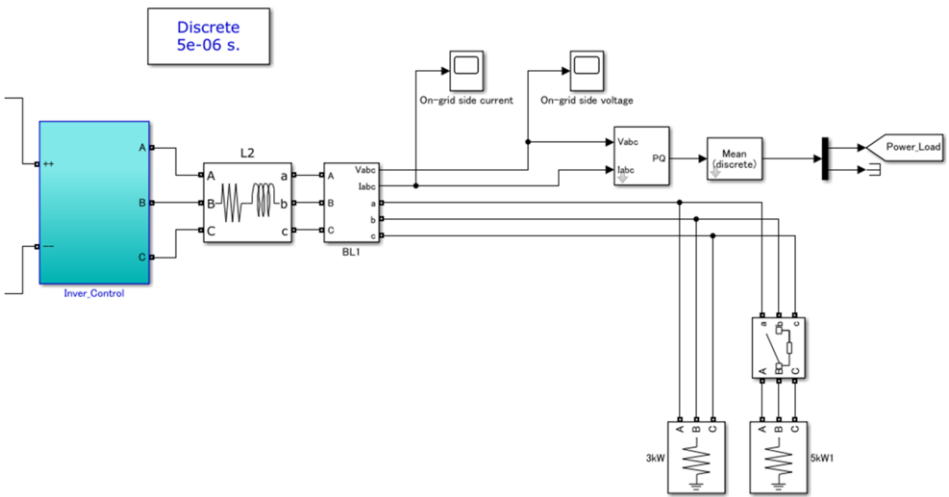


Figure 12. Grid-connected side simulation model.

The simulation result is shown in Fig.13. It can be seen from the figure that the output voltage and current are all standard sinusoidal waveform. At the same time, the line responds quickly, and the voltage and current can quickly return to a stable state. Both can quickly and effectively keep the bus voltage and current stable, and well meet the actual grid connection requirements, and further verify the correctness and effectiveness of the simulation model.

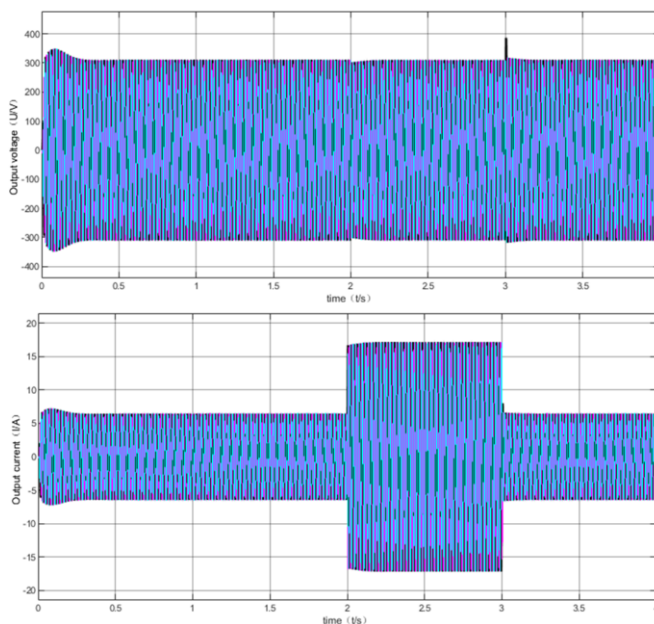


Figure 13. Output voltage and current

5. Conclusion

With the country's deep emphasis on environmental protection and the continuous maturity of micro-grid technology, This paper builds a detailed micro-grid simulation model in MATLAB/Simulink based on the mathematical model of wind turbines and photovoltaic arrays, The wind power and photovoltaic power generation parts of the model adopt the MPPT control strategy of the hill climbing search method and the disturbance observation method respectively, and are verified by simulation, Under the changes of wind speed and light intensity, the maximum power point can be tracked in real time, and the wind energy utilization rate can reach 0.48, and when the load is added and cut off on the grid-connected side, the model can efficiently and quickly restore and maintain the stability of the bus voltage and current, which fully meets the operation of the power grid. It shows that the simulation model built in this paper is correct and the control strategy is effective, There are still some problems and deficiencies in this research, but which has certain reference value for improving and perfecting the modeling and simulation of the new energy ship micro-grid.

References

- [1] Wang Chengshan, "Micro analysis and simulation of grid theory," Beijing: Science Press, 2013, pp.1–62.
- [2] Han Zhou and Ren Yongfeng, "Micro-grid modeling and simulation based on distributed power sources," Computer Simulation, 2014, 31(5), pp. 120–124.
- [3] Yan Juhuai, Tan Yinchao, "Design of ship micro-grid monitoring system based on wind-solar complementary technology," China Water Transport, 2018,18(03), pp.80–82.

- [4] Guo Tianyong, Zhao Gengshen, Zhao Yao, "Modeling and simulation of microgrid system based on wind-solar complementation," *Power System Protection and Control*, 2010, 38(21), pp. 104–108.
- [5] Lin Li, He Yang, Zhou Jianhua, "Modeling and simulation of direct drive permanent magnet synchronous wind turbine side system," *Electric Drive*, 2020, 50(02), pp. 73–76.
- [6] Wang Ling, Li Peiqiang, Li Xinran, "Micro power supply modeling and its application in micro grid simulation," *Journal of Electric Power System and Automation*, 2010, 22(3), pp. 32–38.
- [7] S. Kumari, V. Kushwaha and TN Gupta, "A Maximum Power Point Tracking For a PMSG Based Variable Speed Wind Energy Conversion System," 2018 International Conference on Power Energy, Environment and Intelligent Control(PEEIC), 2018, pp. 789–794.
- [8] Kong Zhendong, Hong Chengcheng, "Grid-connected permanent magnet synchronous wind power generation system and maximum wind energy tracking," *New Industrialization*, 2019, 9(03), pp. 7–12.
- [9] BINAYAK B, SHIVA R P, "Mathematical modeling of hybrid renewable energy system: A review on small hydro-solar-wind power generation," *International Journal of Precision Engineering and Manufacturing-Green Technology*, 2014(1), pp. 157-173.
- [10] Geng Longhai, Li Zhaoxia, Quan Xuezheng, "Photovoltaic cell characteristics and MPPT simulation study of disturbance observation method," *Tibet Technology*, 2020(10), pp. 13-17.

Is the TikTok Hype Real? A Contextual Analysis of the #FordWatchMe Challenge

Markus Rach^{a,1}

^a*University of Applied Sciences and Arts Northwestern Switzerland*

Abstract. The objective of this research project was to spark academic discourse on the need for practitioner-oriented research in big data marketing applications. For this purpose, a specific TikTok Hashtag Challenge, #FordWatchMe, was selected for its over 2.7 billion campaign impressions. Little to no scholarly research was identified to critically appraise the value of TikTok's user engagement and reported campaign metrics, despite TikTok's growing relevancy for marketers. A sequential mixed research method was designed, consisting of interviews, qualitative content reviews and a user engagement experiment to assess the relevancy of the #FordWatchMe campaign for a defined sample. Analyzing over 450 campaign videos resulted in more than 88% campaign unrelated user generated content contributions. The user perception experiment revealed a low probability for both brand recall and content engagement. Findings showcase the need for more scholarly research on the value of superlative impression counts and their implied effect on brand recall, brand perception and purchase intent stimuli.

Keywords. TikTok, Social Media, Marketing, Advertising

1. Introduction

Since early 2020, TikTok established itself as the fastest growing, the most downloaded and the most hyped social media platform on the planet [1]. With over 3 billion downloads, TikTok has catapulted itself to become marketing and advertising mainstream, much supported by the platform's ever-growing business and advertising opportunities [2]. Many showcase campaigns on TikTok, such as the handwash challenge, run by Dettol in 2020, resulted in never heard of marketing reach. In Dettol's case, its paid TikTok Hashtag Challenge generated over 125 billion views [3]. A Hashtag Challenge is one of TikTok's premium advertising products, actively promoting the creation of user generated content, potentially using creative elements such as a campaign soundtrack, a branded effect and of course a challenge for users to creatively answer through their video content. Some other widely featured Hashtag Challenges include Chipotle's #Boorito Hashtag Challenge, or Pringle's #PlayWithPringles.

Despite TikTok's skewed demographic to the younger end [4], brands flock to the platform to capitalize on its still relative affordable reach [5]. Almost every industry, from sports, automotive to medicine, can be found on TikTok, with many engaging in the platform's paid advertising opportunities, or influencer campaigns [6], [7]. Likewise, scholars' interest in TikTok as a marketing and advertising platform has increased [8],

¹ Markus Rach, markus.rach@fnw.ch, Institute of Competitiveness and Communication, University of Applied Sciences and Arts Northwestern Switzerland

[9], [10]. However, very little research questioning the true effectiveness of TikTok, and its impressive reach potential was identified, despite the platform's very restricted access and information sharing information policy. As such, the app raises much ambiguity for marketers and scholars alike. For example, with 2.5 billion app downloads in 2020 [11], how could Dettol's TikTok campaign content have 125 billion views, or the equivalent of 33 views for each of 3.8 billion social media users in 2020 [12]. With less than 700 million reported monthly TikTok users during the campaign's lifetime [3], the above computes to a minimum of 179 views per active TikTok user. Assuming all views are true views, that is in TikTok terms any render of the video on a user's device, how many of these views are qualitative views? Qualitative in terms of target group reach, brand recall and brand favorability? How much of the user generated content, as part the user engagement of a campaign, is truly campaign relevant? These questions are of high relevancy for marketing budget allocations, with regards to optimizing the return on marketing investment. A non-representative survey on LinkedIn with 513 answers, the majority of which came from marketing professionals, revealed a high trust bias towards reported platform metrics. The latter formed the research aim of this paper.

To provide a use case and stimulate further discourse on these questions, the #FordWatchMe Hashtag Challenge, by Ford Germany, has been selected for analysis. The selection was done based on current practitioners' media publications, which this campaign dominated. The campaign had at the time of analysis 2.7 billion views and formed part of a larger product launch by Ford Germany to introduce an all-electric vehicle to the German market. Starting in June, Ford Germany took it to TikTok to run a paid Hashtag Challenge, which got kickstarted with various sponsored influencer postings [13]. At the time of the content analysis, the 23rd July 2021, 455 TikToks were uploaded using the campaign soundtrack, the hashtag #forddeutschland displayed 8.2 million views and the campaign's underlying product, under the hashtag #fordmustangmache, 29.2 million views. Ford Germany did not have an active TikTok account at the time of analysis. The commonality of all clips related to the Hashtag Challenge is the use of the hashtag #FordWatchMe.

2. Research

This research project followed a mixed method research design [14] to instigate exploratory- and explanatory-research into the topic matter, while reducing the potential sequential method bias. Results are likely not representative but meant to stimulate further academic discourse to tighten the academic-practitioners' gap in performance relevant marketing matters. Particularly the wider field of data science is called upon to further investigate marketing decision making relevant metrics in the areas of unstructured data applications, such as short video, audio and other novel social media formats.

2.1. Literature Review

Academic research interest around TikTok amplified since 2017, which is evident through over 15k search findings for TikTok on Google Scholar and almost 5K for TikTok and advertising. A similar search query on ScienceDirect displayed only 82 results. Most research on the topic relates to the impact TikTok holds on digital marketing [5], TikTok's use motivators [15], the impact of TikTok on users [16],

predictors of success of product placement [17], the use of TikTok for politics [18], [19], medical content dissemination [20], its demographic makeup [21], or the TikTok algorithm [22]. No relevant research was identified to critically appraise the value of brands' TikTok engagement, other than optimization product conversion campaigns [17]. No research was identified to question the ambiguity of metrics, or generally unstructured format impacts. A deeper level of research was identified relating to TikTok's Chinese version Douyin [23], [24], which has however little generalization value in the west due to the higher content moderation practice, differing cultural spheres and of course more lenient privacy and data protection laws at work [25], [26]. For this reason, this research project seems highly relevant to stimulate the practitioner-oriented data science community for further research in this area.

A potential rationale for the absence of academic research in the above areas is to be found in TikTok's young age. Academic research requires much time [27], which is evident by the ample of research available for other social media networks, such as Facebook [28].

2.2. Creator Interviews

Pre-dating the campaign analysis, a random selection of 10 campaign contributing TikTok creators were interviewed on their motivation to participate. Creators were randomly selected from the campaign's landing page and contacted through social media. Sponsored content creators were excluded from the preliminary interview round due to their obvious transactional relationship with the brand and campaign.

Out of all interviews, 8 out of 10 participants were unable to explain the Hashtag Challenge's objective. 6 out of 10 participants stated to have participated as a follow up to consumed user generated content. The main stimuli to participate was the campaign's soundtrack. 3 out of 10 participants stated to have participated as a growth hacking attempt to boost views. None of the interview participants' motive of participation was related to either brand liking, brand affiliation, or brand engagement. Further, 4 out of 10 participants were in fact unaware of the Ford brand's sponsorship of the challenge.

It is important to note, that the campaign's creative did not receive further attention in this study. Creative introduces a high subjective bias, which further studies should consider as a moderating variable.

Preliminary interview findings support the need to further research this sample campaign's content relevancy to infer on the quality of generated views.

2.3. Campaign Analysis

Since TikTok does restrict automated third-party analysis of TikTok content and further restricts searchable results, the campaign analysis was conducted using video content found under the campaign soundtrack. Secondly, a random selection of campaign clips, from the Hashtag Challenge's landing page, was analyzed. In total, 301 clips using the campaign soundtrack² and 150 random clips from the campaign landing page³ were selected. The 301 limit marked the maximum number of accessible clips for the campaign soundtrack. The analysis was conducted on pre-defined content criteria, by two independent researchers. Results were combined through an iterative process.

² <https://vm.tiktok.com/ZMRD4NWYp/>

³ <https://vm.tiktok.com/ZMRDXTfXW/>

Out of all clips using the campaign soundtrack, 48% used the branded effect, 2% were sponsored uploads, 5% related to Ford, 10% related to the Hashtag Challenge, 9% had the campaign soundtrack muted or overlaid with other sound and 88% appeared non-campaign related. Out of the 10% uploads relating to the Hashtag Challenge, all but 2 applied the campaign's branded effect.

In all but 19 uploads, both researchers had matching relevancy ratings of uploads. Examples of the category of non-related campaign uploads include clips with a black screen, gaming recordings, advertising of a local fast-food shop, advertising for other businesses, the showcasing of random objects like lamps or bottles, people performing to the soundtrack, unrelated to the challenge, to trend watchers explaining why users should apply the campaign hashtag for a boost in views. The latter is congruent to some of the preliminary interview findings.

Out of the random sample not incorporating the campaign soundtrack, all 150 sampled videos were non campaign related. Some of the sample included dating tips, recordings of famous soccer players, lunchbox preparing instructions, comics and random tv recordings.

Since this sample analysis hints at a low user generated content relevancy to the analyzed campaign, a further user experiment was setup to assess brand recall and relevancy of user generated content to average TikTok users.

2.4. User Experiment, Interviews and Marketing Manager Survey

Following the quantitative campaign analysis, 20 TikTok users were recruited to qualitatively test the impact of branded effects on brand recall and overall perception. Since branded effects provide a visual stimulus, the purpose of these experiments was to assess, whether unrelated user generated content still provokes a positive brand effect. For this test, these 20 users were recruited on pre-defined criteria, such as geographic location, age, TikTok usage. Only users situated in Germany, being above the app's set minimum age of 13 and having an active TikTok account qualified for the experiment. User recruiting was done via an ad-supported network sampling technique on Facebook [29]. Participants were randomly split into two groups. Using videoconferencing systems, each participant was exposed to a total of 15 TikTok videos. 5 TikTok videos were randomly selected clips from the #FordWatchMe campaign. Only clips using the campaign soundtrack were eligible. The other 10 clips were randomly selected TikToks using trending music. These 10 clips were shown to all 20 participants. The 5 #FordWatchMe clips however differed for participants from group A vs. participants from group B. Group A was exposed to campaign clips using the campaign's branded effect, whilst group B was exposed to campaign clips not incorporating the branded effect. Participants were exposed only once to each clip. Following each viewing, participants were asked a standard set of questions about the clip's content, perception, favorability of the perceived content and their likely engagement. Participant interactions were recorded to reduce experiment and interview duration. All recordings were deleted post data analysis, compliant with privacy laws.

Both groups displayed a very similar attitude towards the overall likelihood of content engagement. Across the board this was non-existent for high engagement activities such as video shares, duets, or stitches. The latter are two popular TikTok reaction mechanisms. For low engagement tactics, group B displayed however a much 2 times higher likelihood to engage with the content through likes or comments than group A. Assessing brand recall and brand attitude differed much in weight between both

groups. Group A displayed a 4 times higher brand recall, particularly after seeing the 2nd or 3rd campaign video, as compared to group B. For the latter, brand recall was below 10%, due to the low perception of the Ford brand. Equally, the effect of hashtags on user brand recall behavior proved in this sample experiment very low for both groups. Group A however exhibited a higher sensitivity to the campaign hashtag #FordWatchMe, which participants related to the branded effect group A was exposed to.

Further, a non-representative survey was conducted on LinkedIn with 266 participating B2C marketing managers in Germany. Only 17% questioned a non-qualitative impression metric as sufficient to determine the potential of a platform's paid media options for their brand. The vast majority viewed a high impression number as sufficient to assume a broad reach, justifying potential media investments.

3. Results Discussion

This research project analyzed an accessible sample of the #FordWatchMe campaign on TikTok to estimate ambiguities of marketing practitioners when referring to impression metrics on TikTok for budget allocation decision making.

Whilst the selected campaign has 2.7 billion views, the analyzed sample revealed over 88% of campaign unrelated user generated content. The sample represented 66% of all uploads using the campaign's soundtrack. Campaign relevancy even decreased for a randomly generated, non-representative, sample of 150 clips not using the campaign soundtrack. Whilst the analyzed sample does not infer views, it poises to question the quality of views achieved. A follow up experiment suggested that most sampled users did not actively perceive the sponsoring brand. Visual clues in the form of branded effects provided a noticeable uplift in brand recall, compared to clips not having visual clues.

As existing studies confirmed [30], recall of video advertising is dependent on goal-oriented consumption, which is to a higher degree impacted by product displays, compared to brand displays. This asks for a congruent goal-oriented purpose of branded content.

In summary, the findings of this research project raise various questions. First, on the qualitative side, what is the value of superlative impression metrics on the TikTok platform? How much do impression metrics dilute marketing budget decision making processes in favor of the TikTok platform? Although the views relating to this campaign could not be automatically processed, 88% campaign unrelated user generated content suggests a high ratio of non-qualitative impressions. Nevertheless, the conducted LinkedIn survey findings suggest a high positive bias towards impression metrics.

Second, what are the opportunity costs for marketers initiating non-product related user engagement campaigns with regards to brand recall and quality user engagement. How can these opportunity costs be qualified with regards to marketing return on investment? This study suggested a low brand recall for non-visually supported clips. Thus, marketing managers are advised to increase the use of visual stimuli in paid formats to maximize brand recall effects.

Thirdly, from an operational level, can brands impact the advertising intensity on both product and brand by stimulating a higher level of campaign related user generated content? How, if at all, is the latter perceived by marketing managers sighting competitive campaigns?

4. Conclusion

This research project highlighted two separate issues demanding further research. First, academics and practitioners need to question the ambiguity and quality of impression metrics, particularly on platforms with restricted third-party access. With over 88% of campaign unrelated uploads identified in this project, brand perception and thus potential brand favorability impacts on scale need to be questioned. Particularly practitioners need to demand an impression and engagement quality score to better judge their relevant campaign reach.

Second, in the experiment conducted, visual aids such as the branded effect displayed the highest impact on brand recognition and thus brand recall. It is therefore advisable for practitioners to include visual brand clues in their creations. Due to the current trend to consume much video content without sound [31], visual recall aids are prone to receive an even higher importance in the coming future. The best placement of brand mentions has already been researched on TikTok, however the placement of visual clues to enhance brand recall and favorability demands further scholarly attention.

Finally, this research project evidenced the academic-practitioners' gap [32]. Whilst a lot of research has already been conducted on TikTok, very little focuses on current marketing practitioners' problems.

5. Limitations And Further Research

The following limitations have been noted. First, TikTok's restriction to search and data access did not allow for automated data queries or large-scale analysis of user generated content. Sampling data through a manual analysis of user generated content served as a mitigation measure yet exposing this research project to sampling and self-selection bias.

This research project hopes to spark further interest in the wider research and practitioners' community to expand upon these findings. Besides the quantitative validation of findings, auxiliary research is highly suggested, such as research on predicting factors of impression metrics' quality. It is argued that with the increasing focus on short video and other high impression formats, the stressed thematic becomes even more relevant for marketers.

References

- [1] Rach M. The Influence of Brands and Platform Mechanics on Creator'Content Sovereignty on TikTok. InDigital Marketing & eCommerce Conference 2021 Jun 29 (pp. 35-42). Springer, Cham.
- [2] Ye J. TikTok tops 3 billion downloads worldwide, the first non-Facebook app to do so. South China Morning Post. 2021 Jul 15. Retrieved from <https://www.scmp.com/tech/big-tech/article/3141181/tiktok-tops-3-billion-downloads-worldwide-first-non-facebook-app-do>
- [3] Rach M. #okBoomer: My TikTok experiment and what marketers should know about the platform!. 2020 March. Amazon Self-Publishing.
- [4] Kennedy M. 'If the rise of the TikTok dance and e-girl aesthetic has taught us anything, it's that teenage girls rule the internet right now': TikTok celebrity, girls and the Coronavirus crisis. European Journal of Cultural Studies. 2020 Dec;23(6):1069-76.
- [5] Guarda T, Victor JA, Augusto MF, Mazón LM, Lopes IM, Oliveira P. The impact of tiktok on digital marketing. ICMarkTech 2020. 2021;205:35-44.
- [6] Haenlein M, Anadol E, Farnsworth T, Hugo H, Hunichen J, Welte D. Navigating the New Era of Influencer Marketing: How to be Successful on Instagram, TikTok, & Co. California Management Review. 2020 Nov;63(1):5-25.

- [7] Su Y, Baker BJ, Doyle JP, Yan M. Fan engagement in 15 seconds: Athletes' relationship marketing during a pandemic via TikTok. *International Journal of Sport Communication*. 2020 Aug 27;13(3):436-46.
- [8] Ma R, Kim S. Use, Motivations, and Responses of TikTok as an Advertising Channel. *The Journal of the Korea Contents Association*. 2021;21(2):507-19.
- [9] Hu Y. Research on the commercial value of Tiktok in China. *Academic Journal of Business & Management*. 2020 Nov 6;2(7).
- [10] Ma R, Kim S. Use, Motivations, and Responses of TikTok as an Advertising Channel. *The Journal of the Korea Contents Association*. 2021;21(2):507-19.
- [11] Amore S. TikTok Tops 2.5 Billion in Global Downloads. *THEWRAP*. 2020 Nov 10. Retrieved from <https://www.thewrap.com/tiktok-tops-2-5-billion-in-global-downloads/>
- [12] Hysa B, Karasek A, Zdonek I. Social media usage by different generations as a tool for sustainable tourism marketing in society 5.0 idea. *Sustainability*. 2021 Jan;13(3):1018.
- [13] Bayer C. #FordWatchMe – Ford verlängert Launchkampagne für den Mustang Mach-E mit einer TikTok-Challenge. *MEEDIA*. 2021 Jun 06. Retrieved from <https://meedia.de/2021/06/10/fordwatchme-ford-verlaengert-launchkampagne-fuer-den-mustang-mach-e-mit-einer-tiktok-challenge/>
- [14] Creswell JW. Mixed-method research: Introduction and application. In *Handbook of educational policy 1999* Jan 1 (pp. 455-472). Academic Press.
- [15] Montag C, Yang H, Elhai JD. On the Psychology of TikTok Use: A First Glimpse From Empirical Findings. *Frontiers in Public Health*. 2021 Mar 16;9:62.
- [16] Zhaoying G. The Influence of Short Video Platform on Audience Use and Reflections—Take TikTok as an example. *Academic Journal of Humanities & Social Sciences*. 2021 May 12;4(4).
- [17] Yang J, Zhang J, Zhang Y. INFLUENCER VIDEO ADVERTISING IN TIKTOK. *MIT INITIATIVE ON THE DIGITAL ECONOMY*. 202. Vol. 4
- [18] Gonzalez A, Vandenbosch L. Politics Undercover: Understanding the Role of Social Media and Entertainment Series in Adolescents' Political Socialization. In *International Political Psychology (IPoPsy) working group*, Location: Online 2021.
- [19] Medina Serrano JC, Papakyriakopoulos O, Hegelich S. Dancing to the partisan beat: a first analysis of political communication on TikTok. In *12th ACM conference on web science 2020* Jul 6 (pp. 257-266).
- [20] Zheng DX, Ning AY, Levoska MA, Xiang L, Wong C, Scott JF. Acne and social media: A cross-sectional study of content quality on TikTok. *Pediatric Dermatology*. 2021 Jan;38(1):336-8.
- [21] Kennedy M. 'If the rise of the TikTok dance and e-girl aesthetic has taught us anything, it's that teenage girls rule the internet right now': TikTok celebrity, girls and the Coronavirus crisis. *European Journal of Cultural Studies*. 2020 Dec;23(6):1069-76.
- [22] Klug D, Qin Y, Evans M, Kaufman G. Trick and Please. A Mixed-Method Study On User Assumptions About the TikTok Algorithm. In *13th ACM Web Science Conference 2021* 2021 Jun 21 (pp. 84-92).
- [23] Meng KS, Leung L. Factors influencing TikTok engagement behaviors in China: An examination of gratifications sought, narcissism, and the Big Five personality traits. *Telecommunications Policy*. 2021 Aug 1;45(7):102172.
- [24] Scherr S, Wang K. Explaining the success of social media with gratification niches: Motivations behind daytime, nighttime, and active use of TikTok in China. *Computers in Human Behavior*. 2021 Jun 3;106893.
- [25] Kaye DB, Chen X, Zeng J. The co-evolution of two Chinese mobile short video apps: Parallel platformization of Douyin and TikTok. *Mobile Media & Communication*. 2021 May;9(2):229-53.
- [26] Sun L, Zhang H, Zhang S, Luo J. Content-based analysis of the cultural differences between TikTok and Douyin. In *2020 IEEE International Conference on Big Data (Big Data) 2020* Dec 10 (pp. 4779-4786). IEEE.
- [27] Zhang J, Huang X, Hao J, Crittenden JC. A guide to shortening the time from submission to publication in *Frontiers of environmental science & engineering*. *Frontiers of Environmental Science & Engineering*. 2020 Mar 9;14(2):35.
- [28] Bhattacharyya S, Bose I. S-commerce: Influence of Facebook likes on purchases and recommendations on a linked e-commerce site. *Decision Support Systems*. 2020 Nov 1;138:113383.
- [29] Baltar F, Brunet I. Social research 2.0: virtual snowball sampling method using Facebook. *Internet research*. 2012 Jan 27.
- [30] Zhang X, Yuan SM. An eye tracking analysis for video advertising: Relationship between advertisement elements and effectiveness. *IEEE access*. 2018 Feb 5;6:10699-707.
- [31] Semerádová T, Weinlich P. The (In) Effectiveness of In-Stream Video Ads: Comparison of Facebook and YouTube. In *Research Anthology on Strategies for Using Social Media as a Service and Tool in Business 2021* (pp. 668-687). IGI Global.
- [32] Lawler III EE, Benson GS. The practitioner-academic gap: A view from the middle. *Human Resource Management Review*. 2020 Jun 19:100748.

Design and Implementation of International Trade Virtual Experiment Platform

Meilin Yin¹, Chuting Liang and Ning Luo
Guangdong University of Foreign Studies, China

Abstract. Because of the problems that the current virtual experimental platforms focus on a single situation and small number of compatible users, a virtual experimental platform for international trade is designed. The platform uses desktop virtual reality technology to build the platform, modular to construct it. The platform has improved the international trade course system. Finally, compared with the existing virtual experiment platform, the results show that the designed International Trade Virtual Experiment Platform has more compatible users and faster response speed.

Keywords: Virtual Experiment Platform, international trade, modular, compatibility, stability

1. Introduction

Education currently faces the challenge of adapting to very rapidly changing environments due to technological developments [1]. Virtual Reality (VR) can assist solve this problem. VR can help students understand abstract topics and increase student motivation [2] as well as having a positive impact on the learning outcomes of students' behavior skills training [3]. And VR can enhance self-efficacy and knowledge [4]. However, it has become evident that VR has yet to be implemented in daily teaching routines [5][6]. What's more, it is often hard to customize and integrate into standard educational contexts [6][7]. In recent years, many scholars have also designed virtual experimental platforms for many fields to improve the ability to evaluating physical education[8], help the students learn math [9] and farming culture [10]. What's more, VR improves fire safety awareness[11]. However, there is very little discussion about the virtual experimental platforms of economics and management. They basically focus on imitation of all the internal conditions and processes of enterprises, such as operation, finance, management and so on. This study focuses on the subject of international trade, sets up macro-market economic data and simulates the real environment. It allows students to participate in international trade, and have a better understand the theory they learned.

2. Research Method

VR technologies encompass a range of digital tools that are used to immerse the user in a digitally-generated world. Scientists categorize VR into three types: 1)

¹Corresponding Author: Meilin Yin, Network and Information Center, Experimental Teaching Center, Guangdong University of Foreign Studies, China; Email: 383635698@qq.com; This study was financially supported by the Undergraduate Innovation Training Project of Guangdong University of Foreign Studies in 2021.

non-immersive (desktop): the images are delivered by a screen even if there are 3D images. It is the most common and inexpensive form of VR; 2) semi-immersive (projected): images and effects are projected on a wide big screen, immersion is increased but the level of interaction is affected; and 3) fully Immersive VR: this is the most expensive and the most famous VR [12]. This study uses the desktop virtual reality system to design the virtual experiment platform of international trade. The desktop virtual reality system uses the web technology to realize the online access and operation system. Desktop virtual reality technology takes the display as a tool for external display to show the virtual environment to the visitors. It uses the mouse, keyboard and other output devices for simulation, mainly focusing on giving visitors visual experience and immersive plots. Its cost is low. It is not limited by space and time.

3. Construction of Virtual Experimental Platform Based on Web Technology

The existing virtual experimental platform basically has the phenomenon that too many compatible users will cause the platform to slow down or even crash. In view of this problem, the platform designed in this study will be aimed at solving this situation. In order to improve the number of compatible users, the user framework is designed in this study. Users are divided into administrators, students and teachers, which interact with each other. The administrators manage the platform to ensure the secure operation of the platform. Teachers share resources and use platforms to teach. Students learn through assignments and resources assigned by the teachers.

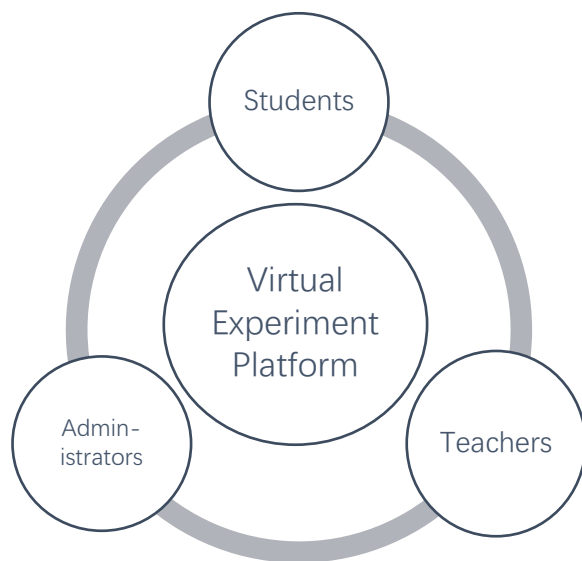


Figure 1. Users' structure chart

From Figure 1. Users' structure chart, the framework and database will be refined, and the platform will be modular. And in the process of user interaction, virtual reality technology is used to enhance the practicality of the platform.

3.1. Platform Framework Design

According to the user structure diagram in Figure 1, the modules are planned in an overall way to build the basic framework of the platform. In order to ensure the rationality of the platform framework, we design the following framework.

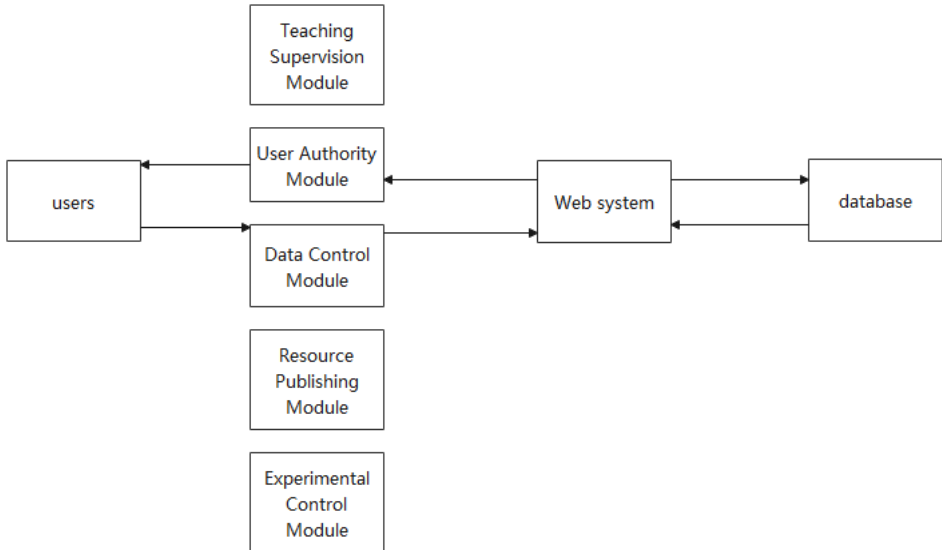


Figure 2. International Trade Virtual Experiment Platform frame diagram

As shown in Figure 2, the framework is divided into four parts: users, module, Web system and database. The users use the system through the module. The module transfers the user usage information to the Web system. The network management system transfers the information to the database. The database feeds the situation back to the Web system. The Web system gives the situation to the user through the module. The modules are divided into user authority module, teaching supervision module, experimental control module, data control module and resource publishing module. The modules affect each other. The modules are all built around the experiment. Students do experiments through the experimental control module. The experimental data is collected by the user authority module and then collated into a report. Report is feedback to the teaching supervision module. Resources released by teachers before the experiment are control by the resource publishing module. Resources data during the experiment is also collected by the data control module. Modules are designed according to the user framework. It can meet users' needs, and to a certain extent to expand the number of compatible users.

3.2. Design of Platform Database

The platform will store the macroeconomic data that has been debugged in advance in the database, and the modified data will also be temporarily stored in the database. Only after the above process can the set situation be simulated. It can be seen that the platform can run normally. It is the key to simulate the situation. In the design of the platform database, this study chooses SQL Server 2013 as the database development software,

and the generated database as the database of the platform. The function of the database is to save, modify the information and maintain the stability of the platform. We must ensure that it conforms to the following principles of database design: the design of the data table is normative; Fewer data tables; Fewer fields in the table.

According to the principles mentioned above, this study sets up corresponding data tables to facilitate unified data management. The data input by the users is planned through the data table, which provides convenience for the subsequent data management.

3.3. Design of Platform modular

Some virtual instrument with an instrument function is encapsulated as a module. Using the modular virtual experimental unit, different experimental objects can be analyzed by the same experimental system. This helps to develop the students' ability to draw inferences from one example. Experimental resources are saved. The International Trade Virtual Experiment Platform is divided into five modules: user authority, teaching supervision, experiment control, data control and resource publishing. The following figure describes the modules and their functions.

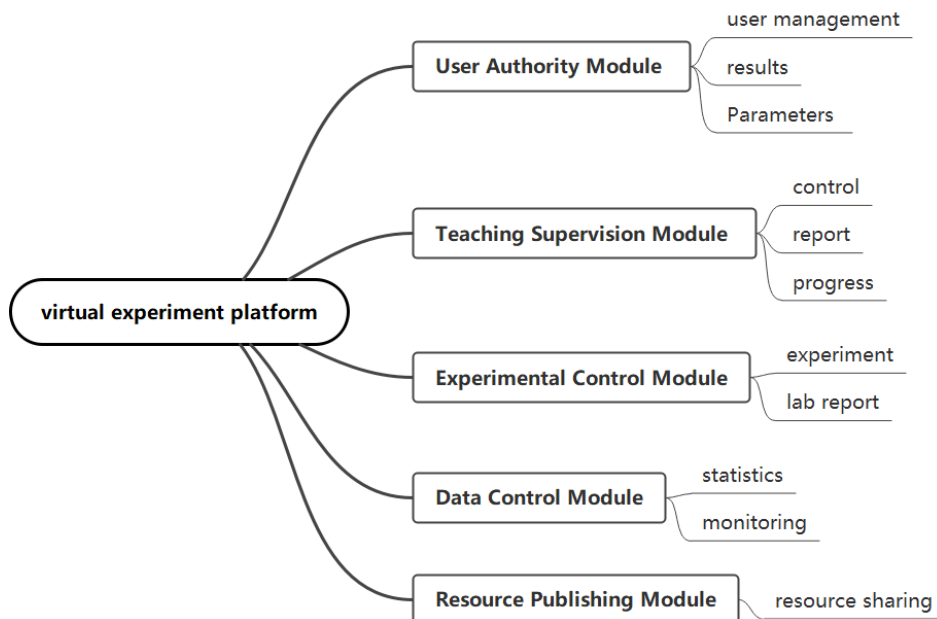


Figure 3. International Trade Virtual Experiment Platform modularization

- **User Authority Module.** Students can join the class through the course code sent by the teachers. The students can also join the virtual experiment platform by introducing the list of information into the system. The teachers can help students better understand the knowledge in the class by publishing the experiment. At the same time, the teachers made the simulated situation closer to reality through parameter restriction. Students' experimental process will also be systematically recorded, organized into a report, and sent to the teachers. Administrators have the highest authority and can create courses.

- Teaching Supervision Module. Teachers can use the system to assist teaching. It is also as a review tool after class. Teachers publish experiments and quizzes in class to understand students' mastery. Students' completion of the quiz will also report back to the teacher. The teachers can better grasp the teaching pace through the error rate and other data. At the same time, students' completion of assignments will also be reflected in the course progress, so that teachers can understand the situation.
- Experimental Control Module. Teachers can add, delete experiments, prolong the experiment time and so on. And the experiment situation will be plotted into a report.
- Data Control Module. The administrators can monitor the operation of the platform through the platform data feedback. And they can use the data to identify problems of the platform.
- Resource Publishing Module. Teachers and students can upload resources to achieve resource sharing.

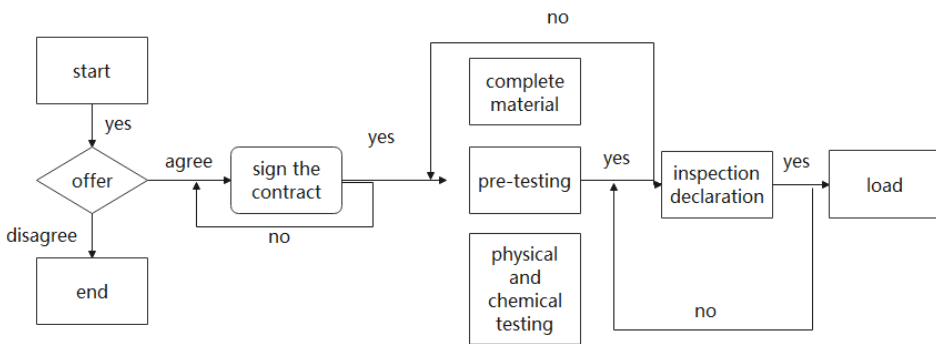


Figure 4. Enterprise export trade interaction diagram

This study takes the enterprise export trade interaction process as an example to illustrate. Users scheme quotation of the production according to the needs of customers. The quotation plan shall be approved by the manager, sales director, etc. and shall be quoted to the customer within the authority. After the customer accepts, the contract is signed and the company begins to produce. Materials are complete before products can be made. After internal pre-testing and finished products through physical and chemical testing, they go to customs broker to check their products. After the inspection, the company can load. After the installation is completed, it can be shipped to the customer.

4. Experimental Results

Modularization solves the problem of poor compatibility of existing virtual experimental platform. It is known that the key to platform stability is the number of users and the number of servers. R is used to represent the platform stability; x is used to represent the remaining user capacity. B is used to represent the number of remaining users, and c is used to represent the number of website servers, then:

$$R = \frac{b}{x} + c \tag{1}$$

Since the remaining user capacity x cannot be obtained directly, the following formula is used to predict the remaining user capacity x, where x₀ represents the initial

user capacity.

$$x = x_0 - \frac{b}{R-c} \tag{2}$$

Administrators can use the preceding formula to monitor the user capacity and avoid system crash. In order to ensure that the International Trade Virtual Experiment Platform is more stable than the virtual experimental platform on the market, this study does an experiment. The stability of the platform is illustrated by comparing the concurrent data of users. The technology used in the test is black box technology, and the key to the test is the number of people they can be compatible with.

4.1. Operating Environment

In this experiment, the first thing is to build an operating environment. The establishment of operating conditions includes server, operating system, database, etc.

4.2. Sample Run

This study takes the number of run-time users as a sample run. Assuming 10 runs, this study sets the maximum and minimum number of users per run in advance. The pre-set sample data is substituted into the virtual experiment platform. The maximum number of compatible users between the two platforms is compared.

4.3. Results Analysis

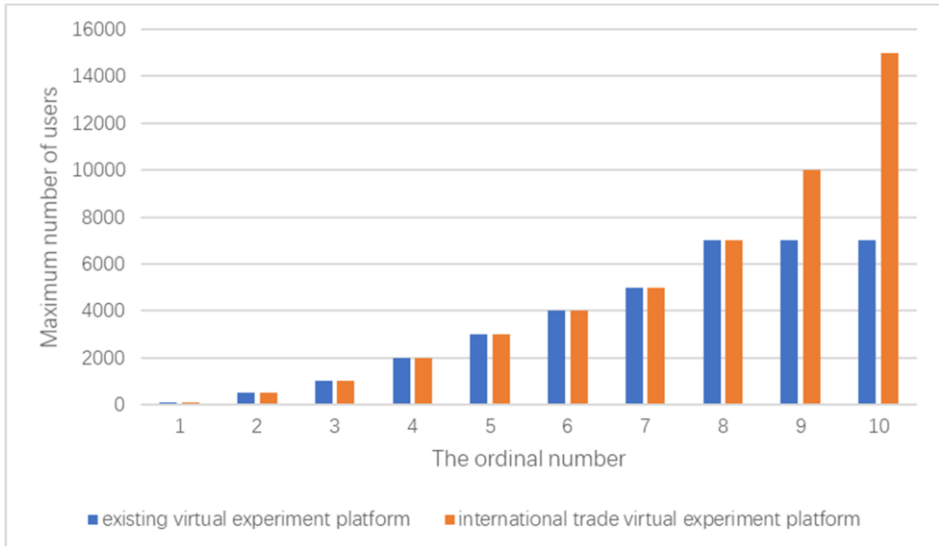


Figure 5. Maximum number of users on two platforms

From the above run, you can see when the number of users is small, both platforms can run smoothly. On the eighth run, the existing virtual experimental platform began to collapse. After the number of users is cleared, the 9th and 10th runs are carried out respectively. The existing virtual experimental platform crashes, but the International

Trade Virtual Experiment Platform can still run smoothly. Therefore, the International Trade Virtual Experiment Platform is relatively stable.

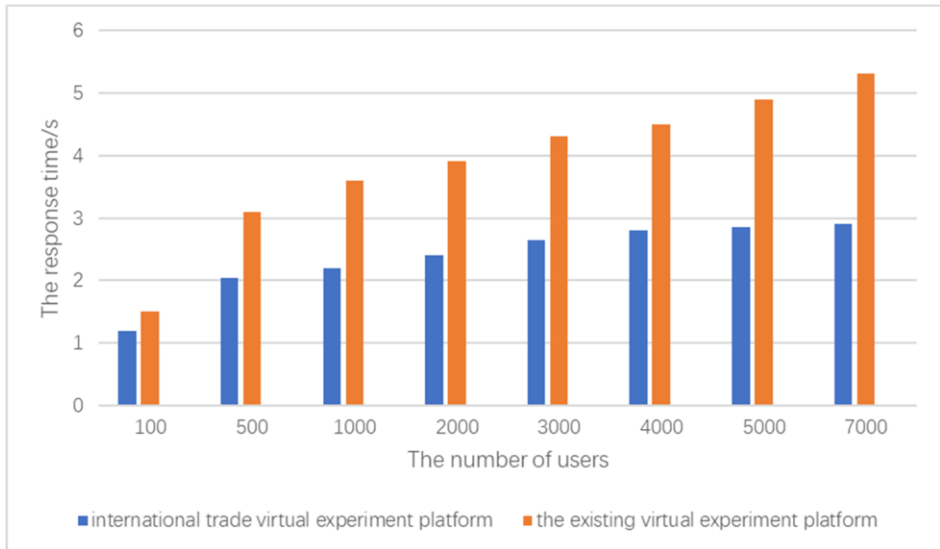


Figure 6. Response time for the same number of users on two platforms

As shown in Figure 6, the response time of the platform designed in this paper is less than 3 seconds under different user numbers. The response time of the existing virtual experimental platform increases as the number of users' increases. Thus, the International Trade Virtual Experiment Platform is more stable.

5. Conclusion

Using the International Trade Virtual Experiment Platform for teaching, students are immersed in the relevant situation. In the process of the experiment, students can choose the role of the government, enterprises and other roles independently. This helps students to experience the behavior decision-making of different subjects. In addition, the experiment can increase the motivation of students to learn and tap their interest and potential. Moreover, compared with the existing virtual experiment platform, the performance of the International Trade Virtual Experiment Platform is better and the running time is more stable.

References

- [1] Sholihin M, Sari R C, Yuniarti N, et al. A new way of teaching business ethics: The evaluation of virtual reality-based learning media. *The International Journal of Management Education*. 2020 Mar; 18(3):100428.
- [2] Makransky G, Lilleholt L. A structural equation modeling investigation of the emotional value of immersive virtual reality in education. *Educational Technology Research and Development*. 2018 May; 66(5):1141-1164.

- [3] Cakiroglu U, Gokoglu S. Development of fire safety behavioral skills via virtual reality. *Computers & Education*.2019 May; 133(5):56-68.
- [4] Ding D, Brinkman W P, Neerinx M A. Simulated thoughts in virtual reality for negotiation training enhance self-efficacy and knowledge. *International Journal of Human-Computer Studies*. 2020; 139:102400.
- [5] Radianti Jaziar, Majchrzak Tim A., Fromm Jennifer, Wohlgenannt Isabell. A systematic review of immersive virtual reality applications for higher education: Design elements, lessons learned, and research agenda. *Computers & Education*.2020;147(C):103778.
- [6] Baceviciute S, Terkildsen T, Makransky G. Remediating Learning from Non-immersive to Immersive Media: Using EEG to Investigate the Effects of Environmental Embeddedness on Reading in Virtual Reality - ScienceDirect. *Computers & Education*. 2021; 164(4):104122.
- [7] Johnston E, Olivas G, Steele P, et al. Exploring Pedagogical Foundations of Existing Virtual Reality Educational Applications: A Content Analysis Study. *Journal of Educational Technology Systems*. 2018; 46(4): 414-439
- [8] J Cheng. Evaluation of Physical Education Teaching Based on Web Embedded System and Virtual Reality. *Microprocessors and Microsystems*. 2021; 83: 103980.
- [9] Buentello-Montoya D.A., Lomeli-Plascencia M.G., Medina-Herrera L.M.. The role of reality enhancing technologies in teaching and learning of mathematics. *Computers and Electrical Engineering*.2021; 94: 107287
- [10] Cheng C, Kang L, Cai S, et al. Virtual Display and Interactive Experience Platform of Farming Culture Based on Unity3D[J]. *IFAC-PapersOnLine*. 2018; 51(17):637-642.
- [11] S Morélot, Garrigou A, Dedieu J, et al. Virtual Reality for Fire Safety Training: Influence of immersion and sense of presence on conceptual and procedural acquisition. *Computers & Education*. 2021, 166(Supplement C):104145.
- [12] Mayne R, Green H. Virtual Reality for Teaching and Learning in Crime Scene Investigation. *Science & Justice*. 2020, 60(5): 466-472.

Personalized Information Recommendation for Chinese Paper Cutting Culture Heritage

Weibo Huang¹, Bairu Xie and Xiaoyue Liao

Guangdong University of Foreign Studies, Guangzhou, China

Abstract. Globalization and information technology are developing rapidly. Chaozhou Chinese paper cutting exists physically. Chaozhou Chinese paper cutting is facing the difficulties of preservation and dissemination. The purpose of this study is to further realize the preservation and personalized recommended dissemination of intangible cultural heritage represented by Chaozhou Chinese paper cutting. In this paper, information technologies such as knowledge graphs, multimedia applications, Bi-RNN neural networks, and probabilistic decomposition models are used. This paper delves into the visual communication and personalized recommendation of intangible culture to preserve, pass on, and spread it better.

Keywords. Chaozhou Chinese paper cutting, Personalized Information Recommendation, Knowledge Graph.

1. Introduction

The trend of economic globalization and world multi-polarization is irreversible, and international competition is a competition of comprehensive national power based on economic strength and scientific and technological strength. In the twenty-first century, to promote Chinese culture and spread Chinese voice, Chaozhou Chinese paper cutting maybe a piece of high ground that cannot be ignored. However, the network platform of Chinese paper cutting mainly displays information about Chinese paper cutting, without a personalized information customization service. How to spread the Chinese paper cutting in Chaozhou vigorously and radiate more and more people is the challenge of Chaozhou Chinese paper cutting heritage.

Yu Fuye and Zhang Xizhong have proposed the importance of establishing a knowledge map and building a database on the inheritance and development of Manchu Chinese paper cutting. In terms of knowledge graph construction, knowledge graphs are built around the domain aspects of various industries, while the knowledge graph construction of Chinese paper cutting information and application services are few and far between. [1]

In terms of personalized recommendation, scholars have mainly divided traditional recommendation algorithms into three main categories. For example, collaborative filtering recommendation algorithms, content-based recommendation algorithms, and hybrid recommendation algorithms are proposed with the shortcomings and defects of the combined recommendation algorithms. Also, personalized recommendation

¹ Corresponding Author: Huang Weibo, Network and Information Center, Experimental Teaching Center, Guangdong University of Foreign Studies, China; Email: hwb444@163.com

systems with multiple sources of big data, and knowledge graphs that fuse contextual information [2]. However, the existing algorithms are not always able to maintain a high accuracy rate due to the dynamic changes of user interests and the long-term instability of user interests and other elements.

This study takes the relationship between information and attributes of Chaozhou paper cuttings as a starting point. This paper composes the relationship between Chaozhou Chinese paper cutting and its attributes. This paper constructs a knowledge graph on this basis and incorporates the knowledge graph into specific algorithms. This paper is constructed in a way to have a better sorting of Chaozhou Chinese paper cutting attributes. This paper is based on the construction of the knowledge graph of Chaozhou Chinese paper cutting and the integration of the personalized recommendation algorithm. This paper will be better and more accurate to make personalized information recommendations for users. [3]

2. Knowledge graph construction

2.1. Definition of Chaozhou Chinese paper cutting attributes

The construction of the knowledge map of Chaozhou Chinese paper cutting starts with defining the attributes of Chaozhou Chinese paper cutting. In other words, the process of defining the attributes of Chaozhou Chinese paper cutting is also the process of extracting and re-understanding the information of Chaozhou Chinese paper cutting.

To identify the attributes of Chaozhou Chinese paper cutting that can be used as entities for the knowledge graph construction of Chaozhou Chinese paper cutting. Knowledge and integration of offline and online information related to Chaozhou Chinese paper cutting are required. By understanding and researching offline and online, it is possible to determine information about the attributes common to Chaozhou paper cutting. Information on the attributes of Chaozhou Chinese paper cutting is Chinese paper cutting types, Chinese paper cutting knives, subject matter, Chinese paper cutting forms, pattern styles, emotional connotations, life uses, and belief customs. [4] By defining the attributes of Chaozhou paper cuttings, entities that can be used for knowledge graph construction are abstracted. These entities will be applied to the subsequent process of knowledge graph construction.

The information from the online platform was analyzed and studied to identify several important attributes of Chaozhou Chinese paper cutting as entities for the knowledge mapping of Chaozhou Chinese paper cutting. The common attributes of Chaozhou Chinese paper cutting information are Chinese paper cutting types, Chinese paper cutting knives, subject matter, Chinese paper cutting forms, pattern styles, emotional connotations, life uses, and belief customs.

2.2. The construction of Chaozhou Chinese paper cutting knowledge graph

To ensure the quality of the Chaozhou Chinese paper cutting knowledge graph, this paper adopts a top-down construction approach. The top-down approach firstly determines the schema layer for the knowledge graph and uses the schema layer for the upper management of the knowledge graph. By upper-level management of the schema layer, valid data and entities can be added to the knowledge base. Furthermore, in the

process of adding data to the knowledge base, invalid data is excluded at the same time. In the process of constructing the knowledge graph, the knowledge graph sick cycle and some characteristics in terms of the Chaozhou Chinese paper cutting domain will also be considered. Because of this, the Chaozhou Chinese paper cutting knowledge graph collusion process is in order of original data acquisition, ontology construction, knowledge extraction, knowledge fusion, and knowledge storage. [5] It is worth mentioning that each step of this construction method develops a suitable scheme according to the actual situation.

3. Chaozhou Chinese paper cutting knowledge graph recommendation algorithm

In recent years, recommendation algorithms, including collaborative filtering algorithms, have suffered from shortcomings in cold-start, overfitting, and data sparsity [6]. These shortcomings lead to inefficient use of data and the inability to effectively match their users' individual needs.

Many researchers use different auxiliary information including Social Networks, the user or item attributes, and Knowledge Graphs to complement the algorithm to improve the recognition of user characteristics. Among them, recommendation algorithms using knowledge graphs are undoubtedly the hot research topic nowadays. The research results of recommendation algorithms for knowledge graphs are also being expanded and applied in industries such as music, film and television, and business. [7] Elena Hernández-Nieves et al. investigate how to use personalized recommendation algorithms (PER) for financial product recommendations. [8] To enhance the information linkage in the recommendation model for the implicit layer, Depeng Dang et al. proposed to use a deep perceptual neural network model (DKN) [9] Wang YueQun et al., on the other hand, tried to use RippleNet and a multi-task recommendation model (MKR) oriented to knowledge graphs. This model enhances the recommendation model's ability to mine user information and interactively combine the knowledge graph with the user's historical data. Thus, this approach improves the performance of the model for movie, music, and book recommendations. [10]

However, the above studies still have certain shortcomings. Subject to the problems of meta-road design and merging of model and auxiliary information, it has some degree of limitation in application scenarios. Moreover, among the existing recommendation algorithms for knowledge graphs, there is a lack of models that can efficiently identify and extract low-level features from user information. To address this situation, this paper proposes the use of collaborative filtering algorithms based on Bi-RNN neural networks to solve the data sparsity problem. In this paper, we improve the cold start problem by measuring the similarity of user features and finally integrate it with the knowledge graph embedding technique (KGE). Thus, this paper makes full use of the contextual relationship between user information and auxiliary information. This approach enhances the mining, identification, and extraction of users' features for the paper-cut recommendation algorithm, and thus improves its recommendation accuracy for the paper-cut algorithm.

3.1 Model design

This model first collects and measures the similarity feature indexes of users, and cross-fuses the knowledge graph feature information with the user information using the knowledge embedding technique.

This model uses a collaborative filtering algorithm based on a Bi-RNN neural network to identify multi-level features in the feature vector of user preferences about Chinese paper cutting mapping and contextual relationships. The model recommends suitable Chinese paper cutting knowledge graphs for different users. The overall framework of the model is shown in Figure 1.

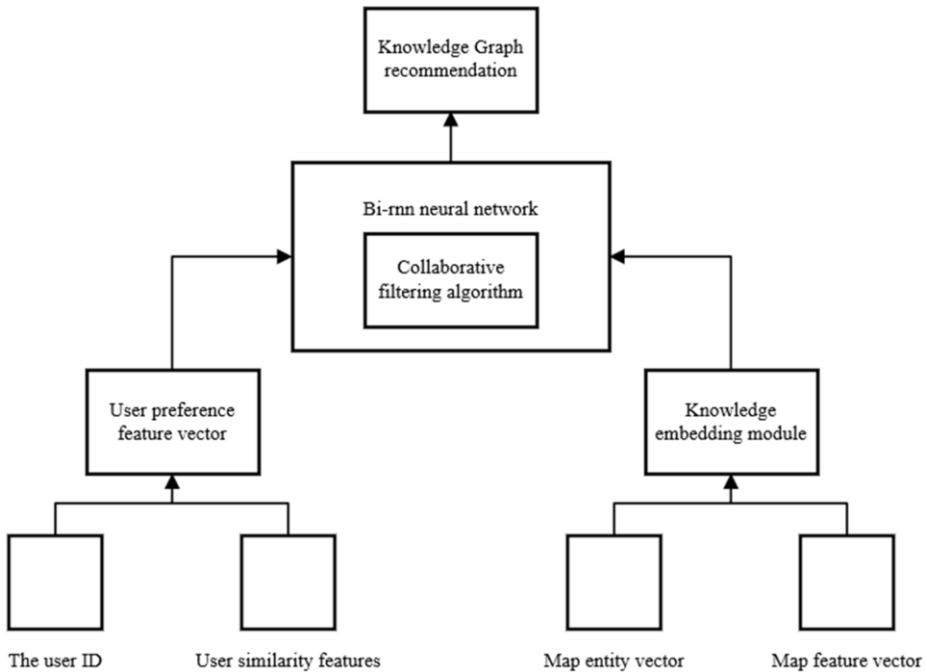


Fig. 1. Recommended model of the paper-cut knowledge graph.

3.1.1 User preference similarity index construction

For users with similar age and educational backgrounds, their preferences for Chinese paper cutting charts are perhaps more similar. Therefore, it makes sense to recommend similar or the same type of clippings to users with similar attribute characteristics. This also improves the cold start problem of the clippings recommendation model very well. For the construction indicators of user attribute characteristics, mainly including age indicators as well as education indicators, the relevant formulas are as follows.

(1) User age similarity measurement

There is a high probability that users of similar age have similar preferences for paper-cut mapping. This model sets the age gap threshold between users to 3. Users with an age gap less than or equal to 3 will be considered as users with the same feature attribute and their similarity is marked as 1. The formula is as follows.

$$SIM(N, U)_{age} = \begin{cases} \frac{3}{|a_N - a_U|}, & |a_N - a_U| > 3 \\ 1, & |a_N - a_U| \leq 3 \end{cases} \quad (1)$$

N, U : User N as well as user U.

a_N, a_U : The ages of user N as well as user U.

$SIM(N, U)_{age}$: The age similarity between user N as well as user U.

(2) Calculation of similarity of users' education

The preferences between users with similar academic qualifications are also likely to be similar, and the similarity for users' academic qualifications is calculated as follows.

$$SIM(N, U)_{Edu} = \begin{cases} 1, & E_N = E_u \\ 0, & E_N \neq E_u \end{cases} \quad (2)$$

N, U : User N as well as User U.

E_N, E_u : User N and the educational status of User U.

$SIM(N, U)_{Edu}$: The similarity of education between user N as well as user U is recorded as 1 if they are the same, and 0 if they are not.

Based on the 2 similarity features mentioned above, the formula used to represent the similarity of the overall user preference features is proposed as follows.

$$SIM(N, U)_{Preference} = \alpha * SIM(N, U)_{age} + \beta * SIM(N, U)_{Edu}, \\ \alpha + \beta = 1 \quad \alpha, \beta \in [0, 1] \quad (3)$$

$SIM(N, U)_{Preference}$: The similarity of the overall preference characteristics of user N as well as user U.

α, β : The weights of different similarity factors.

3.1.2 Chinese paper cutting knowledge graph embedding

The MLP model is used to process the deep-level feature relationship between the entity vector of the paper-cut mapping and the feature vector of the paper-cut mapping. Thus, the deep-level feature representations of the relationship vectors between them can be obtained. Further, the potential feature representations of the data are concatenated to obtain the final paper-cut mapping feature vectors. The formula is as follows.

$$P_T = \Phi_{C \sim E(H)}[M^T(C, P)[P]] \quad (4)$$

$$R_T = S^T(S^{T-1}(\dots S(R))) \quad (5)$$

$$\hat{f} = \sigma(F_{MLP}^Z(P_T, R_T)) \quad (6)$$

$$S^T = \sigma(W_R R + B_R) \quad (7)$$

$$F_{MLP} = \sigma(W_{KGE}(U_T, C_T) + B_{KGE}) \quad (8)$$

P_T : Deep representation of paper-cut mapping entity feature vectors.

M^T : The cross-compression unit of the Lth layer.

$M^T(C, P)$: Paper-cut mapping entity features and deep feature representation of paper-cut mapping obtained by cross-compression cells of T-layer.

R_T : Deep representation of the relation T-vector.

$[P]$: Distinguishing marks for paper cutting entity vectors.

$S(R)$: The network layer in the fully connected state.

F_{MLP}^Z :Z-layer MLP network.

σ : Nonlinear activation function.

W_{KGE}, W_R : Weights.

B_{KGE} : Deviation.

\hat{f} : Prediction vectors for paper-cut mapping.

3.1.3

The user preference feature vector, as well as the mapping feature vector are cross-compressed with the following equation.

(1) For the paper-cut mapping prediction vector as well as the user similarity feature vector, crossover processing is performed.

$$M_Z = \hat{f}_Z S_Z^T = \begin{bmatrix} f_Z^{(1)} S_Z^{(1)} & \dots & f_Z^{(1)} S_Z^{(E)} \\ \vdots & \ddots & \vdots \\ f_Z^{(E)} S_Z^{(1)} & \dots & f_Z^{(E)} S_Z^{(E)} \end{bmatrix} \quad (9)$$

Z : The embedding dimension of the feature vector.

M_Z : The feature matrix obtained by intersecting the user similarity vector and the paper-cut mapping prediction vector.

(2) Compression of the feature vectors after cross-processing.

$$C_{z+1} = M_Z W_Z^{CC} + M_Z^T W_Z^{CP} + B_Z^C = C_Z P_Z^T W_Z^{CC} + P_Z C_Z^T W_Z^{CP} + B_Z^C \quad (10)$$

$$P_{z+1} = M_Z W_Z^{CP} + M_Z^T W_Z^{PP} + B_Z^P = C_Z P_Z^T W_Z^{CP} + P_Z C_Z^T W_Z^{CP} + B_Z^C \quad (11)$$

$$[C_{z+1}, P_{z+1}] = M(C_{z+1}, P_{z+1}) \quad (12)$$

$M(C_{z+1}, P_{z+1})$: The feature vector representation of the paper-cut mapping obtained after cross-compression.

$[C], [P]$: The output of user feature vectors and the output of paper-cut mapping feature vectors.

3.1.4

The cross-compressed processed knowledge mapping feature vectors are fed into the Bi-RNN neural network. Thus, its deep multi-feature representation can be obtained, and the structure of the Bi-RNN neural network is shown in Figure 2.

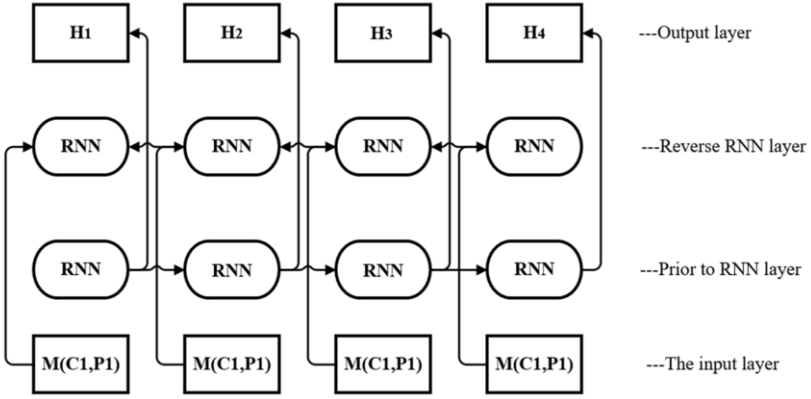


Figure 2. Bi-RNN neural network.

The formula is as follows:

$$\vec{H}_Z = gru(M(C_N, P_N), \vec{H}_{Z-1}) \tag{13}$$

$$\overleftarrow{H}_Z = gru(M(C_N, P_N), \overleftarrow{H}_{Z-1}) \tag{14}$$

$$H_Z = W^T \overleftarrow{H}_Z + W^C \vec{H}_Z \tag{15}$$

$$R = Softmax(W^T M(C_N, P_N)) \tag{16}$$

R: The final value of the weight matrix.

\vec{H}_Z : Forward hidden layer state vector.

\overleftarrow{H}_Z : Backward hidden layer state vector.

W^T, W^C : The weight coefficients of the preceding and following state vectors. And the expressions of users' prediction scores for different knowledge graphs are as follows.

$$\hat{G} = C_N P_N^T = \sum_{a=1}^Z C_{Na} P_{Na} \tag{17}$$

C_N : The number of rows of the matrix where user C is located.

P_N : The number of rows of the matrix where the features P of the map are located.

C_{Na} : The relationship between user C and the ath mapping feature.

P_{Na} : The relationship between the graph feature P and the ath user.

After optimization, the loss function is:

$$Loss = \sum_{(N \in TRAIN)} (G_N - \sum_{a=1}^Z C_{Na} P_{Na} + \theta (||C_N||^2 + ||P_N||^2)) \tag{18}$$

4. Experimental results

The experimental environment is shown in Table 1-1:

Table 1-1. MKFM recommendation algorithm training process.

Category	Parameter
The operating system	10 the 32-bit Windows
The processor	Intel(R) Core(TM) i5-3337U @ 1.80ghz quad Core
GPU	NVIDIA GeForce GT 720M
Memory	6G

4.1 Data set

In this paper, two datasets, the publicly available Chinese paper cutting website 1M and some survey questionnaires 2M made by ourselves, are selected.

The rating file in the dataset includes 3040 users, 22 types of Chaozhou paper cutting, and user rating scores for different paper cutting types. The cumulative number of user ratings in this data set has reached 1327, with ratings ranging from 1 to 5. The higher the rating, the more the user likes paper cutting. The user attributes file contains information about user attributes. For example, age, education, etc. The paper cutting attribute file paper cutting attribute information. For example contains emotions, categories, etc.

4.2 Data pre-processing

The display data in the two obtained datasets 1M, 2M are converted into implicit data. If a user rates a paper cutting, the entry is marked as 1. Then an additional set of unrated paper cutting is matched and marked as 0. The score threshold in dataset 1M is 4. The entry is marked as 1 only when the user rates the paper cutting as 4. This means the user has rated a type of paper cutting positively. The opposite is true for negative ratings. The score and count for all interactions are uniformly marked as 1.

Table 1-2. Data set statistics.

The data set	The number of users	Value of the user feature domain	Number of paper cutting types	Number of interactions	Number of tuples of a knowledge graph
1M	2040	3.1	1,347	754,23	2,873
2M	1000	1	334	34,234	1,231

Building the Knowledge Graph FG database uses Microsoft Satori to build the FG database for each dataset. Further, the names of the paper-cut types are matched with the tail features of the knowledge graph triples. Thereby, the set of IDs in the FG subset is obtained. Then, the IDs of paper-cut types with duplicate matches or missing matches are removed, and the remaining IDs are matched with the head and tail features of the knowledge graph triad. In turn, all the triads with successful matches and good matches are filtered out, as shown in Table 1-2.

4.3 Experimental Results

This algorithm uses both ACC and AUC as the measurement criteria for CTR prediction for 1M as well as 2M. The results are shown in Tables 1-3.

Table 1-3. CTR prediction tasks on the data set.

Model	1M		2M	
	AUC	ACC	AUC	ACC
Bi-RNN	0.834	0.656	0.810	0.687
PER	0.801	0.648	0.802	0.657
CKE	0.768	0.637	0.789	0.643
DKN	0.754	0.571	0.764	0.632

4.4 Analysis of experimental results

The results of the experiments show that the AUC, as well as AAU metrics of this model are higher than the rest of the models, both on 1M and 2M. Even in the case of sparse data, the model can perform the recommendation of a Chinese paper cutting knowledge graph with high accuracy.

5. Conclusion

The art of Chinese paper cutting in Chaozhou is unique in its expression and has certain artistic value. Chaozhou Chinese paper cutting has been included in the list of China's non-material cultural heritage. There is a certain necessity to establish a knowledge graph and personalized recommendation for Chaozhou Chinese paper cutting to realize its modernized communication. In this paper, information technologies such as knowledge graph, multimedia application, Bi-RNN neural network, and collaborative filtering model are used. This paper delves into the visual communication and personalized recommendation of intangible culture to preserve and transmit it better. In addition, the research contents and methods of this project are well-grounded in theory. The project is innovative and highly experimental, with high feasibility of the scheme and a certain prior research foundation. The research of this paper will provide scientific and intellectual support for Chaozhou Chinese paper cutting and the preservation and dissemination of intangible cultural heritage.

Acknowledgement

This study was financially supported by the Undergraduate Innovation Training Project of Guangdong University of Foreign Studies in 2021.

References

- [1] Hussein E., Daoud S. and Alrabaiah H. et al. Exploring Undergraduate Students' Attitudes towards Online Learning during COVID-19: A Case from the UAE. *Children and Youth Services Review*, 2020, 119: 105699.

- [2] Chen Wenyan, Wang Xin, Fu Xueqing, Li Renjie and Zhang Junhai. Multidimensional visualization method of regional intangible cultural heritage landscape. *Science of surveying and mapping*, 2013, 38(01): 87-89+95.
- [3] Depeng Dang, Chuangxia Chen, Haochen Li, Rongen Yan, Zixian Guo and Xingjian Wang. Deep knowledge-aware framework for web service recommendation. *The Journal of Supercomputing*, 2021, May 11 published online. DOI:10.1007/s11227-021-03832-2.
- [4] Elena Hernández-Nieves, Guillermo Hernández, Ana-Belén Gil-González, Sara Rodríguez-González and Juan M. Corchado. Fog computing architecture for personalized recommendation of banking products. *Expert Systems with Applications*, 2019, 140: 112900.
- [5] Jiang Xinjing, Qi Xiaogang and Liu Lifang. *Journal of Intelligent Systems*, 2018, 13 (02):189-195.
- [6] Scatter tiger. Without suitable soil, local art will eventually decline -- shaanxi paper cutting Inheritance dilemma. *Art Observation*, 2014(10):21-22.
- [7] Rendle S. Factorization Machines, The 10th IEEE International Conference on Data Mining, Sydney, Australia, 14-17 December, 2010, IEEE, 995–1000.
- [8] Wang Q., Mao Z. and Wang B et al. Knowledge graph embedding: a survey of approaches and applications. *IEEE Transactions on Knowledge and Data Engineering*, 2017, 29(12): 2724-2743.
- [9] Wang YueQun, Dong LiYan, Li YongLi and Zhang Hao. Multitask feature learning approach for knowledge graph enhanced recommendations with RippleNet. *PLOS ONE, Public Library of Science*, 2021, 16(5): 1-21.
- [10] Yang Yuji, Xu Bin and Hu Jiawei et al., An efficient method for constructing domain knowledge graph, *Journal of Software*, 2018, 29(10): 2931-2947.

Multi-Granularity and Internal-External Correlation Residual Model for Chinese Sentence Semantic Matching

Lan Zhang and Hongmei Chen¹

*School of Information Science and Engineering, Yunnan University
Kunming 650091, China*

Abstract. Sentence semantic matching (SSM) is central to many natural language processing tasks. This is especially the case for Chinese sentence semantic matching due to the complexity of the semantics, missing semantics and semantic confusion are more likely to occur. Existing methods have used enhanced text representations and multiple matching strategies to address these problems but there is still great potential to capture deep semantic information for Chinese text. This paper proposes a Multi-Granularity and Internal-External correlation Residual model (MGIER) to better capture the deep semantic information and to alleviate the missing semantics effectively. First, the MGIER model utilizes character/word granularity to capture fine-grained information. Then, soft alignment attention is employed to enhance the correlation between characters/words in a sentence, called internal correlation, and the correlation between sentences, called external correlation. In particular, this method uses residual connections to preserve more semantic information from the bottom embedding layer to the top prediction layer. Experimental results show that the proposed method achieves state-of-the-art performance for Chinese SSM, and, compared with pre-trained models, the method also achieves better performance with fewer parameters.

Keywords. Chinese text matching, sentence semantic matching, multi-granularity, residual encoding, soft alignment attention, BiLSTM

1. Introduction

Sentence semantic matching (SSM), which is used to identify whether or not two sentences have the same meaning, is widely used in various applications, such as intelligent customer service, information retrieval, and plagiarism detection.

Due to the complexity of the semantics in the Chinese language, missing semantics and semantic confusion are more likely to occur. With the development of deep learning, such as the attention mechanism [1, 2] and Siamese networks [3], it is possible to capture deep semantic information of sentences. In English SSM tasks, [4, 5] lead the way in using multi-granularity to extract fine-grained information. Although the character-granularity is beneficial to enrich English text representation, one single English character does not express meaning. However, a Chinese character is able to represent a definite meaning, which can convey more semantic information. Thus, [6-8]

¹ Corresponding Author, Hongmei Chen, School of Information Science and Engineering, Yunnan University, Kunming 650091, China; Email: hmchen@ynu.edu.cn

utilize character/word granularity to capture semantic information from Chinese text and achieve remarkable performance. In order to capture more semantic information, [2] employs the residual connections to preserve information. [9] preserves semantic information from the bottom layer to the topmost layer. Although existing methods capture deep semantic information from different perspectives, they cannot completely overcome the missing semantics problem.

Motivated by existing methods, we propose a Chinese SSM model, named the Multi-Granularity and Internal-External correlation Residual model (MGIER). We not only alleviate the problem of missing semantics in the encoding process, but also in the information propagation process. Moreover, we capture more sentence correlation information based on multi-granularity. For comparison, we list the core components of related methods in Table 1.

Table 1. Core components of related methods.

Method	Multi-Granularity	Siamese	Residual Connection	Internal correlation	External correlation	From bottom to top	Multi-Residual
MGIER	√	√	√	√	√	√	√
ICE [8]	√	√	×	×	√	×	×
MGF [7]	√	√	×	×	×	×	×
DRCN [9]	×	√	×	×	√	√	×
ESIM [1]	×	√	×	×	√	×	×

In Table 1, the term “Siamese” refers to encoding information by the same network, which is detailed in section 2. “From bottom to top” refers to preserving information in every layer of the models. “Multi-Residual” refers to using residual connections in multiple layers of models.

In summary, we mainly make the following contributions in this work:

- We capture the semantic information of Chinese sentences from the bottom embedding layer to the top prediction layer by using the residual connections.
- We utilize character/word granularity to capture fine-grained information of sentences, and employ soft alignment attention to enhance the internal correlation and the external correlation.

2. Related Work

Earlier SSM methods mainly focused on text representation [3, 10-12]. These obtained the vector representation for two sentences separately at first, and then employed distance measures to compute the semantic similarity of the two sentences. Among them, the Siamese network is still used today because the feature of sharing parameters makes the model smaller and easier to train. A key issue for such models is that there is no explicit interaction between the two sentences.

To enhance interaction of sentences, some methods incorporate attention mechanism into the SSM task [1, 13]. ESIM [1] employs soft alignment attention to enhance the correlation between two sentences. Inspired by ESIM, some methods introduce many complex matching strategies to enhance the correlation between two sentences [2, 5, 13-14]. For these methods, missing semantics is still a difficult issue. To address this problem, researchers discovered that the granularity of text is also crucial for capturing semantic information [4-8], especially for Chinese SSM. In

particular, the MGF model [7] integrates character/word granularity and achieves remarkable results. However, this work does not consider the correlation of sentences. Thus, ICE [8] employs soft alignment attention to extract correlation information, but only considering the internal correlation of sentences is far from adequate. Some methods use residual connections [2] and dense connections [9] to capture semantic information for SSM. However, they do not incorporate multi-granularity and capture sufficient correlation information.

Recently, pre-trained language models (PTMs) have achieved great success in various natural language processing tasks, due to their capacity to capture deep contextualized information [15-19]. Although BERT [15] and NEZHA [17] achieve remarkable results for Chinese SSM, they need to be trained on high-quality datasets and their migration ability is also very limited.

Different from existing methods, we propose the MGIER model to capture more and deeper semantic information. With less computational cost, our method achieves better performance compared with the state-of-the-art methods.

3. MGIER Model

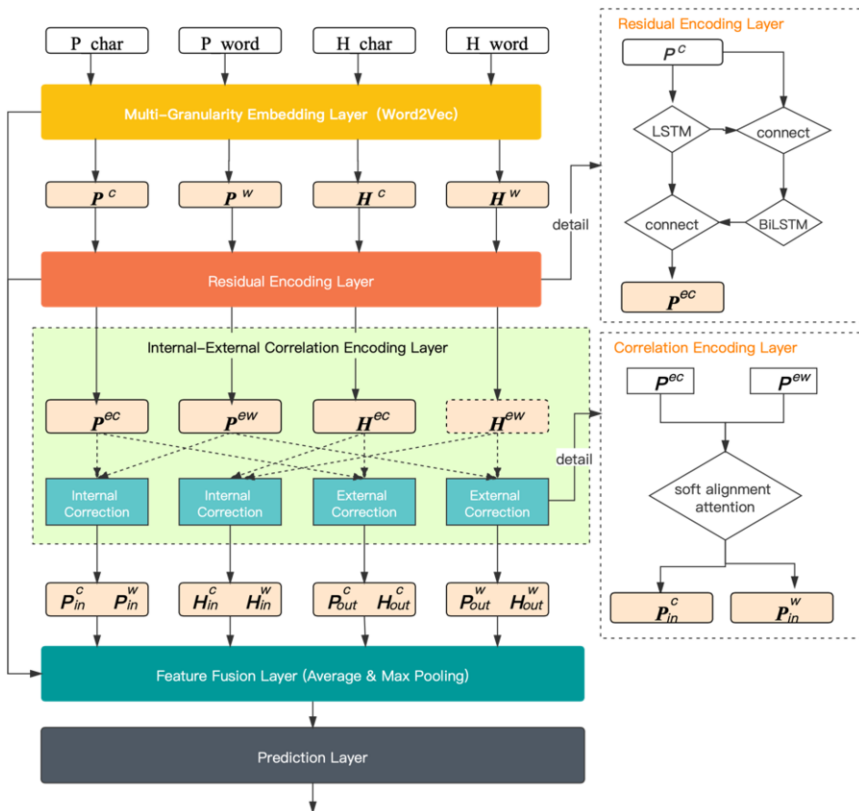


Figure 1. Architecture of the Multi-Granularity and Internal-External correlation Residual Model.

In this section, we introduce the proposed Multi-Granularity and Internal-External correlation Residual model (MGIER) for Chinese SSM.

Given two sentences P and H, we respectively segment P and H to character sequences P_char and H_char, and word sequences P_word and H_word. Then, the MGIER model inputs P_char, P_word, H_char, and H_word, and predicts a label \hat{y} that indicates the semantic relationship between P and H. As shown in Fig. 1, the MGIER model architecture consists of five components: 1) a multi-granularity embedding layer, 2) a residual encoding layer, 3) an internal-external correlation encoding layer, 4) a global feature fusion layer, and 5) a prediction layer. We will detail each component in the following subsections.

3.1. Multi-Granularity Embedding Layer

In this layer, the character/word sequences P_char, P_word, H_char, and H_word of sentences P and H are first padded to the same length N. Then, an l -dimensional embedding vector for a character/word in the sequences is obtained by the pre-trained Word2Vec [20] on the data set, such as BQ [21] and LCQMC [22] in our experiments. It is noted that out-of-vocabulary (OOV) words are initialized with zero vectors. As a result, the sentences P and H are converted to four sequences P^c, P^w, H^c, H^w , where each sequence consists of N l -dimensional character/word embedding vectors. That is to say, each of P^c, P^w, H^c, H^w is a $N \times l$ matrix.

3.2. Residual Encoding Layer

In this layer, we use LSTM [23] and BiLSTM [24] to encode character/word embedding vector sequences in P^c, P^w, H^c, H^w obtained in the previous layer. The formula is shown in Eq. (1).

$$\left. \begin{aligned} P^{ec} &= [\text{BiLSTM}([\text{LSTM}(P^c), P^c]), \text{LSTM}(P^c)], \\ P^{ew} &= [\text{BiLSTM}([\text{LSTM}(P^w), P^w]), \text{LSTM}(P^w)], \\ H^{ec} &= [\text{BiLSTM}([\text{LSTM}(H^c), H^c]), \text{LSTM}(H^c)], \\ H^{ew} &= [\text{BiLSTM}([\text{LSTM}(H^w), H^w]), \text{LSTM}(H^w)]. \end{aligned} \right\} (1)$$

Consider the first line in Eq. (1). First, we use LSTM to encode the character embedding vector sequence P^c , i.e., $\text{LSTM}(P^c)$. Second, we combine $\text{LSTM}(P^c)$ and P^c , i.e., $[\text{LSTM}(P^c), P^c]$. Third, we use BiLSTM to encode the result in the second step, i.e., $\text{BiLSTM}([\text{LSTM}(P^c), P^c])$. Finally, we combine $\text{BiLSTM}([\text{LSTM}(P^c), P^c])$ and $\text{LSTM}(P^c)$ and obtain P^{ec} . As shown in Eq. (1), similar steps are applied to the other character/embedding vector sequences P^w, H^c, H^w . The steps in Eq. (1) are detailed in the top-right of Fig. 1.

3.3. Internal and External Correlation Encoding Layer

In this layer, we employ soft alignment attention [1] to compute the internal correlation between characters/words in a sentence, and the external correlation between sentences.

Internal Correlation Encoding. We capture the internal correlation features between a character and a word in the same sentence.

We first compute the correlation weight via Eq. (2).

$$\left. \begin{aligned} p_{ij} &= (p_i^{ec})^T p_j^{ew}, \quad i, j \in \{1, \dots, N\}, \\ h_{ij} &= (h_i^{ec})^T h_j^{ew}, \quad i, j \in \{1, \dots, N\}. \end{aligned} \right\} (2)$$

where p_i^{ec} and p_j^{ew} are respectively the i -th character encoding vector in P^{ec} and the j -th word encoding vector in P^{ew} for the sentence P , which are obtained in the previous layer. p_{ij} is the correlation weight between p_i^{ec} and p_j^{ew} . Similarly, h_i^{ec} , h_j^{ew} , and h_{ij} for the sentence H . After obtaining the correlation weights p_{ij} and h_{ij} , we compute the internal correlation features via Eq. (3).

$$\left. \begin{aligned} \overline{p}_i^c &= \sum_{j=1}^N \frac{\exp(p_{ij})}{\sum_{k=1}^N \exp(p_{ik})} p_j^{ew}, \quad i \in \{1, \dots, N\}, \\ \overline{p}_j^w &= \sum_{i=1}^N \frac{\exp(p_{ij})}{\sum_{k=1}^N \exp(p_{ik})} p_i^{ec}, \quad j \in \{1, \dots, N\}, \\ \overline{h}_i^c &= \sum_{j=1}^N \frac{\exp(h_{ij})}{\sum_{k=1}^N \exp(p_{ik})} h_j^{ew}, \quad i \in \{1, \dots, N\}, \\ \overline{h}_j^w &= \sum_{i=1}^N \frac{\exp(h_{ij})}{\sum_{k=1}^N \exp(p_{ik})} h_i^{ec}, \quad j \in \{1, \dots, N\}. \end{aligned} \right\} (3)$$

where \overline{p}_i^c , \overline{p}_j^w , \overline{h}_i^c and \overline{h}_j^w are respectively the correlation features of the i -th character or the j -th word in the sentences P and H . With the above operations, we obtain the internal correlation features: P_{in}^c ($\{\overline{p}_i^c\}_{i=1}^N$), P_{in}^w ($\{\overline{p}_j^w\}_{j=1}^N$), H_{in}^c ($\{\overline{h}_i^c\}_{i=1}^N$), and H_{in}^w ($\{\overline{h}_j^w\}_{j=1}^N$).

External Correlation Encoding. We capture the external correlation features between two characters or two words in two different sentences.

We first compute the correlation weight via Eq. (4).

$$\left. \begin{aligned} c_{ii} &= (p_i^{ec})^T h_i^{ec}, \quad i \in \{1, \dots, N\}, \\ w_{jj} &= (p_j^{ew})^T h_j^{ew}, \quad j \in \{1, \dots, N\}. \end{aligned} \right\} (4)$$

where p_i^{ec} and h_i^{ec} are respectively the i -th character encoding vector in P^{ec} for the sentence P and the i -th character encoding vector in H^{ec} for the sentence H . c_{ii} is the correlation weight between p_i^{ec} and h_i^{ec} . Similarly, p_j^{ew} , h_j^{ew} and w_{jj} for the word encoding vectors. After obtaining the correlation weights c_{ii} and w_{jj} , we compute the external correlation features via Eq. (5).

$$\left. \begin{aligned} \overline{p}_i^c &= \sum_{j=1}^N \frac{\exp(c_{ij})}{\sum_{k=1}^N \exp(c_{jk})} h_i^{ec}, \quad i \in \{1, \dots, N\}, \\ \overline{p}_j^w &= \sum_{i=1}^N \frac{\exp(w_{ij})}{\sum_{k=1}^N \exp(w_{kk})} h_j^{ew}, \quad j \in \{1, \dots, N\}, \\ \overline{h}_i^c &= \sum_{j=1}^N \frac{\exp(c_{ij})}{\sum_{k=1}^N \exp(c_{kk})} p_i^{ec}, \quad i \in \{1, \dots, N\}, \\ \overline{h}_j^w &= \sum_{i=1}^N \frac{\exp(w_{ij})}{\sum_{k=1}^N \exp(w_{kk})} p_j^{ew}, \quad j \in \{1, \dots, N\}. \end{aligned} \right\} (5)$$

where \overline{p}_i^c , \overline{p}_j^w , \overline{h}_i^c , and \overline{h}_j^w are respectively the correlation features of characters or words in the sentences P and H . With the above operations, we obtain the external

correlation features: P_{out}^c ($\{\overline{p_i^c}\}_{i=1}^N$), P_{out}^w ($\{\overline{p_j^w}\}_{j=1}^N$), H_{out}^c ($\{\overline{h_i^c}\}_{i=1}^N$), and H_{out}^w ($\{\overline{p_j^c}\}_{j=1}^N$).

3.4. Feature Fusion Layer

We have obtained the residual encoding features and internal-external correlation features in the above layers. Specifically, the residual encoding features are P^{ec} , P^{ew} , H^{ec} , and H^{ew} , the internal correlation features are P_{in}^c , P_{in}^w , H_{in}^c , and H_{in}^w , and the external correlation features are P_{out}^c , P_{out}^w , H_{out}^c , and H_{out}^w .

Internal Correlation Feature Fusion. The average and max pooling operations are able to extract a set of global and key features, respectively.

$$\left. \begin{aligned} In_p &= [avgpool([P^{ec}; P^{ew}; P_{in}^c; P_{in}^w]); maxpool([P^{ec}; P^{ew}; P_{in}^c; P_{in}^w])], \\ In_H &= [avgpool([H^{ec}; H^{ew}; H_{in}^c; H_{in}^w]); maxpool([H^{ec}; H^{ew}; H_{in}^c; H_{in}^w])], \\ In_{global} &= [avgPool([P_{in}^c; P_{in}^w; H_{in}^c; H_{in}^w]); maxpool([P_{in}^c; P_{in}^w; H_{in}^c; H_{in}^w])]. \end{aligned} \right\} (6)$$

Consider the first line in Eq. (6). First, we combine the residual encoding features and internal correlation features of sentence P, i.e., $[P^{ec}; P^{ew}; P_{in}^c; P_{in}^w]$. Second, we perform the average and max pooling operations on the combined feature. Finally, we combine the results of the pooling operations and obtain In_p which is the feature of P. As shown in Eq. (6), similar steps are applied to sentence H and obtain In_H which is the feature of H. For the global internal correlation feature In_{global} , we first combine all the internal correlation features, i.e., $[P_{in}^c; P_{in}^w; H_{in}^c; H_{in}^w]$, and then perform the pooling operations on the combined feature.

$$Sim_{in} = [|In_p - In_H|; In_p \times In_H]. \quad (7)$$

Here, the operations $-$ and \times are performed element-wise to infer the relationship between two sentences. As shown in Eq. (7), we compute the correlation feature Sim_{in} for the tuple $\langle In_p, In_H \rangle$.

$$In = [Sim_{in}; In_{global}]. \quad (8)$$

As shown in Eq. (8), we obtain the internal correlation feature In by combining the correlation feature Sim_{in} and the global internal correlation feature In_{global} .

External Correlation Features Fusion. We integrate the residual encoding features and the external correlation features.

$$\left. \begin{aligned} Out_w &= [avgpool([P^{ew}; H^{ew}; P_{out}^w; H_{out}^w]); maxpool([P^{ew}; H^{ew}; P_{out}^w; H_{out}^w])], \\ Out_c &= [avgpool([P^{ec}; H^{ec}; P_{out}^c; H_{out}^c]); maxpool([H^{ec}; H^{ew}; P_{out}^c; H_{out}^c])], \\ Out_{global} &= [avgPool([P_{out}^c; P_{out}^w; H_{out}^c; H_{out}^w]); maxpool([P_{out}^c; P_{out}^w; H_{out}^c; H_{out}^w])]. \end{aligned} \right\} (9)$$

Consider the first line in Eq. (9). First, we combine the residual encoding features and external correlation features of word-granularity for sentences P and H, i.e., $[P^{ew}; H^{ew}; P_{out}^w; H_{out}^w]$. Second, we perform the average and max pooling operations on the combined feature. Finally, we combine the results of the pooling operations and obtain Out_w , which is the word-granularity feature for sentences P and H. Similar steps are applied to character-granularity for sentences P and H. For the global external correlation feature Out_{global} , we first combine all the external correlation features, i.e., $[P_{out}^c; P_{out}^w; H_{out}^c; H_{out}^w]$, and then perform pooling operations on the combined feature.

$$Sim_{out} = [Out_w - Out_c; Out_w \times Out_c]. \quad (10)$$

As shown in Eq. (10), we compute the correlation feature Sim_{out} for the tuple $\langle Out_w, Out_c \rangle$.

$$Out = [Sim_{out}; Out_{global}]. \quad (11)$$

As shown in Eq. (11), we obtain the external correlation feature Out by combining the correlation feature Sim_{out} and the global external correlation feature Out_{global} .

$$Feature_{total} = [In; Out]. \quad (12)$$

Finally, we obtain the global feature $Feature_{total}$ by combining the internal/external correlation features, as shown in Eq. (12), which is the input of the prediction layer.

3.5. Prediction Layer

The prediction layer is a multi-layer perceptron classifier with three dense sub-layers, in which the first two dense layers are activated with the ReLU function [25] and the last dense layer is connected with the sigmoid activation function in our experiments.

3.6. Loss Function

When training the models, we use two loss functions which have different effects on different datasets. The first one is the modified binary cross-entropy l_{modify} [26] shown in Eq. (13), which can focus on the training samples that are not easy to distinguish.

$$l_{modify} = -\sum \lambda(y_{true}, y_{pred})(y_{true} \log y_{pred} + (1 - y_{true}) \log(1 - y_{pred})). \quad (13)$$

where y_{true} and y_{pred} are the true value and the predicted value, $\lambda(y_{true}, y_{pred})$ is defined as in Eq. (14).

$$\lambda(y_{true}, y_{pred}) = 1 - \theta(y_{true} - m)\theta(y_{pred} - m) - \theta(1 - m - y_{true})\theta(1 - m - y_{pred}). \quad (14)$$

where m is a threshold which is usually set to 0.7, $\theta(x)$ is the unit step function and is defined as shown in Eq. (15).

$$\theta(x) = \begin{cases} 1, & x > 0, \\ 1/2, & x = 0, \\ 0, & x < 0. \end{cases} \quad (15)$$

The second loss function is the equilibrium binary cross-entropy $l_{equilibrium}$ [7] shown in Eq. (16), which can strengthen its ability to distinguish the fuzzy boundary and eliminate the blurring phenomenon in classification tasks.

$$l_{equilibrium} = -\sum_{i=1}^n (l_{mse} \times y_{true} \log y_{pred} + (1 - l_{mse}) \times (1 - y_{true}) \log(1 - y_{pred})). \quad (16)$$

Where n is the count of samples and l_{mse} is the equilibrium factor MSE, defined as in Eq. (17).

$$l_{mse} = \frac{1}{2n} \sum_{i=1}^n (y_{true} - y_{pred})^2. \quad (17)$$

4. Experiments

The goal of the experiments is to evaluate the effect of the performance of the proposed model, MGIER, for Chinese SSM.

4.1. Experiment Setup

Datasets. In the experiments, we use two Chinese datasets BQ [21] and LCQMC [22]. BQ is a Chinese bank question corpus for sentence intention equivalence identification, which comes from Weizhong bank’s online customer service logs. LCQMC is a Chinese question matching corpus collected from Baidu Knows. The two datasets consist of a large number of instances in the form of (P, H, Label), where P and H are two Chinese sentences, and Label indicates whether P and H have the same meaning. We split each dataset into a training set, validation set, and test set by the same proportion mentioned in [24, 25]. A summary of the datasets is shown in Table 2.

Table 2. Experimental data sets

Dataset	Source	Scale(train/validation/test)	Positive:Negative
BQ	Weizhong bank	100,000/10,000/10,000	1:1
LCQMC	Baidu Knows	238,766/8802/12,499	1.35:1

Baseline models. In the experiments, we compare the proposed model with seven baseline models. ESIM [1] employs soft alignment attention to capture deep correlation information between two sentences. Although MGF [7] and ICE [8] use multi-granularity to enhance text representation, only ICE uses soft alignment attention to capture the correlation information of sentences. Both have good performance for Chinese SSM. DRCN [9] utilizes the representational power of recurrent networks and attentive information. ESIM and DRCN also have remarkable performance in English SSM. BiMPM [14] matches two sentences from different directions. ARC-II [27] is a simplification of MatchPyramid. MatchPyramid [28] comes from modeling text matching as image recognition, which takes the matching matrix as an image.

Metrics. The metrics used in the experiments include accuracy, precision, recall and F1_score.

Parameters. In the experiments, the hidden states of LSTM and BiLSTM and the character/word embedding vectors have 300 dimensions. For LSTM, the dropout rates 0.4 and 0 are used for the datasets BQ and LCQMC, respectively. In BiLSTM, the dropout rates are set to 0.55 and 0.25, respectively, for BQ and LCQMC. The dropout rates 0.3 and 0.5 are used for BQ and LCQMC, respectively, in the prediction layer which consists of two densely-connected hidden layers with 600 units and one classifier with a sigmoid activation function. When training the models, we use Adam optimizer, where the number of epochs is 100 and the batch size is 512.

Environment Setting. We implemented the proposed model using Python with the Keras and Tensorflow frameworks, and the baseline models using the Pytorch frameworks. All experiments are run on a workstation equipped with two Intel (R) Xeon (R) gold 6132 CPU, @ 2.60GHz 256GB memory, four pieces of NVIDIA Tesla V100 SXM2 32GB GPU, and CentOS Linux.

4.2. Experimental Results

The effect of loss functions. We compare the effect of two loss functions: the modified binary cross-entropy l_{modify} defined in Eq. (14) and the equilibrium cross-entropy $l_{equilibrium}$ defined in Eq. (18). The results are shown Table 3. From this table, we can see that the modified binary cross-entropy l_{modify} is better than the equilibrium cross-entropy $l_{equilibrium}$ for the dataset BQ, while $l_{equilibrium}$ is better than l_{modify} for the dataset LCQMC. The reasons may be that the modified binary cross-entropy focuses on the training samples that are not easy to distinguish, and the equilibrium cross-entropy distinguishes the fuzzy boundary and eliminates the blurring phenomenon. As a result, we use the modified binary cross-entropy as the loss function for BQ, and the equilibrium cross-entropy for LCQMC.

Table 3. The effect of loss functions

Dataset	Loss Function	Accuracy	Precision	Recall	F1 score
BQ	l_{modify} [8]	84.93	84.96	84.94	84.87
	$l_{equilibrium}$ [7]	81.60	84.97	76.78	80.56
LCQMC	l_{modify} [8]	85.73	80.64	94.04	86.78
	$l_{equilibrium}$ [7]	87.70	88.77	86.49	87.57

The effect of models. We compare the proposed model with the baseline models. The results are shown in Table 4. In most cases, the accuracy, precision, and F1_score of the models using character/word granularity are better than that of other models. This indicates that using multi-granularity can improve the performance of the model. Among the models, the performance of MGIER, ESIM, and ICE using soft alignment attention is also better than that of other models in most cases. Thus, soft alignment attention is beneficial to Chinese SSM. Generally, the accuracy of MGIER, outperforms that of the baseline models for the dataset LCQMC and BQ. This is because MGIER uses multi-granularity and soft alignment attention to capture the fine-

grained information and internal/external correlation information. Also, MGIER employs residual connections to preserve semantic information.

Table 4. The performance of models

Dataset	Model	Accuracy	Precision	Recall	F1 score
BQ	MGIER _{char+word}	84.93	84.96	84.94	84.87
	ESIM _{char} [1]	83.69	78.19	94.22	85.46
	ESIM _{word}	81.59	83.87	78.74	81.23
	MGF _{char+word} [7]	82.61	89.65	73.75	80.83
	ICE _{char+word} [8]	84.05	83.31	85.10	84.12
	DRCN _{char+word} [9]	76.78	78.13	74.38	76.21
	BiMPM _{char} [14]	82.23	80.41	85.74	82.99
	ARC-II _{char} [27]	76.68	75.94	78.10	77.01
	MatchPyramid _{char} [28]	67.09	65.47	72.35	68.74
LCQMC	MGIER _{char+word}	87.70	88.77	86.49	87.57
	ESIM _{char}	84.83	78.19	94.22	85.46
	ESIM _{word}	83.69	75.50	94.42	83.90
	MGF _{char+word}	85.86	81.45	92.89	86.76
	ICE _{char+word}	86.15	81.93	92.70	86.94
	DRCN _{char+word}	78.93	72.10	94.42	81.76
	BiMPM _{char}	82.23	75.53	95.47	84.34
	ARC-II _{char}	82.35	88.53	74.34	80.81
	MatchPyramid _{char}	72.47	67.01	88.43	76.26

Comparison with pre-trained models. We compare MGIER with the pre-trained models as shown in Table 5. From the results in Table 5, we can see that the accuracy of MGIER is higher than that of other pre-trained models, with fewer parameters. This is probably because MGIER can capture more and deeper semantic information.

Table 5. Comparison with pre-trained models

Dataset	Model	Accuracy/Parameters	Dataset	Model	Accuracy/Parameters
BQ	MGIER	84.93 (21.25M)	LCQMC	MGIER	87.70 (21.25M)
	Bert	83.23 (169.62M)		Bert	87.57 (169.62M)
	NEZHA-Base	84.79 (97.16M)		NEZHA-Base	86.07 (97.16M)
	NEZHA-Base-WWM	84.67 (97.16M)		NEZHA-Base-WWM	86.35 (97.16M)
	Roberta-wwm-ext	84.11 (97.16M)		Roberta-wwm-ext	84.86 (97.16M)

Ablation Experiments. We conduct an ablation study for the proposed model MGIER on the datasets BQ and LCQMC. The results in Table 6 demonstrate the effectiveness of the residual encoding layer as well as the internal-external correlation encoding layer.

First, we remove the residual encoding and only preserve the output features of BiLSTM and LSTM, denoted case (1). Table 6 shows that the accuracy, precision, and F1_score drops obviously, which demonstrates the effectiveness of residual encoding.

Next, we remove the internal correlation encoding from MGIER, denoted case (2). The precision drops to 82.77% and 84.65% for the datasets BQ and LCQMC, respectively. We remove the external correlation encoding from MGIER, denoted case (3), and the recall drops to 79.36% for BQ, and the precision drops to 87.3% for LCQMC. This suggests that computing the internal/external correlation of the sentences is useful to improve the performance of the model.

Table 6. Ablation experiments

Dataset	Model	Accuracy	Precision	Recall	F1_score
BQ	MGIER	84.93	84.96	84.94	84.87
	(1) No residual encoding	83.76	84.51	82.62	83.47
	(2) No internal encoding	83.48	82.77	84.55	83.57
	(3) No external encoding	82.81	85.19	79.36	82.11
LCQMC	MGIER	87.70	88.77	86.49	87.57
	(1) No residual encoding	84.35	78.86	93.84	85.65
	(2) No internal encoding	86.81	84.65	89.88	87.15
	(3) No external encoding	87.65	87.30	88.14	87.67

5. Conclusions

We propose a Chinese SSM model, MGIER, to capture deep semantic information from the bottom embedding layer to the top prediction layer. Experimental results for two Chinese datasets demonstrate that the proposed method outperforms the state-of-the-art methods. Moreover, the proposed method is more efficient than pre-trained models. Although the MGIER model has achieved remarkable performance, there are still some important points that need to be considered. Through analyzing the incorrectly-predicted examples by the MGIER model, we find that different parts of a sentence have greater influence on the semantic matching results. For example, if the subject of the sentence does not match but the rest of the sentence does match, the result predicted by the MGIER model is matching when in fact it does not. Moreover, the MGIER model just considers the character and word granularity, but the phrases and themes of the sentence also have important semantic information. In the future, we will attempt to utilize phrases, themes, and subject-verb-objects of sentences to further improve the performance of MGIER for Chinese SSM.

References

- [1] CHEN Q, ZHU X, LING Z, et al.: Enhanced LSTM for natural language inference[C]. Proceedings of the 55th Annual Meeting of the Association for Computational Linguistics, 2017, 1657-1666.
- [2] YANG R, J ZHANG, GAO X, et al.: Simple and Effective Text Matching with Richer Alignment Features[J]. Proceedings of the 57th Annual Meeting of the Association for Computational Linguistics, 2019.

- [3] MUELLER J, THYAGARAJAN A.: Siamese recurrent architectures for learning sentence similarity[C]. Proceedings of the Thirtieth AAAI Conference on Artificial Intelligence, 2016, 2786-2792.
- [4] Kun Zhang, Guangyi Lv, Linyuan Wang, Le Wu, Enhong Chen, Fangzhao Wu, and Xing Xie. 2019. DRr-Net: Dynamic Re-read Network for Sentence Semantic Matching. (2019).
- [5] Yichen Gong, Heng Luo, and Jian Zhang. 2018. Natural language inference over interaction space. In Proceedings of the International Conference on Learning Representations.
- [6] Jiangping Huang, Shuxin Yao, Chen Lyu, and Donghong Ji. 2017. Multi-granularity neural sentence model for measuring short text similarity. In Proceedings of the International Conference on Database Systems for Advanced Applications, pages 439–455.
- [7] ZHANG X, LU W, ZHANG G, et al.: Chinese sentence semantic matching based on multi-granularity fusion model[M]. 2020.
- [8] ZHANG X, LI Y, LU W, et al.: Intra-Correlation Encoding for Chinese Sentence Intention Matching[C]// Proceedings of the 28th International Conference on Computational Linguistics. 2020.
- [9] Kim S, Kang I, Kwak N. Semantic Sentence Matching with Densely-connected Recurrent and Co-attentive Information[J]. 2018.
- [10] HUANG P S, HE X D, GAO J F, et al.: Learning deep structured semantic models for web search using clickthrough data [C] //Proceedings of the 22nd ACM International Conference on Conference on Information & Knowledge Management, 2013: 2333-2338.
- [11] SHEN Y, HE X, GAO J, et al.: A latent semantic model with convolutional-pooling structure for information retrieval[C]. Proceedings of the 23rd ACM international conference on conference on information and knowledge management, 2014, 101-110.
- [12] PALANGI H, DENG L, SHEN Y, et al.: Semantic modelling with long-short-term memory for information retrieval[J]. arXiv preprint arXiv:1412.6629, 2014.
- [13] PENG S, CUI H, XIE N, et al. Enhanced-RCNN: An Efficient Method for Learning Sentence Similarity[C]// WWW '20: The Web Conference 2020. 2020.
- [14] WANG Z, HAMZA W, FLORIAN R.: Bilateral Multi-Perspective Matching for Natural Language Sentences[C]// Twenty-Sixth International Joint Conference on Artificial Intelligence. 2017.
- [15] DEVLIN J, CHANG M, LEE K, et al.: BERT: pre-training of deep bidirectional transformers for language understanding[C]. Proceedings of the 2019 Conference of the North American Chapter of the Association for Computational Linguistics, 2019, 4171-4186
- [16] LIU W, ZHOU P, ZHAO Z, et al. K-bert:enabling language representation with knowledge graph[J]. arXiv preprint arXiv:1909.07606, 2019
- [17] WEI J, REN X, LI X, et al. NEZHA: Neural Contextualized Representation for Chinese Language Understanding[J]. 2019.
- [18] REIMERS N, GUREVYCH I. Sentence-BERT: Sentence Embeddings using Siamese BERT-Networks[J]. Proceedings of the 2019 Conference on Empirical Methods in Natural Language Processing and the 9th International Joint Conference on Natural Language Processing (EMNLP-IJCNLP), 2019.
- [19] Yinhan Liu, Myle Ott, Naman Goyal, Jingfei Du, Mandar Joshi, Danqi Chen, Omer Levy, Mike Lewis, Luke Zettlemoyer, and Veselin Stoyanov. 2019. RoBERTa: A Robustly Optimized BERT Pretraining Approach. arXiv preprint arXiv:1907.11692.
- [20] MIKOLOV T, SUTSKEVER I, CHEN K, et al. Distributed representations of words and phrases and their compositionality[C]. Advances in neural information processing systems, 2013, 3111-3119
- [21] CHEN J, CHEN Q C, LIU X, et al. 2018. The BQ corpus: A large-scale domain-specific Chinese corpus for sentence semantic equivalence identification. In Proceedings of the Conference on Empirical Methods in Natural Language Processing, pages 4946–4951.
- [22] LIU X, CHEN Q C, DENG C, et al. 2018. LCQMC: A large-scale Chinese question matching corpus. In Proceedings of the 27th International Conference on Computational Linguistics, pages 1952–1962.
- [23] Jianpeng Cheng, Li Dong, and Mirella Lapata. 2016. Long short-term memory-networks for machine reading. In Proceedings of the Conference on Empirical Methods in Natural Language Processing, pages 551–561.
- [24] Schuster, Mike, Paliwal, et al. Bidirectional recurrent neural networks. [J]. IEEE Transactions on Signal Processing, 1997.
- [25] Nair V, Hinton G E. Rectified Linear Units Improve Restricted Boltzmann Machines Vinod Nair[C]// International Conference on International Conference on Machine Learning. Omnipress, 2010.
- [26] SU J L. 2017. Text emotion classification (IV): Better loss function. Web page. <https://spaces.ac.cn/archives/4293>.
- [27] Hu, B.; Lu, Z.; Li, H.; and Chen, Q. 2014. Convolutional neural network architectures for matching natural language sentences. In Advances in Neural Information Processing Systems, 2042–2050.
- [28] Liang P, Lan Y, Guo J, et al. Text Matching as Image Recognition. 2016.

Mass Ratio Variance Majority Undersampling and Minority Oversampling Technique for Class Imbalance

Piboon Polvimoltham^a and Krung Sinapiromsaran^{a,1}

^a*Department of Mathematics and Computer Science, Faculty of Science, Chulalongkorn University, Bangkok, Thailand*

Abstract. A sampling method is one of the popular methods to deal with an imbalance problem appearing in machine learning. A dataset having an imbalance problem contains a noticeably different number of instances belonging to different classes. Three sampling techniques are used to solve this problem by balancing class distributions. The first one is an undersampling technique removing noises from a class having a large number of instances, called a majority class. The second one is an over-sampling technique synthesizing instances from a class having a small number of instances, called a minority class, and the third one is the combined technique of both undersampling and oversampling. This research applies the combined technique of both undersampling and oversampling via the mass ratio variance scores of instances from each individual class. For the majority class, instances with high mass ratio variances are removed whereas for the minority class, instances with high mass ratio variances are used in synthesizing minority instances. The results of this proposed sampling technique help improve recall over standard classifiers: a decision tree, a random forest, Linear SVM, MLP on all synthesized datasets; however it may have low precision. So the combined measure of precision and recall is used, F1-score. Recall and F1-scores of synthesized datasets and UCI datasets are significantly better for collections of datasets having small imbalance ratio. Moreover, the Wilcoxon signed-rank test is used to confirm the improvement for datasets having imbalance ratio smaller than or equal to 0.2.

Keywords. Mass ratio variance score, Undersampling, Oversampling, Imbalanced problem, Classification

1. Introduction

A class imbalanced problem[1] is one of the important topics in classification from machine learning. It is a problem of building a classifier in the presence of underrepresented class instances and highly skewed class distributions. This occurs when the number of instances representing an important class is much smaller than those from other classes. In a binary classification, the smaller class is called the minority class or the positive class while another class is called the majority class or the negative class. The main purpose of classification on this problem is to identify the minority instances

¹ Corresponding Author, Krung Sinapiromsaran, Department of Mathematics and Computer Science, Faculty of Science, Chulalongkorn University, Bangkok, Thailand; E-mail: krung.s@chula.ac.th

as accurately as possible. In real world applications, minority instances are important such as fraud transactions in the fraud detection[2], ailing patients in the medical diagnosis[3], default loans in the credit approval[4]. In addition, a class imbalance problem in the medical diagnosis is to detect and diagnose the patterns of certain diseases within patient electronic healthcare records. It is normal that some life threatening diseases are rare among patients. The misclassification of these cases can lead to the patient's death so the ailing patients that identify as healthy should not be occurred, i.e. the number of false negative patients should be small. Traditionally, a minority instance tends to be misclassified when a standard classifier is applied on an imbalanced dataset due to its tiny portion.

There are three main methodologies to deal with an imbalanced problem. First, a data-level methodology[5, 6, 7, 8] resamples the distribution of class instances to make them balance. Then this new dataset can be used to train with any classifier. Many techniques in this approach are an oversampling technique[9, 10, 11] which synthesizes random instances from the minority group avoiding those from majority groups, or an undersampling technique[12, 13] which discards random instances from the majority group to extend the minority region of instances in the minority class or the mixture of an oversampling and undersampling technique[14]. Second, an algorithmic-level methodology upgrades or reimplements the classification algorithms to be more robust to noise while handling minority instances successfully[15, 16, 17, 18, 19]. Third, the hybrid methodology combines both the data-level approach and the algorithmic-level approach such as Adaboost[20], Boosting[21], Bagging[22], etc.

An undersampling algorithm concentrates on removing instances from the majority class, it reduces the total amount of information that the model has to learn from. Currently, there are many undersampling techniques such as DBMUTE 2017, MUTE, 2011, but a random undersampling algorithm (RUS) is the simplest method that removes minority instances randomly without any restriction. There are many intelligent approaches toward undersampling such as Tomek-link[23], it is the method that based on 1-Nearest-Neighbour, groups the borderline minority instance with nearest majority instance then removes those majority instances, this makes borderline unblemish and easy to partition. An oversampling algorithm contrasts this operation by increasing the number of minority instances. The simplest method is the random oversampling algorithm (ROS). It randomly duplicates instances from the minority class, which will not expand the region of the minority class. One of the popular oversampling techniques that expand the region of this class is the Synthetic minority oversampling technique (SMOTE)[5]. It produces artificial minority instances by interpolating between existing minority instances and their nearest minority neighbours. The enhanced SMOTE algorithm has been developed such as Borderline-SMOTE[6] and Safe-Level-SMOTE[7] that deal with some majority instances during the synthetic process.

A misclassified minority instance normally lies further away from other minority instances or abnormal minority instances. An algorithm to help a classifier to recognize them should remove some surrounding majority instances within the overlapping region. In addition, it should also synthesize a small number of minority instances near these minority instances. Hence, the resampling technique is proposed. In addition, the algorithm may be used to identify abnormal instances in the majority class for removal. This can be achieved using the anomaly score, the Mass-ratio variance based outlier factor(MOF)[24]. The algorithm to generate MOF requires no parameter and uses the density to assign high scores to outliers. This makes MOF perfect to detect those abnormal instances for majority and minority classes.

The mass ratio variance majority undersampling and minority oversampling technique (MUOT) is proposed. It uses MOF to detect abnormal instances in both majority and minority classes. An abnormal instance from the majority class is treated as noise which will be removed to clean up the overlapping area between both classes while abnormal instances from the minority class will be packed with synthesized minority instances. To evaluate the performance of the proposed method via precision, recall and F1-score, four standard classifiers will be executed on synthesized datasets and UCI datasets. Finally, the Wilcoxon signed-rank test will be used to demonstrate the effectiveness of the proposed method for unseen instances.

2. Related work and background knowledge

A mass-ratio-variance based outlier factor algorithm[24] is a parameter-free density-based outlier scoring algorithm. It gives scores to all instances from a dataset. The high score is given to an outlier whereas the low score is given to normal instances via the variance of mass-ratio scores. The following definitions are used to define MOF.

Definition 1: Given a dataset $D \subseteq \mathbb{R}^d$ the Euclidean distance of instance $x = (x_1, \dots, x_d) \in D$ to instance $y = (y_1, \dots, y_d) \in D$ denoted as $d(x, y)$ is defined as

$$d(x, y) = \sqrt{\sum_{i=1}^d (x_i - y_i)^2}$$

Definition 2: Given a dataset $D \subseteq \mathbb{R}^d$, the set of all instances within the neighbourhood of instances $x \in D$ with respect to the radius r is defined as the set of points that lies within the ball centred at instance x with the radius r

$$N(x, r) = \{z \in D \mid d(x, z) \leq r\}$$

Definition 1 is the Euclidean distance definition and definition 2 defines the set of neighbourhoods of instance x with respect to the radius r . The next definition defines the mass-ratio of an instance with respect to another instance. The last definition defines the mass-ratio variance score of an instance.

Definition 3: For instance $y \in D$ and instance $x \neq y \in D$, the mass-ratio of instance y with respect to instance x is defined as

$$mr_x(y) = \frac{|N(y, d(x, y))|}{|N(x, d(x, y))|}$$

For instance x , the definition 3 will assign mass-ratios to other instances in the dataset. If this instance x is outlier, the denominator will contribute a small number so that other instances will have high mass-ratios, except the one that is close to x . If this instance x is among other instances in a dataset, this mass-ratio will be close to 1.

Definition 4: $\bar{m}r_x$ is defined as mean of the mass-ratio distribution of other instances, except x and MOF of instance x is defined as the variance of the mass-ratio distribution. These MOFs are used to separate abnormal instances from normal ones. They are used in the proposed method, MUOT, for a class imbalance problem. The criterion to separate abnormal instances from normal instances will explain in detail in the next section.

3. MUOT

MUOT uses mass-ratio-variance scores for undersampling and oversampling. Originally, the mass-ratio-variance score was designed to identify outliers of a static dataset by giving high MOF scores to outliers and low MOF scores to normal instances. MUOT is the algorithm that resamples imbalanced to balanced dataset. Both undersampling and oversampling steps are performed only on abnormal instances. The undersampling step is to remove abnormal instances from the majority class and oversampling step is to synthesize the minority instances into balls using abnormal instances from the minority class as center. To identify abnormal instances, a threshold for MOF scores must be selected. For a univariate data distribution, $Q_3 + 1.5IQR$ is suggested as the IQR rule to identify outliers. Note $IQR = Q_3 - Q_1$ where Q_3 is the 75th percentile and Q_1 is the 25th percentile. Nevertheless, to find an appropriate threshold for MUOT, 50th, 60th, 70th, 80th and 90th percentiles are investigated to compare with $Q_3 + 1.5IQR$ via the decision tree. After resampling techniques are applied to datasets with different thresholds. The one with the highest F1-score will be selected as the appropriate threshold for MUOT, see Figure 1. From these experiments, the best threshold is 90 percentile. So 10% of majority instances will be removed and 10% of minority instances will be used in the oversampling step to make sure that there are enough minority instances for a classifier to recognize these minority outcasts.

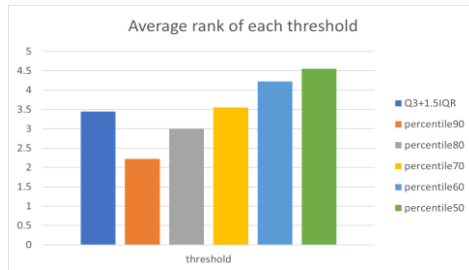


Figure 1: Average rank of each threshold compared

The following pseudocode demonstrates the step-by-step of the MUOT algorithm.

Algorithm MUOT(X, y, p)

Input: Array of data X ; vector of target y ; percentile threshold p (default = 90)

nFeatures = number of features, nPos = number of minority instances, nNeg = number of majority instances

Note: 1. y_i is 0 for a majority instance and 1 for a minority instance

2. # is used for a line comment

3. compute_MOF(S) returns MOF scores of each instance in S

4. percentile(S, p) returns the p^{th} percentile value from S

5. a group of selected instances is represented in a numpy array as Variable_name[*conditions* or *index*]

6. ball($x, nFeatures, r, n$) returns n synthesized instances within a ball centered at x and radius r .

7. enumerate(S) returns a sequence of (i, s) where i is the index of s in S

7. concatenate(S, T) returns the new set that concatenate T to S

Output: the balanced dataset X and y

1. XNeg is the subset of X having target $y = 0$
 2. MOFNeg = compute_MOF(XNeg)
 3. NegThreshold = percentile(MOFNeg, p)
 4. NegAbnormal is the set of instances from XNeg having MOFNeg > NegThreshold
 5. nNegAbnormal = the number of instances from NegAbnormal
 6. $X =$ is the subset of X removing NegAbnormal
-

```

7. nNegNormal = nNeg - nNegAbnormal
8. nSyn = nNegNormal - nPos # nSyn will be the number of synthesized instance
9. if nSyn > 0
10.   then # Do the oversampling step
11.     XPos is the subset of X having target y = 1
12.     MOFPos = compute_MOF(XPos)
13.     PosThreshold = percentile(MOFPos, p)
14.     PosAbnormal is the set of instances from XPos having MOFPos > PosThreshold
15.     nPosAbnormal = the number of instances from PosAbnormal
16.     nSynPos = nSyn*(MOFPos[PosAbnormal] / Sum(MOFPos[PosAbnormal]))
17.     NegIndex = index of nearest majority instance from instances in PosAbnormal
18.     radius = distance[NegIndex] # radius is set as the distance from the minority instance to its
        nearest majority instance
19.     for i, abnormal in enumerate(PosAbnormal)
20.       SynPos = ball(abnormal, nFeatures, radius[i], nSynPos[i])
21.       X = concatenate(X, SynPos)
22.       Y = concatenate(Y, 1)
23.     endfor
24.   endif
25. return X, y
End MUOT

```

4. Experiments and Results

This section reports the experimental results of the MUOT algorithm via four classifiers. The experimental datasets are grouped into three collections having the imbalance ratio (IR) of 0.1, 0.2 and 0.3. Note that the imbalance ratio is defined as the ratio between number of minority instances and number of all instances. IR values represent the ratio of imbalance data, a low IR value means there is a small number of minority instances (highly imbalanced) while a high IR value means the data is more balanced. In each collection, the subcollection is defined based on the number of clusters of 2, 3 and 4. Each collection will contain 3 subcollections, each subcollection is defined in 3D and 5D with 100 or 300 instances. Then the datasets are generated randomly 30 times and the average performance will be reported from these 30 datasets in each subcollection and each collection. The reported results are the average performance measures of each collection by each subcollection based on different classifiers and measures.

$$\text{Imbalanced Ratio}(IR) = \frac{|\text{minority instances}|}{|\text{all instances}|} \quad (1)$$

The performance measures are computed from the confusion matrix shown below. TP is the count of true positive instances: the actual class is positive and the predicted class is also positive. TN is the count of true negative instances: the actual class is negative and the predicted class is negative. FP is the count of false positive instances: the actual class is negative but the predicted class is positive. FN is the count of false negative instances: the actual class is positive but the predicted class is negative.

	Actual Positive	Actual Negative
Predicted Positive	TP: True Positive	FP: False Positive
Predicted Negative	FN: False Negative	TN: True Negative

Figure 2: Confusion matrix

In a class imbalance problem, three measures are more crucial than others which are TP, FN and FP. Note that FP is the number of negative instances that are predicted as positive and FN is the number of positive instances that are predicted as negative which should be very low for a class imbalance problem. So recall, see Equation 3, will be more emphasized than precision, see Equation 2. Nevertheless, to incorporate both measures, F1-score is used as the harmonic mean of precision and recall, see Equation 4.

$$\text{Precision} = \frac{TP}{TP+FP} \quad (2)$$

$$\text{Recall} = \frac{TP}{TP+FN} \quad (3)$$

$$\text{F1 - score} = 2 \times \frac{\text{Precision} \times \text{Recall}}{\text{Precision} + \text{Recall}} \quad (4)$$

4.1 Synthesized data

There are 36 settings in the experiment which are grouped by IR and the number of clusters. Collection 1 has IR = 0.1, Collection 2 has IR = 0.2 and Collection 3 has IR = 0.3. Each collection also has three subcollections grouped by the number of clusters = 2, 3 and 4. In each subcollection, there are 4 settings varying by the number of features = 3 and 5 and the number of instances = 100 and 300 as shown in Table 1. In each setting, 30 datasets are randomly generated based on the provided setting.

Table 1. Information of synthesized datasets used in the experiment

Synthesized data				
Collection (IR)	Subcollection	#clusters	#features	#instances
1 (IR = 0.1)	1.1	2	3, 5	100, 300
	1.2	3	3, 5	100, 300
	1.2	4	3, 5	100, 300
2 (IR = 0.2)	2.1	2	3, 5	100, 300
	2.2	3	3, 5	100, 300
	2.3	4	3, 5	100, 300
3 (IR = 0.3)	3.1	2	3, 5	100, 300
	3.2	3	3, 5	100, 300
	3.3	4	3, 5	100, 300

The average performances of precision, recall and F1-score are reported in Figure 3 over four classifiers: a decision tree, a random forest, linear SVM, MLP comparing between the use of the original dataset and the dataset from the MUOT algorithm.

The results of the experiments are shown in Table 2 and Figure 3. Each cell in Table 2 reports mean±sd from each setting, where mean is the average performance and sd is the standard deviation. To easily see the increase and decrease of performance, Figure 3 shows the barplot of each measurement compared between the original and the MUOT datasets. It has a 3 by 3 barplots by the collections and the subcollections. But in this paper are shows a 2 by 2 barplots which the collection having IR= 0.1 and 0.3 and the subcollection having the number of clusters= 2 and 4. In case of full Figure 3 can be find at this following links[<https://bit.ly/3k2SMv0>].

From Table 2, all experiments show the decrease in precision and the increase in recall. For F1-scores, all experiments show improvement of this performance measure. Notice that for the number of clusters = 2, the improvement of recalls and F1-scores are small with respect to the larger number of clusters for all collections. The reason for this behavior is that by removing majority abnormal instances will expand the minority region so a classifier would be able to classify more minority instances which increases recall. However, this behavior will cause precision to decrease because the more minority

prediction, the more chance that some majority instances will be predicted as minority instances which will decrease precision. Therefore, F1-score should be used to determine the performance of MUOT. This demonstrates that the MUOT algorithm can help classifiers to give a better improvement for the original datasets having IR less than or equal to 0.2 and the more number of clusters the better improvement from MUOT can be obtained.

Table 2. Mean±sd of precision, recall and F1-score of each collection

Collection	Subcollection	Models	Mean±sd		
			precision	recall	F1-score
IR = 0.1	2	Original	0.6030 ± 0.1670	0.3974 ± 0.1077	0.4474 ± 0.1118
		MUOT	0.5035 ± 0.1200	0.5110 ± 0.1175	0.4767 ± 0.1063
	3	Original	0.4403 ± 0.1972	0.2399 ± 0.1054	0.2810 ± 0.1144
		MUOT	0.3774 ± 0.1463	0.3904 ± 0.1330	0.3499 ± 0.1268
	4	Original	0.4591 ± 0.0398	0.3446 ± 0.1746	0.3571 ± 0.1740
		MUOT	0.4368 ± 0.1296	0.5068 ± 0.1740	0.4344 ± 0.1367
IR = 0.2	2	Original	0.7699 ± 0.0949	0.6147 ± 0.0877	0.6608 ± 0.0871
		MUOT	0.6656 ± 0.0917	0.7139 ± 0.0700	0.6675 ± 0.0734
	3	Original	0.6577 ± 0.1086	0.4536 ± 0.0979	0.5046 ± 0.0948
		MUOT	0.5653 ± 0.0975	0.6003 ± 0.0655	0.5562 ± 0.0728
	4	Original	0.6780 ± 0.1435	0.5069 ± 0.1356	0.5485 ± 0.1371
		MUOT	0.5685 ± 0.1200	0.6265 ± 0.1224	0.5743 ± 0.1187
IR = 0.3	2	Original	0.8023 ± 0.0693	0.7254 ± 0.0721	0.7461 ± 0.0670
		MUOT	0.7194 ± 0.0671	0.7942 ± 0.0447	0.7450 ± 0.0556
	3	Original	0.7441 ± 0.0889	0.5938 ± 0.1072	0.6401 ± 0.1024
		MUOT	0.6537 ± 0.0806	0.6963 ± 0.0734	0.6614 ± 0.0761
	4	Original	0.7366 ± 0.0995	0.6277 ± 0.1322	0.6606 ± 0.1191
		MUOT	0.6618 ± 0.0806	0.7052 ± 0.1014	0.6730 ± 0.0905
UCI collection	Original	0.5750 ± 0.2381	0.4774 ± 0.2453	0.4843 ± 0.2559	
	MUOT	0.5646 ± 0.1903	0.6087 ± 0.1939	0.5551 ± 0.2054	

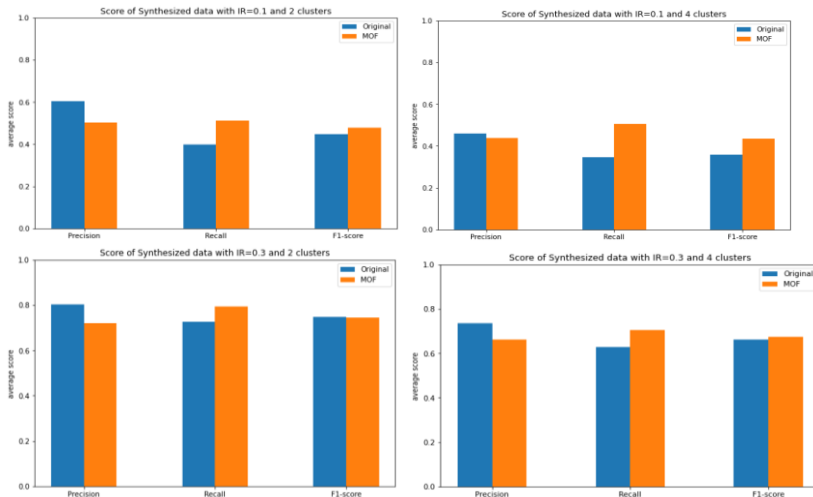


Figure 3: Average precision, recall and F1-score of 4 collection

4.2 Real world datasets

Five UCI datasets are used in the experiment. In contrast with the synthesized data, the minority class must be selected in the experiment. The brief description of five UCI

datasets and their characteristics are shown in Table 3. In real world datasets, consisting of both binary and multiclass datasets. The multiclass datasets are converted to the binary datasets by selecting one class as the minority class and the rest as the majority class. In Table 3, the target class was chosen to be the minority class as in the column of “minority target” and the rest were set as the majority class. The overall IR values of these five datasets is 0.2467. The average performances from the UCI datasets are shown in Figure 4.

Table 3. Information of UCI datasets used in the experiment

Datasets	#instances	#features	minority target	#minority	IR
Wine	178	13	“3”	48	0.2697
Parkinsons	195	22	“0”	48	0.2461
Haberman	306	3	“2”	81	0.2647
E Coli	336	7	“imU”	35	0.1041
Pima	768	8	“1”	268	0.3489
Average					0.2467

From the previous observation, the MUOT algorithm can help classifiers to gain better recall and F1-score for IR less than 0.3 so it is expected to see the improved performance for these five UCI datasets having the average IR as 0.2467. From Figure 4, the improved performance of recall and F1-score are obtained. This can be concluded that the MUOT algorithm can help classifiers improve recall and F1-score.

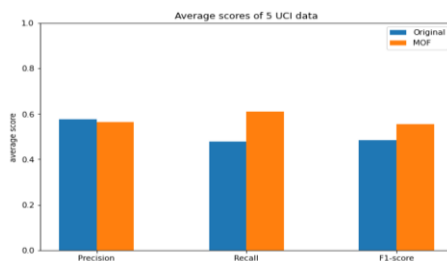


Figure 4: Average precision, recall and F1-score of 5 UCI dataset

4.3 Results

The MUOT algorithm generates a new dataset that increases recall for a classifier since more positive instances can be easily recognized, but it will decrease precision due to the enlarged minority regions so F1-score is the preferred measure which incorporates recall and precision together. All results show the increases of recall and F1-score and the decrease of precision. From three collections varying by IR values, the ranges of recall and F1-score increase corresponding to IR, the more balanced the datasets are, the less improvement MUOT will be. For the result of different numbers of clusters, MUOT exhibits the highest F1-score when the number of clusters is equal to 4. This may come from the spread of minority instances among all clusters. So MOF can be used to help detect abnormal instances very well when more minority instances are spread across the dataset. For UCI datasets, MUOT improves recall and F1-score and decreases precision. To validate these findings, the non-parametric Wilcoxon signed-rank tests are used to find the statistical significance of F1-score between the original datasets and the datasets from the MUOT algorithm with respect to four classifiers.

4.4 The Wilcoxon signed-rank test

The Wilcoxon signed-rank tests are used to evaluate the statistical significant improvement of datasets from the MUOT algorithm against the original datasets. In each test, the original datasets will be evaluated by 4 standard classifiers compared with the datasets generated from the MUOT algorithm based on the same classifier. Table 4 showed the p-values from the Wilcoxon signed-rank test if the p-value is less than 0.05, then it is considered to be significantly different.

Table 4. Wilcoxon signed-rank test, p-values of each dataset

Collection	Subcollection	P-value		
		precision	recall	F1-score
IR = 0.1	#cluster			
	2	0.004181	3.05E-05	0.015503
	3	3.35E-02	6.10E-05	0.000214
IR = 0.2	4	4.04E-01	3.05E-05	0.000305
	2	6.10E-05	3.05E-05	4.04E-01
	3	4.27E-04	3.05E-05	9.16E-05
IR = 0.3	4	6.10E-05	3.05E-05	6.29E-03
	2	3.05E-05	3.05E-05	0.175354
	3	9.16E-05	3.05E-05	0.028992
UCI collection	4	3.05E-05	3.05E-05	0.433197
		4.75E-01	3.62E-05	7.30E-03

For collection 3 with IR = 0.3 and the number of clusters = 2 and 4, it shows no significantly different performances of F1-score since their p-values are higher than 0.05. While all other collections, the p-values are smaller than 0.05 so the significant improvement can be obtained using MUOT. It can be concluded that MUOT is more effective on imbalance datasets having IR value less than or equal 0.2 from the datasets.

5 Conclusion

This paper proposed the undersampling and oversampling techniques using MOF for a class imbalance problem, called MUOT (Mass ratio variance majority undersampling and minority oversampling technique). It selects abnormal instances using MOF from the parameter-free outlier scoring method with the 90 percentile threshold. The undersampling step performs on majority instances having MOF score above 90 percentile and the oversampling step performs on abnormal minority instances using the same threshold setting inside the ball that does not include any majority instance according to MOF scores. This enlarges the minority regions and aids classifiers to recognize more minority instances.

The experiments with different IR values shows the improved performance of MUOT for recall and F1-score. In addition, datasets having IR less than 0.3 will be improved using MUOT. So that MUOT can handle imbalance datasets very effectively when a dataset is imbalanced. More characteristics of datasets should be investigated further via MUOT and the threshold values for undersampling and oversampling should be investigated.

References

- [1] Ali A, Ralescu A, Shamsuddin SM. Classification with class imbalance problem: A review. *Int. J. Advance Soft Compu.* 2015 Jan. vol. 5, no. 3, p.176-204.

- [2] Aweyemi JO, Adetunmbi AO, Oluwadare SA. Credit card fraud detection using machine learning techniques: A comparative analysis. *International Conference on Computing Networking and Informatics (ICCNi)*; 2017 Oct 29-31. p. 1-9.
- [3] Kononenko I. Machine learning for medical diagnosis: history, state of the art and perspective. *Artificial Intelligence in Medicine*. 2001 Aug. vol. 23, no. 1, p. 89-109.
- [4] Mozina M, Zabkar J, Bratko I. Argument based machine learning. *Artificial Intelligence*. 2007 Jul-Oct. vol. 171, no. 10–15, p. 922-937.
- [5] Chawla NV, Bowyer KW, Hall LO, Kegelmeyer WP. SMOTE: Synthetic Minority Over-sampling Technique. *Journal of Artificial Intelligence Research*. 2002. vol. 16, p. 321–357.
- [6] Han H, Wang WY, Mao BH. Borderline-SMOTE: A New Over-Sampling Method in Imbalanced Data Sets Learning. In: Huang DS, Zhang XP, Huang GB, editors. *Advances in Intelligent Computing*. ICIC; 2005. *Lecture Notes in Computer Science*; Berlin, Heidelberg, Springer. vol. 3644, p. 878-887.
- [7] Bunkhumpornpat C, Sinapiromsaran K, Lursinsap C. Safe-Level-SMOTE: Safe-Level-Synthetic Minority Over-Sampling Technique for Handling the Class Imbalanced Problem. In Theeramunkong T, Kijssirikul B, Cercone N, Ho TB, editors. *Advances in Knowledge Discovery and Data Mining*. PAKDD; 2009. *Lecture Notes in Computer Science*; Berlin, Heidelberg, Springer. vol. 5476, p. 475-482.
- [8] Rout N, Mishra D, Mallick MK. Handling Imbalanced Data: A Survey. In: Reddy M, Viswanath K, K.M. S, editors. *International Proceedings on Advances in Soft Computing, Intelligent Systems and Applications*; 2017 Dec 28. *Advances in Intelligent Systems and Computing*; Singapore, Springer. vol 628, p. 431-443.
- [9] Gosain A, Sardana S. Handling class imbalance problem using oversampling techniques: A review, *International Conference on Advances in Computing, Communications and Informatics*; 2017 Sep 13-16. p. 79-85.
- [10] Bunkhumpornpat C, Sinapiromsaran K, Lursinsap C. DBSMOTE: Density-Based Synthetic Minority Over-sampling TEchnique. *Appl Intell* 36. 2012 Apr. p. 664–684.
- [11] Chiamanusorn C, Sinapiromsaran K. Extreme Anomalous Oversampling Technique for Class Imbalance. In *Proceedings of the 2017 International Conference on Information Technology (ICIT 2017)*; 2017 Dec 27. *Association for Computing Machinery*, New York, NY, USA. p. 341–345.
- [12] Liu X, Wu J, Zhou Z. Exploratory Undersampling for Class-Imbalance Learning. In *IEEE Transactions on Systems, Man, and Cybernetics, Part B (Cybernetics)*; 2009 Apr. vol. 39, no. 2, p. 539-550.
- [13] Bunkhumpornpat C, Sinapiromsaran K. DBMUTE: density-based majority under-sampling technique. *Knowl Inf Syst* 50. 2017 Mar. p. 827–850.
- [14] Junsomboon N, Phienthrakul T. Combining Over-Sampling and Under-Sampling Techniques for Imbalance Dataset. In *Proceedings of the 9th International Conference on Machine Learning and Computing*; 2017 Feb 24. USA, New York, *Association for Computing Machinery*. p. 243–247.
- [15] Sahin Y, Bulkan S, Duman E. A cost-sensitive decision tree approach for fraud detection. *Expert Systems with Applications*. 2013 Nov 1. vol. 40, no. 15, p. 5916-5923.
- [16] Boonchuay K, Sinapiromsaran K, Lursinsap C. Decision tree induction based on minority entropy for the class imbalance problem. *Pattern Anal Applic* 20. 2017 Aug. p. 769–782.
- [17] Sagoolmuang A, Sinapiromsaran K. Oblique Decision Tree Algorithm with Minority Condensation for Class Imbalanced Problem. *Engineering Journal*. 2020 Feb 8. vol. 24, no. 1, p. 221-237.
- [18] Sagoolmuang A, Sinapiromsaran K. Decision Tree Algorithm with Class Overlapping-Balancing Entropy for Class Imbalanced Problem. *International Journal of Machine Learning and Computing*. 2020 May 3. vol. 10, no. 3, p. 444-451.
- [19] Suebkul K, Sinapiromsaran K. Recursive Tube-Partitioning Algorithm for a Class Imbalance Problem. *Thai Journal of Mathematics*. 2020. vol. 18, no. 4, p.2041-2051.
- [20] Thanathamathee P, Lursinsap C. Handling imbalanced data sets with synthetic boundary data generation using bootstrap re-sampling and AdaBoost techniques. *Pattern Recognition Letters*. 2013 Sep 1. vol. 34, no. 12, p. 1339-1347.
- [21] Sun Y, Kamel MS, Wong AKC, Wang Y. Cost-sensitive boosting for classification of imbalanced data. *Pattern Recognition*. 2007 Dec. vol. 40, no. 12, p. 3358-3378.
- [22] Breiman L. Bagging Predictors. *Machine Learning* 24. 1996 Aug. p. 123-140.
- [23] Devi D, Biswas S, Purkayastha B. Redundancy-driven modified Tomek-link based undersampling: A solution to class imbalance. *Pattern Recognition Letters*. 2017 Jul 1. vol. 93, p. 3-12.
- [24] Changsakul P, Boonsiri S, Sinapiromsaran K, Mass-ratio-variance based Outlier Factor. 18th *International Joint Conference on Computer Science and Software Engineering (JCSSE)*; 2021 Jul, p. 1-5.

Hierarchical Structure in Fuzzy Multi-Information Granular Computing Model

WEIJIE LIU^a, QINGHAI WANG^{a,1}

^a*School of Computing, Qinghai Normal University, Xining 810001, P.R. China*

Abstract. Granularity analysis and measurements for complex data environment are important tools to describe the essential attributes of the granular computing model(GCM). Firstly, based on fuzzy multiple relations, this paper defines a multi-fuzzy granular structure, and studies the hierarchical characteristics and relates mathematical conclusions of the four fuzzy multiple partial-order relations on the structure; Secondly, the measurement method of multi-fuzzy information granularity is proposed, and its properties of measurements are analyzed; Finally, the axiomatic definition of multi-fuzzy information granularity and its properties are discussed.

Keywords. Granular computing; fuzzy multi-information GCM; multi-fuzzy information granularity; partial-order relationship; axiomatic method

1. Introduction

Zadeh proposed the concept of granular computing in 1996[1]. He elaborated that human cognition has three main concepts, namely granulation (decomposing the whole into parts), organization (integrating the parts into the whole), and causation (connections between parts)[1][2]. Since granular computing covers the research of granular theory, methodology, technology and tools, it has become one of the research hotspots in the field of artificial intelligence in recent years, and has been widely used in machine learning, decision analysis, process control, pattern recognition and data mining, etc. Also the ideological of granular computing is structured thinking, peculiaritied by hierarchical modeling, comprehending, processing and learning[3]. Information system is the carrier for us to obtain the most information resources[4]. In granular computing, it is one of the important ways of knowledge representation[5]. The information granularity of an information system reflects the uncertainty measure of its real structure[6]. In recent years, measurement methods have been widely studied. How to analyze the granular structure and measurement of complex information granular computing models are particularly important for the measurement of information uncertainty of complex data in reality. At present, people have proposed a variety of information granularity measurement forms

¹Corresponding Author: Qinghai Wang, Qinghai Normal University, Xining, The Chinese; E-mail: wangqinghai@qhnu.edu.cn. The authors are grateful to the financial support from the National Social Science Project, 17XTQ013, Phased results.

in information systems for different data environments[7-12]. Qian et al. mainly studied the information granularity in the information system under the fuzzy binary relation, discussed the three partial-order relations on the fuzzy-binary information granularity, and gave the axiomatic definition of the fuzzy binary information granular[13]. Under the framework of Qian's research on information granularity in information systems, other scholars have expanded their research content. Yang et al. proposed the granularity in the intuitionistic fuzzy information system, gave the granularity and its axiomatic definition, and studied related properties[14]. Based on the interval-value hesitant fuzzy binary relation, Lu et al. gave the concept of interval-valued hesitant fuzzy granularity structure, calculated the interval-valued hesitant fuzzy information granularity; Meanwhile lu et al. put forward the partial-order relationship on interval-valued hesitant fuzzy information granularity[15], and further researched its internal hierarchical granularity structure. In view of the constantly quantified multi-data environment, the research on the hierarchical structure of its internal granularity and its measurement is undoubtedly of great significance to reveal the essence of its internal structure.

Yager first proposed fuzzy multiset, its biggest advantage is to allow the membership of elements in the universe to appear multiple times with the same or different membership values[16]. Kim et al. studied the basic relations and operations of fuzzy multisets, and discussed the application of fuzzy multisets in fuzzy relational database systems [17]. Miyamoto gave the definition of the module of fuzzy multiset, and considered the application of commutativity in fuzzy multisets [18]. El-Azab, M.S. defined fuzzy multi correlation measure and many of its properties are investigated[19]. However, few people have discussed the partial-order relation between the multi-fuzzy information granular structure based on the fuzzy multirelation. And few people use information granularity to study the uncertainty measurement of fuzzy multi-information GCM. Therefore, it is necessary to study the multi-fuzzy granular structure of fuzzy multiple information granularity and information measurement.

The main contributions of this paper are as follow:

- The granular structure under fuzzy multiple environments is defined, and three operations are discussed.
- Four partial-order relations between multi-fuzzy granular structures are established, and their properties are proved mathematically.
- Uncertainty measures of fuzzy multi-information are studied by using information granularity.
- Axiomatization method of fuzzy multi-information granularity presented in this paper has important theoretical significance and application value for multi-information granular computing model.

This paper is organized as follows. Section 2 reviews some basic concepts: fuzzy multisets, the number of membership degrees of elements in the fuzzy multisets, the operations between fuzzy multisets, and proposes a fuzzy multirelation. Section 3 studies the multi-fuzzy granular structure and the three operations. In the section 4, we present for the hierarchical characteristics and related mathematical conclusions of the four fuzzy multiple partial-order relations on the structure. In the Section 5, the multi-fuzzy information granularity and its axiomatization method are defined, and under the four partial-order relations proposed above, the properties of multi-fuzzy information granularity are studied. Finally, section 6 gives the conclusion.

2. Preliminaries

In this section, we will review several basic concepts, such as fuzzy multisets, the number of membership degrees of elements in the fuzzy multisets, the operations between fuzzy multisets, and proposes a fuzzy multirelation.

Fuzzy multisets is an extension of multisets, which is defined as follows:

Definition 2.1[20]: Let $U = \{x_1, x_2, \dots, x_n\}$ be a finite and nonempty set. A fuzzy multisets M on U can be defined as $M = \{d_M(x_1)/x_1, d_M(x_2)/x_2, \dots, d_M(x_n)/x_n\}$, in which $d_M(x_i) = \{d_M^1(x_i), d_M^2(x_i), \dots, d_M^k(x_i)\}$ is a finite multiset of the $[0, 1]$, denoting the possible membership degrees of the x_i to the set M , and $d_M^1(x_i) \geq d_M^2(x_i) \geq \dots \geq d_M^k(x_i)$. In this paper, all fuzzy multisets are defined as $FM(U)$.

Example 1: Consider a fuzzy mltiset $A = \{(x_1, 0.3), (x_1, 0.4), (x_1, 0.5), (x_1, 0.5), (x_2, 0.4), (x_2, 0.6)\}$ of $U = \{x_1, x_2\}$. We may write $A = \{\{0.3, 0.4, 0.5, 0.5\}/x_1, \{0.4, 0.6\}/x_2\}$, in which the multiset of memberships $\{0.3, 0.4, 0.5, 0.5\}$ and $\{0.4, 0.6\}$ correspond to x_1 and x_2 .

Definition 2.2: Let $U = \{x_1, x_2, \dots, x_n\}$ be a finite and nonempty set. Let $A, B \in FM(U)$. $A = \{d_A(x_1)/x_1, d_A(x_2)/x_2, \dots, d_A(x_n)/x_n\}$, $B = \{d_B(x_1)/x_1, d_B(x_2)/x_2, \dots, d_B(x_n)/x_n\}$, where $d_A(x_i) = \{d_A^1(x_i), d_A^2(x_i), \dots, d_A^p(x_i)\}$ and $d_B(x_i) = \{d_B^1(x_i), d_B^2(x_i), \dots, d_B^q(x_i)\}$. The number of values in seqence $d_A(x_i)$ is defined as

$$L(x_i, A) = \max\{s : d_A^s(x_i) \neq 0\}.$$

We can get $L(x_i; A, B) = \max\{L(x_i; A), L(x_i; B)\}$. The resulting length for A and B is defined by

$$L(x_i; A, B) = \max\{p, q\}.$$

We sometimes write $L(x_i)$ instead of $L(x_i; A, B)$ when no ambiguity arises.

Definition 2.3[20]: The number of elements, or cardinality of a fuzzy multiset is given by $|M| = \sum_{x_i \in U} \sum_{s=1}^{L(x_i; M)} d_M^s(x_i)$.

Definition 2.4[21]: Let a universe $U = \{x_1, x_2, \dots, x_n\}$ be a finite universe of discourse. Then their basic operations for the membership sequences between A and B are as follows:

$$d_{A \cup B}^s(x_i) = d_A^s(x_i) \vee d_B^s(x_i), s = 1, 2, \dots, L(x_i); \tag{1}$$

$$d_{A \cap B}^s(x_i) = d_A^s(x_i) \wedge d_B^s(x_i), s = 1, 2, \dots, L(x_i); \tag{2}$$

$$\sim d_A^s(x_i) = 1 - d_A^s(x_i), s = 1, 2, \dots, L(x_i; A). \tag{3}$$

Note: If $\forall A, B \in FM(U)$, in order to have a correct comparison and define an operation between two fuzzy multisets A and B , the membership sequences $d_A^1(x_i), d_A^2(x_i), \dots$,

$d_A^p(x_i)$ and $d_B^1(x_i), d_B^2(x_i), \dots, d_B^q(x_i)$ should have the equal length[20]. If $p < q$, we therefore extend $d_A(x_i)$ with maximum element $d_A^p(x_i)$ until it has same length with $d_B(x_i)$.

Definition 2.5: Let $U = \{x_1, x_2, \dots, x_n\}$ be a finite and nonempty set. Then the fuzzy multi-subset defined in the direct product space $U \times U$ is called the fuzzy multirelation \tilde{R}^* on U , \tilde{R}^* is given by $\tilde{R}^* = \{dr(x_{ij})/x_{ij} \mid x_{ij} = (x_i, x_j) \in U \times U, i, j = 1, 2, \dots, n\}$, where $dr(x_{ij})$ is a subset of the power set $[0, 1]$ representing the possible multiple membership degrees of the x_i and x_j .

3. Multi-Fuzzy Granular Structures

In Granular Computing, transformation among granular structures is a significant matter which involves composition, disintegration and transformation. A class of fuzzy information particles produced by fuzzy multiple relations in the universe of discourse is called multi-fuzzy granular structure. The granular structure under multi-fuzzy environment is defined as follow.

Definition 3.1: Suppose $U = \{x_1, x_2, \dots, x_n\}$, \tilde{R}^* is a fuzzy multirelation on U . Then the multi-fuzzy granular structure of U is defined as

$$K(\tilde{R}^*) = (S_{\tilde{R}^*}(x_1), S_{\tilde{R}^*}(x_2), \dots, S_{\tilde{R}^*}(x_n)) \tag{4}$$

where $S_{\tilde{R}^*}(x_i) = (\frac{dr(x_{i1})}{x_i}, \frac{dr(x_{i2})}{x_i}, \dots, \frac{dr(x_{in})}{x_i})$ is a multi-fuzzy information granule, $dr(x_{ij}) = \{d_r^1(x_{ij}), d_r^2(x_{ij}), \dots, d_r^s(x_{ij})\}$ denotes a set about the possible multiple degrees of equivalence and between x_i and x_j .

Definition 3.2: Let $K(\tilde{P}^*), K(\tilde{Q}^*) \in K(U)$, $K(\tilde{P}^*) = (S_{\tilde{P}^*}(x_1), S_{\tilde{P}^*}(x_2), \dots, S_{\tilde{P}^*}(x_n))$, $S_{\tilde{P}^*}(x_i) = (\frac{dp(x_{i1})}{x_i}, \frac{dp(x_{i2})}{x_i}, \dots, \frac{dp(x_{in})}{x_i})$, in which $dp(x_{ij}) = \{d_p^1(x_{ij}), d_p^2(x_{ij}), \dots, d_p^s(x_{ij})\}$, $s = L(x_{ij}; S_{\tilde{P}^*}(x_i))$; $K(\tilde{Q}^*) = (S_{\tilde{Q}^*}(x_1), S_{\tilde{Q}^*}(x_2), \dots, S_{\tilde{Q}^*}(x_n))$, $S_{\tilde{Q}^*}(x_i) = (\frac{dq(x_{i1})}{x_i}, \frac{dq(x_{i2})}{x_i}, \dots, \frac{dq(x_{in})}{x_i})$, $dq(x_{ij}) = \{d_q^1(x_{ij}), d_q^2(x_{ij}), \dots, d_q^t(x_{ij})\}$, and $t = L(x_{ij}; S_{\tilde{Q}^*}(x_i))$. Refer to definition 2.2, the number of values in $dp(x_{ij})$ is defined as

$$L(x_{ij}; S_{\tilde{P}^*}(x_i)) = \max \{m : d_p^m(x_{ij}) \neq 0\}.$$

We can get $L(x_{ij}; S_{\tilde{P}^*}(x_i), S_{\tilde{Q}^*}(x_i)) = \max \{L(x_{ij}; S_{\tilde{P}^*}(x_i)), L(x_{ij}; S_{\tilde{Q}^*}(x_i))\}$. The resulting length for $S_{\tilde{P}^*}(x_i), S_{\tilde{Q}^*}(x_i)$ is defined by

$$L(x_{ij}; S_{\tilde{P}^*}(x_i), S_{\tilde{Q}^*}(x_i)) = \max \{s, t\}.$$

We sometimes write $L(x_{ij})$ instead of $L(x_{ij}; S_{\tilde{P}^*}(x_i), S_{\tilde{Q}^*}(x_i))$ when no ambiguity arises.

Definition 3.3: Let $K(\tilde{R}^*) \in K(U)$, $K(\tilde{R}^*) = (S_{\tilde{R}^*}(x_1), S_{\tilde{R}^*}(x_2), \dots, S_{\tilde{R}^*}(x_n))$, where $S_{\tilde{R}^*}(x_i) = (\frac{dr(x_{i1})}{x_i}, \frac{dr(x_{i2})}{x_i}, \dots, \frac{dr(x_{in})}{x_i})$ is a multi-fuzzy information granule, $dr(x_{ij}) = \{d_r^1(x_{ij}), d_r^2(x_{ij}), \dots, d_r^s(x_{ij})\}$ and $s = L(x_{ij}; S_{\tilde{R}^*}(x_i))$. The cardinality of the multi-fuzzy granule $S_{\tilde{R}^*}(x_i)$ can be calculated with

$$|S_{\tilde{R}^*}(x_i)| = \sum_{j=1}^n \left(\frac{\sum_{s=1}^{L(x_{ij}; S_{\tilde{R}^*}(x_i))} d_r^s(x_{ij})}{L(x_{ij}; \tilde{R}^*)} \right) \tag{5}$$

which is a natural extension of the cardinality of fuzzy sets.

Given a family of fuzzy multi-granular structures $GCM = (U, \tilde{\mathcal{H}}^*)$, we also denote the multi-fuzzy granular structure induced by $\tilde{P}^* \in \tilde{\mathcal{H}}^*$ by $K(\tilde{P}^*) = (S_{\tilde{P}^*}(x_1), S_{\tilde{P}^*}(x_2), \dots, S_{\tilde{P}^*}(x_n))$, where $S_{\tilde{P}^*}(x_i) = (\frac{dp(x_{i1})}{x_i}, \frac{dp(x_{i2})}{x_i}, \dots, \frac{dp(x_{in})}{x_i})$. Moreover, let $K(U)$ be the collection of all multi-fuzzy granular structures on U .

Example 2: Let $K(\tilde{R}^*) = (S_{\tilde{R}^*}(x_1), S_{\tilde{R}^*}(x_2))$.

$$M(\tilde{R}^*) = \left(\begin{array}{cc} \{0.2, 0.2\} & \{0.3, 0.3, 0.6\} \\ \{0.6, 0.6, 0.8\} & \{0.1, 0.3, 0.3, 0.4\} \end{array} \right)$$

where $dr(x_{11}) = \{d_r^1(x_{11}), d_r^2(x_{11})\} = \{0.2, 0.2\}$, $dr(x_{12}) = \{d_r^1(x_{12}), d_r^2(x_{12}), d_r^3(x_{12})\} = \{0.3, 0.3, 0.6\}$ and $S_{\tilde{R}^*}(x_1) = (\frac{dr(x_{11})}{x_1}, \frac{dr(x_{12})}{x_1}) = (\frac{\{0.2, 0.2\}}{x_1}, \frac{\{0.3, 0.3, 0.6\}}{x_1})$. According to the definition of cardinality, we can get $|S_{\tilde{R}^*}(x_1)| = 0.2 + 0.4 = 0.6$.

In fact, Qian [13] proposed four operations of the granular structure, proving that the new fuzzy granular structure can be generated by these four operations. Therefore, three operations(intersection operation, union operation and complement operation) for multi-fuzzy granular structures are given below. Before this, We first give the definition of \sqcap , \sqcup and \sim in the multi-fuzzy granules.

Definition 3.4: Let $K(\tilde{P}^*), K(\tilde{Q}^*) \in K(U)$, $K(\tilde{P}^*) = (S_{\tilde{P}^*}(x_1), S_{\tilde{P}^*}(x_2), \dots, S_{\tilde{P}^*}(x_n))$, $S_{\tilde{P}^*}(x_i) = (\frac{dp(x_{i1})}{x_i}, \frac{dp(x_{i2})}{x_i}, \dots, \frac{dp(x_{in})}{x_i})$, in which $dp(x_{ij}) = \{d_p^1(x_{ij}), d_p^2(x_{ij}), \dots, d_p^s(x_{ij})\}$, and $s = L(x_{ij}; S_{\tilde{P}^*}(x_i))$; Also $K(\tilde{Q}^*) = (S_{\tilde{Q}^*}(x_1), S_{\tilde{Q}^*}(x_2), \dots, S_{\tilde{Q}^*}(x_n))$, $S_{\tilde{Q}^*}(x_i) = (\frac{dq(x_{i1})}{x_i}, \frac{dq(x_{i2})}{x_i}, \dots, \frac{dq(x_{in})}{x_i})$, in which $dq(x_{ij}) = \{d_q^1(x_{ij}), d_q^2(x_{ij}), \dots, d_q^t(x_{ij})\}$ and $t = L(x_{ij}; S_{\tilde{Q}^*}(x_i))$. Three operators \sqcap , \sqcup and \sim on objects in the multi-fuzzy granules are defined as follow:

$$\begin{aligned} S_{\tilde{P}^*}(x_i) \sqcap S_{\tilde{Q}^*}(x_i) &= \left\{ \frac{dp(x_{i1}) \cap dq(x_{i1})}{x_i}, \frac{dp(x_{i2}) \cap dq(x_{i2})}{x_i}, \dots, \frac{dp(x_{in}) \cap dq(x_{in})}{x_i} \right\} \\ &= \left\{ \frac{\{d_{p \cap q}^1(x_{i1}), d_{p \cap q}^2(x_{i1}), \dots, d_{p \cap q}^s(x_{i1})\}}{x_i}, \right. \\ &\quad \left. \frac{\{d_{p \cap q}^1(x_{i2}), d_{p \cap q}^2(x_{i2}), \dots, d_{p \cap q}^s(x_{i2})\}}{x_i}, \right. \\ &\quad \left. \dots, \frac{\{d_{p \cap q}^1(x_{in}), d_{p \cap q}^2(x_{in}), \dots, d_{p \cap q}^s(x_{in})\}}{x_i} \right\} \end{aligned} \tag{6}$$

$$\begin{aligned}
 S_{\tilde{P}^*}(x_i) \sqcup S_{\tilde{Q}^*}(x_i) &= \left\{ \frac{dp(x_{i1}) \cup dq(x_{i1})}{x_i}, \frac{dp(x_{i2}) \cup dq(x_{i2})}{x_i}, \dots, \frac{dp(x_{in}) \cup dq(x_{in})}{x_i} \right\} \\
 &= \left\{ \frac{\{d_{p \cup q}^1(x_{i1}), d_{p \cup q}^2(x_{i1}), \dots, d_{p \cup q}^s(x_{i1})\}}{x_i}, \right. \\
 &\quad \left. \frac{\{d_{p \cup q}^1(x_{i2}), d_{p \cup q}^2(x_{i2}), \dots, d_{p \cup q}^s(x_{i2})\}}{x_i}, \right. \\
 &\quad \left. \dots, \frac{\{d_{p \cup q}^1(x_{in}), d_{p \cup q}^2(x_{in}), \dots, d_{p \cup q}^s(x_{in})\}}{x_i} \right\} \tag{7}
 \end{aligned}$$

$$\sim S_{\tilde{P}^*}(x_i) = \left(\frac{\sim dp(x_{i1})}{x_i}, \frac{\sim dp(x_{i2})}{x_i}, \dots, \frac{\sim dp(x_{in})}{x_i} \right) \tag{8}$$

in which, $\sim dp(x_{ij}) = \{(1 - d_p^1(x_{ij})), (1 - d_p^2(x_{ij})), \dots, (1 - d_p^s(x_{ij}))\}, i, j = 1, 2, \dots, n$.

Note, suppose $t < s$, we therefore extend $d_q(x_{ij})$ with maximum element $d_q^t(x_{ij})$ until it has same length with $d_p(x_{ij})$.

Definition 3.5: Let $K(U)$ be the collection of all multi-fuzzy granular structures on U , $K(\tilde{P}^*), K(\tilde{Q}^*) \in K(U)$. Three operators \cap, \cup and \wr are defined as follow:

$$K(\tilde{P}^*) \cap K(\tilde{Q}^*) = \{S_{\tilde{P}^*}(x_i) \cap S_{\tilde{Q}^*}(x_i)\} \tag{9}$$

$$K(\tilde{P}^*) \cup K(\tilde{Q}^*) = \{S_{\tilde{P}^*}(x_i) \cup S_{\tilde{Q}^*}(x_i)\} \tag{10}$$

$$\wr K(\tilde{P}^*) = \{S_{\tilde{P}^*}(x_i) \mid \wr S_{\tilde{P}^*}(x_i) = \sim S_{\tilde{P}^*}(x_i)\} \tag{11}$$

Note: The offered three operators can be regarded as intersection operation, union operation and complement operation in-between multi-fuzzy granular structures, which are used to refine and roughen multi-fuzzy granular structures and calculate complement of a multi-fuzzy granular structure, respectively. Next, we investigate some basic mathematical properties of these three operators.

Theorem 3.1: Let \cap, \cup and \wr be three operators on $K(U)$, they have the following algebra properties:

- (1) $K(\tilde{P}^*) \cap K(\tilde{P}^*) = K(\tilde{P}^*), K(\tilde{P}^*) \cup K(\tilde{P}^*) = K(\tilde{P}^*);$
- (2) $K(\tilde{P}^*) \cap K(\tilde{Q}^*) = K(\tilde{Q}^*) \cap K(\tilde{P}^*), K(\tilde{P}^*) \cup K(\tilde{Q}^*) = K(\tilde{Q}^*) \cup K(\tilde{P}^*);$
- (3) $K(\tilde{P}^*) \cap (K(\tilde{P}^*) \cup K(\tilde{Q}^*)) = K(\tilde{P}^*), K(\tilde{P}^*) \cup (K(\tilde{P}^*) \cap K(\tilde{Q}^*)) = K(\tilde{P}^*);$
- (4) $(K(\tilde{P}^*) \cap K(\tilde{Q}^*)) \cap K(\tilde{R}^*) = K(\tilde{P}^*) \cap (K(\tilde{Q}^*) \cap K(\tilde{R}^*));$
 $(K(\tilde{P}^*) \cup K(\tilde{Q}^*)) \cup K(\tilde{R}^*) = K(\tilde{P}^*) \cup (K(\tilde{Q}^*) \cup K(\tilde{R}^*)).$

Proof: Item (1)(2)(3) and (4) are straightforward by Definition 3.5.

Theorem 3.2: Let \cap, \cup and \wr be three operators on $K(U)$, then

- (1) $\wr(\wr K(\tilde{P}^*)) = K(\tilde{P}^*);$
- (2) $\wr(K(\tilde{P}^*) \cap K(\tilde{Q}^*)) = \wr K(\tilde{P}^*) \cup \wr K(\tilde{Q}^*);$

$$(3) \ \imath(K(\tilde{P}^*) \cup K(\tilde{Q}^*)) = \imath K(\tilde{P}^*) \cap \imath K(\tilde{Q}^*).$$

Proof: According to these operators of Definition 3.3, we can get (1) $\imath K(\tilde{P}^*) = \{\imath S_{\tilde{P}^*}(x_i) | \imath S_{\tilde{P}^*}(x_i) \sim S_{\tilde{P}^*}(x_i)\}$, where $\sim dp(x_{ij}) = \{(1 - d_p^1(x_{ij})), (1 - d_p^2(x_{ij})), \dots, (1 - d_p^s(x_{ij}))\}$; Then $\sim(\sim dp(x_{ij})) = \{1 - (1 - d_p^1(x_{ij})), 1 - (1 - d_p^2(x_{ij})), \dots, 1 - (1 - d_p^s(x_{ij}))\}$, $\sim(\sim S_{\tilde{P}^*}(x_i)) = (\frac{\sim(\sim dp(x_{i1}))}{x_i}, \frac{\sim(\sim dp(x_{i2}))}{x_i}, \dots, \frac{\sim(\sim dp(x_{in}))}{x_i}) = S_{\tilde{P}^*}(x_i), i, j = 1, 2, \dots, n$. Therefore, $\imath(\imath K(\tilde{P}^*)) = K(\tilde{P}^*)$ holds. Items (2) and (3) are straightforward by Definition 3.4.

4. Partial-Order Relations on Multi-Fuzzy Granular Structures

Partial-order relation is one of the important ways to describe the granular structure. In the following, we propose four partial-order relations on multi-fuzzy granular structures.

Definition 4.1: Let $S_{\tilde{P}^*}(x_i) = (\frac{dp(x_{i1})}{x_i}, \frac{dp(x_{i2})}{x_i}, \dots, \frac{dp(x_{in})}{x_i})$, $S_{\tilde{Q}^*}(x_i) = (\frac{dq(x_{i1})}{x_i}, \frac{dq(x_{i2})}{x_i}, \dots, \frac{dq(x_{in})}{x_i})$. If $dp(x_{ij}) \leq dq(x_{ij})$, then $S_{\tilde{P}^*}(x_i) \subseteq S_{\tilde{Q}^*}(x_i)$.

Definition 4.2: Let $K(\tilde{P}^*), K(\tilde{Q}^*) \in K(U)$, $K(\tilde{P}^*) = (S_{\tilde{P}^*}(x_1), S_{\tilde{P}^*}(x_2), \dots, S_{\tilde{P}^*}(x_n))$, $S_{\tilde{P}^*}(x_i) = (\frac{dp(x_{i1})}{x_i}, \frac{dp(x_{i2})}{x_i}, \dots, \frac{dp(x_{in})}{x_i})$, in which $dp(x_{ij}) = \{d_p^1(x_{ij}), d_p^2(x_{ij}), \dots, d_p^s(x_{ij})\}$, and $s = L(x_{ij}; S_{\tilde{P}^*}(x_i))$; Also $K(\tilde{Q}^*) = (S_{\tilde{Q}^*}(x_1), S_{\tilde{Q}^*}(x_2), \dots, S_{\tilde{Q}^*}(x_n))$, $S_{\tilde{Q}^*}(x_i) = (\frac{dq(x_{i1})}{x_i}, \frac{dq(x_{i2})}{x_i}, \dots, \frac{dq(x_{in})}{x_i})$, where $dq(x_{ij}) = \{d_q^1(x_{ij}), d_q^2(x_{ij}), \dots, d_q^t(x_{ij})\}$, $t = L(x_{ij}; S_{\tilde{Q}^*}(x_i))$ and $i, j = 1, 2, \dots, n$, a partial-order relation \preceq_1 is defined as

$$\begin{aligned} K(\tilde{P}^*) \preceq_1 K(\tilde{Q}^*) &\Leftrightarrow S_{\tilde{P}^*}(x_i) \subseteq S_{\tilde{Q}^*}(x_i) \\ &\Leftrightarrow dp(x_{ij}) \leq dq(x_{ij}) \\ &\Leftrightarrow d_p^1(x_{ij}) \leq d_q^1(x_{ij}), d_p^2(x_{ij}) \leq d_q^2(x_{ij}), \dots, d_p^s(x_{ij}) \leq d_q^s(x_{ij}). \end{aligned}$$

Clearly, $(K(U), \preceq_1)$ is a poset. Furthermore,

$$\begin{aligned} K(\tilde{P}^*) = K(\tilde{Q}^*) &\Leftrightarrow S_{\tilde{P}^*}(x_i) = S_{\tilde{Q}^*}(x_i) \\ &\Leftrightarrow dp(x_{ij}) = dq(x_{ij}) \\ &\Leftrightarrow d_p^1(x_{ij}) = d_q^1(x_{ij}), d_p^2(x_{ij}) = d_q^2(x_{ij}), \dots, d_p^s(x_{ij}) = d_q^s(x_{ij}), i, j = \end{aligned}$$

$1, 2, \dots, n$, which can be written as $\tilde{P}^* = \tilde{Q}^*$.

$$K(\tilde{P}^*) \prec_1 K(\tilde{Q}^*) \Leftrightarrow K(\tilde{P}^*) \preceq_1 K(\tilde{Q}^*) \text{ and } K(\tilde{P}^*) \neq K(\tilde{Q}^*) \text{ is denoted by } \tilde{P}^* \prec_1 \tilde{Q}^*.$$

Theorem 4.1: Let \cup, \cap and \imath be three operators on $K(U)$, the following properties hold.

- (1) If $K(\tilde{P}^*) \preceq_1 K(\tilde{Q}^*)$, then $\imath K(\tilde{Q}^*) \preceq_1 \imath K(\tilde{P}^*)$;
- (2) $K(\tilde{P}^*) \preceq_1 K(\tilde{P}^*) \cup K(\tilde{Q}^*), K(\tilde{Q}^*) \preceq_1 K(\tilde{P}^*) \cup K(\tilde{Q}^*)$;
- (3) $K(\tilde{P}^*) \cap K(\tilde{Q}^*) \preceq_1 K(\tilde{P}^*), K(\tilde{P}^*) \cap K(\tilde{Q}^*) \preceq_1 K(\tilde{Q}^*)$.

Proof:

$$\begin{aligned} K(\tilde{P}^*) \preceq_1 K(\tilde{Q}^*) &\Rightarrow \forall x_i \in U, S_{\tilde{P}^*}(x_i) \subseteq S_{\tilde{Q}^*}(x_i), i = 1, 2, \dots, n. \\ &\Rightarrow \forall x_i \in U, dp(x_{ij}) \leq dq(x_{ij}), i, j = 1, 2, \dots, n. \\ &\Rightarrow \forall x_i \in U, (1 - d_p^1(x_{ij})) \leq (1 - d_q^1(x_{ij})), (1 - d_p^2(x_{ij})) \leq \\ &\quad (1 - d_q^2(x_{ij})), \dots, (1 - d_p^s(x_{ij})) \leq (1 - d_p^s(x_{ij})), i, j = 1, 2, \dots, n. \\ &\Rightarrow \forall x_i \in U, \imath S_{\tilde{Q}^*}(x_i) \preceq_1 \imath S_{\tilde{P}^*}(x_i). \Rightarrow \imath K(\tilde{Q}^*) \preceq_1 \imath K(\tilde{P}^*). \end{aligned}$$

In the same way, items (2) and (3) are easily obtained by the Definition 4.2.

Example 3: Let $K(\tilde{P}^*), K(\tilde{Q}^*) \in K(U)$, \tilde{P}^* and \tilde{Q}^* are fuzzy multirelations on U , where $K(\tilde{P}^*) = (S_{\tilde{P}^*}(x_1), S_{\tilde{P}^*}(x_2))$ and $K(\tilde{Q}^*) = (S_{\tilde{Q}^*}(x_1), S_{\tilde{Q}^*}(x_2))$, The fuzzy multirelation is denoted by the following maxtrix:

$$M(\tilde{P}^*) = \left(\begin{array}{cc} \{0.1, 0.1, 0.2, 0.2\} & \{0.1, 0.1, 0.4\} \\ \{0.2, 0.5\} & \{0.2, 0.5, 0.5, 0.6, 0.7\} \end{array} \right)$$

$$M(\tilde{Q}^*) = \left(\begin{array}{cc} \{0.3, 0.3, 0.4\} & \{0.3, 0.4, 0.4\} \\ \{0.6, 0.6, 0.7, 0.8\} & \{0.3, 0.5, 0.6, 0.7, 0.8\} \end{array} \right)$$

From the values of these knowledge and the definition of \leq_1 , we know that $K(\tilde{P}^*) \leq_1 K(\tilde{Q}^*)$.

Definition 4.3: Let $K(\tilde{P}^*), K(\tilde{Q}^*) \in K(U)$, $K(\tilde{P}^*) = (S_{\tilde{P}^*}(x_1), S_{\tilde{P}^*}(x_2), \dots, S_{\tilde{P}^*}(x_n))$, $S_{\tilde{P}^*}(x_i) = (\frac{dp(x_{i1})}{x_i}, \frac{dp(x_{i2})}{x_i}, \dots, \frac{dp(x_{in})}{x_i})$, $dp(x_{ij}) = \{d_p^1(x_{ij}), d_p^2(x_{ij}), \dots, d_p^s(x_{ij})\}$, $i, j = 1, 2, \dots, n$ and $s = L(x_{ij}; S_{\tilde{P}^*}(x_i))$. then the definition of the mean degree of multiple membership is as follows:

$$\tilde{dp}(x_{ij}) = \frac{1}{L(x_{ij})} \sum_{s=1}^{L(x_{ij}; S_{\tilde{P}^*}(x_i))} d_p^s(x_{ij}) \tag{12}$$

Thus, the multi-fuzzy information granule can also be defined as

$$S_{\tilde{P}^*}(x_i) = (\frac{\tilde{dp}(x_{i1})}{x_i}, \frac{\tilde{dp}(x_{i2})}{x_i}, \dots, \frac{\tilde{dp}(x_{in})}{x_i}) \tag{13}$$

Definition 4.4: Let $S_{\tilde{P}^*}(x_i) = (\frac{\tilde{dp}(x_{i1})}{x_i}, \frac{\tilde{dp}(x_{i2})}{x_i}, \dots, \frac{\tilde{dp}(x_{in})}{x_i})$ and $S_{\tilde{Q}^*}(x_i) = (\frac{\tilde{dq}(x_{i1})}{x_i}, \frac{\tilde{dq}(x_{i2})}{x_i}, \dots, \frac{\tilde{dq}(x_{in})}{x_i})$, if $\tilde{dp}(x_{ij}) \leq \tilde{dq}(x_{ij})$, then $S_{\tilde{P}^*}(x_i) \sqsubseteq S_{\tilde{Q}^*}$.

Definition 4.5: Let $K(\tilde{P}^*), K(\tilde{Q}^*) \in K(U)$, where $K(\tilde{P}^*) = (S_{\tilde{P}^*}(x_1), S_{\tilde{P}^*}(x_2), \dots, S_{\tilde{P}^*}(x_n))$, $S_{\tilde{P}^*}(x_i) = (\frac{\tilde{dp}(x_{i1})}{x_i}, \frac{\tilde{dp}(x_{i2})}{x_i}, \dots, \frac{\tilde{dp}(x_{in})}{x_i})$, $K(\tilde{Q}^*) = (S_{\tilde{Q}^*}(x_1), S_{\tilde{Q}^*}(x_2), \dots, S_{\tilde{Q}^*}(x_n))$ and $S_{\tilde{Q}^*}(x_i) = (\frac{\tilde{dq}(x_{i1})}{x_i}, \frac{\tilde{dq}(x_{i2})}{x_i}, \dots, \frac{\tilde{dq}(x_{in})}{x_i})$, a partial-order relation \leq_2 is defined as $K(\tilde{P}^*) \leq_2 K(\tilde{Q}^*) \Leftrightarrow S_{\tilde{P}^*}(x_i) \sqsubseteq S_{\tilde{Q}^*}(x_i), i = 1, 2, \dots, n$

$$\Leftrightarrow dp(x_{ij}) \leq dq(x_{ij}), i, j = 1, 2, \dots, n,$$

$$\frac{\sum_{s=1}^{L(x_{ij}; S_{\tilde{P}^*}(x_i))} d_p^s(x_{ij})}{L(x_{ij}; S_{\tilde{P}^*}(x_i))} \leq \frac{\sum_{t=1}^{L(x_{ij}; S_{\tilde{Q}^*}(x_i))} d_q^t(x_{ij})}{L(x_{ij}; S_{\tilde{Q}^*}(x_i))}$$

in which $\tilde{dp}_{ij} = \frac{\sum_{s=1}^{L(x_{ij}; S_{\tilde{P}^*}(x_i))} d_p^s(x_{ij})}{L(x_{ij}; S_{\tilde{P}^*}(x_i))}$, $\tilde{dq}_{ij} = \frac{\sum_{t=1}^{L(x_{ij}; S_{\tilde{Q}^*}(x_i))} d_q^t(x_{ij})}{L(x_{ij}; S_{\tilde{Q}^*}(x_i))}$, should be written as $\tilde{P}^* \leq_2 \tilde{Q}^*$.

Furthermore,

$$K(\tilde{P}^*) \simeq K(\tilde{Q}^*) \Leftrightarrow S_{\tilde{P}^*}(x_i) \simeq S_{\tilde{Q}^*}(x_i), i = 1, 2, \dots, n.$$

$$\Leftrightarrow \tilde{dp}(x_{ij}) = \tilde{dq}(x_{ij}), i, j = 1, 2, \dots, n \text{ is written as } \tilde{P}^* \simeq \tilde{Q}^*.$$

$$K(\tilde{P}^*) \prec_2 K(\tilde{Q}^*) \Leftrightarrow K(\tilde{P}^*) \leq_2 K(\tilde{Q}^*) \text{ and } K(\tilde{P}^*) \not\approx K(\tilde{Q}^*) \text{ should be written as } \tilde{P}^* \prec_2 \tilde{Q}^*.$$

Theorem 4.2: Letting $K(U)$ be the collection of all multi-fuzzy granular structures on U , then $(K(U), \leq_2)$ is a poset.

Proof: Let $K(\tilde{P}^*), K(\tilde{Q}^*), K(\tilde{R}^*) \in K(U)$, $K(\tilde{P}^*) = (S_{\tilde{P}^*}(x_1), S_{\tilde{P}^*}(x_2), \dots, S_{\tilde{P}^*}(x_n))$,

$$S_{\tilde{P}^*}(x_i) = (\frac{\tilde{dp}(x_{i1})}{x_i}, \frac{\tilde{dp}(x_{i2})}{x_i}, \dots, \frac{\tilde{dp}(x_{in})}{x_i}), \tilde{dp}_{ij} = \frac{\sum_{s=1}^{L(x_{ij}; S_{\tilde{P}^*}(x_i))} d_p^s(x_{ij})}{L(x_{ij}; S_{\tilde{P}^*}(x_i))}; \text{ Also } K(\tilde{Q}^*) = (S_{\tilde{Q}^*}(x_1),$$

$$S_{\tilde{Q}^*}(x_2), \dots, S_{\tilde{Q}^*}(x_n)), S_{\tilde{Q}^*}(x_i) = (\frac{\tilde{dq}(x_{i1})}{x_i}, \frac{\tilde{dq}(x_{i2})}{x_i}, \dots, \frac{\tilde{dq}(x_{in})}{x_i}), \tilde{dq}_{ij} = \frac{\sum_{t=1}^{L(x_{ij}; S_{\tilde{Q}^*}(x_i))} d_q^t(x_{ij})}{L(x_{ij}; S_{\tilde{Q}^*}(x_i))}.$$

And $K(\tilde{R}^*) = (S_{\tilde{R}^*}(x_1), S_{\tilde{R}^*}(x_2), \dots, S_{\tilde{R}^*}(x_n))$, $S_{\tilde{R}^*}(x_i) = (\frac{\tilde{d}r(x_{i1})}{x_i}, \frac{\tilde{d}r(x_{i2})}{x_i}, \dots, \frac{\tilde{d}r(x_{in})}{x_i})$, $\tilde{d}r_{ij} = \frac{\sum_{m=1}^{L(x_{ij}; S_{\tilde{R}^*}(x_i))} d_r^m(x_{ij})}{L(x_{ij}; S_{\tilde{R}^*}(x_i))}$.

- (1) It can be seen from Definition 4.5, for $x_i \in U$, $S_{\tilde{P}^*}(x_i) \sqsubseteq S_{\tilde{Q}^*}(x_i)$, $\tilde{d}p(x_{ij}) \leq \tilde{d}q(x_{ij})$, $i, j = 1, 2, \dots, n$, holds, we can find $\tilde{P}^* \preceq_2 \tilde{Q}^*$.
- (2) Suppose $\tilde{P}^* \preceq_2 \tilde{Q}^*$ and $\tilde{Q}^* \preceq_2 \tilde{P}^*$, according to Definition 4.5, we can find

$$\begin{aligned} \tilde{P}^* \preceq_2 \tilde{Q}^* &\Leftrightarrow S_{\tilde{P}^*}(x_i) \sqsubseteq S_{\tilde{Q}^*}(x_i) \\ &\Leftrightarrow dp(x_{ij}) \leq dq(x_{ij}); \\ \tilde{Q}^* \preceq_2 \tilde{P}^* &\Leftrightarrow S_{\tilde{Q}^*}(x_i) \sqsubseteq S_{\tilde{P}^*}(x_i) \\ &\Leftrightarrow dq(x_{ij}) \leq dp(x_{ij}) \text{ for } i = 1, 2, \dots, n. \end{aligned}$$

Therefore, we obtain that $\tilde{d}p(x_{ij}) = \tilde{d}q(x_{ij}) = dp(x_{ij})$, which is $\tilde{d}p(x_{ij}) = \tilde{d}q(x_{ij})$. Hence $\tilde{P}^* \simeq \tilde{Q}^*$.

- (3) Suppose $\tilde{P}^* \preceq_2 \tilde{Q}^*$, $\tilde{Q}^* \preceq_2 \tilde{R}^*$. $\tilde{P}^* \preceq_2 \tilde{Q}^* \Leftrightarrow S_{\tilde{P}^*}(x_i) \sqsubseteq S_{\tilde{Q}^*}(x_i) \Leftrightarrow \tilde{d}p(x_{ij}) \leq \tilde{d}q(x_{ij}) \Leftrightarrow$

$$\frac{\sum_{s=1}^{L(x_{ij}; S_{\tilde{P}^*}(x_i))} d_p^s(x_{ij})}{L(x_{ij}; S_{\tilde{P}^*}(x_i))} \leq \frac{\sum_{t=1}^{L(x_{ij}; S_{\tilde{Q}^*}(x_i))} d_q^t(x_{ij})}{L(x_{ij}; S_{\tilde{Q}^*}(x_i))}, \text{ for } i, j = 1, 2, \dots, n. \tilde{Q}^* \preceq_2 \tilde{R}^* \Leftrightarrow S_{\tilde{Q}^*}(x_i) \sqsubseteq$$

$$S_{\tilde{R}^*}(x_i) \Leftrightarrow \tilde{d}p(x_{ij}) \leq \tilde{d}r(x_{ij}) \Leftrightarrow \frac{\sum_{t=1}^{L(x_{ij}; S_{\tilde{Q}^*}(x_i))} d_q^t(x_{ij})}{L(x_{ij}; S_{\tilde{Q}^*}(x_i))} \leq \frac{\sum_{m=1}^{L(x_{ij}; S_{\tilde{R}^*}(x_i))} d_r^m(x_{ij})}{L(x_{ij}; S_{\tilde{R}^*}(x_i))}, \text{ for } i, j =$$

$$1, 2, \dots, n. \text{ So we can get } \frac{\sum_{s=1}^{L(x_{ij}; S_{\tilde{P}^*}(x_i))} d_p^s(x_{ij})}{L(x_{ij}; S_{\tilde{P}^*}(x_i))} \leq \frac{\sum_{t=1}^{L(x_{ij}; S_{\tilde{Q}^*}(x_i))} d_q^t(x_{ij})}{L(x_{ij}; S_{\tilde{Q}^*}(x_i))} \leq \frac{\sum_{m=1}^{L(x_{ij}; S_{\tilde{R}^*}(x_i))} d_r^m(x_{ij})}{L(x_{ij}; S_{\tilde{R}^*}(x_i))},$$
 thus $\tilde{d}p(x_{ij}) \leq \tilde{d}q(x_{ij}) \leq \tilde{d}r(x_{ij})$, $\tilde{d}p(x_{ij}) \leq \tilde{d}q(x_{ij}) \Leftrightarrow S_{\tilde{P}^*}(x_i) \sqsubseteq S_{\tilde{R}^*}(x_i)$. Hence, $\tilde{P}^* \preceq_2 \tilde{R}^*$.

Theorem 4.3: The partial-order relation \preceq_1 is a special instance of partial-order relation \preceq_2 .

Proof: Suppose that $K(\tilde{P}^*), K(\tilde{Q}^*) \in K(U)$ and $K(\tilde{P}^*) \preceq_1 K(\tilde{Q}^*)$. According to the Definition 4.2, we can know $S_{\tilde{P}^*}(x_i) \sqsubseteq S_{\tilde{Q}^*}(x_i)$ and $dp(x_{ij}) \leq dq(x_{ij})$. So, $dq(x_{ij}) \leq dp(x_{ij})$. Hence $S_{\tilde{P}^*}(x_i) \sqsubseteq S_{\tilde{Q}^*}(x_i)$, we obtain that $K(\tilde{P}^*) \preceq_2 K(\tilde{Q}^*)$. Therefore, partial-order relation \preceq_1 is a special instance of partial-order relation \preceq_2 .

Definition 4.6: Let $K(\tilde{P}^*), K(\tilde{Q}^*) \in K(U)$, $K(\tilde{P}^*) = (S_{\tilde{P}^*}(x_1), S_{\tilde{P}^*}(x_2), \dots, S_{\tilde{P}^*}(x_n))$, $S_{\tilde{P}^*}(x_i) = (\frac{dp(x_{i1})}{x_i}, \frac{dp(x_{i2})}{x_i}, \dots, \frac{dp(x_{in})}{x_i})$, in which $dp(x_{ij}) = \{d_p^1(x_{ij}), d_p^2(x_{ij}), \dots, d_p^s(x_{ij})\}$, $s = L(x_{ij}; S_{\tilde{P}^*}(x_i))$; $K(\tilde{Q}^*) = (S_{\tilde{Q}^*}(x_1), S_{\tilde{Q}^*}(x_2), \dots, S_{\tilde{Q}^*}(x_n))$, $S_{\tilde{Q}^*}(x_i) = (\frac{dq(x_{i1})}{x_i}, \frac{dq(x_{i2})}{x_i}, \dots, \frac{dq(x_{in})}{x_i})$, in which $dq(x_{ij}) = \{d_q^1(x_{ij}), d_q^2(x_{ij}), \dots, d_q^t(x_{ij})\}$ and $t = L(x_{ij}; S_{\tilde{Q}^*}(x_i))$. The partial-order relation \preceq_3 is defined as $K(\tilde{P}^*) \preceq_3 K(\tilde{Q}^*) \Leftrightarrow |S_{\tilde{P}^*}(x_i)| \leq |S_{\tilde{Q}^*}(x_i)|, i =$

$$1, 2, \dots, n, \text{ where } |S_{\tilde{P}^*}(x_i)| = \sum_{j=1}^n \left(\frac{\sum_{s=1}^{L(x_{ij}; S_{\tilde{P}^*}(x_i))} d_p^s(x_{ij})}{L(x_{ij}; S_{\tilde{P}^*}(x_i))} \right) \text{ and } |S_{\tilde{Q}^*}(x_i)| = \sum_{j=1}^n \left(\frac{\sum_{t=1}^{L(x_{ij}; S_{\tilde{Q}^*}(x_i))} d_q^t(x_{ij})}{L(x_{ij}; S_{\tilde{Q}^*}(x_i))} \right).$$

Furthermore, $K(\tilde{P}^*) \cong K(\tilde{Q}^*) \Leftrightarrow |S_{\tilde{P}^*}(x_i)| = |S_{\tilde{Q}^*}(x_i)|, i = 1, 2, \dots, n$, is written as $\tilde{P}^* \cong \tilde{Q}^*$. $K(\tilde{P}^*) \prec_3 K(\tilde{Q}^*) \Leftrightarrow K(\tilde{P}^*) \preceq_3 K(\tilde{Q}^*)$ and $K(\tilde{P}^*) \not\cong K(\tilde{Q}^*)$ should be written as $\tilde{P}^* \prec_3 \tilde{Q}^*$.

Theorem 4.4: Let $K(U)$ be the collection of all multi-fuzzy granular structures on U , then $(K(U), \preceq_3)$ is a poset.

Proof: Suppose that $K(\tilde{P}^*), K(\tilde{Q}^*), K(\tilde{R}^*) \in K(U)$, $K(\tilde{P}^*) = (S_{\tilde{P}^*}(x_1), S_{\tilde{P}^*}(x_2), \dots, S_{\tilde{P}^*}(x_n))$, $S_{\tilde{P}^*}(x_i) = (\frac{dp(x_{i1})}{x_i}, \frac{dp(x_{i2})}{x_i}, \dots, \frac{dp(x_{in})}{x_i})$; $K(\tilde{Q}^*) = (S_{\tilde{Q}^*}(x_1), S_{\tilde{Q}^*}(x_2), \dots, S_{\tilde{Q}^*}(x_n))$, $S_{\tilde{Q}^*}(x_i) = (\frac{dq(x_{i1})}{x_i}, \frac{dq(x_{i2})}{x_i}, \dots, \frac{dq(x_{in})}{x_i})$; And $K(\tilde{R}^*) = (S_{\tilde{R}^*}(x_1), S_{\tilde{R}^*}(x_2), \dots, S_{\tilde{R}^*}(x_n))$, $S_{\tilde{R}^*}(x_i) = (\frac{dr(x_{i1})}{x_i}, \frac{dr(x_{i2})}{x_i}, \dots, \frac{dr(x_{in})}{x_i})$.

- (1) According to the definition of the partial-order relation \preceq_3 , we can find $\tilde{P}^* \preceq_3 \tilde{P}^*$.
- (2) Suppose $\tilde{P}^* \preceq_3 \tilde{Q}^*$, $\tilde{Q}^* \preceq_3 \tilde{P}^*$. According the definition of the partial-order relation

$$\preceq_3, \text{ we can find } |S_{\tilde{P}^*}(x_i)| \leq |S_{\tilde{Q}^*}(x_i)| \Leftrightarrow \sum_{j=1}^n \left(\frac{\sum_{s=1}^{L(x_{ij}; S_{\tilde{P}^*}(x_i))} d_p^s(x_{ij})}{L(x_{ij}; S_{\tilde{P}^*}(x_i))} \right) \leq \sum_{j=1}^n \left(\frac{\sum_{t=1}^{L(x_{ij}; S_{\tilde{Q}^*}(x_i))} d_q^t(x_{ij})}{L(x_{ij}; S_{\tilde{Q}^*}(x_i))} \right)$$

$$\text{and } |S_{\tilde{Q}^*}(x_i)| \leq |S_{\tilde{P}^*}(x_i)| \Leftrightarrow \sum_{j=1}^n \left(\frac{\sum_{t=1}^{L(x_{ij}; S_{\tilde{Q}^*}(x_i))} d_q^t(x_{ij})}{L(x_{ij}; S_{\tilde{Q}^*}(x_i))} \right) \leq \sum_{j=1}^n \left(\frac{\sum_{s=1}^{L(x_{ij}; S_{\tilde{P}^*}(x_i))} d_p^s(x_{ij})}{L(x_{ij}; S_{\tilde{P}^*}(x_i))} \right). \text{ So,}$$

$$\sum_{j=1}^n \left(\frac{\sum_{s=1}^{L(x_{ij}; S_{\tilde{P}^*}(x_i))} d_p^s(x_{ij})}{L(x_{ij}; S_{\tilde{P}^*}(x_i))} \right) \leq \sum_{j=1}^n \left(\frac{\sum_{t=1}^{L(x_{ij}; S_{\tilde{Q}^*}(x_i))} d_q^t(x_{ij})}{L(x_{ij}; S_{\tilde{Q}^*}(x_i))} \right) \leq \sum_{j=1}^n \left(\frac{\sum_{s=1}^{L(x_{ij}; S_{\tilde{P}^*}(x_i))} d_p^s(x_{ij})}{L(x_{ij}; S_{\tilde{P}^*}(x_i))} \right). \text{ Therefore,}$$

we obtain that $|S_{\tilde{P}^*}(x_i)| \leq |S_{\tilde{Q}^*}(x_i)| \leq |S_{\tilde{P}^*}(x_i)|$, that is $|S_{\tilde{P}^*}(x_i)| = |S_{\tilde{Q}^*}(x_i)|$. Hence, $\tilde{P}^* \cong \tilde{Q}^*$.

- (3) Suppose $\tilde{P}^* \preceq_3 \tilde{Q}^*$, $\tilde{Q}^* \preceq_3 \tilde{R}^*$, according the definition of the partial-order relation

$$\preceq_3, \text{ we can find } |S_{\tilde{P}^*}(x_i)| \leq |S_{\tilde{Q}^*}(x_i)| \Leftrightarrow \sum_{j=1}^n \left(\frac{\sum_{s=1}^{L(x_{ij}; S_{\tilde{P}^*}(x_i))} d_p^s(x_{ij})}{L(x_{ij}; S_{\tilde{P}^*}(x_i))} \right) \leq \sum_{j=1}^n \left(\frac{\sum_{t=1}^{L(x_{ij}; S_{\tilde{Q}^*}(x_i))} d_q^t(x_{ij})}{L(x_{ij}; S_{\tilde{Q}^*}(x_i))} \right)$$

$$\text{and } |S_{\tilde{Q}^*}(x_i)| \leq |S_{\tilde{R}^*}(x_i)| \Leftrightarrow \sum_{j=1}^n \left(\frac{\sum_{t=1}^{L(x_{ij}; S_{\tilde{Q}^*}(x_i))} d_q^t(x_{ij})}{L(x_{ij}; S_{\tilde{Q}^*}(x_i))} \right) \leq \sum_{j=1}^n \left(\frac{\sum_{m=1}^{L(x_{ij}; S_{\tilde{R}^*}(x_i))} d_r^m(x_{ij})}{L(x_{ij}; S_{\tilde{R}^*}(x_i))} \right), \text{ for}$$

$i, j = 1, 2, \dots, n$. Therefore, we obtain that $|S_{\tilde{P}^*}(x_i)| \leq |S_{\tilde{Q}^*}(x_i)| \leq |S_{\tilde{R}^*}(x_i)|$, that is $|S_{\tilde{P}^*}(x_i)| \leq |S_{\tilde{R}^*}(x_i)|$. Thus, $\tilde{P}^* \preceq_3 \tilde{R}^*$.

Summarizing the (1)-(3), $(K(U), \preceq_3)$ is a poset.

Theorem 4.5: The partial-order relation \preceq_2 is a special instance of partial-order relation \preceq_3 .

Proof: Suppose that $K(\tilde{P}^*), K(\tilde{Q}^*) \in K(U)$ and $K(\tilde{P}^*) \preceq_2 K(\tilde{Q}^*)$. According to the Definition 4.5, we can know $S_{\tilde{P}^*}(x_i) \subseteq S_{\tilde{Q}^*}(x_i)$ and $d_p^1(x_{ij}) \leq d_q^1(x_{ij}), d_p^2(x_{ij}) \leq d_q^2(x_{ij}), \dots, d_p^s(x_{ij}) \leq d_q^s(x_{ij})$. So, $dq(x_{ij}) \leq dp(x_{ij})$. Hence $|S_{\tilde{P}^*}(x_i)| \leq |S_{\tilde{Q}^*}(x_i)|$, we obtain that $K(\tilde{P}^*) \preceq_3 K(\tilde{Q}^*)$. Therefore, partial-order relation \preceq_2 is a special instance of partial-order relation \preceq_3 .

Definition 4.8: Let $K(\tilde{P}^*), K(\tilde{Q}^*) \in K(U)$, in which $K(\tilde{P}^*) = (S_{\tilde{P}^*}(x_1), S_{\tilde{P}^*}(x_2), \dots, S_{\tilde{P}^*}(x_n))$, $S_{\tilde{P}^*}(x_i) = (\frac{dp(x_{i1})}{x_i}, \frac{dp(x_{i2})}{x_i}, \dots, \frac{dp(x_{in})}{x_i})$; $K(\tilde{Q}^*) = (S_{\tilde{Q}^*}(x_1), S_{\tilde{Q}^*}(x_2), \dots, S_{\tilde{Q}^*}(x_n))$, $S_{\tilde{Q}^*}(x_i) = (\frac{dq(x_{i1})}{x_i}, \frac{dq(x_{i2})}{x_i}, \dots, \frac{dq(x_{in})}{x_i})$. A partial-order relation \preceq_4 is defined as

$K(\tilde{P}^*) \preceq_4 K(\tilde{Q}^*) \Leftrightarrow$ for $K(\tilde{P}^*)$, there exists a sequence $K'(\tilde{Q}^*)$ of $K(\tilde{Q}^*)$, such that $|S_{\tilde{P}^*}(x_i)| \leq |S_{\tilde{Q}^*}(x_i')|, i = 1, 2, \dots, n$, where $K'(\tilde{Q}^*) = (S_{\tilde{Q}^*}(x_1'), S_{\tilde{Q}^*}(x_2'), \dots, S_{\tilde{Q}^*}(x_n'))$. Furthermore, $K(\tilde{P}^*) \approx K(\tilde{Q}^*) \Leftrightarrow |S_{\tilde{P}^*}(x_i)| = |S_{\tilde{Q}^*}(x_i')|, i = 1, 2, \dots, n$, which is denoted

by $\tilde{P}^* \approx \tilde{Q}^* . K(\tilde{P}^*) \prec_4 K(\tilde{Q}^*) \Leftrightarrow K(\tilde{P}^*) \preceq_4 K(\tilde{Q}^*)$ and $K(\tilde{P}^*) \not\approx K(\tilde{Q}^*)$, which is written as $\tilde{P}^* \prec_4 \tilde{Q}^*$.

Theorem 4.7: Let $K(U)$ be the collection of all multi-fuzzy granular structures on U , then $(K(U), \preceq_4)$ is a poset.

Proof: According to the definition of order-relation \preceq_4 , it can be proved that $(K(U), \preceq_4)$ is a poset.

Theorem 4.6: The partial-order relation \preceq_3 is a special instance of partial-order relation \preceq_4 .

Proof: It is easy to prove from Definition 4.6 and Definition 4.7.

5. Multi-Fuzzy Information Granularity and Its Axiomatic Method

Information granularity can be regarded as a measure of the degree of aggregation (regularity) of knowledge on the domain classification. Fuzzy multi-information granularity is equally important, and can be used to describe the classification ability of multi-fuzzy granular structure. According to Zadeh’s research on granular computing, information granularity should be expressed the granulation degree of objects from a hierarchical perspective[2]. That is, information granularity should represent the hierarchical relationship between multi-fuzzy granular structures.

From the viewpoint of sizes of information granules, in the following, we introduce the definition of multi-fuzzy information granularity.

Definition 5.1: Suppose $K(\tilde{R}^*) \in K(U)$, in which $K(\tilde{R}^*) = (S_{\tilde{R}^*}(x_1), S_{\tilde{R}^*}(x_2), \dots, S_{\tilde{R}^*}(x_n))$. Then, the multiple fuzzy information granularity of \tilde{R}^* is defined as

$$GK(\tilde{R}^*) = \frac{1}{n} \sum_{i=1}^n \frac{|S_{\tilde{R}^*}(x_i)|}{n} \tag{14}$$

where $|S_{\tilde{R}^*}(x_i)|$ is the cardinality of the muti-fuzzy information granule $S_{\tilde{R}^*}(x_i)$. Axiomatic methods and constructive methods play an equal role in mathematical definition. In the following, we give the axiomatic constraint to define a multi-fuzzy information granularity in the context of multi-fuzzy granular structures by employing the partial-order relation \preceq_3 .

Definition 5.2: Let $K(U)$ be the collection of all multi-fuzzy granular structures on U , if $\forall K(\tilde{P}^*) \in K(U)$, there is a real number $G(\tilde{P}^*)$ with the following properties:

- (1) $G(\tilde{P}^*) \geq 0$ (nonnegative);
- (2) For $\forall K(\tilde{P}^*), K(\tilde{Q}^*) \in K(U)$, if $K(\tilde{P}^*) \cong K(\tilde{Q}^*)$, then $G(\tilde{P}^*) = G(\tilde{Q}^*)$ (invariability);
- (3) For $\forall K(\tilde{P}^*), K(\tilde{Q}^*) \in K(U)$, for $K(\tilde{P}^*) \prec_3 K(\tilde{Q}^*)$, then $G(\tilde{P}^*) < G(\tilde{Q}^*)$ (monotonicity).

then G is called a multi-fuzzy information granularity. Obtained by the above axiomatic method, we come to the following theorem.

Theorem 5.1: Let $\forall K(\tilde{P}^*), K(\tilde{Q}^*) \in K(U)$, if $K(\tilde{P}^*) \preceq_3 K(\tilde{Q}^*)$, then $G(\tilde{P}^*) \leq G(\tilde{Q}^*)$. This also satisfies the partial-order relation \preceq_1, \preceq_2 and \preceq_4 , respectively. It is easy to prove by Definition 5.2 and the definition of partial-order relations $\preceq_1, \preceq_2, \preceq_3$ and \preceq_4 . Furthermore, the information granularity GK given by Definition 5.1 satisfies the axiomatic definition methods. Next, we give proof:

- (1) Obviously, it is nonnegative;

(2) Letting $K(\tilde{P}^*), K(\tilde{Q}^*) \in K(U)$, $K(\tilde{P}^*) = (S_{\tilde{P}^*}(x_1), S_{\tilde{P}^*}(x_2), \dots, S_{\tilde{P}^*}(x_n))$, $K(\tilde{Q}^*) = (S_{\tilde{Q}^*}(x_1), S_{\tilde{Q}^*}(x_2), \dots, S_{\tilde{Q}^*}(x_n))$. According to the definition of partial-order relation \preceq_3 , if $\tilde{P}^* \cong \tilde{Q}^*$, then $|S_{\tilde{P}^*}(x_i)| = |S_{\tilde{Q}^*}(x_i)|$, $i = 1, 2, \dots, n$. Therefore

$$GK(\tilde{P}^*) = \frac{1}{n} \sum_{i=1}^n \frac{|S_{\tilde{P}^*}(x_i)|}{n} = \frac{1}{n} \sum_{i=1}^n \frac{|S_{\tilde{Q}^*}(x_i)|}{n} = \frac{1}{n} \sum_{i=1}^n \frac{|S_{\tilde{Q}^*}(x_i)|}{n} = GK(\tilde{Q}^*).$$

(3) Letting $K(\tilde{P}^*), K(\tilde{Q}^*) \in K(U)$ with $\tilde{P}^* \prec_3 \tilde{Q}^*$, such that

$$\begin{aligned} K(\tilde{P}^*) \prec_3 K(\tilde{Q}^*) &\Leftrightarrow |S_{\tilde{P}^*}(x_i)| < |S_{\tilde{Q}^*}(x_i)|, i = 1, 2, \dots, n. \\ &\Leftrightarrow \sum_{j=1}^n \left(\frac{\sum_{s=1}^{L(x_{ij})} d_{\tilde{P}^*}^s(x_i)}{L(x_{ij})} \right) < \sum_{j=1}^n \left(\frac{\sum_{s=1}^{L(x_{ij})} d_{\tilde{Q}^*}^s(x_{ij})}{L(x_{ij})} \right), \\ GK(\tilde{P}^*) &= \frac{1}{n} \sum_{i=1}^n \frac{|S_{\tilde{P}^*}(x_i)|}{n} < \frac{1}{n} \sum_{i=1}^n \frac{|S_{\tilde{Q}^*}(x_i)|}{n} = GK(\tilde{Q}^*). \end{aligned}$$

Thus, $GK(\tilde{P}^*) < GK(\tilde{Q}^*)$. Through monotonicity, meaning that relation \tilde{Q}^* is more chaotic than relation \tilde{P}^* , so the uncertainty of group \tilde{Q}^* is higher.

In conclusion, the information granularity GK given by Definition 5.1 satisfies the axiomatic definition methods in Definition 5.2.

6. Conclusion

Based on fuzzy multirelations, this paper first proposes a kind of fuzzy information granular structure generated by multi-fuzzy relations in the universe of discourse, namely multi-fuzzy granular structure. Based on this structure, four fuzzy multiple partial-order relations are defined, and the hierarchical characteristics of these four partial order relations and related mathematical conclusions are studied. Secondly, for fuzzy multi-information GCM, a multi-fuzzy information granularity is proposed. Finally, an axiomatic method for defining fuzzy multiple information granularity on the fuzzy multiple granular structure is given, and axiomatic constraints with partial-order relations are established. This paper studies the internal structure nesting relationship and information granularity measurement of fuzzy multi-information GCM, which provides a theoretical basis for the development of artificial intelligence and decision-making theory. In the next step of this paper, the reasoning logic and algorithm design of fuzzy multiple information will be further studied.

References

- [1] Zadeh LA. Fuzzy logic computing with words. IEEE Transactions on Fuzzy Systems. 1996 May;4(2):103–111.
- [2] Zadeh LA. Toward a theory of fuzzy information granulation and its centrality in human reasoning and fuzzy logic. Fuzzy Sets and Systems. 1997 Feb; 90(2):111-127.
- [3] Cunpeng Wang. Data Analysis in Incomplete Information Systems Based on Granular Computing. IEEE 2010 International Conference on System Science, Engineering Design and Manufacturing Informatization (ICSEM). Yichang, China, 2010; pp.153–155.
- [4] Xu W, Li M, Wang X. Information Fusion Based on Information Entropy in Fuzzy Multisource Incomplete Information System. International Journal of Fuzzy Systems, 2016; 19(4):12.

- [5] Yang Weiping, Lin Menglei. Information granularity in intuitionistic fuzzy information system. *Computer Applications*.2012; 2012(01):130-134.
- [6] Lin, Tsau Young. Granular computing I: the concept of granulation and its formal model. *International Journal of Granular Computing, Rough Sets and Intelligent Systems*.2009; 1(1):21–42.
- [7] Jieye Liang, Yuhua Qian. Information granules and entropy theory in information systems. 2008 Jul; 51(10):1427–1444.
- [8] Jiye Liang, Zhongzhi Shi, Xiaodong Li, Wierman MJ. Information entropy, rough entropy and knowledge granulation in incomplete information systems. *International Journal of General Systems*. 2006 Nov; 35(6):641–654.
- [9] Jiye Liang, Zhongzhi shi. The information entropy, rough entropy and knowledge granulation in rough set theory. *International Journal of Uncertainty, Fuzziness Knowledge-Based Systems*. 2004; 12(1):37-46.
- [10] Yuanhua Qian, Jieye Liang, Chuangyin Dang. Knowledge structure, knowledge granulation and knowledge distance in a knowledge base. *International Journal of Approximate Reasoning*. 2009; 50(1):174-188.
- [11] Yuhua Qian, Jiye Liang. Combination entropy and combination granulation in rough set theory. *International Journal of Uncertainty, Fuzziness Knowledge-Based Systems*. 2008; 16(2):179-193.
- [12] Taorong Qiu, Lu wang, shujie Xiong. A method of knowledge hiding based on granular computing. *Journal of Shandong University*. 2010; 45(7):60-64.
- [13] Yuhua Qian, Jiye Liang, et al. Information Granularity in Fuzzy Binary GrC Model. *IEEE Transactions on Fuzzy Systems*. 2011; 19(2):253-264.
- [14] Weiping Yang, Lin Menglei. Information granularity in intuitionistic fuzzy information system. *Computer Applications*.2012; 2012(01):130-134.
- [15] Xiaoyun Lu, Shengling Geng. Information granule and rough entropy in interval hesitating fuzzy information system. *Fuzzy systems and mathematics*. 2016; 45(7):60-64.
- [16] Yager R R. On the theory of bags. *International Journal of General System*, 1986; 13(1):23-27.
- [17] Kim K.S, Miyamoto S. Application of fuzzy multisets to fuzzy database systems. 1996 *Asian Fuzzy Systems Symposium*; 1996 Dec 11-14; Kengding, Taiwan; 115–120.
- [18] Miyamoto S. Remarks on basics of fuzzy sets and fuzzy multisets. *Fuzzy Sets and Systems*.2005; 156(3):427-431.
- [19] El-Azab M. S. , Shokry M. , Khadra R. A.. Correlation measure for fuzzy multisets. *Journal of the Egyptian Mathematical Society*, 2017; 25(3)
- [20] Miyamoto S. Multisets and Fuzzy Multisets as a Framework of Information Systems. *Modeling Decisions for Artificial Intelligence, MDAI 2004, Barcelona, Spain, August 2-4, 2004, Proceedings*.
- [21] S. Miyamoto. Fuzzy multisets with infinite collections of memberships. *Proceedings of the International Conference of the Korean Institute of Intelligent Systems*. 1997; 1:61-66.

Support Vector Machine Technique as Classifier of Impaired Body Fat Percentage

Alexandra LA CRUZ ^{a,1}, Erika SEVEREYN ^b, Mónica HUERTA ^c and Sara WONG ^d

^a *Faculty of Engineering, Universidad de Ibagué, Colombia*

^b *Department of Thermodynamics and Transfer Phenomena, Universidad Simón Bolívar, Venezuela*

^c *Faculty of Engineering, Universidad Politécnica Salesiana, Ecuador*

^d *Department of Electronics and Circuits, Universidad Simón Bolívar, Venezuela*

Abstract. Excess weight and obesity are indicators of an unhealthy or harmful accumulation of fat that can be dangerous to health. Body mass index (BMI) refers to height-to-weight ratio and is often used to identify overweight and obesity in adults. Although BMI is commonly used to diagnose obesity and overweight, it is ineffective in differentiating between high muscle mass and elevated body fat mass. Body fat percentage (BF%) is one of the best predictors of obesity because it quantifies adipose tissue. The Deurenberg equation is among the indirect methods to measure BF%; it uses BMI, age, and sex as parameters to calculate the BF%. Machine learning techniques demonstrated to be a good classifier of overweight, obesity, and diseases related to insulin resistance and metabolic syndrome. This study intends to evaluate anthropometric parameters as classifiers of BF% alteration using support vector machines and the Deurenberg equation for BF% estimation. The database used consisted of 1978 individuals with 24 different anthropometric measurements. The results suggest the SVM as a suitable technique for classifying individuals with normal and abnormal BF% values. Accuracy, F1 score, PPV, NPV, and sensitivity were above 0.8. Besides, the specificity value is below 0.7, which indicates that false positives may occur. As future work, this research intends to apply neural networks as a classification technique.

Keywords. Support vector machine, anthropometric measurements, fat body percentage, Monte Carlo cross validation

1. Introduction

Being overweight and obese are indicators of unhealthy or excessive fat accumulation on the body with the potential to be harmful to health [1]. Body mass index (BMI) is a simple measure of the height-to-weight ratio, commonly used to identify overweight and obesity among adults [2]. Although BMI is usually used to diagnose obesity and overweight, it has the disadvantage of not differentiating between high fat and lean mass [3]. Since those downsides with BMI, two classifications of obesity are reported in the literature,

¹Corresponding Author: Faculty of Engineering Universidad de Ibagué, Carrera 22, Calle 67 B, Av. Amalá, Ibagué, Tolima, Colombia; E-mail: alexandra.lacruz@unibague.edu.co.

the first classification is individuals with high body fat mass but the normal metabolic response, and the second classification endorse individuals that suffer from metabolic obesity with normal weight (MONW) [4,5]. The persons that are MONW have high cardiovascular and metabolic risk factors similar to individuals with abnormal BMI [6,7].

The body fat percentage (BF%) is the indicator that best predicts obesity due it can quantify tissue adipose [8]. Several direct methods measure BF%, including densitometry, dual-energy x-ray absorptiometry, bioelectrical impedance analysis, near-infrared reactance, dual-energy x-ray absorptiometry and magnetic resonance imaging. However, they are unsuitable for epidemiological studies since they are expensive, require specialized equipment and skilled professionals [9]. Some indirect methods to measure BF% use BMI, age, and sex as parameters to calculate the BF% applying the Deurenberg [10], Gallagher [11] and Jackson-Pollock [12] equations. There are high correlations between BF% and anthropometric measurements, among them the hip circumference, waist-to-height ratio, and the abdominal circumference [13]. Further, the SIRI equation calculates the BF% from the skin folds [14]. These studies have all determined an appropriate relationship between measurements of these anthropometric values and BF%.

There is no consensus regarding the cut-off points of BF% because there is no statistically representative database [15]. Some researches proposed 25% for men and 30% for women as a BF% cut off point [8,16]. Other researches suggest that age is a relevant factor to consider in the cut-off point establishment [17,18,19]. In this work, a spectral cut-off point was considered, including sex and age.

Machine learning techniques have been used to classify overweight, obesity, insulin resistance and metabolic syndrome [20,21]. Some studies have used support vector machines (SVM) and decision tree to differentiate individuals with and without metabolic syndrome from variables as waist circumference, waist to height ratio, body mass index, among others [20,22]. The k-means algorithm has also been used to detect individuals with insulin resistance and overweight using as variables waist and hip circumferences [21,23].

This study aims to assess the anthropometric variables as a classifier of impaired BF%. A database used consisted of 1978 individuals with 24 anthropometrics measures (weight, height, body circumferences, and body skinfolds). The SVM method evaluates the predictive ability of anthropometric measure variables. The next section describes the methodology. The results, and discussion are explained in sections 3 and 4. Finally, section 5 presents the conclusions and proposals for future work.

2. Methodology

2.1. Database

The Nutritional Evaluation Laboratory of the Simón Bolívar University collected during the period from 2004 to 2012 [24] the database used in this work. It counted with 1978 participants, of which 678 are men and the rest women. The implemented protocol performed 24 anthropometric measurements in each volunteer, including height, weight, body circumferences, and body folds. Additionally, the BF% is calculated using Deurenberg's equation. Deurenberg's equation, as can be seen in equation (1), uses BMI, age, and sex as variables. The sex variable is equal to one for men and equal to zero for women.

$$BF\% = 1.20 BMI - 10.8 sex - 0.23 age - 5.4 \quad (1)$$

The clinical protocol implemented in the database followed the ethical standards of the Declaration of Helsinki of 1964 and the ethical standards of the ethical committee of the Simón Bolívar University. All participants accepted the conditions of the study by signing informed consent. Table 1 shows the average and standard deviation of anthropometric variables of the subjects with normal and altered BF%.

2.2. Classifier Metrics

For the detection of altered levels of BF%, 24 anthropometric measurements were used, weight and height were excluded since they are variables of the Deurenberg equation. The true positives (TP), false positives (FP), true negatives (TN), and false negatives (FN) were measured. It visualizes the classification discrepancies in the classifier model [25]. The accuracy (ACC), specificity (SPE), sensitivity (SEN), positive predictive value (PPV), negative predictive value (NPV), and F1 score (F1) were calculated using the equations (2), (3), (4), (5), (6), and (7) respectively.

$$ACC = \frac{(TP+TN)}{(TP+FP+TN+FN)} \quad (2) \quad SEN = \frac{TP}{(TP+FN)} \quad (3)$$

$$SPE = \frac{TN}{(TN+FP)} \quad (4) \quad PPV = \frac{TP}{(FP+TP)} \quad (5)$$

$$NPV = \frac{TN}{(FN+TN)} \quad (6) \quad F1 = 2 \frac{(PPV)(SEN)}{(PPV+SEN)} \quad (7)$$

2.3. Implementation of the support vector machine method

The classification-regression method SVM is a classification method used for binary, multiple classifications, and classification-regression problems. SVM has proven to be considered among the best classifiers over a wide range of scenarios, making it one of the benchmarks in both statistical learning and machine learning fields [26].

Support Vector Machine is based on the Maximal Margin Classifier, which turns on the hyperplane concept. In this work, the SVM method allows classifying individuals with normal and abnormal BF% values. For this purpose, a Monte Carlo Cross-Validation (MCCV) [27], and a Gaussian kernel [28] were used. Figure 1 shows the procedure applied in this work. The database was randomly (with a uniform probability) divided 80% for training with SVM and the remaining 20% to test the trained SVM and calculate the metrics. The process was performed 100 times, and the metrics were calculated in each iteration and then averaged.

2.4. Statistical tests

For the statistical analysis, the Mann-Whitney U test was used, since it was assumed that the samples are not paired and have a different distribution than the normal, and a p-value of less than 5% was considered statistically significant [29]. The Tables 1 and 2 are presented as mean and standard deviation values (mean \pm standard deviation).

Table 1. Anthropometric parameters for individuals with normal and abnormal BF%.

Anthropometric parameter	Normal BF% (n=1037)	Impaired BF% (n=941)
Age[years] ^a	24.678±13.832	71.358±18.386
Weight[Kg] ^a	56.064±9.348	62.243±12.867
Height[cm] ^a	162.278±8.699	156.614±9.802
Right arm circumference [cm] ^a	25.820±2.817	27.931±4.023
Left arm circumference[cm] ^a	25.694±2.802	27.749±4.066
Right flexed arm circumference [cm] ^a	26.828±3.026	28.543±4.063
Left flexed arm circumference [cm] ^a	26.576±3.339	28.245±4.093
Waist circumference [cm] ^a	71.119±7.571	88.127±11.557
Hip circumference [cm] ^a	91.763±6.339	95.235±10.105
Right thigh circumference [cm] ^a	44.947±3.321	45.629±5.950
Left thigh circumference [cm] ^a	44.431±3.403	45.447±5.873
Right calf circumference [cm] ^a	33.582±2.938	33.198±4.053
Left calf circumference [cm] ^a	33.549±3.070	33.089±4.063
Right triceps fold [mm] ^a	13.656±5.186	14.953±6.747
Left triceps fold [mm]	13.471±5.129	14.872±6.636
Right subscapular fold [mm] ^a	12.920±4.569	17.293±7.510
Left subscapular fold [mm] ^a	13.031±4.585	17.472±7.426
Right suprailiac fold [mm] ^a	12.148±5.424	18.229±7.725
Left suprailiac fold [mm] ^a	12.198±5.456	18.230±7.663
Right abdominal fold [mm] ^a	22.034±5.927	25.393±8.917
Left abdominal fold [mm] ^a	22.805±6.033	25.318±9.048
Right thigh fold [mm] ^a	19.770±5.847	20.887±9.452
Left thigh fold [mm] ^a	20.530±5.917	21.047±9.532
Right calf fold [mm] ^a	13.184±5.429	15.544±7.832
Left calf fold [mm] ^a	13.591±5.468	15.891±7.816
BMI[Kg/m ²] ^a	21.211±2.551	25.319±4.460
BF% ^a	22.667±5.901	36.988±8.609

^aStatistically significant difference (p-value < 0.05).

Table 2. Metrics of the support vector machine classification and Monte Carlo Cross Validation.

Metrics	BF%
Sensitivity	0.965±0.012
Specificity	0.679±0.044
Accuracy	0.897±0.015
F1 Score	0.935±0.010
NPV	0.855±0.043
PPV	0.907±0.016

3. Results

Table 1 presents the anthropometric values of control individuals and individuals with impaired BF%. The database includes 1978 individuals, 52.43% belongs to the control group, and 47.57% endures impaired BF%. The classification was performed according

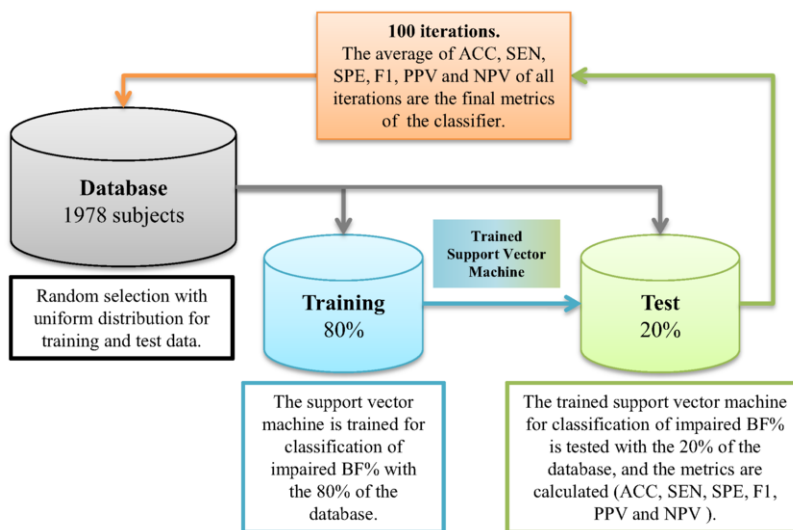


Figure 1. General methodology schematics for support vector machine classification.

to [11,18,17], whereby the cut-off point of the impaired BF% established for women between 20 and 39 years old is above 32%, for women between 40 and 59 years old 34%, and women over 60 years old 35%. On the other hand, the cut-off point of the impaired BF% in men between 20 and 39 years old is above 20%, men between 40 and 59 years old 22%, and men over 60 years old 23%. Table 2 reports the results of the training with the SVM using the 26 anthropometrics parameters displaying the average of sensitivity, specificity, accuracy, F1 score, negative, and positive predictive values performed 100 times.

4. Discussion

Table 1 shows features of subjects with normal and abnormal BF% values. Significant differences were found between groups in all anthropometric variables. Individuals with abnormal values of BF% have higher values of circumferences and folds than subjects with normal values of BF%. This finding corroborates studies that suggest that individuals with a high BF% have a thicker adipose pad than subjects with normal BF% [30,31]. Additionally, the average BMI of the individuals with abnormal BF% values suggests that they are overweight since it exceeds 25 Kg/m^2 .

Furthermore, the waist circumference levels are normal for individuals with normal BF% values but are above 88 cm for individuals with abnormal BF% values. This finding could indicate that individuals with abnormal BF% values have a high accumulation of adipose tissue at the waist, which can be also observed in the abdominal fold, which is significantly higher in individuals with abnormal BF% than in individuals with normal BF% [32].

Table 2 shows the metrics of the SVM evaluation as a classifier of individuals with abnormal BF%. Almost all the metrics are above 0.8. The database used has approximately the same percentage of individuals with normal and abnormal BF%, suggesting that the accuracy is a valid metric to assess the capability of the methods to classify

individuals with abnormal BF%. In this case, the capacity of the classifier method of classifying this metabolic dysfunction is high with an accuracy above 0.89 [33].

Moreover, the probabilities of obtaining a correct classification with individuals with normal and abnormal BF% values are high. Since the NPV, PPV, and F1 score values are above 0.85. The sensitivity value obtained above 0.96, indicates a false-negative rate of about 4%, which is low, and it is convenient for the classifier. Furthermore, specificity was the lowest metric value (< 0.7), indicating a high false-positive rate. Therefore, individuals with normal BF values may be classified as individuals with abnormal BF% values [34].

In other studies, automatic learning techniques have been used to detect other dysfunctions directly related to altered BF% levels. Farzaneh et. al. [20] used decision trees to determine alterations such as metabolic syndrome, obtaining a lower accuracy than the results obtained in this research (0.739 vs. 0.897), suggesting that SVM is the most suitable technique for detecting metabolic dysfunctions related to body composition than decision trees. Seyed-Taghi et. al. [35] used neural networks to classify obesity, obtaining sensitivity values lower than the sensitivity values found in this investigation (0.965 vs. 0.819). In contrast, the specificity values found in [35] are better than the values of specificity values found in this study (0.837 vs. 0.679), suggesting that the neural network technique should be used as future work.

5. Conclusion

In this research, a supervised machine learning technique (Support Vector Machine) was applied, and as a validation method, the Monte Carlo cross-validation technique was used. The results indicate that SVM was a reliable technique for classifying individuals based on body fat percentage (BF%), with an accuracy, F1 score, PPV, NPV, and sensitivity of more than 0.8.

Notwithstanding, the specificity value is less than 0.7, indicating that false positives may occur, this does not affect the classifier, considering that false negatives are the events to avoid. Further work will include the application of neural networks as a classification technique.

6. Acknowledgment

The Research and Development Deanery of the Universidad Politecnica Salesiana from Cuenca, Ecuador, the Research and Development Deanery (DID) of the Universidad Simón Bolívar, Caracas, Venezuela, and the Research Direction of Universidad de Ibagué from Ibagué Colombia are the main founded of this project.

References

- [1] R. S. Chan and J. Woo, "Prevention of overweight and obesity: how effective is the current public health approach," *International journal of environmental research and public health*, vol. 7, no. 3, pp. 765–783, 2010.
- [2] C. B. Weir and A. Jan, "Bmi classification percentile and cut off points," January 2019.
- [3] J. Gómez-Ambrosi, C. Silva, J. Galofré, J. Escalada, S. Santos, D. Millán, N. Vila, P. Ibañez, M. Gil, V. Valentí, et al., "Body mass index classification misses subjects with increased cardiometabolic risk factors related to elevated adiposity," *International journal of obesity*, vol. 36, no. 2, pp. 286–294, 2012.

- [4] E. A. Sims, "Are there persons who are obese, but metabolically healthy?," *Metabolism-Clinical and Experimental*, vol. 50, no. 12, pp. 1499–1504, 2001.
- [5] S. Gómez-Zorita, M. Queral, M. A. Vicente, M. González, and M. P. Portillo, "Metabolically healthy obesity and metabolically obese normal weight: a review," *Journal of physiology and biochemistry*, pp. 1–15, 2021.
- [6] M. Garg and S. Mohale, "Prevalence of metabolic obesity normal weight (monw) in cardiovascular disease patients—a hospital-based case control study.," *Journal of Evolution of Medical and Dental Sciences*, vol. 9, no. 34, pp. 2427–2432, 2020.
- [7] H. S. Sachdev, A. Porwal, A. Sarna, R. Acharya, S. Ramesh, U. Kapil, and A. V. Kurpad, "Intraindividual double-burden of anthropometric undernutrition and "metabolic obesity" in indian children: a paradox that needs action," *European Journal of Clinical Nutrition*, pp. 1–13, 2021.
- [8] P. Macek, M. Biskup, M. Terek-Derszniak, M. Stachura, H. Krol, S. Gozdz, and M. Zak, "Optimal body fat percentage cut-off values in predicting the obesity-related cardiovascular risk factors: A cross-sectional cohort study," *Diabetes, metabolic syndrome and obesity: targets and therapy*, vol. 13, p. 1587, 2020.
- [9] K. González-Ruíz, M. Medrano, J. E. Correa-Bautista, A. García-Hermoso, D. H. Prieto-Benavides, A. Tordecilla-Sanders, C. Agostinis-Sobrinho, M. Correa-Rodríguez, J. Schmidt Rio-Valle, E. González-Jiménez, et al., "Comparison of bioelectrical impedance analysis, slaughter skinfold-thickness equations, and dual-energy x-ray absorptiometry for estimating body fat percentage in colombian children and adolescents with excess of adiposity," *Nutrients*, vol. 10, no. 8, p. 1086, 2018.
- [10] P. Deurenberg, A. Andreoli, P. Borg, K. Kukkonen-Harjula, A. De Lorenzo, W. D. Van Marken Lichtenbelt, G. Testolin, R. Vígano, and N. Vollaard, "The validity of predicted body fat percentage from body mass index and from impedance in samples of five european populations," *European journal of clinical nutrition*, vol. 55, no. 11, pp. 973–979, 2001.
- [11] D. Gallagher, M. Visser, D. Sepulveda, R. N. Pierson, T. Harris, and S. B. Heymsfield, "How useful is body mass index for comparison of body fatness across age, sex, and ethnic groups?," *American journal of epidemiology*, vol. 143, no. 3, pp. 228–239, 1996.
- [12] A. S. Jackson, M. L. Pollock, and L. R. Gettman, "Intertester reliability of selected skinfold and circumference measurements and percent fat estimates," *Research Quarterly. American Alliance for Health, Physical Education and Recreation*, vol. 49, no. 4, pp. 546–551, 1978.
- [13] F. Amirabdollahian and F. Haghighatdoost, "Anthropometric indicators of adiposity related to body weight and body shape as cardiometabolic risk predictors in british young adults: superiority of waist-to-height ratio," *Journal of obesity*, vol. 2018, 2018.
- [14] M. Arroyo, A. M. Rocandio, L. Ansotegui, H. Herrera, I. Salces, and E. Rebato, "Comparison of predicted body fat percentage from anthropometric methods and from impedance in university students," *British Journal of Nutrition*, vol. 92, no. 5, pp. 827–832, 2004.
- [15] B. Dong, Y. Peng, Z. Wang, O. Adegbjaja, J. Hu, J. Ma, and Y.-H. Ma, "Joint association between body fat and its distribution with all-cause mortality: A data linkage cohort study based on nhanes (1988-2011)," *PLoS One*, vol. 13, no. 2, p. e0193368, 2018.
- [16] A. Jia, S. Xu, J. Ming, Y. Xing, J. Guo, M. Zhao, L. Zhang, and Q. Ji, "Body fat percentage cutoffs for risk of cardiometabolic abnormalities in the chinese adult population: a nationwide study," *European journal of clinical nutrition*, vol. 72, no. 5, pp. 728–735, 2018.
- [17] H. Gharote, K. Pushpanshu, R. Kaushik, and R. Gharote, "Estimation of body fat percentage in oral squamous cell carcinoma," *International healthcare research journal*, vol. 2-11, no. 1, pp. 291–296, 2019.
- [18] P. Deurenberg, J. A. Weststrate, and J. C. Seidell, "Body mass index as a measure of body fatness: age-and sex-specific prediction formulas," *British journal of nutrition*, vol. 65, no. 2, pp. 105–114, 1991.
- [19] D. Gallagher, S. B. Heymsfield, M. Heo, S. A. Jebb, P. R. Murgatroyd, and Y. Sakamoto, "Healthy percentage body fat ranges: an approach for developing guidelines based on body mass index," *The American journal of clinical nutrition*, vol. 72, no. 3, pp. 694–701, 2000.
- [20] F. Karimi-Alavijeh, S. Jalili, and M. Sadeghi, "Predicting metabolic syndrome using decision tree and support vector machine methods," *ARYA atherosclerosis*, vol. 12, no. 3, p. 146, 2016.
- [21] J. Velásquez, S. Wong, L. Encalada, H. Herrera, and E. Severein, "Lipid-anthropometric index optimization for insulin sensitivity estimation," in *11th international symposium on medical information processing and analysis*, vol. 9681, p. 96810R, International Society for Optics and Photonics, 2015.
- [22] A. Worachartcheewan, N. Schaduangrat, V. Prachayasittikul, and C. Nantasenamat, "Data mining for

- the identification of metabolic syndrome status," *EXCLI journal*, vol. 17, p. 72, 2018.
- [23] C. Vintimilla, S. Wong, F. Astudillo-Salinas, L. Encalada, and E. Severeyn, "An aide diagnosis system based on k-means for insulin resistance assessment in elderly people from the ecuadorian highlands," in *2017 IEEE Second Ecuador Technical Chapters Meeting (ETCM)*, pp. 1–6, IEEE, 2017.
- [24] H. Herrera, E. Rebato, G. Arechabaleta, H. Lagrange, I. Salces, and C. Susanne, "Body mass index and energy intake in venezuelan university students," *Nutrition research*, vol. 23, no. 3, pp. 389–400, 2003.
- [25] J. Xu, Y. Zhang, and D. Miao, "Three-way confusion matrix for classification: A measure driven view," *Information sciences*, vol. 507, pp. 772–794, 2020.
- [26] W. S. Noble, "What is a support vector machine?," *Nature biotechnology*, vol. 24, no. 12, pp. 1565–1567, 2006.
- [27] Q.-S. Xu and Y.-Z. Liang, "Monte carlo cross validation," *Chemometrics and Intelligent Laboratory Systems*, vol. 56, no. 1, pp. 1–11, 2001.
- [28] S. S. Keerthi and C.-J. Lin, "Asymptotic behaviors of support vector machines with gaussian kernel," *Neural computation*, vol. 15, no. 7, pp. 1667–1689, 2003.
- [29] M. Marusteri and V. Bacarea, "Comparing groups for statistical differences: how to choose the right statistical test?," *Biochemia medica: Biochemia medica*, vol. 20, no. 1, pp. 15–32, 2010.
- [30] W. L. Ripka, L. Ulbricht, and P. M. Gewehr, "Body composition and prediction equations using skinfold thickness for body fat percentage in southern brazilian adolescents," *Plos one*, vol. 12, no. 9, p. e0184854, 2017.
- [31] G. Ojo and O. Adetola, "The relationship between skinfold thickness and body mass index in estimating body fat percentage on bowen university students," *International Biological and Biomedical Journal*, vol. 3, no. 3, pp. 138–144, 2017.
- [32] K. M. Flegal, J. A. Shepherd, A. C. Looker, B. I. Graubard, L. G. Borrud, C. L. Ogden, T. B. Harris, J. E. Everhart, and N. Schenker, "Comparisons of percentage body fat, body mass index, waist circumference, and waist-stature ratio in adults," *The American journal of clinical nutrition*, vol. 89, no. 2, pp. 500–508, 2009.
- [33] K. Michael, M. P. Garcia-Souto, and P. Dabnichki, "An investigation of the suitability of artificial neural networks for the prediction of core and local skin temperatures when trained with a large and gender-balanced database," *Applied Soft Computing*, vol. 50, pp. 327–343, 2017.
- [34] A. G. Lalkhen and A. McCluskey, "Clinical tests: sensitivity and specificity," *Continuing education in anaesthesia critical care & pain*, vol. 8, no. 6, pp. 221–223, 2008.
- [35] S. T. Heydari, S. M. T. Ayatollahi, and N. Zare, "Comparison of artificial neural networks with logistic regression for detection of obesity," *Journal of medical systems*, vol. 36, no. 4, pp. 2449–2454, 2012.

Uncertainty Measure of Pythagorean Fuzzy Sets

Xiaozhuan GAO^{a,d}, Lipeng PAN^a and Yong DENG^{a,b,c,d,1}

^a*Institute of Fundamental and Frontier Science, University of Electronic Science and Technology of China, Chengdu, 610054, China*

^b*School of Education, Shannxi Normal University, Xi'an, 710062, China*

^c*School of Knowledge Science, Japan Advanced Institute of Science and Technology, Nomi, Ishikawa 923-1211, Japan*

^d*Department of Management, Technology, and Economics, ETH Zurich, Zurich, Switzerland*

Abstract. Pythagorean fuzzy sets (PFS) can better express and handle the uncertainty information and has the more lager representation space. Hence, the reasonable and effective method to measure the uncertainty of PFS can better analyze information. From the view of Dempster-Shafer evidence theory, hesitancy degree can include the two focal elements (membership, non-membership). Hence, considering the number of focal elements for hesitancy degree to measure uncertainty is important. In addition, the difference between membership and non-membership degree plays an essential role in uncertainty measure. From the above views, the paper proposed the new uncertainty measure. Based on the new uncertainty measure, cross entropy and divergence of PFS can be presented. In addition, some numerical examples are used to explain the proposed methods by comparing other methods. Finally, the proposed divergence can be used in pattern recognition to verify its effectiveness.

Keywords. Pythagorean fuzzy sets, Dempster-Shafer evidence theory, Uncertainty measure, Cross entropy, Divergence

1. Introduction

Expressing information plays an essential role in knowledge representation. There are a lot of methodologies, such as Dempster-Shafer evidence theory [1,2], fuzzy sets [3] and other methodologies [4,5]. In those methodologies, fuzzy sets can handle the fuzziness information and have become the important methodology in decision-making and control. With the development of fuzzy sets, Atanassov proposed the intuitionistic fuzzy sets which can consider the membership, non-membership and hesitancy degree of information and is the generalization of fuzzy sets [6]. Yager expanded the intuitionistic fuzzy sets into the Pythagorean theme to propose Pythagorean fuzzy sets [7]. Pythagorean fuzzy

¹Corresponding Author: Yong Deng; E-mail: dengentropy@uestc.edu.cn.

sets (PFS) have the larger representation space than intuitionistic fuzzy sets and became the important math tool to handle uncertain information [8,9].

Due to the strong space representation of PFS, how to measure the uncertainty of PFS is interesting. Thao and Smarandache proposed the new fuzzy entropy of PFS by exploiting the concept of probability [10]. Peng et al proposed fuzzy Information Measures [11]. Xiao and Ding proposed the divergence by considering Jensen–Shannon divergence [12]. Yang et al proposed the fuzzy entropy of PFS [13]. Uncertainty measure of PFS should consider all aspects of information, including membership, non-membership and hesitancy degree. Moreover, two PFSs with the same uncertainty of membership, non-membership and hesitancy degree may be quite different. In other words, the difference between membership and non-membership degree should also be considered to measure the distribution of fuzziness [14]. Although there are various methods, they can not fully consider the uncertainty of PFS. Hence, how to measure the uncertainty of PFS is also an open issue.

Based on the above discussion, the paper proposed the new uncertainty measure which can consider all aspects of information as possible. Firstly, from the view of Dempster-Shafer evidence theory, the hesitant information can include the membership and non membership information which means there are two focal elements. Hence, the new uncertainty measure considers the number of focal elements. Secondly, the difference between membership and non-membership degree is computed by the score function. Based on the new uncertainty measure, the paper proposed the cross entropy and divergence of PFS. Moreover, some numerical examples can be used to explain the reasonableness of proposed methods by comparing with other methods. Finally, the new divergence can be applied to the pattern recognition to verify the effectiveness.

The structures of this article are as follows. The preliminaries of PFS and divergence are introduced in section 2. The new uncertainty measure, cross entropy and divergence of PFS are proposed in Section 3. Section 4 introduces the method of pattern recognition. In section 5, the paper can be concluded.

2. Preliminaries

In this section, we briefly recall some essential concepts of PFS and divergence.

2.1. Pythagorean Fuzzy sets

Definition 2.1. (Pythagorean fuzzy sets)

Let $\Theta = \{\lambda_1, \lambda_2, \dots, \lambda_n\}$ be a universe of discourse, a Pythagorean fuzzy set A in Θ can be defined [7]:

$$A = \{(\lambda_i, u_A(\lambda_i), v_A(\lambda_i)) \mid \lambda_i \in \Theta\} \quad (1)$$

where $0 \leq u_A(\lambda_i) \leq 1$ and $0 \leq v_A(\lambda_i) \leq 1$, which represent the membership degree and non-membership degree respectively and should satisfy $u_A(\lambda_i)^2 +$

$v_A(\lambda_i)^2 \leq 1$. Besides, the hesitancy degree can be written as follows $h_A(\lambda_i) = \sqrt{1 - (u_A(\lambda_i)^2 + v_A(\lambda_i)^2)}$ [7].

2.2. Jensen–Shannon divergence

Definition 2.2. (Jensen–Shannon divergence measure)

There are two probability distributions $A = \{a_1, a_2, \dots, a_n\}$ and $B = \{b_1, b_2, \dots, b_n\}$. The Jensen–Shannon divergence between A and B is as follows [15]

$$JS(A, B) = \frac{1}{2} [S(A, \frac{A+B}{2}) + S(B, \frac{A+B}{2})] = H(\frac{A+B}{2}) - \frac{1}{2}H(A) - \frac{1}{2}H(B) \quad (2)$$

where $H(A)$ is the Shannon entropy.

3. The proposed method

This section mainly introduces the new uncertainty measure, cross entropy and divergence of PFSs.

3.1. The Proposed Uncertainty Measure

Definition 3.1. (Uncertainty measure)

Let $\Theta = \{\lambda_1, \lambda_2, \dots, \lambda_n\}$ be a universe of discourse, the PFSs in Θ are $P(\lambda_i) = \langle \lambda_i, u(\lambda_i), v(\lambda_i) \rangle$. The uncertainty measure of PFSs is defined by

$$UM = - \sum_{i=1}^{i=n} (\sum_{j=1}^{j=3} \kappa_j(\lambda_i)^2 \log(\kappa_j(\lambda_i)^2)) + \pi(\lambda_i)^2 \log(\frac{\pi(\lambda_i)^2}{3}) \quad (3)$$

where $\kappa_1(\lambda_i) = u(\lambda_i)$, $\kappa_2(\lambda_i) = v(\lambda_i)$, $\kappa_3(\lambda_i)^2 = \Delta(\lambda_i)^2 = |u(\lambda_i)^2 - v(\lambda_i)^2|$, $\pi(\lambda_i)^2 = 1 - u(\lambda_i)^2 - v(\lambda_i)^2$. In addition, 3 is explained by the power set of Dempster-Shafer evidence theory which can be computed by $2^2 - 1$.

Definition 3.2. (Cross Entropy and Divergence)

There are two PFSs P and Q in Θ , where $P = \{ \langle \lambda_1, u(\lambda_1), v(\lambda_1) \rangle, \dots, \langle \lambda_n, u(\lambda_n), v(\lambda_n) \rangle \}$, $Q = \{ \langle \lambda_1, u(\lambda_1), v(\lambda_1) \rangle, \dots, \langle \lambda_n, u(\lambda_n), v(\lambda_n) \rangle \}$.

The new cross entropy between P and Q is defined by

$$NCE_{PQ} = \sum_{i=1}^{i=n} (\sum_{j=1}^{j=3} \kappa_{Pj}(\lambda_i)^2 \cdot \log(\frac{1}{\kappa_{Qj}(\lambda_i)^2})) + \pi_P(\lambda_i)^2 \cdot \log(\frac{3}{\pi_Q(\lambda_i)^2}) \quad (4)$$

The new divergence between P and Q is defined by

$$ND = \frac{1}{2} \sum_{i=1}^{i=n} \sum_{j=1}^{j=4} \left[\kappa_{Pj}(\lambda_i)^2 \log \frac{2\kappa_{Pj}(\lambda_i)^2}{\kappa_{Pj}(\lambda_i)^2 + \kappa_{Qj}(\lambda_i)^2} + \kappa_{Qj}(\lambda_i)^2 \log \frac{2\kappa_{Qj}(\lambda_i)^2}{\kappa_{Pj}(\lambda_i)^2 + \kappa_{Qj}(\lambda_i)^2} \right] \quad (5)$$

where $\kappa_4(\lambda_i) = \pi(\lambda_i)$. More importantly, the 0 can be regarded as the $1 \cdot 10^{-16}$ if denominator is 0.

3.2. Numerical examples

Some numerical examples are used to explain and discuss the proposed uncertainty measure, cross entropy and divergence of PFS.

Example 1 Supposing there are two PFSs $A = \langle x, 0.45, 0.75 \rangle$, $B = \langle x, 0.55, 0.80 \rangle$, the corresponding uncertainty measures are as follows.

Table 1. Uncertainty measure of Example 1

	$E_1^{[11]}$	$E_2^{[11]}$	$E_3^{[11]}$	$E_4^{[11]}$	UM
A	0.5486	0.4706	0.6400	0.3600	1.6133
B	0.5161	0.4953	0.6625	0.4727	1.2413

Obviously, B should have the smaller uncertainty than A . Because the information of B is more certain due it has the larger membership and non membership than A . From this view, it can be seen that proposed uncertainty measure and E_1 is more reasonable than other methods. Besides, the UM can better express the difference between A and B than E_1 , which can show the effectiveness of new certainty measure.

Example 2 There are some PFSs $A = \langle x, 0.45, 0.75 \rangle$, $B = \langle x, 0.55, 0.80 \rangle$, $C = \langle x, 0.55, 0.78 \rangle$, the corresponding divergences are as follows.

$$D^{[12]}(A, B) = 0.0352, D^{[12]}(A, C) = 0.0225, D^{[12]}(B, C) = 0.0019$$

$$ND(A, B) = 0.0354, ND(A, C) = 0.0236, ND(B, C) = 0.0023$$

The D which is the divergence proposed by Xiao and ND show that B is more similar with the C than A which is reasonable.

Example 3 Supposing there are two PFSs $A = \langle x, 0.5, x \rangle$, $B = \langle x, 0.4, y \rangle$. The uncertainty, cross entropy and divergence of A, B can be discussed.

In this example, x can change from 0 to 0.8660, y can change from 0 to 0.9165. The uncertainty, cross entropy and divergence of *Example 3* are as *Fig. 1*.

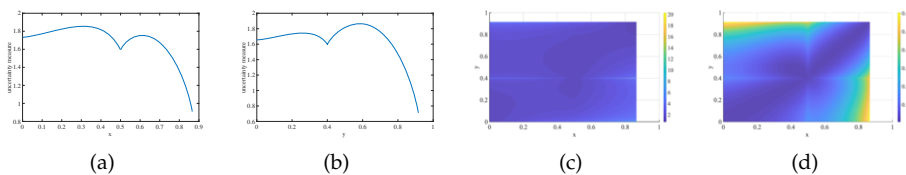


Figure 1. The uncertainty measure, cross entropy and divergence of *Example 3*. (a) uncertainty of A , (b) uncertainty of B , (c) cross entropy, (d) divergence

(a) The uncertainty of A and B can be discussed. For A , there are some conditions, as follows. (1) when x is about 0.3, the PFS is $A = \langle x, 0.5, 0.3 \rangle$. In this case, the hesitancy degree has the maximum value which has the maximum uncertainty. (2) when $x = 0.8660$, the PFS is $A = \langle x, 0.5, 0.8660 \rangle$. In this case, the hesitancy degree is 0 which has the minimum uncertainty. Next, the uncertainty

of B is analyzed. (1) when $y = 0.581$, the PFS is $B = \langle x, 0.4, 0.581 \rangle$. There is the maximum uncertainty. (2) when $y = 0.9165$, the PFS is $B = \langle x, 0.4, 0.9165 \rangle$, which has the minimum uncertainty.

(b) The cross entropy of A, B ($NCE(A,B)$) can be discussed as Fig. 1(c). (1) when $y = 0.4$, the $\Delta_B = 0$, the change of cross entropy can be shown in Fig. 2(a). It is obvious that there is the minimum cross entropy when $x = 0.5$. (2) when $x = 0.5$, the $\Delta_A = 0$. In this case, the change of cross entropy can be shown in Fig. 2(b). It can be seen that the change of cross entropy is symmetric about 0.5.

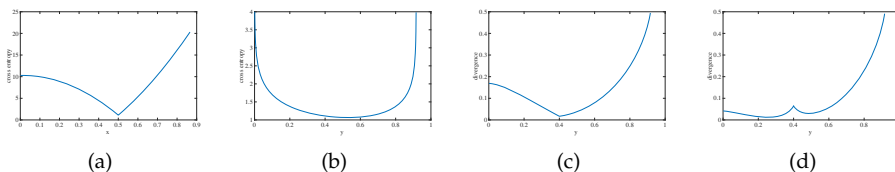


Figure 2. The cross entropy of Example. 3. (a) $y = 0.4$, (b) $x = 0.5$. The divergence of Example. 3. (a) $x = 0.5$, (b) $x = 0.3$.

(c) The divergence of A and B can be discussed, as shown in Fig. 1(d). (1) when $x = 0.5, y = 0.4, A = \langle x, 0.5, 0.5 \rangle, B = \langle x, 0.4, 0.4 \rangle$. In this case, $\Delta_A = 0, \Delta_B = 0$. Hence, the score function can not express the difference between A and B . However, hesitancy degree can help us distinguish the difference. (2) Fig. 2(c) and (d) discussed the change of divergence with y when $x = 0.5$ and $x = 0.3$. When $y = 0.4$, the divergence of $x = 0.5$ is more than $x = 0.3$, which reflects the importance of score function.

4. Application

This section introduced the method of pattern recognition based on the proposed divergence to explain its effectiveness.

4.1. Method of pattern recognition based on proposed method

Problem Statement : There are some patterns $P = \{p_1, p_2, \dots, p_m\}$ which can be expressed by PFS $p_j = \{x_i, \mu_j(x_i), v_j(x_i)\}$. Given n samples $S = \{s_1, s_2, \dots, s_n\}$ which can be expressed by PFSs $s_t = \{x_i, \mu_t(x_i), v_t(x_i)\}$. The samples should be recognised to the certain pattern. The specific steps are as follows.

Step 1 : Compute the distance between samples and patterns
The distance can be computed by using the view of Xiao [12], as follows.

$$d_{jt}(x_i) = \sqrt{\frac{1}{n} \sum ND(p_j, s_t)}$$

Step 2 : Determine the minimum value of distance

There are some distances between every sample and all patterns. The minimum distance can be determined as

$$\tilde{D}(p_\alpha, s_t) = \min_{1 \leq j \leq m} D(p_j, s_t)$$

Step 3 : Obtain the results of recognition

The sample can be classified as the pattern with minimum distance.

$$s_t \leftarrow p_\alpha$$

4.2. Application of medical diagnosis

Medical diagnosis can be used to explain the proposed pattern recognition which can be introduced simply. There are four patients $P = \{p_1, p_2, p_3, p_4\}$ with the five symptoms $S = \{s_1 : \text{Temperature}, s_2 : \text{Headache}, s_3 : \text{Stomachpain}, s_4 : \text{Cough}, s_5 : \text{Chestpain}\}$. The possible diagnosis $D = \{d_1 : \text{Viral fever}, d_2 : \text{Malaria}, d_3 : \text{Typhoid}, d_4 : \text{Stomachproblem}, d_5 : \text{Chestproblem}\}$. The more related information can be obtained in [12]. The results of medical diagnosis by using proposed method are as Tab. 2.

Table 2. The results of pattern recognition

	D_1	D_2	D_3	D_4	D_5	Results
p_1	0.3055	0.2501	0.3885	0.4776	0.5337	D_2
p_2	0.4388	0.5223	0.4178	0.1864	0.4734	D_4
p_3	0.3878	0.4223	0.3888	0.4797	0.5068	D_3
p_2	0.3296	0.4030	0.4528	0.4519	0.5466	D_1

To further explore the reasonableness and effectiveness of proposed method, there are some comparisons with other methods as Tab. 3. It can be seen that the results of proposed method are similar to those of most methods which proves the proposed method is practical in dealing with medical diagnosis.

Table 3. The results of different methods

	Own ^[16]	Deetal. ^[17]	Szmidtetat. ^[18]	Weietal. ^[19]	Mondaletal. ^[20]	Xiao ^[12]	Proposed
p_1	D_2	D_2	D_2	D_2	D_2	D_2	D_2
p_2	D_4	D_4	D_4	D_4	D_4	D_4	D_4
p_3	D_3	D_2	D_3	D_3	D_3	D_3	D_3
p_4	D_2	D_2	D_1	D_1	D_1	D_1	D_1

5. Conclusion

In Pythagorean fuzzy sets (PFS), how to measure uncertainty is important and an open issue. PFS can include the membership, non-membership and hesitancy degree. Hence considering them comprehensively can help us better analyze the uncertainty of PFS. The paper proposed the uncertainty measure of PFS by considering the membership, non-membership, hesitancy degree and difference

between membership and non-membership degree. Besides, from the view of Dempster-Shafer evidence theory, the number of focal elements of hesitancy information which can include the membership and non-membership information is considered. Based on the proposed uncertainty measure, the cross entropy and divergence of PFS can be also presented. In addition, the new uncertainty measure can be compared with the other methods, which shows the new uncertainty measure can better reflect the difference between PFSs and is reasonable. Finally, the medical diagnosis can be applied to the method of proposed the pattern recognition based on the new divergence. The results are used to compare with other methods to verify reasonableness and effectiveness of the new method.

References

- [1] A. P. Dempster, Upper and lower probabilities induced by a multivalued mapping, *The Annals of Mathematical Statistics* 38 (2) (1967) 325–339.
- [2] G. Shafer, *A mathematical theory of evidence*, Vol. 42, Princeton university press, 1976.
- [3] L. A. Zadeh, Fuzzy sets, in: *Fuzzy sets, fuzzy logic, and fuzzy systems: selected papers by Lotfi A Zadeh*, World Scientific, 1996, pp. 394–432.
- [4] K. Ullah, T. Mahmood, N. Jan, Similarity measures for t-spherical fuzzy sets with applications in pattern recognition, *Symmetry* 10 (6) (2018) 193.
- [5] X. Gao, Y. Deng, Quantum model of mass function, *International Journal of Intelligent Systems* 35 (2) (2020) 267–282.
- [6] K. T. Atanassov, *On intuitionistic fuzzy sets theory*, Vol. 283, Springer, 2012.
- [7] R. R. Yager, Pythagorean fuzzy subsets, in: *2013 joint IFSA world congress and NAFIPS annual meeting (IFSA/NAFIPS)*, IEEE, 2013, pp. 57–61.
- [8] H. Garg, Linguistic pythagorean fuzzy sets and its applications in multiattribute decision-making process, *International Journal of Intelligent Systems* 33 (6) (2018) 1234–1263.
- [9] L. Pan, X. Gao, Y. Deng, K. H. Cheong, The constrained pythagorean fuzzy sets and its similarity measure, *IEEE Transactions on Fuzzy Systems* (2021) DOI: 10.1109/TFUZZ.2021.3052559.
- [10] N. X. Thao, F. Smarandache, A new fuzzy entropy on pythagorean fuzzy sets, *Journal of Intelligent & Fuzzy Systems* 37 (1) (2019) 1065–1074.
- [11] X. Peng, H. Yuan, Y. Yang, Pythagorean fuzzy information measures and their applications, *International Journal of Intelligent Systems* 32 (10) (2017) 991–1029.
- [12] F. Xiao, W. Ding, Divergence measure of pythagorean fuzzy sets and its application in medical diagnosis, *Applied Soft Computing* 79 (2019) 254–267.
- [13] M.-S. Yang, Z. Hussain, Fuzzy entropy for pythagorean fuzzy sets with application to multi-criterion decision making, *Complexity* 2018 (2018).
- [14] Y. Song, Q. Fu, Y.-F. Wang, X. Wang, Divergence-based cross entropy and uncertainty measures of atanassov's intuitionistic fuzzy sets with their application in decision making, *Applied Soft Computing* 84 (2019) 105703.
- [15] J. Lin, Divergence measures based on the shannon entropy, *IEEE Transactions on Information theory* 37 (1) (1991) 145–151.
- [16] C.-M. Own, Switching between type-2 fuzzy sets and intuitionistic fuzzy sets: an application in medical diagnosis, *Applied Intelligence* 31 (3) (2009) 283.
- [17] S. K. De, R. Biswas, A. R. Roy, An application of intuitionistic fuzzy sets in medical diagnosis, *Fuzzy sets and Systems* 117 (2) (2001) 209–213.
- [18] E. Szmidt, J. Kacprzyk, Intuitionistic fuzzy sets in intelligent data analysis for medical diagnosis, in: *International conference on computational science*, Springer, 2001, pp. 263–271.
- [19] C.-P. Wei, P. Wang, Y.-Z. Zhang, Entropy, similarity measure of interval-valued intuitionistic fuzzy sets and their applications, *Information Sciences* 181 (19) (2011) 4273–4286.
- [20] K. Mondal, S. Pramanik, Intuitionistic fuzzy similarity measure based on tangent function and its application to multi-attribute decision making, *Global journal of advanced research* 2 (2) (2015) 464–471.

Open Access Digital Thesaurus on Ethnic Groups in the Mekong River Basin

Wirapong Chansanam^{a,1}, Kanyarat Kwiecien^a, Marut Buranarach^b and Kulthida Tuamsuk^a

^a*Department of Information Science, Faculty of Humanities and Social Sciences, Khon Kaen University, Khon Kaen 40002, Thailand*

^b*National Electronics and Computer Technology Center, Pathumthani 12120, Thailand*

Abstract. The ethnic group domain, in particular, is characterized by rich and diverse data sets in the Mekong River Basin (MRB). Ethnic groups' vocabulary and relevant data come from various sources that cross history, language, and geography. As a result, distinct language is used by specialized groups to characterize their artifacts. Data interoperability among multiple catalogs is highly challenging as a result of this. The usage of controlled vocabularies and thesauri is generally considered a major practice for making preparations for standardization, which is essential for data reuse and sharing. In contrast, when used together, thesauri eliminate ambiguity in natural language, making it easier to identify and integrate data from different sources and allow scholars and computer programs to understand data more efficiently. This paper describes the modeling process of the EGMRB Thesaurus, its integration and role in the infrastructure, its publication as Linked Open Data, and the results of this work after six months of development. This paper presents the rationale behind the realization of this thesaurus. Thesaurus EGMRB (<http://thesaurus.asiana.net/vocab/>) provides a semantic resource on ethnic groups in the Mekong river basin. EGMRB is the outcome of interdisciplinary cooperation of specialists from the domains of ethnic groups and information science, who collaborated in the context of collaborative research. The thesaurus was developed in Simple Knowledge Organization System (SKOS), a standard data format based on the Resource Description Framework (RDF), using semantic web standard technologies. EGMRB is freely available online, with a SPARQL endpoint (<http://thesaurus.asiana.net/vocab/sparql.php>) for querying and an API (<http://thesaurus.asiana.net/vocab/services.php>) for system integration. Digital collections, digital exhibits, and a virtual study environment are being built as part of a digital platform that will give scholars and the general users search and content curation services. EGMRB, which provides unified ideas with related unique and resolvable URIs, can profoundly reduce the barriers to data discovery, integration, and sharing if adopted as a standard and carefully implemented and expanded by the academic community.

Keywords. Thesaurus, Mekong River Basin, Digital Platform, Linked Data, Web service

¹ Corresponding Author, Wirapong Chansanam, Department of Information Science, Faculty of Humanities and Social Sciences, Khon Kaen University, Khon Kaen 40002; E-mail: wirach@kku.ac.th.

1. Introduction

An online platform providing search and content curation services will be available for free to anybody who wishes to use it via the EGMRB Thesaurus. This will feature digital displays, digital collections, and access to a virtual study environment for scholars and the general users. The EGMRB Thesaurus infrastructure will be used to help project researchers in the development of data open access management strategies and to disseminate any data by the KOS principles. According to [1] DCAT 2 (Data Catalogue Vocabulary) specifications like the Getty Thesaurus will be easier to locate and utilize because of the DCAT 2 specifications.

Nowadays, information can be transferred rapidly and simply according to such new technologies as the Internet and electronic data records. To conduct effective research and analysis, users must have access to the appropriate datasets and efficient methods for properly explaining and exploring basic concepts inside and across datasets [2, 3]

Metadata, controlled vocabularies, thesauri, or even ontologies are used in this method since they complement one another [4]. A thesaurus is a controlled and structured vocabulary that contains concepts by terms. It is delivered so that concepts are interconnected so that links between them may be made clear. Preferred terms are accompanied with comes entries for synonyms or "quasi-synonyms" [5]. By reducing ambiguity in plain language, thesauri are essential method for discovering and organizing information, especially for discovering material in non-literary, uncategorized formats. They help academics and the public to discover data and other materials consistently.

The process of building a thesaurus is rather complicated. It involves identifying terms from a specific area, analyzing and linking those phrases into a categorization model that can be used to classify resources from the same domain. The form and characteristics of monolingual and multilingual thesauri have changed throughout the years to normalize these structures [5-8]. ISO 25964, the most current international standard for thesauri, describes five fundamental kinds of thesaurus ideas, thesaurus terms, thesaurus arrays, and notes and sets forth a data format and derived XML schema. There is an explicit distinction between "terms" and "concepts" in the data model. The data model includes information on additional elements that might be considered a part of a thesaurus, including ConceptGroup, a unique grouping for terms related to a particular domain, theme, or other categories [5-8]. While it does not have a specific building technique proposed, the ISO 25964 does not offer specific advice on developing and maintaining thesauri but does provide guidelines for both aspects.

Initiatives in development for digital platform assistance for content discovery and management will be using the EGMRB Thesaurus. A helpful way to share and link to controlled vocabularies in the Semantic Web is by using the W3C recommendation, the SKOS (Simple Knowledge Organization System), as a model [9]. The thesaurus of the EGMRB is detailed in this article, including how it functions inside the infrastructure and as Linked Open Data (LOD). The second section of this paper will consider similar work that has modeled thesauri and other controlled vocabularies and other research infrastructures and LOD initiatives in the framework of other projects and initiatives addressing specific ethnic group. Section 3 will discuss the methods and tools used to manage and publish vocabularies in the infrastructure. This section details our preliminary findings. Our findings and recommendations conclude with this section.

2. Related work

In GLAM (Galleries, Libraries, Archives, and Museums) applications, subject indexing, keyword-based search in local databases, and federated search across multiple databases [10, 11] are extensively used through the use of thesauri and other knowledge organization systems, such as taxonomies, classification schemes, and classifications. Within LOD efforts, it is estimated that SKOS is one of the most often used vocabularies and is widely utilized by other Semantic Web vocabularies. Using controlled vocabularies for Semantic Web applications such as query expansion, search term recommendations, and semantic search engines is possible through the 'skosification' of those vocabularies [12, 13, 14]. Here, the Getty Vocabularies Project is a classic case, as it contains reference vocabularies that describe the work of artists and architects, such as the Art and Architecture Thesaurus (AAT).

The two publication models identified by Pohorec, Zorman, and Kokol include both inline and parallel Web publications (2013). Another popular approach of making massive datasets available as Linked Data is by publishing them in parallel, as machine-processable collections of RDF data. However, the findings of this study include an observation that RDF material published using this method is not often indexed by standard search engines and has limited exposure [15]. Instead of just utilizing an established standard like Microdata or Resource Description Framework (RDF), authors can use an extension like the Microdata or RDF markup to add semantic markup to HTML text and create structured data. As a result, the Linked Data concepts are syntax agnostic, making the technology compatible with many markup languages and serialization methods.

Linked Data is defined as a method of publishing and interconnecting structured information while also encouraging the growth and contribution of other participants in the Linked Data ecosystem [16]. The machines can "understand" the meaning of the relationships by making inferences about the content and then interlinking that data to new information automatically, discovering connections that were previously hidden [17, 18].

3. Methodology

Development of the EGMRB Thesaurus

EGMRB Thesaurus development follows the procedure in Fig. 1, based on standard for building multilingual thesauri [19-21].

In the beginning, we are just getting started when we are synthesizing several language resources provided by our partnering academic institutes and various KOS from the domains of humanities and social sciences. Mapping or alignment can be performed with regard to the words and ideas included in the following canonical sources: these sources serve not only as reference material for terms and concepts in the EGMRB Thesaurus but also as subjects of that mapping or alignment. A comprehensive mapping of the ideas included in LOD to reference and top-level concept schemes, such as the AAT and the BBT, should be achievable. In our process, we include interactions with subject matter experts and information professionals. It will be essential to provide the local topic heading lists, thesauri and validate third-party subject heading lists. It will also help test EGMRB Thesaurus macro and microstructure.

This thesaurus contains approximately 4,609 ethnic terms organized hierarchically, although other essential ideas are also included. A collaborative working team method was employed throughout the development of the EGMRB Thesaurus. Different duties were divided up amongst editors and knowledge engineers, who worked together. As a result, editors have knowledge of many ethnic groups' subjects, and they are responsible for planning, design, implementation, and maintenance of the thesaurus.

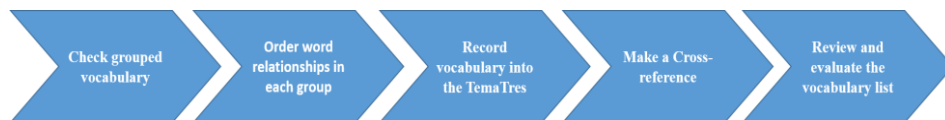


Figure 1. The EGMRB digital thesaurus development

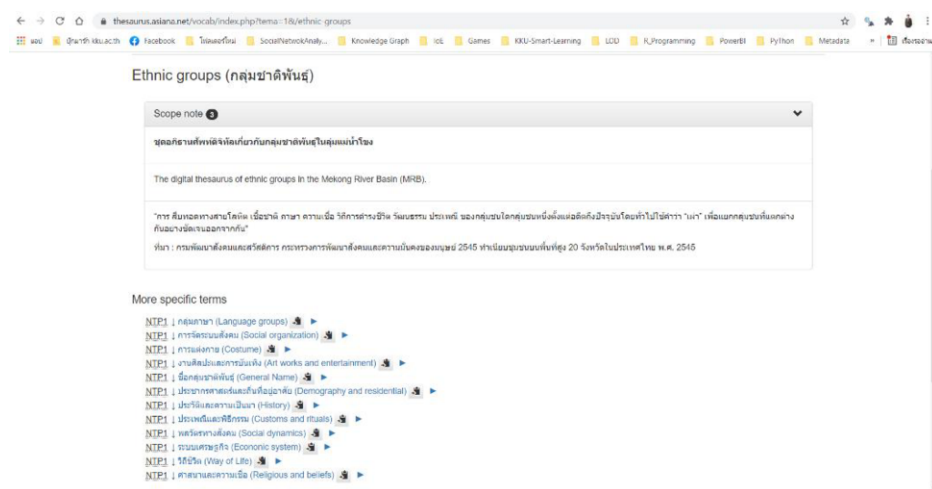


Figure 2. The screen shot of hierarchical structure with narrower terms and meta terms for “Ethnic groups” respectively.

TemaTres (<http://www.vocabularyserver.com/>) was chosen to make SKOS thesaurus' development less difficult [22]. TemaTres' relative simplicity, and the fact that it was possible to interact with it through the web, made it a good option for developing EGMRB Thesaurus. Fig. 3 presents the TemaTres user interface, which contains a basic but helpful feature for modifying ideas. As shown, it has advanced search capabilities and the possibility to link to external concepts (e.g., SKOS-Core, JSON, JSON-LD). In addition, the TemaTres allows a little more basic taxonomy input for tab-indented files or RDF/XML encoded SKOS documents [23].

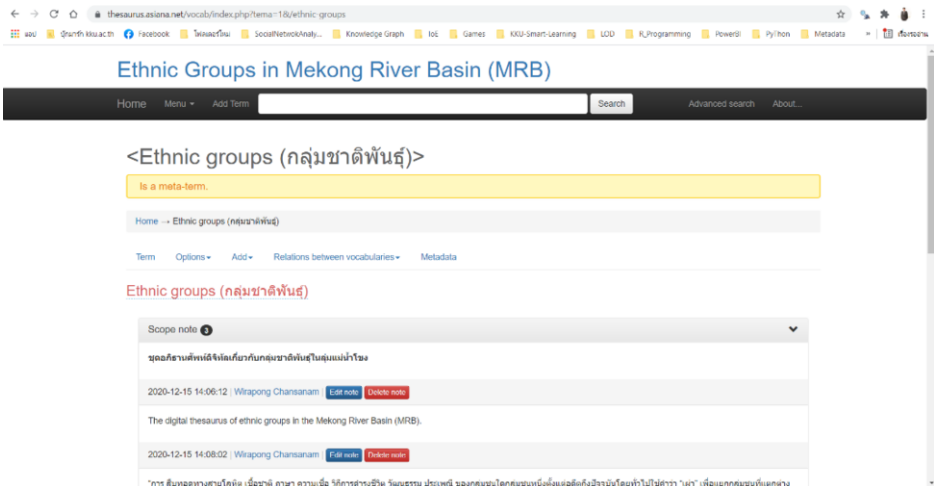


Figure 3. In the admin interface of the EGMRB thesaurus main page, there are several tabs on the screen.

SPARQL endpoints are also accessible, enabling anybody (human or otherwise) to utilize the SPARQL language to search the thesaurus [24]. Results are often delivered in machine-processable forms. In addition to the SPARQL interface, TemaTres also provides an online form that knowledge engineers may use to query the thesaurus (Fig. 5). While inexperienced users will generally handle both the formulation of questions and the human-readable display of results, developing ad-hoc user interfaces and software are required for more proficient users.

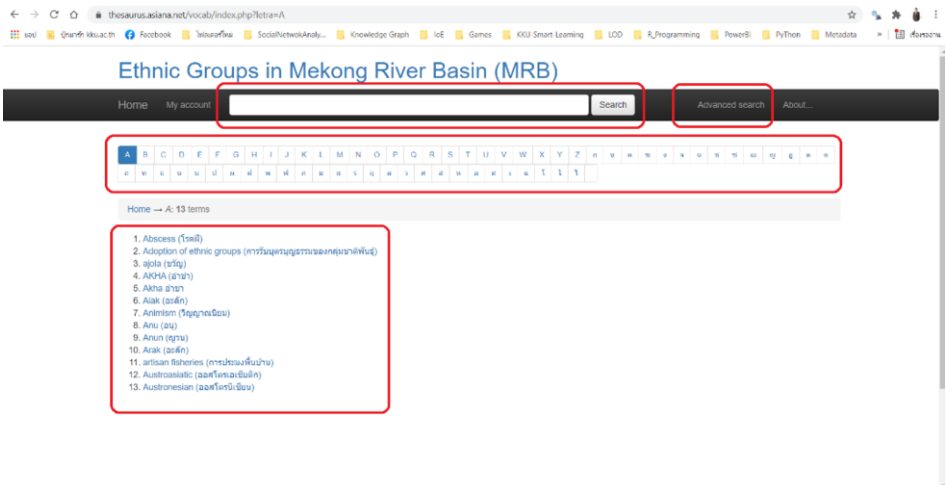


Figure 4. EGMRB Thesaurus's variety of user-friendly search engines included: simple search engine; auto-completed text box search, alphabetic index, and advanced search.

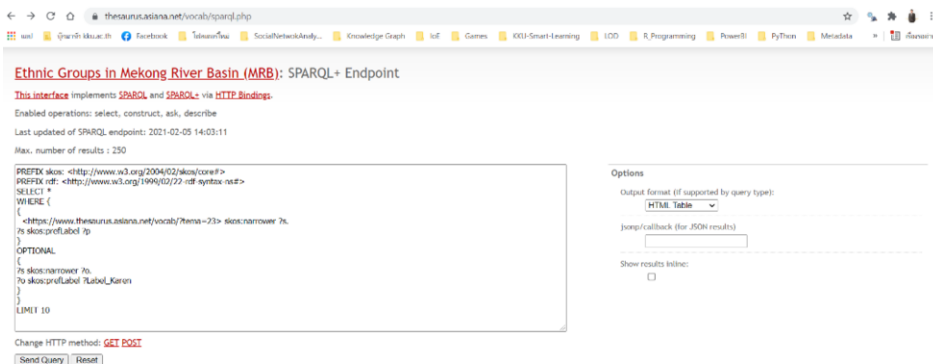


Figure 5. SPARQL endpoint interface for the concept "Karen" which offers an example of a query in the form of a query string, with a response in HTML table format.

We assigned attributes and relations to the terms, then changed them based on how they were relevant to the webpage's structure. Editorial touch-ups: Users could modify the structural elements of each term (preferred term, non-preferred term, definition, associated bibliographic note, etc.) by using the TemaTres user interface, while simultaneously restructuring the hierarchical structure if applicable. Each of the chosen terms was accompanied by a definition that frequently linked to a bibliographic reference and was presented within a hierarchical relationship. In addition, preferred terminology such as related terms and a synonym were given where it is usual to use those phrases.

When the thesaurus was built, editors sent it to the knowledge engineer, who went through and assessed various terms and their structural elements, then confirmed or excluded them and submitted revisions to the editors in the form of private notes from TemaTres. The knowledge engineers submitted their comments, and the editors evaluated the information, after which the stable version of the thesaurus was issued. Codes and Uniform Resource Identifiers (URIs) are published, and each code and URI changes are monitored.

EGMRB Thesaurus is accessible over the internet at the URL <https://thesaurus.asiana.net/vocab/>. This feature is flexible and might be applied to many uses. Additionally, we utilize the EGMRB Thesaurus as well as other existing controlled vocabularies to help manage data sources, including databases, research documents, and to support semantic interoperability at the Princess Maha Chakri Sirindhorn Anthropology Centre (Public Organization) (<https://www.sac.or.th/databases/ethnic-groups/ethnicGroups>)

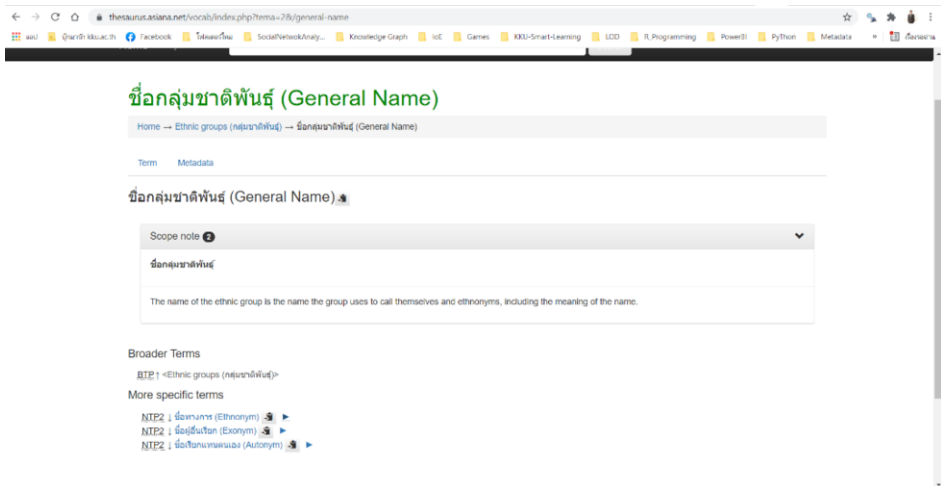


Figure 6. A screenshots of vocabulary provided for the concept “General Name”.

INSPIRE, the national standard of metadata, includes guidelines for SAC metadata which meet these guidelines (Drafting Team Metadata and European Commission Joint Research Centre, 2013). The “Dataset Metadata” user interface incorporates an approved user input form, as well as a synonym entry form from the EGMRB Thesaurus, within its “Dataset Metadata” section to allow authorised users to describe datasets in line with SAC Metadata Schema. While the metadata standard does not specify where to put metadata terms like “keyword” for the explanation of datasets on ethnic groups variety or correlated domains, EGMRB Thesaurus can be used for metadata annotations, and the process of identifying terms to use for metadata annotations begins by looking for relevant metadata terms in the data. If the user uses clear terms from shared thesauri for their metadata schema's population, searchers' efforts will be helped tremendously in data discovery and retrieval.

Additional anthropological thesauri and controlled vocabularies are necessary to the academic community. Furthermore, the EGMRB Thesaurus is utilized by the Linked Data system for data annotation [25]. When contributors uploading data resources through the portal utilize the data ingestion web interface, they must name their dataset's fields after the taxonomies, which are located inside the thesauri. These ideas, when put together, form the "EGMRB Data Schema". The examples shown in figure 7 illustrate the annotation of data accessible via the data portal by leveraging APIs (JSON format).

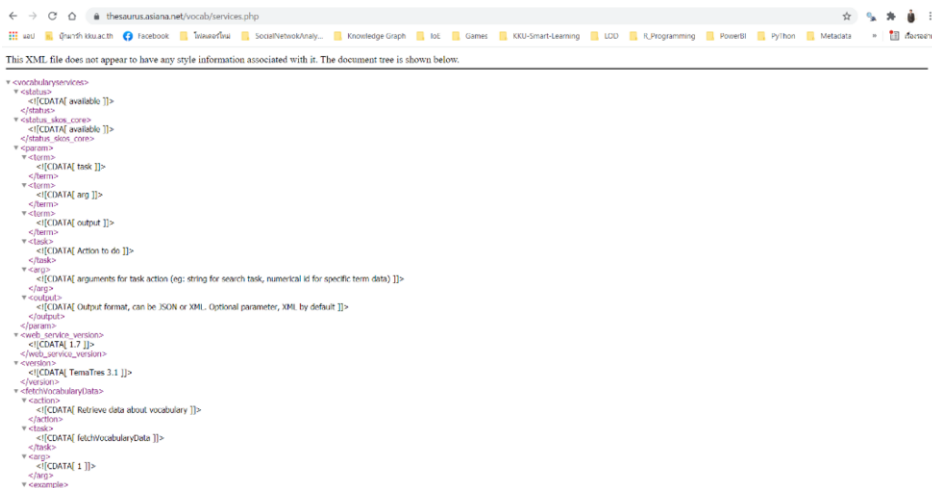


Figure 7. A portion of the database's schema description including information on the semantic annotations of fields with thesauri concepts.

In addition, while searching for the ethnic group concept, all these terms will be returned. The terminology and URIs in a standardized data markup are connected explicitly with one another, allowing records to be understood by the machine. The potential for computer-aided change, distribution, and long-term reuse opens up with the opening of datasets to a larger universe of possibilities.

The EGMRB Thesaurus has a stated objective of developing a web portal that will increase the amount of ethnic historical MRB resources in the public domain and help in the advanced search and display of information linked to this inheritance. To enhance the quality of the study, it seeks to utilize as many scientific references as feasible. This thesaurus is specifically designed for academics, students, and anthropologists. For example, the researcher may connect words they may have found in manuscript documentation with thesaurus entries, which are more modern and conventional in their nomenclature. Standardizing vocabulary in a monument requires the use of a thesaurus. Students in the humanities and social sciences will learn about many ethnic groups. In addition, this vocabulary's ultimate goal is to promote the knowledge, conservation, and distribution of ethnic groups information.

The EGMRB Thesaurus has an increasingly international terminology, implying that all terms have to be translated. Initially, simple words, synonyms, and related ideas were translated directly. In other situations, specialized resources provide translations in between Thai and English. Because terms only existed in the original ethnic language or needed more than one translation, difficulties occurred while translating them.

4. Discussion

This project aims to ensure its long-term sustainability. The project's initial goal was to create the EGMRB Thesaurus to address ambiguity concerns with natural language by standardizing how words, meanings, and relationships are constructed.

As a result, building upon the various semantic resources, such as the EGMRB Thesaurus, is essential for facilitating the discovery and interchange of existing and new knowledge and accomplishing a more thorough consideration within the particular domain as well as a greater understanding of the broader context. The first step towards semantic interoperability is dataset annotation using taxonomies [17].

This perspective argues that the EGMRB Thesaurus is created according to LOD principles to ensure that computers may run in a way that assists data users in finding and processing relevant material [26]. In addition, EGMRB Thesaurus, maintaining standards about Web development, boosts interoperation and use of automatic data interchange across various sources. EGMRB Thesaurus ideas for the semantic annotation of their data enable simultaneous searches on various data.

The thematic thesaurus is expected to be an essential initial step in creating an ethnic group knowledge base for the Mekong River Basin. While [27] talk about creating ontologies, they also suggest using thesauri as a starting point. In this view, EGMRB Thesaurus employed knowledge structure [28] based on ethnicity in six countries, moreover utilized semantic data categorization using a LOD framework [25], expanding researchers' boundaries.

5. Conclusion and future work

The purpose of this article is to construct the EGMRB Thesaurus. Instead, they aim to enable the discovery and administration of different content types in the EGMRB Thesaurus database, providing resources for topics such as politics, liberal arts, linguistics, and culture. We hope that our resource will become a valuable part of the Linked Open Data cloud and function as a reference tool in subjects of anthropology domain. While important work remains to be done in creating and publishing the EGMRB Thesaurus, significant progress has been made. The first complete edition of the thesaurus is expected to be released in October 2021. The EGMRB Thesaurus digital platform will have another assignment: integration of the thesaurus into the platform. This means that academics will be able to comment on virtual exhibits, virtual collections, and other content developed on the platform. In order to increase the reach of our platform, we will employ the thesaurus to expand search throughout our existing collection and the semantic domain by accessing a smaller dataset given by a researcher of the Digital Humanities Research Group (DHRG) who specializes in folktales.

References

- [1] R. Albertoni et al., "Data Catalog Vocabulary (DCAT)-Version 2," W3C Candidate Recommendation, vol. 3, 2019.
- [2] M. B. Jones, M. P. Schildhauer, O. Reichman, and S. Bowers, "The new bioinformatics: integrating ecological data from the gene to the biosphere," *Annu. Rev. Ecol. Evol. Syst.*, vol. 37, pp. 519–544, 2006.
- [3] J. Madin, S. Bowers, M. Schildhauer, S. Krivov, D. Pennington, and F. Villa, "An ontology for describing and synthesizing ecological observation data," *Ecological informatics*, vol. 2, no. 3, pp. 279–296, 2007.
- [4] B. Haslhofer and W. Klas, "A survey of techniques for achieving metadata interoperability," *ACM Computing Surveys (CSUR)*, vol. 42, no. 2, pp. 1–37, 2010.

- [5] ISO 25964-1: Information and documentation - Thesauri and interoperability with other vocabularies - Part 1: Thesauri for information retrieval. ISO, Geneva (2011)
- [6] BS 8723-1, 2005. Structured vocabularies for information retrieval - Guide - Part 1: Definitions, symbols and abbreviations. British Standards Institution, London.
- [7] E. G. Fayen, "Guidelines for the construction, format, and management of monolingual controlled vocabularies: A revision of ANSI/NISO Z39. 19 for the 21st century," *Information Wissenschaft und Praxis*, vol. 58, no. 8, p. 445, 2007.
- [8] I. O. for Standardization, ISO 25964-2:2013: Information and Documentation: Thesauri and Interoperability with Other Vocabularies. Interoperability with other vocabularies, no. pt. 2. ISO, 2013. [Online]. Available: <https://books.google.co.th/books?id=703ooAEACAAJ>
- [9] A. Miles and S. Bechhofer, "SKOS simple knowledge organization system reference," W3C recommendation, 2009.
- [10] Coudyzer, E.: First release GLAM sector reference terminologies (Sep 2013), <https://www.athenaplus.eu/getFile.php?id=187>
- [11] P. Harpring, Introduction to controlled vocabularies: terminology for art, architecture, and other cultural works. Getty Publications, 2010.
- [12] D. Koutsomitropoulos, G. Solomou, and K. Kalou, "Federated semantic search using terminological thesauri for learning object discovery," *Journal of Enterprise Information Management*, 2017.
- [13] H. Nagy, T. Pellegrini, and C. Mader, "Exploring structural differences in thesauri for SKOS-based applications," in *Proceedings of the 7th International Conference on Semantic Systems*, 2011, pp. 187–190.
- [14] Y. Yang, J. Xiong, and S. Wang, "A semantic search engine based on SKOS model ontology in agriculture," in *International Conference on Computer and Computing Technologies in Agriculture*, 2010, pp. 110–118.
- [15] S. Pohorec, M. Zorman, and P. Kokol, "Analysis of approaches to structured data on the web," *Computer Standards & Interfaces*, vol. 36, no. 1, pp. 256–262, 2013.
- [16] C. Bizer, T. Heath, and T. Berners-Lee, "Linked data: The story so far," in *Semantic services, interoperability and web applications: emerging concepts*, IGI global, 2011, pp. 205–227.
- [17] T. Berners-Lee, J. Hendler, and O. Lassila, "The semantic web," *Scientific american*, vol. 284, no. 5, pp. 34–43, 2001.
- [18] W3.org. 2021. Ontologies - W3C. [online] Available at: <http://www.w3.org/standards/semanticweb/ontology> [Accessed 19 June 2021].
- [19] E. G. Fayen, "Guidelines for the construction, format, and management of monolingual controlled vocabularies: A revision of ANSI/NISO Z39. 19 for the 21st century," *Information Wissenschaft und Praxis*, vol. 58, no. 8, p. 445, 2007.
- [20] J. Aitchison, D. Bawden, and A. Gilchrist, *Thesaurus construction and use: a practical manual*. Routledge, 2003.
- [21] V. Broughton, *Essential thesaurus construction*. Facet Publishing, 2006.
- [22] A. Gonzales-Aguilar, M. Ramírez-Posada, and D. Ferreyra, "TemaTres: software para gestionar tesoros," *Profesional de la Información*, vol. 21, no. 3, pp. 319–325, 2012.
- [23] D. Beckett and B. McBride, "RDF/XML syntax specification (revised)," W3C recommendation, vol. 10, no. 2.3, 2004.
- [24] E. Prud'hommeaux, "SPARQL query language for RDF, W3C recommendation," <http://www.w3.org/TR/rdf-sparql-query/>, 2008.
- [25] W. Chansanam, K. Tuamsuk, and J. Chaikhambung, "Linked Open Data Framework for Ethnic Groups in Thailand Learning," *International Journal of Emerging Technologies in Learning (iJET)*, vol. 15, no. 10, pp. 140–156, 2020.
- [26] E. Garnier et al., "Towards a thesaurus of plant characteristics: an ecological contribution," *Journal of Ecology*, vol. 105, no. 2, pp. 298–309, 2017.
- [27] W. Chansanam, K. Tuamsuk, K. Kwiecien, T. Ruangritpakorn, and T. Supnithi, "Development of the Belief Culture Ontology and Its Application: Case Study of the GreaterMekong Subregion," in *Joint International Semantic Technology Conference*, 2014, pp. 297–310.
- [28] J. Chaikhambung and K. Tuamsuk, "Knowledge classification on ethnic groups in Thailand," *Cataloging & Classification Quarterly*, vol. 55, no. 2, pp. 89–104, 2017.

Semantic Repeatability Screening Mechanism of Intelligent Learning Platform Based on Bi-LSTM

Jianghui Liu^{a,1} Bairu Xie^b and Yuqing Shi^c

^aNetwork and Information Center, Experimental Teaching Center, Guangdong University of Foreign Studies, Guangzhou, China

^bSchool of Economics and Trade, Guangdong University of Foreign Studies, Guangzhou, China

^cSchool of English Education, Guangdong University of Foreign Studies, Guangzhou, China

Abstract. To solve the excessive utilization of back-end data caused by the sharp increase in the visit and consultation on the intelligent learning platform in the era of novel coronavirus epidemic, this study proposed to introduce Co-attention mechanism (Co-attention) into the Bidirectional Long Short Term Memory model (Bi-LSTM). The study employed Multi-layer Perception Network (MLP) for classification and screening to accurately judge the semantic repeatability. Lastly the study carried out contrast experiments for different models, using 1150 consultation posts about transposed determinant, using Newton's Leibniz formula to calculate definite integral, using Laplace's theorem to calculate determinant, how to do model analysis of STATA panel data, under what circumstances is the weighted least square method applicable, how to realize the Pareto optimality and finding the area of trapezoid with curve side from MOOC platform of Chinese universities. Results show that this model performs better than other existing models on the judgment accuracy and its accuracy is up to 89.42%.

Keywords. Intelligent learning platform, Bi-LSTM, Co-attention, Sentence vector, Semantic repeatability

1. Introduction

To meet the development needs of Chinese students in the new era, online education industry has gradually become a new trend in China's education. According to the survey of China Internet Network Information Center (CNNIC), the number of online education users in China has increased from 117 million in 2016 to 351 million in 2020, increasing by nearly three times. And the usage rate has increased from 16.6% to nearly 30%.

The rise of online smart teaching platforms has provided new ideas for solving the dilemmas faced by the traditional education industry under the new crown epidemic. Major online smart learning platforms should also begin to think about how to better improve the efficiency of platform operations, so as to efficiently support the large

¹ Corresponding Author: Jianghui Liu, Network and Information Center, Experimental Teaching Center, Guangdong University of Foreign Studies, China; Email: maggyliu1978@163.com

influx of students. [1] A survey of opinions on online learning conducted by undergraduates of Guangdong University of Foreign Studies revealed that while students generally recognized the safety and high participation of online learning platforms, they also raised questions about the knowledge of students on the platform by teachers. Questions are not answered in time. [2] Therefore, how to effectively improve the system operating efficiency of the online intelligent learning platform plays a crucial role in improving the efficiency and enthusiasm of learners in online learning.

In the process of learning on the online learning platform, students will also send consultation posts to seek answers to the questions encountered during the online course learning. But among the countless consultation posts, there was inevitably a large number of repeated or similar questions that had been answered [3]. Learners may use completely different statements to ask the same or similar questions. The difficulties in detecting semantic similarity are as follows: First, similar or identical questions may contain completely different grammar, vocabulary or statement structures. Second, a single approach may be appropriate for different types of problems. Third, some teachers had answered the consulting contents before the repeatability screening of these uploaded contents, which caused the difficulty and burden of data processing. Fourth, it's hard to efficiently screen out the repeated statements from the numerous consultation posts.

Rather than expanding the capacity of back-end data from the aspect of information overload, it is better to improve the filtering system for duplicate values. In the processing of natural language, the detection of equivalent semantics has always been a difficult problem. In order to detect similar data in the smart medical platform, an innovative security mechanism called HealthGuard came into being. [3] In addition to the detection of semantic differences, an end-to-end multi-channel deep learning model SDCM is also applied to deal with the differences between image pairs. [4]

In recent years, various neural network models have also been widely used to process the semantic similarity of natural language. Existing research has tried to merge the CNN model and the RNN model to solve the problem of superimposing multiple convolutional layers when the CNN model recognizes the correlation between sentences. [5]

And the adoption of Siamese neural network to detect the semantic similarity of statements had become the focus of research in this field.[6] Many scholars have used neural network models to improve the repeatability detection mechanism of Quora and Stack Overflow platforms.[7,8] There are also studies that have improved related technologies from the perspective of models, such as DupPredictorRep and DupeRep models based on DupPredictor and Dupe models.[9] Some scholars have further proposed that introducing the attention mechanism into the deep learning model to screen the similarity of sentences.[10,11] Then, the ESIM model came into being. This model further improves the ability of the Bi-LSTM model to obtain the semantic information of sentences at different time steps. [12]

According to the literature review, the current research on the use of deep learning models to repetitively screen online learning platform consulting issues still has the following shortcomings. First, the optimization of the intelligent learning platform system is mainly focused on the recommendation system of learning paths and learning resources, and there is a lack of research on the optimization of the processing system of student consulting data. Second, the attention mechanism introduced in the current deep learning model is limited to obtaining semantic information from a single

direction of the sentence, and the inference of the similarity of sentence meaning is prone to large errors. Third, the current deep learning model mainly uses the Word2Vec model or the GloVe model to convert sentences into word vector representations, but the word vector representation cannot efficiently process large-scale sentence data and lacks the ability to identify the connection between sentence context information Ability to effectively improve the prediction rate.

To solve the above problems, this study introduced the Siamese sub-neural network into the twin growth short-term memory model Bi-LSTM, and used the DM model in the sentence vector technology (doc2vec) to improve the prediction rate of the model, sentence vector technology and two-way mutual attention. The introduction of the mechanism enabled the model to effectively obtain the context information of the sentence, thereby achieving accurate semantic recognition. The study also optimized the hidden layer, so that the model can have a higher operating efficiency than the existing model. Finally, the Euclidean distance function was used to measure the similarity between the question sentences, and the characteristic information was obtained, so as to judge whether the sentences had repeated values.

2. System design

In this system, the input question statement will firstly pass through the word vector layer DM to produce the corresponding word vector feature representation. And it will be transformed from the discrete word vector into continuous one-dimensional vector by Embedding.

Then, the produced characteristic vector will be inputted into the neural network of Bi-LSTM. And then the result of the Bi-LSTM output will be introduced into Co-attention mechanism to generate corresponding statement's Co-attention representation. Then the system will use the weighted Euclidean Distance function to measure the similarity degree between characteristic vectors. Lastly, the system will employ Multi-layer Perception Network (MLP) for classification and screening to judge whether the problem statement has duplicate values or not. The process is shown in Figure 1:

2.1. Assume that there is a set of problem statements W_1 and W_2 in the consultation posts

Denote as: $S(W_1, W_2)$ (1)

Meanwhile when $S(W_1, W_2) \rightarrow 1$, it means that the semantics of the two sentences are similar or the same, that is, the two sentences W_1 and W_2 may have different grammatical structures, but their meanings are similar or the same. In this case, there are duplicate values between this set of statements.

When $S(W_1, W_2) \rightarrow 0$, it means that the semantics of the two sentences are not the same, that is, whether the two sentences W_1 and W_2 have similar grammatical structures, the meanings expressed are not similar or the same. In this case, there are no duplicate values between this group of statements.

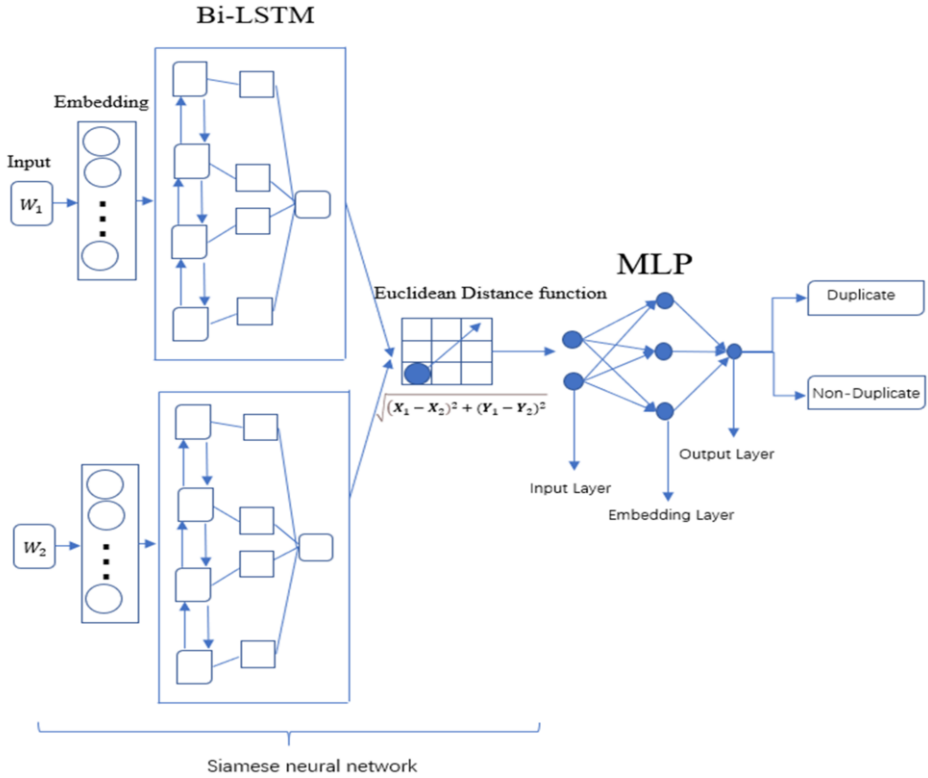


Figure 1. Question-and-answer system based on Bi-LSTM and Co-attention model.

2.2. Input layer

Each question statement is separately put into the sub-network of Siamese neural network, and the parameter and weight in each sub-network is the same. Siamese neural network is mainly used to measure the similarity between the two inputs of the model. The two inputs correspond to two sub-networks, which map the input statements into the new space, thus forming the sentence feature vectors in the new space. In Siamese neural network, the contrastive loss function it used can achieve the matching degree between samples well and also be effectively used for the training model. Because the problem statements are character-level text, statements in this layer are placed in the form of individual characters or symbols into the sub-networks.

2.3. sentence vector layer

This study adopts the DM model of doc2Vec technology, and its framework is shown in Figure 2:

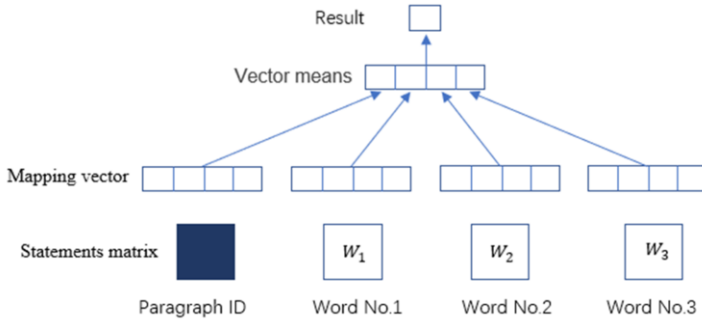


Figure 2. DM model.

In the training process of DM model, Paragraph ID will generate a statement recognition vector with the same dimension as the word vector at first. And then all the sentence vectors and word vectors will be accumulated to obtain the corresponding sentence vector. Finally the corresponding sentence vector will be transferred to the next coding layer. Moreover, during the training of a sentence, its Paragraph ID will remain fixed and share the same sentence vector with other sentences. So in each probability prediction of the words in the statements, the model can make complete use of the full meaning of the statements.

2.4 Coding layer

The system will transfer the sentence vectors obtained by DM model in the sentence vector layer to the Bidirectional Long Short Term Memory model (Bi-LSTM). And the semantic information of the bidirectional tense of the sentence vector is read and encoded to obtain it more completely. Then, the feature vector output from the Bi-LSTM model will be introduced into the Co-attention model to further obtain the body information of the statements.

2.4.1. Introduce the Co-attention mechanism into the Bi-LSTM model

The traditional one-direction LSTM model cannot go forward and backward from the statement at the same time to get the semantic information. We cannot fully use the coded information of a statement if we only use time step information of the statements on a single direction. [11] Based on the above shortcomings, this study decided to use multi-layer and bidirectional Bi-LSTM model. This model has two sub-networks, allowing it to get the information both forward and backward. So the model can obtain the statement semantics on two voice directions, that is, the past and the future. And it can also connect state of hidden layers of the time step in both directions, so as to gain more accurate semantic information.

$$q_t = \sigma(p_{q_y}y_t + p_{q_h}h_{t-1} + B_q) \tag{2}$$

$$d_t = \sigma(p_{d_y}y_t + p_{d_h}h_{t-1} + B_d) \tag{3}$$

$$o_t = \sigma(p_{o_y}y_t + p_{o_h}h_{t-1} + B_o) \tag{4}$$

$$s_t = \tan h(p_{s_y}y_t + p_{s_h}h_{t-1} + B_s) \tag{5}$$

$$B_t = d_t \odot B_{t-1} + q_t \odot s_t \tag{6}$$

$$h_t = \tan h(b_t) \odot o_t \tag{7}$$

\odot : corresponding product of elements
 $p_q p_d p_o p_s$: Weight factors in the hidden layer
 $B_q B_d B_o B_s$: Deviation vector
 σ : S-shaped function as an activation function
 $\tan h$: Hyperbolic tangent function

$X_t = [h_{t-n}, h_{t-(n-1)}, \dots, h_{t-2}, h_{t-1}]$ is the output of the LSTM layer, which represents the vector of all output results.

Then, we use the LSTM model to connect the state of hidden layer of each time step backward and forward. And through (8), we can calculate each vector output by Bi-LSTM.

$$X_t = ((h_t)^\rightarrow \odot (h_t)^\leftarrow) \tag{8}$$

\odot : Connection function between two output results
 $h^\rightarrow, h^\leftarrow$: It respectively represents the calculation output results of the forward sequence from the t-n time period to the t-1 time period and the reverse input of the forward layer

Therefore, the output vector of Bi-LSTM can be expressed as:

$$X_t = [x_{t-n}, x_{t-(n-1)}, \dots, x_{t-2}, x_{t-1}] \tag{9}$$

2.4.2. Co-Attention Mechanism

In this part, the system will encode the input statement to form the intermediate content vector, so as to distribute different weights to different parts of the statement and then effectively obtain the topic information of it. The Co-attention mechanism is used to optimize the Bi-LSTM model, and the semantic similarity matrix is constructed as follows:

$$s_{ij} = E(\bar{n}_i)^T \cdot E(\bar{m}_j)^T, s \in R^{1_n \times 1_m} \tag{10}$$

\bar{n}_i, \bar{m}_j : Respectively represent the i-th and j-th words in statements n and m.
 $E(\cdot)$: Single-hidden Layer Feedforward Neural Network and meanwhile $e(x) = \text{Relu}(p(x) + g)$.

Maximum pooling is carried out for row and column s to extract the features of the pooling layer. The process is as follows:

$$n' = S(\max_{col}(s))^T n \tag{11}$$

$$m' = S(\max_{row}(s))^T m \tag{12}$$

s_{ij} : The similarity matrix of n and m statements, and $s \in R^{1_n \times 1_m}$.
 $S(\cdot)$ is the softmax function.
 n', m' : Respectively the Co-attention representations of n and m statements

2.4.3. Measurement of semantic similarity

The weighted Euclidean Distance function is used to measure the similarity distance between feature vectors. The formula is as follows:

$$u(x, y) = \sqrt{\sum_{i=0}^{n-1} (x(i) - y(i))^2} \quad (13)$$

x, y : vectors in K -dimensional space

The Euclidean Distance of x and y is defined as the real distance between x and y in space. If x and y are vectors in two-dimensional space, the value of $u(x, y)$ can be measured using the Pythagorean theorem. Even if the statements are not similar, when the Euclidean distance between the feature vectors is small, the loss value of the Contrastive loss function in the neural network will still increase, so that the degree of similarity between the statements can still be well judged.

2.5. Output layer

Multi-layer perception network (MLP) is used for classification and screening to achieve prediction. The hybrid Siamese neural network and multi-layer perception network (MLP) are generated, which enables the output of the Siamese encoder to be passed to the MLP and thus simulate the interaction between the two problem statements. Thus, the MLP model can obtain the vector representation of the problem statement and the connection between the similarity distance of its semantics as the input of the model, namely:

$$V = [f(w_1); f(w_2); d(w_1, w_2)] \quad (14)$$

Then the matching probability between the two question statements is printed as the output. Finally a single 1×2 vector is printed to determine whether there are duplicate values or not.

3. Model experiment

3.1. Experimental environment

This experiment adopted the TensorFlow system, which realizes the programming of machine learning algorithm through the programming of data flow and symbol teaching. And C++ was chosen to speed up its operation efficiency, and advanced machine learning application program interface (API) was used to maximize the efficiency of model training.

3.2. Collection and processing of experimental data

The experiment selected 1150 consultation posts sent in the MOOC platform of Chinese universities about "transposed determinant", "using Newton's Leibniz formula to calculate definite integral", "using Laplace's theorem to calculate determinant", "how to do model analysis of STATA panel data", "under what circumstances is the weighted least square method applicable", "how to realize the Pareto optimality" and "finding the area of trapezoid with curve side" as the experimental data, and integrated the

statements from the question-and-answer results of the posts. And this resulted in two text documents, respectively named question text and answer text.

A total of about 6400 pieces of consulting data, 4800 pieces of data were selected for training, and 1600 pieces of data were tested for about 6400 iterations of data. Use the jieba tokenizer to segment the sentences in the text, and then delete punctuation marks, etc., to prepare for the subsequent generation of sentence vectors.

Then the Euclidean Distance function was used to measure the similarity of the output results of the Bi-LSTM model based on the Co-attention mechanism. And the MLP filter was used to judge whether there were duplicate statements.

3.3. Model training results and analysis

The TensorFlow technology was used to train the model. And when the network convergence was achieved, the model data was saved. Parameter settings of the model are shown in Table 1:

Table 1. Parameter of model

Parameter	Value
Initial learning rate	0.001
Iteration	6400
Dimension	256
Dimension of sentence vector	256

In addition, in order to better evaluate the performance of the model proposed above, the experimental results are shown in Table 2:

Table 2. Comparison with other models

Model	Vector	Result
Bi-LSTM	Word vector	76.26%
Attention-Bi-LSTM	Word vector	81.13%
Co-attention-Bi-LSTM	Word vector	86.76%
Bi-LSTM	sentence vector	80.61%
Attention-Bi-LSTM	sentence vector	85.86%
Co-attention-Bi-LSTM	sentence vector	89.42%

Moreover, according to Table 2, Bi-LSTM model introduced with the Co-attention mechanism had higher accuracy compared with the other two models no matter word vectors or sentence vectors were used in the same way. What’s more, for the above three models, when sentence vectors were used, they all had a higher judgment accuracy of semantic repeatability than when word vectors were used.

Then use Stata to test the significance of the experimental results. The test results show that, under the control of variables such as corpus size, number of iterations, and number of query sentences, the accuracy of repeatability prediction using sentence vectors and Bi-LSTM is significantly positive at the 2.5% level. It shows that the use of word vectors can improve the prediction accuracy of Bi-LSTM based on the mutual attention mechanism. And, according to whether the attention mechanism is introduced

for different models to perform sub-sample regression, the regression results show that after the attention mechanism is introduced, the prediction accuracy of the model is significantly positive at the 1% level. The use of sentence vectors can effectively improve the prediction accuracy of models based on the attention mechanism. For the model without the attention mechanism, its prediction accuracy is significantly positive at the level of 1% when compared with the sentence vector, indicating that the use of the sentence vector can also effectively improve the prediction accuracy of the non-attention mechanism model. The results of the significance test fully illustrate that the core conclusion that the use of word vectors and the introduction of the attention mechanism has a positive effect on the model's prediction accuracy is robust.

In addition, the prediction accuracy rate of Bi-LSTM based on the mutual attention mechanism and the more widely used neural network model are compared and tested. The experimental results are shown in Table 2. Comparative experiments show that, compared with other neural network models, the Bi-LSTM model has a better accuracy in the detection of sentence repeatability.

4. Conclusion

This study carried out a control experiment for the designed model to obtain the accuracy of judging statement duplicate values. The results showed that the use of sentence vector and the introduction of bidirectional Co-attention mechanism both significantly improved the judgment accuracy of the model. This model is expected to be used in the online intelligent learning platform for semantic repetitive screening, thereby improving the operating efficiency of the background system and efficiently assisting students in personalized learning. However, the training results of this model in a large-scale corpus are not ideal. As a result, its efficiency in large-scale repetitive screening tasks needs to be improved, and its applicable consulting platform is too single to efficiently identify consulting sentences in different fields. In future work, we will focus on introducing the dynamic attention mechanism and the attention mechanism based on the capsule network into the Bi-LSTM model, so as to better improve the efficiency of model detection. It will also increase the size of the corpus used for model training and try to apply it to different intelligent consulting platform fields.

Acknowledgement

This study was financially supported by the Undergraduate Innovation Training Project of Guangdong University of Foreign Studies in 2021 (NO. S202111846022).

References

- [1] Hussein E , Daoud S , Alrabaiah H , et al. Exploring Undergraduate Students' Attitudes towards Online Learning during COVID-19: A Case from the UAE[J]. *Children and Youth Services Review*, 2020, vol. 119, 105699
- [2] Li Ruiqian. Research on the Evaluation of Online Education Platform by University Students: Based on Technology Acceptance Model [J]. *Continue Education Research*. 2021, No. 257(01):116-119.

- [3] A.I. Newaz, A.K. Sikder, M.A. Rahman, A.S. Uluagac. Healthguard: a machine learning-based security framework for smart healthcare systems, in: 2019 Sixth International Conference on Social Networks Analysis, Management and Security, SNAMS, IEEE, 2019, pp. 389-396.
- [4] Oluwasanmi A , Aftab M U , Alabdulkreem E , et al. CaptionNet: Automatic End-to-End Siamese Difference Captioning Model With Attention[J]. IEEE Access, 2019, vol. 7, pp.106773-106783.
- [5] Hassan A , Mahmood A . Convolutional Recurrent Deep Learning Model for Sentence Classification [J]. IEEE Access, 2018, vol.6, pp13949-13957.
- [6] Zhu P , Tan Y , Zhang L , et al. Deep Learning for Multilabel Remote Sensing Image Annotation With Dual-Level Semantic Concepts[J]. IEEE Transactions on Geoscience and Remote Sensing, 2020, (99) pp.1-14.
- [7] Imtiaz Z , Umer M , Ahmad M , et al. Duplicate Questions Pair Detection Using Siamese MaLSTM[J]. IEEE Access, 2020, PP (99):1-1.
- [8] M. Ahasanuzzaman, M. Asaduzzaman, C.K. Roy, K.A. Schneider, Mining duplicate questions in stack overflow, in: Proceedings of the 13th International Conference on Mining Software Repositories, ACM, 2016, pp. 402-412.
- [9] K. R.F. Silva, M. de Almeida Maia, Duplicate question detection in stack overflow: A reproducibility study, in: IEEE 25th International Conference on Software Analysis, Evolution and Reengineering (SANER), 2018, pp. 572-581.
- [10] Ning Chunmei. Research and Application of Text Similarity Algorithm Based on Deep Learning [D].Chongqing University.2019.
- [11] Wenpeng Yin, Hinrich Schütze, Bing Xiang, et al. ABCNN: Attention-Based Convolutional Neural Network for Modeling Sentence Pairs. 2016, 4:259-272.
- [12] CHEN Q, ZHU X D, LING Z H, et al. Enhanced LSTM for natural language inference[C]//Proceedings of the 55th Annual Meeting of the Association for Computational Linguistics. 2016: 1657-1668.

Short Note on “Nonlinear Optimization Problem Subjected to Fuzzy Relational Equations Defined by Dubois-Prade Family of t-Norms”

Xiaoling LIU^a, Khizar HAYAT^b and Xiaopeng YANG^{a,1}

^a*School of Mathematics and Statistics, Hanshan Normal University, Chaozhou, China*

^b*Department of Mathematics, University of Kotli, Azad Jammu and Kashmir, Pakistan*

Abstract. This short note aims to make some modification for improving the results presented in [1]. A. Ghodousian et al. discussed the resolution of a system of max-Dubois-Prade fuzzy relation equations based on their proposed index sets J_i , $i \in I$. It is found that not every $e \in E = J_1 \times J_2 \times \dots \times J_m$ corresponds to a solution. To overcome this flaw, we modify the expression of the index sets, denoted by J_i^- , $i \in I$. Based on the modified index sets, resolution of the max-Dubois-Prade fuzzy relation equations becomes easier, regarding the computational cost.

Keywords. fuzzy relation equation, max-Dubois-Prade composition, solution set, minimal solution

1. Introduction

In a recent paper [1], A. Ghodousian et al. studied the nonlinear optimization problem subject to a system of max-Dubois-Prade fuzzy relation equations as follows

$$\begin{aligned} & \min f(x) \\ & \text{s.t. } A\varphi x = b, \\ & \quad x \in [0, 1]^n. \end{aligned} \tag{1}$$

Denote the index sets $I = \{1, 2, \dots, m\}$ and $J = \{1, 2, \dots, n\}$. In above the fuzzy relation equations system

$$A\varphi x = b, \tag{2}$$

$A = (a_{ij})_{m \times n} \in [0, 1]^{m \times n}$ represents a fuzzy matrix, while $b = (b_i)_{m \times 1} \in [0, 1]^m$ is a m -dimensional fuzzy vector. The max-Dubois-Prade composition φ is defined as

¹Corresponding Author: Xiaopeng Yang; E-mail: 706697032@qq.com. This work was supported by the National Natural Science Foundation of China (61877014) and the funds provided by the Education Department of Guangdong Province (2017KTSCX124, 2019KZDXM013, ZD201802).

$$\varphi(x, y) = T_{DP}^{\gamma}(x, y) = \frac{xy}{\max\{x, y, \gamma\}}, \quad \forall x, y \in [0, 1], \quad (3)$$

where $\gamma \in (0, 1)$ is some fixed parameter. Notice that $T_{DP}^0(x, y) = \min\{x, y\}$ and $T_{DP}^1(x, y) = xy$. That is to say, when $\gamma = 0$, the composition $\varphi = T_{DP}^0$ becomes "min", while $\gamma = 1$, $\varphi = T_{DP}^1$ turns out to be "product" composition. The authors first presented the resolution of the constraint, i.e. system (2). Based on the properties of the solution set of (2), they further applied the genetic algorithm to search an approximate optimal solution of problem (1). After carefully examination, we found that some of the result in [1] could be improved, for making it always true for the general case.

Searching all the solutions of a fuzzy relation system, including equations system or inequalities system, is an lasting research topic [2]-[6]. In the resolution of a fuzzy relation system, the composition plays important role. The composition has been extended from the initial *max-min* operator to the general *max-t-norm* one. Recently, fuzzy relation systems with *addition-min* [4]-[6] or *max-Dubois-Prade* [1,7] were also investigated. Especially, the solution set of consistent fuzzy relation inequalities system with addition-min composition is no longer non-convex, but convex [4]. Moreover, the number of its minimal solutions (when non-unique) are no longer finite, but infinite [4]. However, resolution of all its solutions remains an open problem [5].

When applying the fuzzy relation system in some application field, the relevant optimization problem might be dealt. S.-C. Fang and G. Li first introduced the optimization problem minimizing a linear function with fuzzy relation equations constraint [8]. There are much research focusing on such a topic [8]-[11]. The Branch-and-Bounded approach is one of the most applied resolution methods. However, it is no longer suit for optimization problem with addition-min composition [10,11,12]. For fuzzy relation programming with general nonlinear objective function, the generic algorithm is an common method to search its approximate optimal solution [1,7,13,14]. Computation complexity and accuracy are important criterions for evaluation of a generic algorithm. Other specific fuzzy relation nonlinear programming problems could be handled according to their special objective functions and structure of the feasible regions [15]-[20].

The optimization problem with a linear objective function and a group of max-product fuzzy relation equation constraints was first studied by J. Loetamonphong and S.-C. Fang [21]. The imitated the resolution approach presented in [8]. In recent years, the fuzzy relation inequalities system with max-product composition was further applied to the foodstuff management in a given city [20,22,23] and the wireless communication station system [24,25,26]. The linear objective function was replaced by a nonlinear one [22,23,24,25]. Obviously, the resolution method presented in [21] was no longer effective for those nonlinear fuzzy relation optimization problems [22,23,24,25]. J. Qiu et al. further investigated the fuzzy relation optimization problem with a bi-level objective function [26]. Fuzzy relation inequality with addition-min composition was another challenging researching topic. As pointed out in [4], in most cases, a system of addition-min fuzzy relation inequalities has an infinite number of minimal solutions. As we know, there is no efficient method for obtaining all the minimal solutions till now. Hence, one is not able to find its complete solution set. However, searching some specific solutions of the addition-min fuzzy relation inequalities is interesting and achievable. Several resolution method were proposed for the optimization problem with a linear objective function and the addition-min fuzzy relation inequality constraints [10,11,27]. For decreasing the network congestion in the P2P file sharing system, X. Yang et al. [12,28,29]

further established and investigated the corresponding min-max programming subject to the addition-min fuzzy relation inequalities system. Moreover, the relevant multiple objective optimization problem was also studied, which allowed the system manager to consider three objectives (system congestion, cost, and penalty) simultaneously [30]. Besides, some other issues with respect to the addition-min fuzzy relation inequalities system were introduced and investigated [31,32].

The contribution and novelty of this work are summarized as follows.

(i) Point out the drawbacks of the existing work [1].

The following Theorem 2 and its relevant assertion are adopted from [1] (see pages 169-170 in [1]).

- *Theorem 2.* $S_{T_{DP}^\gamma}(A, b) = \bigcup_{e \in E} [\underline{X}(e), \bar{X}]$.
- *As a consequence, it turns out that \bar{X} is the unique maximum solution and $\underline{X}(e)$ ($e \in E$) are the minimal solutions of $S_{T_{DP}^\gamma}(A, b)$. Moreover, we have the following corollary that is directly resulted from Theorem 2.*

We have found that the results in the above “Theorem 2” and its relevant assertion might be incorrect.

(ii) Give the reason causing the above drawbacks.

In fact, $\underline{X}(e)$ might not be a feasible solution of problem (1). In other words, it is possible that $\underline{X}(e) \notin S_{T_{DP}^\gamma}(A, b)$. This is the reason causing the above-presented drawbacks. If $\underline{X}(e) \notin S_{T_{DP}^\gamma}(A, b)$ holds, then $\underline{X}(e)$ is not a solution of system (2). As a consequence, the result that $S_{T_{DP}^\gamma}(A, b) = \bigcup_{e \in E} [\underline{X}(e), \bar{X}]$, in Theorem 2, is invalid. In addition, $\underline{X}(e)$ is not a minimal solution of $S_{T_{DP}^\gamma}(A, b)$.

(iii) Make some corresponding corrections.

In this work, we have made some modifications to the index sets J_1, J_2, \dots, J_m and the Definition 4 in [1]. The modified index sets are denoted by $J_1^=, J_2^=, \dots, J_m^=$. After these modifications, it has been further proved that for any $e \in E^= = J_1^= \times J_2^= \times \dots \times J_m^=$, it holds that $\underline{X}(e) \in S_{T_{DP}^\gamma}(A, b)$. Consequently, the corresponding results in the above theorem and assertion turn out to be correct.

We organized our paper as follows. Section 2 provides some necessary preliminaries on the max-Dubois-Prade fuzzy relation equations. The main results of this paper are set in Section 2, including three parts: Phenomenon, Reason and Correction. Section 4 is the simple conclusion.

2. Preliminaries

In this section we recall some concepts and results which are presented in [1].

The max-Dubois-Prade fuzzy relation equations (2) could be written as

$$\varphi(a_i, b_i) = \varphi(a_{i1}, x_1) \vee \varphi(a_{i2}, x_2) \vee \dots \vee \varphi(a_{in}, x_n) = b_i, \quad i \in I,$$

where $\varphi(a_{ij}, x_j) = \frac{a_{ij}x_j}{\max\{a_{ij}, x_j, \gamma\}}$.

Let

$$S_{T_{DP}^\gamma}(A, b) = \{x \in [0, 1]^n \mid A\varphi x = b\}$$

be the complete solution set of system (2). Denote the solution set of the i th equation of system (2), i.e.

$$\varphi(a_{i1}, x_1) \vee \varphi(a_{i2}, x_2) \vee \cdots \vee \varphi(a_{in}, x_n) = b_i, \tag{4}$$

by $S_{T_{DP}^\gamma}(a_i, b_i)$, for all $i \in I$. Then it is clear that

$$S_{T_{DP}^\gamma}(A, b) = \bigcap_{i \in I} S_{T_{DP}^\gamma}(a_i, b_i). \tag{5}$$

Definition 1. For each $i \in I$, we define the following index sets

$$\begin{aligned} J_i^{1,1} &= \{j \in J : a_{ij} > b_i \text{ and } \gamma > a_{ij}\}, \\ J_i^{1,2} &= \{j \in J : a_{ij} > b_i \text{ and } \gamma \leq a_{ij}\}, \\ J_i^{2,1} &= \{j \in J : a_{ij} = b_i \text{ and } b_i \neq 0\}, \\ J_i^{2,2} &= \{j \in J : a_{ij} = b_i = 0\}. \end{aligned}$$

Let $J_i = J_i^{1,1} \cup J_i^{1,2} \cup J_i^{2,1} \cup J_i^{2,2}$. Additionally we set

$$l_{ij} = \begin{cases} \frac{\gamma b_i}{a_{ij}} & j \in J_i^{1,1}, \\ b_i & j \in J_i^{1,2}, \\ \max\{b_i, \gamma\} & j \in J_i^{2,1}, \\ 0 & j \in J_i^{2,2}, \end{cases} \quad \text{and} \quad u_{ij} = \begin{cases} \frac{\gamma b_i}{a_{ij}} & j \in J_i^{1,1}, \\ b_i & j \in J_i^{1,2}, \\ 1 & j \in J_i^{2,1} \cup J_i^{2,2}. \end{cases} \tag{6}$$

Lemma 1. Let $i \in I$. If $j \notin J_i$, then $T_{DP}^\gamma(a_{ij}, x_j) < b_i, \forall x_j \in [0, 1]$.

Lemma 2. Suppose that $i \in I$ and $j \in J_i$.

- (a) $x_j > u_{ij}$ iff $T_{DP}^\gamma(a_{ij}, x_j) > b_i$.
- (b) $x_j < l_{ij}$ iff $T_{DP}^\gamma(a_{ij}, x_j) < b_i$.
- (c) $l_{ij} \leq x_j \leq u_{ij}$ iff $T_{DP}^\gamma(a_{ij}, x_j) = b_i$.

Lemma 3. For a fixed $i \in I$, $S_{T_{DP}^\gamma}(a_i, b_i) \neq \emptyset$ if and only if $J_i \neq \emptyset$.

Definition 2. Suppose that $i \in I$ and $S_{T_{DP}^\gamma}(a_i, b_i) \neq \emptyset$ (hence, $J_i \neq \emptyset$ from Lemma 3). Let $\hat{x}_i = [(\hat{x}_i)_1, (\hat{x}_i)_2, \dots, (\hat{x}_i)_n] \in [0, 1]^n$ where the components are defined as follows:

$$(\hat{x}_i)_k = \begin{cases} u_{ij} & k \in J_i, \\ 1 & k \notin J_i, \end{cases} \quad \forall k \in J. \tag{7}$$

Also, for each $j \in J_i$, we define $\check{x}_i(j) = [\check{x}_i(j)_1, \check{x}_i(j)_2, \dots, \check{x}_i(j)_n] \in [0, 1]^n$ such that

$$\check{x}_i(j)_k = \begin{cases} l_{ij} & k = j, \\ 0 & \text{otherwise,} \end{cases} \quad \forall k \in J. \tag{8}$$

The solution set of the i th single fuzzy relation equation (4) could be characterized as below.

Theorem 1. Let $i \in I$. If $S_{T_{DP}^\gamma}(a_i, b_i) \neq \emptyset$, then $S_{T_{DP}^\gamma}(a_i, b_i) = \bigcup_{j \in J_i} [\check{x}_i(j), \hat{x}_i]$.

According to Theorem 1, \hat{x}_i is the unique maximum solution of $S_{T_{DP}^\gamma}(a_i, b_i)$, while $\check{x}_i(j)$'s ($j \in J_i$) are the minimal solutions.

Definition 3. Let \hat{x}_i ($i \in I$) be the unique maximum solution of $S_{T_{DP}^\gamma}(a_i, b_i)$. We define $\bar{X} = \min_{i \in I} \hat{x}_i$.

Definition 4. Let $e : I \rightarrow J_i$ so that $e(i) = j \in J_i, \forall i \in I$. Let E be the set of all vectors e . For the sake of convenience, we represent each $e \in E$ as an m -dimensional vector $e = [j_1, j_2, \dots, j_m]$ in which $j_k = e(k)$.

Definition 5. Let $e = [j_1, j_2, \dots, j_m] \in E$. We define $\underline{X}(e) = [\underline{X}(e)_1, \underline{X}(e)_2, \dots, \underline{X}(e)_n] \in [0, 1]^n$, where $\underline{X}(e)_j = \max_{i \in I} \{\check{x}_i(e(i))_j\} = \max_{i \in I} \{\check{x}_i(j_i)_j\}, \forall j \in J$.

Theorem 2. $S_{T_{DP}^\gamma}(A, b) = \bigcup_{e \in E} [\underline{X}(e), \bar{X}]$.

Theorem 2 gives the complete characterization of the solution set of system (2). It follows from Theorem 2 that \bar{X} is the unique maximum solution (if it is consistent), “and $\underline{X}(e)$ ($e \in E$) are the minimal solutions of $S_{T_{DP}^\gamma}(A, b)$ ” [1]. Moreover, the consistency of system (2) could be checked by the feasibility of \bar{X} , according to the following Corollary 1.

Corollary 1. (first necessary and sufficient condition) $S_{T_{DP}^\gamma}(A, b) \neq \emptyset$ if and only if $\bar{X} \in S_{T_{DP}^\gamma}(A, b)$.

3. Main result

In this section, we will show that some results presented in Ref. [1] are invalid for some specific cases regarding the system of max-Dubois-Prade fuzzy relation equations. In order to make sure the results valid for all cases, we point out the causing reason and further make some modifications of the definitions in [1].

3.1. Phenomenon: $\underline{X}(e)$ might not be a (minimal) solution for some specific $e \in E$

As mention above, it was pointed out in [1] that the vectors $\{\underline{X}(e) : e \in E\}$ are the minimal solutions of system (2), i.e. $\underline{X}(e) \in S_{T_{DP}^\gamma}(A, b), \forall e \in E$. However it is found that this assertion is uncorrect in some specific case. In other words, there might exit some $e \in E$, such that $\underline{X}(e)$ is not a solution of (2).

Now we declare our assertions as follows:

- (i) It is possible that $\underline{X}(e) \notin S_{T_{DP}^\gamma}(A, b)$ for some $e \in E$.
- (ii) Even if $\underline{X}(e) \in S_{T_{DP}^\gamma}(A, b)$ holds for some $e \in E$, the solution $\underline{X}(e)$ might not be a minimal solution of system (2).

We take the example from [1] to support our above-mentioned assertions.

Example 1. [1] Consider the problem below with Dubois-Prade t-norm

$$\begin{bmatrix} 0.9 & 0.4 & 0.6 & 0.7 & 0.4 & 0.4 \\ 0.5 & 0.1 & 0.2 & 0.3 & 0.5 & 0.2 \\ 0.2 & 0.8 & 0.4 & 0.4 & 0.6 & 0.9 \\ 0.9 & 0.7 & 0.3 & 0.8 & 0.8 & 0.5 \\ 0 & 0.4 & 0.2 & 0.2 & 0.1 & 0.7 \end{bmatrix} \varphi x = \begin{bmatrix} 0.7 \\ 0.5 \\ 0.6 \\ 0.8 \\ 0.4 \end{bmatrix}, \tag{9}$$

where $\varphi(x, y) = T_{DP}^{0.5}(x, y) = \frac{xy}{\max\{x, y, 0.5\}}$ (i.e. $\gamma = 0.5$).

By simple computation, it could be obtained that $J_1 = \{1, 4\}$, $J_2 = \{1, 5\}$, $J_3 = \{2, 5, 6\}$, $J_4 = \{1, 4, 5\}$, $J_5 = \{2, 6\}$. Maximum solutions of the equations in system (9) are

$$\begin{aligned} \hat{x}_1 &= [0.7, 1, 1, 1, 1, 1], \\ \hat{x}_2 &= [1, 1, 1, 1, 1, 1], \\ \hat{x}_3 &= [1, 0.6, 1, 1, 1, 0.6], \\ \hat{x}_4 &= [0.8, 1, 1, 1, 1, 1], \\ \hat{x}_5 &= [1, 1, 1, 1, 1, 0.4], \end{aligned}$$

respectively. On the other hand, all the minimal solutions are as

$$\begin{aligned} \check{x}_1(1) &= [0.7, 0, 0, 0, 0, 0], \check{x}_1(4) = [0, 0, 0, 0.7, 0, 0], \\ \check{x}_2(1) &= [0.5, 0, 0, 0, 0, 0], \check{x}_2(5) = [0, 0, 0, 0, 0.5, 0], \\ \check{x}_3(2) &= [0, 0.6, 0, 0, 0, 0], \check{x}_3(5) = [0, 0, 0, 0, 0.6, 0], \check{x}_3(6) = [0, 0, 0, 0, 0, 0.6], \\ \check{x}_4(1) &= [0.8, 0, 0, 0, 0, 0], \check{x}_4(4) = [0, 0, 0, 0.8, 0, 0], \check{x}_4(5) = [0, 0, 0, 0, 0.8, 0], \\ \check{x}_5(2) &= [0, 0.5, 0, 0, 0, 0], \check{x}_5(6) = [0, 0, 0, 0, 0, 0.4]. \end{aligned}$$

Based on \hat{x}_i ($i = 1, 2, \dots, 5$), it is easy to find the maximum solution of system (9), i.e.

$$\bar{X} = \hat{x}_1 \wedge \hat{x}_2 \wedge \dots \wedge \hat{x}_5 = [0.7, 0.6, 1, 1, 1, 0.4].$$

By Definition 4, $|E| = |J_1| \times |J_2| \times \dots \times |J_5| = 2 \times 2 \times 3 \times 3 \times 2 = 72$. As a consequence, the authors said "we have 72 solutions $\underline{X}(e)$ associated to 72 vectors e " in [1].

In fact, this statement is incorrect. For example, take $e_1 = [1, 1, 2, 1, 2] \in E$, then we have $\underline{X}(e_1) = \check{x}_1(1) \vee \check{x}_2(1) \vee \check{x}_3(2) \vee \check{x}_4(1) \vee \check{x}_5(2) = [0.8, 0.6, 0, 0, 0, 0]$. Substituting $\underline{X}(e_1)$ in system (9), it is found that the first equation doesn't hold. Hence $\underline{X}(e_1)$ is not a solution of (9).

Moreover, take $e_2 = [4, 1, 5, 5, 2] \in E$. Even though the corresponding vector $\underline{X}(e_2) = [0.5, 0.5, 0, 0.7, 0.8, 0]$ is a solution of (9), it is not a minimal solution. It is easy to check that $x = [0, 0.5, 0, 0.7, 0.8, 0]$ is also a solution of (9). But it holds that $x \leq \underline{X}(e_2)$ and $x \neq \underline{X}(e_2)$. □

Next we will explain the reason causing the above conflict and provide some necessary modification to improve the results in [1].

3.2. Reason: it is possible that $\underline{X}(e) \not\leq \bar{X}$

What is the reason causing the non-membership relation $\underline{X}(e) \notin S_{T_{DP}^\gamma}(A, b)$?

In fact, whether $\underline{X}(e)$ belongs to $S_{T_{DP}^\gamma}(A, b)$ is determined by availability of the inequality that $\underline{X}(e) \leq \bar{X}$. Furthermore, we provide the following Theorem 3 to show the necessary and sufficient condition that ensures the vector $\underline{X}(e)$ to be a solution of (2), for a given $e \in E$.

Lemma 4. A vector $x \in [0, 1]^n$ is a solution of system (2), if and only if for any $i \in I$, $a_{ij}\varphi x_j$ holds for all $j \in J$ and $a_{ij_i}\varphi x_{j_i}$ holds for some $j_i \in J$.

Proof. The proof is trivial. □

Theorem 3. Let $e \in E$. Then $\underline{X}(e) \in S_{T_{DP}^\gamma}(A, b)$ if and only if $\underline{X}(e) \leq \bar{X}$.

Proof. Since \bar{X} is the maximum solution, $\underline{X}(e) \in S_{T_{DP}^\gamma}(A, b) \Rightarrow \underline{X}(e) \leq \bar{X}$ is straightforward. Next we just verify the contrast implication. Assume that $\underline{X}(e) \leq \bar{X}$ for some $e \in E$. We have to prove that $\underline{X}(e) \in S_{T_{DP}^\gamma}(A, b)$.

Take arbitrary $i \in I$.

(i) By Lemma 4, $\bar{X} \in S_{T_{DP}^\gamma}(A, b)$ implies that $a_{ij}\varphi\bar{X}_j \leq b_i, \forall j \in J$. On the other hand, the assumption that $\underline{X}(e) \leq \bar{X}$ indicates $\underline{X}(e)_j \leq \bar{X}_j, \forall j \in J$. Due to the monotonicity of the operator φ , we have

$$a_{ij}\varphi\underline{X}(e)_j \leq a_{ij}\varphi\bar{X}_j \leq b_i, \forall j \in J.$$

(ii) Suppose $e = [j_1, j_2, \dots, j_m]$. By Definition 5, $\underline{X}(e) = \bigvee_{k \in I} \check{x}_k(j_k)$. Thus

$$\underline{X}(e)_{j_i} = \bigvee_{k \in I} \check{x}_k(j_k)_{j_i} \geq \check{x}_i(j_i)_{j_i}. \tag{10}$$

According to (8), it holds that

$$\check{x}_i(j_i)_{j_i} = l_{ij_i}. \tag{11}$$

Since $j_i \in J_i$, it follows from (7) that

$$\bar{X}_{j_i} = \left(\bigwedge_{k \in I} \hat{x}_k\right)_{j_i} = \bigwedge_{k \in I} (\hat{x}_k)_{j_i} \leq (\hat{x}_i)_{j_i} = u_{ij_i}. \tag{12}$$

Combining (10), (11) and (12), we have

$$l_{ij_i} = \check{x}_i(j_i)_{j_i} \leq \underline{X}(e)_{j_i} \leq \bar{X}_{j_i} \leq u_{ij_i}. \tag{13}$$

According to Lemma 2, it holds that $a_{ij_i}\varphi\underline{X}(e)_{j_i} = b_i$.

By Lemma 4, the above-proved (i) and (ii) contribute to $\underline{X}(e) \in S_{T_{DP}^\gamma}(A, b)$. □

3.3. Correction: modification of the index set J_i

In this subsection we aim to make some modification for improving the results in [1]. To make the above-mention assertion presented in [1] correct, we just need to modified the index set J_i used in Definition 4.

For arbitrary $i \in I$, let

$$J_i^- = \{j \in J_i | l_{ij} \leq \bar{X}_j\}. \tag{14}$$

It is clear that $J_i^- \subseteq J_i, \forall i \in I$. Moreover, it is possible that $J_i^- \neq J_i$, e.g. J_3^- and J_4^- are not equal to J_3 and J_4 , respectively, in Example 2.

We replace J_i in Definition 4 by J_i^- in (14). Then the Definition 4 turns out to be Definition 4' as below.

Definition 4'. Let $e : I \rightarrow J_i^-$ so that $e(i) = j \in J_i^-, \forall i \in I$. Let $E^=$ be the set of all vectors e . For the sake of convenience, we represent each $e \in E^=$ as an m-dimensional vector $e = [j_1, j_2, \dots, j_m]$ in which $j_k = e(k)$.

The set $E^=$ could be simply viewed as

$$E^= = J_1^- \times J_2^- \times \dots \times J_m^-. \tag{15}$$

Based on the modified Definition 4', we further provide a theorem to illustrate the correction.

Theorem 4. Let $e = [j_1, j_2, \dots, j_m] \in E^=$, where $E^=$ is as defined in Definition 4'. Then the corresponding vector

$$\underline{X}(e) = [\underline{X}(e)_1, \underline{X}(e)_2, \dots, \underline{X}(e)_n] = [\bigvee_{i \in I} \check{x}_i(j_i)_1, \bigvee_{i \in I} \check{x}_i(j_i)_2, \dots, \bigvee_{i \in I} \check{x}_i(j_i)_n] = \bigvee_{i \in I} \check{x}_i(j_i)$$

is a solution of system (2), i.e. $\underline{X}(e) \in S_{DP}^\gamma(A, b)$.

Proof. According to Definition 5, $\underline{X}(e) = \check{x}_1(j_1) \vee \check{x}_2(j_2) \vee \dots \vee \check{x}_m(j_m)$. By (8), for arbitrary $i \in I$, there exists at most one nonzero component in the vector $\check{x}_i(j_i)$. If there exists, the unique non-zero component is indeed the j_i th component, i.e. $\check{x}_i(j_i)_{j_i} = l_{ij_i} \neq 0$. Notice that $\bar{X}_j \geq 0$ for all $j \in J$. Moreover, since $j_i \in J_i^-$, it follows from (14) that $\check{x}_i(j_i)_{j_i} = l_{ij_i} \leq \bar{X}_{j_i}$. As a result, we have $\check{x}_i(j_i) \leq \bar{X}$. Due to the arbitrariness of i , we further get $\underline{X}(e) = \check{x}_1(j_1) \vee \check{x}_2(j_2) \vee \dots \vee \check{x}_m(j_m) \leq \bar{X}$. According to Theorem 3, $\underline{X}(e)$ is a solution of system (2) □

Example 2. Continue to discuss the system (9) in Example 1, based on the modified Definition 4'.

According to (14), we get

$$J_1^- = \{1, 4\}, J_2^- = \{1, 5\}, J_3^- = \{2, 5\}, J_4^- = \{4, 5\}, J_1^- = \{2, 6\}. \tag{16}$$

Hence, the cardinality of $E^=$ is

$$|E^-| = J_1^- \times J_2^- \times \cdots \times J_5^- = 2^5 = 32.$$

That is to say, there are 32 solutions corresponding the 32 vectors e in E^- . These 32 solutions could be represented by

$$\{\underline{X}(e) | e \in E^-\}.$$

Recall that in Ref. [1], one should compute 72 vectors based on E . But by our modified set E^- , we just need to compute 32 ones. It is much easier to compute the solution set of system (9). \square

4. Conclusion

Max-Dubois-Prade fuzzy relation equations system with parameter γ and its corresponding optimization problem were recently investigated in [1]. For characterizing the solution set of system (2), the authors constructed the index set $E = J_1 \times J_2 \times \cdots \times J_m$ and asserted that all vectors in $\{\underline{X}(e) : e \in E\}$ are minimal solutions. However, it is found that $\underline{X}(e)$ might not be a solution for some specific $e \in E$. In order to make every vector $\underline{X}(e)$ be a solution of the corresponding fuzzy relation system, we modify the index set E to $E^- = J_1^- \times J_2^- \times \cdots \times J_m^-$. Moreover, we have verified that for each $e \in E^-$, the corresponding vector $\underline{X}(e)$ is a solution of system (2). Finding the solution set based on E^- should be easier than that based on E .

The limitation of this study and Ref. [1] is that the proposed resolution algorithm is only able to find an approximate (optimal) solution of the relevant optimization problem, but not an exact solution. Moreover, Ref. [1] hasn't explained the influence of the parameter γ to the resolution process or results. In our future works, there are some interesting researching topics, including but not limited to (i) the influence of the parameter γ , (ii) the sensitivity analysis with respect to A or/and b ; (iii) the optimization problems subject to other kinds of fuzzy relation systems; (iv) the potential industrial applications of the fuzzy relation optimization problems.

References

- [1] A. Ghodousian, M. Naeimi, A. Babalhavaeji, Nonlinear optimization problem subjected to fuzzy relational equations defined by Dubois-Prade family of t-norms, *Computers & Industrial Engineering* 119 (2018) 167-180.
- [2] E. Bartl, Minimal solutions of generalized fuzzy relational equations: Probabilistic algorithm based on greedy approach, *Fuzzy Sets and Systems* 260 (2015) 25-42.
- [3] A. A. Molai, Resolution of a system of the max-product fuzzy relation equations using $L \circ U$ -factorization, *Information Sciences* 234 (2013) 86-96.
- [4] X.-P. Yang, H.-T. Lin, X.-G. Zhou, B.-Y. Cao, Addition-min fuzzy relation inequalities with application in BitTorrent-like Peer-to-Peer file sharing system, *Fuzzy Sets and Systems* 343 (2018) 126-140.
- [5] X.-B. Yang, X.-P. Yang, K. Hayat, A New Characterisation of the Minimal Solution Set to Max-min Fuzzy Relation Inequalities, *Fuzzy Information and Engineering* 9 (2017) 423-435.
- [6] S.-J. Yang, Some Results of the Fuzzy Relation Inequalities With Addition-Min Composition, *IEEE Transactions on Fuzzy System* 26(1) (2018) 239-245.
- [7] A. Ghodousian, A. Babalhavaeji, An efficient genetic algorithm for solving nonlinear optimization problems defined with fuzzy relational equations and max-Łukasiewicz composition, *Applied Soft Computing* 69 (2018) 475-492.

- [8] S.-C. Fang, G. Li, Solving fuzzy relation equations with a linear objective function, *Fuzzy Sets and Systems* 103 (1999) 107-113.
- [9] A. Ghodousian, E. Khorram, Solving a linear programming problem with the convex combination of the max-min and the max-average fuzzy relation equations, *Applied Mathematics and Computation* 180 (2006) 411-418.
- [10] S.-M. Guu, Y.-K. Wu, A Linear Programming Approach for Minimizing a Linear Function Subject to Fuzzy Relational Inequalities With Addition-Min Composition, *IEEE Transactions on Fuzzy System* 25(4) (2017) 985-992.
- [11] S.-J. Yang, An algorithm for minimizing a linear objective function subject to the fuzzy relation inequalities with addition-min composition, *Fuzzy Sets and Systems* 255 (2014) 41-51.
- [12] X.-P. Yang, Optimal-vector-based algorithm for solving min-max programming subject to addition-min fuzzy relation inequality, *IEEE Transactions on Fuzzy Systems* 25(5) (2017) 1127-1140.
- [13] J. Lu, S.-C. Fang, Solving nonlinear optimization problems with fuzzy relation equations constraints, *Fuzzy Sets and Systems* 119 (2001) 1-20.
- [14] E. Khorram, R. Ezzati, Z. Valizadeh, Solving nonlinear multi-objective optimization problems with fuzzy relation inequality constraints regarding Archimedean triangular norm compositions, *Fuzzy Optimization and Decision Making* 11 (2012) 299-335.
- [15] X.-P. Yang, X.-G. Zhou, B.-Y. Cao, Single-variable term semi-latticized fuzzy relation geometric programming with max-product operator, *Information Sciences* 325 (2015) 271-287.
- [16] X.-P. Yang, Linear programming method for solving semi-latticized fuzzy relation geometric programming with max-min composition, *International Journal of Uncertainty, Fuzziness and Knowledge-Based Systems* 23 (2015) 781-804.
- [17] E. Shivanian, E. Khorram, Monomial geometric programming with fuzzy relation inequality constraints with max-product composition, *Computer & Industrial Engineering* 56 (2009) 1386-1392.
- [18] Y.-K. Wu, Optimizing the geometric programming problem with single-term exponents subject to max-min fuzzy relational equation constraints, *Mathematical and Computer Modelling* 47 (2008) 352-362.
- [19] X.G. Zhou, R. Ahat, Geometric programming problem with single-term exponents subject to max-product fuzzy relational equations, *Mathematical and Computer Modelling* 53 (2011) 55-62.
- [20] A. Abbasi Molai, A new algorithm for resolution of the quadratic programming problem with fuzzy relation inequality constraints, *Computers & Industrial Engineering* 72 (2014), 306-314.
- [21] J. Loetamonphong, S.-C. Fang, Optimization of fuzzy relation equations with max-product composition, *Fuzzy Sets and Systems* 118 (2001) 509-517.
- [22] B. Hedayatfar, A. Abbasi Molai, S. Aliannezhadi, Separable programming problems with the max-product fuzzy relation equation constraints, *Iranian Journal of Fuzzy Systems*, 16(1) (2019) 1-15.
- [23] S. Aliannezhadi, A. Abbasi Molai, Geometric programming with a single-term exponent subject to bipolar max-product fuzzy relation equation constraints, *Fuzzy Sets and Systems* 397 (2020) 61-83.
- [24] X.-P. Yang, D.-H. Yuan, B.-Y. Cao, Lexicographic optimal solution of the multi-objective programming problem subject to max-product fuzzy relation inequalities, *Fuzzy Sets and Systems* 341 (2018) 92-112.
- [25] X.-P. Yang, X.-G. Zhou, B.-Y. Cao, Latticized linear programming subject to max-product fuzzy relation inequalities with application in wireless communication, *Information Sciences* 358C359 (2016) 44-55.
- [26] J. Qiu, H. Xue, G. Li, X. Yang, Fuzzy relation bilevel optimization model in the wireless communication station system, *IEEE Access*, 8 (2020) 60811-60823.
- [27] F.-F. Guo, J. Shen, A Novel Smoothing Approach for Linear Objective Optimizations Subject to Fuzzy Relation Inequalities With Addition-Min Composition, *IEEE Transactions on Fuzzy System* 29(8) 2021 2444-2450.
- [28] Y.-L. Chiu, S.-M. Guu, J. Yu, Y.-K. Wu, A single-variable method for solving min-max programming problem with addition-min fuzzy relational inequalities, *Fuzzy Optimization and Decision Making* 18 (2019) 433-449.
- [29] X. Yang, J. Qiu, H. Guo, X. Yang, Fuzzy relation weighted minimax programming with addition-min composition, *Computers & Industrial Engineering* 147 (2020) 106644.
- [30] S.-M. Guu, Y.-K. Wu, Multiple objective optimization for systems with addition-min fuzzy relational inequalities, *Fuzzy Optimization and Decision Making* 18 (2019) 529-544.
- [31] X.-P. Yang, Z.-F. Hao, Supereigenvalue problem to addition-min fuzzy matrix with application in P2P file sharing system, *IEEE Transactions on Fuzzy System* 28(8) (2020) 1640-1651.
- [32] X.-P. Yang, Leximax minimum solution of addition-min fuzzy relation inequalities, *Information Sciences* 524 (2020) 184-198.

A New Group Fuzzy-Delphi Analytic Hierarchy Process Method with Its Application in Enterprise Intellectual Property Financing Decision Analysis

Bo FENG ^{a,b}, Zhipeng HUI ^a, Junwen FENG ^{a,b,1}

^a*Nanjing University of Science and Technology, 210094, China*

^b*Nanjing Audit University Jinshen College, 210023, China*

Abstract. The traditional analytic hierarchy process (AHP), fuzzy evaluation method and the Delphi method of group decision-making are organically combined and a new method of system analysis called Fuzzy Delphi Analytic Hierarchy Process (FDAHP) is proposed. Based on the Delphi survey of group decision-making information, the group's pairwise judgment of objects is fuzzily processed, and the results of the group's overall judgment are used as decision-making environmental parameters. Furthermore, the group's comprehensive weight of objects is determined according to the optimistic coefficient of group decision-making consideration. A simple example is given to illustrate the specific implementation steps and feasibility of the method. Finally, the advantages and disadvantages of the method are briefly discussed, and the possible research topics in the future are proposed.

Keywords. Analytic hierarchy process; Fuzzy evaluation; Delphi analysis; Determination of weights; Sorting, Fuzzy Delphi analytic hierarchy process

1. Introduction

Analytic Hierarchy Process (AHP) is a systematic decision analysis method combining both qualitative analysis and quantitative analysis, which was put forward by T. L. Saaty, an outstanding American operations researcher and professor of Business School, University of Pittsburgh in the early 1970s, saw Saaty (1980) [1] and Wang (1990) [2]. Analytic hierarchy process is a kind of multi-objective group decision-making thought and method in essence. In the practical application of group decision making method, there are two ways to deal with the pairwise judgment matrix of the group decision information. One is to first determine the individual weight according to the individual judgment matrix and then synthesize the individual weight; the other is to first synthesize the individual judgment matrix and then determine the weight of the group decision information. In recent years, scholars such as Corvin (2021) [3], Li (2012) [4], Zhou (2020) [5], Wang (2006) [6], have been improving the analytic hierarchy process to make it more convenient to use, such as establishing the order relationship between indicators, multi-attribute variable weight decision making methods, but these methods are

¹ Corresponding Author, Nanjing University of Science and Technology, Nanjing, China; E-mail: 313472714@qq.com

artificially adjusted to meet the consistency of the judgment matrix, this adjustment will lead to the original discriminant information is tampered with, the reliability of the conclusion is reduced. In the early stage, aiming at the difficult problems of consistency test in AHP, some researchers such as Li (2012) [3], Lu (2002) [7], Qin (2021) [8], Zhang (2000) [9] also proposed the method of using fuzzy consistency matrix to solve them, and formed the fuzzy analytic hierarchy process. Some of them put forward the idea and principle of fuzzy analytic hierarchy process from fuzzy number. Based on these improvements, analytic hierarchy process has a more mature application in many fields, but one problem is that after experts put forward judgment matrix, weight synthesis and so on seem to be the matter of decision analysts, who play the role of half decision makers. Another problem is that these so-called fuzzy analytic hierarchy process is only fuzzy in some steps of the traditional analytic hierarchy process. In particular, the calculated weight is still certain, such as mentioned by Singh (2021) [10], Tang (2002) [11], Tao (2002) [12]. Without fuzziness, it is difficult to reflect the participation of decision makers in the later stage of weight determination. As for the consistency of the expert judgment matrix, the traditional analytic hierarchy process (AHP) requires consistency test. In fact, from the perspective of behavioral decision analysis, decision-makers should be allowed to have large inconsistencies, because inconsistencies also reflect a kind of decision-making behavior. If the process of weight determination is regulated artificially by revising the judgment range matrix, it will affect the decision judgment formed by the decision maker before.

This paper presents a decision-making method which can fully involve decision makers in weight determination and analysis. The basic idea is to form a group fuzzy pairwise judgment range matrix by synthesizing the definite pairwise judgment range matrix given by various experts in the form of fuzzy triangular number, Then, according to the properties of fuzzy trigonometric numbers and some operation methods, the fuzzy weight vector of fuzzy judgment matrix of the group is determined. The fuzzy weight vector is processed according to the thought of group decision making, and then an interactive weight vector decision analysis process is formed, and finally the decision maker is satisfied with the weight vector of group decision. This process of decision interaction can be carried out under any single criterion in the hierarchy.

2. Basic approaches of fuzzy Delphi analytic hierarchy process

The hierarchical structure of the problem is established, and the groups have given their pairwise judgment matrices according to the traditional analytic hierarchy process. We assume that the weight determination of the corresponding decision scheme under a certain criterion is considered. Assuming that the relative importance of i and j elements in the sub-level of the k th expert has been determined as B_{ijk} under a certain criterion by expert investigation, forming the pairwise comparisons judgment matrix $B(k) = (B_{ijk})$ of the k th expert. Assuming that there are m decision schemes or evaluation indexes to be considered, the purpose is to determine the decision weight of the m decision schemes on the decision criterion. The specific steps are as follows:

Step 1: Building Fuzzy Judgment Matrix of Population

The pairwise comparison judgment matrix contains the opinions of experts involved in decision making, and the judgment of relative importance is uncertain. In this method, the fuzzy triangular number is used to integrate the opinions of experts, in order to

establish a more objective fuzzy group judgment matrix on the basis of the subjective opinions of decision makers. The pairwise judgment matrix of the group represented by triangular fuzzy number is as follows:

$B = (B_{ij})$, where B_{ij} is triangular fuzzy number, which is determined by the following method:

$B_{ij} = [T_{ij}, U_{ij}, V_{ij}]$, $T_{ij} \leq U_{ij} \leq V_{ij}$, & $T_{ij}, U_{ij}, V_{ij} \in [1/9, 1] \cup [1, 9]$, B_{ij} is triangular fuzzy number; $T_{ij} = \min_k(B_{ijk})$.

$U_{ij} = \text{Geomean}_k(B_{ijk})$, Here Geomean denotes geometric mean, and can also consider the weight of each expert using weighted geometric mean.

$$V_{ij} = \max_k(B_{ijk}) \tag{1}$$

Step 2: Determining Group Fuzzy Weight Vector

Based on the group fuzzy judgment matrix $B = (B_{ij})$, the corresponding fuzzy weight vector is determined by the column vector geometric average method as follows :

For any $j, j = 1, 2, \dots, m$, to calculate $r_j = (B_{1j} \cdot B_{2j} \cdot \dots \cdot B_{mj})^{1/m}$, Where \cdot denotes the product operation relation between fuzzy triangular numbers. Further standardize r_j to w_j :

$$w_j = r_j / (r_1 + r_2 + \dots + r_m), j = 1, 2, \dots, m \tag{2}$$

Step 3: Single- weight decision analysis

Firstly, the concept of cut sets in fuzzy analysis is used to defuzzify the weights, let $T \in [0, 1]$ be a truncated parameter, assuming $w_i = (w_i^L, w_i^M, w_i^U)$,

$$w_i^L(T) = (w_i^M - w_i^L)T + w_i^L \tag{3}$$

$$w_i^U(T) = (w_i^U - w_i^M)T + w_i^M \tag{4}$$

$$(T, \lambda) = \lambda w_i^U(T) + (1 - \lambda)w_i^L(T) \tag{5}$$

Where λ is the optimistic coefficient of weight for decision makers. Further, $w_i(T, \lambda)$ is normalized to get the normalized weight vector:

$$(T, \lambda) = w_i(T, \lambda) / (\sum_i w_i(T, \lambda)) \tag{6}$$

The decision weights now depend on two parameters T and λ . They mean:

The weight of the change degree of decision-making expert’s judgment is reflected by T . When $T = 0$, the comprehensive weight contains the decision-making weight information of each expert, and the change range of decision-making is the largest. When $T = 1$, the comprehensive weight contains the least decision-making weight information of each expert, which is actually equivalent to the synthesis method of expert decision-making weight without fuzzification. Therefore, T is a decision-making environmental parameter.

λ represents a parameter that integrates the decision-making weights of decision makers. When $\lambda = 0$, the opinions of experts take the upper limit of the weights, and the experts are the most optimistic. When $\lambda = 1$, experts take a conservative attitude, and take the lower limit of their weights. Therefore, λ can be called the decision-making optimism coefficient.

In the process of determining the actual weight, if the expert group has a high consensus on the problem, it can choose a larger T, otherwise it can choose a smaller T. The choice of λ reflects the degree of optimism of decision makers in evaluating the problem. The more optimistic it is, the larger its corresponding value.

3. Operational treatments in fuzzy Delphi analytic hierarchy process

Let $a = [a_1, a_2, a_3]$ and $b = [b_1, b_2, b_3]$ be two triangular fuzzy numbers, T is any positive real number, then according to the triangular fuzzy number theory, there are the following operational properties:

$$a \cdot b = [a_1 + b_1, a_2 + b_2, a_3 + b_3] \tag{7}$$

$$T_a = [T_{a1}, T_{a2}, T_{a3}] \tag{8}$$

$$a \cdot b = [a_1b_1, a_2b_2, a_3b_3] \tag{9}$$

$$1/a = a^{-1} = [1/a_3, 1/a_2, 1/a_1] \tag{10}$$

The standardized vector of a is w, w is a fuzzy triangular number, $w = (w_1, w_2, w_3)$, where $w_i = (a_i / (a_1 + a_2 + a_3))$.

In addition, it is easy to verify that the fuzzy group judgment matrix determined in the first step is a fuzzy antisymmetric matrix, that is, $B = (B_{ij})$ satisfies $B_{ij} = 1/B_{ji}$. In addition, when $i = j$, $B_{ij} = 1$.

The consistency test of the judgment matrix is not carried out in the decision-making method designed above. This is because from the perspective of behavioral decision-making, decision makers are allowed to make pairwise judgments that are not rational.

4. An application in enterprise intellectual property financing decision analysis

Consider a Decision-making problem of enterprise intellectual property financing. There are four decision strategies to be considered: (1) IP securitization, (2) IP Pledge financing, (3) IP Product Business Sharing, (4) IP franchising. Four experts, denoted as E1, E4, E2 and E3, are employed to evaluate the importance of the intellectual property financing strategies. The pairwise judgment matrices given by the experts are as follows:

$$E1 = \begin{bmatrix} 1 & 1/2 & 1/3 & 1/4 \\ 2 & 1 & 2/3 & 1/2 \\ 3 & 3/2 & 1 & 3/4 \\ 4 & 2 & 4/3 & 1 \end{bmatrix}, E2 = \begin{bmatrix} 1 & 2 & 2/3 & 1/2 \\ 1/2 & 1 & 1/3 & 1/4 \\ 3/2 & 3 & 1 & 3/4 \\ 2 & 4 & 4/3 & 1 \end{bmatrix}$$

$$E3 = \begin{bmatrix} 1 & 1/3 & 1/2 & 1/4 \\ 3 & 1 & 3/2 & 3/4 \\ 2 & 2/3 & 1 & 1/2 \\ 4 & 4/3 & 2 & 1 \end{bmatrix}, E4 = \begin{bmatrix} 1 & 4/3 & 2 & 4 \\ 3/4 & 1 & 3/2 & 3 \\ 1/2 & 3/2 & 1 & 2 \\ 1/4 & 1/3 & 1/2 & 1 \end{bmatrix}$$

Accordingly, the group fuzzy pairwise judgment matrix $B = (B_{ij})$ of the expert group is constructed as follows:

$$(T_{ij}) = \begin{bmatrix} 1.00 & 0.33 & 0.33 & 0.25 \\ 0.50 & 1.00 & 0.33 & 0.25 \\ 0.50 & 0.67 & 1.00 & 0.50 \\ 0.25 & 0.33 & 0.50 & 1.00 \\ 1.00 & 2.00 & 2.00 & 4.00 \end{bmatrix}, (U_{ij}) = \begin{bmatrix} 1.00 & 0.82 & 0.69 & 0.60 \\ 1.23 & 1.00 & 0.84 & 0.78 \\ 1.46 & 1.46 & 1.00 & 0.80 \\ 1.68 & 1.37 & 1.55 & 1.00 \end{bmatrix}$$

$$(V_{ij}) = \begin{bmatrix} 3.00 & 1.00 & 1.50 & 4.00 \\ 3.00 & 3.00 & 1.00 & 2.00 \\ 4.00 & 2.00 & 2.00 & 1.00 \end{bmatrix}$$

The standardized fuzzy weight vector of the population can be obtained as follows:
 $w_1 = (0.13, 0.24, 0.63)$, $w_2 = (0.13, 0.27, 0.60)$
 $w_3 = (0.17, 0.30, 0.53)$, $w_4 = (0.13, 0.32, 0.55)$

Assuming that the decision-making environment parameter is $T = 0.5$, and the decision-making optimism coefficient is $\lambda = 0.8$, we can get the normalized weight vector of group decision-making as $w = (0.24, 0.25, 0.25, 0.26)$, which means that strategy (4) is more important and the first choice. Assuming that the decision environment parameter is $T = 0.2$ and the decision optimism coefficient is $\lambda = 0.9$, the normalized weight vector of group decision is $w = (0.23, 0.25, 0.26, 0.26)$, which means that strategy (3) and (4) are equal important. Different choices of T and λ by decision makers will lead to different decision weights. We can also make the influence curves of decision environment parameter T and decision optimism coefficient λ on decisions weight DW on the plane. It is easy to prove that for a fixed T , the decision weight is a strictly monotonically increasing linear function of λ . Similarly, for a fixed λ , the decision weight is a strictly monotonically increasing linear function of T . These linear functions can be directly derived.

5. Conclusion

In this paper, a fuzzy group analytic hierarchy process (FAHP) is designed based on analytic hierarchy process (AHP), fuzzy evaluation principle and Delphi group decision method. Through Delphi investigation, the deterministic pairwise comparison judgment matrix of the group or expert to the evaluation object is obtained, and then the fuzzy mathematics method is used to process and analyze the group survey results, and then the environmental decision parameters and decision optimism coefficient are added to form an interactive weight decision analysis process to determine the comprehensive weight of the group to the evaluation object.

There are two approaches to group decision-making and evaluation based on analytic hierarchy process in the past literature. One is to integrate the pairwise judgment matrix of experts to form a group pairwise judgment matrix, and then determine the

decision weight or evaluation of the group to the evaluation object. The other is to determine the decision weight or evaluation of each expert based on the pairwise judgment matrix of each expert, and then integrate the decision weight of each expert to form the decision weight of the group. The workload of the two methods is large, and these methods assume a fact that the group's decision-making can be determined according to the one-time judgment of each individual in the group. The method given in this paper is not the same. On the basis of the individual investigation in the group, when the final evaluation results are determined, the group is also required to carry out decision analysis as a whole, reflecting the idea of a democracy and the unity of the main body of the concentration. The group can correct the previous judgment that is not appropriate in the final concentration process, so that the analytic hierarchy process has truly become an interactive decision analysis tool.

This paper only discusses the problem based on a single criterion, which can be easily extended to a multi-level and multi-criteria decision-making environment. In addition, the previous common group decision-making methods based on analytic hierarchy process are special cases in this paper under different combinations of decision-making environment parameters and decision-making optimism coefficients. In addition, this paper applies fuzzy triangular numbers to the fuzzy processing of expert information, and can also use other fuzzy processing methods to obtain different types of weight decision analysis processes.

The fuzzy group analytic hierarchy process (FDAHP) discussed in this paper has been compiled into a spreadsheet-based software, and interactive decision analysis can be easily carried out by means of Microsoft Excel.

References

- [1] Saaty, T. L., *The Analytic Hierarchy Process: Planning, Priority Setting, Resource Allocation*, 1980
- [2] Wang Lianfen, Xu Shubai. *Introduction to analytic hierarchy process* [M]. Beijing: People's University of China Press, 1990.
- [3] Corvin Jaime A et al. Analytic hierarchy process: An innovative technique for culturally tailoring evidence-based interventions to reduce health disparities.[J]. *Health expectations: an international journal of public participation in health care and health policy*, 2021, 24 Suppl 1: 70-81.
- [4] Li Chunhao, Du Yuanwei, Sun Yonghe, Tian Shuo. Multiple Attribute Implicit Variable Weight Decision Analysis Method [J]. *China Management Science*, 2012, 20 (05) : 163-172.
- [5] Zhou Lianchun and Jinshan Zhang and Konrad Fröhling. Evaluation of coal mine pollution abatement benefit based on analytic hierarchy process [J]. *Arabian Journal of Geosciences*, 2020, 13(19) : 71-86.
- [6] Wang Xuejun, Guo Yajun. Consistency analysis of judgment matrix based on G1 method [J]. *Chinese management science*, 2006 (03) : 65-70.
- [7] Lu Yuejin. Ranking of fuzzy analytic hierarchy process based on fuzzy consistent matrix [J]. *Fuzzy systems and mathematics*, 2002, 16 (2) : 79-85.
- [8] Qin Guangyu et al. Comprehensive evaluation of regional energy internet using a fuzzy analytic hierarchy process based on cloud model: A case in China[J]. *Energy*, 2021, 228.
- [9] Zhang Jijun. Fuzzy Analytic Hierarchy Process (FAHP) [J].*Fuzzy System and Mathematics*, 2000,14 (2) : 80-88.
- [10] Singh Rajbala and Kumar Deepak and Sagar Bharat Bhushan. Fuzzy analytical hierarchical process based two way assessment for agile testing[J]. *Journal of Discrete Mathematical Sciences and Cryptography*, 2021, 24(3) : 745-762.
- [11] Tang Youwen. Fuzzy Analytic Hierarchy Process [J]. *Journal of Qinghai Normal University (Natural Science Edition)*, 2002, (3) : 19-23.
- [12] Tao Shehui. How to construct fuzzy consistent matrix in fuzzy analytic hierarchy process [J].*Journal of Sichuan Normal University (Natural Science Edition)*, 2002, 23 (3) : 282-285.

Category of $\mathbf{CFR}(Y)^C$ and Weak Topos¹

Shao-Jun YANG^{a,2}, Xinyi HUANG^{a,3}

^aThe Fujian Provincial Key Laboratory of Network Security and Cryptology, College of Mathematics and Informatics, Fujian Normal University, Fuzhou 350117, P.R. China

Abstract. Topos theory plays an important role in modern mathematics. It can be viewed as a generalization of set from the category aspect. However, the category of all fuzzy sets do not form topos. In order to investigate the category properties about fuzzy sets, the notion of weak topos is introduced. Factor space is an effective approach in knowledge representation and factor ratten is a crucial concept of a factor space. Rattans over Y could be viewed as an abstraction of factor ratten. In addition, the category of rattans over Y is not a topos. In this paper, two comments about the paper titled "Factor rattans, category $\mathbf{FR}(Y)$, and factor space" (J MATH ANAL APPL, 1994) are presented, and the notion of ratten over Y is revised to complete ratten over Y . The corresponding category is denoted $\mathbf{CFR}(Y)$. Topoi properties of the functor category $\mathbf{CFR}(Y)^C$ are investigated and it is proved that $\mathbf{CFR}(Y)^C$ is a weak topos, but not a topos.

Keywords. Factor space, Ratten over Y , category of fuzzy sets, Weak topos

1. Introduction

Set theory is an important field in modern mathematics and provides a general fundamental framework of mathematics. The notion of fuzzy sets, which can be considered as a generalization of classical sets, was first introduced in 1965 by Zadeh [1].

The sets with the functions between two sets could construct a category **Set**. Topoi, which are cartesian closed categories with subobject classifiers, can be regarded as categories which are "essentially the same" as **Set** [2, 3]. That is, topoi can be viewed as another generalization of sets. Topoi theory plays an important role in mathematics, especially in logic. By the notion of topos, the logical operators (such as implication, negation) of classical sets can be obtained. More generally, each topos carries its own logical calculus [2].

Some correlations between fuzzy sets and topoi are inspected by various researchers [4–11]. However, the logical operators can not be obtained reasonably by the theory of topoi since **Fuz** which is the category of fuzzy sets is not a topos. To address this issue, the concepts of middle object and weak topos are introduced [9, 11, 12]. It is proved that **Fuz** is a weak topos and middle object can serve a similar function as the

¹This work is supported by National Natural Science Foundation of China (61822202, 61872089), Science and Technology Program of Fujian Province, China (2019J01428, 2020J02016), and State Key Laboratory of Cryptology Research Fund (MMKFKT202008)

²E-mail: shaojunyang@outlook.com

³Corresponding Author; E-mail: xyhuang81@yahoo.com

subobject classifier in a topos. Besides, the category **FuzFuz** of morphisms in category **Fuz** and the functor category \mathbf{Fuz}^C from a small category **C** to **Fuz** are also weak topoi [10, 12].

Another important instance of weak topos is $\mathbf{FR}(Y)$, which is the category of rattans over Y [13]. With the background of factor spaces [14], the notion of rattans over Y is introduced in [13]. Factor space is an important concept and It can be widely applied to various fields, such as knowledge representation, information science and big data [15–18]. Factor rattan is a crucial concept of a factor space, and rattans over Y [13] could be viewed as an abstraction of factor rattan. It is proved that the category of rattans over Y is a weak topos [13].

Definition 1.1 ([13]). Let Y be a fixed non-empty set and let X be any set. (X, ξ) is called a rattan over Y if $\xi : \mathcal{P}(X) \rightarrow \mathcal{P}(Y)$ is a mapping satisfying the following conditions.

- (1) $\xi(\emptyset) = Y$ and there exists a fixed element $y_0 \in Y$ such that $y_0 \in \xi(A)$ for any $A \in \mathcal{P}(X)$.
- (2) $\xi(A \cup B) = \xi(A) \cap \xi(B)$ for any $A, B \in \mathcal{P}(X)$.

A rattan over Y is called a Y -rattan for short.

The purpose of this paper is to inspect the topos properties of the category $\mathbf{FR}(Y)^C$, which is the functors category from a small category **C** to $\mathbf{FR}(Y)$. Two comments about [13] are proposed. Then the notion of complete rattans over Y is given, and the corresponding category is denoted by $\mathbf{CFR}(Y)$. It is proved that $\mathbf{CFR}(Y)^C$ is not a topos since it has no subobject classifier. However there exists a middle object in $\mathbf{CFR}(Y)^C$. Therefore, $\mathbf{CFR}(Y)^C$ forms a weak topos.

2. Topos and weak topos

A topos **C** is a category satisfying the following properties.

- 1. **C** has all finite products.
- 2. There is a terminal object t in **C**.
- 3. An equalizer exists in **C** for any $f, g \in \mathcal{M}(a, b)$ with $a, b \in \mathcal{O}(\mathbf{C})$.
- 4. Exponentials exist in **C**.
- 5. There is a subobject classifier in **C**. Specifically, there is an object s and a morphism ν from t to s such that for each monomorphism $f \in \mathcal{M}(a, b)$ with $a, b \in \mathcal{O}(\mathbf{C})$, there exists a unique morphism $\chi_f \in \mathcal{M}(b, s)$ so that the following diagram is a pullback.

$$\begin{array}{ccc}
 a & \longrightarrow & t \\
 f \downarrow & & \downarrow \nu \\
 b & \xrightarrow{\chi_f} & s
 \end{array}$$

Topoi have a great influence on logic. However, some significant categories, such as **Fuz**, **FuzFuz**, are not topoi since there is no subobject classifier in those categories. The notion of middle object defined in [12] can be viewed as a generalization of subobject classifier.

Definition 2.1 ([12]). A middle object in a category \mathbf{C} is a monomorphism $m \in \mathcal{M}(c_1, c_2)$ where $c_1, c_2 \in \mathcal{O}(\mathbf{C})$ satisfy the following conditions.

1. $\mathcal{M}(c, c_2)$ is partially ordered for all object $c \in \mathcal{O}(\mathbf{C})$.
2. For any $c \in \mathcal{O}(\mathbf{C})$, there is an unique smallest morphism $\alpha \in \mathcal{M}(c, c_2)$ such that the square is a pullback.

$$\begin{array}{ccc}
 c & \longrightarrow & c_1 \\
 1_c \downarrow & & \downarrow m \\
 c & \xrightarrow{\alpha} & c_2
 \end{array}$$

3. For any monomorphism $f \in \mathcal{M}(c, d)$ with any $c, d \in \mathcal{O}(\mathbf{C})$, there is an unique characteristic mapping $\chi_f \in \mathcal{M}(d, c_2)$ such that $\chi_f \leq \alpha$ and the following square is a pullback.

$$\begin{array}{ccc}
 c & \longrightarrow & c_1 \\
 f \downarrow & & \downarrow m \\
 d & \xrightarrow{\chi_f} & c_2
 \end{array}$$

With the definition of middle object, the concept of weak topos was also introduced.

Definition 2.2 ([12]). A weak topos is a category which satisfies the first four properties in the definition of topos and has a middle object.

In fact, a weak topos is a cartesian closed category with middle object.

3. Comments on “Factor rattans, category $\mathbf{FR}(Y)$, and factor space” (J MATH ANAL APPL, 1994)

The category of rattans over Y is denoted by $\mathbf{FR}(Y)$ where the morphisms from (X_1, ξ_1) to (X_2, ξ_2) are mappings $f : X_1 \rightarrow X_2$ satisfying $\xi_2(f^{-1}(A)) \supseteq \xi_1(A)$ for any $A \in \mathcal{P}(X_1)$. In addition, it is proved that $\mathbf{FR}(Y)$ is a weak topos.

The topic of [13] is meaningful and the results are beautiful. However, we think that there are two minor errors neglected by the authors.

Comment 1. It is proved in [13] that $\mathbf{FR}(Y)$ has finite product (Theorem 3.1 in [13]). Specifically, the product of any two rattans (X_1, ξ_1) and (X_2, ξ_2) can be denoted by (X, ξ) such that $X = X_1 \times X_2$ and $\xi(A) = \xi_1(A_1) \cap \xi_2(A_1)$ for any $A \in \mathcal{P}(X)$, where $A_1 = \{x_1 \in X_1 : \exists x_2 \in X_2 \text{ with } (x_1, x_2) \in A\}$ and $A_2 = \{x_2 \in X_2 : \exists x_1 \in X_1 \text{ with } (x_1, x_2) \in A\}$. However, the products do not always satisfy condition (1) in Definition 1.1 (see the following example).

Example 3.1. Let $Y = \{\perp, \top\}$, $X_1 = X_2 = \{x\}$ and let $\xi_i : \mathcal{P}(X_i) \rightarrow \mathcal{P}(Y)$ ($i = 1, 2$) such that $\xi_1(\emptyset) = \xi_2(\emptyset) = Y$, $\xi_1(X_1) = \{\top\}$ and $\xi_2(X_2) = \{\perp\}$. It is trivial to verify that (X_1, ξ_1) and (X_2, ξ_2) are two rattans over Y . However, we have $\xi(X) = \xi_1(X_1) \cap \xi_2(X_2) = \emptyset$ where (X, ξ) is the product of (X_1, ξ_1) and (X_2, ξ_2) .

Indeed, according to the definitions of factor spaces and factor rattans, we can see “there exists a fixed element $y_0 \in Y$ such that $y_0 \in \xi(A)$ for any $A \in \mathcal{P}(X)$ ” is not a pivotal property. Thus we can drop this condition in Definition 1.1.

Comment 2. It is proved that a middle object exists in **FR**(Y) (Theorem 3.2 in [13]). More specifically, let $M = \{\{y_0\} \cup A : A \in \mathcal{P}(Y)\}$, $N = \mathcal{P}(Y)$ and let $\xi_M : \mathcal{P}(M) \rightarrow \mathcal{P}(Y)$ be a mapping such that $\xi_M(\mathcal{A}) = \bigcap \mathcal{A}$ if $\emptyset \neq \mathcal{A} \in \mathcal{P}(M)$ and $\xi_M(\mathcal{A}) = Y$ if $\mathcal{A} = \emptyset$. Then (M, ξ_M) and (N, ξ_N) with $\xi_N(A) = Y$ for any $A \subseteq Y$, are two rattans. Besides, let $l_M : M \rightarrow N$ be a mapping such that $l_M(A) = A$ for any $A \in M$. Thus l_M is a morphism from (M, ξ_M) to (N, ξ_N)

Let (X_1, ξ_1) and (X, ξ) be two rattans and let $m : X_1 \rightarrow X$ be a monomorphism. Then two morphisms, $\phi_m : X \rightarrow N$ and $f_1 : X_1 \rightarrow M$ are defined in [13], where

$$\phi_m(x) = \begin{cases} \xi_1(\{x_1\}) & \exists x_1 \in X_1 \text{ s.t. } m(x_1) = x; \\ \emptyset & \text{otherwise,} \end{cases}$$

and $f_1(x_1) = \xi_1(\{x_1\})$ for any $x \in X$ and $x_1 \in X_1$, respectively. Thus we deduce that $\phi_m \cdot m = l_M \cdot f_1$. For any rattan (X', ξ') and any two morphisms $n : X' \rightarrow X$ and $f' : X' \rightarrow M$ with $\phi_m \cdot n = l_M \cdot f'$, let $\bar{n} : X' \rightarrow X_1$ be the mapping such that $n = m \cdot \bar{n}$. Then we can deduce that $\bar{n}(x') = x_1$ where x_1 satisfies $m(x_1) = n(x')$ for any $x' \in X'$. According to the definitions, \bar{n} is well-defined. Besides, it is said in [13] that “ \bar{n} is a morphism”. However, \bar{n} is not always a morphism (see the following example).

Example 3.2. Let $Y = [0, +\infty] = [0, +\infty) \cup \{+\infty\}$ with $a < +\infty$ for any $a \in [0, +\infty)$ and let $y_0 = +\infty$. Let $X_1 = X = [0, +\infty)$ with $\xi_1(A) = (\bigvee A, +\infty) \cup \{+\infty\}$ and $\xi(A) = [\bigvee A, +\infty]$ for any $A \subseteq [0, +\infty)$. Thus (X_1, ξ_1) and (X, ξ) form two rattans, and the mapping $m : X_1 \rightarrow X$ with $m(x) = x$ for any $x \in [0, +\infty)$ is a monomorphism. Besides, according to the definitions in [13], we have $M = \{\{+\infty\} \cup A : A \subseteq [0, +\infty)\}$, $N = \mathcal{P}([0, +\infty])$, $f_1(x) = (x, +\infty]$ and $\phi_m(x) = (x, +\infty]$, $\forall x \in [0, +\infty)$. Thus we have $\phi_m \cdot m = l_M \cdot f_1$.

Let $X' = [0, +\infty)$ and $\xi' : \mathcal{P}(X') \rightarrow \mathcal{P}(Y)$ such that:

$$\xi'(A) = \begin{cases} [\bigvee A, +\infty], & \text{if } \bigvee A \notin A, \\ (\bigvee A, +\infty) \cup \{+\infty\}, & \text{if } \bigvee A \in A, \end{cases}$$

for any $A \in \mathcal{P}(X')$. It is easy to verify that (X', ξ') is a rattan over Y . Then we get $\phi_m \cdot n = m \cdot f'$ where $n : X' \rightarrow X$ and $f' : X' \rightarrow M$ such that $n(x) = x$, $f'(x) = \xi'(\{x\})$ are two morphisms.

Then according to the definition of \bar{n} in [13], we get $\bar{n}(x) = x$ for any $x \in [0, +\infty)$. However, \bar{n} is not a morphism since $\xi_1(\bar{n}^{-1}([0, 1))) = \xi_1([0, 1)) = (1, +\infty] \subsetneq [1, +\infty] = \xi'([0, 1))$.

The main reason is that ξ satisfies $\xi(A \cup B) = \xi(A) \cap \xi(B)$ but not $\xi(\bigcup_{i \in I} A_i) = \bigcap_{i \in I} \xi(A_i)$ for any index set I . However, according to the definition of factor rattan, ξ and η satisfy $\xi(\bigcup_{i \in I} A_i) = \bigcap_{i \in I} \xi(A_i)$ and $\eta(\bigcup_{i \in I} A_i) = \bigcap_{i \in I} \eta(A_i)$ for any index set I , respectively.

According to the Comment 1 and Comment 2, we can revise the definition of rattan over Y as follows.

Definition 3.3. Let Y be a fixed non-empty set and let X be any set. (X, ξ) is called an complete rattan over Y if $\xi : \mathcal{P}(X) \rightarrow \mathcal{P}(Y)$ is a mapping satisfying the following conditions.

1. $\xi(\emptyset) = Y$.
2. $\xi(\bigcup_{i \in I} A_i) = \bigcap_{i \in I} \xi(A_i)$ for any $A_i \in \mathcal{P}(X)$ ($i \in I$) where I is an index set.

Under this revised definition, all complete rattans over Y also form a category, and we denote it by $\mathbf{CFR}(Y)$.

Remark 3.4. This concept is equivalent to a relation R from X to Y : $\xi_R(A) = \{y \in Y \mid A \times \{y\} \subseteq R\}$ and $(x, y) \in R_\xi$ iff $y \in \xi(\{x\})$ [19].

4. Topoi properties of category $\mathbf{CFR}(Y)^C$

Let \mathbf{C} be a small category and $\mathbf{CFR}(Y)^C$ be the functor category from \mathbf{C} to $\mathbf{CFR}(Y)$.

Theorem 4.1. Category $\mathbf{CFR}(Y)^C$ has all topoi properties except subobject classifiers.

Proof. We only need to prove that category $\mathbf{FR}(Y)^C$ has exponentials since others are trivial.

Let $F, G \in \mathcal{O}(\mathbf{CFR}(Y)^C)$ be two functors from \mathbf{C} to $\mathbf{CFR}(Y)$ with $F(c) = (X_c^F, \xi_c^F)$ and $G(c) = (X_c^G, \xi_c^G)$ for any $c \in \mathcal{O}(\mathbf{C})$. $c \uparrow \mathbf{C}$ denotes the comma category.

Let F_c, G_c be two “forgetful” functors from $c \uparrow \mathbf{C}$ to \mathbf{Set} . More specifically, for any $f : c \rightarrow d \in \mathcal{O}(c \uparrow \mathbf{C})$ and $h \in \mathcal{M}(f : c \rightarrow d, g : c \rightarrow e)$, we have $F_c(f) = X_d^F$, $F_c(h) = F(h)$, $G_c(f) = X_d^G$ and $G_c(h) = G(h)$. In addition, let $\text{Nat}[F_c, G_c]$ be the family of natural transformations from F_c to G_c . Then for any $A \subseteq \text{Nat}[F_c, G_c]$, we define:

$$\Sigma_c^A = \left\{ C \in \mathcal{P}(Y) : \begin{array}{l} \xi_d^F(B) \cap C \subseteq \xi_d^G(A_f^\rightarrow(B)) \\ \text{for any } f : c \rightarrow d, B \in \mathcal{P}(X_d^F) \end{array} \right\}$$

where $A_f^\rightarrow(B) = \bigcup_{\tau \in A} \tau_f^\rightarrow(B)$. In addition, let $\xi_c(A) = \bigcup \Sigma_c^A$.

According to the definition of ξ_c , it is trivial that $\xi_c(\emptyset) = Y$. Moreover, for any index set I , $A_i \subseteq \text{Nat}[F_c, G_c]$, $C_i \in \Sigma_c^{A_i}$ ($i \in I$), $f : c \rightarrow d$ and any $B \in \mathcal{P}(X_d^F)$, we can get $\xi_d^F(B) \cap \bigcap_{i \in I} C_i = \bigcap_{i \in I} \xi_d^F(B) \cap C_i \subseteq \bigcap_{i \in I} \xi_d^G((A_i)_f^\rightarrow(B)) = \xi_d^G((\bigcup_{i \in I} A_i)_f^\rightarrow(B))$. Thus $\bigcap_{i \in I} C_i \in \Sigma_c^{\bigcup_{i \in I} A_i}$, which implies $\bigcap_{i \in I} \xi_c(A_i) = \bigcap_{i \in I} \bigcup \Sigma_c^{A_i} \subseteq \bigcup \Sigma_c^{\bigcup_{i \in I} A_i} = \xi_c(\bigcup_{i \in I} A_i)$. Besides,

$\xi_c(A_1) \cap \xi_c(A_2) \supseteq \xi_c(A_1 \cup A_2)$ is trivial. Thus $(Nat[F_c, G_c], \xi_c) \in \mathcal{O}(\mathbf{CFR}(Y))$ is a Y -rattan.

For any $c \in \mathcal{O}(\mathbf{C})$ and $f : c \rightarrow d \in \mathcal{M}(c, d)$, let $G^F(c) = (Nat[F_c, G_c], \xi_c)$ and $G^F(f) : Nat[F_c, G_c] \rightarrow Nat[F_d, G_d]$, where $(G^F(f)(\tau))_g = \tau_{g \cdot f}$ for any $\tau \in Nat[F_c, G_c]$ and any $g : d \rightarrow e \in \mathcal{O}(d \uparrow \mathbf{C})$. Then for any $A \subseteq Nat[F_c, G_c]$, we have

$$\begin{aligned} \Sigma_d^{(G^F(f))^{-1}(A)} &= \left\{ C \in \mathcal{P}(Y) : \begin{array}{l} \xi_e^F(B) \cap C \subseteq \xi_e^G \left(\left((G^F(f))^{-1}(A) \right)_g^{-1}(B) \right), \\ \forall g : d \rightarrow e, B \in \mathcal{P}(X_e^F) \end{array} \right\} \\ &\supseteq \left\{ C \in \mathcal{P}(Y) : \begin{array}{l} \xi_e^F(B) \cap C \subseteq \xi_e^G(A_h^{-1}(B)), \\ \forall h : c \rightarrow e, B \in \mathcal{P}(X_e^F) \end{array} \right\} \\ &= \Sigma_c^A. \end{aligned}$$

Hence, for any $A \subseteq Nat[F_c, G_c]$, we get: $\xi_d \left((G^F(f))^{-1}(A) \right) = \bigcup \Sigma_d^{(G^F(f))^{-1}(A)} \supseteq \bigcup \Sigma_c^A = \xi_c(A)$. Thus we know that $G^F(f)$ is a morphism from $G^F(c)$ to $G^F(d)$. In addition, it is trivial that G^F preserves the identity and composition of morphisms. So G^F is a functor from category \mathbf{C} to category $\mathbf{CFR}(Y)$.

For any $c \in Ob(\mathbf{C})$, let $ev_c : Nat[F_c, G_c] \times X_c^F \rightarrow X_c^G$, $(\tau, x) \mapsto \tau_{1_c}(x)$, where $1_c : c \rightarrow c$ is the identity of c . For any $A \subseteq Nat[F_c, G_c] \times X_c^F$, we denote $A_1 = \{\tau \in Nat[F_c, G_c] : \text{there exists } x \in X_c^F \text{ s.t. } (\tau, x) \in A\}$ and $A_2 = \{x \in X_c^F : \text{there exists } \tau \in Nat[F_c, G_c] \text{ s.t. } (\tau, x) \in A\}$. Then we get that $\xi_c^G(ev_c^{-1}(A)) = \xi_c^G(\{\tau_{1_c}(x) : (\tau, x) \in A\}) \supseteq \xi_c^G(\bigcup_{\tau \in A_1} \tau_{1_c}^{-1}(A_2)) \supseteq \bigcup_{B \in \Sigma_c^{A_1}} \xi_c^F(A_2) \cap B = \xi_c \times \xi_c^F(A)$. Thus $ev_c \in \mathcal{M}(G^F(c) \times F(c), G(c))$.

For any $f : c_1 \rightarrow c_2 \in \mathcal{M}(c_1, c_2)$ and any $(\tau, x) \in G^F(c_1) \times F(c_1)$, according to the definition of τ , we can reduce that $G(f) \cdot \tau_{(1_{c_1})}(x) = \tau_f \cdot F(f)(x)$ for any $x \in X_{c_1}^F$, which implies that $G(f) \cdot ev_{c_1}(\tau, x) = G(f) \cdot \tau_{(1_{c_1})}(x) = \tau_{(1_{c_2} \cdot f)} \cdot F(f)(x) = ev_{c_2}(G^F(f)(\tau), F(f)(x)) = ev_{c_2} \cdot (G^F \times F)(f)(\tau, x)$. So $ev : G^F \times F \rightarrow G$ is a natural transformation from $G^F \times F$ to G .

Now let $H : \mathbf{C} \rightarrow \mathbf{CFR}(Y)$ be a functor from \mathbf{C} to $\mathbf{CFR}(Y)$, where $H(c) = (X_c^H, \xi_c^H)$ for any $c \in \mathcal{O}(\mathbf{C})$, and let $\sigma : H \times F \rightarrow G$ be a natural transformation. Then we define $\bar{\sigma}_c : X_c^H \rightarrow Nat[F_c, G_c]$ such that for any $y \in X_c^H$ and any $f : c \rightarrow d \in \mathcal{M}(c, d)$, $(\bar{\sigma}_c(y))_f : X_d^F \rightarrow X_d^G$ is a mapping where $(\bar{\sigma}_c(y))_f(x) = \sigma_d(H(f)(y), x)$ for any $x \in X_d^F$.

For any $f : c \rightarrow d \in \mathcal{M}(c, d)$, $g : c \rightarrow e \in \mathcal{M}(c, e)$ and any $h : d \rightarrow e \in \mathcal{M}(d, e)$ with $g = h \cdot f$, we have $(\bar{\sigma}_c(y))_g \cdot F(h)(x) = \sigma_e(H(g)(y), F(h)(x)) = \sigma_e(H(h) \cdot H(f)(y), F(h)(x)) = G(h) \cdot (\bar{\sigma}_c(y))_f(x)$ for any $x \in X_d^F$. Hence, we have $\bar{\sigma}_c(y) : F_c \rightarrow G_c$ is a natural transformation. So $\bar{\sigma}_c : X_c^H \rightarrow Nat[F_c, G_c]$ is well-defined.

For any $A \in \mathcal{P}(X_c^H)$, $f : c \rightarrow d \in \mathcal{M}(c, d)$ and any $B \in \mathcal{P}(X_d^F)$, we get $\xi_d^G \left((\bar{\sigma}_c^{-1}(A))_f^{-1}(B) \right) = \xi_d^G(\{\sigma_d(H(f)(y), x) : x \in B, y \in A\}) = \xi_d^G(\sigma_d^{-1}(\{H(f)^{-1}(A)\} \times B)) \supseteq \xi_d^H(\{H(f)^{-1}(A)\}) \cap \xi_d^F(B)$, which implies $\xi_c(\bar{\sigma}_c^{-1}(A)) = \bigcup \Sigma_c^{\bar{\sigma}_c^{-1}(A)} \supseteq \xi_d^H(H(f)^{-1}(A)) \supseteq \xi_c^H(A)$. Hence, we get $\bar{\sigma}_c \in \mathcal{M}(H(c), G^F(c))$.

For any $c \in \text{Ob}(\mathbf{C})$, $f : c \rightarrow d \in \mathcal{M}(c, d)$, $y \in X_c^H$, $g : d \rightarrow e \in \mathcal{M}(d, e)$ and any $x \in X_e^F$, we have $(G^F(f) \cdot \bar{\sigma}_c(y))_g(x) = (\bar{\sigma}_c(y))_{g \cdot f}(x) = \sigma_e(H(g \cdot f)(y), x) = \sigma_e(H(g) \cdot H(f)(y), x) = (\bar{\sigma}_d \cdot H(f)(y))_g(x)$. It follows that $\bar{\sigma} : H \rightarrow G^F$ is a natural transformation, and according to the definition of $\bar{\sigma}$, the following diagram is commutative.

$$\begin{array}{ccc}
 G^F \times F & \xrightarrow{ev} & G \\
 \bar{\sigma} \times 1_F \uparrow & \searrow \sigma & \\
 H \times F & &
 \end{array}$$

In addition, it is easy to verify such $\bar{\sigma}$ is unique. So, $\{G^F, ev\}$ is an exponential of F and G . It follows the theorem. □

From [13], we know that $\mathbf{CFR}(Y)$ has no subobject classifier. Similarly, we also have the following proposition.

Proposition 4.2. *Let Y be a non-empty setting. Category $\mathbf{CFR}(Y)^{\mathbf{C}}$ has no subobject classifier.*

Proof. Let $T : \mathbf{C} \rightarrow \mathbf{CFR}(Y)$ be the terminal object in $\mathbf{CFR}(Y)^{\mathbf{C}}$. That is, for any $c \in \mathcal{O}(\mathbf{C})$, $T(c) = (\{\top\}, \xi_0)$ where $\xi_0(\emptyset) = \xi_0(\{\top\}) = Y$. If $\mathbf{CFR}(Y)^{\mathbf{C}}$ has a subobject classifier, then there exists a functor $F : \mathbf{C} \rightarrow \mathbf{CFR}(Y)$ and a natural transformation $\omega : T \rightarrow F$ such that F is a subobject classifier.

Let $F_i : \mathbf{C} \rightarrow \mathbf{CFR}(Y)$ ($i = 1, 2, 3$) be three functors such that $F_i(c) = (X_i, \xi_i)$ for any $c \in \mathcal{O}(\mathbf{C})$, where $X_1 = X_2 = X_3 = \{\top\}$ and $\xi_1(\{\top\}) = \emptyset$, $\xi_2 = \xi_3 = \xi_0$. It is trivial that $\iota : F_1 \rightarrow F_2$ such that $\iota_c : X_1 \rightarrow X_2$ with $\iota_c(\top) = \top$ for any $c \in \mathcal{O}(\mathbf{C})$ is a natural transformation. In addition, ι is a monomorphism in $\mathbf{CFR}(Y)^{\mathbf{C}}$. Thus there exists a natural transformation $\chi_\iota : F_2 \rightarrow F$ such that $\chi_\iota \cdot \iota = \omega \cdot !$. Similarly, we can define a natural transformation $\kappa : F_3 \rightarrow F_2$ such that $\chi_\iota \cdot \kappa = \omega \cdot !$. Thus there exists a unique natural transformation $\bar{\kappa} : F_3 \rightarrow F_1$ with $\kappa = \iota \cdot \bar{\kappa}$. So for any $c \in \mathcal{O}(\mathbf{C})$, $\xi_1(\bar{\kappa}_c^{\rightarrow}(\{\top\})) \supseteq \xi_3(\{\top\})$. However, according to the definitions, we have $\xi_1(\bar{\kappa}_c^{\rightarrow}(\{\top\})) = \xi_1(\{\top\}) = \emptyset \subsetneq Y = \xi_3(\{\top\})$, which is a contradiction. Thus there is no subobject classifier in $\mathbf{CFR}(Y)^{\mathbf{C}}$. □

5. Category $\mathbf{CFR}(Y)^{\mathbf{C}}$ is a weak topos

In this section, we prove $\mathbf{CFR}(Y)^{\mathbf{C}}$ is a weak topos.

Theorem 5.1. *Category $\mathbf{CFR}(Y)^{\mathbf{C}}$ has a middle object.*

Proof. Let $*$ be an universal element and $\mathcal{P}(Y)^* = \mathcal{P}(Y) \cup \{*\}$. For convenience, we stipulate that $* \subseteq \emptyset$.

For any $c \in \mathcal{O}(\mathbf{C})$, let $M(c) = (X_c^M, \xi_c^M)$ and $N(c) = (X_c^N, \xi_c^N)$, where

$$\begin{aligned}
 X_c^M &= \left\{ f : \mathcal{O}(c \uparrow \mathbf{C}) \longrightarrow \mathcal{P}(Y) : \begin{array}{l} f(k \cdot l) \supseteq f(l), \forall l \in \mathcal{M}(c, a), \\ \forall k \in \mathcal{M}(a, b) \end{array} \right\}, \\
 X_c^N &= \left\{ f : \mathcal{O}(c \uparrow \mathbf{C}) \longrightarrow \mathcal{P}(Y)^* : \begin{array}{l} f(k \cdot l) \supseteq f(l), \forall l \in \mathcal{M}(c, a), \\ \forall k \in \mathcal{M}(a, b) \end{array} \right\}, \\
 \xi_c^M(A) &= \bigcap_{f \in A} f(1_c), \forall A \in \mathcal{P}(X_c^M), \\
 \xi_c^N(B) &= Y, \forall B \in \mathcal{P}(X_c^N).
 \end{aligned}$$

It is trivial that (X_c^M, ξ_c^M) and (X_c^N, ξ_c^N) are two Y -rattans.

In addition, for any $c, a \in \mathcal{O}(C)$ and $k \in \mathcal{M}(c, a)$, let $M(k) : X_c^M \longrightarrow X_a^M$ and $N(k) : X_c^N \longrightarrow X_a^N$ be two mappings such that $M(k)(f)(g) = f(g \cdot k)$ and $N(k)(f)(g) = f(g \cdot k)$. Thus for any $A \in \mathcal{P}(X_c^M)$, we have $\xi_a^M(M(k)^{\rightarrow}(A)) = \bigcap_{f \in A} M(k)(f)(1_a) = \bigcap_{f \in A} f(1_a \cdot k) = \bigcap_{f \in A} f(k) = \bigcap_{f \in A} f(k \cdot 1_c) \geq \bigcap_{f \in A} f(1_c) = \xi_c^M(A)$. So $M : \mathbf{C} \longrightarrow \mathbf{CFR}(Y)$ is a functor, and analogously, $N : \mathbf{C} \longrightarrow \mathbf{CFR}(Y)$ is also a functor.

For any $c \in \mathcal{O}(C)$, we define $m_c : X_c^M \longrightarrow X_c^N$ such that $m_c(f) = f$ for any $f \in X_c^M$. Then we get $N(k) \cdot m_c = m_a \cdot M(k)$ for any $k \in \mathcal{M}(C)$, which implies that $m : M \longrightarrow N$ is a natural transformation. Besides, it is clear that m is a monomorphism.

Now we want to prove that $m : M \longrightarrow N$ is a middle object.

(1) Let $F : \mathbf{C} \longrightarrow \mathbf{CFR}(Y)$ be a functor and let $\iota, \kappa \in \mathcal{M}(F, N)$ be two natural transformations. Besides, we let $\iota \leq \kappa \iff \iota_c \leq \kappa_c, \forall c \in \mathcal{O}(C) \iff \iota_c(x) \leq \kappa_c(x), \forall x \in X_c^F, c \in \mathcal{O}(C) \iff \iota_c(x)(k) \subseteq \kappa_c(x)(k), \forall k \in \mathcal{O}(c \uparrow \mathbf{C}), x \in (X_c^F), c \in \mathcal{O}(C)$. Then the pair $(\mathcal{M}(F, N), \leq)$ forms a partial order set.

(2) Let $F : \mathbf{C} \longrightarrow \mathbf{CFR}(Y)$ be a functor and let $a, c \in \mathcal{O}(C)$. For any $x \in X_c^F$ and $k \in \mathcal{M}(c, a)$, we define $\alpha_c(x)(k) = \xi_a^F(\{F(k)(x)\})$. Thus for any $l \in \mathcal{M}(a, b)$, we reduce that $\alpha_c(x)(l \cdot k) = \xi_b^F(\{F(l \cdot k)(x)\}) = \xi_b^F(F(l)^{\rightarrow}\{F(k)(x)\}) \geq \xi_a^F(\{F(k)(x)\}) = \alpha_c(x)(k)$, which implies $\alpha_c(x) \in X_c^N$. Besides, we have $(\alpha_a \cdot F(k)(x))(l) = \xi_b^F(\{F(l) \cdot F(k)(x)\}) = \xi_b^F(\{F(l \cdot k)(x)\}) = \alpha_c(x)(l \cdot k) = (N(k) \cdot \alpha_c(x))(l)$. Thus $\alpha : F \longrightarrow N$ is a natural transformation since $\alpha_c \in \mathcal{M}(F(c), N(c))$ is trivial.

Let $\tau_c(x) = \alpha_c(x) \in X_c^M$ for any $c \in \mathcal{O}(C)$ and $x \in X_c^F$. Hence, for any $A \in \mathcal{P}(X_c^F)$, we know that $\xi_c^M(\tau_c^{\rightarrow}(A)) = \bigcap_{x \in A} \tau_c(x)(1_c) = \bigcap_{x \in A} \xi_c^F(\{F(1_c)(x)\}) = \bigcap_{x \in A} \xi_c^F(\{x\}) = \xi_c^F(A)$, which implies $\tau_c \in \mathcal{M}(F(c), M(c))$. Similarly, we can prove $\tau : F \longrightarrow M$ is a natural transformation.

It is clear that $1_F : F \longrightarrow F$ with $(1_F)_c = F(1_c) : X_c^F \longrightarrow X_c^F$ for any $c \in \mathcal{O}(C)$ is the identical morphism in $\mathbf{CFR}(Y)^{\mathbf{C}}$. According to the definition of m, α and τ , we can get $m_c \cdot \tau_c = \alpha_c \cdot F(1_c)$. In addition, it is trivial to verify that this is a pullback.

If there exist α' and τ' such that the following diagram is a pullback.

$$\begin{array}{ccc}
 F & \xrightarrow{\tau'} & M \\
 \downarrow 1_F & & \downarrow m \\
 F & \xrightarrow{\alpha'} & N
 \end{array}$$

Thus for any $c \in \mathcal{O}(\mathbf{C})$ and $x \in X_c^F$, we have $\alpha'_c(x) = (\alpha'_c \cdot F(1_c))(x) = (m_c \cdot \tau'_c)(x) = \tau'_c(x)$. Thus for any $k \in \mathcal{M}(c, a)$, we have $\alpha'_c(x)(k) = \tau'_c(x)(k) = \tau'_c(x)(1_a \cdot k) = (M(k) \cdot \tau'_c(x))(1_a) = (\tau'_a \cdot F(k)(x))(1_a) = \xi_a^M(\{(\tau'_a \cdot F(k)(x))\}) \supseteq \xi_a^F(\{F(k)(x)\}) = \alpha_c(x)(k)$, which means $\alpha' \geq \alpha$.

(3) Let $\sigma : F \rightarrow G$ be a monomorphism in $\mathbf{CFR}(Y)^{\mathbf{C}}$ with $F, G \in \mathcal{O}(\mathbf{CFR}(Y)^{\mathbf{C}})$. For any $c \in \mathcal{O}(\mathbf{C})$, $y \in X_c^G$ and any $k : c \rightarrow a \in \mathcal{O}(c \uparrow \mathbf{C})$, we define

$$(\chi_\sigma)_c(y)(k) = \begin{cases} \xi_a^F(\{z\}) & \exists z \in X_a^F \text{ s.t. } G(k)(y) = \sigma_a(z), \\ * & \text{else.} \end{cases}$$

Since $\sigma : F \rightarrow G$ is a monomorphism, then $(\chi_\sigma)_c(y)(k)$ is well-defined. Thus if $(\chi_\sigma)_c(y)(k) \neq *$, we have $(\chi_\sigma)_c(y)(l \cdot k) = \xi_b^F(\{F(l)(z)\}) \geq \xi_a^F(\{z\}) = (\chi_\sigma)_c(y)(k)$ for any $l : a \rightarrow b \in \mathcal{M}(a, b)$. This implies $(\chi_\sigma)_c(y) \in X_c^N$. Besides, it is trivial to verify $\chi_\sigma : G \rightarrow N$ is a natural transformation.

For any $c \in \mathcal{O}(\mathbf{C})$ and $x \in X_c^F$, let $\varsigma_c(x) = (\chi_\sigma)_c \cdot \sigma_c(x) \in X_c^M$. Then for any $A \in \mathcal{P}(X_c^F)$, we have $\xi_c^M(\varsigma_c^{\rightarrow}(A)) = \bigcap_{x \in A} \varsigma_c(x)(1_c) = \bigcap_{x \in A} ((\chi_\sigma)_c \cdot \sigma_c(x))(1_c) = \bigcap_{x \in A} \xi_c^F(\{x\}) = \xi_c^F(A)$. Thus we get $\varsigma_c : X_c^F \rightarrow X_c^M \in \mathcal{M}(F(c), M(c))$. Therefore, $\varsigma : F \rightarrow M$ is a natural transformation. Besides, we have $\chi_\sigma \cdot \sigma = m \cdot \varsigma$.

Let $\eta : H \rightarrow G$ and $\theta : H \rightarrow M$ be two natural transformations with $\chi_\sigma \cdot \eta = m \cdot \theta$. Then we have $\theta_c(x)(k) = ((\chi_\sigma)_c \cdot \eta_c(x))(k)$ for any $x \in X_c^H$ and any $k \in \mathcal{O}(c \uparrow \mathbf{C})$ with any $c \in \mathcal{O}(\mathbf{C})$. Thus $((\chi_\sigma)_c \cdot \eta_c(x))(1_c) \neq *$. So there exists a unique $y \in X_c^F$ such that $\eta_c(x) = \sigma_c(y)$. Let $\bar{\eta}_c(x) = y$. Then $\bar{\eta}_c$ is well-defined and $\eta_c(x) = \sigma_c \cdot \bar{\eta}_c(x)$. So $\theta_c(x) = m_c \cdot \theta_c(x) = (\chi_\sigma)_c \cdot \eta_c(x) = (\chi_\sigma)_c \cdot \sigma_c \cdot \bar{\eta}_c(x) = m_c \cdot \varsigma_c \cdot \bar{\eta}_c(x) = \varsigma_c \cdot \bar{\eta}_c(x)$. In addition, for any $A \in \mathcal{P}(X_c^H)$, we have $\xi_c^F(\bar{\eta}_c^{\rightarrow}(A)) = \bigcap_{x \in A} ((\chi_\sigma)_c \cdot \eta_c(x))(1_c) = \bigcap_{x \in A} (\theta_c(x))(1_c) = \xi_c^M(\theta_c^{\rightarrow}(A)) \supseteq \xi_c^H(A)$, which implies $\bar{\eta}_c \in \mathcal{M}(H(c), F(c))$.

For any $k \in \mathcal{M}(c, a)$ and $x \in X_c^H$, we have $(\bar{\eta}_a \cdot H(k))(x) = y \iff \sigma_a(y) = (\eta_a \cdot H(k))(x) \iff \sigma_a(y) = G(k) \cdot \eta_c(x) \iff \sigma_a(y) = G(k) \cdot \sigma_c \cdot \bar{\eta}_c(x) \iff \sigma_a(y) = \sigma_a \cdot F(k) \cdot \bar{\eta}_c(x) \iff F(k) \cdot \bar{\eta}_c(x) = y$. Thus $\bar{\eta} : H \rightarrow F$ is a natural transformation with $\eta = \sigma \cdot \bar{\eta}$ and $\theta = \varsigma \cdot \bar{\eta}$. The proof of uniqueness of $\bar{\eta}$ is trivial. \square

Theorem 5.2. $\mathbf{CFR}(Y)^{\mathbf{C}}$ is a weak topos.

Proof. The proof of this theorem follows from Theorem 4.1 and Theorem 5.1. \square

6. Conclusion

In this paper, we present two comments about category of rattan over Y in [13] by two counter-examples. According to those comments and the background of rattan over Y , we revise the definition of rattan over Y . Then we show that $\mathbf{CFR}(Y)^{\mathbf{C}}$, which is the functors category from a small category to the category of rattan over Y (revised), is a weak topos, but it is not a topos since there is no subobject classifier in it. More specifically, it is a cartesian closed category with a middle object.

References

- [1] L.A. Zadeh. Fuzzy sets. *Information and Control*, 8(3):338–353, 1965.
- [2] Robeart Goldblatt. *Topoi: the categorical analysis of logic*. North-Holland, Amsterdam, 1984.
- [3] Saunders Mac Lane. *Categories for the working mathematician*. Springer-Verlag New York, 1998.
- [4] M. Barr. Fuzzy set theory and topos theory. *Canadian Mathematical Bulletin*, 29(29):501–508, 1986.
- [5] Ulrich Höhle and Lawrence Neff Stout. Foundations of fuzzy sets. *Fuzzy Sets and Systems*, 40(40):257–296, 1991.
- [6] Ulrich Höhle. Fuzzy sets and sheaves. I: basic concepts. *Fuzzy Sets and Systems*, (11):1143–1174, 2007.
- [7] Ulrich Höhle. Fuzzy sets and sheaves. part II: sheaf-theoretic foundations of fuzzy set theory with applications to algebra and topology. *Fuzzy Sets and Systems*, 158(11):1175–1212, 2007.
- [8] Lawrence N. Stout. A survey of fuzzy set and topos theory. *Fuzzy Sets and Systems*, 42(1):3–14, 1991.
- [9] X. H. Yuan and E. S. Lee. Categorical analysis of logic operators on fuzzy sets. *Journal of Mathematical Analysis and Applications*, 177(2):600–607, 1993.
- [10] Xue Hai Yuan and E. Stanley Lee. Category Fuz, wtopos, and category FuzFuz. *Journal of Mathematical Analysis and Applications*, 201(2):489–501, 1996.
- [11] Xue Hai Yuan. Comparisons between category Fuz and category Set. *The Journal of Fuzzy Mathematics*, 5(4):907–914, 1997.
- [12] Xue Hai Yuan, Hongxing Li, and E. Stanley Lee. Categories of fuzzy sets and weak topos. *Fuzzy Sets and Systems*, 127(3):291–297, 2002.
- [13] X. H. Yuan, E. S. Lee, and P. Z. Wang. Factor rattans, category $FR(Y)$, and factor space. *Journal of Mathematical Analysis and Applications*, 186(1):254–264, 1994.
- [14] Pei Zhuang Wang. A factor spaces approach to knowledge representation. *Fuzzy Sets and Systems*, 36(1):113–124, 1990.
- [15] A. Kandel, X. T. Peng, Z. Q. Cao, and P. Z. Wang. Representation of concepts by factor spaces. *Journal of Cybernetics*, 21(1):43–57, 1990.
- [16] Xue Hai Yuan, Pei Zhuang Wang, and E. S. Lee. Factor space and its algebraic representation theory. *Journal of Mathematical Analysis and Applications*, 171(1):256–276, 1992.
- [17] Pei-Zhuang Wang, Zeng-Liang Liu, Yong Shi, and Si-Cong Guo. Factor space, the theoretical base of data science. *Annals of Data Science*, 1(2):233–251, 2014.
- [18] Pei-Zhuang Wang and Alex Jiang. Rules detecting and rules-data mutual enhancement based on factors space theory. *International Journal of Information Technology & Decision Making*, 01(01):73–90, 2002.
- [19] Bernhard Ganter and Rudolf Wille. *Formal Concept Analysis*. Number 1. Springer-Verlag Berlin Heidelberg, 1999.

Control Design for One Class of Uncertain Metzler-Takagi-Sugeno Time-Delay Systems

Dušan KROKAVEC¹ and Anna FILASOVÁ

Technical University of Košice, Slovakia

Abstract. This paper presents a new approach to synthesize the control for one class of uncertain Metzler-Takagi-Sugeno time-delay systems. The structural parametric constraints of the closed-loop system, their diagonal matrix representations as well as the interval system parameter bounds are accounted into an associated set of the linear matrix inequalities. After sorting out the relevant preliminaries in the uncertain structure of the Metzler systems and the specific properties of the time-delay positive system representations, the design conditions reflecting quadratic system stability of the considered system class are proven in the matrix inequality framework. The main result of the control law parameter design is shown in detail by the numerical example in order to characterize potential adaptation of the method for purely Metzler matrix parameter structures.

Keywords. Metzler-Takagi-Sugeno systems, positive systems, quadratic stability, point state delay, diagonal stabilization, linear matrix inequalities.

1. Introduction

Time-delay systems are used to model the time lag phenomenon in thermodynamics [1] and ecology [2] and in modeling of interactions between species in mathematical biology [3]. In order to control, a number of approaches are proposed to solve the problems fixed with time-delay systems (see, e.g., [4]). In this paper the time-delay phenomena is considered as a point delay in the state vector [5].

Due to uncertainty existence, the uncertain plant stabilization have attracted many attentions to solve simultaneously this problem, reflecting LQR control [6], H_2 cost control [7] and H_∞ control principle [8]. In the sense of these prerequisites along with techniques for simultaneous quadratic stabilization of time-delay systems, the key concepts in stabilization and tracking conditions have been developed in [9] and the delay-dependent stabilization has been investigated in [10].

Positive systems represent the dynamical plants whose states and outputs have to be positive [11], [12]. The problem of positive systems usually deals with positive control structure and positive system state estimation [13]. Since existence of the system posi-

¹Corresponding Author: Dušan Krokavec, Department of Cybernetics and Artificial Intelligence, Faculty of Electrical Engineering and Informatics, Technical University of Košice, Letná 9, 042 00, Košice Slovakia; E-mail: dusan.krokavec@tuke.sk

tivity depends on the constraints in nonnegativity of the system matrix parameters, constrained design approaches are proposed to solve these problems [14]. Among the main features of positive systems can be mentioned the facts that the stability of delayed positive systems does not depend on the amplitude of delays [15], the asymptotical stability of positive systems is equivalent to diagonal stability (systems are not only stable but also positive) [16] and the system positivity can be interpreted through the model parametric constraints [17]. Since these models prioritize theory of matrices of Metzler structure [18], such systems are denoted oftentimes as Metzler systems. A similar approach one can find in development of control for the Metzler time-delayed systems [19].

Using the Takagi-Sugeno fuzzy model [20] a nonlinear system is represented as the collection of fuzzy rules, where each rule utilizes the local dynamics by a linear system model. Since Takagi-Sugeno fuzzy models can well approximate a large class of interval nonlinear systems the relevant design methodologies exploit fully advantage of the modern control theory, especially in the constrained control of positive T-S systems with delays [21] and in the positive system state estimation and fault diagnosis [22].

From the previous overview of methods and principles it can see how many different aspects have to be covered in the control design for uncertain Metzler-Takagi-Sugeno time-delay systems. Although the principle of diagonal stabilization provides a way to represent the parametric constraints of linear positive systems using the linear programming method [23], its direct adaptation to this system class is hardly limited. To overcome these limitations an original, new approach is established to give explicit design conditions in the form of linear matrix inequalities (LMI) to guaranty the strictly positive closed-loop system matrices if the uncertain system model takes the time-delay strictly Metzler-Takagi-Sugeno form. Note that, this LMIs structure cover the system structural constraints, the parameter uncertainties, the point-delay in system state, the quadratic stability and the diagonal stabilisation principle. The primary goal is to find the controller for stabilisation of the system under consideration while being consistent with the positive configuration. Although such defined class of systems prescribes the set of strong structural parametric constraints, the proposed design conditions allow the numerical solution in straightforward access. It is authors' belief that further extensions can be done through the given theoretical framework.

The remaining of the article is lay out as follows: Section 2 deals with the problem formulation and representative preliminaries related to Metzler-Takagi-Sugeno time-delay dynamic systems. The control problem, the resulting system parameter constraint formats and the relevant synthesis formulation are given in Section 3. The performance of the proposed technique and the system parameters representation are illustrated by carrying out a detailed numerical example in Section 4, also supporting related outlines of new points of view and conclusions, drafted in Section 5.

For sake of convenience, throughout the paper used notations reflect usual conventionality so that x^T , X^T denotes the transpose of the vector x , and the matrix X , respectively, X^{-1} , $\rho(X)$ signifies the inverse and the eigenvalue spectrum of a square matrix X , respectively, for a symmetric square matrix $X \prec 0$ means that X is negative definite matrix, $\text{diag}[\cdot]$ marks the elements of a (block) diagonal matrix, $*$ represents the block in a square symmetric matrix that is readily inferred by the matrix symmetry, the symbol I_n indicates the n -th order unit matrix, \mathbb{R} (\mathbb{R}_+) qualifies the set of (nonnegative) real numbers, $\mathbb{R}_+^{n \times r}$ refers to the set of $n \times r$ positive (nonnegative) real matrices and $\mathbb{M}_{-+}^{n \times n}$ is the set of (strictly or pure) Metzler matrices.

2. Basic Preliminaries

The system class under consideration is multi-input, multi-output (MIMO) uncertain Metzler-Takagi-Sugeno time-delay dynamic systems, represented in state-space form as

$$\dot{q}(t) = \sum_{i=1}^s h_i(\vartheta(t))(A_i + \Delta_i A_i(t))q(t) + (A_s + \Delta A_s(t))q(t - \tau) + (B + \Delta B(t))u(t), \quad (1)$$

$$y(t) = Cq(t), \quad (2)$$

where the point delay in the state vector is constant and satisfies the condition $0 < \tau \in \mathbb{R}_+$, the system input variable vector $u(t) \in \mathbb{R}^r$ and the uncertainties $\Delta A_i(t), \Delta B(t), \Delta A_s(t)$ are matching uncertainties. The system trajectory $q(t) \in \mathbb{R}_+^n$, and the output $y(t) \in \mathbb{R}_+^m$ are nonnegative, $C \in \mathbb{R}_+^{m \times n}$, $B, \Delta B(t) \in \mathbb{R}_+^{n \times r}$ and $\Delta A_i(t), \Delta A_s(t) \in \mathbb{R}_+^{n \times n}$ are nonnegative matrices, $A, A_s \in \mathbb{M}_{-+}^{n \times n}$ are strictly Metzler and $r = m$. Moreover, $h_i(\theta(t))$ is averaging weight for the i -th rule, representing the normalized grade of membership, where

$$0 \leq h_i(\vartheta(t)) \leq 1, \quad \sum_{i=1}^s h_i(\vartheta(t)) = 1 \quad \text{for all } i \in \langle 1, s \rangle, \quad (3)$$

while s is the number fuzzy rules (linear sub-models) and

$$\vartheta(t) = [\theta_1(t) \theta_2(t) \cdots \theta_q(t)] \quad (4)$$

is q -dimensional vector of premise variables, where the premise variables are measurable. More details can be found, e.g., in [24], [25].

Definition 1. [18] A square matrix $A \in \mathbb{M}_{-+}^{n \times n}$ is purely Metzler if its diagonal elements are negative and its off-diagonal elements are nonnegative. A Metzler matrix $A \in \mathbb{M}_{-+}^{n \times n}$ is strictly Metzler if its diagonal elements are negative and its off-diagonal elements are positive. A Metzler matrix is stable if it is Hurwitz.

Definition 2. [26] Given any nonnegative initial condition $\phi(t) \in \mathbb{R}_+^n$ such that $q(t) = \phi(t)$ for $-\tau \leq t \leq 0$, the externally forced system (1) is said to be positive if the corresponding trajectory is nonnegative ($q(t) \in \mathbb{R}_+^n$ for all $t \geq 0$).

Definition 3. (adapted from [8]) If the uncertainties of the system (1), (2) satisfy for every time-instant $t > 0$ the condition

$$[\Delta A_i(t) \quad \Delta B(t) \quad \Delta A_s(t)] = M \Xi(t) [N_{ai} \quad N_b \quad N_s], \quad (5)$$

where $M \in \mathbb{R}_+^{n \times s}$, $N_{ai} \in \mathbb{R}_+^{p \times n}$, $N_b \in \mathbb{R}_+^{p \times r}$, $N_s \in \mathbb{R}_+^{p \times n}$ are known nonnegative real matrices characterizing the uncertainties structure, $\Xi(t) \in \mathbb{R}^{s \times p}$ is a time varying matrix satisfying the bound

$$\Xi^T(t) \Xi(t) \leq I_p \quad (6)$$

and the elements of $\Xi(t)$ are Lebesgue measurable, then the uncertainties $\Delta A_i(t), \Delta B(t), \Delta A_s(t)$, are matching uncertainties.

Note, as a rule, for point time-delay Metzler-Takagi-Sugeno systems with strictly positive A_i, A_s and nonnegative B all the matrices $M \in \mathbb{R}_+^{n \times s}$, $N_{ai} \in \mathbb{R}_+^{p \times n}$, $N_b \in \mathbb{R}_+^{p \times r}$, $N_s \in \mathbb{R}_+^{p \times n}$ have to be non-negative.

Since Metzler-Takagi-Sugeno systems are defined to satisfy affine combination of matrix elements [27], this suggests the following.

Lemma 1. (adapted from [26]) Assuming that the externally forced system (1) is asymptotically stable and the matrices $A_s \in \mathbb{M}_{-+}^{n \times n}$ and $A_i \in \mathbb{M}_{-+}^{n \times n}$ for $i = 1, \dots, s$ are strictly Metzler then the composed matrix

$$A_i^\diamond = A_i + A_s \tag{7}$$

is strictly Metzler and Hurwitz

Remark 1. Obviously, if all matrices in (7) are strictly Metzler then their sum must have the form of a strictly Metzler matrix. In dependence on positions of zero elements in these matrices, there can be a strictly Metzler matrix A_i^\diamond even for the case where both matrices are only purely Metzler, or one from them is strictly Metzler and the other is purely Metzler. This means different interpretations of the tasks of analysis and synthesis of such class of systems and leads to solutions with different parametric boundaries on Metzler structures [4], [28], [29]. Unless otherwise stated below, the both above given matrices in (7) are considered to be strictly Metzler for all i .

Remark 2. In general, a strictly Metzler matrix $A \in \mathbb{M}_{-+}^{n \times n}$ is so confronted with n^2 boundaries implying from the structural constraints

$$a_{lh} < 0, l = h, \quad a_{lh} > 0, l \neq h, \quad \forall l, h \in \langle 1, n \rangle. \tag{8}$$

This just means in consequence to apply diagonal stabilization principle [30] in control or observer design task. This principle can be adapted for the control design task if a strictly Metzler matrix $A \in \mathbb{M}_{-+}^{n \times n}$ is represented with the following rhombic form, constructed by circular shifts of the rows of the strictly Metzler A as follows

$$A_\Theta = \begin{bmatrix} -a_{11} & a_{12} & a_{13} & \cdots & a_{1n} \\ & -a_{22} & a_{23} & \cdots & a_{2n} & a_{21} \\ & & -a_{33} & \cdots & a_{3n} & a_{31} & a_{32} \\ & & & \ddots & \vdots & \vdots & \vdots \\ & & & & -a_{nn} & a_{n1} & a_{n2} & \cdots & a_{n,n-1} \end{bmatrix}, \tag{9}$$

where the diagonal matrices

$$A_\Theta(l, l) = \text{diag} [-a_{11} \ -a_{22} \ \cdots \ -a_{nn}] < 0, \tag{10}$$

$$A_\Theta(l, l+h) = \text{diag} [a_{1,1+h} \cdots a_{n-h,n} \ a_{n-h+1,1} \cdots a_{n,h}] > 0, \quad h = 1, \dots, n-1, \tag{11}$$

are related to diagonals of A_Θ and $\Theta = (1 \leftrightarrow n)/n$ notes summation in the sense of the sum of modulo $(n+1)$.

Moreover, it can see that generally n^2 parametric Metzler constraints (8) can be defined by the negativeness of (10) and positiveness of the set of diagonal matrices (11).

Definition 4. [31] A square matrix $L \in \mathbb{R}_+^{n \times n}$ is the permutation matrix if exactly one element in each column and each row is equal to 1 and all others are equal to 0. The permutation matrix L is called circulant if

$$L = \begin{bmatrix} 0^T & 1 \\ I_{n-1} & 0 \end{bmatrix}. \tag{12}$$

Remark 3. If $X \in \mathbb{R}^{n \times n}$ is a diagonal matrix and L is the circulant permutation matrix (12) then

$$L^T \text{diag} [x_1 \ x_2 \ \cdots \ x_n] L = \text{diag} [x_2 \ \cdots \ x_n \ x_1]. \tag{13}$$

Lemma 2. [32] *Let the matrix $A \in \mathbb{M}_{-+}^{n \times n}$ is strictly Metzler then it is Hurwitz if and only if there exists the positive definite diagonal matrix $S \in \mathbb{R}_{+}^{n \times n}$ that for $h = 1, \dots, n-1$ and the circulant $L \in \mathbb{R}_{+}^{n \times n}$ the following sets of LMIs is feasible*

$$S \succ 0, \quad SA^T + AS \prec 0, \tag{14}$$

$$A_{\Theta}(l, l)S \prec 0, \quad L^h A_{\Theta}(l, l+h)L^{hT}S \succ 0. \tag{15}$$

Lemma 3. [33] *If the strictly Metzler $A \in \mathbb{R}_{-+}^{n \times n}$, the nonnegative $B \in \mathbb{R}_{+}^{n \times r}$ and a positive $K \in \mathbb{R}_{+}^{r \times n}$ guarantee that $A_c = A - BK \in \mathbb{R}_{-+}^{n \times n}$ is strictly Metzler then it is satisfied for the defined h and j*

$$A_c = \sum_{h=0}^{n-1} (A_{\Theta}(l, l+h) - \sum_{j=0}^r B_{dj}K_{djh})L^{hT}, \tag{16}$$

where with $K_{dj}, B_{dj} \in \mathbb{R}_{+}^{n \times n}$

$$A_{\Theta}(l, l) - \sum_{j=0}^r B_{dj}K_{dj} \prec 0, \tag{17}$$

$$A_{\Theta}(l, l+h) - \sum_{j=0}^r B_{dj}K_{djh} \succ 0, \tag{18}$$

$$K = \begin{bmatrix} k_1^T \\ \vdots \\ k_r^T \end{bmatrix}, \quad K_{dj} = \text{diag} [k_j^T] = \text{diag} [k_{j1} \cdots k_{jn}], \quad K_{djh} = L^{hT}K_{dj}L^h \tag{19}$$

$$B = [b_1 \cdots b_r], \quad B_{dj} = \text{diag} [b_j] = \text{diag} [b_{j1} \cdots b_{jn}] \tag{20}$$

Note, (17), (18) force parameter constraints of the Metzler A_c and do not guaranty that A_c is Hurwitz. Equation (16) together with (19)–(20) give the relations between the square and the rhombic matrix representation of A_c .

Summarizing, in this section are fixed the basis notations and terminologies used in the paper, clarified the necessary background theoretical preliminaries from the assorted points of interpretation and recalled a number of relevant definitions. In order to commonly formalize control synthesis for the uncertain Metzler-Takagi-Sugeno time-delay systems in the following section, everything is defined on the common state-space basis.

3. Control Design for the Class of Uncertain Metzler-Takagi-Sugeno Time-delay Systems

This section presents the conditions on control existence for considered class of systems with constant time-delays and the LMI based formulation for computing the control law parameters. The considered problem is connected with the control law

$$u(t) = -Kq(t) - K_s q(t - \tau) \tag{21}$$

such that in the closed-loop structure

$$\begin{aligned} \dot{q}(t) &= \sum_{i=1}^s h_i(\vartheta(t))(A_i - BK)q(t) + \sum_{i=1}^s h_i(\vartheta(t))(\Delta A_i(t) - \Delta B(t)K)q(t) + \\ &+ (A_s - BK_s)q(t - \tau) + (\Delta A_s(t) - \Delta B(t)K_s)q(t - \tau) \\ &= \sum_{i=1}^s h_i(\vartheta(t))A_{ci}q(t) + \sum_{i=1}^s h_i(\vartheta(t))A_{\Delta ci}(t)q(t) + A_{cs}q(t - \tau) + A_{\Delta cs}(t)q(t - \tau), \end{aligned} \tag{22}$$

where

$$A_{ci} = A_i - BK, A_{\Delta ci}(t) = \Delta A_i(t) - \Delta B(t)K, A_{cs} = A_s - BK_s, \Delta A_{cs}(t) = \Delta A_s(t) - \Delta B(t)K_s, \tag{23}$$

the matrices $A_{ci}, A_{cs}, A_{ci}^\circ, A_{cs}^\circ \in \mathbb{R}_{-+}^{r \times n}$ are strictly Metzler, the control law gains $K, K_s \in \mathbb{R}_{+}^{r \times n}$ are positive and

$$A_{ci}^\circ = A_{ci} + A_{cs} \tag{24}$$

are strictly Metzler and Hurwitz for all i .

The relation (5) then admits the uncertainty models if $p = r$

$$\Delta A_{ci}(t) = M\Xi(t)(N_{ai} - N_bK) = M\Xi(t)N_{ci}, \tag{25}$$

$$\Delta A_{cs}(t) = M\Xi(t)(N_s - N_bK_s) = M\Xi(t)N_{cs}. \tag{26}$$

where

$$N_{ci} = N_{ai} - N_bK, N_{cs} = N_s - N_bK_s. \tag{27}$$

Reflecting the diagonal stabilisation principle, then to the above introduced relations (19), (20) the additional terms are defined

$$A_{ci} = A_i - \sum_{j=1}^r b_j k_j^T = A_i - \sum_{j=1}^r B_{dj} l_n l_n^T K_{dj}, \tag{28}$$

$$A_{cs} = A_s - \sum_{j=1}^r b_j k_{sj}^T = A_s - \sum_{j=1}^r B_{dj} l_n l_n^T K_{sdj}, \tag{29}$$

$$N_{ci} = N_{ai} - \sum_{j=1}^r n_{bj} k_j^T = N_{ai} - \sum_{j=1}^r N_{bdj} l_r l_n^T K_{dj}, \tag{30}$$

$$N_{cs} = N_s - \sum_{j=1}^r n_{bj} k_{sj}^T = N_s - \sum_{j=1}^r N_{bdj} l_r l_n^T K_{sdj}, \tag{31}$$

$$A_{\Theta_i}(l, l) = \text{diag} [-a_{i11} \quad -a_{i22} \quad \cdots \quad -a_{inn}], \tag{32}$$

$$A_{\Theta_i}(l, l+h) = \text{diag} [a_{i,1,1+h} \quad \cdots \quad a_{i,n-h,n} \quad a_{i,n-h+1,1} \quad \cdots \quad a_{i,nh}], \tag{33}$$

$$A_{\Theta_s}(l, l) = \text{diag} [-a_{s11} \quad -a_{s22} \quad \cdots \quad -a_{smn}], \tag{34}$$

$$A_{\Theta_s}(l, l+h) = \text{diag} [a_{s,1,1+h} \quad \cdots \quad a_{s,n-h,n} \quad a_{s,n-h+1,1} \quad \cdots \quad a_{s,nh}], \tag{35}$$

$$K_s = \begin{bmatrix} k_{s1}^T \\ \vdots \\ k_{sr}^T \end{bmatrix}, K_{sdj} = \text{diag} [k_{sj}^T] = \text{diag} [k_{sj1} \quad \cdots \quad k_{sjn}], K_{sdjh} = L^{hT} K_{sdj} L^h \tag{36}$$

$$N_b = [n_{b1} \quad \cdots \quad n_{bp}], N_{bdj} = \text{diag} [n_{bj}] = \text{diag} [n_{bj1} \quad \cdots \quad n_{bjp}]. \tag{37}$$

$$l_n^T = [1 \ 1 \quad \cdots \ 1], l_r^T = [1 \ 1 \quad \cdots \ 1], l_n \in \mathbb{R}_+^n, l_r \in \mathbb{R}_+^r \tag{38}$$

and (7) is reformulated as:

$$A_{ci}^\circ = A_{ci} + A_{cs}. \tag{39}$$

To simply constructing under defined matching uncertainties the following lemma can be applied.

Lemma 4. [34] *Let the real matrices X, Y, Z of consistent dimensions are bound by the relation*

$$Z = X^T Y + Y^T X, \tag{40}$$

then for positive $\gamma \in \mathbb{R}_+$ the following inequality is satisfied

$$Z \preceq \gamma^{-1} X^T X + \gamma Y^T Y. \tag{41}$$

Thus, considering (19), (20), (32)–(39) and the circulant $L \in \mathbb{R}_+^{n \times n}$ from (12) it can prove the following.

Theorem 1. *If for strictly Metzler $A_i, A_s \in \mathbb{M}_+^{n \times n}$ and nonnegative $B \in \mathbb{R}_+^{n \times r}, M \in \mathbb{R}_+^{n \times s}, N_{ai} \in \mathbb{R}_+^{p \times n}, N_b \in \mathbb{R}_+^{p \times r}, N_s \in \mathbb{R}_+^{p \times n}$ there exist positive definite diagonal matrices $S, R_j, R_{sj} \in \mathbb{R}_+^{n \times n}$ and a positive scalar $\delta \in \mathbb{R}_+$ such that for $h = 1, \dots, n - 1, i = 1, \dots, s$ is feasible the following set of linear matrix inequalities*

$$S \succ 0, \quad R_j \succ 0, \quad R_{sj} \succ 0, \quad \delta > 0, \tag{42}$$

$$\begin{bmatrix} [(A_i + A_s)S - \sum_{j=1}^r B_{dj} l_n l_n^T (R_j + R_{sj})] + [*] + \delta M M^T & * \\ (N_{ai} + N_s)S - \sum_{j=1}^r N_{bdj} l_r l_n^T (R_j + R_{sj}) & -\delta I_r \end{bmatrix} \prec 0, \tag{43}$$

$$A_{\Theta_i}(l, l)S - \sum_{j=0}^r B_{dj} R_j \prec 0, \tag{44}$$

$$A_{\Theta_s}(l, l)S - \sum_{j=0}^r B_{dj} R_{sj} \prec 0, \tag{45}$$

$$L^h A_{\Theta_i}(l, l+h)S - \sum_{j=0}^r L^h B_{dj} L^{hT} R_j \succ 0, \tag{46}$$

$$L^h A_{\Theta_s}(l, l+h)S - \sum_{j=0}^r L^h B_{dj} L^{hT} R_{sj} \succ 0, \tag{47}$$

then the positive control gains $K, K_s \in \mathbb{R}_+^{r \times n}$ are given as

$$K_{dj} = R_j S^{-1}, \quad k_j^T = l_n^T K_{dj}, \quad K = \begin{bmatrix} k_1^T \\ \vdots \\ k_r^T \end{bmatrix}, \tag{48}$$

$$K_{sdj} = R_{sj} S^{-1}, \quad k_{sj}^T = l_n^T K_{sdj}, \quad K_s = \begin{bmatrix} k_{s1}^T \\ \vdots \\ k_{sr}^T \end{bmatrix} \tag{49}$$

and force the strictly Metzler and Hurwitz matrices (39) and Metzler matrices A_{ci}, A_{cs} .

*Hereafter, * denotes the symmetric item in a symmetric matrix.*

Proof. It quickly follows from (7), (14) that

$$(A_i + A_s + \Delta_i A_i(t) + \Delta A_s(t))S + S(A_i + A_s + \Delta A_i(t) + \Delta A_s(t))^T \prec 0, \tag{50}$$

where $S \succ 0$ is a positive definite diagonal matrix. Combining associated parts of uncertainties in (50) it can write

$$\begin{aligned}
 & (\Delta A_i(t) + \Delta A_s(t))S + S(\Delta A_i(t) + \Delta A_s(t)) \\
 & = M\Xi(t)(N_{ai} + N_s)S + S(N_{ai} + N_s)^T \Xi(t)^T M^T \\
 & \preceq \gamma^{-1} M\Xi(t)\Xi(t)^T M^T + \gamma S(N_{ai} + N_s)^T (N_{ai} + N_s)S \\
 & \preceq \gamma^{-1} MM^T + \gamma S(N_{ai} + N_s)^T (N_{ai} + N_s)S,
 \end{aligned} \tag{51}$$

where the final relation follows from (41) taking a positive scalar $\gamma \in \mathbb{R}_+$ into account. Then, in the view of condition (50)

$$(A_i + A_s)S + S(A_i + A_s)^T + \gamma^{-1} MM^T + \gamma S(N_{ai} + N_s)^T (N_{ai} + N_s)S \prec 0 \tag{52}$$

and it is apparent that

$$\begin{bmatrix} (A_i + A_s)S + S(A_i + A_s)^T + \gamma^{-1} MM^T & S(N_{ai} + N_s)^T \\ (N_{ai} + N_s)S & -\gamma^{-1} I_r \end{bmatrix} \prec 0, \tag{53}$$

when the Schur complement property is applied.

To govern the closed-loop system then (53) has to be satisfied with exchange for $A_i \leftarrow A_{ci}, A_s \leftarrow A_{cs}, N_{ai} \leftarrow N_{cai}, N_s \leftarrow N_{cs}$ and $\delta = \gamma^{-1}$ that is

$$\begin{bmatrix} (A_{ci} + A_{cs})S + S(A_{ci} + A_{cs})^T + \delta MM^T & S(N_{cai} + N_{cs})^T \\ (N_{cai} + N_{cs})S & -\delta I_r \end{bmatrix} \prec 0. \tag{54}$$

Since it can check the following hold from (28)–(31)

$$A_{ci}S = A_iS - \sum_{j=1}^r b_j k_j^T S = A_iS - \sum_{j=1}^r B_{dj} l_n l_n^T K_{dj} S = A_iS - \sum_{j=1}^r B_{dj} l_n l_n^T R_j, \tag{55}$$

$$A_{cs}S = A_sS - \sum_{j=1}^r b_j k_{sj}^T S = A_sS - \sum_{k=1}^m B_{dj} l_n l_n^T K_{sdj} S = A_sS - \sum_{j=1}^r B_{dj} l_n l_n^T R_{sj}, \tag{56}$$

$$N_{cai}S = N_{ai}S - \sum_{j=1}^r n_{bj} k_j^T S = N_{ai}S - \sum_{j=1}^r N_{bdj} l_r l_n^T K_{dj} S = N_{ai}S - \sum_{j=1}^r N_{bdj} l_r l_n^T R_j, \tag{57}$$

$$N_{cs}S = N_sS - \sum_{j=1}^r n_{bj} k_{sj}^T S = N_sS - \sum_{j=1}^r N_{bdj} l_r l_n^T K_{sdj} S = N_sS - \sum_{j=1}^r N_{bdj} l_r l_n^T R_{sj} S, \tag{58}$$

where

$$R_j = K_{dj}S, \quad R_{sj} = K_{sdj}S. \tag{59}$$

then LMI (57) conditioned by (58)-(59) imply (43).

The inequalities (17), (18) and the relation (19) in turn give the similar expressions for actual parametric constraints

$$A_{\Theta_i}(l, l) - \sum_{j=0}^r B_{dj} K_{dj} \prec 0, \quad A_{\Theta_s}(l, l) - \sum_{j=0}^r B_{dj} K_{sdj} \prec 0, \tag{60}$$

$$A_{\Theta_i}(l, l+h) - \sum_{j=0}^r B_{dj} K_{djh} \succ 0, \quad A_{\Theta_s}(l, l+h) - \sum_{j=0}^r B_{dj} K_{sdjh} \succ 0, \tag{61}$$

where

$$K_{djh} = L^{hT} K_{dj} L^h, \quad K_{sdjh} = L^{hT} K_{sdj} L^h. \tag{62}$$

Then, multiplying the right side of (60) by S it yields

$$A_{\Theta_i}(l, l)S - \sum_{j=0}^r B_{dj} K_{dj} S \prec 0, \quad A_{\Theta_s}(l, l)S - \sum_{j=0}^r B_{dj} K_{sdj} S \prec 0 \tag{63}$$

and replacing with (59) then (60) imply (44) and (45).

Pre-multiplying the left side by L^h and post-multiplying the right side by $L^{hT}S$ then (61) is rewritten as

$$A_{\Theta_i}(l, l+h)S - \sum_{j=0}^r B_{dj}K_{djh}L^{hT}S \succ 0, \quad A_{\Theta_s}(l, l+h)S - \sum_{j=0}^r B_{dj}K_{sdjh}L^{hT}S \succ 0, \quad (64)$$

Thus, substituting (62)

$$A_{\Theta_i}(l, l+h)S - \sum_{j=0}^r B_{dj}L^{hT}K_{dj}S \succ 0, \quad A_{\Theta_s}(l, l+h)S - \sum_{j=0}^r B_{dj}L^{hT}K_{sdj}S \succ 0, \quad (65)$$

where $L^hL^{hT} = I_n$ and replacing with (59) then (64) imply (46) and (47). This completes the proof. \square

Remark 4. *If the set of LMIs (42)–(47) is feasible, the conditions (44)–(47) cover that the matrices A_{ci}, A_i are strictly Metzler, the matrix inequality (43) clamps that A_{ci}° is Metzler and Hurwitz and the positive definite diagonal matrix variables S, R_j, R_{sj} guaranty that $K, K_s \in \mathbb{R}_+^{r \times n}$ are positive. Thus, the given problem can be solved by (42)–(47), guaranteeing quadratically stable closed-loop system.*

Potentially, the given task formulation can be extended for models with the interval uncertainties in time-delays and inputs using the concept of parallel distributed compensation [25].

Corollary 1. *Consider that $B \in \mathbb{R}_+^{n \times r}$ is nonnegative and that $A_i, A_s \in \mathbb{M}_{-+}^{n \times n}$ are pure Metzler but all are mutually compatible in the position of a zero value off-diagonal element (zero element falls in all these matrices on the position with the row number z and the column number y).*

If the z -th row of B is zero vector ($b_z^T = 0^T$), the design conditions (42)–(47) remain valid and the results in the feasible case are positive K, K_s , pure Metzler matrices $A_{ci}, A_s \in \mathbb{M}_{-+}^{n \times n}$ and pure Metzler and Hurwitz $A_{ci}^\circ \in \mathbb{M}_{-+}^{n \times n}$.

If elements of the z -th row of B are nonzero and an off-diagonal (z, y) -element is equal to zero in mutually compatible $A_i, A_s \in \mathbb{M}_{-+}^{n \times n}$ then the design conditions have to be reformulated for the structural positive semi-definite diagonal matrix variables R_j, R_{sj} , defined as

$$R_j = \text{diag} [r_{j1} \cdots r_{j,z-1} \quad r_{jz} \quad r_{j,z+1} \cdots r_{jn}] \succeq 0 \quad (66)$$

$$R_{sj} = \text{diag} [r_{s,j1} \cdots r_{s,j,z-1} \quad r_{s,jz} \quad r_{s,j,z+1} \cdots r_{s,jn}] \succeq 0 \quad (67)$$

where for all j and given z

$$r_{jz} = 0, \quad r_{s,jz} = 0 \quad (68)$$

The results in the last noted case guaranty nonnegative K, K_s , pure Metzler and Hurwitz $A_{ci}^\circ \in \mathbb{M}_{-+}^{n \times n}$ and pure Metzler matrices $A_i, A_s \in \mathbb{M}_{-+}^{n \times n}$. The inclusion of the reference [35] makes up for the omitted details of the explanation.

Other cases, if they are solvable, can be done "ad hoc" in definition of distinct structural positive semi-definite diagonal matrix variables R_j, R_{sj} for different $j \in \langle 1, s \rangle$.

The aim of the proposed methodology is to stabilize the systems of the given class at the defined parameters of the system model. In the solved task, the task validation is included inherently in the synthesis conditions - if the considered system is stabilizable, there must be positive definite diagonal matrix variables such that the proposed set of LMI is feasible. Only if the system has uncontrollable modes the validation would be

more involved. For the control approach, the quadratic stability of the overall closed-loop error dynamics is proven using by the system matrix eigenvalue emplacement criterion.

Remark 5. For application use in the control theory, this type of design task does not define the principle of LMI algorithm implementation, but only their boundaries [36]. The final characteristics are defined by the choice of a standard LMI solver, which defines the computational complexity of the implemented algorithms. In this case the algorithm solves the design task in polynomial time with respect to the cardinality of the state space, the number of matrix variables and applied LMI solver. Using the LMI solver SeDuMi the computational complexity is $O(h_{dv}^2 h_{ar}^{2.5} + h_{ar}^{3.5})$, where h_{dv} is the number of decision variables and h_{ar} is the number of active rows in the LMIs [37], while the computational complexity of MATLAB LMI Toolbox is $O(h_{dv}^3 h_{ar})$ [38]. The former algorithm is so more efficient for problems with a large number of LMI variables.

Because the principle is not intended for use in an adaptive control structure with the real-time control parameter calculation, this computational complexity is not applicable limiting.

The proposed method provides a novel, original, constructive and nontrivial formulation, where the computation of the control gains reduces to a feasibility problem over a set of LMIs. The solution depends on the positive parameter δ , corresponding to an upper bound for the matching uncertainty condition and is optimized in the nominally defined design task. The parameter δ can be fixed in the design step interactively in the case it is necessary to modify (usually slow down) the dynamics of a closed loop.

4. Illustrative Example

To illustrate the effectiveness of the proposed method the design principle is applied to the system model (1), (2) defined by the system parameters

$$A_1 = \begin{bmatrix} -0.27 & 1.94 & 1.45 \\ 0.08 & -3.96 & 0.20 \\ 0.45 & 0.70 & -2.91 \end{bmatrix}, A_2 = \begin{bmatrix} -0.26 & 2.06 & 1.55 \\ 0.14 & -3.64 & 0.36 \\ 0.25 & 0.78 & -2.55 \end{bmatrix}, L^T = \begin{bmatrix} 0 & I_2 \\ 1 & 0^T \end{bmatrix}, l_r = \begin{bmatrix} 1 \\ 1 \end{bmatrix},$$

$$A_s = \begin{bmatrix} -0.01 & 0.12 & 0.15 \\ 0.01 & -0.38 & 0.03 \\ 0.04 & 0.07 & -0.31 \end{bmatrix}, B = \begin{bmatrix} 0.5 & 1.0 \\ 1.0 & 0.9 \\ 0.7 & 1.1 \end{bmatrix}, C^T = \begin{bmatrix} 1 & 0 \\ 0 & 1 \\ 0 & 0 \end{bmatrix}, l_n = \begin{bmatrix} 1 \\ 1 \\ 1 \end{bmatrix}, M = \begin{bmatrix} 0 & 0 \\ 1 & 0 \\ 0 & 1 \end{bmatrix},$$

$$N_{a1} = \begin{bmatrix} 0.02 & 0 & 0 \\ 0 & 0.01 & 0 \end{bmatrix}, N_{a2} = \begin{bmatrix} 0.01 & 0 & 0 \\ 0 & 0.02 & 0 \end{bmatrix}, N_s = \begin{bmatrix} 0.02 & 0 & 0 \\ 0 & 0.02 & 0 \end{bmatrix}, N_b = \begin{bmatrix} 0.2 & 0 \\ 0 & 0.2 \end{bmatrix},$$

where A_1, A_2, A_s are strictly Metzler but not Hurwitz.

With the synthesis focusing points, of immediate consequences are primary the common matrix auxiliary parameters

$$A_{\Theta 1}(l, l) = -\text{diag} [0.27 \ 3.96 \ 2.91], \quad A_{\Theta 2}(l, l) = -\text{diag} [0.26 \ 3.64 \ 2.55],$$

$$A_{\Theta 1}(l, l+1) = \text{diag} [1.94 \ 0.20 \ 0.45], \quad A_{\Theta 2}(l, l+1) = \text{diag} [2.06 \ 0.36 \ 0.25],$$

$$A_{\Theta 1}(l, l+2) = \text{diag} [1.45 \ 0.08 \ 0.70], \quad A_{\Theta 2}(l, l+2) = \text{diag} [1.55 \ 0.14 \ 0.78],$$

$$A_{\Theta s}(l, l) = -\text{diag} [0.01 \ 0.38 \ 0.31],$$

$$A_{\Theta s}(l, l+1) = \text{diag} [0.12 \ 0.03 \ 0.04], \quad A_{\Theta s}(l, l+2) = \text{diag} [0.15 \ 0.01 \ 0.07],$$

$$B_{d1} = \text{diag} [0.5 \ 1.0 \ 0.7], \quad B_{d2} = \text{diag} [1.0 \ 0.9 \ 1.1],$$

$$N_{bd1} = \text{diag} [0.2 \ 0], \quad N_{bd2} = \text{diag} [0 \ 0.02].$$

Solving (42)-(47), applying SeDuMi package in MATLAB environment, the feasible task admits the solution with the following positive definite diagonal matrix variables

$$S = \text{diag} [3.3558 \ 0.4667 \ 0.6948],$$

$$R_1 = \text{diag} [0.0879 \ 0.1008 \ 0.0422], \quad R_2 = \text{diag} [0.1190 \ 0.0813 \ 0.0496],$$

$$R_{s1} = \text{diag} [0.0115 \ 0.0132 \ 0.0066], \quad R_{s2} = \text{diag} [0.0119 \ 0.0093 \ 0.0070].$$

Using relations (48), (49) the positive gain matrices of the common control law are computed as

$$K = \begin{bmatrix} 0.0023 & 0.0426 & 0.0078 \\ 0.0079 & 0.0208 & 0.0167 \end{bmatrix}, \quad K_s = \begin{bmatrix} 0.0296 & 0.1861 & 0.0614 \\ 0.0352 & 0.1583 & 0.0659 \end{bmatrix}$$

and it is trivial to construct the matrices $A_{c1}^\circ, A_{c2}^\circ$

$$A_{c1}^\circ = \begin{bmatrix} -0.3338 & 1.7437 & 1.4834 \\ 0.0253 & -4.7589 & 0.0865 \\ 0.4264 & 0.3854 & -3.3588 \end{bmatrix}, \quad \rho(A_{c1}^\circ) = \begin{bmatrix} -0.1231 \\ -3.5463 \\ -4.7821 \end{bmatrix},$$

$$A_{c2}^\circ = \begin{bmatrix} -0.3238 & 1.8637 & 1.5834 \\ 0.0853 & -4.4389 & 0.2465 \\ 0.2264 & 0.4654 & -2.9988 \end{bmatrix}, \quad \rho(A_{c2}^\circ) = \begin{bmatrix} -0.1459 \\ -3.0848 \\ -4.5308 \end{bmatrix}.$$

The design condition guaranties only that A_{c1}, A_{c2}, A_{cs} be strictly Metzler, but for such given system parameters it is obtained

$$A_{c1} = \begin{bmatrix} -0.3186 & 1.6578 & 1.3483 \\ 0.0219 & -4.3328 & 0.0750 \\ 0.3927 & 0.3572 & -3.0310 \end{bmatrix}, \quad \rho(A_{c1}) = \begin{bmatrix} -0.1226 \\ -3.2068 \\ -4.3529 \end{bmatrix},$$

$$A_{c2} = \begin{bmatrix} -0.3086 & 1.7778 & 1.4483 \\ 0.0819 & -4.0128 & 0.2350 \\ 0.1927 & 0.4372 & -2.6710 \end{bmatrix}, \quad \rho(A_{c2}) = \begin{bmatrix} -0.1452 \\ -2.7440 \\ -4.1032 \end{bmatrix},$$

$$A_{cs} = \begin{bmatrix} -0.0153 & 0.0859 & 0.1352 \\ 0.0034 & -0.4262 & 0.0115 \\ 0.0337 & 0.0283 & -0.3277 \end{bmatrix}, \quad \rho(A_{cs}) = \begin{bmatrix} -0.0003 \\ -0.3396 \\ -0.4293 \end{bmatrix},$$

which all are strictly Metzler and Hurwitz, but this results is not guaranteed in general.

One can verify that using slightly different parameter matrix with the time-delay relation A_s in the form

$$A_s = \begin{bmatrix} -0.01 & 0.12 & 0.15 \\ 0.01 & -0.38 & 0.03 \\ 0.04 & 0.07 & -0.31 \end{bmatrix} \leftarrow \begin{bmatrix} -0.01 & 0.12 & 0.15 \\ 0.01 & -0.38 & 0.03 \\ 0.04 & 0.07 & -0.30 \end{bmatrix},$$

the solution mean strictly Metzler and Hurwitz $A_{c1}^\circ, A_{c2}^\circ, A_{c1}, A_{c2}$, but A_{cs} is only strictly Metzler, since in this case

$$A_{cs} = \begin{bmatrix} -0.0153 & 0.0859 & 0.1352 \\ 0.0034 & -0.4262 & 0.0115 \\ 0.0337 & 0.0283 & -0.3177 \end{bmatrix}, \quad \rho(A_{cs}) = \begin{bmatrix} 0.0001 \\ -0.3302 \\ -0.4291 \end{bmatrix}.$$

Note, the matrix A_{cs} does not need to be a Hurwitz matrix since the main idea is to construct a stable augmented matrix A_{ci}° .

Real negative system eigenvalues are conditional on the use of positive Metzler systems because they guarantee the aperiodic positive trajectories of state variables for a

non-negative initial state of the system with convergence to the system equilibrium only in the positive subspace \mathbb{R}_+^n . For this reason, the graphical presentation of state trajectories appears to be redundant. The given example contains all the parameters so that interesting readers can verify this fact.

Note, the potentially comparable method for stabilization of time-delay positive continuous-time systems presented in [39] produces in general the non-negative gains and the nonnegative closed-loop system matrices although the description of the system is based on the strictly Metzler matrix structures. As a result, there is no comparison base of the design methods for the results presented in this paper for uncertain Metzler-Takagi-Sugeno time-delay systems.

For sake of readability, in the example is only treated the case of strictly Metzler system matrices, but the authors are convinced that this explicit example helps interesting readers in understanding such defined design problem in the whole complexity.

5. Concluding Remarks

In the paper, a novel method is proposed for design of control law parameters for uncertain Metzler-Takagi-Sugeno time-delay systems with a constant point time-delay in state and it is showed that it preserves principle of diagonal stabilization. Structural properties of the considered systems with uncertainties are reflected to ensure the closed-loop quadratic stability when defining the LMIs structure which cover the system structural constraints, the parameter uncertainties and the point-delay in system state. What seems perhaps specific is additional conditions to find state feedbacks with positive system gains, preserving the closed-loop system positivity for strictly Metzler system matrices. The parameter uncertainty domination as well as quadratic stability are guaranteed by using the proposed structure of the state feedback. The illustrative example confines to the theoretical starting points. To the best of authors' knowledge, no comparable theoretical results are available for design of state control of this class of systems with strictly Metzler matrix structures.

The reason justifying the use of uncertain Metzler-Takagi-Sugeno time-delay model is the need to minimize potentially the time-delay impact on the control with distributed sensor structures of nonlinear systems. In this sense the account of the uncertainties in Metzler-Takagi-Sugeno models allows adjusting the system state so that the system parameter constraints imposed by the system positivity are satisfied. This is also the main topic for the future research.

The limitation of the presented structure of LMIs is tied to the positive definiteness of the diagonal variables $R_j, R_{s,j}$, which in the case of the purely Metzler structure of the matrices may mean a marginal feasibility of the solution. Corollary 1 outlines an approach of solving this problem by defining these variables as structured in an ad hoc manner for a specific case. Another disadvantage limiting their widespread use is the problem of selecting the nonnegative uncertainty matching conditions.

Solving under given system parametric constraints and the boundlessness of system uncertainties substantially limits a control parameter tuning by reexpressing the design conditions with an additive tuning parameter. However, such a path must be used for uncertain Metzler-Takagi-Sugeno time-delay systems with a polytopic region of uncertainty as this introduces another scalar tuning parameter when using the slack matrix

principle. If an unknown disturbance is acting on the uncertain Metzler-Takagi-Sugeno time-delay systems, adjusting to the H_∞ norm of the disturbance transfer function must be done by even more tuning scalar parameter. The ideas presented can be potentially extended to a more general class of Metzler-Takagi-Sugeno time-delay systems with interval time-delays or to design a non-fragile memory feedback controller for the considered system class and to the system reference trajectory problem. These cases are partly a topic for future research.

Acknowledgements

The work presented in the paper was supported by VEGA, the Grant Agency of the Ministry of Education and the Academy of Science of Slovak Republic, under Grant No. 1/0463/21. This support is very gratefully acknowledged.

References

- [1] Zheng F, Frank P.M. Robust control of uncertain distributed delay systems with application to the stabilization of combustion in rocket motor chambers. *Automatica*. 2002; 38(3):487-497.
- [2] Hale JK, Lunel S.M.V. *Introduction to Functional Differential Equations*. New York: Springer; 1993, 458 p.
- [3] Wang Y, Zou X. On a predator-prey system with digestion delay and anti-predation strategy. *Journal of Nonlinear Science*. 2020, 30:1579-605.
- [4] Fridman E. *Introduction to Time-Delay Systems: Analysis and Control*, Cham: Springer Nature; 2014 378 p.
- [5] Li X, Yurkovich S. Sliding mode control of delayed systems with application to engine idle speed control. *IEEE Transactions on Control Systems Technology*. 2001, 9(6):802-10.
- [6] Miller DA, Rossi, M. Simultaneous stabilization with near optimal LQR performance. In: *Proceedings of the 38th Conference on Decision & Control*; 1999 December 07-10; Woenix, Arizona, USA: p. 2300-5.
- [7] Geromel JC, Peres PLD, Souza SR. H_2 guaranteed cost control for uncertain continuous-time linear systems. *Systems & Control Letters*. 1992; 19(1):23-27.
- [8] Khargonekar PP, Petersen IR, Zhou K. Robust stabilization of uncertain systems and H_∞ optimal control. *IEEE Transactions on Automatic Control*. 1990; 35(3): 356-61.
- [9] Xu S, Lam J, Yang C. Quadratic stability and stabilization of uncertain linear discrete-time systems with state delay. *Systems & Control Letters*, 2001; 43(1):77-84.
- [10] Cao SG, Rees NW, Feng G. H_∞ control of uncertain fuzzy continuous-time systems. *Fuzzy Sets and Systems*. 2020; 115:171-90.
- [11] Nikaido H. *Convex Structures and Economic Theory*. New York: Academic Press; 1968, 422 p.
- [12] Smith H.L. *Monotone Dynamical Systems: An Introduction to the Theory of Competitive and Cooperative Systems*. Providence: American Mathematical Society; 1995, 178 p.
- [13] Hmamed A, Ait Rami M, Benzaouia A, F. Tadeo F. Stabilization under constrained states and controls of positive systems with time delays. *European Journal of Control*. 2012; 18(2):182-90.
- [14] Anderson BDO. Positive system realizations. In: *Open Problems in Mathematical Systems and Control Theory*. London: Springer; 1999, p. 7-10.
- [15] Haddad W.M, Chellaboina V. Stability theory for nonnegative and compartmental dynamical systems with time delay. *Systems & Control Letters*. 2004; 51(5):355-61.
- [16] Liu X, Lam J. Relationships between asymptotic stability and exponential stability of positive delay systems. *International Journal of General Systems*. 2013; 42(2):224-38.
- [17] Farina L, Rinaldi S. *Positive Linear Systems: Theory and Applications*. New York: John Wiley & Sons; 2000, 300 p.
- [18] Berman A, Neumann M, Stern R. *Nonnegative Matrices in Dynamic Systems*. New York: John Wiley & Sons, New York; 1989, 167 p.

- [19] Peet MM, Papachristodoulou A, Lall S. Positive forms and stability of linear time-delay system. *SIAM Journal on Control and Optimization*. 2009; 47(6):3237-58.
- [20] Takagi T, Sugeno M. Fuzzy identification of systems and its applications to modeling and control. *IEEE Transactions on Systems, Man, and Cybernetics*. 1985; 15(1):116-32.
- [21] Liu X. Constrained control of positive systems with delays. *IEEE Transactions on Automatic Control*. 2009; 54(7):1596-600.
- [22] Krokavec D, Filasová A. On observer design methods for a class of Takagi-Sugeno fuzzy systems. *Computer Science & Information Technology*. 2014; 4(11):279-90.
- [23] Vanderbei RJ. *Linear Programming: Foundations and Extensions*. Cham: Springer Nature; 2020, 466 p.
- [24] Tanaka K, Wang, HO. *Fuzzy Control Systems Design and Analysis: A Linear Matrix Inequality Approach*. New York: John Wiley & Sons; 2001. 305 p.
- [25] Krokavec D, Filasová A. Optimal fuzzy control for a class of nonlinear systems. *Mathematical Problems in Engineering*. 2012; 2012:1-29.
- [26] Ait Rami M, Helmke U, Tadeo F. Positive observation problem for linear time-delay positive systems. In: *Proceedings of the 15th Mediterranean Conference on Control & Automation MED2007*; 2007 June 27-29; Athens, Greece: p. 1-6.
- [27] Gallier J. *Geometric Methods and Applications: For Computer Science and Engineering*. New York: Springer; 2011, 709 p.
- [28] Ebihara Y. Stability analysis of neutral type time-delay positive systems with commensurate delays. *IFAC PapersOnLine*. 2017; 50(1):3093-98.
- [29] Briat, C. Stability and performance analysis of linear positive systems with delays using input-output methods. *International Journal of Control*. 2018; 91(7):1669-92.
- [30] Mason O. Diagonal Riccati stability and positive time-delay systems. *Systems & Control Letters*. 2012; 61(1):6-10.
- [31] Horn RA, Johnson C.R. *Matrix Analysis*. New York: Cambridge University Press; 1985, 643 p.
- [32] Krokavec D, Filasová A. LMI based principles in strictly Metzlerian systems control design. *Mathematical Problems in Engineering*. 2018; 2018:1-14.
- [33] Krokavec D, Filasová A. Control design for linear strictly Metzlerian descriptor systems. In: *Proceedings of the 18th EUCA European Control Conference ECC2020*; 2020 May 12-15; Saint-Petersburg, Russia: p. 2092-97.
- [34] Amato A, Pironti A, Scala S. Necessary and sufficient conditions for quadratic stability and stabilizability of uncertain linear time-varying systems. *IEEE Transactions on Automatic Control*. 1996; 41(1):125-28.
- [35] Krokavec D, Filasová A. H_∞ norm principle in residual filter design for discrete-time linear positive systems. *European Journal of Control*. 2019; 45:17-29.
- [36] VanAntwerp JG, Braatz RD. A tutorial on linear and bilinear matrix inequalities. *Journal of Process Control*. 2000; 10(4):363-85.
- [37] Peaucelle D, Henrion D, Labit Y, Taitz K. *User's Guide for SeDuMi Interface*. Toulouse: LAAS-CNRS; 2002, 37 p.
- [38] Gahinet PM, Nemirovski A, Laub AJ, Chilali M. *LMI Control Toolbox User's Guide*. Natick: The MathWorks; 1995, 357 p.
- [39] Elloumi W, Benzaouia A, Chaabane M. Delay-dependent stabilization conditions of controlled positive continuous-time systems. *International Journal of Automation and Computing*. 2014; 11(6):653-60.

A Deep Learning Approach to Recognize Human Activity Using Inertial Sensors and Motion Capture Systems

M. Jaén-Vargas ^{a,1}, K. Reyes Leiva ^{a,b}, F. Fernandes ^c,

S.B. Gonçalves ^c, M. Tavares Silva ^c, D.S. Lopes ^{c,d}, J. Serrano Olmedo ^{a,f}

^a*Bioinstrumentation and Nanomedicine Laboratory (LBN), Center for Biomedical Technology (CTB), Universidad Politécnica de Madrid, Madrid, Spain*

^b*Engineering Faculty, Universidad Tecnológica Centroamericana UNITEC, San Pedro Sula, Honduras*

^c*INESC-ID, Lisbon, Portugal*

^d*Instituto Superior Técnico, University of Lisbon, Lisbon, Portugal*

^e*IDMEC, Instituto Superior Técnico, University of Lisbon, Lisbon, Portugal*

^f*Centro de Investigación Biomédica en Red en Bioingeniería, Biomateriales y Nanomedicina, (CIBER-BBN), Madrid, España*

Abstract. Human Activity Recognition (HAR) plays an important role in behavior analysis, video surveillance, gestures recognition, gait analysis, and posture recognition. Given the recent progress of Artificial Intelligence (AI) applied to HAR, the inputs that are the data from wearable sensors can be treated as time-series from which movement events can be classified with high accuracy. In this study, a dataset of raw sensor data served as input to four different deep learning networks (DNN, CNN, LSTM, and CNN-LSTM). Differences in accuracy and learning time were then compared and evaluated for each model. An analysis of HAR was made based on an attempt to classify three activities: walking, sit-to-stand, and squatting. We also compared the performance of two different sensor data types: 3-axis linear acceleration measured from two inertial measurement units (IMUs) versus 3D acceleration of two retro-reflective markers from the high-end optoelectronic motion capture system (MOCAP). The dataset created from observations of ten subjects was preprocessed with labelling and sliding windows and then used as input to the four frameworks. The results indicate that, for HAR prediction, linear accelerations estimated using IMUs are as reliable as those measured using the MOCAP system. Also, the use of the hybrid CNN-LSTM framework for both methods resulted in higher accuracy (99%).

Keywords. human activity recognition; motion capture; inertial measurement unit; artificial intelligence, deep learning.

1. Introduction

Currently, devices that aim to identify human activities play an important role in understanding how people perform their daily activities. The growing applications of Human Activity Recognition (HAR) include behavior analysis, video surveillance,

¹ Corresponding Author: Universidad Politécnica de Madrid, Parque Científico y Tecnológico de la UPM 28223, Pozuelo de Alarcón, Madrid, Spain; E-mail: milagros.jaen@ctb.upm.es

gestures recognition, gait analysis, and posture recognition [1]. Consequently, there are two types of HAR: that based on data extracted from video and that based on motion sensors (e.g., wearable sensors, smartphones, radio frequency (RF) sensors (Wi-Fi, RFID), LED light sensors, cameras [2]. For HAR based on motion sensors, the raw data obtained translates into signal patterns that represent the movement of the sensed area of the body.

The application of AI for HAR has revolutionized the way researchers segment and identify information extracted from wearable motion sensors. Machine Learning techniques first were used to extract features, and later to apply classifiers and obtain predictions (i.e., Support Vector Machines, k-Nearest Neighbor, and Artificial Neural Networks) [3]. However, the use of Deep Learning is recommended for feature extraction due to the power that these networks offer [4]. In Deep Learning, the raw data is managed as *time series sequences*. Hence, sliding windows must be created to organize this raw data [5]. The literature suggests using special networks to work with this type of data: these include Deep Neural Networks (DNN), Convolutional Neural Networks (CNN), and Recurrent Neural Networks (RNN). Lately, a hybrid model has been used that is based on the combination of two deep neural networks: CNN-LSTM (Long Short-Term Memory). This hybrid model allows for the achievement of high recognition scores in image processing and video-based HAR [6].

Overall, by using deep learning frameworks, it is possible to obtain high accuracy predictions and avoid the manual feature extraction process that occurs when applying Machine Learning [7]. In other words, this process overcomes the disadvantages of basic Machine learning algorithms, so that data scientists need not perform feature engineering manually. Given that, this study aimed to evaluate the performance of four deep learning networks (DNN, CNN, LSTM, CNN-LSTM) for HAR and, specifically, their ability to predict three different activities: walking, sit-to-stand, and squatting. The experimental data acquired includes 3D acceleration values from two different systems: a low-cost inertial measurement system composed of two IMUs, and an optoelectronic MOCAP system.

2. Materials and Methods

2.1. Experimental Acquisition:

The performance of the different networks was tested by evaluating the linear acceleration data of three daily movements: walking, sit-to-stand, and squatting. The experimental acquisitions were done in the Lisbon Biomechanics Laboratory at Instituto Superior Técnico using two motion capture systems: a low-cost inertial measurement system based on two MetaMotionR sensors (MBIENTLAB INC, San Francisco, CA., USA) and a high-end optoelectronic system composed of 14 infrared ProReflex 1000 cameras (Qualisys[®], Göteborg, Sweden). The study was approved by the ethics committee of Instituto Superior Técnico in January 2020 (Ref. nr. 1/2020 (CE-IST)). All volunteers expressed their agreement to participate by signing an informed consent after a detailed explanation of the study objectives and experimental protocol.

The inertial measurement acquisition protocol consisted in the use of two wearable sensors placed on the left wrist and left ankle. Simultaneously, a 2D full body protocol, composed of 24 retro-reflective markers placed on anatomical landmarks as suggested by ISB [8] [9], was implemented to acquire the volunteer's motion with the optoelectronic system. Two more markers were placed over the IMUs to directly compare the neural network predictions from the two systems (see Fig. 1). Ten healthy volunteers (M:6, F:4;



Figure 1. Representation of the experimental protocol: a) Ankle sensor; b) Wrist Sensor

Age: 30.0 ± 6.3 years; Height: 1.70 ± 0.11 m.; Weight: 69.7 ± 15.3 kg.) were selected based on the inclusion/exclusion criteria defined in the ethics committee proposal. The acquisitions with the two systems were done simultaneously using a sampling frequency of 100 Hz. The MOCAP data was processed using the Qualisys Tracking Manager software and the IMU data with the MetaBase App. For the gait analysis, volunteers were instructed to walk continuously for 60 seconds; this procedure was repeated three times. For the remaining movements, volunteers performed three series of ten repetitions each. All the trials were performed after a period of adaptation to the laboratory environment.

2.2. Data Preprocessing:

All acquisition files were processed using Python programming language (Google Colab). A unified dataset was created, including all the frames in a file. Next, each activity was labeled, following the labelling technique [10], adding the information corresponding to the activity to which the sample belongs. The raw data was processed using sliding windows [11]. To create sliding windows it was necessary to divide the input signal into segments of a certain time duration. For this study, a window of 100 samples in length was used. Six columns (x_1 , y_1 , z_1 , x_2 , y_2 , z_2) and the final column named label, corresponding to the variable y , contained the three classes of expected activity (walking, sit-to-stand, squatting).”

IMU data consisted of 3D vector accelerations in csv format. As the dataset was obtained using two MBIENTLAB INC sensors, the acquisition control was managed via Low Energy Bluetooth through the MetaBase App and, thus, in some cases the start time for recording the samples differed. The raw data was manually synchronized to adjust for this discrepancy.

Because the MOCAP system does not directly provide acceleration values, the acquired trajectories were processed using in-house routines developed in MATLAB software (MathWorks[®], Natick, USA). The trajectories were smoothed using a 2nd order Butterworth filter with a cutoff frequency of 6 Hz and were posteriorly splined using cubic polynomials. Finally, the linear accelerations were computed as the 2nd order derivative of the spline functions.

2.3. Choosing the artificial intelligence architecture:

Several studies have suggested that time series data should be processed with Deep Learning networks [5,12,13] because these types of networks directly learn the mapping (between the inputs of time-series and class outputs) with the feature engineering technique [14]. First, a DNN architecture was implemented with fully connected layers. Second, CNN was used to treat the data as a times series and build them into 1 dimension temporal convolution (1D-CNN) to capture dependences among input data [13]. This type of architecture is recommended to learn detailed feature representations and patterns from images [15]. Third, a LSTM is the type of RNN that helps in training the model over lengthy sequences and in the retention of the memory from previous time steps of

input fed to the model [16]. Hence, this last architecture is the one most often recommended to treat time series data. However, four networks with different architectures were tested, including a new approach combining CNN and LSTM. The CNN-LSTM is a hybrid model that uses CNN layers for feature extraction on input data combined with LSTMs to support sequence prediction [6]. Thus, the CNN-LSTM model reads subsequences of the main sequence as blocks: CNN extract features from each block, and then allows the LSTM to interpret the features extracted from each block. For this, a TimeDistributed wrapper was used that allows reuse of the CNN model, once per each subsequence. The CNN output serves as input to the LSTM, which provides the final prediction.

Two metrics were chosen to measure the classification performance of each algorithm: accuracy and F1 score. Accuracy is the ratio of the number of correct predictions to the total number of input samples [17]. The F1 score combines two measures defined in terms of the total number of correctly recognized samples, which are known in the information retrieval community as precision and recall. Precision is defined as $\frac{TP}{TP+FP}$, and recall corresponds to $\frac{TP}{TP+FN}$, where TP, FP are the number of true and false positives, respectively, and FN corresponds to the number of false negatives [18]. Class imbalance is countered by weighting classes according to their sample proportion:

$$F1 = \sum_i 2 * w_i \frac{precision_i * recall_i}{precision_i + recall_i}$$

where i is the class index and $w_i = n_i/N$ is the proportion of samples of class i , with n_i being the number of samples of the i -th class and N being the total number of samples.

3. Results

3.1. Deep Learning Networks for IMU and MOCAP:

The IMU-system database contained 304,135 samples and the MOCAP 315,334 samples. To train the algorithm, data from 8 volunteers was used and split in a relation of 80% for training and 20% for testing. Once trained, the algorithm was validated using data from an additional 2 volunteers. Early-stopping was added in the training phase to avoid overfitting.

Although the number of epochs and batch normalization were not the same for each network type, the remaining configuration used the same parameter settings for the two types of data. First, the basic DNN architecture was settled with the following parameters: 4 Dense fully connected layers with a dimension of 32 neurons, each built alongside a flatten layer. This model was trained with 50 epochs using a batch size of 64. The number of network parameters was 11,939. Also, the loss function used was sparse categorical crossentropy, which is commonly used for categorical problems. The activation function was ReLU, and the optimizer function was Adam. Using this configuration, an accuracy of 0.999 was obtained for both acquisition systems (Figure 2, DNN IMU vs. DNN MOCAP). An F1 score of 91.856% was obtained for IMU and 87.198% for MOCAP. Second, a CNN architecture was created using a sequential model of one Convolutional 1D layer with 32 filters, using a kernel of size 3 and ReLU activation. Besides a dropout of 0.5, a Max pooling 1D of size 2 and a flatten layer were used. In the end, a dense 8 units layer with ReLU activation function and another dense layer using the number of classes (in this case 3 classes) using as activation SoftMax were used for obtaining the prediction. This network was trained for 20 epochs using a

batch size of 32. Also, as in DNN, the loss function used was sparse categorical crossentropy. Using this configuration, an accuracy of 0.913 for IMU and 0.989 for MOCAP was obtained in the prediction as shown in Figure 2 (CNN IMU vs CNN MOCAP). F1 score values of 91.352% and 86.303%, respectively, were obtained. Third, an LSTM architecture was created using a sequential model of one LSTM layer with 100

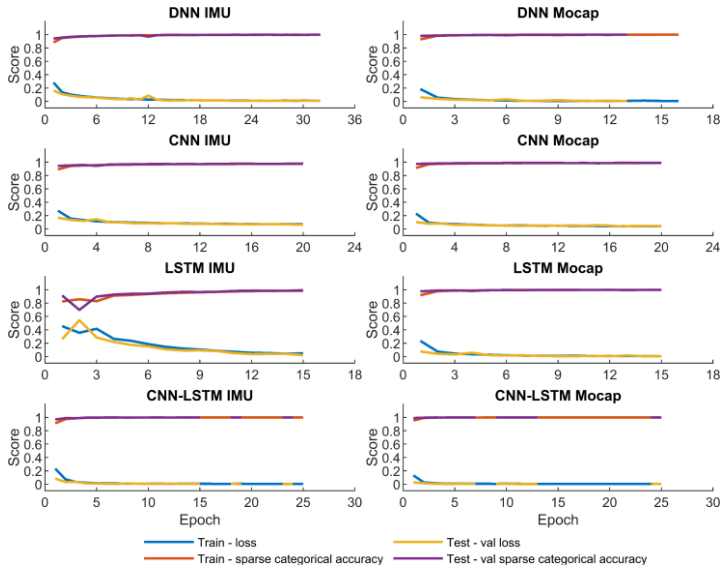


Figure 2. Accuracy and Loss metrics for the four Deep Learning networks of IMU and MOCAP data.

neurons. In addition, it featured a dropout of 0.5 and two dense layers: the first one with 100 and activation function ReLU, and the last one with the number of classes and a SoftMax activation function. The number of network parameters was higher, totaling 53,203. This network was trained for 15 epochs, using a batch size of 64. Also, as in the DNN and CNN architecture, the loss function used was sparse categorical crossentropy. Using this configuration resulted in a prediction accuracy of 0.993 (Figure 2: LSTM IMU vs LSTM MOCAP), and F1 scores of 91.856% and 86.303%, respectively.

Finally, when creating the CNN-LSTM network, we highlight the necessity of treating the data, which is in windows of 100-time steps, into subsequences using 4 steps and length 25 to feed a sequential model followed by a 1D CNN wrapped into two Time Distributed layers. Also, as in the 3 models mentioned above, the loss function used was sparse categorical crossentropy. This configuration resulted in prediction accuracies of 0.993 and 0.993 (Figure 2: CNN-LSTM IMU vs CNN-LSTM MOCAP) and F1 scores of 99.97% and 88.63%, respectively.

4. Discussion

Although the first three classification networks returned acceptable accuracies (between 91 and 99%), the F1 score, due to its robustness in the face of class imbalance, is the sole parameter that proves that a network is able to classify well, [19].

According to the accuracy metric, all values, except for CNN, are around 99% (Table 1). This is most likely due to the early-stopping settings, although it is expected

that the accuracy percentage would also reach 99% if it were allowed to train for more epochs.

Table 1. Accuracy and F1 Score results

Performance Measurements Parameters	Acquisition System	DNN	CNN	LSTM	CNN-LSTM
Accuracy	IMU	0.999	0.913	0.993	0.999
	MOCAP	0.999	0.989	0.999	0.999
F1 Score	IMU	91.856	91.352	91.856	99.97
	MOCAP	87.198	86.303	87.830	88.629

The *F1 score* metric for IMU performance surpasses 90% for all four networks; however, for MOCAP all networks (DNN, CNN, LSTM, CNN-LSTM) do not perform as expected because the samples were not sufficiently balanced (Table 1). For example, there were fewer walking frames than sitting and squatting frames. Prediction was most powerful with the last network (CNN-LSTM) for both systems, achieving a 99.97% prediction score for IMU and 88.63% for MOCAP.

Comparing our results to the literature, Deep & Zheng [20] used a UCI_HAR dataset implementing 4 different LSTM and the hybrid framework CNN-LSTM. Their CNN-LSTM model achieved the highest accuracy value with respect to the resting frameworks (93.40%); in contrast, we achieved 99% accuracy for all 4 networks tested. On the other hand, due to the imbalanced condition of our dataset, the calculated F1 score proves that the CNN-LSTM model is the best at recognition: hybrid models present higher scores [21]. Overall, using low-cost inertial sensor data with a complex Deep Learning hybrid model (CNN-LSTM) results in a good accuracy that is equal in reliability to a higher-cost and more complex MOCAP data system more specialized in motion capture.

5. Conclusion

Using Deep Learning methods, it was possible to recognize human activities such as walking, sit-to-stand, and squatting using only two IMUs and two markers located in the same place on the human body. This was accomplished by using Deep Learning Networks and processing the raw data as time series through sliding windows to extract relevant features from the segmented sequences. Accurate results were achieved with sensor data from IMUs, and the results validated with high quality MOCAP data. Using deep learning networks (DNN, CNN, LSTM), accuracies of above 91% was achieved. It was proven that, using the hybrid CNN-LSTM model, predictions can be achieved with the same accuracy (99%) as with the MOCAP system. Further research on the implementation of automatic labelling of human activities is required.

Acknowledgements

We acknowledge the support provided by the BeHealSy Program of EIT Health that promoted the collaboration between the Universidad Politécnica de Madrid and the University of Lisbon. Additionally, this work was supported by Fundação para a Ciência e a Tecnologia (FCT) with references UIDB/50021/2020 (INESC-ID) and UIDB/50022/2020 (Lisbon Biomechanics Laboratory and IDMEC under LAETA). Also, the first author thanks the IFARHU-SENACYT Panama program for supporting her PhD

scholarship and the second author acknowledges scholarship support from the Fundación Carolina FC and the Universidad Tecnológica Centroamericana UNITEC.

References

- [1] Wang J, Chen Y, Hao S, Peng X, Hu L. Deep learning for sensor-based activity recognition: A survey. *Pattern Recognit Lett* [Internet]. 2019;119:que bue:3–11. Available from: <https://doi.org/10.1016/j.patrec.2018.02.010>
- [2] Wan S, Qi L, Xu X, Tong C, Gu Z. Deep Learning Models for Real-time Human Activity Recognition with Smartphones. *Mob Networks Appl*. 2020;25(2):743–55.
- [3] Kale H, Mandke P, Mahajan H, Deshpande V. Human Posture Recognition using Artificial Neural Networks. *Proc 8th Int Adv Comput Conf IACC 2018*. 2018;272–8.
- [4] Wu Q, Wang F. Concatenate convolutional neural networks for non-intrusive load monitoring across complex background. *Energies*. 2019;12(8).
- [5] Ortiz Laguna J, Olaya AG, Borrajo D. A dynamic sliding window approach for activity recognition. *Lect Notes Comput Sci (including Subser Lect Notes Artif Intell Lect Notes Bioinformatics)*. 2011;6787 LNCS:219–30.
- [6] Yao S, Hu S, Zhao Y, Zhang A, Abdelzaher T. DeepSense: A unified deep learning framework for time-series mobile sensing data processing. *26th Int World Wide Web Conf WWW 2017*. 2017;351–60.
- [7] Brownlee J. *Deep Learning for Time Series Forecasting*. Machine Learning Mastery. 2018.
- [8] Wu G, Siegler S, Allard P, Kirtley C, Leardini A, Rosenbaum D, Whittle M, D’Lima DD, Cristofolini L, Witte H, Schmid O, Stokes I. ISB recommendation on definitions of joint coordinate system of various joints for the reporting of human joint motion—part I: ankle, hip, and spine. *J Biomech* [Internet]. 2002;35(4):543–8. Available from: <https://www.sciencedirect.com/science/article/pii/S0021929001002226>
- [9] Wu G, van der Helm FCT, (DirkJan) Veeger HEJ, Makhsous M, Van Roy P, Anglin C, Nagels J, Karduna AR, McQuade K, Wang X, Werner FW, Buchholz B. ISB recommendation on definitions of joint coordinate systems of various joints for the reporting of human joint motion—Part II: shoulder, elbow, wrist and hand. *J Biomech* [Internet]. 2005;38(5):981–92. Available from: <https://www.sciencedirect.com/science/article/pii/S002192900400301X>
- [10] Woodward K, Kanjo E, Oikonomou A, Chamberlain A. LabelSens: enabling real-time sensor data labelling at the point of collection using an artificial intelligence-based approach. *Pers Ubiquitous Comput*. 2020;24(5):709–22.
- [11] Niemann F, Reining C, Rueda FM, Nair NR, Steffens JA, Fink GA, Hoppel M Ten. Lara: Creating a dataset for human activity recognition in logistics using semantic attributes. *Sensors (Switzerland)*. 2020;20(15):1–42.
- [12] Xu C, Chai D, He J, Zhang X, Duan S. InnoHAR: A deep neural network for complex human activity recognition. *IEEE Access*. 2019;7:9893–902.
- [13] Murad A, Pyun JY. Deep recurrent neural networks for human activity recognition. *Sensors (Switzerland)*. 2017;17(11).
- [14] Chao-Lung Yang Z-XC and C-YY. Sensor Classification Using Convolutional Neural Network by Encoding Multivariate Time Series as Two-Dimensional Colored Images. *Sensors (Switzerland)*. 2019;(1).
- [15] Gollapudi S, Gollapudi S. Deep Learning for Computer Vision. In: *Learn Computer Vision Using OpenCV*. 2019. p. 51–69.
- [16] Goyal P, Pandey S, Jain K. Deep learning for natural language processing: Creating neural networks with Python [Internet]. 2018. 290 p. Available from: <https://proquest-safaribooksonline-com.cyber.usask.ca/9781484236857>
- [17] Mishra A. Metrics to evaluate your machine learnign algorithm [Internet]. 2018. Available from: <https://towardsdatascience.com/metrics-to-evaluate-your-machine-learning-algorithm-f10ba6e38234>
- [18] Ordóñez FJ, Roggen D. Deep convolutional and LSTM recurrent neural networks for multimodal wearable activity recognition. *Sensors (Switzerland)*. 2016;16(1).
- [19] Dehghani A, Sarbishei O, Glatard T, Shihab E. A quantitative comparison of overlapping and non-overlapping sliding windows for human activity recognition using inertial sensors. *Sensors (Switzerland)*. 2019;19(22):10–2.
- [20] Deep S, Zheng X. Hybrid Model Featuring CNN and LSTM Architecture for Human Activity Recognition on Smartphone Sensor Data. *Proc - 2019 20th Int Conf Parallel Distrib Comput Appl Technol PDCAT 2019*. 2019;259–64.
- [21] Abbaspour S, Fotouhi F, Sedaghatbaf A, Fotouhi H, Vahabi M, Linden M. A comparative analysis of hybrid deep learning models for human activity recognition. *Sensors (Switzerland)*. 2020;20(19):1–14.

Tracking Control Design for Positive T-S Fuzzy Systems Under H_∞ Performance

Lining FU ^a, Fucai LIU ^a, Aiwen MENG ^{a,1}, H.K. LAM ^b and Jilong XU ^a

^a*Institute of Electrical Engineering, Yanshan University, Qinghuangdao, Hebei, China*

^b*Department of Informatics, King's College London, London, WC2R 2LS, UK*

Abstract. This paper is dedicated to study the tracking control problem of the positive T-S Fuzzy systems under H_∞ performance. Compared with general systems, the limitation of the positive systems will bring non-convex conditions into the stability analysis. In order to overcome the challenge brought by the transformation of non-convex conditions into convex conditions, a feasible solution is presented. In addition, by using the piecewise-linear membership functions (PLMFs) technology, more effective information of membership functions (MFs) is introduced, which effectively weakens the conservativeness of the stability conditions and achieves satisfactory tracking results. Ultimately, a simulation example is shown to confirm the reliability of the design method.

Keywords. Positive T-S Fuzzy Systems, H_∞ Performance, Tracking Control, PLMFs

1. Introduction

Positive systems are ubiquitous in the real world, such as social demographic, network communication systems, etc [1]. These systems have the inherent property that their state variables are always positive under non-negative initial conditions [2]. Due to the limitation of the positivity, when positive conditions and stability conditions exist at the same time, the generation of non-convex conditions is inevitable [3], which will make the analysis of positive nonlinear systems more complicated and scarce. Therefore, the study of positive nonlinear systems has both practical value and challenges in theory.

Among all the nonlinear control strategies, the T-S fuzzy-model-based (TSFMB) control has attracted the attention of more and more scholars [4]-[6]. Therefore, this paper naturally uses the TSFMB to analyze the tracking control issue of positive systems. Although the application of tracking control can be seen everywhere [7]-[9], such as missile trajectory control [10] and aircraft attitude tracking [11], the existing literature on tracking control of positive systems is quite lacking. Thus, starting from the actual needs, the research on tracking control of positive systems have aroused our attention. In the existing literature, due to the insufficient introduction of the original membership function (MFs) information, the results achieved are extremely conservative. In this paper, more effective information of MFs is brought into the analysis condition, which is

¹Corresponding Author: Meng Aiwen, The Key Laboratory of Industrial Computer Control Engineering of Hebei Province, Yanshan University, Qinghuangdao, Hebei 066004, China; E-mail: 1309494495@qq.com.

helpful to realize a satisfactory tracking effect. In summary, the research motivation of the tracking control of the positive system is mature.

In order to distinguish from the previous work, the main contribution of this paper is to successfully extend the research of tracking control from general systems to positive systems that are rarely discussed. Correspondingly, for dealing with the non-convex problem generated by positive systems, this paper presents an effective approach so that feasible solutions can be found. In addition, for the purpose of achieving better tracking effect, this paper uses PLMFs technology to introduce more effective MFs information into the analysis conditions.

The following notations will refer to the full paper. $\delta_{r,s}$ represents the r -th row and s -th column of the matrix $\Delta \in \mathfrak{R}^{n \times m}$. $\Delta \prec 0$, $\Delta \succ 0$, $\Delta \preceq 0$ and $\Delta \succeq 0$ represent that each element $\delta_{r,s}$ is negative, positive, non-positive and non-negative, respectively. The Metzler matrix means that its off diagonal elements are all non-negative. \check{d} represents $\check{d} = \{1, 2, \dots, d\}$.

2. Preliminaries

2.1. Positive T-S Fuzzy Model

The dynamic behavior of nonlinear plants is described by using p rules, where the i -th rule is as follows:

$$\begin{aligned} \text{Rule } i, i \in \check{p} : & \text{ IF } \varphi_1(\mathbf{x}(t)) \text{ is } M_1^i \text{ AND } \dots \text{ AND } \varphi_\psi(\mathbf{x}(t)) \text{ is } M_\psi^i \\ \text{ THEN } & \dot{\mathbf{x}}(t) = \mathbf{A}_i \mathbf{x}(t) + \mathbf{B}_i \mathbf{u}(t), \mathbf{x}(t) = \boldsymbol{\phi}(t), \end{aligned} \tag{1}$$

where M_l^i is the fuzzy set, $\varphi_l(\mathbf{x}(t))$ is the premise variable, $l \in \check{\psi}$, $\boldsymbol{\phi}(t)$ is the vector valued initial function. \mathbf{A}_i and \mathbf{B}_i are the system matrices with matching dimensions.

The whole system dynamics is shown as follows:

$$\dot{\mathbf{x}}(t) = \sum_{i=1}^p w_i(\mathbf{x}(t)) (\mathbf{A}_i \mathbf{x}(t) + \mathbf{B}_i \mathbf{u}(t)), \tag{2}$$

where $w_i(\mathbf{x}(t)) = \prod_{l=1}^\psi \mu_{M_l^i}(\varphi_l(\mathbf{x}(t))) / \sum_{k=1}^p \prod_{l=1}^\psi \mu_{M_l^k}(\varphi_l(\mathbf{x}(t)))$. $w_i(\mathbf{x}(t)) \in [0 \ 1]$ and $\sum_{i=1}^p w_i(\mathbf{x}(t)) = 1, \forall i$.

Definition 1 [12]: If the condition $\boldsymbol{\phi}(\cdot) \succcurlyeq 0$ satisfy corresponding $\mathbf{x}(t) \succcurlyeq 0, \forall t \geq 0$, then the system is regarded as a positive system.

Lemma 1 [13]: System (2) is positive if it satisfies the following: \mathbf{A}_i is a Metzler matrix and $\mathbf{B}_i \succeq 0, \forall i$ when $\mathbf{u}(t) \succeq 0$.

2.2. Positive Stable Reference Model

The stable positive reference model is given:

$$\dot{\mathbf{x}}_r(t) = \mathbf{A}_r \mathbf{x}_r(t) + \mathbf{B}_r \mathbf{r}(t), \tag{3}$$

where $\mathbf{A}_r \in \mathfrak{R}^{n \times n}$, $\mathbf{B}_r \in \mathfrak{R}^{n \times m}$, $\mathbf{r}(t) \in \mathfrak{R}^{m \times 1}$ and $\mathbf{x}_r(t) \in \mathfrak{R}^{n \times 1}$. It is worth emphasizing that the reference model should be guaranteed to be stable.

2.3. Fuzzy Controller Design

By using c rules to describe the T-S fuzzy controller, where the j -th rule is:

$$\begin{aligned} &\text{Rule } j, j \in \check{c}: \text{IF } \vartheta_1(\mathbf{x}(t)) \text{ is } N_1^j \text{ AND} \cdots \text{AND } \vartheta_\Omega(\mathbf{x}(t)) \text{ is } N_\Omega^j \\ &\text{THEN } \mathbf{u}(t) = \mathbf{F}_j \mathbf{e}(t) + \mathbf{G}_j \mathbf{x}_r(t), \end{aligned} \quad (4)$$

where $\vartheta_d(\mathbf{x}(t))$ is the premise variable, N_d^j is the fuzzy set, $\mathbf{e}(t) = \mathbf{x}(t) - \mathbf{x}_r(t)$. $\mathbf{F}_j \in \mathfrak{R}^{m \times n}$ and $\mathbf{G}_j \in \mathfrak{R}^{m \times n}$ are the feedback gains, $d \in \check{\Omega}$.

The overall T-S fuzzy controller is displayed as follows:

$$\mathbf{u}(t) = \sum_{j=1}^c m_j(\mathbf{x}(t)) (\mathbf{F}_j \mathbf{e}(t) + \mathbf{G}_j \mathbf{x}_r(t)), \quad (5)$$

where $m_j(\mathbf{x}(t)) = \prod_{d=1}^{\check{\Omega}} \mu_{N_d^j}(\vartheta_d(\mathbf{x}(t))) / \sum_{k=1}^c \prod_{d=1}^{\check{\Omega}} \mu_{N_d^k}(\vartheta_d(\mathbf{x}(t)))$. $m_j(\mathbf{x}(t)) \in [0 \ 1]$, $\sum_{j=1}^c m_j(\mathbf{x}(t)) = 1, \forall j$, and $m_j(\mathbf{x}(t))$ is the normalized grade of membership. In the following analysis, if there is no confusion, the time t in each variable will be omitted.

3. Positivity and Stability Analysis

Combining (2) and (5), the closed-loop system is given:

$$\dot{\mathbf{x}} = \sum_{i=1}^p \sum_{j=1}^c w_i m_j \left((\mathbf{A}_i + \mathbf{B}_i \mathbf{F}_j) \mathbf{x} + \mathbf{B}_i (\mathbf{G}_j - \mathbf{F}_j) \mathbf{x}_r \right). \quad (6)$$

In order to study the stability of the error system, $\dot{\mathbf{e}}$ can be obtained:

$$\dot{\mathbf{e}} = \dot{\mathbf{x}} - \dot{\mathbf{x}}_r = \sum_{i=1}^p \sum_{j=1}^c w_i m_j (\mathbf{A}_i + \mathbf{B}_i \mathbf{F}_j) \mathbf{e} + \sum_{i=1}^p \sum_{j=1}^c w_i m_j (\mathbf{A}_i - \mathbf{A}_r + \mathbf{B}_i \mathbf{G}_j) \mathbf{x}_r - \mathbf{B}_r \mathbf{r}. \quad (7)$$

Since positive conditions and stability conditions are met at the same time, non-convex conditions will arise. Thus, for coping with this problem, a diagonally positive definite matrix $\mathbf{X} \in \mathfrak{R}^{n \times n}$ is defined. Defining $\mathbf{F}_j \mathbf{X} = \mathbf{M}_j$ and $\mathbf{G}_j \mathbf{X} = \mathbf{N}_j$, according to Lemma 1, post-multiplying both sides of all positive conditions by \mathbf{X} at the same time, then the positive conditions can be obtained, i.e., $(\mathbf{A}_i + \mathbf{B}_i \mathbf{F}_j) \mathbf{X} = \mathbf{A}_i \mathbf{X} + \mathbf{B}_i \mathbf{M}_j$ is Metzler matrix and $(\mathbf{B}_i (\mathbf{G}_j - \mathbf{F}_j)) \mathbf{X} = \mathbf{B}_i (\mathbf{N}_j - \mathbf{M}_j) \succeq 0, \forall i, j$.

For further dealing with the non-convex stability conditions, based on the previous definition, (7) will be analyzed as:

$$\begin{aligned} \dot{\mathbf{e}} &= \sum_{i=1}^p \sum_{j=1}^c w_i m_j (\mathbf{A}_i \mathbf{X} + \mathbf{B}_i \mathbf{M}_j) \mathbf{X}^{-1} \mathbf{e} + \sum_{i=1}^p \sum_{j=1}^c w_i m_j (\mathbf{A}_i \mathbf{X} - \mathbf{A}_r \mathbf{X} + \mathbf{B}_i \mathbf{N}_j) \mathbf{X}^{-1} \mathbf{x}_r \\ &\quad - \mathbf{B}_r \mathbf{r} = \sum_{i=1}^p \sum_{j=1}^c w_i m_j \Psi_{ij} \mathbf{Z}, \end{aligned} \quad (8)$$

where $\Psi_{ij} = [\Psi_{ij}^{(1)} \ \Psi_{ij}^{(2)} \ \Psi_{ij}^{(3)}]$, $\Psi_{ij}^{(1)} = \mathbf{A}_i \mathbf{X} + \mathbf{B}_i \mathbf{M}_j$, $\Psi_{ij}^{(2)} = \mathbf{A}_i \mathbf{X} - \mathbf{A}_r \mathbf{X} + \mathbf{B}_i \mathbf{N}_j$, $\Psi_{ij}^{(3)} = -\mathbf{B}_r$ and $\mathbf{Z}^T = [\mathbf{Z}_1^T \ \mathbf{Z}_2^T \ \mathbf{Z}_3^T]$, $\mathbf{Z}_1 = \mathbf{X}^{-1} \mathbf{e}$, $\mathbf{Z}_2 = \mathbf{X}^{-1} \mathbf{x}_r$, $\mathbf{Z}_3 = \mathbf{r}$.

The following Lyapunov function candidate were selected for stability analysis:

$$V(t) = \mathbf{e}^T(t) \mathbf{X}^{-1} \mathbf{e}(t). \tag{9}$$

For facilitating the stability analysis, we define $\mathbf{e}_1 = [\mathbf{I}_n \ \mathbf{0} \ \mathbf{0}]$, $\mathbf{e}_2 = [\mathbf{0} \ \mathbf{I}_n \ \mathbf{0}]$ and $\mathbf{e}_3 = [\mathbf{0} \ \mathbf{0} \ \mathbf{I}_m]$. At the same time, $\dot{V}(t)$ is derived as:

$$\dot{V}(t) = \sum_{i=1}^p \sum_{j=1}^c w_i m_j \mathbf{Z}^T (\Psi_{ij}^T \mathbf{e}_1 + \mathbf{e}_1^T \Psi_{ij}) \mathbf{Z} = \sum_{i=1}^p \sum_{j=1}^c w_i m_j \mathbf{Z}^T \mathbf{\Xi}_{ij} \mathbf{Z}. \tag{10}$$

For checking the tracking effect, the H_∞ performance is utilized. Meanwhile, the variable Θ will be defined: $\Theta = \dot{V} + \mathbf{Z}_1^T \mathbf{Z}_1 - \rho_1 \mathbf{Z}_2^T \mathbf{Z}_2 - \rho_2 \mathbf{Z}_3^T \mathbf{Z}_3$, where $\rho_1 > 0$ and $\rho_2 > 0$.

Considering $\Theta < 0$, then $\dot{V}(t) \leq -\mathbf{Z}_1^T \mathbf{Z}_1 + \rho_1 \mathbf{Z}_2^T \mathbf{Z}_2 + \rho_2 \mathbf{Z}_3^T \mathbf{Z}_3$. Set t_f as the terminal time, thus, the H_∞ performance [14] is given:

$$\frac{\int_0^{t_f} \mathbf{Z}_1^T \mathbf{Z}_1 dt - V(0)}{\int_0^{t_f} (\rho_1 \mathbf{Z}_2^T \mathbf{Z}_2 + \rho_2 \mathbf{Z}_3^T \mathbf{Z}_3) dt} \leq 1. \tag{11}$$

Remark 1 : In order to meet the H_∞ performance, inequality $\Theta < 0$ must be guaranteed.

where $\Theta = \sum_{i=1}^p \sum_{j=1}^c w_i m_j \mathbf{Z}^T \mathbf{\Lambda}_{ij} \mathbf{Z}$,

$$\mathbf{\Lambda}_{ij} = \mathbf{\Xi}_{ij} + \mathbf{e}_1^T \mathbf{e}_1 - \rho_1 \mathbf{e}_2^T \mathbf{e}_2 - \rho_2 \mathbf{e}_3^T \mathbf{e}_3. \tag{12}$$

4. Relaxed Positivity and Stability Analysis by PLMFs

To relax the analysis conditions, PLMFs, explained in detail in [15], will be used as a method to extract more effective information of MFs. This includes digging the boundary information of $w_i(\mathbf{x})$, $m_j(\mathbf{x})$ and $\Delta h_{ij}(\mathbf{x})$ respectively, so that the conservativeness of the results can be weakened.

$$\underline{\gamma}_{ij} \leq \Delta h_{ij}(\mathbf{x}) \leq \bar{\gamma}_{ij}, 0 \leq \underline{\sigma}_i \leq w_i(\mathbf{x}) \leq \bar{\sigma}_i \leq 1, 0 \leq \underline{\tau}_j \leq m_j(\mathbf{x}) \leq \bar{\tau}_j \leq 1, \forall i, j, \tag{13}$$

where $h_{ij}(\mathbf{x}) = w_i(\mathbf{x})m_j(\mathbf{x})$, $\tilde{h}_{ij}(\mathbf{x})$ and $\Delta h_{ij}(\mathbf{x}) = h_{ij}(\mathbf{x}) - \tilde{h}_{ij}(\mathbf{x})$ are the approximation function and the error function, respectively. $\underline{\gamma}_{ij}$, $\bar{\gamma}_{ij}$, $\underline{\sigma}_i$, $\bar{\sigma}_i$, $\underline{\tau}_j$ and $\bar{\tau}_j$ respectively represent the lower and upper boundaries of the corresponding functions.

To relax the research conditions, the above-mentioned boundary information of MFs is introduced through the following slack matrices $0 < \mathbf{P}_{ij} = \mathbf{P}_{ij}^T$, $0 < \mathbf{Q}_{ij} = \mathbf{Q}_{ij}^T$ and $0 < \mathbf{R}_{ij} = \mathbf{R}_{ij}^T$, $\mathbf{R}_{ij} \geq (\mathbf{\Lambda}_{ij} - \mathbf{P}_{ij} + \mathbf{Q}_{ij})$. Thus, Θ can be dealt with as:

$$\begin{aligned} \Theta &= \sum_{i=1}^p \sum_{j=1}^c w_i m_j \mathbf{Z}^T \mathbf{\Lambda}_{ij} \mathbf{Z} \leq \sum_{i=1}^p \sum_{j=1}^c \mathbf{Z}^T \left((\tilde{h}_{ij}(\mathbf{x}) + \underline{\gamma}_{ij}) (\mathbf{\Lambda}_{ij} - \mathbf{P}_{ij} + \mathbf{Q}_{ij}) \right. \\ &\quad \left. + (\bar{\gamma}_{ij} - \underline{\gamma}_{ij}) \mathbf{R}_{ij} + \bar{\sigma}_i \bar{\tau}_j \mathbf{P}_{ij} - \underline{\sigma}_i \underline{\tau}_j \mathbf{Q}_{ij} \right) \mathbf{Z}. \end{aligned} \tag{14}$$

It can be seen from (14) that inequality $\Theta < 0$ can be satisfied if $\sum_{i=1}^p \sum_{j=1}^c \left((\tilde{h}_{ij}(\mathbf{x}) + \underline{\gamma}_{ij}) (\mathbf{A}_{ij} - \mathbf{P}_{ij} + \mathbf{Q}_{ij}) + (\bar{\gamma}_{ij} - \underline{\gamma}_{ij}) \mathbf{R}_{ij} + \bar{\sigma}_i \bar{\tau}_j \mathbf{P}_{ij} - \underline{\sigma}_i \underline{\tau}_j \mathbf{Q}_{ij} \right) < 0$ holds. In a word, the tracking control analysis results of the positive T-S fuzzy systems are given by the following theorem.

Theorem 1 *Through scalars $\rho_1 > 0$, $\rho_2 > 0$, the tracking control of the positive T-S fuzzy system is guaranteed under satisfying the H_∞ performance (11), if there is a diagonal positive definite matrix $\mathbf{X} \in \mathfrak{R}^{n \times n}$, the feedback gains $\mathbf{M}_j \in \mathfrak{R}^{m \times n}$, $\mathbf{N}_j \in \mathfrak{R}^{m \times n}$, $j \in \check{c}$, symmetric matrices of matching dimensions $\mathbf{P}_{ij} = \mathbf{P}_{ij}^T$, $\mathbf{Q}_{ij} = \mathbf{Q}_{ij}^T$ and $\mathbf{R}_{ij} = \mathbf{R}_{ij}^T$ such that the GEVP has the feasible solution:*

Minimize $\rho_1 + \rho_2$

Subject to

- 1) $\rho_1 > 0$, $\rho_2 > 0$; 2) $\xi^T (\mathbf{X} - \varepsilon_1 \mathbf{I}) \xi$ is SOS;
- 3) $a_{irs} \mathbf{X} + b_{ir} \mathbf{M}_j$ is SOS; $\forall r \neq s$; 4) $\xi^T (\mathbf{b}_{ir} (\mathbf{N}_j - \mathbf{M}_j) - \varepsilon_2 \mathbf{I}) \xi$ is SOS;
- 5) $\xi^T (\mathbf{P}_{ij} - \varepsilon_3 \mathbf{I}) \xi$ is SOS; 6) $\xi^T (\mathbf{Q}_{ij} - \varepsilon_3 \mathbf{I}) \xi$ is SOS; 7) $\xi^T (\mathbf{R}_{ij} - \varepsilon_3 \mathbf{I}) \xi$ is SOS;
- 8) $\xi^T (\mathbf{R}_{ij} \geq (\mathbf{A}_{ij} - \mathbf{P}_{ij} + \mathbf{Q}_{ij}) - \varepsilon_3 \mathbf{I}) \xi$ is SOS; 9) $-\xi^T \left(\sum_{i=1}^p \sum_{j=1}^c \left((\tilde{h}_{ij}(\mathbf{x}) + \underline{\gamma}_{ij}) (\mathbf{A}_{ij} - \mathbf{P}_{ij} + \mathbf{Q}_{ij}) + (\bar{\gamma}_{ij} - \underline{\gamma}_{ij}) \mathbf{R}_{ij} + \bar{\sigma}_i \bar{\tau}_j \mathbf{P}_{ij} - \underline{\sigma}_i \underline{\tau}_j \mathbf{Q}_{ij} \right) + \varepsilon_4 \mathbf{I} \right) \xi$ is SOS, $\forall i, j$, (15)

where the controller gains can be obtained by $\mathbf{F}_j = \mathbf{M}_j \mathbf{X}^{-1}$, $\mathbf{G}_j = \mathbf{N}_j \mathbf{X}^{-1}$.

Remark 2 : When only sub-conditions 1) to 4) in Theorem 1 and $\mathbf{A}_{ij} < 0$ in (12) are satisfied, the situation where PLMFs are not used will be obtained, that is, the information of MFs is not applied to the analysis conditions.

5. Simulation Example

A simulation example is presented to confirm the reliability of the controller design. Under $\mathbf{x} = [x_1 \quad x_2]^T$, three-rule positive T-S fuzzy model is shown as follows:

$$\mathbf{A}_1 = \begin{bmatrix} 1.18 & 0.46 \\ 6.72 & -13.63 \end{bmatrix}, \mathbf{A}_2 = \begin{bmatrix} 0.85 & 1.25 \\ 4.59 & -12.6 \end{bmatrix}, \mathbf{A}_3 = \begin{bmatrix} 0.69 & 0.35 \\ 7.21 & -8.86 \end{bmatrix},$$

$$\mathbf{B}_1 = \begin{bmatrix} 3.63 \\ 0.05 \end{bmatrix}, \mathbf{B}_2 = \begin{bmatrix} 1.42 \\ 0.12 \end{bmatrix}, \mathbf{B}_3 = \begin{bmatrix} 2.85 \\ 0.86 \end{bmatrix}.$$

The positive reference model is set to:

$$\mathbf{A}_r = \begin{bmatrix} -3.5 & 1.06 \\ 6.35 & -12.5 \end{bmatrix}, \quad \mathbf{B}_r = \begin{bmatrix} 1.26 \\ 0.31 \end{bmatrix}, \quad \mathbf{r}(t) = 1 + 0.5 \sin(0.2t).$$

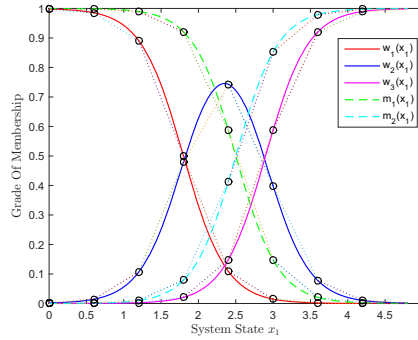


Figure 1. Positive fuzzy model: $w_1(x_1)$, $w_2(x_1)$, $w_3(x_1)$. Fuzzy controller: $m_1(x_1)$, $m_2(x_1)$. The sampling points are set to $x_1(t) = \{0; 0.6; \dots; 4.8\}$.

The MFs of the positive fuzzy model and the controller are respectively set as: $w_1(x_1) = 1 - \frac{1}{1+e^{-3.5(x_1-1.8)}}$, $w_2(x_1) = 1 - w_1(x_1) - w_3(x_1)$, $w_3(x_1) = \frac{1}{1+e^{-3.5(x_1-2.9)}}$, and $m_1(x_1) = 1 - \frac{1}{1+e^{-3.5(x_1-2.5)}}$, $m_2(x_1) = 1 - m_1(x_1)$, which are shown in Figure 1. Set the initial condition to $\mathbf{x}(0) = [0.3 \ 0.5]$ and $\mathbf{x}_r(0) = [0.3 \ 0]$, by using the designed controller, the state-time simulation results obtained under Remark 2 and Theorem 1 are presented in Figure 2 and Figure 3, respectively, which proves that the tracking effect is satisfactory.

By comparing Figure 2 and Figure 3, it can be concluded that the tracking effect of Figure 3 is significantly better, which proves the importance of MFs information introduced by the PLMFs method. It is worth mentioning that the more segments in the PLMFs method, the smaller the approximation error obtained, and the better the tracking effect obtained.

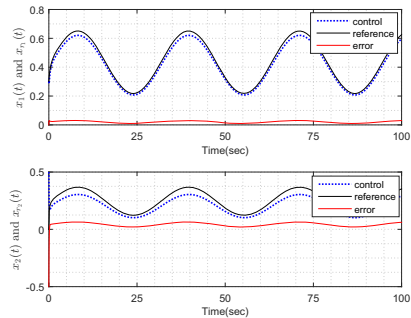
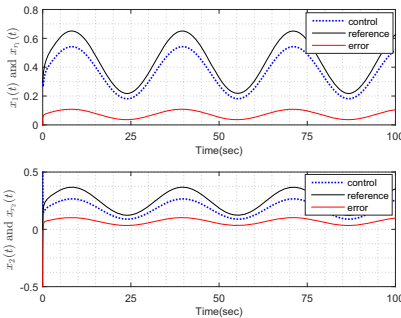


Figure 2. Tracking effect and tracking error **Figure 3.** Tracking effect and tracking error with $\rho_1 = 0.3111$ and $\rho_2 = 0.2086$. Top panel: with $\rho_1 = 0.4248$ and $\rho_2 = 0.1855$. Top panel: $e_{1max} = 0.1087$, $RMSE1 = 0.0778$. Bottom panel: $e_{1max} = 0.0305$, $RMSE1 = 0.0220$. Bottom panel: $e_{2max} = 0.1021$, $RMSE2 = 0.0860$. $e_{2max} = 0.0640$, $RMSE2 = 0.0647$.

6. Conclusion

This paper is dedicated to the design of the tracking control of the positive T-S fuzzy system. To suppress tracking errors, a method of combining the MFs information with the H_∞ performance is adopted. In addition, the non-convex problem due to the constraints of the positive system has been overcome. On the other hand, in order to weaken the conservativeness of the analysis results brought by the lack of MFs, the PLMFs method has been considered to introduce more effective information of MFs into the stability analysis. A simulation example has verified the reliability of the control strategy.

This work was supported by Natural Science Foundation of Hebei Province under Project Number F2019203505 and Kings College London.

References

- [1] Y. Ebihara, D. Peaucelle and D. Arzelier, "Analysis and Synthesis of Interconnected Positive Systems," in IEEE Transactions on Automatic Control, vol. 62, no. 2, pp. 652-667, Feb. 2017, doi: 10.1109/TAC.2016.2558287.
- [2] Forni F, Sepulchre R. Differentially positive systems[J]. Automatic Control IEEE Transactions on, 2014, 61(2):346-359.
- [3] L. Fu, H.K.Lam, F.Liu, B.Xiao and Z.Zhong, "Static Output-Feedback Tracking Control For Positive Polynomial Fuzzy Systems," in IEEE Transactions on Fuzzy Systems, doi: 10.1109/TFUZZ.2021.3065521.
- [4] Kang M. Structure identification of fuzzy model[J]. Fuzzy Sets and Systems, 1988.
- [5] Ghorbal H , Hajjaji A E , Souissi M , et al. Robust Tracking Control for Takagi-Sugeno Systems With Unmeasurable Premise Variables: Application to Tank System[J]. Journal of Dynamic Systems Measurement Control, 2014, 136(4).
- [6] S. Dong, C. L. P. Chen, M. Fang and Z. -G. Wu, "Dissipativity-Based Asynchronous Fuzzy Sliding Mode Control for T-S Fuzzy Hidden Markov Jump Systems," in IEEE Transactions on Cybernetics, vol. 50, no. 9, pp. 4020-4030, Sept. 2020, doi: 10.1109/TCYB.2019.2919299.
- [7] Y. Yu, H. Lam and K. Y. Chan, "T-S Fuzzy-Model-Based Output Feedback Tracking Control With Control Input Saturation," in IEEE Transactions on Fuzzy Systems, vol. 26, no. 6, pp. 3514-3523, Dec. 2018, doi: 10.1109/TFUZZ.2018.2835761.
- [8] C. Zhang, H.K. Lam, J. Qiu, P. Qi and Q. Chen, "Fuzzy-Model-Based Output Feedback Steering Control in Autonomous Driving Subject to Actuator Constraints," in IEEE Transactions on Fuzzy Systems, vol. 29, no. 3, pp. 457-470, March 2021, doi: 10.1109/TFUZZ.2019.2955044.
- [9] Karimi, Hamid-Reza Rathinasamy, Sakthivel Palanisamy, Selvaraj. (2016). EID based repetitive tracking control for Takagi-Sugeno fuzzy systems with saturating actuator. IET Control Theory Applications. 10. 10.1049/iet-cta.2016.0036.
- [10] Tseng C, Chen B S, Uang H J. Fuzzy tracking control design for nonlinear dynamic systems via T-S fuzzy model[J]. IEEE Transactions on Fuzzy Systems, 2001.
- [11] Lee T, Leok M, M Cc Lamroch N H. Geometric Tracking Control of a Quadrotor UAV on SE(3)[J]. IEEE, 2010.
- [12] Mao Y, Zhang H, Dang C. Stability Analysis and Constrained Control of a Class of Fuzzy Positive Systems with Delays Using Linear Copositive Lyapunov Functional[J]. Circuits Systems Signal Processing, 2012, 31(5):1863-1875.
- [13] Li X, Lam H K, Ge S, et al. Stability Analysis of Positive Polynomial Fuzzy-Model-Based Control Systems with Time Delay under Imperfect Premise Matching[J]. IEEE Transactions on Fuzzy Systems, 2018, 26(4):2289-2300.
- [14] Lam, H. K, Hongyi. Output-Feedback Tracking Control for Polynomial Fuzzy-Model-Based Control Systems.[J]. IEEE Transactions on Industrial Electronics, 2013.
- [15] Zhao Y , Bo X , Liu C , et al. Relaxed LMI-based stability conditions for fuzzy-model-based control systems under imperfect premise matching: Approximated membership function approach[C]// Intelligent Control Automation. IEEE, 2015.

An Aspect of Bilevel Indefinite Quadratic Transportation Problem Under Intuitionistic Fuzzy Environment

Ritu ARORA ^{a,1}, Aakanksha SINGH ^b and Shalini ARORA ^c

^a*Keshav Mahavidyalaya, University of Delhi, Delhi, India*

^b*Research Scholar, Indira Gandhi Delhi Technical University for Women, Kashmere Gate, New Delhi and Aryabhata College, University of Delhi, Delhi, India*

^c*Indira Gandhi Delhi Technical University for Women, Kashmere Gate, New Delhi, India*

Abstract. In this paper, a bilevel problem is exhibited wherein both the manufacturers and e-traders want to minimize the cost of transportation as well as deterioration cost. In today's world, reliability on online ordering has increased manifold. The "app culture" has lured the common man to prefer virtual shopping over the physical one. The consumers can order the necessities or the goods of their choice through electronic delivery apps. The manufacturers have tied up with e-traders who in turn satisfy the consumers demand. With this aim, a bilevel indefinite quadratic transportation problem is dened. Sometimes it is difficult to estimate the daily demand of perishable products on a regular basis. Therefore, demand and supply parameters become fluctuating in nature. To tackle this situation, bilevel indefinite quadratic transportation problem with intuitionistic fuzzy demand and supply parameters is formulated. This problem is dealt by converting fuzzy parameters into crisp ones. The transformed problem is then solved by two methods, intuitionistic fuzzy programming and fuzzy goal programming approach. To support the results, an example is also illustrated numerically representing the practical application of the problem. A comparative analysis of the solutions obtained from the two techniques is also presented. The problem is solved by computing software.

Keywords. bilevel programming, indefinite quadratic transportation, intuitionistic fuzzy programming, fuzzy goal programming, uncertainty

1. Introduction

Bilevel Programming Problem (BLPP) is a non-convex optimization problem. It is a decision making problem which involves the decision makers at two levels, upper level and lower level. The decision maker at lower level executes its policies after the decision maker at upper level propounds his plan of action. BLPP has numerous applications in varied practical scenarios like agriculture, banking sector, medicine, economy, energy sector as in electricity market, so on and so forth. The implementation of BLPP can also be seen in the field of transportation. Calvete et al. [1] applied ant colony optimization for production-distribution problem by formulating it as a bilevel model. Sun [2] designed the transport network problem as a bilevel model and solved it.

¹Corresponding Author: Associate Professor, Keshav Mahavidyalaya, University of Delhi, Delhi, India; E-mail: ritu.arora@keshav.du.ac.in.

Transportation plays an important role in any economic system bridging the gap between the consumers and the producers. Transportation models and distinct techniques for solving them have been presented by numerous authors. The simplest form of transportation problem was presented by Hitchcock [3]. Transportation problem with mixed constraints was considered by Brigden [4]. Ji and Chu [5] solved the transportation problem by the method of dualmatrix. Multi-objective transportation problem has been considered by various researchers and fuzzy programming techniques has been employed by them for solving these problems. Verma et al. [6] employed non-linear membership functions for solving multi-objective transportation problem by fuzzy programming. Ringuest and Rinks [7] proposed the algorithms for multi-objective transportation problems. Mousa [8] solved the multiobjective transportation problem by genetic algorithm and the method of TOPSIS. Kundu et al. [9] represented the multi-objective solid transportation problem in an uncertain environment and applied fuzzy programming techniques to obtain the optimal solution. Yu et al. [10] computed the compromise solution for multi-objective transportation problem where the decision makers have described the uncertainty in parameters as interval values. Shojaie and Raoofpanah [11] solved the fuzzy transportation problem by the approach of simulated annealing and genetic algorithm.

Fuzzy programming technique is a tool which facilitates the decision makers to find satisfactory solution in an optimization problem. Tanaka and Asai [12] instigated the technique of fuzzy programming. Fuzzy logic has also been used by Nittymaki and Kikuchi [13] to regulate the timings for traffic signal. In 2004, Tang et al. [14] exhibited the significance of fuzzy optimization by summarizing the models and their solution methodologies. Rommelfanger [15] described the benefits of modelling real life scenarios by fuzzy approach. Liu et al. [16] generated the optimal solution for solid transportation problem where parameters are considered as type-2 fuzzy variables. Aviso et al. [17] developed a bilevel model and applied fuzzy approach to utilize the resources and managing the waste in eco-industrial parks. The application of fuzzy approach can be seen in Ruan et al. [18] in which authors have considered the problem of medical supplies in disaster areas. Du et al. [19] solved the bilevel fuzzy programming problem for the transportation of hazardous material. Nayak and Ojha [20] solved the multi-objective non-linear programming problem by fuzzy goal programming approach. Muneeb et al. [21] formulated a fuzzy bilevel model for advertisement planning.

Although transportation problems were solved by the fuzzy programming approach, the concept of intuitionistic fuzzy sets emerged when the parameters are not precise. The perception of intuitionistic fuzzy sets was given by Atanassov [22] in 1986. Angelov [23] solved the mathematical programming problem as an application of the intuitionistic fuzzy set. In 2010, Zhang and Liu [24] applied the triangular fuzzy number for multi-attitude decision making problem. Razmi et al. [25] solved the multi-objective problem by intuitionistic fuzzy approach. In 2018, Bharati and Singh [26] formulated and solved the transportation problem by intuitionistic fuzzy procedure. Ebrahimnejad and Verdegay [27] solved the transportation problem under trapezoidal intuitionistic fuzzy environment. Muthuperumal et al. [28] explained the optimization technique for unbalanced transportation problem with triangular fuzzy numbers.

Transportation problem has been considered by researchers for minimizing the cost of transportation while carrying goods from one place to another. With time it was observed that goods like fruits and vegetables may get perished or essential commodities like medicines and medical equipments such as PPE kits, oxygen cylinders etc. may get

damaged due to poor conditions of roads or unfavourable weather conditions. The need arises to decrease the cost of damaged goods along with the cost of transportation. Thus, indefinite quadratic transportation problem (IQTP) was defined. The objective function in IQTP is a product of two linear functions, thus, minimizing the transportation cost and deterioration cost simultaneously. To the best of author’s knowledge, there are not many published papers on IQTP. Bhatia [29] explained the procedure for finding the locally optimal solution for IQTP. Khurana and Arora [30] described an algorithm for finding cost-time trade off pairs for bi-criterion IQTP with fixed charge. Sokolov et al. [31] presented the solution technique for non-linear transportation problems. Table 1 represents the summary of related literature by different authors.

Table 1. Summary of related literature

Author & References	Method Used	Problem Type
Liu & Zhang[32]	Exact penalty method	Bilevel transportation model
Zhang & Gao [33]	Penalty function method	Mixed-integer non-linear BLPP
Biswas & Bose [34]	Fuzzy goal programming	Quadratic BLPP
Xu & Gang [35]	Particle swarm optimization	Fuzzy random multiobjective BLPP
Yue et al.[36]	Fuzzy programming	Type-2 fuzzy mixed-integer BLPP
Zhao et al.[37]	Interactive intuitionistic fuzzy method	Multilevel programming problem
Maiti & Roy [38]	Intuitionistic fuzzy programming	Interval and multi-choice BLPP
Chhibber et al.[39]	Intuitionistic fuzzy programming	Multi-objective fixed-charge solid transportation problem under intuitionistic fuzzy environment
Proposed paper	Intuitionistic fuzzy programming	Bilevel indefinite quadratic transportation problem under intuitionistic fuzzy environment

In the proposed problem, a bilevel model is conferred, defining IQTP at both the levels of the problem. The upper level represents the manufacturers transporting the goods like grocery, medicines, fruits, vegetables etc. to e-traders and lower level depicts the transportation from e-traders to customers in different regions of the country. The novelty of this paper is that besides minimizing the cost of transportation while carrying goods from source to destination, it also aims at minimization of the cost due to damaged goods. Moreover, due to Covid-19 pandemic, the present market scenario is fluctuating in nature. This uncertainty in supply and demand of goods is represented by intuitionistic fuzzy parameters in bilevel IQTP. The uncertain parameters are dealt using (α, β) - cut. The converted problem is then solved by intuitionistic fuzzy programming approach. The satisfactory solution for bilevel IQTP can be obtained for different values of α and β provided that $\alpha + \beta \leq 1$. The paper is divided in the following sections: section 2 represents the definition of bilevel IQTP. Section 3 presents the definitions of fuzzy numbers which are vital in the elucidation of bilevel IQTP with uncertain parameters. Section 4 presents bilevel IQTP with intuitionistic fuzzy parameters and its solution methodology. Application of intuitionistic fuzzy bilevel IQTP is exhibited in section 5 followed by conclusions and prospective work in section 6.

2. Definition of Bilevel Indefinite Quadratic Transportation Problem

In this section, bilevel indefinite quadratic transportation problem (BIQTP) is defined. During transportation, unpleasant weather or bad roads results in perished goods. In or-

der to minimize the cost of damaged goods while transportation along with the transportation cost, indefinite quadratic transportation problem is considered at both the levels of (BIQTP). The objective functions at both the levels are product of two linear factors and are quasi-concave in nature. Thus, the minimum of bilevel problem will be obtained at an extreme point of the feasible region. Mathematically, (BIQTP) is defined as:

$$(BIQTP) : \min_{Y_1} Z_{11}(Y_1, Y_2) = (e_1^T Y_1 + e_2^T Y_2) (f_1^T Y_1 + f_2^T Y_2)$$

where Y_2 solves

$$\min_{Y_2} Z_{12}(Y_1, Y_2) = (g_1^T Y_1 + g_2^T Y_2) (h_1^T Y_1 + h_2^T Y_2) \quad (\text{for a given } Y_1)$$

subject to

$$\sum_{k \in K'} y_{jk} \leq c'_j \quad \forall j \in J' \tag{1}$$

$$\sum_{j \in J'} y_{jk} \geq d'_k \quad \forall k \in K' \tag{2}$$

$$\sum_{k \in K''} y_{jk} \leq c''_j \quad \forall j \in J'' \tag{3}$$

$$\sum_{j \in J''} y_{jk} \geq d''_k \quad \forall k \in K'' \tag{4}$$

$$y_{jk} \geq 0 \quad \forall (j, k) \in J \times K \tag{5}$$

Here, $(e_1^T Y_1 + e_2^T Y_2)$ represents the cost of transportation of goods from j^{th} origin to k^{th} destination and $(f_1^T Y_1 + f_2^T Y_2)$ represents the cost of damaged goods at upper level. Similarly at the lower level, $(g_1^T Y_1 + g_2^T Y_2)$ is the cost of transportation and $(h_1^T Y_1 + h_2^T Y_2)$ is the cost of damaged goods.

Notations : The notations used in this mathematical model are as follows :

J, K = Total number of sources and destinations respectively.

J', K' = Number of sources and destinations at upper level respectively.

J'', K'' = Number of sources and destinations at lower level respectively.

$e_1 = [e'_{jk}] ; f_1 = [f'_{jk}] ; g_1 = [g'_{jk}] ; h_1 = [h'_{jk}] \forall j \in J', k \in K'.$

$e_2 = [e''_{jk}] ; f_2 = [f''_{jk}] ; g_2 = [g''_{jk}] ; h_2 = [h''_{jk}] \forall j \in J'', k \in K''.$

$J = J' \cup J'' ; J' = \{1, 2, \dots, r_1\} ; J'' = \{r_1 + 1, \dots, r\}.$

$K = K' \cup K'' ; K' = \{1, 2, \dots, s_1\} ; K'' = \{s_1 + 1, \dots, s\}.$

$e'_{jk} > 0 ; f'_{jk} > 0 ; g'_{jk} > 0 ; h'_{jk} > 0$ are the cost parameters for the upper level problem.

$e''_{jk} > 0 ; f''_{jk} > 0 ; g''_{jk} > 0 ; h''_{jk} > 0$ are the cost parameters for the lower level problem.

$Y_1 = [y_{jk}] , y_{jk} \geq 0 \forall j \in J', k \in K'$ is the quantity transported from j^{th} origin to k^{th} destination at the upper level.

$Y_2 = [y_{jk}] , y_{jk} \geq 0 \forall j \in J'', k \in K''$ is the quantity transported from j^{th} origin to k^{th} destination at the lower level.

$c'_j > 0, d'_k > 0 \forall j \in J', k \in K'$ are the supply and demand parameters at the upper level.

$c''_j > 0, d''_k > 0 \forall j \in J'', k \in K''$ are the supply and demand parameters at the lower level.

Feasibility conditions :

$$\sum_{j \in J} c_j \geq \sum_{k \in K} d_k ; \sum_{j \in J'} c'_j \geq \sum_{k \in K'} d'_k ; \sum_{j \in J''} c''_j \geq \sum_{k \in K''} d''_k.$$

3. Basic Definitions

Definition-1[22]: Let the universe of discourse be represented by Z . An intuitionistic fuzzy set in Z is given by the set of three elements defined as follows:

$$\tilde{B}^I = \{ \langle z, \mu_{\tilde{B}^I}(z), \gamma_{\tilde{B}^I}(z) \rangle : z \in Z \},$$

where $\mu_{\tilde{B}^I}(z) : Z \rightarrow [0, 1]$ & $\gamma_{\tilde{B}^I}(z) : Z \rightarrow [0, 1]$ are functions such that $0 \leq \mu_{\tilde{B}^I}(z) + \gamma_{\tilde{B}^I}(z) \leq 1 \forall z \in Z$. For each z , $\mu_{\tilde{B}^I}(z)$ and $\gamma_{\tilde{B}^I}(z)$ indicates the degree of membership and degree of non-membership respectively.

Also, the degree of uncertainty of the element z in the set \tilde{B}^I is denoted by the function $\pi_{\tilde{B}^I}(z)$ and is defined as $\pi_{\tilde{B}^I}(z) = 1 - (\mu_{\tilde{B}^I}(z) + \gamma_{\tilde{B}^I}(z))$. If $\pi_{\tilde{B}^I}(z) = 0 \forall z \in Z$, then the intuitionistic fuzzy set reduces to a fuzzy set.

Definition-2[26]: Triangular Intuitionistic Fuzzy Number (TIFN)

An intuitionistic fuzzy number (IFN) of the form $\tilde{B}^I = (b_1, b_2, b_3), (\bar{b}_1, \bar{b}_2, \bar{b}_3)$ where $\bar{b}_1 \leq b_1 \leq b_2 \leq b_3 \leq \bar{b}_3$ is said to be a TIFN if its membership and non-membership functions, $\mu_{\tilde{B}^I}(z)$ and $\gamma_{\tilde{B}^I}(z)$ respectively are defined as follows :

$$\mu_{\tilde{B}^I}(z) = \begin{cases} \frac{z-b_1}{b_2-b_1} & b_1 \leq z \leq b_2 \\ \frac{b_3-z}{b_3-b_2} & b_2 \leq z \leq b_3 \\ 0 & \text{Otherwise} \end{cases} \quad \& \quad \gamma_{\tilde{B}^I}(z) = \begin{cases} \frac{b_2-z}{b_2-b_1} & \bar{b}_1 \leq z \leq \bar{b}_2 \\ \frac{z-\bar{b}_2}{\bar{b}_3-\bar{b}_2} & \bar{b}_2 \leq z \leq \bar{b}_3 \\ 1 & \text{Otherwise} \end{cases}$$

Definition-3[22]: (α, β) - cut of a triangular intuitionistic fuzzy number $\tilde{B}^I = (b_1, b_2, b_3), (\bar{b}_1, \bar{b}_2, \bar{b}_3)$ is the set of all z whose degree of membership is greater than or equal to α and degree of non-membership is less than or equal to β . It is defined as : $\tilde{B}^I_{(\alpha, \beta)} = \{ z : \mu_{\tilde{B}^I}(z) \geq \alpha ; \gamma_{\tilde{B}^I}(z) \leq \beta ; \alpha + \beta \leq 1, z \in Z \}$. The membership and non-membership functions are defined as $\mu_{\tilde{B}^I}(z) : Z \rightarrow [0, 1]$ and $\gamma_{\tilde{B}^I}(z) : Z \rightarrow [0, 1]$. These functions are defined such that $0 \leq \mu_{\tilde{B}^I}(z) + \gamma_{\tilde{B}^I}(z) \leq 1$. Therefore, $\alpha + \beta \leq 1$.

4. Bilevel IQTP with Intuitionistic Fuzzy Parameters

In fluctuating marketing scenario and due to prevailing Covid-19 pandemic conditions, the demand and the supply of goods in markets are uncertain in nature. Therefore, to address fluctuating market situations, intuitionistic fuzzy bilevel indefinite quadratic transportation problem (IFBIQTP) is defined. In this problem, uncertainty in demand and supply parameters are represented as intuitionistic fuzzy numbers.

Mathematically, intuitionistic fuzzy bilevel indefinite quadratic transportation problem with fuzzy supply and demand parameters is denoted as (IFBIQTP) and is represented as follows:

$$(IFBIQTP) : \min_{Y_1} Z_{11}(Y_1, Y_2) = (e_1^T Y_1 + e_2^T Y_2) (f_1^T Y_1 + f_2^T Y_2)$$

where Y_2 solves

$$\min_{Y_2} Z_{12}(Y_1, Y_2) = (g_1^T Y_1 + g_2^T Y_2) (h_1^T Y_1 + h_2^T Y_2) \quad (\text{for a given } Y_1)$$

subject to

$$\sum_{k \in K'} y_{jk} \leq \tilde{c}_j^I \quad \forall j \in J' \tag{6}$$

$$\sum_{j \in J'} y_{jk} \geq \tilde{d}_k^I \quad \forall k \in K' \tag{7}$$

$$\sum_{k \in K''} y_{jk} \leq \tilde{c}_j^{II} \quad \forall j \in J'' \tag{8}$$

$$\sum_{j \in J''} y_{jk} \geq \tilde{d}_k^{II} \quad \forall k \in K'' \tag{9}$$

Also, $y_{jk} \geq 0 \quad \forall (j, k) \in J \times K$. In this defined problem (IFBIQTP), the supply and the demand parameters are uncertain and therefore, they are represented as intuitionistic fuzzy numbers (IFN).

The membership and the non-membership functions for the supply parameters at the upper level (see Fig 1) are defined as follows with t_{j1} as the range of acceptance for the non-membership function of \tilde{c}_j^I [26]:

$$\mu_{\tilde{c}_j^I}^I(y) = \begin{cases} 1 & y \leq c_{j1} \\ \frac{c_{j2}-y}{c_{j2}-c_{j1}} & c_{j1} \leq y \leq c_{j2} \\ 0 & y \geq c_{j2} \end{cases} \quad \& \quad \gamma_{\tilde{c}_j^I}^I(y) = \begin{cases} 0 & y \leq c_{j1} + t_{j1} \\ \frac{y-(c_{j1}+t_{j1})}{c_{j2}-(c_{j1}+t_{j1})} & c_{j1} + t_{j1} \leq y \leq c_{j2} \\ 1 & y \geq c_{j2} \end{cases}$$

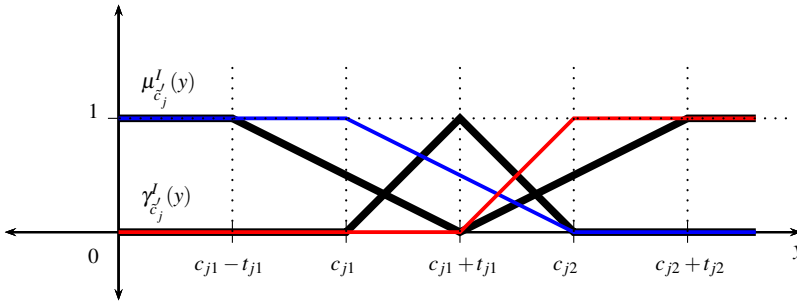


Figure 1

Again, the membership and non-membership functions for the demand parameters at the upper level (see Fig 2) are defined as follows with t_{k1} is the range of acceptance for the non-membership function of \tilde{d}_k^I [26]:

$$\mu_{\tilde{d}_k^I}^I(y) = \begin{cases} 0 & y \leq d_{k1} \\ \frac{y-d_{k1}}{d_{k2}-d_{k1}} & d_{k1} \leq y \leq d_{k2} \\ 1 & y \geq d_{k2} \end{cases} \quad \& \quad \gamma_{\tilde{d}_k^I}^I(y) = \begin{cases} 1 & y \leq d_{k1} \\ \frac{(d_{k2}-t_{k1})-y}{(d_{k2}-t_{k1})-d_{k1}} & d_{k1} \leq y \leq d_{k2} - t_{k1} \\ 0 & y \geq d_{k2} - t_{k1} \end{cases}$$

Similarly, the membership function for the supply and demand parameters at the lower level can also be defined.

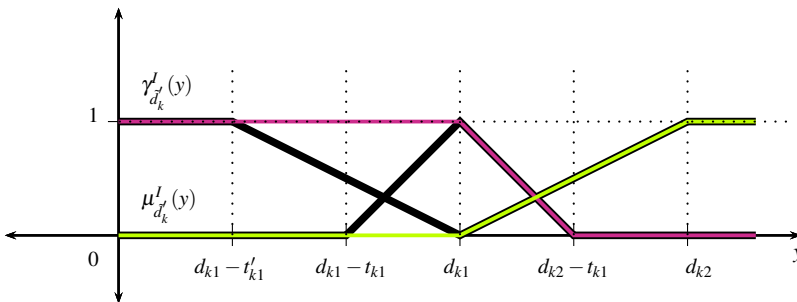


Figure 2

4.1. Solution Methodology

To solve (IFBIQTP), apply (α, β) - cut to the intuitionistic fuzzy supply and demand parameters at both the levels. This will transform the set of fuzzy parameters into crisp set of elements. Applying Def(3) to fuzzy supply parameter at upper level we have $\mu_{c_j}^I(y) \geq \alpha$ and $\gamma_{c_j}^I(y) \leq \beta$. We will get $y \leq c_{j2} - \alpha(c_{j2} - c_{j1})$ and $y \leq (c_{j1} + t_{j1}) + \beta(c_{j2} - c_{j1} - t_{j1})$. Thus, the supply constraints at the upper level becomes

$$\sum_{k \in K'} y_{jk} \leq C_j^1 \quad \forall j \in J' \tag{10}$$

Here, $C_j^1 = \text{Min}\{c_{j2} - \alpha(c_{j2} - c_{j1}), (c_{j1} + t_{j1}) + \beta(c_{j2} - c_{j1} - t_{j1})\}$. Similarly, demand constraints at the upper level problem is given by

$$\sum_{j \in J'} y_{jk} \geq D_k^1 \quad \forall k \in K' \tag{11}$$

Here, $D_k^1 = \text{Max}\{d_{k1} + \alpha(d_{k2} - d_{k1}), (d_{k2} - t_{k1}) - \beta(d_{k2} - t_{k1} - d_{k1})\}$. Likewise, (α, β) - cut can be applied to the intuitionistic fuzzy supply and demand parameters at the lower level which will transform them into crisp sets. The problem (IFBIQTP) gets converted into the problem crisp bilevel indefinite quadratic transportation problem (CBIQTP) where supply and demand parameters at both the levels are crisp sets. (CBIQTP) is defined as follows:

$$(CBIQTP) : \min_{Y_1} Z_{11}(Y_1, Y_2) = (e_1^T Y_1 + e_2^T Y_2) (f_1^T Y_1 + f_2^T Y_2)$$

where Y_2 solves

$$\min_{Y_2} Z_{12}(Y_1, Y_2) = (g_1^T Y_1 + g_2^T Y_2) (h_1^T Y_1 + h_2^T Y_2) \quad (\text{for a given } Y_1)$$

subject to

$$\sum_{k \in K'} y_{jk} \leq C_j^1 \quad \forall j \in J' \tag{12}$$

$$\sum_{j \in J'} y_{jk} \geq D_k^1 \quad \forall k \in K' \tag{13}$$

$$\sum_{k \in K''} y_{jk} \leq C_j^2 \quad \forall j \in J'' \tag{14}$$

$$\sum_{j \in J''} y_{jk} \geq D_k^2 \quad \forall k \in K'' \tag{15}$$

Also, $y_{jk} \geq 0 \quad \forall (j, k) \in J \times K$. From Eq.(10) and Eq.(11), we get $\sum_{k \in K'} D_k^1 \leq \sum_{j \in J'} \sum_{k \in K'} y_{jk} \leq \sum_{j \in J'} C_j^1$.

Thus, we get $\sum_{j \in J'} C_j^1 \geq \sum_{k \in K'} D_k^1$. Similarly, we can have $\sum_{j \in J''} C_j^2 \geq \sum_{k \in K''} D_k^2$. Since the feasibility condition at the upper level and lower level problem is described, problem (CBIQTP) is a **well defined problem**.

4.2. Intuitionistic Fuzzy Programming Approach

We will solve the problem (CBIQTP) by Intuitionistic Fuzzy Programming Approach (IFPA). Firstly, find the maximum and minimum values of the objective functions at both the levels of (CBIQTP) with respect to the constraint set (12-15). The membership and nonmembership functions for the objective functions at both the levels are described as follows: (for $i = 1,2$)

$$\mu(Z_{1i}) = \begin{cases} 1 & Z_{1i} \leq Z_{1i}^{Min} \\ \frac{Z_{1i}^{Max} - Z_{1i}}{Z_{1i}^{Max} - Z_{1i}^{Min}} & Z_{1i}^{Min} \leq Z_{1i} \leq Z_{1i}^{Max} \\ 0 & Z_{1i} \geq Z_{1i}^{Max} \end{cases} \quad \& \quad \gamma(Z_{1i}) = \begin{cases} 0 & Z_{1i} \leq Z_{1i}^{Min} \\ \frac{Z_{1i} - Z_{1i}^{Min}}{Z_{1i}^{Max} - Z_{1i}^{Min}} & Z_{1i}^{Min} \leq Z_{1i} \leq Z_{1i}^{Max} \\ 1 & Z_{1i} \geq Z_{1i}^{Max} \end{cases}$$

Let the minimum degree of satisfaction for the membership and non-membership function for the upper level problem be η_{11} and η'_{11} respectively. Let η_{12} and η'_{12} be the degree of satisfaction for the membership and non-membership function for the lower level problem respectively.

Let $\delta_1 = \text{Max}(\eta_{11}, \eta_{12})$ and $\delta_2 = \text{Min}(\eta'_{11}, \eta'_{12})$. The intuitionistic fuzzy programming problem for (CBIQTP) is denoted as (IFTP) and it is represented as follows :

$$(IFPP) : \text{Max}(\delta_1 - \delta_2)$$

subject to

$$\mu(Z_{11}) \geq \delta_1, \quad \mu(Z_{12}) \geq \delta_1 \tag{16}$$

$$\gamma(Z_{11}) \leq \delta_2, \quad \gamma(Z_{12}) \leq \delta_2 \tag{17}$$

$$\sum_{k \in K'} y_{jk} \leq C_j^1 \quad \forall j \in J' \tag{18}$$

$$\sum_{j \in J'} y_{jk} \geq D_k^1 \quad \forall k \in K' \tag{19}$$

$$\sum_{k \in K''} y_{jk} \leq C_j^2 \quad \forall j \in J'' \tag{20}$$

$$\sum_{j \in J''} y_{jk} \geq D_k^2 \quad \forall k \in K'' \tag{21}$$

$$\delta_1 \geq \delta_2; \delta_1 + \delta_2 \leq 1; \delta_1, \delta_2 \in [0, 1] \ \& \ y_{jk} \geq 0 \ \forall (j, k) \in J \times K. \tag{22}$$

(IFPP) is solved to obtain the satisfactory solution for the problem (IFBIQTP). The computing software LINGO 17.0 is used to solve the problem (IFPP).

4.3. Fuzzy Goal Programming Approach

(IFBIQTP) is also solved by the fuzzy goal programming method. It is described as follows:

$$\text{Min } \xi$$

subject to

$$Z_{11} - d_1^+ + d_1^- = Z'_{11} \tag{23}$$

$$Z_{12} - d_2^+ + d_2^- = Z'_{12} \tag{24}$$

$$\sum_{k \in K'} y_{jk} \leq C_j^1 \quad \forall j \in J' \tag{25}$$

$$\sum_{j \in J'} y_{jk} \geq D_k^1 \quad \forall k \in K' \tag{26}$$

$$\sum_{k \in K''} y_{jk} \leq C_j^2 \quad \forall j \in J'' \tag{27}$$

$$\sum_{j \in K''} y_{jk} \geq D_k^2 \quad \forall k \in K'' \tag{28}$$

$$\xi - d_1^+ \geq 0; \xi - d_2^+ \geq 0; d_1^+ d_1^- = 0; d_2^+ d_2^- = 0 \tag{29}$$

$$0 \leq \xi \leq 1; y_{jk} \geq 0 \quad \forall (j, k) \in J \times K. \tag{30}$$

Here, $d_1^+, d_1^-, d_2^+, d_2^-$ are deviational variables introduced in the objective functions. Z'_{11}, Z'_{12} are the aspired goals of the decision makers.

5. Application of Intuitionistic Fuzzy Bilevel IQTP

Consider a milk manufacturing company Sukanya. The company has four plants located in Gurugram, Faridabad, Kundli and Sonipat. It transports milk and milk products like cheese, ice-cream etc. to e-traders like easy mart, milk mart, fresh mart and large basket. Due to Covid-19 pandemic, the common man place their order for their daily needs to these e-traders through electronic delivery apps. These e-traders distribute milk and milk products to customers in four different regions of Delhi; North Delhi, South Delhi, West Delhi and North-west Delhi. While delivering milk and milk product from plants to e-traders and then to customers, there is a possibility of deterioration of products like mishandling, expiry dates, temperature imbalance, melting of ice-cream and so on. The aim of the company and e-traders is to minimize the cost of transportation of products as well as the cost of deterioration. Suppose that Z_{11} represents the objective function at the upper level (from plants to e-traders) and Z_{12} be the objective function at the lower level (delivering products from e-traders to customers in four regions of Delhi). Table 2 and Table 3 represents the costs(in thousands) of the objective function at the upper level and at lower level respectively.

The membership functions and non-membership functions for supply and demand constraints at two levels are respectively given as follows:

$$\mu_{c_1}(y) = \begin{cases} 1 & y \leq 31 \\ \frac{35-y}{35-31} & 31 \leq y \leq 35 \\ 0 & y \geq 35 \end{cases} \quad \gamma_{c_1}(y) = \begin{cases} 0 & y \leq 33 \\ \frac{y-33}{35-33} & 33 \leq y \leq 35 \\ 1 & y \geq 35 \end{cases}$$

$$\mu_{c_2}(y) = \begin{cases} 1 & y \leq 21 \\ \frac{25-y}{25-21} & 21 \leq y \leq 25 \\ 0 & y \geq 25 \end{cases} \quad \gamma_{c_2}(y) = \begin{cases} 0 & y \leq 23 \\ \frac{y-23}{25-23} & 23 \leq y \leq 25 \\ 1 & y \geq 25 \end{cases}$$

$$\mu_{c_3}(y) = \begin{cases} 1 & y \leq 40 \\ \frac{44-y}{44-40} & 40 \leq y \leq 44 \\ 0 & y \geq 44 \end{cases} \quad \gamma_{c_3}(y) = \begin{cases} 0 & y \leq 42 \\ \frac{y-42}{44-42} & 42 \leq y \leq 44 \\ 1 & y \geq 44 \end{cases}$$

Table 2. Cost table for the upper level

Plants \ E-traders	Easy mart		Milk mart		Fresh mart		Large basket	
	Gurugram	5	4	1	3	7	1	5 → e_{jk}
Faridabad	6	1	3	3	4	5	5	4
Kundli	5	1	1	5	4	4	2	6
Sonipat	3	4	4	2	1	3	5	4

→ f_{jk}

Table 3. Cost table for the lower level

E-traders \ Regions	North Delhi		South Delhi		West Delhi		North-west Delhi	
	Easy mart	3	3	4	5	6	1	3 → g_{jk}
Milk mart	1	1	2	4	3	5	6	4
Fresh mart	3	1	2	5	5	5	3	6
Large basket	1	3	6	1	4	6	5	1

→ h_{jk}

$$\mu_{\bar{e}_4}(y) = \begin{cases} 1 & y \leq 31 \\ \frac{37-y}{37-31} & 31 \leq y \leq 37 \\ 0 & y \geq 37 \end{cases} \quad \gamma_{\bar{e}_4}(y) = \begin{cases} 0 & y \leq 32 \\ \frac{y-32}{37-32} & 32 \leq y \leq 37 \\ 1 & y \geq 37 \end{cases}$$

$$\mu_{\bar{d}_1}(y) = \begin{cases} 0 & y \leq 20 \\ \frac{y-20}{24-20} & 20 \leq y \leq 24 \\ 1 & y \geq 24 \end{cases} \quad \gamma_{\bar{d}_1}(y) = \begin{cases} 1 & y \leq 20 \\ \frac{22-y}{22-20} & 20 \leq y \leq 22 \\ 0 & y \geq 22 \end{cases}$$

$$\mu_{\bar{d}_2}(y) = \begin{cases} 0 & y \leq 17 \\ \frac{y-17}{21-17} & 17 \leq y \leq 21 \\ 1 & y \geq 21 \end{cases} \quad \gamma_{\bar{d}_2}(y) = \begin{cases} 1 & y \leq 17 \\ \frac{19.5-y}{19.5-17} & 17 \leq y \leq 19.5 \\ 0 & y \geq 19.5 \end{cases}$$

$$\mu_{\bar{d}_3}(y) = \begin{cases} 0 & y \leq 18 \\ \frac{y-18}{24-18} & 18 \leq y \leq 24 \\ 1 & y \geq 24 \end{cases} \quad \gamma_{\bar{d}_3}(y) = \begin{cases} 1 & y \leq 18 \\ \frac{21.5-y}{21.5-18} & 18 \leq y \leq 21.5 \\ 0 & y \geq 21.5 \end{cases}$$

$$\mu_{\bar{d}_4}(y) = \begin{cases} 0 & y \leq 24 \\ \frac{y-24}{28-24} & 24 \leq y \leq 28 \\ 1 & y \geq 28 \end{cases} \quad \gamma_{\bar{d}_4}(y) = \begin{cases} 1 & y \leq 24 \\ \frac{26.5-y}{26.5-24} & 24 \leq y \leq 26.5 \\ 0 & y \geq 26.5 \end{cases}$$

The intuitionistic fuzzy problem is formulated and it is solved by a computing software LINGO 17.0. Table 4 represents the satisfactory solution for the decision makers at two levels by varying the values of α and β . The decision makers at two levels can choose the solution best suited to them according to the demand and supply parameters. It has been

observed from Table 4 that the values of the objective functions Z_{11} and Z_{12} obtained from intuitionistic fuzzy programming approach is minimum.

Table 4. Comparative Analysis

Parameters		Intuitionistic Fuzzy Programming Approach		Fuzzy Goal Programming	
α	β	Z_{11}	Z_{12}	Z_{11}	Z_{12}
0.2	0.4	69230	51436	179703	185238
0.2	0.5	71920	37300	186744	205738
0.4	0.3	81939	51744	177996	191893
0.5	0.2	71775	53720	180268	193154
0.6	0.4	77580	62220	169212	173430
0.8	0.1	85748	70132	168432	173591

6. Conclusions and Prospective Work

Bilevel IQTP has been scrutinized in this paper when the parameters are uncertain in nature. An effort is made to exhibit the relevance of the model when e-traders are supplying milk to the consumers at their door steps. In doing so, it is required that minimum amount of milk gets deteriorated to minimize the loss. In todays world especially in this pandemic time, demand of delivery of essential commodities at door steps has upsurged exponentially. The method can also be applied to other merchandising streams involving home-delivery services. The aim of the problem is to find a satisfactory solution for the manufacturers at upper level and e-traders at lower level. Distinct values of α and β ($\alpha + \beta \leq 1$) will yield varied satisfactory solutions for the decision makers at two levels. The problem is solved by two approaches. One is intuitionistic fuzzy approach and another is fuzzy goal programming method. The satisfactory solution obtained by two modes is compared. It has been observed that the objective function values are minimum when the problem is solved by intuitionistic fuzzy method.

Bilevel IQTP has been considered in this paper under intuitionistic fuzzy environment. The concept of this paper can be extended to trilevel IQTP with intuitionistic fuzzy demand and supply parameters. Moreover, indeterminacy in cost coefficients can also be contemplated. Bilevel IQTP in this paper has been solved by interactive fuzzy programming technique. Authors would like to solve the problem by other methods like TOPSIS. Other algorithmic approaches like genetic algorithm, particle swarm optimization, etc. could also be examined for solving bilevel/trilevel IQTP. A similar situation with respect to time minimizing transportation problem could also be depicted.

Acknowledgements The authors are readily grateful to the reviewers for their valuable suggestions, incorporating which has helped us in improving the quality of the paper to a great extent.

References

[1] Calvete HI, Gale C, Oliveros MJ. Bilevel model for production-distribution planning solved by using ant-colony optimization. *Computers & Operations Research*. 2011; 38(1): 320-327.

- [2] Sun Z. Continuous transport network design problem based on bi-level programming model. *Procedia Engineering*. 2016; 137: 277-282.
- [3] Hitchcock, FL. The distribution of a product from several sources to numerous localities. *Journal of Mathematics and Physics*. 1941; 20: 224-230.
- [4] Brigden MEB. A variant of the transportation problem in which the constraints are of mixed type. *Journal of the Operational Research Society*. 1974; 25(3): 437-445.
- [5] Ji P, Chu KF. A dual-matrix approach to the transportation problem. *Asia- Pacific Journal of Operational Research*. 2002; 19: 35-45.
- [6] Verma R, Biswal MP, Biswas A. Fuzzy programming technique to solve multi-objective transportation problems with some non-linear membership functions. *Fuzzy Sets and Systems*. 1997; 91(1):37-43.
- [7] Ringuest JL, Rinks DB. Interactive solutions for the linear multi-objective transportation problem. *European Journal of Operational Research*. 1987; 32(1): 96-106.
- [8] Mousa AA. Using genetic algorithms and TOPSIS technique for multi-objective transportation problem: a hybrid approach. *International Journal of Computer Mathematics*. 2010; 87(13): 3017-3029.
- [9] Kundu P, Kar S, Maiti M. Multi-objective solid transportation problems with budget constraints in uncertain environment. *International Journal of Systems Science*. 2014; 45(8): 1668-1682.
- [10] Yu VF, Hu KJ, Chang AY. An interactive approach for the multi-objective transportation problem with interval parameters. *International Journal of Production Research*. 2015; 53(4): 1051-1064.
- [11] Shojaie AA, Raoofpanah H. Solving a two-objective green transportation problem by using meta-heuristic methods under uncertain fuzzy approach. *Journal of Intelligent & Fuzzy Systems*. 2018; 34(1): 1-10.
- [12] Tanaka H, Asai K. Fuzzy linear programming problems with fuzzy numbers. *Fuzzy Sets and Systems*. 1984; 13(1): 1-10.
- [13] Nittymaki J, Kikuchi S. Application of fuzzy logic to the central of a pedestrian crossing signal. *Transportation Research Record: Journal of the transportation Research Board*. 1998; 1651(1): 30-38.
- [14] Tang J, Wang D, Fung RYK, Yung KL. Understanding of fuzzy optimization: theories and methods. *Journal of Systems Science and Complexity*. 2004; 17(1): 117-136.
- [15] Rommelfanger HJ. The advantages of fuzzy optimization in practical use. *Fuzzy optimization and Decision making*. 2004; 3, 295-309.
- [16] Liu P, Yang L, Wang L, Li S. A solid transportation problem with type-2 fuzzy variables. *Applied Soft computing*. 2014; 24: 543-558.
- [17] Aviso KB, Tan RR, Culaba AB, Cruz Jr. JB. Bi-level fuzzy optimization approach for water exchange in eco-industrial parks. *Process Safety and Environmental Protection*. 2010; 88(1): 31-40.
- [18] Ruan JH, Wang XP, Chan FTS, Shi Y. Optimising the intermodal transportation of emergency medical supplies using balanced fuzzy clustering. *International Journal of production Research*. 2016; 54(14): 4368-4386.
- [19] Du J, Li X, Yu L, Dan R, Zhou J. Multi-depot routing problem for hazardous material transportation : A fuzzy bilevel programming. *Information Sciences*. 2017; 399: 201-218.
- [20] Nayak S, Ojha A. An approach of fuzzy and TOPSIS to bi-level multi-objective non-linear fractional programming problem. *Soft Computing*. 2019; 23: 5605-5618.
- [21] Muneeb SM, Adhami AY, Asam Z, Jalil SA. Bi-level decision making models for advertising allocation problem under fuzzy environment. *International Journal of System Assurance Engineering and Management*. 2019; 10: 160-172.
- [22] Atanassov KT. Intuitionistic fuzzy sets. *Fuzzy Sets and Systems*. 1986; 20(1): 87-96.
- [23] Angelov PP. Optimization in an intuitionistic fuzzy environment. *Fuzzy Sets and Systems*. 1997; 66(3): 299-306.
- [24] Zhang X, Liu P. Method for aggregating triangular fuzzy intuitionistic fuzzy information and its application to decision making. *Technological and economic Development of economy*. 2010; 16(2): 280-290.
- [25] Razmi J, Jafarian E, Amin SH. An interactive fuzzy goal programming approach for finding pareto-optimal solutions to multi-objective programming problems. *Expert Systems with Applications*. 2016; 65: 181-193.
- [26] Bharati, SK, Singh, SR. Transportation problem under interval-valued intuitionistic fuzzy environment. *International Journal of Fuzzy Systems*. 2018; 20: 1511-1522.
- [27] Ebrahimnejad A, Verdegay, JL. A new approach for solving fully intuitionistic fuzzy transportation problems. *Fuzzy optimization and decision making*. 2018; 17(4): 447-474.
- [28] Muthuperumal S, Titus P, Venkatchalopathy M. An algorithmic approach to solve unbalanced triangular fuzzy transportation problems. *Soft Computing*. 2020; 24: 18689-18698.

- [29] Bhatia HL. Indefinite quadratic solid transportation problem. *Journal of Information and Optimization Sciences*. 1981; 2(3): 297-303.
- [30] Khurana A, Arora SR. Fixed charge bi-criterion indefinite quadratic transportation problem with enhanced flow. *Investigacion Operacional*. 2011; 32(2): 133-145.
- [31] Sokolov AA, Tizik AP, Tsurkov VI. Iterative method for the transportation problem with additional supply and consumption points and quadratic cost. *Journal of Computer and Systems Science International*. 2013; 52: 588-598.
- [32] Liu GS, Zhang JZ. Decision making of transportation plan, a bilevel transportation problem approach. *Journal of Industrial & Management Optimization*. 2005; 1(3) : 305-314.
- [33] Zhang H, Gao Z. Bilevel programming model and solution method for mixed transportation network design problem. *Journal of Systems Science and Complexity*. 2009; 22: 446-459.
- [34] Biswas A, Bose K. A fuzzy programming approach for solving quadratic bilevel programming problems with fuzzy resource constraints. *International Journal of Operational Research*. 2011; 12(2): 142-156.
- [35] Xu J, Gang J. Multi-objective bilevel construction material transportation scheduling in large-scale construction projects under a fuzzy random environment. *Transportation Planning and Technology*. 2013; 36(4): 352-376.
- [36] Yue Q, Wang Y, Liu L, Niu J, Guo P, Li P. Type-2 fuzzy mixed integer bi-level programming approach for multi-source multi-user water allocation under future climate change. *Journal of Hydrology*. 2020; 591: 125332.
- [37] Zhao X, Zheng Y and Wan Z. Interactive intuitionistic fuzzy methods for multilevel programming problems. *Expert Systems with Applications*. 2017; 72: 258-268.
- [38] Maiti SK, Roy SK. Analysing interval and multi-choice bi-level programming for Stackelberg game using intuitionistic fuzzy programming. *International Journal of Mathematics in Operational Research*. 2020; 16(3): 354375.
- [39] Chhibber D, Bisht DC and Srivastava PK. Pareto-optimal solution for fixed-charge solid transportation problem under intuitionistic fuzzy environment. *Applied Soft Computing*. 2021; 107, 107368.

A Secure Image Authentication Scheme with Tamper Localization and Recovery

Neena Raj N. R.^a and Shreelekshmi R.^{b,1}

^a *Department of Computer Science and Engineering, College of Engineering Trivandrum (Affiliated to APJ Abdul Kalam Technological University), Thiruvananthapuram - 695016, Kerala, India*

^b *Department of Computer Science and Engineering, Government Engineering College (Affiliated to APJ Abdul Kalam Technological University), Thrissur - 680009, Kerala, India*

Abstract. This paper proposes a secure image authentication scheme that can locate the tampered regions, recover the lost contents and hide application-specific sensitive data. In this scheme, an encrypted watermark that comprises tamper localization, recovery and application-specific information is placed in the selected pixels, which is extracted and decrypted to identify the tampered regions, recover the tampered regions approximate to original image contents and extract the hidden data. The watermark is highly secure and sensitive to any modification in the image. The proposed scheme ensures lossless recovery of the original image and data from an untampered image. The experimental results show that this scheme generates watermarked image of high quality and has high resistance to copy-move, image splicing, vector quantization and collage attacks. As compared with state-of-the-art schemes, the proposed scheme provides better recovered image quality under extensive tampering.

Keywords. Image authentication, Fragile watermarking, Tamper localization, Image recovery, Data hiding

1. Introduction

Rapid growth in communication and digital imaging technology enables anyone to share images on various platforms like e-healthcare, e-commerce, e-governance, social media, etc. Security of these images is a serious concern since the availability of powerful image manipulation software enables anyone to tamper images without leaving visual traces. Tampering the image contents misleads its purpose in medical diagnosis, forensic investigation, military applications, etc. These situations demand content authentication and verification of image integrity.

Fragile watermarking is an effective solution for strict content authentication since any modifications in the protected image lead to changes in the embedded watermark [1,2]. D. Singh and S. K. Singh proposed a fragile watermarking scheme [3] in which the recovery information is generated using Discrete Cosine Transform (DCT). They proposed another scheme [4] using Block Truncation Coding (BTC). In these schemes,

¹ Corresponding Author: Shreelekshmi R., Department of Computer Science and Engineering, Government Engineering College, Thrissur - 680009; E-mail: shreelekshmir@gmail.com

the watermark generated for a block is placed in another block known as a mapping block to resist collage attack [5]. This causes misclassification of untampered blocks if their mapping block is tampered. Low tamper localization accuracy causes degradation in the recovered image quality.

To increase recovery rate under extensive tampering, Haghghi et al. [6] generated recovery information using Lifting Wavelet Transform (LWT) and halftoning. This scheme cannot resist collage attack. Qin et al. [7] proposed a scheme in which the recovery information is generated using an Optimal Iterative Block Truncation Coding (OIBTC) algorithm and distributed over the image. This scheme provides high quality recovered image under extensive tampering. But this scheme cannot resist collage attack. Rajput and Ansari [8] proposed a recovery scheme in which four copies of the recovery information are placed in the different parts of the image. The watermarked image quality is low since the watermark is placed in the 4 Least Significant Bits (LSB) of image pixels. This scheme is vulnerable to four scanning attack since the watermark is less secure [5]. Shen et al. [9] generated authentication information using Singular Value Decomposition (SVD) and recovery information using block average.

Gul and Ozturk [10] proposed a pixel-wise authentication scheme in which recovery information is generated using the average value of image blocks. Kim and Yang [11] proposed a scheme based on Absolute Moment Block Truncation Code (AMBTC). The recovery information is computed using AMBTC and placed in the LSBs using Optimal Pixel Adjustment Process (OPAP). This scheme provides low recovered image quality under extensive tampering. The schemes [3,4,6,7,8,9,10,11] cannot recover original image from an untampered received image. The schemes [12,13] can hide sensitive data like Electronic Patient Record (EPR) along with tamper localization. But these schemes are vulnerable to copy-move, Vector Quantization (VQ), collage and chosen cover-image attacks since the watermark is not protected [5].

Most of the existing schemes have limitations such as low watermarked image quality, low tamper detection accuracy, less security and poor recovery ability under extensive tampering. The majority of schemes focus on grayscale images only. In this scenario, we propose a fragile watermarking scheme that can locate the tampered regions, recover the lost contents and also hide data in the image. The scheme can support both grayscale and color and can be effectively used in images carrying sensitive information like medical, biometric. The major highlights of the proposed scheme include:

1. High watermarked image quality.
2. High security.
3. High tamper detection accuracy.
4. Lossless recovery of the original image contents and sensitive information from the untampered watermarked image.
5. High recovered image quality under extensive tampering.
6. High resistance to copy-move, image splicing, VQ and collage attacks.

The remaining part of this paper is organized as follows. Section 2 presents the proposed scheme. Section 3 discusses experimental results and performance comparison with state-of-the-art schemes before concluding in section 4.

2. Proposed Scheme

The proposed scheme creates a cover image C from the original image I of size $h \times w \times c$ with b bits per channel where h , w and c represent height, width and number

of channels in I respectively, using Pixel to Block conversion (PTB) technique [12]. The cover image is divided into N blocks of size 4×4 and a watermark of length 24 bits is generated for each channel in the image block. The watermark contains an 8-bit Tamper Localization Code (TLC), 14-bit Self Recovery Code (SRC) and two bits from the application-specific sensitive data. The TLC is computed from the image pixels using SVD [14] and logistic map to make it sensitive to the changes in the image contents. The SRC contains the recovery information of two different blocks which are randomly selected using a block mapping sequence generation procedure. The watermark is encrypted using the logistic map and is embedded into the 2 LSBs of 12 pixels in the image block. The remaining 4 pixels are kept unchanged to ensure the recovery of image pixels in the original image from untampered regions of the watermarked image. A smoothing function is used to enhance the watermarked image quality. The tamper localization is performed in multilevel to increase the localization accuracy and resist various tampering attacks. The recovery is carried out in two levels for improving the recovery rate under extensive tampering. The major phases in the proposed scheme are watermarked image generation, tamper localization and image recovery.

2.1. Watermarked image generation

The watermarked image generation phase includes chaotic sequence generation, block mapping sequence generation, cover image generation, watermark generation, encryption and embedding.

1. Chaotic sequence generation: In the proposed scheme, a chaotic sequence S of length $31N$ is generated using a logistic map $x_{n+1} = \mu x_n(1 - x_n)$, where $n \geq 0$, $0 \leq x_0 \leq 1$ and $0 \leq \mu \leq 4$ [15]. The value of μ is selected from the range $[3.57, 4]$ to ensure the chaotic nature of S . Initial condition x_0 and the control parameter μ together forms k_1 , which is used as a key in the chaotic sequence generation. Further S is partitioned into SM, ST, SE of length $N, 4N, 26N$ respectively from front to rear.
2. Block mapping sequence generation: A look-up table L of size $\frac{h}{2} \times \frac{w}{2}$ is constructed to store terms in the block mapping sequence. Initially, L is assigned with $1, 2, \dots, N$ in row-major order. Odd columns in the left half are swapped with corresponding columns of the right half to maximize the recovery rate. Then L is partitioned into sub-blocks TL, TR, BL, BR each of size $\frac{h}{4} \times \frac{w}{4}$. The cells in each sub-block are scrambled using SM to provide security and randomness in block mapping. To eliminate mapping to the same block, a cell in the left half of L which is mapped to itself is swapped with the corresponding cell in the right half. Similarly, cells in the right half which are mapped to itself are swapped with cells in the left half.
3. Cover image generation: PTB conversion technique [12] is used to generate the cover image C of size $2h \times 2w \times c$ from the original image I . Further C is divided into 4×4 blocks C_1, C_2, \dots, C_N in row-major order.
4. Watermark generation and embedding: Watermark of length 24 bits is generated for each channel d in C_i 's mapping block C_j and placed in C_j after encrypting the watermark.
 - (a) TLC computation: The TLC is computed by using pixels in the image block and a randomly selected chaotic terms in ST . It ensures sensitivity of TLC towards changes in image contents and key which in turn helps to resist copy-move,

image splicing, VQ and collage attacks. To compute TLC, the sequence ST is partitioned into N sets and a set is chosen at random using random numbers in $[1, N]$ generated based on key k_2 , image identifier and d . The block C_j is divided into 2×2 sub-blocks and matrix A of size 2×2 is formed using the first pixel from each sub-block of C_j in row-major order. A is changed to A' by applying XOR operation to each element with $[(ST_l \times 10^{k_3}) \bmod 2^b]$ where $ST_l, l = 1, 2, 3, 4$ are the terms in selected subset of ST . Then $msv' = [msv \times (2^{2b} - 1) / 2(2^b - 1)]$ is computed, where msv is the maximum singular value of A' obtained by applying SVD. msv' is converted into binary format of length $2b$ and partitioned into 8 groups. The members of each group are XORed together to form 8 bit TLC.

- (b) SRC generation: Applying the same procedure in TLC computation, matrices A and B are created from the block C_i and its partner block C_k respectively. Here $k = i + \frac{N}{2}$ if $i \leq \frac{N}{2}$ and $i - \frac{N}{2}$ otherwise. The 7 Most Significant Bits (MSBs) of A 's average and B 's average together form 14 bit SRC.
- (c) Watermark formation: A 24 bit watermark $W = TLC || SRC || SD$ is computed where SD represents two bits from sensitive data.
- (d) Watermark encryption: The generated watermark W for each channel d is encrypted using the sequence SE . The sequence is partitioned into N sets and a set R is selected using random numbers in $[1, N]$ generated based on key k_4 , image identifier and d . Compute $t_l = [(R_l \times 10^{k_5}) \bmod 2^{12}]$ for $l = 1, 2$ in which key $k_5 > 3$. The binary values of t_1 and t_2 are concatenated to form t . Then t and W are XORed to obtain T . A permutation p is computed based on the new indices obtained after sorting the last 24 terms in R . The encrypted watermark W' is obtained by applying p to the bits in T . Since the chaotic sequence SE is sensitive to the control parameter and initial condition the encrypted watermark is highly key sensitive and secure.
- (e) Watermark embedding: The mapped block C_j is divided into 2×2 sub-blocks and the first pixel of each sub-block is classified as unchangeable pixels and remaining as changeable pixels. The encrypted watermark W' is placed in 2 LSBs of changeable pixels. A smoothing function is applied to improve the watermarked image quality. The difference between the changeable pixel and the unchangeable pixel is computed. The value of changeable pixel is decreased by 4 if the result is 3 and increased by 4 if the difference is -3 .

2.2. Tamper detection and localization

The tamper detection and localization procedure includes watermark extraction, decryption and a multilevel tamper localization process. The suspected image G is divided into non overlapping blocks $G_i, i = 1, 2, \dots, N$ of size 4×4 .

1. Watermark extraction: The watermark E for each channel is extracted from the 2 LSBs of 12 changeable pixels in the block G_i in row-major order.
2. Watermark decryption: To decrypt the extracted watermark E corresponding to the mapped block of G_i, t and p are computed as per the watermark encryption procedure in section 2.1. The inverse permutation of p is applied to E and the result is XORed with t to obtain the decrypted watermark. The first 8 bits of the decrypted

watermark form the TLC, the next 14 bits indicate SRC and the remaining 2 bits represent bits from the sensitive data.

3. Tamper localization: Initially each block G_i is considered as valid.

Level 1: The block G_i is divided into 2×2 sub-blocks and the first sub-block is chosen. The 2 LSBs from a changeable pixel are extracted and inserted into the 2 LSBs of the unchangeable pixel. Then the smoothing function is applied. If the obtained value is different from the value of changeable pixel, the block is considered invalid. Otherwise, repeat the process with the remaining changeable pixels. If no mismatch is found, repeat the process with the next sub-block. This level helps to resist image splicing attack.

Level 2: For each valid block after the first level, the extracted TLC is compared with the computed TLC. If a mismatch is found, the block is considered invalid. Since TLC depends on block contents and position this level helps to resist copy-move attack.

Level 3: For each block that remained as valid after the second level, if at most one among the neighboring blocks is valid, the block is changed as invalid.

Level 4: For each valid block G_i , the average value of unchangeable pixels is computed and the 7 MSBs are stored in a . Then a is compared with the first 7 bits in the SRC of the mapped block if G_i is located in the upper half, otherwise with the last 7 bits in the SRC. If a mismatch is found G_i is changed as invalid. For a valid block, if the number of invalid neighboring blocks is greater than or equal to the number of invalid neighboring blocks of its mapped block, the block is considered invalid. If only less than 3 neighboring blocks of an invalid block are invalid, the block is turned as valid and if more than 5 neighboring blocks of a valid block are invalid, it is considered invalid. Since embedded recovery information enables block-wise dependency, this level helps to resist VQ and collage attacks.

A block is considered as tampered if it becomes invalid either in level 3 or 4.

2.3. Image recovery

The recovered image R of size $h \times w \times c$ is initialized with zeros and divided into 2×2 blocks $R_i, i = 1, 2, \dots, N$.

Level 1: For each i , if G_i is not tampered, then the unchangeable pixels in the sub-blocks constitute pixels in R_i . For a tampered block G_i with untampered mapping block G_j , R_i is obtained from the retrieved SRC of G_j . If G_i is located in the upper half, $b - 7$ zeros are appended to the first 7 bits in SRC to form b bits intensity. Otherwise, the intensity is obtained from the last 7 bits in SRC. The new intensity value is assigned to R_i . If G_i and G_j are tampered and the mapping block G_k of G_i 's partner block is not tampered, then SRC is retrieved from G_k and R_i is formed as per the previous case.

Level 2: The blocks which are not recovered in the first stage are recovered using an inpainting algorithm [16].

3. Experimental results

To evaluate the performance of the proposed scheme for tamper detection and recovery, the experiments are conducted on 96 grayscale and 61 color images selected from CVG-UGR database [17]. The proposed scheme is implemented in MATLAB R2017b

environment. In the experiments, the parameters are randomly initialized as $k_1 = (x_0, \mu) = (0.8566, 3.998)$, $k_2 = 100$, $k_3 = 6$, $k_4 = 101$, $k_5 = 6$ and image identifier is the file name in the database.

Watermarked image quality analysis: Peak Signal to Noise Ratio (PSNR) is used to measure the imperceptibility of the watermark in the cover image. The average PSNR of watermarked image for grayscale images is 45.37 dB and is enhanced to 47.46 dB after applying smoothing function. In the case of color images, it is enhanced to 47.32 dB from 44.98 dB.

Resistance against tampering attacks: To measure the resistance of the proposed scheme against tampering attacks, we used three metrics viz. True Positive Rate (TPR) or Tamper Detection Rate (TDR), True Negative Rate (TNR) and precision (p) [5]. PSNR is used to measure the similarity between recovered and original images. Copy-move, image splicing, VQ and collage attacks [5] are simulated in each watermarked image at various tamper ratios. **Figure 1** shows the visual performance of proposed scheme on tamper localization and recovery on sample images from CVG-UGR database [17].

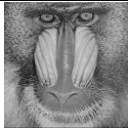
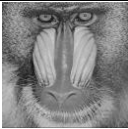

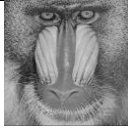






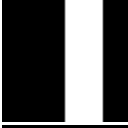













Watermarked image	PSNR (dB)	Tampered image	Tamper ratio	Tamper localization	TPR TNR p	Recovered image	PSNR (dB)
	47.62		0%		100 100 100		∞
	47.61		10%		100 100 100		40.16
	47.61		30%		100 100 100		36.86
	47.62		50%		99.99 100 100		31.04
	47.62		70%		99.99 100 100		26.1
	47.61		90%		100 100 100		23.3

Figure 1. Visual performance of the proposed scheme on tamper localization and recovery on sample images from CVG-UGR database [17].

Table 1 shows the average TPR, TNR and p under various tamper ratios on grayscale images and color images separately. The obtained results are above 99.9% and 100% in

almost all cases. This shows that the proposed scheme has high resistance against copy-move, image splicing, VQ and collage attacks.

Table 1. Tamper detection performance against various attacks

Attacks	Metric	Grayscale images					Color images				
		Tamper ratio (%)									
		10	30	50	70	90	10	30	50	70	90
Copy-move	TPR	99.9933	99.9926	99.9965	99.9917	99.995	100	100	100	99.9997	100
	TNR	100	100	100	100	100	100	100	100	100	100
	p	100	100	100	100	100	100	100	100	100	100
Image Splicing	TPR	99.9959	99.9976	99.9968	99.9991	99.9983	100	100	100	100	100
	TNR	100	100	100	100	100	100	100	100	100	100
	p	100	100	100	100	100	100	100	100	100	100
VQ	TPR	99.9964	99.994	99.9972	99.9979	99.9968	100	100	100	100	100
	TNR	100	100	100	100	100	100	100	100	100	100
	p	100	100	100	100	100	100	100	100	100	100
Collage	TPR	100	99.9969	99.9969	99.9997	99.9978	100	100	100	100	100
	TNR	100	100	100	100	100	100	100	100	100	100
	p	100	100	100	100	100	100	100	100	100	100

Comparison with state-of-the-art schemes: The performance of the proposed scheme is compared with recent schemes [12,7,6,8,4] in terms of watermarked and recovered image quality. To compare the recovery performance, each watermarked image is replaced with white pixels at various tamper ratios from left to right. Table 2 shows the average PSNR of the watermarked image and recovered image on grayscale images. From the table, it is evident that the watermarked image quality of the proposed scheme is higher than other schemes. The proposed scheme and scheme proposed by Parah et al. [12] provide lossless recovery of original image from an untampered watermarked image. It is also observed that the recovered image quality of the proposed scheme is better than the other schemes under extensive tampering.

Table 2. Performance comparison of proposed scheme with state-of-the-art schemes

Schemes	Watermarked image quality	Recovered image quality with various tamper ratio									
		0	10	20	30	40	50	60	70	80	90
Parah et al. [12]	46.39	∞	16	12.76	10.75	9.32	8.2	7.3	6.47	5.76	5.14
Qin et al. [7]	44.12	44.12	38.18	35.82	33.8	32.41	31.26	19.7	18.81	13.32	12.77
Haghighi et al. [6]	46.41	42.81	35.25	32.74	30.8	29.22	28.32	22.62	18.49	15.56	13.05
Rajput and Ansari [8]	32.52	28.22	24.93	22.59	21.69	20.49	21.22	10.77	7.1	5.39	4.8
D. Singh and S. K. Singh [4]	37.24	37.24	16.37	12.99	10.97	9.56	8.43	7.42	6.6	5.84	5.2
Proposed scheme	47.46	∞	40.2	36.32	34.01	32.16	30.79	28.74	26.91	25.07	22.87

4. Conclusion

A highly secure fragile watermarking based image authentication scheme for tamper localization, recovery of tampered regions and hiding sensitive information is proposed in this paper. The generated fragile watermark is highly sensitive to any modification in the image. This scheme ensures lossless recovery of the original image and hidden data from an untampered received image. Experimental results show that the proposed scheme generates watermarked image with high perceptual quality and can locate the tampered regions precisely. This scheme has high resistance against copy-move, image splicing, VQ and collage attacks. It has better recovered image quality under extensive

tampering as compared with state-of-the-art schemes and can be applied to color, grayscale and DICOM images. The proposed scheme can be used in sensitive applications which need image authentication scheme that ensures 100% recovery of image and hidden data, high security, precise tamper localization and high recovery rate.

Acknowledgement

Authors extend gratitude to the Department of Higher Education, Government of Kerala, for granting the research fellowship.

References

- [1] Raj NN, Shreelekshmi R. Blockwise fragile watermarking schemes for tamper localization in digital images. In 2018 International CET Conference on Control, Communication, and Computing (IC4); 2018. p. 441-446.
- [2] Raj NN, Shreelekshmi R. Security Analysis of Hash Based Fragile Watermarking Scheme for Image Integrity. In 2019 2nd International Conference on Intelligent Computing, Instrumentation and Control Technologies (ICICT); 2019. p. 651-654.
- [3] Singh D, Singh SK. DCT based efficient fragile watermarking scheme for image authentication and restoration. *Multimedia Tools and Applications*. 2017; 76(1): p. 953-977.
- [4] Singh D, Singh SK. Block Truncation Coding based effective watermarking scheme for image authentication with recovery capability. *Multimedia Tools and Applications*. 2019; 78(4): p. 4197-4215.
- [5] Raj NN, Shreelekshmi R. A survey on fragile watermarking based image authentication schemes. *Multimedia Tools and Applications*. 2021; 80: p. 19307-19333.
- [6] Haghighi BB, Taherinia AH, Harati A. TRLH: Fragile and blind dual watermarking for image tamper detection and self-recovery based on lifting wavelet transform and halftoning technique. *Journal of Visual Communication and Image Representation*. 2018; 50: p. 49-64.
- [7] Qin C, Ji P, Chang CC, Dong J, Sun X. Non-uniform watermark sharing based on optimal iterative BTC for image tampering recovery. *IEEE MultiMedia*. 2018; 25(3): p. 36-48.
- [8] Rajput V, Ansari IA. Image tamper detection and self-recovery using multiple median watermarking. *Multimedia Tools and Applications*. 2020; 79(47): p. 35519-35535.
- [9] Shen JJ, Lee CF, Hsu FW, Agrawal S. A self-embedding fragile image authentication based on singular value decomposition. *Multimedia Tools and Applications*. 2020; 79(35): p. 25969-25988.
- [10] Gul E, Ozturk S. A novel pixel-wise authentication-based self-embedding fragile watermarking method. *Multimedia Systems*. 2021;: p. 1-15.
- [11] Kim C, Yang CN. Self-embedding fragile watermarking scheme to detect image tampering using AMBTC and OPAP approaches. *Applied Sciences*. 2021; 11(3): p. 1-21.
- [12] Parah SA, Ahad F, Sheikh JA, Bhat GM. Hiding clinical information in medical images: a new high capacity and reversible data hiding technique. *Journal of biomedical informatics*. 2017; 66: p. 214-230.
- [13] Geetha R, Geetha S. Embedding electronic patient information in clinical images: an improved and efficient reversible data hiding technique. *Multimedia Tools and Applications*. 2020; 79(19): p. 12869-12890.
- [14] Klema V, Laub A. The singular value decomposition: Its computation and some applications. *IEEE Transactions on automatic control*. 1980; 25(2): p. 164-176.
- [15] Mandal MK, Banik GD, Chattopadhyay D, Nandi D. An image encryption process based on chaotic logistic map. *IETE Technical Review*. 2012; 29(5): p. 395-404.
- [16] Shen J, Chan TF. Mathematical models for local nontexture inpaintings. *SIAM Journal on Applied Mathematics*. 2002; 62(3): p. 1019-1043.
- [17] The CVG-UGR Image Database. [Online]. [Accessed on January 2021]. Available from: <https://ccia.ugr.es/cvg/dbimagenes/index.php>.

Securing Mobile Adhoc Networks from Black-Hole Attacks

Fahmina Taranum^{a,1} and Khaleel Ur Rahman Khan^b

^a*Muffakham Jah College of Engineering and Technology, Osmania University, India*

^b*Ace Engineering College, Jawahar Lal Nehru Technological University, India*

Abstract. MANETs are in-secure and vulnerable to attacks, as it lacks a central trusted authority. Providing security to such a network becomes an essential task and formulate the origin of the proposed work. The proposed system attempts to secure MANETs using route validation and cryptographic techniques. One of the most crucial, and primary concerns in today's times is to be able to detect an attacker at its initial stages. With this focus point in mind, the approach used is to prevent such an attacks by detecting in initial stage and preventing from network degradation. The novelty of the proposal is the use of cryptographic techniques for improving the security, along a reverse-AODV for reducing path fail correction, and machine learning concepts for validation of results. Many of the existing malware detection techniques proposed by the researchers were executed either on machine independent platform, or on an available dataset with machine dependent approaches. This drawback has been addressed in the existing proposal, where in machine learning is used with self-generated data-set, to eliminate contingent problems. The proposed system includes a network that is free from malware. Justification of the results were generated using classifier tools that were trained with the obtained dataset. For secured communication, an Elliptical curve cryptographic algorithm is applied to reverse ad-hoc on-demand distance vector with reverse multiple route replies that have been generated from the destination to the source node. An investigation to ensure the correct delivery of data can be done by diverting the traffic through the shortest alternative secured path. The metrics used for statistical analysis include average transmission-delay, overhead, packet forwarding rate and packet-delivery-rate, based on which the conclusion is theorized for the detection. The major finding includes the process of selecting an appropriate condition for detecting a malicious node, observing the network behavior with varying number of suspicious nodes and then validating the correctness. The implementation gives us varied results, both when the suspicious node is deferred for some time, and then on its complete elimination. The limitation of the proposal is that the suspicious nodes are uncoordinated.

Keywords. ECC, AODV, R-AODV, Enhanced AODV

1. Introduction

Networking is a vast domain, which deals with finite number of interconnected devices for communication through wired or wireless medium. The communication is managed by using data transmission through nodes in MANETs. A mobile adhoc network consists of mobile devices that move freely in multi-direction, while communicating among each other. MANET is a dynamically configurable system where the mobile

¹ Corresponding Author, Fahmina Taranum, Muffakham Jah College of Engineering and Technology, Osmania University, India; Email: ftaranum@mjccollege.ac.in

nodes are bridged to each other via wireless links. They do not have any definite infrastructure and is with no centralized administrative authority to monitor the network. MANET can serve as a standalone network or can also be a fragment of some larger network.

With the furtherance in mobile technology in future generation, people will have a facilely, widespread, and non-discrete access to information heading towards secure communication. In the modern society, with the advancement in technologies there is an increase in the issues to be addressed. Paucity of security is one of the major issues in MANET. Security includes the discerning of possible attacks, threats and sensitivity of the system against illicit access and alterations. The attacker may drop or access data packets with wrong intention. The attacks on the MANETs can identified based on norms like location, type, behavior, intention or on the layer onto which they befall, etc. The issues encountered like limited wireless transmission range, hidden terminal problems, and packet loss due to reasons like transmission errors, mobility-induced, route changes, and battery constraints. There has been huge amount of work done by the researchers in Manets using in-secure AODV routing Protocols. The designed strategy is novel as it highlights the new approach showing the various aspects of selecting the path using routing protocols, authentication of route and node, followed by validation process. Malicious attacks in the network need to be examined by exploring its type, aim, nature, cause and effects to handle security threats in an appropriate way. The attack could be just for an acquaintance or with fortitude to maltreatment a network. The type of attack implemented is black-hole, in which the traffic is attracted by the node using false dissemination and destination is kept deprived of the transmission. Black hole usually assimilates traffic of the network around it and tries to harm the network by reducing the performance metrics of the system.

The simulators used for implementation includes Ns2, Qualnet and Matlab. The proposal portrays the usage of DYMO routing protocol which provide a specific and much effective route with reduced power consumption. Dymo is a power aware routing algorithm works on the concept of selecting the shortest path to destination for transmitting data. The second novelty of the system is Reverse-AODV in which a reverse route exploration works to select the path from destination to the source node for storing multicast routes that can be used in case of link or path failure. The route obtained after applying R-AODV eliminates the scope of any malicious path selection since the routing table is updated simultaneously by comparison with the highest sequence number or the shortest hop count. The path thereby prevents Black-hole nodes to participate in reverse route discovery, thereby eliminating the chances of attacker in the path. The purpose of adding encryption is to secure the data transmission. The collaboration of the strategies used is Reverse AODV with ECC and validation of the datasets is done using Matlab tool as shown in figure 1. The approach used to do the route discovery of safe path is shown in figure 2.

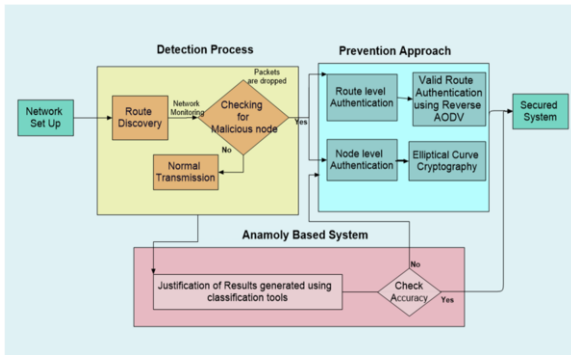


Figure 1. Architecture of the System

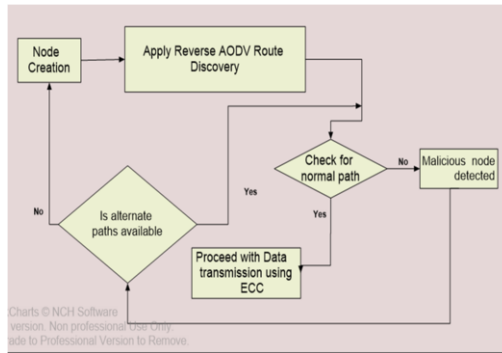


Figure 2. Malicious node detection using R-AODV

Black hole node consumes less time for packet processing and queuing delay. Packet processing here being the time for processing and extracting content from packet header, or time consumed during lookup between routing tables or to link to next node, and queuing delay refers to the time spent in queue at layers (Network and MAC) before it is forwarded to physical layer.

Q.D (Queuing delay) is the time a job waits in a queue until it can be executed, P.D (Processing delay) is the time router takes to process the packet header or time for one bit to travel, T.D (Transmission delay) is the time taken to put a packet onto link. It depends on length of packet and bandwidth of network, which can also be considered in designing. The average packet processing delay and queueing delay time threshold value is represented as ΔdTh .

Black hole attack is detected by checking the following conditions:

- If $\Delta d < \Delta dTh$, then the node is said to be authenticated, otherwise non-authenticated
- If the node is not authenticated, then the conditions (i) and (ii) mentioned below are checked for the possibility of black hole attack
- If $Th < R$, where R is the broadcasting radius of the node, H is the hop distance, $Th = \text{distance}(S, D) / H$, where distance (S, D) is the Euclidian distance
- If $DSN < (sn_{max} + \mu)$, where sn_{max} is the maximum SN value of all entries in routing table and μ is the number of data flows

If both the two conditions are true, then the node is said to be honest, otherwise it is considered a black hole node.

2. Literature Survey

This section of the chapter presents a literature study to highlight the work explored and implemented by researchers. The idea is to fetch the limitation or area of further extension, and then to compare it with the existing approaches. The promising technological areas identified for the proposed system during the literature addresses intrusion detection, prevention and validation.

In [1] the Fuzzy logic is used to define rules for filtering an attacker. It is a way of representing information as it appears in human mind. In [2] the proposal is to deactivate the attacker in its worst effecting period and outcomes are justified using Anomaly based method. The Authors in [3] have worked on validating the accuracy of the results generated. Author in [4] has worked on multiple traffic generators and has evaluated performance in normal and malicious scenarios, the extension to the work would be to coordinate the attackers. In [5] Rmayti et al. accords a scenario of using a coordinated behavior through tunnel for worm hole attack, which is adapted here to check the performance degradation in coordination. Poongothai et al. in [6] aimed at designing an Anomaly based detection system for Routing attacks in MANETs to identify the normal or attacker nodes in the system using different values in the class, i.e. class with different values to represent behaving nodes. V.Saranya et al. in [7] aimed to eliminate a misbehaving node by using a reverse route tracing algorithm and the data is routed through an alternate path. ECC algorithm is used for authentication and integrity. Thanh Tu and Thai et al in [8] has worked on the threshold of the formula for distance and hop count to get the shortest path. Ningrinla et al. in [9] has used the concept of monitoring the behavior using neighbors to detect and eliminate a malicious node from transmission. This idea is applied in the proposal to take a node in a loop of deactivation upon detecting its anomalous nature. Nagendranath and Ramesh et al. in [10] has used a packet leash mechanism to detect the intruder, but the system was prone to fake replies too. This drawback is catered by using multicast approach for route reply in our proposal. Opinder et al. in [11], proposed that for each node with public and private key used for encrypting and decrypting transmitted data with ECC. Dhiraj et al. in [12] has proposed a detection and mitigation approach against Black-hole attacks using DYMO routing protocol.

3. Proposed System

The overview of the proposed approach is depicted in figure 1. Algorithm 1 is used for route level authentication and algorithm 2 for secure data transmission.

Algorithm 1 (EA-AODV)

- Step 1: Route Discovery Process: Source sends RREQ towards Destination
- Step 2: If intermediate node N_{in} receives RREQ, Forwards to $N_{in} + 1$, end if;
- Step 3: If Destination is reached, then it responds with RREP end if;

- Step 4: Source gets RREP from various paths P_m , $m=1, 2, \dots, N$
 For each path P_m
 For each intermediate N_{in} along P_m source computes the per hop time
 S computes Euclidian distance between every two nodes
 Calculate $Th = \text{Euclidian Distance} / \text{No. of Hops}$ end for; end for;
 Step 5: If $\text{Threshold} < \text{per hop time}$ then N_{in} is authenticated else
 If $(Th < R)$ and $DSN < (sn_{max} + \mu)$ then N_{in} is a non-poisonous
 else N_{in} is a malicious
 Remove N_{in} from the routing table of P_m end if; end if;
 Step 6: Fetch an alternate path for valid shortest route from routing table or
 invoke new route discovery process.
 Step 7: Use the validation techniques to test the results

Algorithm 2 (Elliptical Curve Cryptography for Secured Data Transmission)

- Step 1: Point Compression for Y, $Y = Y \% 2$ //selecting a point on curve
 Step 2: Point Decompression for y using x and y
 $Z = (X3 + X + 6) \% p$, $Dy = Z3$, $Dy = dy \% p$, If $(y - dy) \% 2 == 0$
 then $dy = dy$ else $Dy = p - dy$ end if;
 Step 3: Encryption using public key //Selecting co-ord for data enc/dec
 $kp = \text{rand} \% \text{endseq}$; //Identifying point kP's and kQ's seq. No.
 $kq = (\text{rand} * q) \% \text{end seq}$; (where q is the quotient =4) Calling the point
 compress on x and y coordinate of kp Cipher text is $((kpx), \text{compress}(kpy),$
 $quo, kqx \% p)$
 Step 4: Decryption
 i. Decrypted point is $mx, my, pdy = \text{ptdecomp}(x,y)$;
 ii. $\text{Intmedpt} = (\text{key} * \text{arr}[x][pdy]) \% 13$; //calc seq no. of intermediate Pt
 iii. $qu = quo$; for i, j in 0.10 if $(\text{arr}[i][j] == \text{medpt})$ then
 $mx = i; my = j$; end if, end for;

The security to data transmission is applied by data encryption and decryption using logarithmic functions at the multiple points on the curve. ECC is difficult to broken down and even harder to assume. It is based and generated using mathematical logic and hence difficult to predict by an intruder. Finally, the result-set is imported to Matlab for justification of correct detection.

4. Results and Analysis

The results generated using the algorithms are statistically represented by parameters like Packet Delivery Ratio, Overhead, Throughput, Drop and Packet Forwarding Ratio.

$$PDR\% = \frac{\text{No.of collected packets}}{\text{No.of dispatched packets}} * 100 \tag{1}$$

$$\text{Overhead} = \text{No. of Routing packets} \div \text{No. of received datapackets} \tag{2}$$

$$\text{Drop} = (\text{No. of packets sent}) - (\text{No. of packets Received}) \quad (3)$$

$$\text{Packet forwarding rate} = (\text{No. of pack. received}) \div (\text{No. of pack. forwarded}) * 100 \quad (4)$$

$$\text{Throughput} = \text{No. of packets dispatched} \div \text{second} \quad (5)$$

$$Q.D = \text{no. of packets} * \text{size of packet} / (2 * BW) \quad (6)$$

4.1 Result Analysis with Algorithm 1

Attacks are targeted in the system to design it counteract and to provide security. The attack can be a member or an outsider, targeting the network to cause harm to it or retrieve information. The type of attack implemented, detected and avoided in the proposal is the Black hole attack. Additionally, security is added to the path through which the data is to be transmitted. In the Route Request process of route discovery, the source node initiates transmission by broadcasting a RREQ message searching for destination node, after which the destination node unicasts the route reply to the source node. This path is cached in the routing table for packet transmission from source to destination node. The route validity is checked using the destination sequence number and hop count generated in RREP. (In addition the detection of a malicious node assumes that the attacker pretends to take less propagation and queuing delay)

Authentication mechanism helps in checking the validity of the route using the following conditions,

- Actual neighbor: Two nodes N_j and N_k are actual neighbors, if $d(N_j, N_k) < \min(RN_j, RN_k)$; where R is the radius of coverage
- Nodes are said to be normal, if they are neighbors
- $DSN \leq \max(D.Seqno., \mu)$, where μ represents in & out node traffic

In figure 3 throughput is analyzed for avoidance scenario with different simulation times. The inferences are EA-AODV out performs with 258 kbps, VRA-AODV with 84 kbps and AODV with 42 kbps maximum The Higher Packet forwarding ratio determines the drop and signifies that the packets are not furthered.

In figure 4 packet forwarding ratio is analyzed for detection scenario with varying simulation time. The values noted for EA-AODV is 74% maximum, VRA-AODV is 29% maximum and AODV a hike of 18%, where VRA references [8] in bibliography. The equations (1) to (6) are used in the result analysis

The figure 5 depicts a comparative analysis of all the four classifiers (Decision tree(DT), KNN (K nearest neighbor), SVM (Support vector machine) and NN (Neural networks)). From the graph it is clearly perceived that the SVM model holds high accuracy rates compared to the rest of the algorithms. The models are trained with datasets where nodes possess mobility speeds of 5, 10, 15, 20 and 25 seconds.

From the Figure 6, it is clearly interpreted that for any value of speed the SVM provides the highest accuracy rates comparatively. As this network is significantly populated with an increase number of malicious nodes, which are prone to attack network; it results in decrementing the accuracy rate of the network.

4.2 Results for Algorithm 2

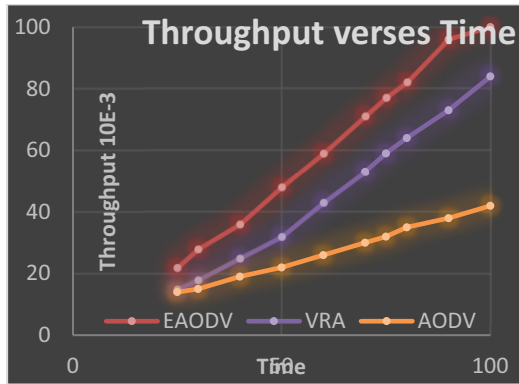


Figure 3. Comparison of Throughput

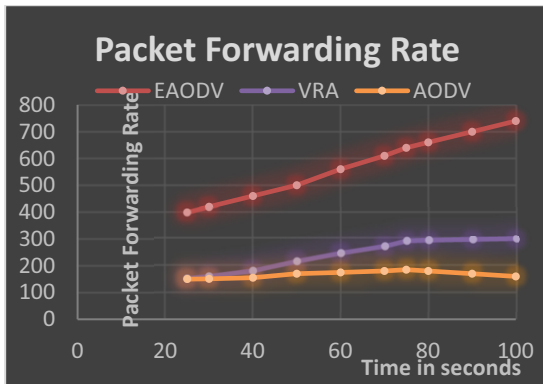


Figure 4. Packet Forwarding Rate

For both the prevention(p) and attack(a) scenario. It can be inferred from the graphs that the performance analysis is better, when a secured path is selected for data transmission. The analysis in figure 7 and figure 8 helps us to conclude that the loss rate is reduced and overhead is brought to zero after applying the prevention mechanism on selecting the sheltered path. Overhead is determined by the number of routing packets. In case of detection scenario with respect to change in simulation time in figure 8 the proposed method shows more overhead compared to the existing ones. The avoidance scenario is experimented over varying number of attackers and multiple simulation time. The reverse R-AODV end to end delay is as shown in figure 9. The delay is initially greater and later becomes linear. As the reverse path is cached at the source node in the R-AODVs, the rediscovery is not initiated unless all the reverse stored paths are used, hence the proposal is considered efficient. The throughput is compared between a Black-hole(green) and reverse AODV(red) with interpretation that after applying the reverse path algorithm, about a tremendous increase in the throughput is seen in figure 10.

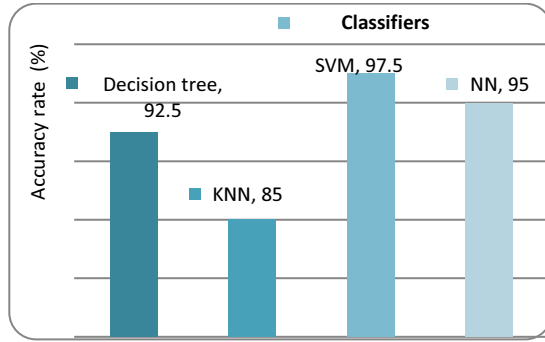


Figure 5. Accuracy versus Classifiers.

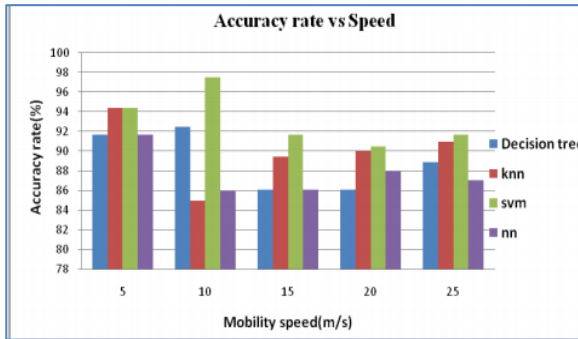


Figure 6. Accuracy versus Speed.

To design a better algorithm for prevention of malicious node, appropriate performance analysis parameters must be selected. Any malicious activity degrades the performance, but the parameters used are different for varying type of attacks. The attack type implemented in this proposal is Black hole in which the traffic sinks at the malicious node. The aim of this malicious node is to attract the traffic by making a false or fake dissemination in the network about having the short path. The node further affects the network transmission by retaining or by dropping the data, which results in the drop of packet forwarding rate. In [4] author has selected the height of antenna as ≥ 3 meter to capture the traffic along with increasing the storage of the buffer size of the node as parameters to inhibit malicious behavior. Figure 6 depicts the results obtained with different classifiers on varying speed of the mobile nodes to analyze the accuracy and it has been found that SVM performs the best in all the considered classifiers. The self-generated data from the network simulator is used to check the best classifier for prediction. The classes used in training are binary in nature with 0 for normal and 1 for malicious.

Advanced routing protocol like DYMO is a popular reactive routing protocol in wireless networks, developed with aim to enhance the performance of ad-hoc network by being more energy efficient. Unlike secure protocols, DYMO lacks the security related features like authentication, integrity, and confidentiality. DYMO has certain vulnerabilities which makes security a major concern here. Outside attackers interfere and interrupt the legitimate traffic due to an open nature of wireless medium. One of such widely known attacks is the Black hole attack. As security is a major concern in wireless

networks, it is provided in the proposal at the node level and at route level by using some encryption algorithms like ECC. Open Shortest Path First(OSPF) routing protocol can also be used to apply security in networks as it includes or inherits authentication facilities as MD5 and simple authentication mechanisms to prevent against the Black hole attack. but OSPF protocol does not support wireless networks

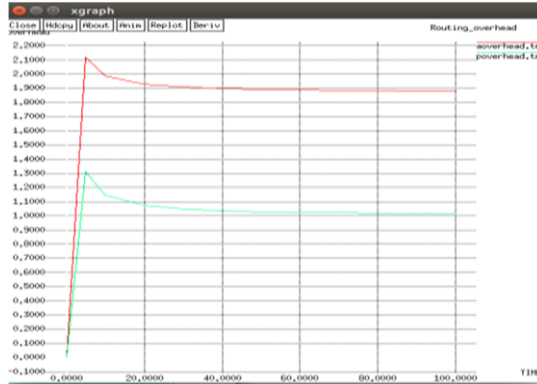


Figure 7. Loss-Ratio for Attack and Prevent.

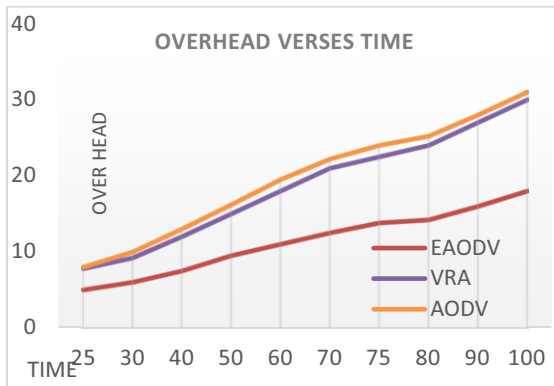


Figure 8. Overhead with Attack and prevention.

When ECC is used to make the transmission secure, it is observed that the throughput gives better values on comparison with AODV. The complete work is implemented in Adhoc wireless networks. The graphs depicted in figure 9 and 10 signifies that the results show a better analysis when the network is secured using prevention algorithm. The security can be applied at the node level or the route level. ECC helps to secure the data at the transmission level using the process of encryption and decryption based on mathematical logistics. The throughput is compared between a Black-hole (in green) and reverse AODV (in red) with conclusion that after applying the reverse path algorithm, about a tremendous increase in the throughput is noted.

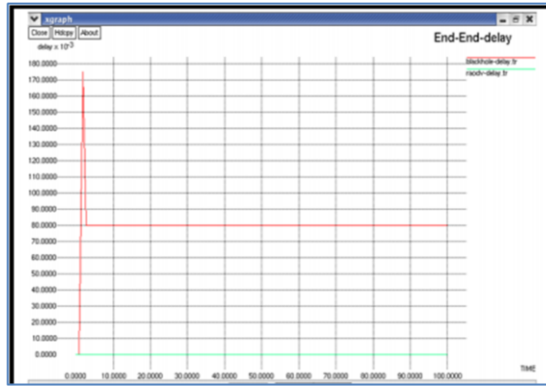


Figure 9. End to End Delay

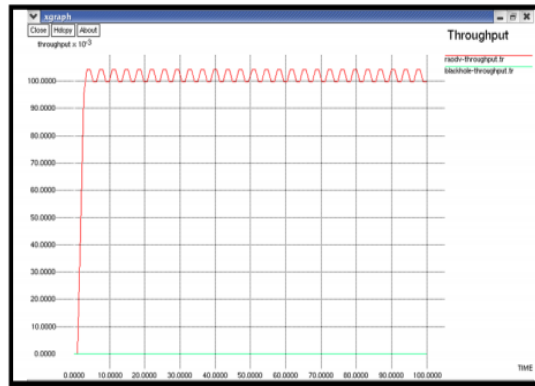


Figure 10. Throughput with ECC and R-AODV

5. Conclusion

The collaboration of two algorithms yields a secured system with good performance metrics. R-AODV helps in storing the routing information of each node thereby reducing the time taken to reinitiate the route discovery process using request retires and helps in transmitting the data at a faster rate when compared to AODV. Further the addition of ECC helps to increase the security of the data transmission, thereby making it difficult for the intruder to interpret the data. The results obtained from these algorithms are imported as data-sets to Matlab to check its efficiency and was found to give good accuracy with SVM classifier. The extension to this work could be to implement coordinated attacks.

References

[1]. Zainab, Fahmina Taranum and Khaleel Ur Rahman. Legitimate-path Formation for AODV under black hole attack in MANETS. Fourth International Conference on Electronics, Communication and Aerospace Technology; ISBN: 978-1-7281-6386-4. 2021 Dec.; p. 1489-1496.

- [2]. Fahmina Taranum, Ayesha Sarvath and Noora Ali. Detection and Prevention of Blackhole node. International Conference on Electronics, Materials Engineering and Nano-Technology; IEEE Xplore. 2020 Oct.; ISBN:978-1-7281-9287-1.
- [3]. Hajira, Fahmina Taranum and Khaleel Ur Rahman. Detection and Interception of Black Hole Attack with Justification using Anomaly based Intrusion Detection System in MANETs. International Journal of Recent Technology and Engineering; ISSN: 2277-3878. 2019 Sept.; 8(2s11). p. 2392-2398.
- [4]. Fahmina Taranum and Khaleel Ur Rahman. Maneuvering Black hole attack using different traffic generators in MANETs. Intelligent Systems Technology and Applications; Springer Germany; 2019 Feb.
- [5]. M. Rmayti, Y. Begriche, Rida Khatoun and Lyes Khoukhi. Graph-Based Wormhole Attack Detection in MANETs. 4th International Conference on Mobile and Secure Services; 2018. p. 1-6.
- [6]. T. Poongothai and K. Jayarajan. Intrusion Detection System for Mobile Ad Hoc Networks using Cross Layer and Machine Learning Approach. International Journal of Computer Applications; 2018; 179(34). p. 5-13.
- [7]. V. Saranya and S.Sharmila. Detection of Black-Hole Attack in MANETs using AODV & Path Tracing Algorithm. International Journal of Pure and Applied Mathematics; 2018; 119(12). p.1355-1371.
- [8]. Thanh Tu and Thai Ngoc Luong. VRA-AODV- Routing Protocol Detects Black-hole& Gray Hole Attacks in Mobile Ad Hoc Network. Journal of Computers; 2018 Feb.; 13(2). p. 222-235.
- [9]. Ningrinla Marchang, Raja Datta and Sajal K Das. A Novel Approach for Efficient Usage of Intrusion Detection System in Mobile Ad Hoc Networks. IEEE Transactions on Vehicular Technology; 2017; 66(2). p. 1684-1696.
- [10]. M. V. S. S Nagendranath, B. Ramesh and V. Aneesha. Detection of Packet Dropping and Replay Attacks in MANET. International Conference on Current Trends in Electronics & Commun'n; 2017. p. 933-938.
- [11]. Opinder Singh, Singh J. and Singh R. Multi-Level Trust Based Intelligence Intrusion Detection System to Detect the Malicious Nodes using Elliptic Curve Cryptography in MANET. Springer; 2018. p. 51-63.
- [12]. Dhiraj Nitnaware and Anitha Thakur. Black-hole Attack Detection & Prevention Strategy in DYMO for MANET. 3rd International Conference On Signal Processing & Integrated Networks, 2016; p. 279- 284.

Performance Evaluation of Radar Range-Bearing Centroid Processing Using Time Series Analysis

Nguyen VAN LOI¹, Tran QUOC TUAN, Tran TRUNG KIEN,
Tran VAN TRUONG, Tran VU HOP

^a*Radar Center, Viettel High Technology Industries Corporation, Hanoi, Vietnam*

Abstract. The paper deals with a problem of performance evaluation of the range-bearing centroid processing for a surveillance radar. First, we review several techniques for centroid processing that are Moving window estimator, Beam shape centroid estimator, Center of mass correlation and Recursive least-squares centroid estimator. Then we point out that the range root-mean-square error (RMSE) and bearing RMSE are not sufficient for performance evaluation of the range-bearing centroid processing. Further, a new parameter using time series analysis for evaluation of structural stability of the centroid processing is proposed. As an illustration, a test with data from an X-band coastal surveillance radar is given.

Keywords. Radar measurement, plot extractor, centroid processing, time series analysis

1. Introduction

Radar [1] is a system that uses the radio waves to detect the objects of various types such as aircraft, spacecraft, guided missiles, ships, motor vehicles, weather formations and terrain. A radar system consists of a transmitter producing electromagnetic waves in the radio or microwaves domain, a transmitting antenna, a receiving antenna (for a pulse radar the same antenna is used for transmitting and receiving) and a receiver and processor (see Figure 1).

¹ Corresponding Author. E-mail: loinv12@viettel.com.vn

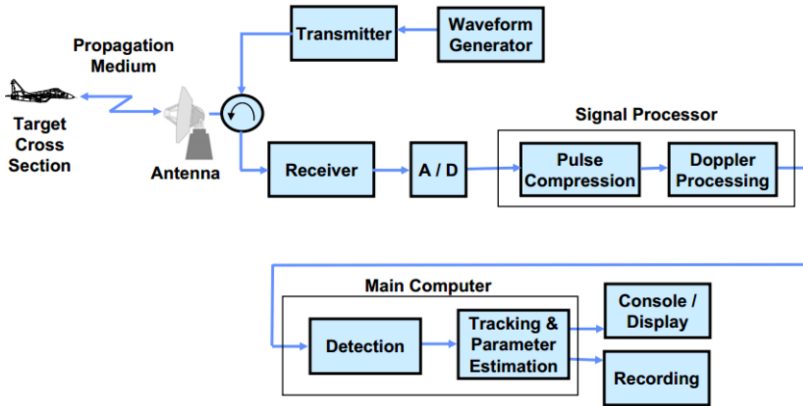


Figure 1. Radar block diagram [2]

The block “Detection” in Figure 1 contains the “Plot detector” and the “Plot extractor” modules (see Figure 2).

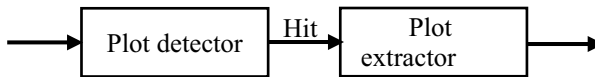


Figure 2. “Detection” block [3]

When the antenna scans across any target, there may be threshold crossings at the “Plot detector” in several inter pulse periods, and in several adjacent range and azimuth resolution cells. The output of “Plot detector” is called *detected hits*. The “Plot extractor” (or range-bearing centroid processing, centroid processing) takes the output of the signal processor of a radar system. Its function is to correlate all threshold crossings (all detected hits), grouping together all those which appear to come from the same target and to estimate range-bearing centroid for generating plot reports such as range, azimuth, power and radial velocity information on all validated targets. Then, the plot reports are used as input for “Tracking and Parameter estimation” block (see Figure 1) to perform object’s trajectories which are displayed on the radar monitor. The more accurate plot reports of range-bearing centroid processing are, the better performance of a radar system is.

The present paper deals with the problem of performance evaluation of the “Plot extractor”. Since the “Plot extractor” has an important role for the performance of a radar system, there are a lot of numbers in the literature concerning the problem of range-bearing centroid processing (see [4-8,10-12]). However, for performance evaluation there is only an approach mentioned in the literature which is based on the range and azimuth (bearing) RMSEs. As illustration in Section 2 (see Figure 7) the range and bearing RMSEs are not sufficient for evaluation of centroid processing. In fact, the target plot reports over scans form a time series and any break-point (change-point) will strongly influence to the “Tracking and Parameter estimation” block. But the range and bearing RMSEs do not give us information about the existence of change-points in a time series. In this paper, a new parameter using time series analysis for evaluation of structural stability of range-bearing centroid processing is introduced.

The paper is organized in the following way. In the next section, we recall the common approaches for range-bearing centroid processing and its evaluation. The main contribution of the paper is presented in section 3. Last section gives out the conclusion and future works.

2. Related works

The “Moving window estimator” is one of the earliest methods of correlating hits to form plot reports (see [4,5]). For each pulse repetition time (PRT), the detected hits are stored as “1”s in the range-cell dimension (see Figure 3). At every range cell, a window in the time-cell dimension is applied to count the number of “1” that are present in the window. The size of the window equals the number of reflected pulses when the radar antenna scans across a target. The target azimuth is estimated by (see [4,6]):

$$\hat{B}(k) = \frac{B(k_1)+B(k_2)}{2} \tag{1}$$

where $B(k_1)$ and $B(k_2)$ are the beginning and end azimuth angles of the targets.

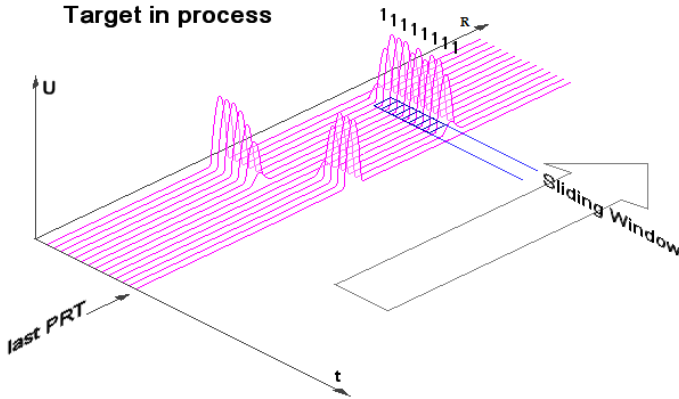


Figure 3. Moving window estimator process [5]

The moving window estimator has many disadvantages. For example, the estimated azimuth in (1) depends only on the first and last detected azimuths of the target. Therefore, the error of the estimated azimuth does not significantly decrease with increasing signal-to-noise ratio.

To avoid the disadvantages of the Moving window estimator, the “Beam shape centroid estimator” based on the collection of association and clustering algorithm was introduced for surveillance radar with coherent processing (see [7, 8]). However, both the Moving window and Beam shape centroid estimators give only the target azimuth estimate, it can not be applied for high range resolution radars, i.e. targets may spread over several adjacent range cells. For these cases, a more modern plot processor needs to be used for the correlation process than the simple sliding window.

One possible method is the Center of mass correlation [9]. The correlator is grouped first in range direction and then in azimuth direction (see Figures 4-6). The plot report is computed by using the center of mass of the signal processor output.

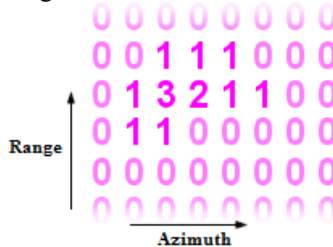


Figure 4. The Signal Processor provides hits including information about received power [9]

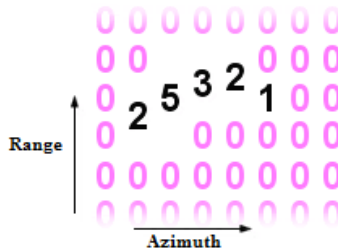


Figure 5. A range correlation provides groups [9]

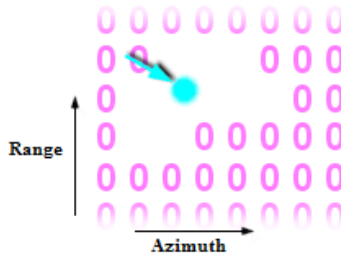


Figure 6. An azimuth correlation provides plots [9]

Some extensions of the *Center of mass correlation* can be found in [8-12].

For evaluation of the above mentioned methods researchers use the simulation data and calculate the range *root-mean-square error* (*range RMSE*) and bearing *RMSE*. However, the range-bearing centroid processing produces a series of time-dependent plot reports for each target (at every radar scan a plot for each target is reported). Therefore, the range and bearing RMSEs may not be enough to evaluate performance of the range-bearing centroid processing. Figure 7 presents two time series with the same RMSEs. But they have different behaviors. In fact, one of them (the dash-line) contains a shock (change-point), i.e. it is not structural stable.

So, in relation with the performance evaluation of range-bearing centroid processing there is a need to consider new parameters than RMSEs. In the next section, we propose the use of time series analysis for this purpose.

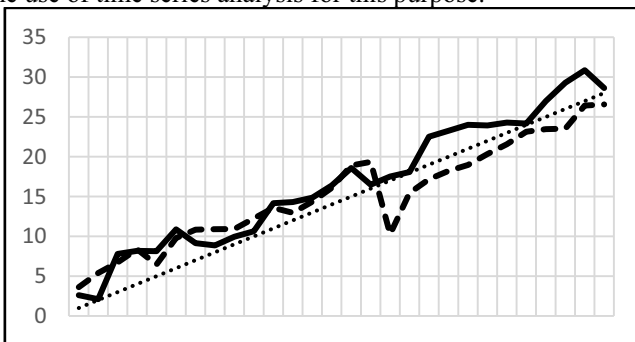


Figure 7. Two time series have the same RMSEs, but different behaviors. The dash-line series has a change-point.

3. Application of time series analysis for performance evaluation of range-bearing centroid processing

Let $\{(R(k), B(k), P(k))\}$ be the range (in meter), bearing angle (in degree) and power (in Watt) of a target centroid (target plot report) at radar scan k . Three time series are available for analysis that are $\{(R(k))\}$, $\{(B(k))\}$ and $\{(R^4(k)P(k))\}$. The reason for considering the series $\{(R^4(k)P(k))\}$ follows from the radar equation. It is well known (see [13], [14]) that the received signal power reflected from a target is determined by

$$P_r = \frac{P_t G_t G_r \sigma \lambda^2}{(4\pi)^3 R^4} \tag{2}$$

where:

- P_r is the received signal power (W) at the radar receiver.
- P_t is the radar transmitting power (W).
- G_t, G_r are the gain of the transmitting and receiving antennas, respectively.
- σ is the radar cross section (m^2).
- λ is the wavelength (m) of the radar electromagnetic energy.
- R is the target range (m).

From (2) it follows that $P_r R^4$ is (theoretical) constant if the radar cross section σ does not change. Two types of targets satisfied for the analysis are (see Figure 8):

- Type 1: targets that move along a straight line toward or away from the radar.
- Type 2: targets that move with a constant range to the radar.

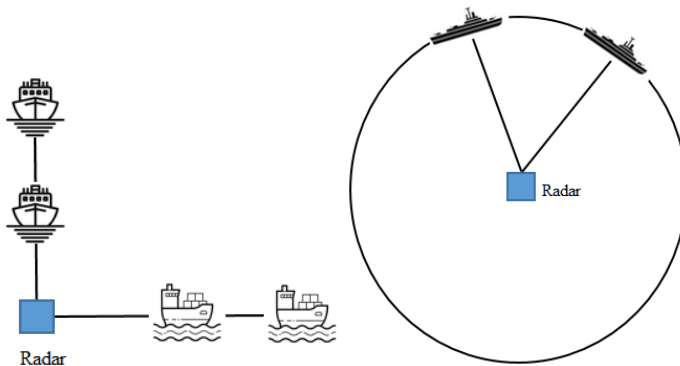


Figure 8. Illustration of targets of Type 1 (left) and of Type 2 (right)

The targets of type 1 and type 2 have (theoretical) constant radar cross section. Moreover, targets of type 1 do not change their bearing angles, so their series of bearing angles are useful for analysis while targets of type 2 do not change their ranges, so their series of ranges are used for evaluation.

We propose the *new approach for the performance evaluation* of the range-bearing centroid processing, which consists of

- accuracy evaluation using range RMSE and bearing RMSE;
- structural stability evaluation using time series analysis.

The Change-Point Ratio (CPR) is used for the evaluation of structural stability. Three values of CPR are estimated, that are bearing CPR (for a target of type 1), range CPR (for a target of type 2) and power CPR (for both types):

$$\text{Range CPR} = \frac{\text{number of change - points of series } \{R(k)\}}{\text{Total number of points in series } \{R(k)\}}$$

$$\text{Bearing CPR} = \frac{\text{number of change - points of series } \{B(k)\}}{\text{Total number of points in series } \{B(k)\}}$$

$$\text{Power CPR} = \frac{\text{number of change - points of series } \{P(k)R^4(k)\}}{\text{Total number of points in series } \{P(k)R^4(k)\}}$$

The Matlab function *findchangepts* is applied for detection of change-points (see [15-17]). This function minimizes

$$J(K) = \sum_{r=0}^K \sum_{i=k_r}^{k_{r+1}-1} \Delta(x_i; \chi([x_{k_r} \cdots x_{k_{r+1}-1}])) + \beta K$$

Where K is the number of change-points; k_0 and k_K are respectively the first and the last samples of the data; Δ and χ denote the deviation measurement and the empirical estimate which depend on the statistical property. For example,

- if ‘Statitlcal property’ is specified as ‘mean’:

$$\Delta(x_i; \chi([x_{k_r} \cdots x_{k_{r+1}-1}])) = (x_i - \text{mean}([x_{k_r} \cdots x_{k_{r+1}-1}]))^2$$

- if ‘Statitlcal property’ is specified as ‘linear’: Let the best-fit line through $x_{k_r}, \dots, x_{k_{r+1}-1}$ be

$$\hat{x}(t) = \frac{S_{xt}|_{k_r}^{k_{r+1}-1}}{S_{tt}|_{k_r}^{k_{r+1}-1}} (t - \text{mean}([t_{k_r} \cdots t_{k_{r+1}-1}])) + \text{mean}([x_{k_r} \cdots x_{k_{r+1}-1}])$$

where

$$S_{xy}|_{k_r}^{k_{r+1}-1} = \sum_{k_r}^{k_{r+1}-1} (x_i - \bar{x})(y_i - \bar{y})$$

$$\bar{x} = \text{mean}([x_{k_r} \cdots x_{k_{r+1}-1}])$$

$$\bar{y} = \text{mean}([y_{k_r} \cdots y_{k_{r+1}-1}])$$

then

$$\Delta(x_i; \chi([x_{k_r} \cdots x_{k_{r+1}-1}])) = (x_i - \hat{x}(t_i))^2$$

Test result. For the test we use the data from an X-band coastal surveillance radar in which the *center of mass correlation* is used for the range-bearing centroid processing. A target of type 1 (see Figure 9) is chosen for the evaluation of structural stability of centroid processing. In real scenario, we understand that type 1 contains all targets that move in a straight line with a small change of their bearing angles (not exceeding 5 degree). The bearing angles of the test target are in the interval from 110 degree to 115 degree.

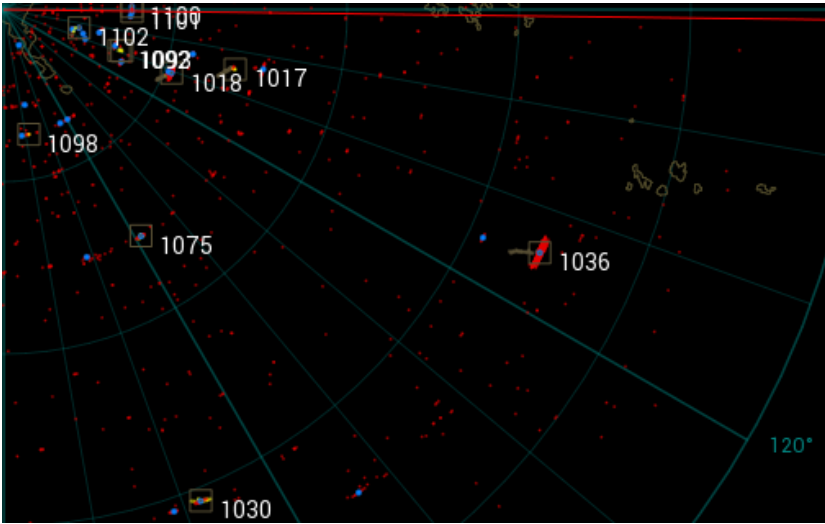


Figure 9. The test target (ID 1036) in the radar screen

Two data series $\{(B(k))\}$ and $\{(P(k)R^4(k))\}$ are used for analysis of structural stability of range-bearing centroid processing. The parameters for the function *findchangepts* are set by:

- ‘Statistic’ = ‘linear’ (since the target moves in a straight line);
- ‘MinThreshold’ = 0 (to find all possible change-points);
- ‘MinDistance’ = 30 (to reject the random noises in the change-points. The value 30 means that minimum number of samples between change-points is 30, or equivalent to 5 minutes of radar scan data. Each radar scan is 10 seconds).

The test results are given in Figures 10 and 11.

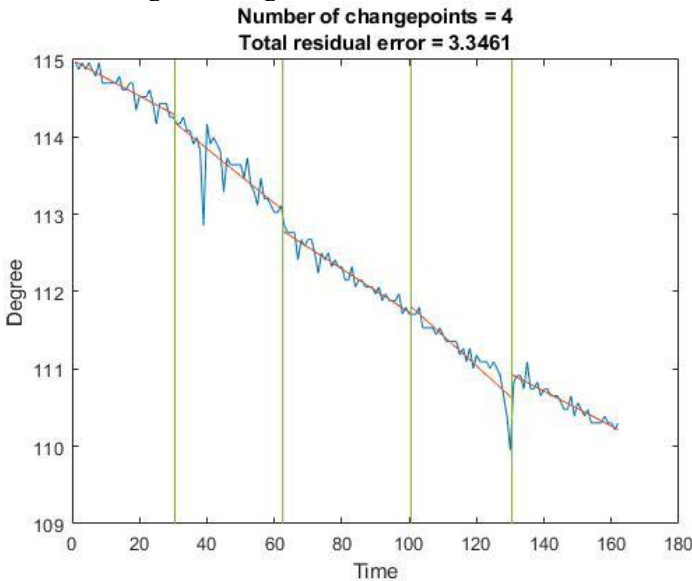


Figure 10. The change-points for the series $\{(B(k))\}$ of the test target. Bearing CPR = 4/162.

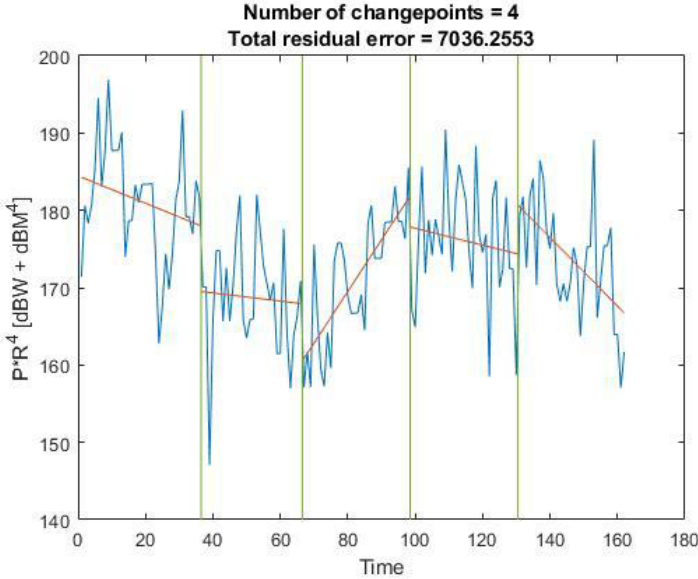


Figure 11. The change-points for the series $\{(P(k)R^4(k))\}$ of the test target. Power CPR = 4/162.

From Figures 10 and 11 it follows that the series $\{(B(k))\}$ and $\{(P(k)R^4(k))\}$, and hence the range-bearing centroid processing, are not structural stable. The causes of the instability of range-bearing centroid processing may occur in “Plot detector” or “Plot extractor” (see Figure 2). If the causes are in “Plot extractor” the radar designers need to use another centroid processing algorithm to avoid the structural instability. For comparison, it is clear that the evaluation method used in [4]-[12] could not be able to detect the change-points while the proposed method gives us the detailed structural stability of the centroid processing. The instability of the centroid processing will lead to a poor performance of “Tracking and Parameter estimation” block.

4. Conclusion and Future works

We have proposed a new (offline) approach for evaluation of range-bearing centroid processing for a radar system that consists of the accuracy evaluation using range and bearing RMSEs and the structural stability evaluation using time series analysis. A test with data from an X-band coastal surveillance radar is given for illustration.

In future works, we will study the online performance evaluation and its application for automatic calibration of a radar system. This will use the online time series analysis which is intensively investigated recently.

Acknowledgement. The authors would like to thank the reviewers for their valuable comments and suggestions to improve the manuscript.

References

- [1] <https://en.wikipedia.org/wiki/Radar>
- [2] O'Donnell RM. Introduction to Radar Systems. Massachusetts Institute of Technology: MIT OpenCourseWare. 2007; <http://ocw.mit.edu>
- [3] <https://www.radartutorial.eu/10.processing/sp08.en.html>
- [4] Walker CM, Atkin J, Bickel H. Comparative evaluation of several azimuth estimating procedures using digital processing and search radar simulation. IRE Transactions on Aeronautical and Navigation Electronics. 1958 Jun; p. 114-121.
- [5] <https://www.radartutorial.eu/10.processing/sp11.en.html>
- [6] Galati G, Struder FA. Angular accuracy of the binary moving window radar detector. IEEE Transactions on Aerospace and Electronic Systems; 1982 July; 18: 416-422.
- [7] Cole EL, Hodges MJ, Oliver RG, Sullivan AC. Novel accuracy and resolution algorithms for the third generation MTD. Proc. of the 1986 National Radar Conference; 1986; p. 41-47.
- [8] Slocumb BJ. Surveillance radar range-bearing centroid processing. Proc. SPIE 4473; Signal and Data Processing of Small Targets 2001; 2001 Nov. 26th.
- [9] <https://www.radartutorial.eu/10.processing/sp13.en.html>
- [10] Slocumb BJ, Macumber DL. Surveillance radar range-bearing centroid processing: Part II, Merged measurements. Proc. SPIE 6236; Signal and Data Processing of Small Targets 2006; 2006 Apr.
- [11] Jian T, Xu X, Zhang L, Han Z. Two algorithms of plots centroid based on mass centre. J. of Air Force Radar Academy 2009; 23: 20-21.
- [12] Liu HB, Li JB, Zhang P. A new algorithm of plots centroid for radar targets. Proc. of 9th Int. Congress on Image and Signal Processing, BioMedical Engineering and Informatics; Datong, China; 2006 Oct. 15-17, p. 1268-1272.
- [13] Skolnik MI (Edi. in Chief). Radar Handbook. McGraw-Hill; 2008; 3rd ed.
- [14] Barton DK. Radar Equation for Modern Radar. Artech House; 2013.
- [15] Lavielle M. Using penalized contrasts for the change-point problem. Signal Processing 2005; 85: 1501-1510.
- [16] Killick R, Fearnhead P, Ecklay IA. Optimal detection of change-points with a linear computational cost. J. of the American Statistical Association 2012; 107(500): 1590-1598.
- [17] <https://www.mathworks.com/help/signal/ref/findchangepts.html>

The Prime Ideals of QMV*-algebras

Yingying Jiang^a and Wenjuan Chen^{a,1}

^a*School of Mathematical Sciences, University of Jinan, P.R. China*

Abstract. QMV*-algebras were introduced in [1] as the extension of MV*-algebras and quasi-MV algebras. In the present paper, the concepts of prime ideals are introduced into QMV*-algebras. First some related properties of QMV*-algebras are listed. Second the properties of prime ideals of a QMV*-algebra are investigated and the quotient algebra by a prime ideal is characterized. Finally, maximal ideals of a QMV*-algebra are discussed.

Keywords. MV*-algebras, Quasi-MV algebras, QMV*-algebras, Ideals, Prime ideals

1. Introduction

Chang had introduced MV*-algebras in [2] for the purpose of providing a convenient abstraction of the algebra defined on the real interval $[-1, 1]$, endowed with the truncated addition $\zeta \oplus v = \max\{-1, \min\{1, \zeta + v\}\}$ and the negation $-\zeta$, paralleling similar work done for MV-algebras in [3]. In [4], the algebraic study of MV*-algebras had been made by Lewin et al., and the logic L^* as a natural extension of Łukasiewicz logic was also investigated in [5]. On the other hand, quasi-MV algebras deriving from quantum computation were introduced in [6] and they were another generalization of MV-algebras. Since they were proposed, lots of properties of quasi-MV algebras were investigated in [7–10] and their corresponding logics were discussed in [11]. In [6], a standard completeness theorem for a quasi-MV algebra was shown: an equation holds in any quasi-MV algebra if and only if it holds in the standard quasi-MV algebra \mathbf{D} . The standard quasi-MV algebra \mathbf{D} whose universe is the set $\mathcal{C}_1 = \{\langle \zeta, v \rangle \in \mathbf{R} \times \mathbf{R} \mid (1 - 2\zeta)^2 + (1 - 2v)^2 \leq 1\}$ is a subalgebra of the standard quasi-MV algebra \mathbf{S} and \mathbf{S} is defined as follows: $\mathbf{S} = \langle [0, 1] \times [0, 1]; \oplus, ', 0, 1 \rangle$ where $\langle \zeta, v \rangle \oplus \langle \kappa, \lambda \rangle = \langle \min\{(1, \zeta + \kappa), \frac{1}{2}\}, \langle \zeta, v \rangle' = \langle 1 - \zeta, 1 - v \rangle, 0 = \langle 0, \frac{1}{2} \rangle$ and $1 = \langle 1, \frac{1}{2} \rangle$.

Notice that the universe of \mathbf{S} is $[0, 1] \times [0, 1]$, it is natural to ask whether we can generalize it to $[-1, 1] \times [-1, 1]$. What is the relationship between the new algebraic structure and \mathbf{S} ? More general, whether we can generalize quasi-MV algebras similarly as MV*-algebras extended MV-algebras. If we can, whether new algebraic structures can be obtained by quasi-MV algebras? In order to solve these questions, we introduced QMV*-algebras in [1] as an extension of quasi-MV algebras. Meanwhile, QMV*-algebras can also be viewed as a generalization of MV*-algebras.

It is well-known that ideals, especially prime ideals, play an important part in studying the algebraic structures. To take a closer look of QMV*-algebras, we introduce the

¹Corresponding Author: Wenjuan Chen, School of Mathematical Sciences, University of Jinan, No.336 West Road of Nan Xinzhuang, 250022 Jinan, Shandong, P.R. China; E-mail: wjchenmath@gmail.com.

notions of prime ideals into QMV*-algebras in the present paper. The properties of prime ideals of a QMV*-algebra are investigated and the quotient algebra using a prime ideal is characterized. The maximal ideals of a QMV*-algebra are also discussed. All results obtained in this paper will generalize the known results in MV*-algebras and expand the contents in quasi-MV algebras.

2. Preliminary

This section recalls some results of QMV*-algebras which will be used in what follows.

Definition 2.1. [1] Let $\Gamma = \langle \Gamma; \oplus, -, 0, 1 \rangle$ be an algebra of type $\langle 2, 1, 0, 0 \rangle$. If for any $\zeta, v \in \Gamma$, we define

$$\begin{aligned} \zeta^+ \in \Gamma \text{ with } \zeta^+ \oplus 0 &= (\zeta \oplus 0)^+ = 1 \oplus ((-1) \oplus \zeta), \\ \zeta^- \in \Gamma \text{ with } \zeta^- \oplus 0 &= (\zeta \oplus 0)^- = (-1) \oplus (1 \oplus \zeta), \\ \zeta \sqcup v &= (\zeta^+ \oplus (-\zeta^+ \oplus v^+)^+) \oplus (\zeta^- \oplus (-\zeta^- \oplus v^-)^+), \end{aligned}$$

and the following equations hold for any $\zeta, v, \kappa \in \Gamma$,

$$\begin{aligned} \text{(QMV*1)} \quad \zeta \oplus v &= v \oplus \zeta, \\ \text{(QMV*2)} \quad (1 \oplus \zeta) \oplus (v \oplus (1 \oplus \kappa)) &= ((1 \oplus \zeta) \oplus v) \oplus (1 \oplus \kappa), \\ \text{(QMV*3)} \quad (\zeta \oplus 1) \oplus 1 &= 1, \\ \text{(QMV*4)} \quad (\zeta \oplus v) \oplus 0 &= \zeta \oplus v, \\ \text{(QMV*5)} \quad \zeta \oplus v &= (\zeta^+ \oplus v^+) \oplus (\zeta^- \oplus v^-), \\ \text{(QMV*6)} \quad 0 &= -0, \\ \text{(QMV*7)} \quad \zeta \oplus (-\zeta) &= 0, \\ \text{(QMV*8)} \quad -(\zeta \oplus v) &= (-\zeta) \oplus (-v), \\ \text{(QMV*9)} \quad -(-\zeta) &= \zeta, \\ \text{(QMV*10)} \quad (-\zeta \oplus (\zeta \oplus v))^+ &= -(\zeta^+) \oplus (\zeta^+ \oplus v^+), \\ \text{(QMV*11)} \quad \zeta \sqcup v &= v \sqcup \zeta, \\ \text{(QMV*12)} \quad \zeta \sqcup (v \sqcup \kappa) &= (\zeta \sqcup v) \sqcup \kappa, \\ \text{(QMV*13)} \quad \zeta \oplus (v \sqcup \kappa) &= (\zeta \oplus v) \sqcup (\zeta \oplus \kappa), \end{aligned}$$

then Γ is called a *quasi-MV* algebra* (QMV*-algebra for short).

Obviously, any MV*-algebra $\Lambda = \langle \Lambda; \oplus, -, 0, 1 \rangle$ is a QMV*-algebra. Conversely, if $\zeta \oplus 0 = \zeta$ holds in a QMV*-algebra Γ , then it is immediate to see that Γ is an MV*-algebra.

On a QMV*-algebra $\Gamma = \langle \Gamma; \oplus, -, 0, 1 \rangle$, we can define some operations on Γ by $\zeta \sqcap v = -((-\zeta) \sqcup (-v))$, $\zeta \ominus v = \zeta \oplus (-v)$ and $|\zeta| = \zeta \sqcup (-\zeta)$ for any $\zeta, v \in \Gamma$. We also define a relation $\zeta \leq v$ by $\zeta \sqcup v = v \oplus 0$, or equivalently, $\zeta \sqcap v = \zeta \oplus 0$. It is obvious to see that the relation \leq is reflexivity and transitivity. For any $\zeta \in \Gamma$, if $0 \leq \zeta$, then the element ζ is called *non-negative* and if $\zeta \leq 0$, then the element ζ is called *non-positive*. We know that a QMV*-algebra does not satisfy the associativity of \oplus in general. However, if ζ and κ are either non-negative or non-positive, then the equality $(\zeta \oplus v) \oplus \kappa = \zeta \oplus (v \oplus \kappa)$ always holds, we call it *restricted associativity* in this case.

Proposition 2.1. [1] Let $\Gamma = \langle \Gamma; \oplus, -, 0, 1 \rangle$ be a QMV*-algebra. Then for any $\zeta, v, \kappa, \lambda \in \Gamma$, we have

$$\begin{aligned} (1) \quad \zeta \oplus v &= (\zeta \oplus 0) \oplus v = \zeta \oplus (v \oplus 0) = (\zeta \oplus 0) \oplus (v \oplus 0), \\ (2) \quad \zeta \sqcap v &= (\zeta \sqcap v) \oplus 0 = (\zeta \oplus 0) \sqcap v = \zeta \sqcap (v \oplus 0) = (\zeta \oplus 0) \sqcap (v \oplus 0), \end{aligned}$$

- (3) $\kappa \ominus (\zeta \sqcup \nu) = (\kappa \ominus \zeta) \sqcap (\kappa \ominus \nu)$ and $\kappa \ominus (\zeta \sqcap \nu) = (\kappa \ominus \zeta) \sqcup (\kappa \ominus \nu)$,
- (4) $(\zeta \sqcup \nu) \ominus \kappa = (\zeta \ominus \kappa) \sqcup (\nu \ominus \kappa)$ and $(\zeta \sqcap \nu) \ominus \kappa = (\zeta \ominus \kappa) \sqcap (\nu \ominus \kappa)$,
- (5) $\zeta \sqcup \zeta = \zeta \oplus 0 = \zeta \sqcap \zeta$,
- (6) $1 \oplus 0 = 1$ and $1 \oplus 1 = 1$,
- (7) $0^+ = 0 = 0^-$,
- (8) $(-\zeta)^+ \oplus 0 = -(\zeta^-) \oplus 0$,
- (9) $\zeta \oplus 0 = (\zeta \oplus 0)^+ \oplus (\zeta \oplus 0)^-$,
- (10) $\zeta \sqcup 0 = \zeta^+ \oplus 0$ and $\zeta \sqcap 0 = \zeta^- \oplus 0$,
- (11) $\zeta^- \leq 0 \leq \zeta^+$,
- (12) $-1 \leq \zeta \leq 1$ and $0 \leq |\zeta| \leq 1$,
- (13) $\zeta \oplus 0 \leq \zeta \leq \zeta \oplus 0$,
- (14) $\zeta \sqcap \nu \leq \zeta \leq \zeta \sqcup \nu$,
- (15) If $\zeta \leq \nu$, then $\zeta^+ \leq \nu^+$, $\zeta^- \leq \nu^-$ and $-\nu \leq -\zeta$,
- (16) If $\zeta \leq \nu$ and $\kappa \leq \lambda$, then $\zeta \oplus \kappa \leq \nu \oplus \lambda$, $\zeta \sqcup \kappa \leq \nu \sqcup \lambda$ and $\zeta \sqcap \kappa \leq \nu \sqcap \lambda$,
- (17) If $\zeta \leq 0$, then $\zeta \oplus 0 = \zeta^- \oplus 0$ and $\zeta^+ \oplus 0 = 0$,
if $0 \leq \zeta$, then $\zeta \oplus 0 = \zeta^+ \oplus 0$ and $\zeta^- \oplus 0 = 0$,
- (18) $\zeta \leq \nu$ iff $0 \leq \nu \ominus \zeta$,
- (19) If $\zeta = \nu$, then $\nu \ominus \zeta = 0$, if $\nu \ominus \zeta = 0$, then $\zeta \oplus 0 = \nu \oplus 0$,
- (20) $(\zeta \oplus \nu^+) \ominus \nu^+ \leq \zeta \leq (\zeta \oplus \nu^+) \oplus \nu^+$,
- (21) $|\zeta| \leq \kappa$ iff $-\kappa \leq \zeta \leq \kappa$.

Let $\Gamma = \langle \Gamma; \oplus, -, 0, 1 \rangle$ be a QMV*-algebra and $\emptyset \neq \Lambda \subseteq \Gamma$. We denote the set $|\Lambda| = \{|\lambda| \mid \lambda \in \Lambda\}$ and define an operation \neg on $|\Lambda|$ by $\neg|\lambda| = 1 \ominus |\lambda|$ for any $|\lambda| \in |\Lambda|$. Below we will discuss the structure of $|\Gamma|$.

Lemma 2.1. *Let $\Gamma = \langle \Gamma; \oplus, -, 0, 1 \rangle$ be a QMV*-algebra. Then $|\Gamma|$ is closed under operations \oplus and \neg .*

Proof. For any $|\zeta|, |\nu| \in |\Gamma|$, then $|\zeta|, |\nu| \in \Gamma$ and we have $|\zeta| \oplus |\nu| \in \Gamma$, so $||\zeta| \oplus |\nu|| \in |\Gamma|$. Since $0 \leq |\zeta| \oplus |\nu|$ by Proposition 2.1(12),(16), we have $-(|\zeta| \oplus |\nu|) \leq 0$, it turns out that $||\zeta| \oplus |\nu|| = (|\zeta| \oplus |\nu|) \sqcup (-(|\zeta| \oplus |\nu|)) = (|\zeta| \oplus |\nu|) \oplus 0 = |\zeta| \oplus |\nu|$, so $|\zeta| \oplus |\nu| \in |\Gamma|$. For any $|\zeta| \in |\Gamma|$, then $|\zeta| \in \Gamma$, it follows that $\neg|\zeta| = 1 \ominus |\zeta| \in \Gamma$, so $|\neg|\zeta|| \in |\Gamma|$. Since $|\zeta| \leq 1$, we have $-1 \leq -|\zeta|$, it turns out that $0 \leq 1 \ominus |\zeta| = \neg|\zeta|$, so $|\neg|\zeta|| = (\neg|\zeta|) \sqcup (-(\neg|\zeta|)) = (\neg|\zeta|) \oplus 0 = \neg|\zeta|$. Hence $\neg|\zeta| \in |\Gamma|$.

Proposition 2.2. *Let $\Gamma = \langle \Gamma; \oplus, -, 0, 1 \rangle$ be a QMV*-algebra. Then $|\Gamma| = \langle |\Gamma|; \oplus, \neg, 0 \rangle$ is an MV-algebra. Moreover, the relation \leq restricted on $|\Gamma|$ is partial-ordering.*

Proof. We only need to check the condition: $\neg(\neg|\zeta| \oplus |\nu|) \oplus |\nu| = \neg(\neg|\nu| \oplus |\zeta|) \oplus |\zeta|$ for any $|\zeta|, |\nu| \in |\Gamma|$. Since $\neg(\neg|\nu| \oplus |\zeta|) \oplus |\zeta| = (1 \ominus ((1 \ominus |\nu|) \oplus |\zeta|)) \oplus |\zeta| = (1 \oplus ((-1 \oplus |\nu|) \oplus (-|\zeta|))) \oplus |\zeta| = (1 \oplus (-1 \oplus (-|\zeta| \oplus |\nu|))) \oplus |\zeta| = (\neg|\zeta| \oplus |\nu|)^+ \oplus |\zeta|$ by restricted associativity and $|\zeta| \sqcup |\nu| = (|\zeta|^+ \oplus (-(|\zeta|^+) \oplus |\nu|^+)^+) \oplus (|\zeta|^- \oplus (-(|\zeta|^-) \oplus |\nu|^-)^+) = |\zeta| \oplus (-|\zeta| \oplus |\nu|)^+$ by Proposition 2.1(12),(17), we have $\neg(\neg|\nu| \oplus |\zeta|) \oplus |\zeta| = |\zeta| \sqcup |\nu|$. Similarly, we can show $\neg(\neg|\zeta| \oplus |\nu|) \oplus |\nu| = |\nu| \sqcup |\zeta|$. Since $|\zeta| \sqcup |\nu| = |\nu| \sqcup |\zeta|$, we get $\neg(\neg|\zeta| \oplus |\nu|) \oplus |\nu| = \neg(\neg|\nu| \oplus |\zeta|) \oplus |\zeta|$. Moreover, if $|\zeta| \leq |\nu|$ and $|\nu| \leq |\zeta|$, then $|\zeta| \sqcup |\nu| = |\nu| \oplus 0 = |\nu|$ and $|\zeta| \sqcup |\nu| = |\zeta| \oplus 0 = |\zeta|$, it turns out that $|\zeta| = |\nu|$, so the relation \leq restricted on $|\Gamma|$ is antisymmetry. Hence the relation \leq restricted on $|\Gamma|$ is partial-ordering.

Definition 2.2. [1] Let $\Gamma = \langle \Gamma; \oplus, -, 0, 1 \rangle$ be a QMV*-algebra. The set $\emptyset \neq L \subseteq \Gamma$ is called an *ideal* of Γ , if L satisfies: (I1) If $\zeta, \nu \in L$, then $\zeta \oplus \nu \in L$; (I2) If $\zeta \in L$, then $\zeta^+ \in L$; (I3) If $\zeta, \kappa \in L$ and $\nu \in \Gamma$ with $\zeta \leq \nu \leq \kappa$, then $\nu \in L$.

Proposition 2.3. [1] Let $\Gamma = \langle \Gamma; \oplus, -, 0, 1 \rangle$ be a QMV*-algebra and L be an ideal of Γ . Then we have

- (1) $0 \in L$, (5) If $\zeta \in L$, then $|\zeta| \in L$,
- (2) If $\zeta \in L$, then $-\zeta \in L$, (6) If $\zeta \oplus \nu \in L$ and $\nu \in L$, then $\zeta \in L$,
- (3) If $\zeta, \nu \in L$, then $\zeta \oplus \nu \in L$, (7) If $\zeta \oplus \nu \in L$ and $\nu \oplus \kappa \in L$, then $\zeta \oplus \kappa \in L$.
- (4) If $\zeta, \nu \in L$, then $\zeta \sqcup \nu \in L$,

Proposition 2.4. Let $\Gamma = \langle \Gamma; \oplus, -, 0, 1 \rangle$ be a QMV*-algebra. If L is an ideal of Γ , then (I3) is equivalent to the following: (I3') If $\zeta \in L$ and $\nu \in \Gamma$ with $|\nu| \leq \zeta$, then $\nu \in L$.

Proof. (I3) \Rightarrow (I3') If $\zeta \in L$ and $\nu \in \Gamma$ with $|\nu| \leq \zeta$, then $-\zeta \in L$ using Proposition 2.3(2) and $-\zeta \leq \nu \leq \zeta$ by Proposition 2.1(21). Thus we have $\nu \in L$ by (I3).

(I3') \Rightarrow (I3) If $\zeta, \kappa \in L$ and $\nu \in \Gamma$ with $\zeta \leq \nu \leq \kappa$, then $|\zeta|, |\kappa| \in L$ using Proposition 2.3(5). Since $\zeta \leq \nu \leq \kappa$, we have $-\kappa \leq -\nu \leq -\zeta$ by Proposition 2.1(15) and then $|\nu| = \nu \sqcup (-\nu) \leq \kappa \sqcup (-\zeta) \leq |\kappa| \sqcup |\zeta|$ by Proposition 2.1(16),(14). Because $|\zeta|, |\kappa| \in L$, we have $|\kappa| \sqcup |\zeta| \in L$ by Proposition 2.3(4). Thus $\nu \in L$ by (I3').

Recall that an ideal L of an MV-algebra $\Lambda = \langle \Lambda; \oplus, -, 0 \rangle$ is a non-empty subset of Λ satisfying: (1) $0 \in L$; (2) If $\zeta, \nu \in L$, then $\zeta \oplus \nu \in L$; (3) If $\zeta \in L$ and $\nu \in \Lambda$ with $\nu \leq \zeta$, then $\nu \in L$.

Proposition 2.5. Let $\Gamma = \langle \Gamma; \oplus, -, 0, 1 \rangle$ be a QMV*-algebra. If L is an ideal of Γ , then $|L|$ is an ideal of $|\Gamma|$.

Proof. Since $0 \in L$, we have $0 = |0| \in |L|$. If $|\zeta|, |\nu| \in |L|$, then $\zeta, \nu \in L$ and then $|\zeta|, |\nu| \in L$ by Proposition 2.3(5), so $|\zeta| \oplus |\nu| \in L$ by Proposition 2.3(3). Since $0 \leq |\zeta| \oplus |\nu|$ by Proposition 2.1(12),(16), we obtain $|\zeta| \oplus |\nu| = ||\zeta| \oplus |\nu|| \in |L|$. If $|\zeta| \in |L|$ and $|\nu| \in |\Gamma|$ with $|\nu| \leq |\zeta|$, then $|\zeta| \in L$ and then $\nu \in L$ by Proposition 2.4, so $|\nu| \in |L|$. Hence $|L|$ is an ideal of $|\Gamma|$.

Let $\Gamma = \langle \Gamma; \oplus, -, 0, 1 \rangle$ be a QMV*-algebra. For any $\emptyset \neq \Lambda \subseteq \Gamma$, we define $\langle \Lambda \rangle = \bigcap \{L \mid \Lambda \subseteq L \text{ and } L \text{ is any ideal of } \Gamma\}$. Then $\langle \Lambda \rangle$ is the least ideal of Γ which contains the set Λ and is called the *ideal generated* by Λ . For any $\zeta \in \Gamma$, denote $0 \cdot \zeta = 0$, $1 \cdot \zeta = \zeta$ and $n \cdot \zeta = (n - 1) \cdot \zeta \oplus \zeta$ for some integer $n \geq 2$.

Proposition 2.6. [1] Let $\Gamma = \langle \Gamma; \oplus, -, 0, 1 \rangle$ be a QMV*-algebra and $\emptyset \neq \Lambda \subseteq \Gamma$. Then $\langle \Lambda \rangle = \{\zeta \in \Gamma \mid |\zeta| \leq |\lambda_1| \oplus |\lambda_2| \oplus \dots \oplus |\lambda_n|, \text{ where } \lambda_1, \lambda_2, \dots, \lambda_n \in \Lambda\}$.

Proposition 2.7. Let $\Gamma = \langle \Gamma; \oplus, -, 0, 1 \rangle$ be a QMV*-algebra. If L is an ideal of Γ and $\lambda \in \Gamma \setminus L$, then we have $\langle L \cup \{\lambda\} \rangle = \{\zeta \in \Gamma \mid |\zeta| \leq |\nu| \oplus n \cdot |\lambda|, \text{ where } \nu \in L \text{ and for some integer } n \geq 1\}$.

Given that L is an ideal of $\Gamma = \langle \Gamma; \oplus, -, 0, 1 \rangle$. For any $\zeta \in \Gamma$, we denote the equivalence class of ζ with respect to L by $\zeta/L = \{\nu \in \Gamma \mid \nu \oplus \zeta \in L\}$ and $\Gamma/L = \{\zeta/L \mid \zeta \in \Gamma\}$. For any $\zeta/L, \nu/L \in \Gamma/L$, we define $(\zeta/L) \oplus_L (\nu/L) = (\zeta \oplus \nu)/L$, $-_L(\zeta/L) = (-\zeta)/L$ and $(\zeta/L) \sqcup_L (\nu/L) = (\zeta \sqcup \nu)/L$, then $\Gamma/L = \langle \Gamma/L; \oplus_L, -_L, 0/L, 1/L \rangle$ is a QMV*-algebra.

Proposition 2.8. *Let L be an ideal of a QMV*-algebra $\Gamma = \langle \Gamma; \oplus, -, 0, 1 \rangle$. Then the quotient algebra Γ/L is an MV*-algebra.*

Proof. We only check the condition: $(\zeta/L) \oplus_L (0/L) = \zeta/L$ for any $\zeta/L \in \Gamma/L$. Since $\zeta/L \in \Gamma/L$, we have $(\zeta/L) \oplus_L (0/L) = (\zeta \oplus 0)/L = \zeta/L$. Indeed, $v \in (\zeta \oplus 0)/L$ iff $v \oplus (\zeta \oplus 0) \in L$ iff $v \oplus \zeta \in L$ iff $v \in \zeta/L$ by Proposition 2.1(1). Hence Γ/L is an MV*-algebra.

Definition 2.3. [1] Let $\Gamma = \langle \Gamma; \oplus, -, 0, 1 \rangle$ and $\Lambda = \langle \Lambda; \oplus, -, 0, 1 \rangle$ be QMV*-algebras. A function $\phi : \Gamma \rightarrow \Lambda$ is called a QMV*-homomorphism, if for any $\zeta, v \in \Gamma$, we have: (1) $\phi(0) = 0$; (2) $\phi(1) = 1$; (3) $\phi(\zeta \oplus v) = \phi(\zeta) \oplus \phi(v)$; (4) $\phi(-\zeta) = -\phi(\zeta)$.

Proposition 2.9. [1] *Let $\Gamma = \langle \Gamma; \oplus, -, 0, 1 \rangle$ and $\Lambda = \langle \Lambda; \oplus, -, 0, 1 \rangle$ be QMV*-algebras and $\phi : \Gamma \rightarrow \Lambda$ be a homomorphism. For any $\zeta, v \in \Gamma$, then*

- (1) $\phi(\zeta \ominus v) = \phi(\zeta) \ominus \phi(v)$, (5) $\phi(\zeta \sqcap v) = \phi(\zeta) \sqcap \phi(v)$,
- (2) $\phi(\zeta^+ \oplus 0) = (\phi(\zeta))^+ \oplus 0$, (6) $\phi(|\zeta|) = |\phi(\zeta)|$,
- (3) $\phi(\zeta^- \oplus 0) = (\phi(\zeta))^- \oplus 0$, (7) *If $\zeta \leq v$, then $\phi(\zeta) \leq \phi(v)$.*
- (4) $\phi(\zeta \sqcup v) = \phi(\zeta) \sqcup \phi(v)$,

Lemma 2.2. [1] *Let $\Gamma = \langle \Gamma; \oplus, -, 0, 1 \rangle$ and $\Lambda = \langle \Lambda; \oplus, -, 0, 1 \rangle$ be QMV*-algebras and $\phi : \Gamma \rightarrow \Lambda$ be a homomorphism. If $\phi(\zeta) = \phi(v)$, then $\zeta \ominus v \in \ker(\phi) = \{\kappa \in \Gamma \mid \phi(\kappa) = 0\}$. Conversely, if $\zeta \ominus v \in \ker(\phi)$, then $\phi(\zeta) \oplus 0 = \phi(v) \oplus 0$.*

Proposition 2.10. [1] *Let $\Gamma = \langle \Gamma; \oplus, -, 0, 1 \rangle$ and $\Lambda = \langle \Lambda; \oplus, -, 0, 1 \rangle$ be QMV*-algebras and $\phi : \Gamma \rightarrow \Lambda$ be a homomorphism. If L is an ideal of Λ , then $\phi^{-1}(L)$ is an ideal of Γ .*

Suppose that L is an ideal of a QMV*-algebra $\Gamma = \langle \Gamma; \oplus, -, 0, 1 \rangle$. We define a function $\phi_L : \Gamma \rightarrow \Gamma/L$ by $\phi_L(\zeta) = \zeta/L$ for any $\zeta \in \Gamma$. Then ϕ_L is the epimorphism, we call it natural homomorphism. Moreover, we have the following results.

Lemma 2.3. *Let L be an ideal of a QMV*-algebra $\Gamma = \langle \Gamma; \oplus, -, 0, 1 \rangle$. If $\phi_L : \Gamma \rightarrow \Gamma/L$ is the natural homomorphism and $v \in \zeta/L$ for any $\zeta \in \Gamma$, then $v/L = \zeta/L$.*

Proof. For any $\kappa \in v/L$, then $\kappa \ominus v \in L$. Since $v \in \zeta/L$, we have $v \ominus \zeta \in L$, it turns out that $\kappa \ominus \zeta \in L$ by Proposition 2.3(7), so $\kappa \in \zeta/L$ which means that $v/L \subseteq \zeta/L$. For any $\kappa \in \zeta/L$, then $\kappa \ominus \zeta \in L$. Since $v \in \zeta/L$, we have $v \ominus \zeta \in L$ and then $\zeta \ominus v \in L$ by Proposition 2.3(2), it turns out $\kappa \ominus v \in L$, so $\kappa \in v/L$ which means that $\zeta/L \subseteq v/L$. Hence $v/L = \zeta/L$.

Proposition 2.11. *Let L be an ideal of a QMV*-algebra $\Gamma = \langle \Gamma; \oplus, -, 0, 1 \rangle$ and $\phi_L : \Gamma \rightarrow \Gamma/L$ be the natural homomorphism. Then $\phi_L(L) = \{0/L\}$ and $L = \ker(\phi_L)$.*

Proof. It is evident that $\{0/L\}$ is an ideal of Γ/L . Now we verify that $\phi_L(L) = \{0/L\}$. For any $v/L \in \phi_L(L)$, there exists $\zeta \in L$ with $v/L = \phi_L(\zeta) = \zeta/L$. Since $v \in v/L = \zeta/L$, we have $v \ominus \zeta \in L$ and then $v \in L$ by Proposition 2.3(6), it turns out that $v \ominus 0 \in L$, so $v \in 0/L$ and then $v/L = 0/L$ by Lemma 2.3. Hence $\phi_L(L) \subseteq \{0/L\}$. Conversely, since ϕ_L is a natural homomorphism and $0 \in L$, we have $0/L = \phi_L(0) \in \phi_L(L)$, so $\{0/L\} \subseteq \phi_L(L)$. Hence $\phi_L(L) = \{0/L\}$. For any $v \in \ker(\phi_L)$, then $\phi_L(v) = 0/L$, we have $v \ominus 0 \in L$ and then $v \in L$, so $\ker(\phi_L) \subseteq L$. Note that $L \subseteq \ker(\phi_L)$, we have $L = \ker(\phi_L)$.

Proposition 2.12. *Let L be an ideal of a QMV*-algebra $\Gamma = \langle \Gamma; \oplus, -, 0, 1 \rangle$. Then the mapping $T \mapsto \phi_L(T)$ is a bijection correspondence between the set of ideals of Γ containing L and the set of ideals of the quotient algebra Γ/L .*

Proof. Suppose that T is an ideal of Γ with $L \subseteq T$. For any $\zeta/L, v/L \in \phi_L(T)$, then there are $\kappa, \tau \in T$ such that $\zeta/L = \phi_L(\kappa)$ and $v/L = \phi_L(\tau)$, we have $(\zeta/L) \ominus (v/L) = \phi_L(\kappa) \ominus \phi_L(\tau) = \phi_L(\kappa \ominus \tau) \in \phi_L(T)$. Moreover, because $(\zeta/L)^+ = (\zeta/L)^+ \oplus 0/L$ and $\kappa^+ \in T$, we get $(\zeta/L)^+ = (\phi_L(\kappa))^+ \oplus 0/L = \phi_L(\kappa^+ \oplus 0) \in \phi_L(T)$. For any $\zeta/L, \lambda/L \in \phi_L(T)$ and $v/L \in \Gamma/L$ with $\zeta/L \leq v/L \leq \lambda/L$, then there exist $\kappa, \omega \in T$ and $\tau \in \Gamma$ such that $\zeta/L = \phi_L(\kappa)$, $v/L = \phi_L(\tau)$ and $\lambda/L = \phi_L(\omega)$. Since $\phi_L(\kappa) \leq \phi_L(\tau) \leq \phi_L(\omega)$, we have $\phi_L(\kappa) = \phi_L(\kappa) \sqcap \phi_L(\tau) = \phi_L(\kappa \sqcap \tau)$ and $\phi_L(\omega) = \phi_L(\tau) \sqcup \phi_L(\omega) = \phi_L(\tau \sqcup \omega)$ by Proposition 2.9(4),(5), it turns out $(\kappa \sqcap \tau) \ominus \kappa \in \ker(\phi_L) = L$ and $(\tau \sqcup \omega) \ominus \omega \in \ker(\phi_L) = L$ using Proposition 2.11. Notice that $\kappa, \omega \in T$ and $L \subseteq T$, we have $\kappa \sqcap \tau \in T$ and $\tau \sqcup \omega \in T$ by Proposition 2.3(6). Since $\kappa \sqcap \tau \leq \tau \leq \tau \sqcup \omega$ by Proposition 2.1(14) and T is an ideal of Γ , we have $\tau \in T$ and then $v/L = \phi_L(\tau) \in \phi_L(T)$. Hence $\phi_L(T)$ is an ideal of Γ/L . For any $\zeta \in T$, we have $\zeta \in \phi_L^{-1}(\phi_L(\zeta)) \subseteq \phi_L^{-1}(\phi_L(T))$. Then $T \subseteq \phi_L^{-1}(\phi_L(T))$. Conversely, for any $\zeta \in \phi_L^{-1}(\phi_L(T))$, we have $\phi_L(\zeta) \in \phi_L(T)$, then there is $v \in T$ such that $\zeta/L = \phi_L(v) = v/L$, it follows that $\zeta \ominus v \in L \subseteq T$. Note that $v \in T$, we have $\zeta \in T$ by Proposition 2.3(6), so $\phi_L^{-1}(\phi_L(T)) \subseteq T$. Hence $T = \phi_L^{-1}(\phi_L(T))$. Now, for any ideal T' of Γ/L , we have $\phi_L^{-1}(T')$ is an ideal of Γ by Proposition 2.10. Meanwhile, since $L = \ker(\phi_L) = \phi_L^{-1}(0/L) \subseteq \phi_L^{-1}(T')$, we have $L \subseteq \phi_L^{-1}(T')$. For any $v \in \phi_L(\phi_L^{-1}(T'))$, then there exists $\zeta \in \phi_L^{-1}(T')$ such that $v = \phi_L(\zeta) \in T'$, so $\phi_L(\phi_L^{-1}(T')) \subseteq T'$. Conversely, for any $v \in T' \subseteq \Gamma/L$, since ϕ_L is surjective, there exists $\zeta \in \Gamma$ such that $v = \phi_L(\zeta)$, we have $\zeta \in \phi_L^{-1}(T')$ and then $v = \phi_L(\zeta) \in \phi_L(\phi_L^{-1}(T'))$, so $T' \subseteq \phi_L(\phi_L^{-1}(T'))$. Hence $\phi_L(\phi_L^{-1}(T')) = T'$.

3. Prime ideals and maximal ideals of QMV*-algebras

In this section, we introduce prime ideals and maximal ideals of a QMV*-algebra and investigate their related properties.

In any QMV*-algebra $\Gamma = \langle \Gamma; \oplus, -, 0, 1 \rangle$, an ideal L of Γ is *prime* if L is proper (i.e., $L \neq \Gamma$) and for any $\zeta \in \Gamma$, either $\zeta^+ \in L$ or $\zeta^- \in L$.

Proposition 3.1. *Let L be a proper ideal of a QMV*-algebra $\Gamma = \langle \Gamma; \oplus, -, 0, 1 \rangle$. Then L is prime iff the quotient algebra Γ/L is totally ordered.*

Proof. Suppose that L is a prime ideal of Γ . For any $\zeta, v \in \Gamma$, then we have $(\zeta \ominus v)^+ \in L$ or $(\zeta \ominus v)^- \in L$. If $(\zeta \ominus v)^- \in L$, then $(v \ominus \zeta)^+ = -(\zeta \ominus v)^- \in L$ by Proposition 2.1(8) and Proposition 2.3(2). Since $(\zeta \sqcup v) \ominus v = (\zeta \ominus v) \sqcup (v \ominus v) = (\zeta \ominus v) \sqcup 0 = (\zeta \ominus v)^+$ and $(\zeta \sqcup v) \ominus \zeta = (\zeta \ominus \zeta) \sqcup (v \ominus \zeta) = 0 \sqcup (v \ominus \zeta) = (v \ominus \zeta)^+$ by Proposition 2.1(4),(10), we have $(\zeta \sqcup v) \ominus v \in L$ or $(\zeta \sqcup v) \ominus \zeta \in L$, it follows that $((\zeta/L) \sqcup (v/L)) \ominus (v/L) = ((\zeta \sqcup v) \ominus v)/L = 0/L$ or $((\zeta/L) \sqcup (v/L)) \ominus (\zeta/L) = ((\zeta \sqcup v) \ominus \zeta)/L = 0/L$. Note that Γ/L is an MV*-algebra, we have $(\zeta/L) \sqcup (v/L) = v/L$ or $(\zeta/L) \sqcup (v/L) = \zeta/L$ by Proposition 2.1(19), so $\zeta/L \leq v/L$ or $v/L \leq \zeta/L$. Hence Γ/L is totally ordered. Conversely, if the algebra Γ/L is totally ordered, then we have $\zeta/L \leq v/L$ or $v/L \leq \zeta/L$ for any $\zeta/L, v/L \in \Gamma/L$, it follows that $(\zeta \sqcup v)/L = v/L$ or $(\zeta \sqcup v)/L = \zeta/L$, so $((\zeta \sqcup v) \ominus v)/L = 0/L$ or $((\zeta \sqcup v) \ominus \zeta)/L = 0/L$ by Proposition 2.1(19) and then $(\zeta \sqcup v) \ominus v \in L$ or $(\zeta \sqcup v) \ominus \zeta \in L$ by Proposition 2.11. Since $(\zeta \ominus v)^+ = (\zeta \sqcup v) \ominus v$ and $(v \ominus \zeta)^+ = (\zeta \sqcup v) \ominus \zeta$, we have $(\zeta \ominus v)^+ \in L$ or $(v \ominus \zeta)^+ \in L$. Hence for any $\zeta \in \Gamma$, we have $\zeta^+ \oplus 0 = (\zeta \ominus 0)^+ \in L$ or $\zeta^- \oplus 0 = -(0 \ominus \zeta)^+ \in L$. Since $\zeta^+ \oplus 0 \leq \zeta^+ \leq \zeta^+ \oplus 0$ and $\zeta^- \oplus 0 \leq \zeta^- \leq \zeta^- \oplus 0$ by Proposition 2.1(13), we have $\zeta^+ \in L$ or $\zeta^- \in L$. So the ideal L of Γ is prime.

Proposition 3.2. *Let V be a prime ideal of a QMV*-algebra $\Gamma = \langle \Gamma; \oplus, -, 0, 1 \rangle$. Then the set of all ideals of Γ/V with respect to the inclusion is totally ordered.*

Proof. It is easy to get that the set of all ideals of Γ/V with respect to the inclusion is partial order. If it is not totally ordered, we may suppose that L, T are ideals of Γ/V such that $L \not\subseteq T$ and $T \not\subseteq L$. So there exist $\zeta/V, v/V \in \Gamma/V$ such that $\zeta/V \in T \setminus L$ and $v/V \in L \setminus T$. Since Γ/V is totally ordered by Proposition 3.1, we have $\zeta/V \leq v/V$ or $v/V \leq \zeta/V$, it turns out that $|\zeta/V| \leq |v/V|$ or $|v/V| \leq |\zeta/V|$. Indeed, if $0/V \leq \zeta/V \leq v/V$, then $-(\zeta/V) \leq 0/V \leq \zeta/V$ and $-(v/V) \leq 0/V \leq v/V$, we have $|\zeta/V| = (\zeta/V) \sqcup (-\zeta/V) = (\zeta/V) \oplus (0/V) = \zeta/V$ and $|v/V| = (v/V) \sqcup (-v/V) = v/V$, so $|\zeta/V| \leq |v/V|$. If $\zeta/V \leq v/V \leq 0/V$, then $\zeta/V \leq 0/V \leq -(\zeta/V)$, $v/V \leq 0/V \leq -(v/V)$ and $0/V \leq -(v/V) \leq -(\zeta/V)$, we have $|\zeta/V| = (\zeta/V) \sqcup (-\zeta/V) = (-\zeta/V) \oplus (0/V) = -(\zeta/V)$ and $|v/V| = (v/V) \sqcup (-v/V) = -(v/V)$, so $|v/V| \leq |\zeta/V|$. If $\zeta/V \leq 0/V \leq v/V$, then we have $-(v/V) \leq 0/V \leq -(\zeta/V)$, so $|\zeta/V| = (\zeta/V) \sqcup (-\zeta/V) = -(\zeta/V)$ and $|v/V| = (v/V) \sqcup (-v/V) = v/V$. Since Γ/V is totally ordered and $-(\zeta/V), v/V \in \Gamma/V$, we have $0/V \leq -(\zeta/V) \leq v/V$ or $0/V \leq v/V \leq -(\zeta/V)$, so $|\zeta/V| \leq |v/V|$ or $|v/V| \leq |\zeta/V|$. The case of $v/V \leq \zeta/V$ can be proved similarly. If $|\zeta/V| \leq |v/V|$, since $v/V \in L$, we have $|v/V| \in L$ by Proposition 2.3(5) and then $\zeta/V \in L$ by Proposition 2.4. Likewise, if $|v/V| \leq |\zeta/V|$, since $\zeta/V \in T$, we have $|\zeta/V| \in T$ and then $v/V \in T$. This is a contradiction with $\zeta/V \notin L$ and $v/V \notin T$. Hence the set of all ideals of Γ/V with respect to the inclusion is totally ordered.

Proposition 3.3. *Let $\Gamma = \langle \Gamma; \oplus, -, 0, 1 \rangle$ be a QMV*-algebra. Then we have:*

- (1) *Any proper ideal of Γ containing a prime ideal is prime.*
- (2) *The set of all ideals of Γ containing a prime ideal is totally ordered by the inclusion.*

Proof. (1) Suppose that L is a proper ideal of Γ and a prime ideal V of Γ with $V \subseteq L$. For any $\zeta \in \Gamma$, we have $\zeta^+ \in V$ or $\zeta^- \in V$, it follows that $\zeta^+ \in L$ or $\zeta^- \in L$. So L is prime.

(2) Suppose that V is a prime ideal of Γ . Then the set of all ideals of Γ/V with respect to the inclusion is totally ordered from Proposition 3.2. Hence we get that the set of all ideals containing V is totally ordered by Proposition 2.12.

Lemma 3.1. *Let $\Gamma = \langle \Gamma; \oplus, -, 0, 1 \rangle$ be a QMV*-algebra. Then for any $\zeta \in \Gamma$ and some integers $n, m \geq 1$, we have $(n \cdot \zeta^+) \sqcap (m \cdot (-\zeta)^+) = 0$.*

Proof. First, we prove $\zeta^+ \sqcap (-\zeta)^+ = 0$ for any $\zeta \in \Gamma$. Since $0 \leq \zeta^+ \sqcap (-\zeta)^+$, we have $0 \sqcap (\zeta^+ \sqcap (-\zeta)^+) = 0 \oplus 0 = 0$. Based on Proposition 2.1(20),(4),(8),(9),(10), we have $\zeta^+ \sqcap (-\zeta)^+ \leq ((\zeta^+ \sqcap (-\zeta)^+) \oplus (-\zeta)^+) \oplus (-\zeta)^+ = ((\zeta^+ \oplus (-\zeta)^+) \sqcap 0) \oplus (-\zeta)^+ = ((\zeta^+ \oplus \zeta^-) \sqcap 0) \oplus (-\zeta)^+ = (\zeta \sqcap 0) \oplus (-\zeta)^+ = \zeta^- \oplus (-\zeta^-) = 0$, so $(\zeta^+ \sqcap (-\zeta)^+) \sqcap 0 = (\zeta^+ \sqcap (-\zeta)^+) \oplus 0 = \zeta^+ \sqcap (-\zeta)^+$, then $\zeta^+ \sqcap (-\zeta)^+ = 0$. Assume $((n-1) \cdot \zeta^+) \sqcap (-\zeta)^+ = 0$ for any $\zeta \in \Gamma$ and some integer $n \geq 2$. Then $\zeta^+ \oplus 0 = (((n-1) \cdot \zeta^+) \sqcap (-\zeta)^+) \oplus \zeta^+ = (n \cdot \zeta^+) \sqcap ((-\zeta)^+ \oplus \zeta^+)$ by Proposition 2.1(4), so $\zeta^+ \sqcap (-\zeta)^+ = ((n \cdot \zeta^+) \sqcap ((-\zeta)^+ \oplus \zeta^+)) \sqcap (-\zeta)^+ = (n \cdot \zeta^+) \sqcap (((-\zeta)^+ \oplus \zeta^+) \sqcap (-\zeta)^+) = (n \cdot \zeta^+) \sqcap ((-\zeta)^+ \oplus 0) = (n \cdot \zeta^+) \sqcap (-\zeta)^+$, it turns out that $(n \cdot \zeta^+) \sqcap (-\zeta)^+ = 0$. Moreover, just like the previous, we verify that $(n \cdot \zeta^+) \sqcap (m \cdot (-\zeta)^+) = 0$ for any $\zeta \in \Gamma$ and some integers $n, m \geq 1$. Since $(n \cdot \zeta^+) \sqcap (-\zeta)^+ = 0$, we suppose that $(n \cdot \zeta^+) \sqcap ((m-1) \cdot (-\zeta)^+) = 0$ for any $\zeta \in \Gamma$ and some integer $m \geq 2$, then we can conclude that $(n \cdot \zeta^+) \sqcap (m \cdot (-\zeta)^+) = 0$ by induction.

Proposition 3.4. *Let L be a proper ideal of a QMV*-algebra $\Gamma = \langle \Gamma; \oplus, -, 0, 1 \rangle$. If $\lambda \notin L$, then there is a prime ideal V satisfying $L \subseteq V$ and $\lambda \notin V$.*

Proof. By Zorn’s Lemma we know that there is an ideal V satisfying $L \subseteq V$ and is maximal with the property $\lambda \notin V$. If V is not a prime ideal of Γ , then assume $\zeta^+ \notin V$ and $\zeta^- \notin V$ for any $\zeta \in \Gamma$. Define $V_1 = \langle V \cup \{\zeta^+\} \rangle$ and $V_2 = \langle V \cup \{\zeta^-\} \rangle$. Since $V \subsetneq V_1$, $V \subsetneq V_2$ and V is maximal with the property $\lambda \notin V$, we have $\lambda \in V_1 \cap V_2$, then there exist $\nu, \kappa \in V$ and some integers $n, m \geq 1$ with $|\lambda| \leq |\nu| \oplus (n \cdot |\zeta^+|)$ and $|\lambda| \leq |\kappa| \oplus (m \cdot |\zeta^-|)$, so $|\lambda| \leq |\nu| \oplus (n \cdot \zeta^+)$ and $|\lambda| \leq |\kappa| \oplus (m \cdot (-\zeta)^+)$ by Proposition 2.1(8). Denote $\tau = |\nu| \sqcup |\kappa|$. Then $\tau \in V$ and we have $|\lambda| \leq \tau \oplus (n \cdot \zeta^+)$ and $|\lambda| \leq \tau \oplus (m \cdot (-\zeta)^+)$, it follows that $|\lambda| \leq (\tau \oplus (n \cdot \zeta^+)) \sqcap (\tau \oplus (m \cdot (-\zeta)^+))$ by Proposition 2.1(16), thus we have $|\lambda| \leq \tau \oplus ((n \cdot \zeta^+) \sqcap (m \cdot (-\zeta)^+)) = \tau \oplus 0$ by Lemma 3.1, so $|\lambda| \leq \tau$. Because V is an ideal of Γ and $\tau \in V$, we have $\lambda \in V$ by Proposition 2.4, this is a contradiction with $\lambda \notin V$. Hence $\zeta^+ \in V$ or $\zeta^- \in V$ and then V is prime.

Corollary 3.1. *Let $\Gamma = \langle \Gamma; \oplus, -, 0, 1 \rangle$ be a QMV*-algebra. Then any proper ideal of Γ is an intersection of prime ideals.*

Proof. Suppose that T is a proper ideal of Γ . Denote $\Phi = \bigcap_{i \in I} \{V_i \mid V_i \text{ is any prime ideal of } \Gamma \text{ and } T \subseteq V_i\}$. Then we have $T \subseteq \Phi$. Below we verify that $\Phi \subseteq T$. If not, then there exists $\zeta \in \Phi \setminus T$. Since $\zeta \notin T$, there exists a prime ideal V with $T \subseteq V$ and $\zeta \notin V$ by Proposition 3.4, so $\zeta \notin \Phi$, this is a contradiction with $\zeta \in \Phi$.

In any QMV*-algebra $\Gamma = \langle \Gamma; \oplus, -, 0, 1 \rangle$, an ideal T of Γ is maximal if it is proper and for any ideal L of Γ with $T \subsetneq L$, then $L = \Gamma$.

Proposition 3.5. *Let T be a proper ideal of a QMV*-algebra $\Gamma = \langle \Gamma; \oplus, -, 0, 1 \rangle$. Then the following conditions are equivalent:*

- (1) T is a maximal ideal of Γ ,
- (2) For any $\zeta \in \Gamma$, $\zeta \notin T$ iff $1 \ominus (n \cdot |\zeta|) \in T$ for some integer $n \geq 1$.

Proof. (1) \Rightarrow (2) Suppose that T is a maximal ideal of Γ . Then for any $\zeta \notin T$, we have $T \subsetneq \langle T \cup \{\zeta\} \rangle$. Because T is maximal, we get $\langle T \cup \{\zeta\} \rangle = \Gamma$ and then $|\nu| \oplus n \cdot |\zeta| = 1$ for some $\nu \in T$ and $n \geq 1$. Since $0 \leq n \cdot |\zeta| \leq 1$, we have $n \cdot |\zeta| = (n \cdot |\zeta|)^+$ and then $|1 \ominus (n \cdot |\zeta|)| = 1 \ominus (n \cdot |\zeta|) = (|\nu| \oplus n \cdot |\zeta|) \ominus (n \cdot |\zeta|) \leq |\nu|$ by Proposition 2.1(17),(20). Because $\nu \in T$, we have $|\nu| \in T$ and then $1 \ominus (n \cdot |\zeta|) \in T$ by Proposition 2.4. Conversely, let $1 \ominus (n \cdot |\zeta|) \in T$ for some integer $n \geq 1$. If $\zeta \in T$, then $|\zeta| \in T$ and then $n \cdot |\zeta| \in T$ by Proposition 2.3(5),(3), so $1 = (1 \ominus (n \cdot |\zeta|)) \oplus (n \cdot |\zeta|) \in T$ which is a contradiction with T is proper.

(2) \Rightarrow (1) Suppose that L is an ideal of Γ and $T \subsetneq L$. Then for any $\zeta \in L \setminus T$, we have $1 \ominus (n \cdot |\zeta|) \in T$ for some integer $n \geq 1$. Since $\zeta \in L$, we have $|\zeta| \in L$ and then $n \cdot |\zeta| \in L$, so $1 = (1 \ominus (n \cdot |\zeta|)) \oplus (n \cdot |\zeta|) \in L$ which means that $L = \Gamma$. Hence T is maximal.

Proposition 3.6. *Let $\Gamma = \langle \Gamma; \oplus, -, 0, 1 \rangle$ be a QMV*-algebra. Then any proper ideal of Γ is contained in a maximal ideal.*

Proof. Denote $\mathcal{S}(\Gamma)$ the ordered set of all proper ideals in Γ . Since the union of any chain of proper ideals is a proper ideal, we conclude that any chain of elements in $\mathcal{S}(\Gamma)$ has an upper bound in $\mathcal{S}(\Gamma)$. Hence for any proper ideal $T \in \mathcal{S}(\Gamma)$, there exists a maximal element $L \in \mathcal{S}(\Gamma)$ by Zorn’s Lemma, i.e., L is a maximal ideal of Γ such that $T \subseteq L$.

Proposition 3.7. *Let $\Gamma = \langle \Gamma; \oplus, -, 0, 1 \rangle$ be a QMV*-algebra and T be any maximal ideal of Γ . Then T is also a prime ideal.*

Proof. Assume that T is a maximal ideal of Γ which is not a prime ideal of Γ . Then there is $\zeta \in \Gamma$ such that $\zeta^+ \notin T$ and $\zeta^- \notin T$, so we have a prime ideal V such that $T \subseteq V$ and $\zeta^+ \notin V$ by Proposition 3.4. However, because V is a prime ideal of Γ and $\zeta^+ \notin V$, we obtain $\zeta^- \in V$, which means that $T \subsetneq V$, this is a contradiction with the maximality of T . Thus T is a prime ideal of Γ .

4. Conclusion

In the present paper, the ideals of QMV*-algebras are investigated. We mainly study the properties of prime ideals and maximal ideals. It is known that filters are dual notions of ideals in MV-algebras. However, the correspondence between filters and ideals in QMV*-algebras is different from the case in MV-algebras. Hence we will focus on the filters of QMV*-algebras and characterize the prime filters in the future.

Acknowledgement

This study was funded by Shandong Provincial Natural Science Foundation, China (No. ZR2020MA041), China Postdoctoral Science Foundation (No. 2017M622177) and Shandong Province Postdoctoral Innovation Projects of Special Funds (No. 201702005).

References

- [1] Jiang YY, Chen WJ. QMV*-algebras: a generalization of MV*-algebras. *Soft Comput.* 2020; submitted.
- [2] Chang CC. A logic with positive and negative truth values. *Acta Philos Fenn Fasc.* 1963;16:19-39.
- [3] Chang CC. Algebraic analysis of many-valued logics. *Trans Amer Math Soc.* 1958;88:467-90.
- [4] Lewin R, Sagastume M, Massey P. MV*-algebras. *Log J IGPL.* 2004;12:461-83.
- [5] Lewin R, Sagastume M, Massey P. Chang's \mathcal{L}^* Logic. *Log J IGPL.* 2004;12:485-97.
- [6] Ledda A, Konig M, Paoli F, Giuntini R. MV algebras and quantum computation. *Stud Log.* 2006;82:245-70.
- [7] Paoli F, Ledda A, Giuntini R, Freytes H. On some properties of quasi-MV algebras and \sqrt{I} quasi-MV algebras. Part I. *Rep Math Logic.* 2009;44:31-63.
- [8] Bou F, Paoli F, Ledda A, Freytes H. On some properties of quasi-MV algebras and \sqrt{I} quasi-MV algebras. Part II. *Soft Comput.* 2008;12:341-52.
- [9] Kowalski T, Paoli F. On some properties of quasi-MV algebras and \sqrt{I} quasi-MV algebras. Part III. *Rep Math Logic.* 2010;45:161-99.
- [10] Jipsen P, Ledda A, Paoli F. On some properties of quasi-MV algebras and \sqrt{I} quasi-MV algebras. Part IV. *Rep Math Logic.* 2013;48:3-36.
- [11] Bou F, Paoli F, Ledda A, Spinks M, Giuntini R. The logic of quasi-MV algebras. *J Log Comput.* 2010;20:619-43.

A Novel Method for Mining Fuzzy Co-Location Patterns

Jinyu GUO and Lizhen WANG¹

School of Information Science and Engineering, Yunnan University, Yunnan, China

Abstract. As an important branch of the spatial data mining, spatial co-location pattern mining refers to discovering a subset of the set of features whose instances are often neighbor in space. In many practical scenes, the instances of spatial features include not only location information, but also attribute information. Some scholars use the type-1 fuzzy membership function to mine fuzzy co-location patterns from spatial instances with attribute information. However, the type-1 membership function itself is uncertain. Therefore, there is some deviation in describing the membership degree of attributes of spatial instances by using a type-1 membership function. To solve this problem, we propose a fuzzy co-location pattern mining method based on type-2 fuzzy membership function. Firstly, we collected interval evaluation values of interval data of attribute information from 1000 experts, and formed granular data. Then, on the basis of the original type-1 membership function, a type-2 fuzzy membership function based on elliptic curve is expanded, and the parameters of the type-2 fuzzy membership function are adjusted by using a gradual method, so that the footprint of uncertainty (FOU) in the function meets the connectivity and the threshold given by the user. After that, we design a fuzzy co-location pattern mining algorithm incorporating type-2 fuzzy membership function into the traditional Join-based algorithm. In which, we define the concepts of fuzzy feature, fuzzy co-location pattern, upper bound participation index, lower bound participation index. In order to improve the efficiency of our method, we also put forward a pruning strategy. We have done a lot of experiments on synthetic and real data sets, which proves the effectiveness and efficiency of our proposed algorithm.

Key words: Spatial data mining; Fuzzy co-location pattern; Type-2 fuzzy set; Pruning

1. Introduction

Spatial co-location pattern mining is a very important branch in the field of spatial data mining. A spatial co-location pattern is a set of spatial features, and the instances of these features are often neighbor in space. For example, {convenience store, pharmacy} may be a prevalent co-location pattern, because convenience stores and pharmacies are often neighbor to each other in a city central. Spatial co-location pattern mining has a wide range of applications, such as geographic information science, symbiotic plant distribution, urban facility distribution, and so on.

We find that spatial data often contains attribute information besides spatial location information, such as the content of heavy metals in topsoil at a certain spatial location, which is usually expressed by specific numerical values. However, people are usually

¹ Corresponding author: Lizhen Wang, School of Information Science and Engineering, Yunnan University, Dongwaihuan SouthRoad, Kunming, Yunnan 650500, China. E-mail: lzhwang@ynu.edu.cn

less sensitive to a specific value of attribute information, but when the attribute value changes fundamentally, that is, when it changes from a certain range to a new range, people are sensitive and attach importance to the result. In this paper, a method of mining fuzzy spatial co-location pattern based on type-2 fuzzy membership function and Join-based algorithm is proposed, which is used to mine fuzzy co-location pattern from spatial data sets with attribute information.

In recent years, spatial co-location pattern mining methods can be roughly divided into two categories, one is Apriori-like method [1,2], which first generates candidate co-location patterns, and then generate row-instances of candidate patterns and check their prevalence. The second method is to generate maximal cliques from spatial data to find prevalent co-location patterns [3,4]. However, these two kinds of mining methods almost only emphasize the spatial location information of spatial data, while ignoring their attribute information. In the traditional methods of mining co-location patterns, we can only find the spatial association of different functional areas, but not the spatial association of functional areas with attribute information. For example, whether there is a correlation between the content of heavy metals in industrial area and the content of heavy metals in residential area, etc. Therefore, we mine fuzzy co-location pattern based on the type-2 fuzzy membership function, which not only reduces the deviation caused by the uncertainty of the type-1 fuzzy membership function, but also accurately mines fuzzy co-location pattern.

In this paper, the heavy metal content in a surface soil is taken as an example to illustrate the application of the proposed method. Through questionnaire survey, 1000 geological researchers were counted to evaluate the membership of two heavy metals (Cu and Zn) in topsoil, that is, the evaluation data of particle type [5]. Aiming at mining more reasonable fuzzy co-location patterns from spatial data sets with attribute information, this paper makes the following contributions to the field of spatial co-location pattern mining:

- (1). In the fuzzy processing of corresponding attribute information, on the basis of the original type-1 membership function, a type-2 membership function based on elliptic curve is expanded from the evaluation data of particle type. Among them, we use a gradual method to adjust the parameters of the function, so that the footprint of uncertainty (FOU) in the type-2 membership function not only satisfies the connectivity [6], but also makes its confidence reach the given threshold (the default is 80%).
- (2). According to the constructed type-2 membership function, this paper defines the concepts of upper bound participation ratio and lower bound participation ratio of fuzzy features, and upper bound participation index and lower bound participation index of fuzzy co-location patterns. Furthermore, because our fuzzy co-location patterns have both upper and lower membership degrees, according to the given prevalence threshold, we divide the fuzzy co-location pattern into three kinds of patterns: absolute non-prevalent fuzzy co-location patterns, fuzzy co-location patterns with prevalent tendency degree and absolute prevalent fuzzy co-location patterns.
- (3). We propose a method based on type-2 fuzzy membership function and traditional Join-based algorithm of mining prevalent co-locations, which is used to mine spatial fuzzy co-location patterns. The fuzzy co-location pattern composed of fuzzy features between different fuzzy sets of the same attribute in the same functional area has no practical significance. Therefore, we propose a bucket-based candidate fuzzy co-location generation method, which puts fuzzy features

of the same attribute in the same bucket, and then selects fuzzy features from different buckets to form candidate fuzzy co-location patterns. Then, prevalent fuzzy co-location patterns are generated by filtering. In order to improve the efficiency of our algorithm, we propose a pruning strategy.

2. Related work

In recent years, there are some researches that apply fuzzy sets to attribute data mining [7,8]. We introduce the related work of fuzzy co-location pattern mining method based on type-2 membership function from two parts: constructing type-2 fuzzy membership function and discovering spatial co-location patterns.

2.1. Constructing type-2 fuzzy membership function

Type-2 membership functions are usually characterized by the shape of the footprint of uncertainty (FOU). Therefore, many type-2 fuzzy membership functions have been proposed, for example, ladder type, triangle type, Gaussian type [9,10], π type [11], etc. We find that these functions have a common shortcoming: there are many parameters that determine the confidence and uncertainty width, which makes it very difficult to select the appropriate parameter values. However, the parameters of the type-2 membership function based on elliptic curve are relatively simple [12] (there is only one parameter). Therefore, we symmetrically expand from the original type-1 membership function [13] to generate type-2 membership function based on elliptic curve.

2.2. Spatial co-location pattern mining algorithm

Spatial co-location pattern mining algorithms are mainly divided into two categories: one is Apriori-like algorithm, for example, Join-based algorithm [2], Join-less algorithm [1], etc., and another is prefix tree-based algorithm, for example, CPI-Tree algorithm [14], ordered clique-based algorithm [15], etc. As the fuzzy co-location pattern mining based on type-2 membership function is still in the preliminary exploration stage, we improve the Join-based algorithm and propose a fuzzy co-location pattern mining method based on type-2 fuzzy membership function and Join-based.

3. Related definitions and lemmas

We take the contents of heavy metals copper and zinc in the topsoil of an area as an example. We divided the area into agricultural area (The number of the functional area is A), residential area(The number of the functional area is B), industrial area(The number of the functional area is C), and then sampled the topsoil of each functional areas, and measured the heavy metal content at each sampling point. The attribute information of sampling points is shown in Table 1.

Table 1. Attribute information of sampling points

The number of the functional area	The number of sampling points	The content of copper	The content of zinc
A	1	62	226
A	2	31	105
A	3	46	136

B	4	86	183
B	5	29	112
C	6	63	210
C	7	51	155

Traditional co-location pattern mining algorithm can mine patterns like {A, B, C}, which means that the instances of functional areas A、B and C are often neighbor. This pattern can reflect the spatial relevance of instances, but ignores the influence of attribute information in instances on mining results. For example, the relationship of heavy metal content among functional areas (for example, what is the relationship between the copper content in functional area B and the zinc content in functional area C). Obviously, the traditional co-location pattern mining method cannot directly solve this kind of problem. Therefore, we give the following definitions.

Definition 1 (Data fuzzification) The most important step in fuzzifying attribute data is to determine the membership function. Assuming that the fuzzy set on the domain is F , the membership function is expressed as U_F , we use the membership function U_F to describe the fuzzy set F , that is $U_F: x \rightarrow [0,1]$.

Suppose there is any $x \in X$, when $U_F(x)=0$, x does not belong to fuzzy set F at all; when $U_F(x)=0.4$, 40% of the tendency of x belongs to fuzzy set F ; when $U_F(x)=1$, x completely belongs to fuzzy set F .

In previous studies, there were the following problems in obtaining type-1 membership function by expert experience: Different experts' evaluation of membership degree of specific value is likely not completely consistent; Experts may give specific membership degrees to specific values, which may cause some deviations (for example, The experts gave the evaluation of low Cu content with membership degree of 0.3 for the Cu content of 25ug/g, which may have some deviations). Therefore, we use the upper and lower bounds of the footprint of uncertainty (FOU) to deal with the problem in this paper, that is, we introduce two membership functions (one is called the upper bound membership function $\bar{U}_F(x)$, which is used to represent the upper bound of the membership degree of an instance's attribute; the another is called lower bound membership function $\underline{U}_F(x)$, which is used to represent the lower bound of the membership degree of an instance's attribute).

Definition 2 (Granular evaluation data) We divide the attribute of heavy metal content into three fuzzy sets: low、middle and high. The divided attributes are called fuzzy attributes, such as Zn(L)、Zn(M) and Zn(H). Then, in the form of questionnaire, we invited 1000 geologists to evaluate the interval membership of the interval content of heavy metals copper and zinc in surface soil, to form granular evaluation data. For example, for the interval value of Cu content [15, 20], 21 people think that the degree of middle membership is [0, 0.1], and 573 people think that the degree of middle membership is [0.1, 0.2], 391 people thought that the degree of low membership was [0.2, 0.3], and 15 people thought that the degree of low membership was [0.3, 0.4].

Definition 3 (Fuzzy feature) Fuzzy features refer to different type of things with fuzzy attributes. A set of fuzzy feature is represented as $Fuz_Fea = \{Fuz_f_1, Fuz_f_2, \dots, Fuz_f_n\}$, a fuzzy feature is represented as $Fuz_f_i (1 \leq i \leq n)$.

For example, the fuzzy feature B.Zn(L) represents the functional area B with low zinc content. The instance of fuzzy feature refers to the sampling point with the fuzzy feature property in the space.

Definition 4 (Neighborhood Relationship) For any two instances s_1 and s_2 in space, if the Euclidean distance between the two instances is less than the given threshold min_dist , that is the distance $(s_1, s_2) \leq min_dist$, it indicates that the two instances are neighbor each other, denoted by $R(s_1, s_2)$.

Definition 5 (Fuzzy co-location pattern) The fuzzy co-location pattern Fuz_c is a set of fuzzy features, and the size of the fuzzy co-location pattern is the number of fuzzy features contained in the fuzzy pattern, denoted by $|Fuz_c|$. For example, The size of fuzzy co-location pattern $\{A.Zn(M), B.Zn(M), C.Cu(M), E.Cu(H)\}$ is 4.

Definition 6 (Row-instance and Table-instance) Suppose there is a set of spatial instances $S = \{s_1, s_2, \dots, s_n\}$, where any two instances are neighbor, if S contains all fuzzy features of a fuzzy co-location pattern, and any subset of S cannot contain all the fuzzy features of Fuz_c , then S is called a row-instance of Fuz_c . All row-instances of Fuz_c constitute the table-instance of Fuz_c .

Definition 7 (upper bound participation ratio and lower bound participation ratio) For a fuzzy pattern $Fuz_c = \{Fuz_f_1, Fuz_f_2, \dots, Fuz_f_n\}$, The lower bound participation ratio of the fuzzy feature $Fuz_f_i (1 \leq i \leq n)$ in this fuzzy pattern is expressed as $PR(Fuz_c, Fuz_f_i)$, defined as ratio of the sum of the lower bound membership degrees of the non-repeated instances of fuzzy feature Fuz_f_i in the table-instance of fuzzy co-location pattern Fuz_c to the sum of the lower bound membership degrees of all the instances of Fuz_f_i . The upper bound participation ratio of the fuzzy feature $Fuz_f_i (1 \leq i \leq n)$ is expressed as $\overline{PR}(Fuz_c, Fuz_f_i)$, defined as the ratio of the sum of the upper bound membership degrees of the non-repeated instances of fuzzy feature Fuz_f_i in the table-instance of fuzzy co-location pattern Fuz_c to the sum of the upper bound membership degrees of all the instances in Fuz_f_i .

Definition 8 (upper bound participation index and lower bound participation index) The upper bound participation index of fuzzy co-location pattern Fuz_c is expressed as $\overline{PI}(Fuz_c)$, which is defined as the minimum of the upper bound participation ratio of all fuzzy features Fuz_f_i in Fuz_c . the lower bound participation index of fuzzy co-location pattern Fuz_c is expressed as $PI(Fuz_c)$, which is defined as the minimum of the lower bound participation ratio of all fuzzy features Fuz_f_i in Fuz_c .

Definition 9 (Prevalent fuzzy co-location patterns) According to Definition 8, a fuzzy co-location pattern Fuz_c has upper bound participation index and lower bound participation index. When the user gives a threshold min_prev , when the upper bound participation index $\overline{PI}(Fuz_c) < min_prev$, Fuz_c is called an absolute non-prevalent fuzzy pattern; when the lower bound participation index $PI(Fuz_c) \geq min_prev$, Fuz_c is called an absolute prevalent fuzzy pattern; when the lower bound participation index $PI(Fuz_c) < min_prev \leq$ upper bound participation index $\overline{PI}(Fuz_c)$, Fuz_c is called a pattern with prevalent tendency degree, and the prevalent tendency degree of the pattern is:

$$\sigma = (\overline{PI}(Fuz_c) - min_prev) / (\overline{PI}(Fuz_c) - PI(Fuz_c))$$

We call absolute prevalent fuzzy co-location patterns and fuzzy co-location patterns with prevalent tendency degree as prevalent fuzzy co-location patterns.

Lemma 1 In a candidate fuzzy co-location pattern Fuz_c , if the upper bound participation index of its any fuzzy sub-patterns is less than the prevalence threshold min_prev , the Fuz_c is absolute non-prevalent.

Proof: For a n size pattern Fuz_c , and a $n+1$ size pattern contain it is Fuz_c' , according to the downward closure, $\overline{PI}(Fuz_c') \leq \overline{PI}(Fuz_c)$, if the n size pattern Fuz_c

is absolute non-prevalent, then $\overline{PI}(Fuz_c) < min_prev$. Therefore, $\overline{PI}(Fuz_c') \leq \overline{PI}(Fuz_c) < min_prev$, then $n+1$ size pattern Fuz_c' is also absolute non-prevalent.

This lemma can be used as our pruning strategy.

4. A fuzzy Co-location mining algorithm based on type-2 fuzzy membership function and Join-based

4.1. Construct type-2 fuzzy membership function

Based on the original type-1 membership function, we adopt the equal expansion method to generate the type-2 membership function based on elliptic curve, and use a gradual method to adjust the parameters of the function, so as to ensure that the footprint of uncertainty (FOU) in the type-2 membership function meets the connectivity and given threshold. We take the interval membership degree of fuzzy set Cu(M) as an example when the copper content is 10 to 50 (we choose the length of interval content as 5 and the length of interval membership degree as 0.1). This example is used to illustrate the steps of constructing type-2 fuzzy membership function.

We have counted the data of 1000 geologists who evaluated the interval value of copper content under the fuzzy set Cu(M). The darker the color is, the more people are evaluated in this interval. Figure 1 shows the number of evaluators for the interval membership of the interval data.

According to the construction method of type-1 fuzzy membership function of the content of heavy metal copper in [7], we get the type-1 fuzzy membership function of heavy metal copper. We draw the type-1 membership function, which is expressed as $y = \frac{x-a}{b-a} = \frac{x-10}{40}$, As shown in Figure 2. Among them, a is the lowest value that experts believe the heavy metal content tends to belong to middle content, and b is the value that experts believe the copper content must belong to middle content.

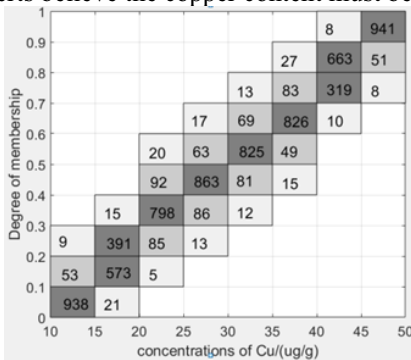


Figure 1. the number of evaluators for the interval membership of the interval data

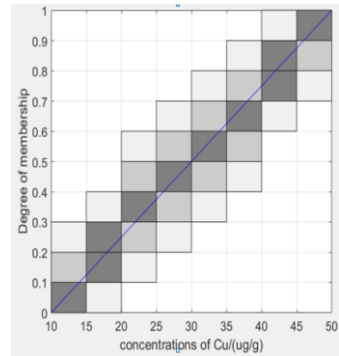


Figure 2. type-1 fuzzy membership function

We construct a type-2 membership function based on the original type-1 membership function. The type-2 membership function we proposed is represented by the upper bound membership function and the lower bound membership function. When the original type-1 membership function is a decreasing function, the formula is expressed as:

$$\text{Upper bound function } \bar{u}(x) = \sqrt[1 - (\frac{x-a}{b-a})^\eta]$$

$$\text{Lower bound function } \underline{u}(x) = 1 - \sqrt[\eta]{1 - \left(\frac{b-x}{b-a}\right)^\eta} \quad (a \leq x \leq b)$$

When the original type-1 membership function is an increasing function, the formula is expressed as:

$$\text{Upper bound function } \bar{u}(x) = \sqrt[\eta]{1 - \left(\frac{b-x}{b-a}\right)^\eta}$$

$$\text{Lower bound function } \underline{u}(x) = 1 - \sqrt[\eta]{1 - \left(\frac{x-a}{b-a}\right)^\eta} \quad (a \leq x \leq b)$$

Where, a is the lowest value that experts start to believe it has a tendency to belong to the fuzzy set, and b is the value that experts believe it must belong to the fuzzy set.

The area covered by the upper bound function and the lower bound function is expressed as the footprint of uncertainty (FOU). Among them, η determines the degree of expansion and contraction of the elliptic curve. The larger the η , the larger the FOU; the smaller the η , the smaller the FOU. For example, when $\eta = 1.1$, our type-2 membership function is shown in Figure 3.

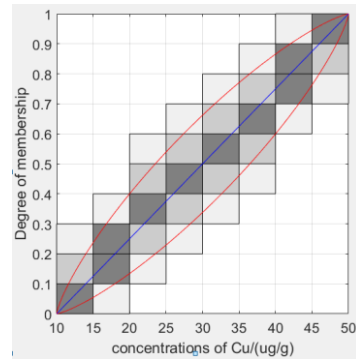
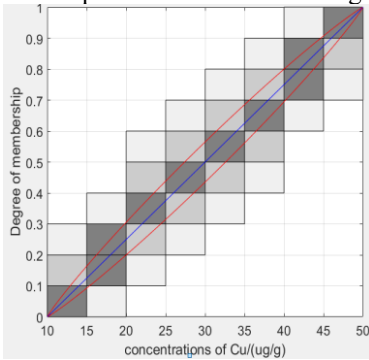


Figure 3. Type-2 membership function when $\eta = 1.1$

Figure 4. Type-2 membership function when $\eta = 1.283$

The granular data indicates that for any specific value in the interval data, the possibility of taking any specific membership value in the interval membership is the same. Therefore, for an interval data, the confidence of the type-2 membership function = $\sum_{i=1}^m \text{Area ratio } S_i \text{ of particles in FOU} * \text{The number } x \text{ of evaluators in this particle}$. Among them, m is the number of particles in each interval data. Within a range, the average of the confidence of all interval data is the confidence of the type-2 membership function in this range.

We use the gradual method to determine the unique parameter η . First, we set an increment $\alpha = 0.1$, when $\eta = 1 + k_1\alpha$ ($k_1 = 1, 2, \dots, n$), Observe whether the FOU is continuous. If there is φ ($\varphi \in \{1, 2, \dots, n\}$), when $\eta = 1 + \varphi\alpha$, FOU is continuous, when $\eta = 1 + (\varphi + 1)\alpha$, FOU is not continuous, then set the gradual value to one-tenth of the original (i.e. $\beta = 0.1\alpha$), $\eta = 1 + \varphi\alpha + k_2\beta$ ($k_2 \in \{1, 2, \dots, 10\}$), and so on, until the accuracy reaches the user's requirement and the FOU is connected. This process is shown in Table 2.

Table 2. connectivity of FOU with different values

η	1.1	1.2	1.3	1.4	1.5	1.6	1.7	1.8	1.9	2.0
Is it connected?	Yes	Yes	No	No	No	No	No	No	No	No
η	1.21	1.22	1.23	1.24	1.25	1.26	1.27	1.28	1.29	1.3
Is it connected?	Yes	Yes	Yes	Yes	Yes	Yes	Yes	Yes	No	No
η	1.281	1.282	1.283	1.284	1.285	1.286	1.287	1.288	1.289	1.29
Is it connected?	Yes	Yes	Yes	No	No	No	No	No	No	No

When $\eta=1.283$, the FOU of the type-2 membership function is connected. At this time, the data in the FOU accounts for 85.13% of the total evaluation data, that is, the confidence of FOU is 0.8513, which reaches the default threshold of 0.8. As shown in Figure 4.

The type-2 fuzzy membership function we get is shown in Figure 5 and Figure 6.

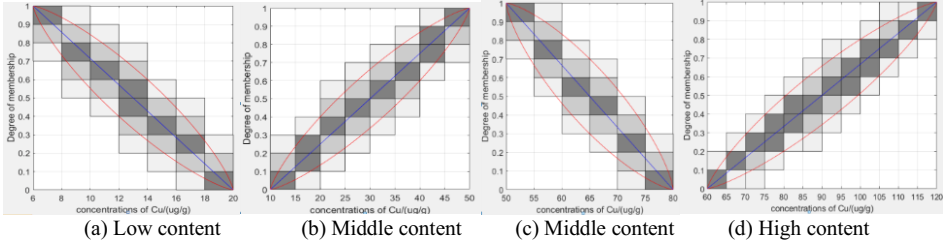


Figure 5. type-2 membership function of Cu

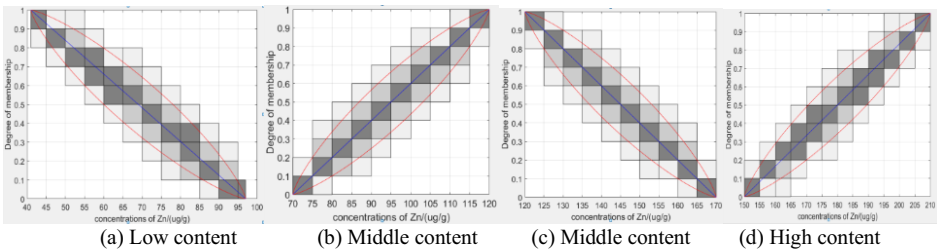


Figure 6. type-2 membership function of Zn

As shown in Figure 5 and Figure 6, the red lines represent the upper bound membership function and the lower bound membership function of the type-2 membership function. The parameters of Cu's type-2 membership function are $\eta_1=1.296$, $\eta_2=1.283$, $\eta_3=1.272$, $\eta_4=1.272$; the parameters of Zn's type-2 membership function are $\eta_5=1.28$, $\eta_6=1.284$, $\eta_7=1.284$, $\eta_8=1.272$. The confidence of the type-2 membership function of Cu are 0.8502, 0.8513, 0.8172, 0.8953, and the confidence of the type-2 membership function of Zn are 0.8605, 0.8904, 0.8910, and 0.9022, respectively.

4.2. Prevalent fuzzy Co-location pattern mining method based on Join-based

In this section, we propose a fuzzy co-location pattern mining method based on type-2 fuzzy membership function and Join-based.

A. Fuzzy co-location pattern mining algorithm

Input: (1) Fuzzy feature set $Fuz_Fea = \{Fuz_f_1, Fuz_f_2, \dots, Fuz_f_n\}$

(2) Instance set of Fuzzy features $S = \{s_1, s_2, \dots, s_n\}$

(3) Minimum distance threshold min_dist

(4) Minimum prevalence threshold min_prev

Output: prevalent fuzzy co-location pattern set Fre_P

Variable:

C_n : n -size candidate fuzzy co-location patterns

T_n : Table instance of C_n

P_n : Prevalent n -size fuzzy co-location patterns

Step:

1. $n = 1$; $Fre_P = \emptyset$; $C_1 = Fuzz_Fea$, $P_1 = Fuzz_Fea$;

2. while($P_n \neq \Phi$) {
3. $C_{n+1} = \text{Gen_Candidate}(P_n, n)$;
4. $T_{n+1} = \text{Gen_table_instance}(C_{n+1}, T_n, \text{min_dist})$;
5. $P_{n+1} = \text{select_prev_pattern}(C_{n+1}, T_{n+1}, \text{min_prev})$;
6. $\text{Fre_P} = \text{Fre_P} \cup P_{n+1}$;
7. $n = n + 1$;}
8. Return Fre_P

Step 1 initializes size-1 candidate fuzzy pattern and size-1 prevalent fuzzy pattern (all fuzzy features are considered as the first size prevalent pattern). Then, the following steps are carried out: In step 3, Apriori-like method is used to generate $n+1$ size candidate fuzzy patterns from n size prevalent fuzzy patterns; Step 4 generates the table-instance of $n+1$ size candidate fuzzy pattern from the table-instance of n size prevalent fuzzy pattern by connecting; In Step 5, we calculate the upper bound participation index and the lower bound participation index of $n+1$ size candidate fuzzy patterns according to the table-instances of $n+1$ size candidate fuzzy patterns. By comparing the prevalence threshold given by the user, we filter out $n+1$ size prevalent fuzzy patterns.

B. Generate candidate fuzzy patterns

When generating candidate fuzzy patterns, some of them have no practical significance, such as $\{A.Cu(L), A.Cu(M), A.Cu(H)\}$, that is, the fuzzy co-location pattern composed of fuzzy features of the same functional area between different fuzzy sets of the same attribute has no practical significance. In order to avoid producing such meaningless candidate fuzzy patterns, we propose a bucket-based candidate fuzzy pattern generation algorithm, which puts the fuzzy features of the same attribute in the same functional area into the same bucket, and then selects the fuzzy features from different buckets to form the candidate fuzzy patterns. The steps of this algorithm are as follows:

- Input: (1) Fuzzy feature set $\mathbf{Fuzz_Fea} = \{Fuz_f_1, Fuz_f_2, \dots, Fuz_f_n\}$
 (2) Fuzzy feature instances' set of $\mathbf{S} = \{s_1, s_2, \dots, s_n\}$
 (3) Minimum distance threshold min_dist
 (4) Minimum prevalence threshold min_prev

Output: C_{n+1} : $n+1$ size candidate fuzzy co-location patterns

Step:

1. if($n == 1$)
2. for each $\mathbf{Fuz_f}$ in $\mathbf{Fuzz_Fea}$ do
3. Initialize_bucket($\mathbf{Fuz_f}$)
4. SetId($\mathbf{Fuz_f}$)
5. else if($n == 2$)
6. for each $\mathbf{Fuz_c}_1$ in bucket
7. for each $\mathbf{Fuz_c}_2$ in other bucket
8. Generate a candidate pattern from $\mathbf{Fuz_c}_1$ and $\mathbf{Fuz_c}_2$
9. else
10. for($i=1$; $i < \text{bucket_count}$; $i++$)
11. for each fuzzy pattern $\mathbf{Fuz_c}_1$ in bucket[i]
12. for each fuzzy pattern $\mathbf{Fuz_c}_2$ in bucket[i]
13. Generate a pattern $\mathbf{Fuz_c}_{n+1}$
14. if(check($n-1$, $\mathbf{Fuz_c}_{n+1}$, bucket))
15. $\mathbf{Fuz_c}_{n+1}$ is a new candidate pattern

Steps 2 to 4 first initialize each bucket, and then number all fuzzy features in the bucket. Among them, for any two fuzzy features in the same bucket, there are $\text{Id}(\text{Fuz}_{f_i})\% \text{bucket_count} = \text{Id}(\text{Fuz}_{f_j})\% \text{bucket_count}$, that is, put all fuzzy features with the same features and the same attributes into the same bucket.

In Step 6 to Step 8, we select two fuzzy features from different buckets in order, to form a size-2 fuzzy pattern. Step 10 to 15 generate $n+1$ size candidates from n size prevalent fuzzy patterns: first, for any two prevalent fuzzy patterns, check whether the fuzzy features of the first $n-1$ of the two fuzzy patterns are same, if they are same, then connect them to generate a $n+1$ size candidate. At the same time, check whether all its n size subsets are prevalent.

C. Generate table-instance

As we know, for a fuzzy co-location pattern, all of its row-instances constitute its table-instance. The process of obtaining the row-instances of fuzzy co-location candidates can be divided into the following 4 steps:

- (1) First, we materialize the neighborhood relationship between instances, and then we can get all row-instances of size-2 co-location patterns.
- (2) For a candidate fuzzy pattern, we find the co-location pattern consisting of all the non-recurring features in the fuzzy candidate pattern. Then, we find the row-instances that have all the fuzzy features of the fuzzy candidate pattern from the table-instance of the co-location pattern, these row-instances are the row-instances of the candidate fuzzy pattern. For example, for the fuzzy pattern $\{C.Cu(L), C.Zn(L), D.Cu(M)\}$, the row-instances whose attributes satisfy C.Cu(L), C.Zn(L) and D.Cu(M) are found in all row-instances of pattern $\{C, D\}$ as row-instances of candidate fuzzy pattern.
- (3) If there is only one feature in the size-2 candidate fuzzy pattern, in this feature, the instances that satisfy all the fuzzy features in the candidate fuzzy pattern are found as the row-instances of the candidate fuzzy pattern. For example, for the fuzzy pattern $\{B.Cu(M), B.Zn(H)\}$, in the instances of feature B, find the instances that satisfy both Cu(L) and Zn(M) simultaneously as the row-instances of the fuzzy pattern $\{B.Cu(M), B.Zn(H)\}$.

4.3. Time performance analysis

The time cost of our proposed method is mainly divided into three parts: generating candidate fuzzy co-location patterns, generating all row-instances through connection and finding table-instances of the candidates. The computational complexity of generating candidate patterns is $O(C)$, where C is the number of candidates generated by our method; The computational complexity of generating table-instances of candidates is $O(R)$, where R is the number of row-instances generated by connection operations; The computational complexity of finding the table-instance of the candidates is $O(T)$, T is the number of all row-instances found for all candidates.

5. Experimental Evaluation

In this section, in order to verify the effectiveness and efficiency of our proposed algorithm, a wide range of experiments have been done. We used a method similar to [6] to generate synthetic data sets. We also used the real data set of heavy metal content of

topsoil samples in Quanzhou to evaluate our method.

All our experiments are carried out on C#, The Intel PC we use has windows 10 operating system and Intel Core i5-4258@ 2.40GHz and 8GB memory.

5.1. Results on synthetic data sets

First of all, we set the size of the instance distribution area to $D*D$, We divide the entire region into grids of size $min_dist*min_dist$, where, min_dist is the distance threshold of instance proximity. After determining the number of features and instances, we determine the number of instances of each feature according to Poisson distribution.

(1) The effect of distance threshold on results

We change the distance threshold to find the effect of different distance threshold on the execution time and the pruning rate. As shown in Figure 7, we find that with the increase of distance thresholds, the execution time of our method will continue to increase, because with the increase of distance thresholds, the number of neighbor instances will increase, so the time consumption will also increase.

(2) The effect of the prevalence threshold on the results

We change the prevalence threshold to find the effect of different prevalence threshold on the execution time and the pruning rate. As shown in Figure 8, we find that the execution time of our methods decreases with the increase of the prevalence threshold. In the case of higher prevalence thresholds, our method can prune a lot of candidate fuzzy co-location patterns, so when the prevalence threshold increases, the time consumption of our method will reduce rapidly.

(3) The effect of the number of fuzzy features on the results

We change the number of fuzzy features to find the effect of different number of fuzzy features on execution time and the pruning rate. As shown in Figure 9, we find that the execution time of our method first increases and then decreases. This is because when the number of fuzzy features increases from 18 to 36, the number of candidate fuzzy co-location patterns increases rapidly, and the generation of row-instances of candidate patterns also increases. When the number of fuzzy features continues to grow (when the number of fuzzy features increases from 36 to 90), the average number of row-instances of candidate patterns will be greatly reduced. Our proposed method has downward closure, so it can quickly prune the absolute non-prevalent candidate patterns. The number of fuzzy features is equal to the number of features multiply the number of fuzzy attributes multiply the number of fuzzy sets. In this experiment, the number of fuzzy attributes is 2, the number of fuzzy sets is 3, and the number of features selected are 3,6,9,12,15 respectively.

(4) The effect of the number of instances on the results

We change the number of instances to find the effect of different instance number on execution time and the pruning rate. As shown in Figure 10, we find that with the increase of the number of instances, the execution time of our method continues to increase. This is because in a region, with the increase of the number of instances, the number of neighbor instances will also increase, that is, the number of row-instances of candidate patterns will increase, and the time consumption will also increase greatly.

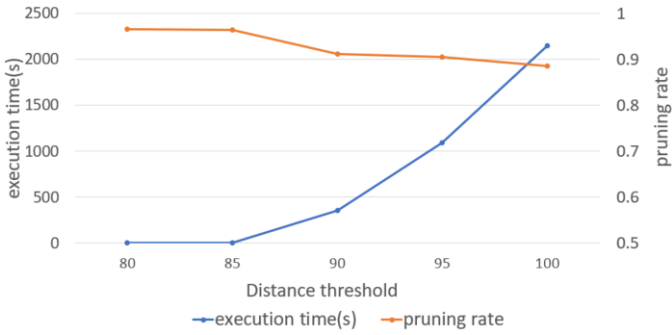


Figure 7. Execution time and the pruning rate varies with the distance threshold

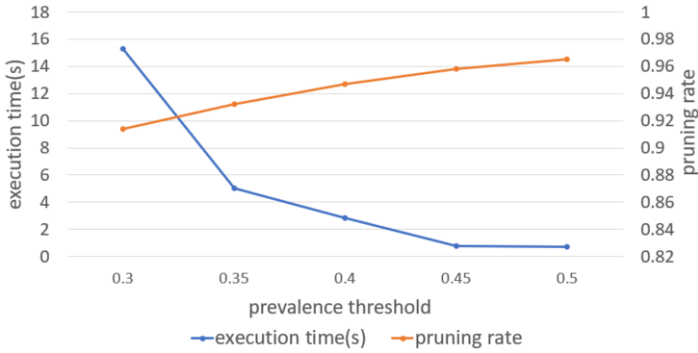


Figure 8. Execution time and the pruning rate varies with the prevalence threshold

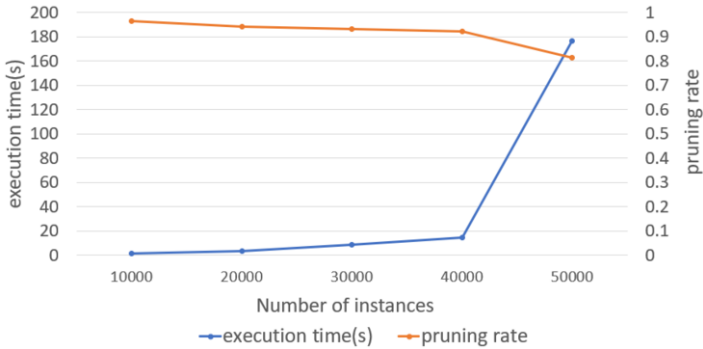


Figure 9. Execution time and the pruning rate varies with the number of instances

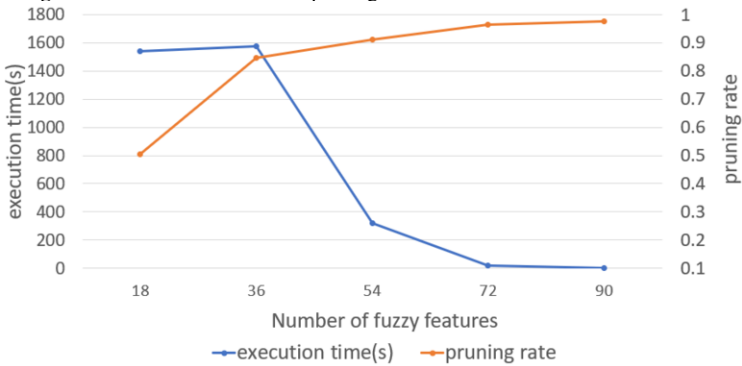


Figure 10. Execution time and the pruning rate varies with the number of fuzzy features

5.2. Results on real data sets

In this section, we use the spatial distribution data set of heavy metals in the topsoil of Jiayuguan City as the real data set to test the effectiveness of our method. As shown in Figure 11, it is divided into four functional areas: industrial area, agricultural area, living area and Gobi area. According to the proportion of the length of the area, we project these data on the space of 850 * 670.

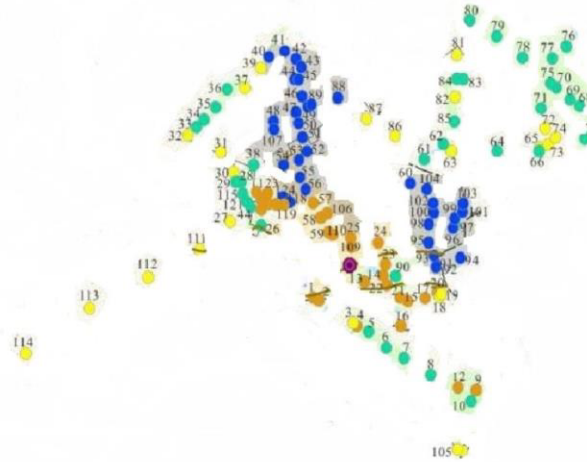


Figure 11. data set of heavy metals in the topsoil of Jiayuguan City

Table 3. Mining results of the real data set

Prevalent fuzzy co-location pattern	Prevalence tendency degree	Lower participation index and Upper participation index	Participation index in traditional method
{A.Cu(L), C.Cu(L)}	0.6125	0.0709,0.6621	0.2312
{A.Cu(L), D.Cu(L)}	0.2328	0.036,0.3801	0.1169
{A.Cu(M), C.Cu(M)}	0.2636	0.1567,0.3513	0.2384
{D.Cu(M), D.Zn(H)}	1	0.4781,0.9135	0.6599
{D.Cu(L), D.Zn(M)}	0.9096	0.2414,0.8896	0.6681
{A.Zn(L), A.Cu(M), C.Zn(L)}	0.2636	0.1567,0.3513	0.2384
{A.Zn(L), C.Zn(L), D.Cu(M)}	0.2167	0.1749,0.3346	0.2492
{B.Cu(L), B.Zn(L), C.Zn(L)}	0.8586	0.2597,0.5448	0.4342
{B.Cu(M),B.Zn(L),C.Cu(M),C.Zn(M)}	0.7039	0.1804,0.5844	0.3358
{B.Cu(M),B.Zn(L),C.Cu(M),C.Zn(L)}	1	0.3933,0.738	0.5726

In the real data set, we set the distance threshold to 50 and the prevalence threshold to 0.3, 112 prevalent fuzzy co-location patterns (26 absolutely prevalent fuzzy co-location patterns and 86 fuzzy co-location patterns with prevalence tendency degree) were mined according to our measurement method, some of which are shown in Table 3, and 63 prevalent fuzzy co-location patterns were mined according to the traditional measurement method. The sampling points of functional area A are represented by blue

dots, the sampling points of functional area B are represented by green dots, the sampling points of functional area C are represented by brown dots, the sampling points of functional area D are represented by yellow dots. A, B, C and D represent industrial area, agricultural area, residential area and Gobi area respectively in this data set. For example, the fuzzy pattern $\{A.Cu(M), C.Cu(M)\}$ indicates that the industrial area with middle copper content and the residential area with middle copper content are prevalently located together, and the prevalence tendency degree of this pattern is 0.2636. $\{B.Cu(M), B.Zn(L), C.Cu(M), C.Zn(M)\}$ indicate agricultural areas with low zinc content and middle copper content, residential areas with middle zinc content and middle copper content tend to be often located together, and the degree of this tendency is 0.7039.

When the fuzzy membership function is uncertain, our method can find the fuzzy co-location pattern that is always prevalent, which is helpful for us to find the stable prevalent fuzzy co-location pattern. Our method can also find the fuzzy co-location pattern that has a certain tendency to be prevalent, which is helpful for us to find the potential fuzzy co-location pattern and predict the occurrence of some prevalent fuzzy co-location patterns. However, the method of mining fuzzy co-location pattern based on type-1 fuzzy membership function can only divide the fuzzy patterns into prevalent fuzzy patterns and non-prevalent fuzzy patterns according to the participation index and prevalence threshold. When there is uncertainty in the fuzzy membership function, this method cannot judge which fuzzy patterns are stable prevalent, which fuzzy patterns have certain tendency are prevalent.

6. Conclusion

Traditional spatial co-location pattern mining methods can not directly mine fuzzy co-location patterns. Therefore, in this paper, we propose a fuzzy co-location pattern mining algorithm based on type-2 fuzzy sets and join-based algorithm to mine prevalent fuzzy co-location patterns from spatial instances with attribute information. Since the fuzzy attributes of spatial data are uncertain, we propose the concepts of upper and lower bound participation ratios of fuzzy features, upper and lower bound participation indexes of fuzzy co-location patterns, to measure the prevalence degree of fuzzy patterns. We also propose a pruning strategy, which effectively prunes the absolute non-prevalent fuzzy co-location patterns in the process of mining prevalent fuzzy co-location patterns.

The method of mining fuzzy co-location pattern based on type-2 fuzzy membership function has great practical significance. For example, it can help us find out whether the industrial areas will cause heavy metal pollution to the surrounding residential areas, and then find out whether the pollutants in the industrial area are related to the epidemic of the surrounding residents; In the distribution of urban facilities, we can see whether the per capita consumption level of the commercial areas is related to the housing prices of the surrounding residential areas, and so on. Our method also has some limitations: generating table-instances of candidate fuzzy patterns require a lot of connection operations, so the efficiency is not high; It does not consider how to mine fuzzy co-location patterns when different features have different attributes.

In the future work, we consider that there are several directions for further researches:

- (1) Propose new fuzzy co-location pattern mining algorithms to improve the efficiency of the fuzzy co-location pattern mining method.
- (2) Use more real data sets to verify the effectiveness of our proposed methods, for example, a data set of tumor diseases in a certain area and pollutant emissions from

surrounding factories.

References

- [1] J.S. Yoo, S. Shekhar, M. Celik. A join-Less approach for co-location pattern mining: a summary of results, in: Proc. IEEE ICDM, 2005, pp. 813-816.
- [2] Y. Huang, S. Shekhar, H. Xiong. Discovering colocation patterns from spatial datasets: a general approach, IEEE Trans. Knowl. Data Eng. 2004, 16 (12): 1472-1485.
- [3] X. Bao and L. Wang. A clique-based approach for co-location pattern mining. 2019, 490 (2019): 244-264.
- [4] A. Berry, R. Pogorelcnik. A simple algorithm to generate the minimal separators and the maximal cliques of a chordal graph, Inf. Process. Lett. 2011, 111 (11): 508-511.
- [5] Cenk Ulu, Müjde Güzelkaya, Ibrahim Eksin. Granular type-2 membership functions: A new approach to formation of footprint of uncertainty in type-2 fuzzy sets. 2013, 13(8): 3713-3728.
- [6] F. Wang, H. Mo. Some basic questions about type-2 fuzzy sets. Acta Automatica Sinica, 2017, 43(07): 1114-1141.
- [7] Z. Wang, Kwong-Sak Leung, George J. Klir. Applying fuzzy measures and nonlinear integrals in data mining. Fuzzy Sets and Systems, 2005, 156(3): 371-380.
- [8] F. E. Petry, L. Zhao. Data mining by attribute generalization with fuzzy hierarchies in fuzzy databases. Fuzzy Sets and Systems, 2009, 160(15): 2206-2223.
- [9] C. Lee, H. Pan. Performance enhancement for neural fuzzy systems using asymmetric membership functions. Fuzzy Sets and Systems 2009, 160 (7): 949-971.
- [10] J. M. Mendel and H. Wu. "Type-2 Fuzzistics for Symmetric Interval Type-2 Fuzzy Sets: Part 1, Forward Problems," IEEE Transactions on Fuzzy Systems, 2006, 14(6): 781-792.
- [11] T.W. Liao. A Procedure for the Generation of Interval Type-2 Membership Functions from Data, Applied Soft Computing Journal <http://dx.doi.org/10.1016/j.asoc.2016.09.034>.
- [12] E. Kayacan, A. Sarabakha, S. Coupland, et al. Type-2 fuzzy elliptic membership functions for modeling uncertainty[J]. Engineering Applications of Artificial Intelligence, 2018, 70:170-183.
- [13] P. Wu, L. Wang, Y. Zhou. Research on mining spatial co-location patterns with fuzzy attributes. Computer Science and Exploration, 2013, 7(04): 348-358.
- [14] L. Wang, Y. Bao, J. Lu. et al. A new join-less approach for co-location pattern mining. In Proc. of the IEEE 8th International Conference on Computer and Information Technology (CIT2008), Piscataway, NJ: the IEEE Computer Society Press, 2008: 197-202.
- [15] L. Wang, L. Zhou, J. Lu. et al. An Order-clique-based Approach for Mining Maximal Co-locations Information Sciences, 2009, 179 (19): 3370-3382

An Optimization of Several Distance Function on Fuzzy Subtractive Clustering

Sugiyarto SURONO^{a,1} and Annisa Eka HARYATI^b, Joko ELIYANTO^b

^a*Department of Mathematics, FAST Ahmad Dahlan University Yogyakarta, Indonesia*

^b*Magister Math. Education Ahmad Dahlan University Yogyakarta, Indonesia*

Abstract. Fuzzy Subtractive Clustering (FSC) is a technique of fuzzy clustering where the cluster to be formed is unknown. The distance function in the FSC method has an important role in determining the number of points that have the most neighbors. Therefore, this study uses several distance functions. The results obtained indicate that the DBI results indicate that the Euclidean distance has a good cluster evaluation result in the number of clusters 4. Meanwhile, for the PC value the combination of the Minkowski Chebysev distance produces a good PC value in the number of clusters 2.

Keywords. Fuzzy subtractive clustering, partition coefficient, Davies-Bouldin index

1. Introduction

The classification method by applying the similarities between data in certain dataset is called clustering technique. The intention of this process is to determine certain pattern in the dataset by separating data into few number of clusters [1]. Clustering has basic concept where data in the same cluster will have high level of similarities and low level of similarities towards data in different cluster [2].

Clustering method which based on the classification with the application of fuzzy set membership degree is known as fuzzy clustering. The probability of the data to be included in one cluster is not absolute, which means data can be included as the member of one or more clusters [3].

Fuzzy subtractive clustering is one of the fuzzy clustering method where the cluster created through this method is still unidentified [4]. This method does not apply the membership matrix which initialized randomly [5]. The basic concept of this method is determining the cluster centroid through searching the data coordinate which have the most density and number of neighboring coordinates. The density of the coordinates which already selected as the cluster centroid will be reduced so that this coordinate will be ineligible to become the next cluster centroid. Then, algorithm will run again to measure the density and the number of neighboring coordinate in each data to be selected as the next cluster centroid. This iteration will be applied until all of the data in the dataset is tested [6].

There are already many research which studied FSC as its main topics. One previous research which worked by [7] applied FSC to classify Wavelet adaptive nerves to improve low-cost and high speed INS/GPS navigation system. Then, FSC was also used

¹ Corresponding Author: Sugiyarto Surono; E-mail: sugiyarto@math.uad.ac.id

by [8] to do grouping and is used by [9] to perform fuzzy-based classification. Furthermore, FSC also applied by [10] to do a classification of ad hoc mobile network based on the akaike information criteria and used by [11] to make predictions on the stock market.

Fuzzy subtractive clustering method requires the distance similarity measurement to determine the number of coordinates which have the most neighboring dots. The most common applied distance parameter to determine the similarity measurement is Euclidean distance. Aside from Euclidean distance, Minkowski distance also had been applied by [12] to do an optimization. Furthermore, Hamming distance also had been applied by [13] to detect malware in android. In addition to that, Minkowski-Chebysev combination distance also had been worked on by [14] to do a classification with KNN, by [15] to do clustering with FCM on categorical data, and by [16] to do clustering with FCM by applying dimension reduction through PCA. Based on these statement, we decided to apply fuzzy subtractive clustering method with the application of few distance function parameter. Then, the results of the cluster evaluation are used to determine which cluster has good quality.

2. Method

The method applied in this research is Fuzzy Subtractive Clustering with the application of few distance functions, such as Euclidean distance, Minkowski distance, Hamming distance, and Minkowski-Chebysev combination distance. Data simulation applied in this research is worked through Python programming language.

2.1. Fuzzy Subtractive Clustering (FSC)

Fuzzy Subtractive Clustering in literature [17] defined as one of the clustering method where the applied algorithm is considered as supervised algorithm. The number of cluster which will be created is initially unidentified, so it is necessary to do a radius simulation for acquiring the expected clusters. There are two comparison factors applied in FSC, which are accept ratio and reject ratio valued between 0 to 1. Accept ratio is the lower limit where certain data coordinates considered as cluster centroid candidate is allowed to be defined as cluster centroid. In the other hand, reject ratio is the upper limit where certain data coordinates considered as cluster centroid candidate is prohibited to be defined as cluster centroid.

There are 3 criteria which can occur in FSC method, there are:

- If $\text{ratio} > \text{accept ratio}$, then the data coordinate is accepted as new cluster centroid.
- If $\text{reject ratio} < \text{ratio}$, then the data coordinate will be accepted as new cluster centroid only if this new data coordinate is located far enough with the other cluster centroid. This minimum distance requirement can be measured through the addition between the ratio and the closest distance of this data coordinate to other existing cluster centroid. If the result of the addition between the ratio and the closest distance of the data coordinate to other existing cluster centroid is < 1 , then this analyzed data coordinate will not be accepted as the new cluster centroid. This data coordinate also won't be reconsidered to become the new cluster centroid (the potential value of this data will be set to 0).

- If ratio \leq reject ratio, then there will be no another data coordinate which will be considered as the new cluster centroid. This means that the iteration process will be terminated.

2.2. Fuzzy Subtractive Clustering Algorithm

- Determining the parameter value which will be applied, such as radius (r), squash factor (q), accept ratio (ar), and reject ratio (rr).
- Transforming data into fuzzy number through this following equation [18]:

$$\mu(x) = \begin{cases} 1 & x \leq a \\ e^{-\frac{(x-a)}{(b-a)} - e^{-s}} & a \leq x \leq b \\ 0 & x \geq b \end{cases} \tag{1}$$

Where a and b are the lowest and highest value from the data.

- Determining the potential value of each coordinate $D_i; i = 1,2,3, \dots, n$ through this following equation:

$$D_i = \sum_{k=1}^n e^{-4\left(\sum_{j=1}^m \left(\frac{\text{distance}}{r}\right)^2\right)} \tag{2}$$

Where D_i is potential data i .

- Measuring the maximum value on each iteration and the Ratio number (R) with this following equation:

$$R = \frac{Z}{M} \tag{3}$$

- Testing the appropriateness of the cluster centroid candidate with 3 criteria which already mentioned before. Specifically for condition 2, to determine whether the data coordinate is fit to be considered as cluster centroid or not, this following equation needs to be applied.

$$Sd_k = \sum_{j=1}^m \left(\frac{V_j - C_{kj}}{r}\right)^2 \tag{4}$$

With $k = 1,2, \dots, p$ and $p =$ the number of clusters. Sd_k is the distance between the coordinate of the cluster centroid candidate and the previous cluster centroid. V_j and C_{kj} are the cluster centroid candidate and the cluster centroid of k in variable of j . If $(Md < 0)$ or $(Sd_k < Md)$, then $Md = Sd_k$.

$$Mds = \sqrt{Md};$$

Where Mds is the closest distance between the cluster centroid candidate and other existing cluster centroid. If $(ratio + Mds) \geq 1$, then the cluster centroid candidate is accepted as the new cluster centroid. While if jika $(ratio + Mds) < 1$, then the cluster centroid candidate is not allowed to be defined as

the new cluster centroid and will not be reconsidered to be the new cluster centroid (the potential value of this data will be set to 0)

- When the new cluster centroid is acquired, the subtraction of the potential value of the data around the previous cluster centroid will be initiated through this following equation [17]:

$$D_i^t = D_i^{t-1} - Z * e^{-4 \left[\sum_{j=1}^m \left(\frac{C_{kj} - x_{ij}}{r * q} \right)^2 \right]} \tag{5}$$

- D_i^t = Data potential of $-i$ in iteration of $-t$.
- D_i^{t-1} = Data potential of $-i$ in iteration of $-(t-1)$.
- $D_{c_{ki}}$ = Data potential of $-k$ in iteration of $-i$.
- C_{kj} = Cluster centroid of $-k$ in variable of $-j$.
- x_{ij} = Data $-i$ in variable $-j$.
- r = Radius.
- q = Squash factor.

- Measuring the value of sigma cluster on each variables by applying an equation as follows [17]:

$$\sigma_j = \frac{r * (X_{max_j} - X_{min_j})}{\sqrt{8}}, j = 1, 2, \dots, m \tag{6}$$

- σ_j = Sigma in variable of $-j$.
- X_{max_j} = The maximum value in variable $-j$.
- X_{min_j} = The minimum value in variable $-j$.

- Measuring the membership degree by applying equation (9) as follows:

$$\mu_{k_i} = e^{-\sum_{j=1}^m \left(\frac{x_{ij} - C_{kj}}{\sqrt{2}\sigma_j} \right)^2} \tag{7}$$

Where μ_{k_i} is the membership value of cluster k on data i and x_{ij} is data of i on variable of j .

2.3. Distance Function

There are few distance function applied in this research which are:

- Euclidean distance
Euclidean distance is the most common and used distance. This distance is defined for x and y coordinate as [19]:

$$d_{euclidean}(x, y) = \sqrt{\sum_{k=1}^n (x_k - y_k)^2} \tag{8}$$

Where x_k and y_k are the value of x and y on dimension n . This distance considered as the standard distance applied for fuzzy C-means clustering method.

- Minkowski distance
Minkowski distance is defined as [20]:

$$d_{\text{minkowski}}(p, x, y) = \sqrt[p]{\sum_{k=1}^n |x_k - y_k|^p} \tag{9}$$

With p is the minkowski parameter. In Euclidean distance, ($p = 2$). As for in Manhattan distance and Chebysev distance, ($p = 1$) and ($p \rightarrow \infty$) respectively. The metric condition of this function is fulfilled as long as $p \geq 1$.

- Hamming distance
Hamming distance in [18] is defined as:

$$d_{\text{hamming}}(x, y) = |x_k - y_k|, k = 1, 2, \dots, n \tag{10}$$

With x_k and y_k are the value for x dan y in n number of data.

- Minkowski-Chebysev combination distance
Minkowski-Chebysev combination distance is defined by [14], [16] as:

$$d_{\text{minkowski-chebysev}} = t_1 \sqrt[p]{\sum_{m=1}^k |x_m - y_m|^p} + t_2 \max_{m=1}^k |x_m - y_m| \tag{11}$$

With t_1 and t_2 are the weight, and x_m and y_m are the value of x and y in m number of data.

2.4. Cluster Evaluation

Evaluation cluster is applied to measure how good the quality of the formed cluster centroid. The cluster evaluation methods applied in this research are described as:

- Partition Coefficient (PC)
This cluster evaluation is invented by [21] to evaluate the data membership value on each cluster. The higher the value of PC (close to 1) indicate that the quality of the formed cluster is better. The partition coefficient for this research is conducted through this following equation:

$$PC = \frac{1}{N} \left(\sum_{i=1}^N \sum_{j=1}^K \mu_{ij}^2 \right) \tag{12}$$

Where N is the number of research objects, K is the number of clusters, and μ_{ij} is the membership degree in i with the cluster centroid j .

- **Davies Bouldin Index (DBI)**
 Davies Bouldin Index (DBI) is one of the method to measure the cluster validity in clustering method. The objective of this method is to maximize the distance between clusters and minimize the distance between data in the same cluster. The formed cluster will have good quality of cluster if the DBI value is minimum or close to 0 [16]. The equation of this cluster evaluation method is defined as follows:

$$DBI = \frac{1}{c} \sum_{i=1}^c \max_{i \neq j} (R_{ij}) \tag{13}$$

With

$$R_{i,j} = \frac{SSW_i + SSW_j}{SSB_{i,j}} \tag{14}$$

$$SSW_i = \frac{1}{m} \sum_{j=1}^{m_i} d(x_j, c_i) \tag{15}$$

$$SSB_{i,j} = d(c_i, c_j) \tag{16}$$

where:

m_i = the amount of data in the i -th cluster

c_i = center of cluster i

c_j = j cluster

$d(x_j, c_i)$ = data distance with cluster center

3. Result and Discussion

The data applied for the simulation in this research is a hypertension data taken from one of the health center in Yogyakarta. There are total of 100 data with 5 main variables, which are X_1 (age), X_2 (gender), X_3 (systolic pressure), X_4 (diastolic pressure), and X_5 (body weight). Clustering process with FSC will resulting in an output of few different formed clusters. The distance function applied in this research are Euclidean distance, Minkowski distance, Hamming distance, and Minkowski-Chebyshev combination distance. The result of the dataset which transformed into fuzzy number is illustrated as follows:

Table 1. Fuzzy number result

X_1	X_2	X_3	X_4	X_5
0	0	0.4609	0.1289	0.4018
0.3913	1	0.5516	0.4785	0.1468

⋮	⋮	⋮	⋮	⋮
0.5734	0	0.3775	0.2862	0.6813

Next, the data in table 1 will be processed by FSC method. In this research, radius simulation is needed to determine how many clusters are able to be acquired. The simulation result from few number of radius is illustrated in table 2 below.

Table 2. The cluster result for each distance function

Distance	Radius	Number of formed cluster	Time
Euclidean	1.07	2	0.47
	0.83	3	0.57
	0.67	4	0.71
Minkowski	1.55	2	0.42
	1.25	3	0.63
	1.02	4	0.90
Hamming	0.97	2	0.39
	0.79	3	0.62
	0.72	4	0.85
Minkowski-Chebyshev	1.6	2	0.43
	1.31	3	0.66
	1.12	4	0.78

The application of Euclidean distance resulting in the creation of 2 clusters with radius 1.07, 3 clusters with radius 0.83, and 4 clusters with radius 0.63. In Minkowski distance, there are 2 clusters, 3 clusters, and 4 clusters formed with the radius 1.55, 1.25, and 1.02 respectively. As for Hamming distance, there are 2 clusters, 3 clusters, and 4 clusters formed with the radius 0.97, 0.79, and 0.72 respectively. Lastly, the application of Minkowski-Chebyshev combination distance resulting in the formation of 2 clusters, 3 clusters, and 4 clusters with the radius 1.6, 1.31, and 1.12 respectively.

Running time for each distance has a different time. Based on Table 2, in general the Euclidean distance has less running time than the other distances. This can be seen in the number of clusters 3 and 4 at the Euclidean distance each takes 0.57 and 0.71.

Furthermore, all of the cluster which already formed through the distance function are evaluated through the application of Partition Coefficient (PC) and Davies Boulding Index (DBI). This evaluation process is necessary to observe which cluster can be considered as high quality cluster. The output value of PC and DBI evaluation process can be observed in Figure 1 to Figure 3.

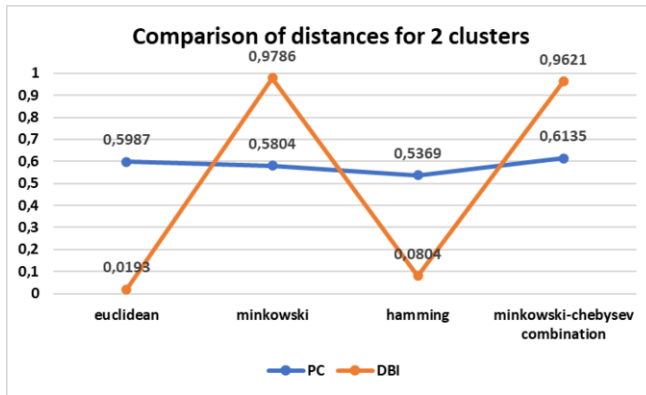


Figure 1. PC and DBI value comparison for 2 formed clusters.

Figure 1 illustrate the comparison between the PC and DBI value for 2 formed clusters in each distance function. Based on the figure 1 above, the PC value for Euclidean distance, Minkowski distance, Hamming distance, and Minkowski-Chebysev distance are 0.5987, 0.5804, 0.5369, and 0.6135 respectively. While the DBI value for each distance function are 0.0193, 0.9786, 0.0804, and 0.9621 respectively.

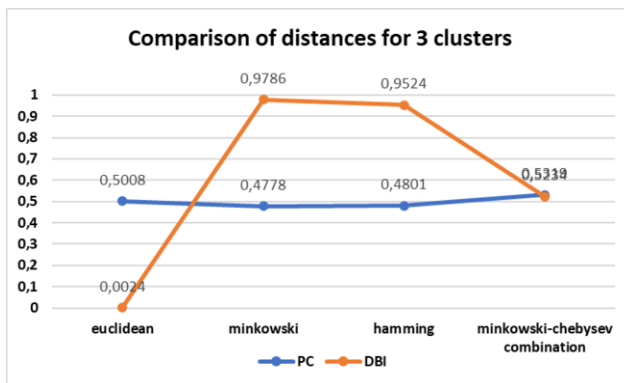


Figure 2. PC and DBI value comparison for 3 formed clusters.

Comparison of the PC and DBI value for 3 formed clusters in each of the distance function is depicted in figure 3. The PC value in the application of Euclidean distance, Minkowski distance, Hamming distance, and Minkowski-Chebysev distance are 0.5008, 0.4778, 0.4801, and 0.5319. As for the DBI value in these four distance function are 0.0024, 0.9786, 0.9524, and 0.5234 respectively.

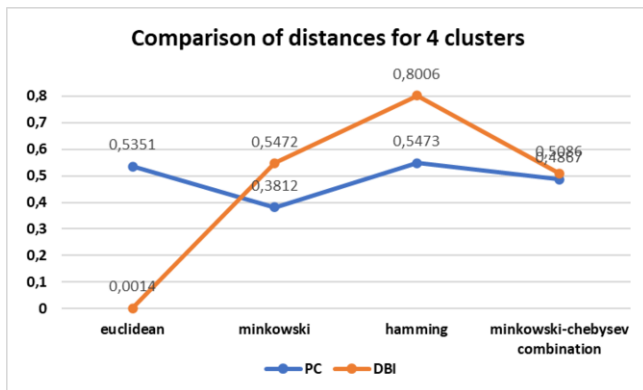


Figure 3. PC and DBI value comparison for 4 formed clusters.

Figure 3 shows the comparison of PC and DBI value for 4 formed cluster in each of the distance function. The PC value in the application of Euclidean distance is 0.5351, Minkowski distance is 0.3182, Hamming distance is 0.5473, and Minkowski-Chebysv distance is 0.4867. Furthermore, the DBI value for Euclidean distance, Minkowski distance, Hamming distance, and Minkowski-Chebysev distance are 0.0014, 0.5472, 0.8006, and 0.5086 respectively.

In this study, the proposed method will produce clusters with different radius for each distance used. The radius values must be simulated one by one to get the desired number of clusters.

4. Conclusions

This research provides the study on the application of Fuzzy Subtractive Clustering which implemented on 4 different distance function, Euclidean distance, Minkowski distance, Hamming distance, and Minkowski-Chebysev distance. The acquired clusters then evaluated through the application of Partition Coefficient (PC) method and Davies Bouldin Index (DBI) method. In this research, the DBI result in the application of Euclidean distance provides good cluster evaluation value for the 4 formed clusters with DBI 0.0014. This conclusion is suitable with the criteria in DBI where the lower the DBI value (close to 0), the better the quality of the formed cluster. From the PC cluster evaluation, the best quality cluster created in the application of Minkowski-Chebysev distance for the two formed clusters with 0.06135 PC value. This conclusion also based on the criteria where the higher the PC value (close to 1), the better the quality of the formed cluster. In future research, it can be done by simulating at another distance with several data sets.

References

- [1] A. C. Rencher and W. F. Christensen, *Methods of Multivariate Analysis*. Wiley, 2012.
- [2] R. Sharma and K. Verma, "Fuzzy shared nearest neighbor clustering," *Int. J. Fuzzy Syst.*, vol. 21, no. 8, pp. 2667–2678, 2019, doi: 10.1007/s40815-019-00699-7.
- [3] J. S. R. Jang, C. T. Sun, and E. Mizutani, "Neuro-Fuzzy and Soft Computing-A Computational Approach

- to Learning and Machine Intelligence [Book Review],” *IEEE Trans. Automat. Contr.*, vol. 42, no. 10, pp. 1482–1484, Oct. 1997, doi: 10.1109/TAC.1997.633847.
- [4] K. Benmouiza and A. Cheknane, “Clustered ANFIS network using fuzzy c-means, subtractive clustering, and grid partitioning for hourly solar radiation forecasting,” *Theor. Appl. Climatol.*, vol. 137, no. 1–2, pp. 31–43, 2019, doi: 10.1007/s00704-018-2576-4.
- [5] S. Zeng, S. M. Chen, and M. O. Teng, “Fuzzy forecasting based on linear combinations of independent variables, subtractive clustering algorithm and artificial bee colony algorithm,” *Inf. Sci. (Nij.)*, vol. 484, pp. 350–366, 2019, doi: 10.1016/j.ins.2019.01.071.
- [6] M. Ghane’i Ostad, H. Vahdat Nejad, and M. Abdolrazzagah Nezhad, “Detecting overlapping communities in LBSNs by fuzzy subtractive clustering,” *Soc. Netw. Anal. Min.*, vol. 8, no. 1, pp. 1–11, 2018, doi: 10.1007/s13278-018-0502-5.
- [7] E. S. Abdolkarimi and M. R. Mosavi, “Wavelet-adaptive neural subtractive clustering fuzzy inference system to enhance low-cost and high-speed INS/GPS navigation system,” *GPS Solut.*, vol. 24, no. 2, pp. 1–17, 2020, doi: 10.1007/s10291-020-0951-y.
- [8] S. M. M. Alam and M. H. Ali, “A new subtractive clustering based ANFIS system for residential load forecasting,” *2020 IEEE Power Energy Soc. Innov. Smart Grid Technol. Conf. ISGT 2020*, 2020, doi: 10.1109/ISGT45199.2020.9087653.
- [9] H. Salah, M. Nemissi, H. Seridi, and H. Akdag, “Subtractive Clustering and Particle Swarm Optimization Based Fuzzy Classifier,” *Int. J. Fuzzy Syst. Appl.*, vol. 8, no. 3, pp. 108–122, 2019, doi: 10.4018/ijfsa.2019070105.
- [10] L. Banteng, H. Yang, Q. Chen, and Z. Wang, “Research on the subtractive clustering algorithm for mobile ad hoc network based on the akaike information criterion,” *Int. J. Distrib. Sens. Networks*, vol. 15, no. 9, 2019, doi: 10.1177/1550147719877612.
- [11] S. K. Chandar, “Stock market prediction using subtractive clustering for a neuro fuzzy hybrid approach,” *Cluster Comput.*, vol. 22, no. s6, pp. 13159–13166, 2019, doi: 10.1007/s10586-017-1321-6.
- [12] H. Xu, W. Zeng, X. Zeng, and G. G. Yen, “An evolutionary algorithm based on Minkowski distance for many-objective optimization,” *IEEE Trans. Cybern.*, vol. 49, no. 11, pp. 3968–3979, 2019, doi: 10.1109/TCYB.2018.2856208.
- [13] R. Taheri, M. Ghahramani, R. Javidan, M. Shojafar, Z. Pooranian, and M. Conti, “Similarity-based Android malware detection using Hamming distance of static binary features,” *Futur. Gener. Comput. Syst.*, vol. 105, pp. 230–247, 2020, doi: 10.1016/j.future.2019.11.034.
- [14] O. Rodrigues, “Combining minkowski and cheyshev: new distance proposal and survey of distance metrics using k-nearest neighbours classifier,” *Pattern Recognit. Lett.*, vol. 110, pp. 66–71, 2018, doi: 10.1016/j.patrec.2018.03.021.
- [15] P. Noviyanti, *Fuzzy c-Means Combination of Minkowski and Chebyshev Based for Categorical Data Clustering*. Yogyakarta: Universitas Ahmad Dahlan, 2018.
- [16] S. Surono and R. D. A. Putri, “Optimization of fuzzy c-means clustering algorithm with combination of minkowski and chebyshev distance using principal component analysis,” *Int. J. Fuzzy Syst.*, 2020, doi: 10.1007/s40815-020-00997-5.
- [17] S. Kusumadewi and H. Purnomo, *Aplikasi logika fuzzy untuk pendukung keputusan*. Yogyakarta: Graha Ilmu, 2010.
- [18] K. Rezaei and H. Rezaei, “New distance and similarity measures for hesitant fuzzy soft sets,” vol. 16, no. 6, pp. 159–176, 2019.
- [19] G. Gan, C. Ma, and J. Wu, “Data clustering: theory, algorithms, and applications,” *Soc. Ind. Appl. Math.*, 2020.
- [20] T. Brunello, D. Bianchi, and E. Enrico, *Introduction To Computational Neurobiology and Clustering*. Singapore: World Scientific Publishing, 2007.
- [21] J. C. Bezdek, *Pattern recognition with fuzzy objective function algorithms*. New York: Plenum Press, 1981.

Optimization Model of Unmanned Aerial Vehicle Distribution Path with Integrated Loading and Unloading

Lei WU^a, Ming WEI^{b1}, Xiang CHEN^a

^a *Information Science and Technology College, Nantong University, Nantong 2260191, China*

^b *Air Traffic Management College, Civil Aviation University of China, Tianjin 300300, China*

Abstract. Unmanned aerial vehicle (UAV) delivery has the advantages of small size, high speed, and low cost. A new drone delivery path optimization model with loading and unloading integration is proposed in this study to make full use of UAV(drone) delivery by improving its efficiency. The model considers drone range constraints and loading capacity limitations, analyzes the start and end points of multiple orders, assigns orders to drones from the optimal distribution centers, calculating the order and time to visit all sets and delivery points, and pursuing the least transportation mileage. The ant colony optimization (ACO) algorithm is adopted to solve the problem in two stages. In the first stage, construction rules and pheromones of the solution are defined, and the orders to the UAVs are assigned. In the second stage, by adding constraints to the ACO algorithm, the sequence order of the UAVs visiting the set and delivery points is determined to obtain the optimal path. Finally, a GIS-based delivery platform is developed using Java Development Kit, which is used to produce the optimal scheduling scheme for an example case. A sensitivity analysis of the model parameters is conducted, which proves the proposed model effectiveness.

Keywords. UAV distribution path, Integrated loading and unloading, Ant colony algorithm, Scheduling platform development

1. Introduction

Unmanned aerial vehicle (UAV) or drone delivery is a new industry that has developed rapidly in recent years. In the context of the global epidemic outbreak in 2020, drone delivery has gained even more attention. Making full use of drone delivery to deliver items to customers efficiently and safely has become a major problem. Compared with conventional vehicle (truck) delivery, drone delivery is not restricted by the road network traffic operation situation of space and time, which can solve the 'last mile' delivery efficiency, cost, safety, and other issues. There are differences between truck and drone delivery models. Thus, despite some commonalities between traditional vehicle and UAV delivery path theories, the available findings and approaches concerning the former (truck delivery) cannot be

¹ Corresponding Author: Ming WEI, Air Traffic Management College, Civil Aviation University of China, Tianjin 300300, China; Email: mingtian911@163.com

directly applied to the UAV delivery problem. Therefore, the UAV delivery path optimization problem has attracted extensive attention from scholars worldwide.

In 2015, Murray and Chu [1] proposed the flying sidekick traveling salesman problem (FSTSP) as a new variant of the TSP problem for solving the path planning of cooperative truck-and-drone transportation. Due to the problem complexity, they considered only one truck and one drone, and the drone carried only a single package for delivery. Then, Agatz [2] formulated the traveling salesman problem with drone (TSP-D) problem and solved it using dynamic programming methods. Like the FSTSP problem, TSPD considered the use of a single truck and a single drone. Ha et al. [3] proposed two heuristics for TSPD to optimize the operation cost. Marinelli et al. [4] studied the TSP-D where the drone take-off and return locations could be different and designed a so-called greedy algorithm. Wang et al. [5] reported that the time of the joint truck-and-drone delivery was less than that of truck delivery, even in the worst case. Ferrandez et al. [6] assumed that all goods/parcels were delivered by drones only, while trucks were used as movable delivery points carrying drones, packages, and charging devices. The K-means clustering algorithm was used to determine the truck delivery points, and then a genetic algorithm was applied to optimize the truck. Chang and Lee [7] used the K-means clustering to optimize the truck delivery path by minimizing the delivery time after classifying the customers.

In all the above studies, it was assumed that the UAV could only carry one package at a time for a single-point delivery. However, single-point delivery will increase the flight distance between UAVs' supply and demand points, causing a waste of UAV flight resources. While relevant studies have shown that full operation of multiple UAVs could effectively improve distribution efficiency [8,9], some researchers [10,11,12] have considered that UAVs could carry multiple parcels at a time. Still, these studies did not consider the simultaneous UAV pick-up and delivery, which would envision that upon completing the delivery task, each UAV could go to another location to pick up the parcels to be delivered before completing the subsequent task. In the UAV multipoint delivery operation, route planning is a key factor that directly affects the efficiency of delivery. Kitjacharoenchai et al. [13] proposed a mixed integer planning method for UAV multipoint delivery route search to reduce truck-and-UAV delivery operation time. Salama et al. [14] used an unsupervised machine-learning heuristic algorithm to study UAV's warehouse's location' points and UAV multipoint delivery routes.

The existing approaches have the following two main shortcomings: (1) they involve separated loading and unloading and separated analyses of the UAV collection and delivery paths; (2) they ignore the presence of no-fly zones in the UAV delivery paths.

To mitigate the above shortcomings, this paper formulates the integrated loading and unloading UAV delivery path optimization problem with the account of no-fly zones, as well as applies the ant colony optimization (ACO) algorithm to solve this problem. When several customers place orders involving the start and end points and the number of parcels, the orders are assigned to drones. Such constraints as no-fly zones and drone performance parameters are considered to determine from which distribution center the drones should depart. The order and time to visit all sets and delivery points are calculated to pursue the least distribution cost. Finally, a GIS-based distribution platform developed in Java script is applied to a simple delivery task example to yield the optimal scheduling scheme. Finally, the parameter sensitivity analysis of the model is performed to verify its effectiveness and feasibility.

2. Problem Formulation

The global problem studied in this paper has several constraints and separate subtasks. There are one or more distribution centers and several customer orders, each with information on the origin and destination (collection and delivery points) and the number of parcels to be delivered (cargo). If there is a no-fly zone between any set and delivery points, no direct UAV flight is allowed. Realistic constraints such as no-fly zone, maximum mileage, and maximum load weight of the UAV are considered. Using the drone delivery platform, one has to collect customer order information, assign orders to drones, determine any drone from the best distribution center, calculate the order and time to visit all sets and delivery points and pursue the least distance of drone delivery [10]. When a drone visits the delivery point of a customer order, it must ensure that there is a sufficient number of parcels on the drone to be unloaded, i.e., the drone needs to visit the collection point of that customer order in advance and pick up a sufficient number of parcels. For the spatio-temporal distribution of customer order demands, it is urgent to reveal the intrinsic relationship between the number of drones in the distribution center, the delivery path, and the transportation cost to optimize the resource allocation and pursue the highest system efficiency. Without loss of generality, the following assumptions can be used to make the model more realistic:

(1) Through the online website or mobile client, collect the starting and ending points of all customer orders and the number of goods, distribute the goods (parcels) according to the unified time window, and ignore the impact of the customer's personalized time window on the distribution plan.

(2) Considering the no-fly zone effect on the flight distance between any collection and delivery points, the actual distance can be obtained through available digital maps (e.g., Baidu maps in China or Google maps elsewhere), ignoring the take-off or landing distance.

(3) The effect of the waiting time of UAV in the collection and delivery points on the distribution plan can be ignored.

To illustrate the mechanism of this problem's solution, two alternative scheduling schemes, namely LBU (loading before unloading) and ILU (integrated loading and unloading), are applied to a simple case. The case comprises one distribution center (D) and four customer orders with collection and delivery points of (S1, E1), (S2, E2), (S3, E3), and (S4, E4), with respective parcel (cargo) weights of 2, 3, 2, and 1 kg. The delivery routes of two available drones, UAV1 and UAV 2, are D-S1-S2-E2-E1-D and D-S3-S4-E4-E3-D for the ILU mode versus D-S1-E1-S2-E2-D and D-S3-E3-S4-E4-D for LBU mode. Combined with the air traffic network travel distance, the objective function can be calculated accordingly.

The definitions and symbols of all parameters and variables used in this study are explained as follow.

In terms of Index, i and j represent Pick-up or delivery index, k represents UAV index, o represents Order index, D represents Set of distribution centers, N represents Set of pick-up or delivery points, K represents Set of UAV. In terms of Parameter, w_i^k represents Weight of the UAV k at pick-up or delivery point i , d_{ij} represents Flight distance between pick-up or delivery points i and j , q_o represents Number of parcels at the order o , u_i^o represents The pick-up point i of order o , v_j^o represents The delivery point j of order o , Q represents Maximum cargo load, L represents Maximum mileage,

M represents Fixed large constant. In terms of Decision variable, z_i^k represents Whether the UAV k visits the pick-up or delivery point i, x_{ij}^k represents Whether the UAV k sequentially visits the pick-up or delivery points i and j, y_o^k represents Whether the customer order o is assigned to the UAV k, s_{ij} represents Whether there is a no-fly zone between pick-up or delivery points i and j.

The mathematical model of the problem solution, using the relevant variables and symbols, can be described as follows.

In the proposed model, the objective function of the problem, which seeks to minimize the total travel distance, is derived via equation (1):

$$\min f = \sum_{\forall k \in K} \sum_{\forall i, j \in \text{DUN}} d_{ij} \cdot x_{ij}^k \quad (1)$$

The problem's constraints are formulated via equations (2)-(11) as follows.

Equation (2) implies that each customer order is uniquely assigned to a drone:

$$\sum_{\forall k \in K} y_o^k = 1 \quad \forall o \in O \quad (2)$$

Equations (3) and (4) indicate that the origin and destination of each order are ensured to be visited by a drone:

$$u_i^o + (1 - y_o^k) \cdot M \leq z_i^k \quad \forall o \in O, \forall i \in N, \forall k \in K \quad (3)$$

$$v_j^o + (1 - y_o^k) \cdot M \leq z_j^k \quad \forall o \in O, \forall j \in N, \forall k \in K \quad (4)$$

Equation (5) indicates that the set, delivery point visited by a drone is in the path:

$$2x_{ij}^k \leq z_i^k + z_j^k \quad \forall i, j \in N, \forall k \in K \quad (5)$$

Equation (6) indicates that each drone departs from the distribution center after completing the task and finally returns to the distribution center:

$$\sum_{\forall j \in \text{DUN}} x_{ij}^k = \sum_{\forall j \in \text{DUN}} x_{ji}^k = z_i^k \quad \forall i \in N, \forall k \in K \quad (6)$$

Equations (7) and (8) indicate the load variation relationship between the UAV's adjacent collection and delivery points:

$$w_i^k + \sum_{\forall o \in O} y_o^k \cdot u_i^o \cdot q_o - \sum_{\forall o \in O} y_o^k \cdot v_i^o \cdot q_o + (1 - x_{ij}^k) \cdot M \leq w_j^k \quad \forall i, j \in N, \forall k \in K \quad (7)$$

$$w_i^k + \sum_{\forall o \in O} y_o^k \cdot u_i^o \cdot q_o - \sum_{\forall o \in O} y_o^k \cdot v_i^o \cdot q_o + (1 - x_{ij}^k) \cdot M \geq w_j^k \quad \forall i, j \in N, \forall k \in K \quad (8)$$

Equation (9) indicates that the UAV visits the delivery points to ensure that the cargo is unloaded, while the maximum cargo weight is not exceeded at the collection point:

$$0 \leq w_i^k \leq Q \quad \forall i \in N, \forall k \in K \quad (9)$$

Equation (10) provides that the UAV's travel mileage does not exceed its upper limit:

$$\sum_{\forall i, j \in \text{DUN}} d_{ij} \cdot x_{ij}^k \leq L \quad \forall k \in K \quad (10)$$

Equation (11) implies that no UAV is allowed to pass through the no-fly zone:

$$s_{ij} \leq x_{ij}^k \quad (11)$$

3. The Ant Colony Optimization Heuristic Algorithm

In 1991, Dorigo and Stützle introduced the ant colony optimization (ACO) algorithm[15,16]. It has been widely used in the field of vehicle routing problems. According to the relevant problem characteristics, the three decision variables z_i^k , x_{ij}^k , and y_o^k are involved, where y_o^k determines z_i^k and x_{ij}^k . However, the problem formulated in this study is an NP-hard problem, i.e., its large-scale case cannot be solved by an exact algorithm, while a non-deterministic Turing machine can solve it in

polynomial time. Given this, we designed an ACO-based heuristic algorithm for minimizing the delivery distance. It should assign orders to UAVs in the first stage and determine the set of orders, and the order of delivery points to be visited by UAVs by making constraints on the “ant pheromone-based” pathfinding’ in the second stage. The latter constraints require that there should be a sufficient number of parcels available to be unloaded when UAVs visit the delivery points. The original ACO algorithm is refined by defining the corresponding solution construction rules, pheromones, heuristic data, and selection probabilities. The specific algorithm solution process is further described and discussed in detail.

3.1. Deconstruction rules

Within the ACO approach framework, each UAV (drone) is simulated by a pheromone-producing ant. In the initial stage, any ant starts from a certain distribution center. When the particular ant is located at the collection point $i(u_i^o)$ of a certain order o ($\forall o \in O$), it will find the feasible UAV sets *allowed* that it is allowed to access. It selects a UAV k to execute the order $o(y_o^k)$ with a certain probability and adds its delivery point $j(v_j^o)$ to the alternative path set of the UAV. If *allowed* $\neq \emptyset$, it sends a new UAV to execute the order to establish the feasible solution continuously. Therefore, the two stages of the deconstruction process are as follows:

Stage 1: Order matching with UAV

Step 1: Randomly select an order $\forall o \in O$.

Step 2: When the ant is located in the collection point of an order o ($\forall o \in O$), it finds the accessible, feasible UAV set *allowed* according to the constraints described by equations (9) and (10).

Step 3: To get y_o^k means to select a UAV k from *allowed* to execute order o with a certain probability.

Step 4: When $O = O - \{o\}$, if $O \neq \emptyset$, go to Step 1. Otherwise, the Stage 1 algorithm is terminated, and the

Stage 2: Path Planning of UAV

Step 1: When the ant is located at the delivery point j of an order o ($\forall o \in O$), if the order has been allocated, it will be transferred to Step 2. Otherwise (if no order has been allocated), it will be transferred to Step 3.

Step 2: Check the execution UAV k of the order o , determine the last visited set and the delivery point $i(z_i^k)$, and add them to the path x_{ij}^k , that is, go to Step 4.

Step 3: Remove the delivery point j of the current order o ($\forall o \in O$) from the current path of the ant.

Step 4: The ant randomly accesses the collection point i or delivery point j of a new order o' ($\forall o' \in O$) again.

3.2. The algorithm flow

Step 1: Initialize the parameters such as the maximum number of iterations nc_{\max} , pheromone α and heuristic information β . Set the UAV performance and order data to $t = 0$.

Step 2: Let M ants be randomly located in the distribution center, and let $m = 1$.

Step 3: Each ant selects the next vertex j according to the corresponding p_{ij}^m in different stages via equation (12) and puts j in the current solution set until all the order sets and delivery points are traversed.

$$p_{ij}^m = \begin{cases} \tau_{ij}^\alpha(t)\eta_{ij}^\beta / \sum_{l \in \text{all}} \tau_{ij}^\alpha(t)\eta_{ij}^\beta, & \text{others} \\ \operatorname{argmax}_{l \in \text{all}} \{ \tau_{ij}\eta_{ij}^\beta \}, & \text{if rand} \leq g_o \end{cases} \quad (12)$$

To accelerate the convergence of the initial algorithm, ant m tends to select the edge calculated according to $\operatorname{argmax}_{l \in \text{all}} \{ \tau_{ij}\eta_{ij}^\beta \}$ with a certain probability g_o . In equation (12), the heuristic data $\eta_{ij} = 1/d_{ij}$ represent the cost of UAV's sequential access set, delivery points i and j ; the pheromone τ_{ij} is the expectation of UAV's sequential access set, delivery points i and j ; while all correspond to the delivery points that have not visited the order or the collection points that have visited the order.

Step 4: Calculate the objective function of the solution constructed by the ant, perform a local update of the pheromone via equation (13) and record the local optimal solution $m = m + 1$, if $m \leq M$, then go to Step 3.

$$\tau_{ij}(t+1) = (1 - \varepsilon(\tau_{ij}(t)))\tau_{ij}(t) + \varepsilon(\tau_{ij}(t)) \cdot Q / f^{\text{nn}} \quad (13)$$

Step 5: Perform a global update of pheromone via equation (14):

$$\tau_{ij}(t+1) = (1 - \gamma(\tau_{ij}(t)))\tau_{ij}(t) + \gamma(\tau_{ij}(t)) \cdot Q / f^{\text{bs}} \quad (14)$$

In equations (13) and (14), parameters $\varepsilon(\tau_{ij}(t))$, and $\gamma(\tau_{ij}(t))$ are positive proportional functions located at (0,1) with $\tau_{ij}(t)$ as the independent variable; f^{nn} and f^{bs} are the optimal solutions searched by the nearest neighbor method and ACO algorithm at present, while Q is a constant.

Step 6: When $t = t + 1$, if $t \leq nc_{\text{max}}$, go to Step 2.

4. Example Analysis

4.1. Test environment and example introduction

To verify the model feasibility and effectiveness, a GIS-based distribution platform was elaborated in the Java Development Kit (JDK 1.8), with the main functions, including order management, traffic network management, UAV management, parameter setting, path optimization, and visualization.

Taking the epidemic emergency supply distribution as an example, three distribution centers (D1-D3), five collection points (S1-S5), 29 delivery points (E1-E29), and 30 customer order data were added to this platform. A certain type of UAV with a maximum mileage of 50km and a maximum cargo weight of 10kg was selected. The ACO algorithm basic parameters were taken from [15], including the maximum number of iterations of 500, the number of ants of 100, the pheromone importance factor $\alpha = 1$, and the heuristic function importance factor $\beta = 4$.

4.2. Analysis of experimental results

Comparing the optimal dispatching plans of the ILU and LBU modes listed in Table 1, it was found that four UAVs in total were needed to complete 30 orders.

(1) The total delivery mileage in the ILU mode was 34.1km, and two UAVs were needed in D3, one UAV in D1, and one UAV in D2.

(2) The total delivery mileage in the LBU mode was 36.3km, and two UAVs were needed in D3, one UAV in D1 and one UAV in D2.

The experimental results show that the ILU mode implied less mileage than the LBU one (34.1 vs 36.3 km) with the same number of drones (4) under the constraint of the maximum operating mileage (50 km) and the maximum cargo weight (10kg) of each drone.

Table 1. The delivery plan optimization in the ILU and LBU modes

UAV No.	Integrated loading and unloading (ILU)			Loading before unloading (LBU)		
	Path	Number of orders	Mileage (km)	Path	Number of orders	Mileage (km)
1	D2(0)-S3(4)-S6(10)-E9(8)-E5(6)-E2(5)-E3(3)-E3(2)-E11(1)-E4(1)-D2(0)	7	4.4	D2(0)-S3(1)-S6(4)-S5(10)-E25(9)-E26(8)-E24(6)-E23(5)-E10(4)-E6(3)-E4(2)-E9(0)-D2(0)	8	10.6
2	D3(0)-S1(5)-E14(4)-E13(3)-E12(1)-E8(0)-S2(5)-E7(3)-E19(2)-E22(0)-D3(0)	7	6.2	D3(0)-S2(3)-S6(5)-S3(101)-E5(8)-E3(7)-E2(6)-E2(5)-E3(3)-E11(2)-E7(0)-D3(0)	7	7.2
3	D3(0)-S2(3)-E2(2)-E15(0)-S3(1)-E6(0)-S5(6)-E25(5)-E26(4)-E24(2)-E23(1)-E10(1)-D3(0)	8	13.3	D3(0)-S1(3)-S2(4)-S4(10)-E29(9)-E28(8)-E19(7)-E22(5)-E18(4)-E21(3)-E17(2)-E14(1)-E13(0)-D3(0)	9	10.1
4	D1(0)-S4(8)-E29(7)-E1(6)-S2(7)-E18(6)-S1(7)-E17(6)-E21(5)-E28(4)-E27(1)-E16(0)-D1(0)	8	10.2	D1(0)-S4(5)-S2(7)-S1(10)-E12(8)-E15(6)-E8(5)-E1(4)-E16(3)-E27(0)-D1(0)	6	8.4

4.3. Parameter sensitivity analysis

The effect of the number of distribution centers on the mileage distribution via the ILU and LBU modes was also analyzed in detail. According to the data in Table 2, the following conclusions were made.

(1) The total distributed mileage gradually increased as the number of distribution centers decreased, because the UAVs could not depart from the nearest distribution center, which increased the mileage.

(2) The total distributed mileage of the ILU was less than that of LBU, because the latter mode implied visiting the collection point first and then the delivery point, discarding a part of the return path to the distribution center.

Table 2. The effect of the number of dispatch centers on scheduling results

Number of dispatch centers	Integrated loading and unloading (ILU)			Loading before unloading (LBU)		
	Number of UAVs	Dispatch centers	Total mileage (km)	Number of UAVs	Dispatch centers	Total mileage (km)
1	5	D2	37.1	4	D2	41.1
2	4	D2, D3	35.0	4	D2, D3	37.0
3	4	D1, D2,D3	34.1	4	D1, D2, D3	36.3

The effect of applying several UAVs types with varying maximum mileages and cargo weights via the ILU and LBU modes on the delivery efficiency was also analyzed. The results are summarized in Table 3.

Table 3. The effect of different drone types on scheduling results

UAV types		Integrated loading and unloading (ILU)			Loading before unloading (LBU)		
Weight (kg)	Mileage (km)	Number of UAVs	Dispatch center	Total mileage (km)	Number of UAVs	Dispatch center	Total mileage (km)
10	50	4	D1, D2, D3	34.1	4	D1, D2, D3	36.3
10	20	5	D1, D2, D3	34.3	5	D1, D3	37.1
20	20	2	D2, D3	29.6	2	D1,D3	32.1

It can be concluded from results in Table 3 that:

(1) for the UAVs with the same cargo weight limit, when their maximum mileage decreases, more UAVs are needed to fulfill the same number of orders, and the total delivery mileage grows because the return to the distribution center increases the invalid mileage

(2) for the UAVs with the same maximum mileage limit, when their maximum load decreases, more UAVs are also needed to fulfill the same number of orders. Besides, the differences between the ILU and LBU scheduling schemes are consistent with the above analysis.

In addition, the impact of different order sizes on the computation time was analyzed, as shown in Table 4.

Table 4. The effect of different order sizes on computation time

Number of orders	Integrated loading and unloading (ILU)		Loading before unloading (LBU)	
	Computation time(s)		Computation time(s)	
30	195.459		221.921	
60	251.237		394.518	
120	719.255		1099.798	

As seen in Table 4, the computation time increased gradually with the problem scale. However, it was within the acceptable time range, thus proving the proposed model and algorithm effectiveness. Besides, the ILU total computation time was less than the LBU one, since the latter implied the increased attribute discrimination operation time of some nodes by traversing the loading and unloading separately. The computation results are in line with the intuitive analysis.

5. Conclusions

In this study, the ant colony optimization (ACO) algorithm was used to solve the UAV distribution path optimization model with an integrated loading and unloading (ILU), taking into account the no-fly zone that increased the flight mileage and UAVs' performance origin and destination of customer orders, and other realistic constraints. Comparing the ILU and LBU (loading before unloading) distribution modes, the relationships between the number of UAVs in distribution centers, distribution routes, and transportation costs were identified. The results show that the ILU mode can effectively reduce transportation mileage, make full use of UAVs for pick-up and delivery services, and improve the efficiency of UAVs. Finally, the GIS-based distribution platform using Java Development Kit was elaborated and tested. The following conclusions were drawn:

(1) The proposed model could effectively integrate the collection and delivery tasks and calculate the best scheduling plans for the ILU and LBU modes. The parameter sensitivity analysis for the multipoint pick-up and delivery by UAV was performed. The total transportation mileage of the ILU mode was systematically less than that of LBU, which is considered instrumental in drone delivery optimization practice.

(2) The heuristic algorithm designed in this paper successfully found feasible solutions to the large-scale problem in an acceptable time.

However, this paper addressed the logistics distribution problem for a single type of UAVs and cargo. In reality, the types of UAVs and the diversity of items in the distribution demand greatly impact the distribution scheme. The interrelations among the above factors are vital in finding the best resource allocation, which will be our future research direction.

Acknowledgements:

This paper is funded by the Central College Basic Scientific Research Operating Expenses Fund in Civil Aviation University of China 3122019126.

References

- [1] Murray C C, Chu A G. The flying sidekick traveling salesman problem: Optimization of drone-assisted parcel delivery. *Transportation Research Part C Emerging Technologies*, 2015, 54(5): 86-109.
- [2] Agatz N, Bouman P, Schmidt M. Optimization approaches for the traveling salesman problem with drone. *Transportation Science*, 2018, 52(4): 965-981.
- [3] Ha Q M, Deville Y, Pham Q D, et al. On the min-cost traveling salesman problem with drone. *Transportation Research Part C*, 2018, 86: 597-621.
- [4] Marinelli M, Caggiani L, Ottomanelli M, et al. En route truck drone parcel delivery for optimal vehicle routing strategies. *IET Intelligent Transport Systems*, 2018, 12(4):253-261.
- [5] Wang K, Yuan B, Zhao M, et al. Cooperative route planning for the drone and truck in delivery services: A bi-objective optimisation approach. *Journal of the Operational Research Society*, 2019, 5:1-18.
- [6] Ferrandez S M, Harbison T, Weber T, et al. Optimization of a truck-drone in tandem delivery network using K-means and genetic algorithm. *Journal of Industrial Engineering and Management*, 2016, 9(2):374-388.
- [7] Chang Y S, Lee H J. Optimal delivery routing with wider drone delivery areas along a shorter truck route. *Expert Systems with Applications*, 2018, 104:307-317.
- [8] Ham Andy M. Integrated scheduling of m-truck, m-drone, and m-depot constrained by time-window, drop-pickup, and m-visit using constraint programming. *Transportation Research Part C*, 2018, 91(4): 1-14.
- [9] González P, Canca D, Andrade J, et al. Truck-drone team logistics: A heuristic approach to multi-drop route planning. *Transportation Research Part C*, 2020, 114(7): 657-680.
- [10] Dorling K, Heinrichs J, Messier G G, et al. Vehicle routing problems for drone delivery. *IEEE Transactions on Systems Man & Cybernetics Systems*, 2017, 47(1): 70-85.
- [11] Rabta B, Wankmüller C, Reiner G.A Drone fleet model for lastmile distribution in disaster relief operations. *International Journal of Disaster Risk Reduction*, 2018, 28:107-112.
- [12] Wen T, Zhang Z, Wong K K L. Multi-objective algorithm for blood supply via unmanned aerial vehicles to the wounded in an emergency situation. *Plos One*, 2016, 11(5):1-22.
- [13] Kijjacharoenchai P, Min B C, Lee S. Two echelon vehicle routing problem with drones in last-mile delivery. *International Journal of Production Economics*, 2020, 225(12): 1-14.
- [14] Salama M, Srinivas S. Joint optimization of customer location clustering and drone-based routing for last-mile deliveries. *Transportation Research Part C*, 2020, 114(7): 620-642.
- [15] Tang L, Hao P, Zhang X J. Path planning method for mountain UAV Based on improved ant colony algorithm. *Transportation system engineering and information*, 2019, 19 (1): 158-164.
- [16] Song A, Bao X Z. Elite diffusion ant colony algorithm for three-dimensional path planning of transportation drones. *Computer Engineering and Science*, 2020.

Responses of Climate Indicators to Droughts in SF Bay Area

Patrick Li^{1 a} and Gang Li^b

^a*Basis Independent Silicon Valley, High School Student*

^b*Panyi Technology Inc, San Jose, VP of Engineering*

Abstract. Droughts have appeared in many different regions that increase the chances of wildfires and other health risks like heat strokes. With satellite imaging and more collections on the Google Earth Engine (GEE) library, more information is available to discover trends. This study analyzes different causes and signs of historical drought data in the San Francisco Bay Area then uses several machine learning tools to model the drought.

Keywords. Google Earth Engine, Drought, Climate Change, Cloud Computing, Large-Scale Data Mining.

1. Introduction

The research in the paper was done on Google Earth Engine (GEE) [1] because of its big data parallel computing power. GEE combines multi-petabyte satellite imagery and geospatial datasets with planetary-scale analysis capability [1] making it a good platform to research global and regional climate change. Several GEE datasets were used to analyze the drought in California San Francisco Bay Area with hopes of providing insight on certain climate change indicators. The results might affect this technology innovation center and provide the fundamentals for policy makers on future droughts.

2. Related Works

There are a lot of researches to analyze and predict droughts in different regions and using different methods including machine learning. Peiyu Lai et al. [2] analyzed seasonal indicators related to droughts in Southwest China. Their work performed comprehensive survey on changes of variety of variables including surface water area, vegetation, meteorological factors and human activities, and whether these changes match the start and end of drought period on record without providing a mathematical modeling for predicting drought. Researches [3] have been made with Internet of Things (IoT) sensors that transfer meteorological information to a fog layer. These sensors include temperature, humidity, precipitation, and water levels. This fog layer would compress the data and then transfer it to the cloud for computations. This work's main focus is on building infrastructure for real-time data collection and computing. Another

¹ Corresponding Author, Patrick Li, Basis Independent Silicon Valley, High School Student; Email: patrick.h.li@gmail.com

study [4] uses the Canadian Earth System Model (CanESM2) produced by ClimEx project by Ouranos with the Canadian Regional Climate Model (CRCM5) as well as CanESM2-LE's monthly sea level pressures, to create accurate drought predictions when combined with artificial neural networks. Data captured with satellites have also been used. Their major contribution is applying an Artificial Neural Network drought model to two European domains, Munich and Lisbon. Sumin *et al.* in their research [5], the Scaled Drought Condition Index (SDCI), Standard Precipitation Index (SPI), and topographic characteristics were used in convolutional long short-term memory (convLSTM) and random forest models to generate predictions. Their area of study focused on East Asia.

The study in this paper focuses in San Francisco Bay Area, one of the most populated and important high-tech economic regions, the water shortage has become more frequent in recent years impacting both daily life and economic activities. This area is not studied in related researches. The method proposed uses readily available massive satellite and geo-sensing data to extract information including permanent water area (PWA), seasonal water area (SWA), temperature, precipitation, and drought area and index. The study of this research tries to use these publicly available, valuable datasets to do the data mining, avoiding the need for extra sensor installation or data collection which were performed by some related researches [3]. The extracted data is analyzed against the drought historic records. This data is also feed into the proposed model using a linear regression to train and predict drought patterns. The result is evaluated with correlation coefficient and shows competitive or better performance compared to some earlier researches as in [5] for example.

3. Proposed Methodology

3.1. Datasets Used

In this study, we choose to use the satellite imagery and geospatial datasets readily available in Google Earth Engine (GEE) database. The datasets contain massive global data and we utilize GEE parallel computing capability to extract the data specifically for our region of interest (RoI) – San Francisco Bay Area, and use the powerful GEE API to reduce the multi-dimensional imagery and geospatial data to several easy-to-process indicators such as surface water area, temperature and precipitation. We call this step data extraction stage with GEE. The program is written in JavaScript using GEE Code Editor platform seen in Table 1.

Table 1. Experiment Details

	Tools/Library	Language	Platform/Framework
Data Extraction Stage	Ge Code Editor	JavaScript	Google Earth Engine
Data Condition Stage	Pandas, Numpy, Jupyter	Python	None
Training Stage	Keras, XGBRegressor	Python	XGBoost/Tensorflow

The datasets include JRC Yearly Water Classification History v1.2 [6], TIGER: US Census Counties 2018 [7], GRIDMET DROUGHT: CONUS drought indices [8], and ERA5 Monthly aggregates – Latest climate reanalysis produced by ECMWF / Copernicus Climate Change Service [9]. Most of the data are from satellite remote sensing images and contain huge amount of information. A single step of data processing usually takes hours even with power of GEE parallel computing. Once the data is

processed and extracted, a model using decision-tree ensemble model is constructed with XGBoost to compute predictions, the linear regression and squared error objective were used to train the model.

The JRC Yearly Water dataset [6] contains occurrence of permanent surface water (PSW), seasonal surface water (SSW) and No-Water. The GEE satellite image of geographic region map is split into small tiles, and each tile is labeled with the occurrence of either PSW, SSW or No-Water. The tiles marked with PSW are integrated into total Permanent Water Area (PWA) in the region of interest (RoI). The integration is calculated by GEE Reducer function parallel computing engine. Similarly, SSW labels are used to compute SWA, and No-Water for No-Water Area. In order to focus our analysis on SF bay area, only the areas within the 6 counties of the SF Bay area were included as RoI: Alameda, Contra Costa, Marin, Napa, San Francisco, and Santa Clara. The outlines of these counties were extracted from the TIGER: US Census Counties 2018 dataset [7] as a polygon into GEE and used as a region of interest (RoI) for the data reducer. Figure 1 shows graphs of the areas of No-Water Area, SWA, and PWA which are blue, orange, and gray respectively. The areas are in kilometers squared for each year from 1985 to 2018.

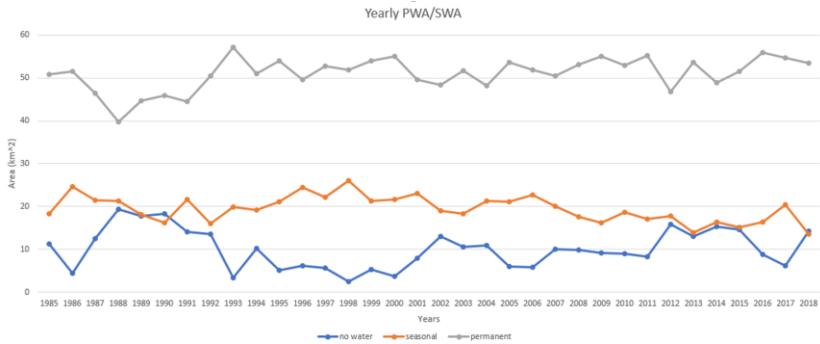


Figure 1. Yearly PWA, SWA and No-Water Area in SF bay area.

ERA5 monthly aggregates dataset [9] contains several global climate parameters, among which the 2-meter (2m) air temperature and total precipitation data were used to analyze the climate change. The monthly air temperature in Santa Clara County were extracted, integrated, averaged and shown in Figure 2. Similarly, monthly precipitation in Santa Clara County change were shown in Figure 3.

To find the drought period and area, the GRIDMET DROUGHT: CONUS drought indices dataset [8] was used. It contains the Evaporative Drought Demand Index (EDDI) around every 5 days from 1985 to 2020. Using the monthly 30-day average, the EDDI drought index from 1985 to 2020 was calculated. Index less than -1.3 is considered a moderate drought, -1.99 to -1.6 is a severe drought, and -2.0 or below is an extreme drought. EDDI was used to mark drought locations [7] in Santa Clara County, and the locations were then integrated to compute the monthly drought area in Figure 4. The drought period could then be identified and compared to PWA and SWA change in Figure 1. A drought is expected to be an increase in drought area, the No-Water Area, and monthly temperature, and drop in precipitation, PWA and SWA. However, many factors lead to the result of a drought and some droughts with changes in one factor are less noticeable than ones with large differences.

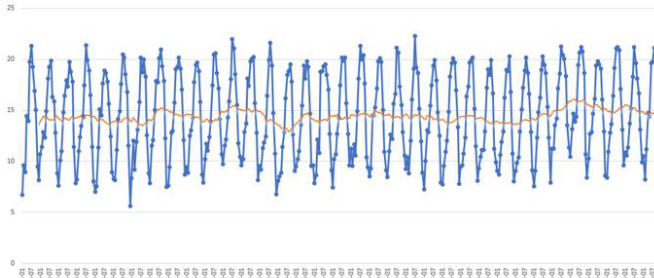


Figure 2. Monthly Temperature (blue curve) and 12-month moving average (orange curve) in Santa Clara County

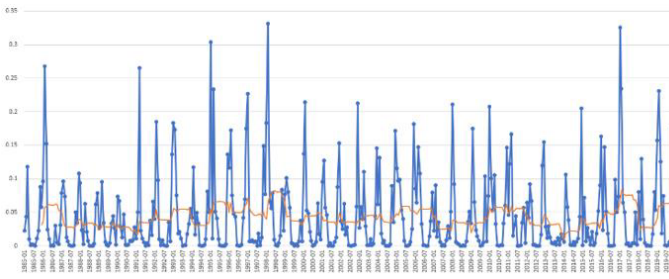


Figure 3. Monthly Precipitation (blue curve) and 12-month moving average (orange curve) in Santa Clara County

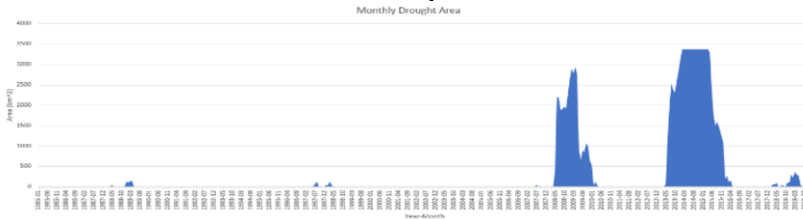


Figure 4. Monthly Drought Area in Santa Clara County

3.2. Proposed Model

This paper’s interest is to find the correlation between the drought occurrence time and pattern with respect to the geo-sensing and climate data such as surface water area, temperature and precipitation. A model was made with decision-tree ensemble in XGBoost’s library, and uses the collected data to train itself. XGBoost is highly effective and widely used machine learning method [10]. The training process is fast and easy to fit variety of target data. The tree ensemble structure is also stable and fast to train and fine-tune whenever new data are added or revised. Since this research is an on-going work, the XGBoost method is chosen so that more data could be easily added and evaluated. The XGBoost is not like Convolutional Neural Network (CNN) or Recurrent Neural Network (RNN) which is hard to interpret, the trained model can actually provide many insights into the mechanism under study, for example the most important or influential input factors to the result. At the end of this section, the experiment of another popular RNN model is also provided.

The input data includes time series (1985-2018) of temperature, precipitation, PWA, SWA and No-Water Area. Month as numbers (1-12) is also added as input to include the

impact of seasonal change. The target ground truth is the calculated drought area as in Figure 4. Temperature and precipitation data is pre-processed using 12-month moving average to remove intrinsic fluctuation noises. Since all this data has different unit and range, they are normalized to facilitate the model training. The normalized data is converted to pandas DataFrame format before fed into the model. Normalized example data is shown in Table 2. This step is the data conditioning stage. The code is written in Python and uses libraries listed in Table 1.

Table 2. Normalized input data and drought ground truth.

MONTH	TEMP	RAINX100	PWA	SWA	NOWATER	DROUGHT
1	6.7224	2.2597	50.8733	18.2422	11.2207	0.0
2	9.6151	4.3679	50.8732	18.2422	11.2207	0.0
3	8.9493	11.7706	50.8732	18.2422	11.2207	0.0
4	14.438	0.9999	50.8732	18.2422	11.2207	0.0
5	13.951	0.1271	50.8732	18.2422	11.2207	0.0

The model is constructed in XGBoost and trained with objective of squared error to the ground truth. The model parameter `colsample_bytree` is set to 0.6 such that 60% of the data is used for training to avoid overfitting. Maximum tree depth, regulation weight `alpha`, number of estimators are adjusted to find the optimal model setting. The model is constructed with `XGBRegressor()` function and trained with `fit()` procedure. In order to evaluate the accuracy of the model prediction, correlation coefficient (r) is used as statistical metric.

$$r = \frac{n(\Sigma y \hat{y}) - (\Sigma y)(\Sigma \hat{y})}{\sqrt{[n\Sigma y^2 - (\Sigma y)^2][n\Sigma \hat{y}^2 - (\Sigma \hat{y})^2]}}$$

n is the number of the samples, y and \hat{y} are the values of reference and predicted drought area. The modeling and training program is written in Python using XGBoost library package as listed in Table 1. We call this step modeling and training stage.

We also evaluated a RNN model which is widely used for analyzing time series sequential data. The model is constructed using 3 layers of Long Short-Term Memory (LSTM) with 20 units each and a Dense fully-connected layer at the end to output the predicated drought area value. The input data is re-arranged with 5 features (PWA, SWA, No-Water Area, Temperature, Precipitation) and 10 time-steps as a 2-dimensional array before fed into the model. ‘‘Adam’’ was used as the optimizer for training with learning rate set at 0.001. To facilitate the training, we added dropout after each layer to avoid overfitting. LSTM models are hard to train and are prone to weight explosions, so we used gradient clipping with a value of 0.2 and normalized the input data by scaling it to ± 0.25 range. Different LSTM cell units, learning rates, dropout rates and clipping values are experimented with. However, the training of this model was not stable and was hard to converge within a reasonable number of epochs. Based on evaluations above, as well as other advantages of XGBoost described at the beginning of this section, XGBoost is chosen in this research.

4. Analysis and Experiment

4.1. Analysis

There is no obvious visual trending correlation between the extracted data and the drought record. Any single input data does not show strong correlation to start or end of

the two drought periods: May 2008 – June 2010, May 2013 – April 2014 shown in Figure 4.

For example, PWA shows the permanent water levels had actually risen slightly during drought period of May 2008 – June 2010 which is counter-intuitive, while drought period of May 2013 – April 2014 could be seen from a peak in No-Water Area or drop in PWA. No-Water Area shows some peaks before the drought period, while the time interval length from the peak to the actual drought start varies. On the other hand, some data correlation could be observed. The average data of No-Water Area was 11.056 km^2 with PWA being 53.629 km^2 , during the drought No-Water Area increased to 14.923 km^2 with the PWA dropping to 50.180 km^2 .

Looking at the temperature data itself in Figure 2, it is hard to identify the drought period. Even though the drought period of May 2013 - April 2014 can be seen from the slight increase of temperature in the winter from 8.099°C to 8.913°C and increase in summer from 20.253°C to 21.202°C , the drought of May 2008 - June 2010 could not be identified, which means that there is not a strong relationship between droughts and the temperatures data alone during them. We see similar characteristics in precipitation data.

The monthly temperature (as in Figure 2), monthly precipitation (as in Figure 3), PWA, SWA and No-Water Area (as in Figure 1), and the drought levels were all gathered into a dataset and put into a model. Because the temperatures were constantly changing through the different seasons in the year the model produced with the data would not be have seen a pattern of sudden spikes of temperature. The solution was to take the moving average in intervals of 12 months to smooth the data points and make it easier to spot periods of drought. The same method of taking the moving average was used on the monthly precipitation for the model. Figures 2 and 3 shows the actual data as blue lines and the calculated average as the orange line. Month as number (1-12) is also used as input to take the seasonal change into account.

4.2. Experiment and Results

Three model parameters were adjusted in order to find the model with the most accuracy, which was tested by comparing the correlation coefficient of the model. These three were the max depth of the model (*max_depth*), L1 regularization (*alpha*), and number of estimators (*n_estimators*). The *max_depth* controls how many levels there are in the model, because the XGBoost model uses decision-trees, the larger the max depth, the more complex the model is. The *alpha* value controls L1 regularization on the weights so weights would not have too much of an influence on a result to avoid overfitting and to make the model more conservative. The *n_estimator* value is the number of decision trees that the model uses together to make a prediction. Larger *n_estimator* results in more complex model. We choose [3,8] for *max_depth*, [10-30] for *alpha* and [5-30] for *n_estimator* as data range in this experiment. After testing different values, increasing the *max_depth* of the model increased the correlation coefficient (*r*) up to 0.99478 with a *max_depth* of 8, however this could be the cause of overfitting. Changing the *alpha* values had little effect as the correlation coefficient did not change much. The last parameter changed was the *n_estimators*. Like the *max_depth*, increasing this value would also improve correlation coefficient because there are more decision trees together. While the parameters changed, the feature importance were also captured, this would give what the model deemed the biggest contributor to its prediction. All correlation values above 0.96 had temperature as their most important feature, with high f scores as shown in Figure 5. As the final result, we choose the model with less complexity while

correlation coefficient (r) is above 0.96: $max_depth=6$, $alpha=15$, $n_estimator=26$, $r=0.966$. The calculated drought area output from this model vs. the ground true is shown in Figure 6.

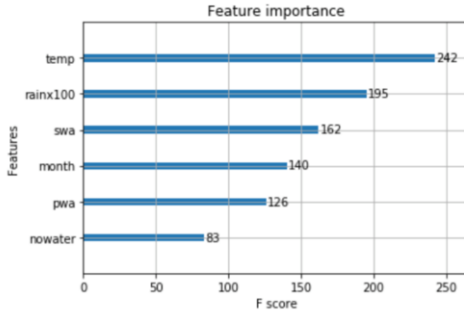


Figure 5. Feature Importance in XGBoost model.

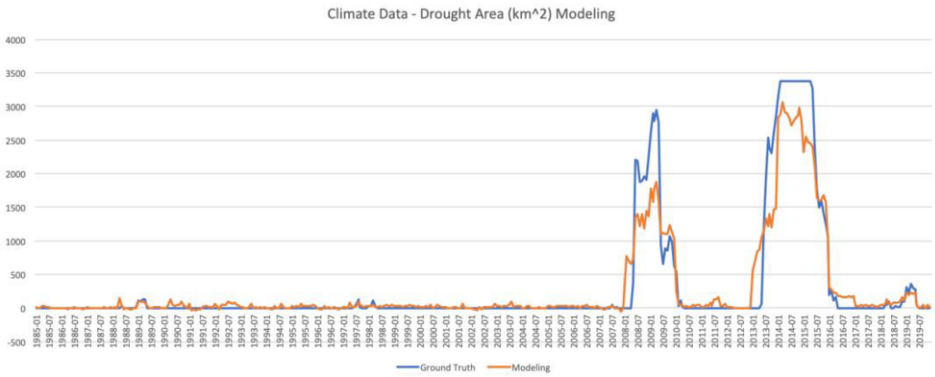


Figure 6. Drought Model vs Drought Ground Truth.

In practical application, predicting future drought based on past and current climate data could enable policy maker to take action in advance. To meet this purpose, the target is shifted 2 years in time axis and similar model is trained. As shown in Figure 7, the model could predict the drought occurrence 2 years in advance.

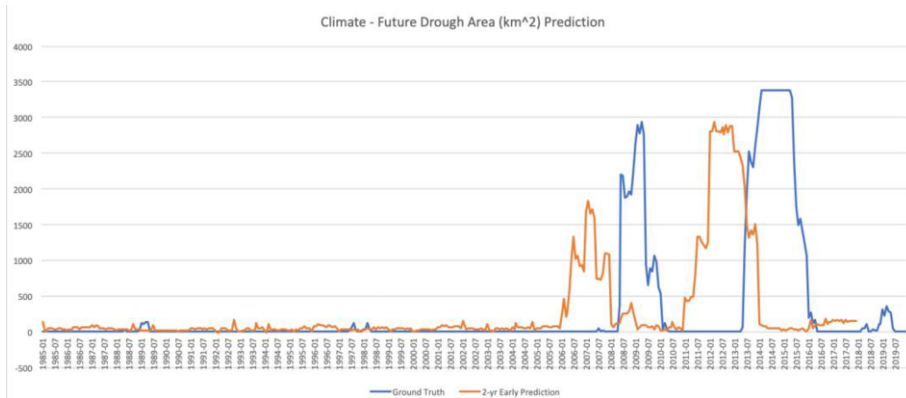


Figure 7. Drought 2-yr Early Prediction vs Drought Ground truth.

5. Conclusion and Future Work

In this work, the author extracted several climate data from GEE satellite imagery and geospatial datasets, including surface water area, precipitation, temperature and drought area in SF bay area. The climate data vs. drought area/occurrence is modeled using decision tree ensemble with XGBoost, trained with linear regression and squared error objective. With time shift in target data, the model is also able to predict the drought occurrence in advance. The model prediction shows good results in terms of r (around 0.96), competitive to other research results [5] (r is around 0.9). Since climate change has long term and complicated impact, more advanced models like RNN/LSTM would be explored to add the accumulation effect, and the prediction would be more robust and precise. More data would be incorporated in the future work, such as vegetation area, cloud area, and possibly the human activity data to explore the more complex drought occurrence mechanism. Due to the fact that the climate change is in larger geographic scale, the author also plans to expand the region of interest to include more surrounding counties' impact and model more accurate models.

References

- [1] Google Earth Engine Documents, <https://developers.google.com/earth-engine/>
- [2] Peiyu Lai, Miao Zhang *et al.*, "Responses of Seasonal Indicators to Extreme Droughts in Southwest China", in remote sensing, March 3rd, 2020
- [3] Amandeep Kaur and Sandeep K. Sood, "Artificial Intelligence-Based Model For Drought Prediction and Forecasting", The British Computer Society 2019, Advance Access publication on 17 November 2019
- [4] Elizaveta Felsche and Ralf Ludwig, "Applying machine learning for drought prediction using data from a large ensemble of climate simulations", Natural Hazard and Earth System Science, 15 April 2021
- [5] Sumin Park, Jungho Im, Daehyeon Han and Jinyoung Rhee, "Short Term Forecasting of Satellite-Based Drought Indices Using Their Temporal Patterns and Numerical Model Output", MDPI Remote Sensing, 24 October 2020
- [6] JRC Yearly Water Classification History, https://developers.google.com/earth-engine/datasets/catalog/JRC_GSW1_2_YearlyHistory
- [7] TIGER: US Census Counties 2018, https://developers.google.com/earth-engine/datasets/catalog/TIGER_2018_Counties
- [8] GRIDMET DROUGHT: CONUS drought indices, https://developers.google.com/earth-engine/datasets/catalog/GRIDMET_DROUGHT
- [9] ERA5 Monthly aggregates – Latest climate reanalysis produced by ECMWF/Copernicus Climate Change Service, https://developers.google.com/earth-engine/datasets/catalog/ECMWF_ERA5_MONTHLY#:~:text=ERA5%20MONTHLY%20provides%20aggregated%20values,10m%20v%2Dcomponent%20of%20wind.&text=All%20other%20parameters%20are%20provided%20as%20monthly%20averages.
- [10] Tianqi Chen, Carlos Guestrin, "XGBoost: A Scalable Tree Boosting System", Cornell University arXiv.org, 10 Jun 2016

Social Media User Profiling Based on Genre Extraction

Konstantin BELOUSOV and Ivan LABUTIN ¹

Perm State University, Perm, Russia

Abstract. The task of automatic user profiling (in particular, determining their psychological parameters from their texts) in Social Networking Services (SNS) is of great practical importance in many fields (PR and marketing, advertising, politics, social relations and recommendations, etc.). However, this problems' solution is often complicated by the need to process large amounts of data and the inability to explain the results achieved. Our article presents a new extensible fuzzy classification method for social media user profiling based on preliminary expert analysis of the linguistic behavior of such users. The proposed method is akin to topic modelling, but is not computationally expensive (so it can be used for large-scale data / web text analysis) and produces results that are relatively easy to interpret. Comparison with the other methods presented in literature also testifies in favor of the approach. The profiling accuracy reaches 65-70% on a relatively small dataset for such kind of studies.

Keywords. Fuzzy Classification, Text Mining, Information Extraction, User Profiling, Social Media, Behavioural Analysis

1. Introduction

Existing works on the user behavior profiling of social network services (SNS) are based on the analysis of social, psychological and behavioral (social circle, likes, the amount of time spent on the network, etc.) aspects (see [1,2]), while the linguistic component of the communication process is not considered. We apply the approach of the unity of behavior (including that determined by social and psychological characteristics) and cognition that exists in the cognitive sciences [3,4]. With regard to our context, we can talk about the relationship between the psychological characteristics of a person and the parameters of his speech behavior in a social media. Confirmation of this hypothesis would open up the possibility of auto-tagging content and profiling of Social Networking Services users.

This formulation of the hypothesis poses the problem of analyzing text arrays consisting of user-generated content from social media. The problem is solved by using the information system of graphosemantic modeling “Semograph” [5] developed by the team. The cornerstone of “Semograph” is a concept of *semantic fields* – sets of linguistic units (words, phrases and even more compound constructions) with meanings that share common semantic feature. Semantic fields can comprehensively describe textual and hy-

¹Corresponding Author: Ivan Labutin, Perm State University, Bukireva Str. 15, 614990 Perm, Russia; E-mail: i.a.labutin@yandex.ru.

peritextual content in terms of semantics, syntax, graphics (for example, the use of special punctuation or emoticons), stylistics (for example, message genres²), etc. This complex description makes it possible to use the sets of semantic fields as the representations of contexts that have been marked up with these fields.

In this work, our task was to implement methods for determining the psychological parameters of a person based on the expert analysis³ of their speech behavior in social media performed in the IS “Semograph”. This article is a continuation of our research [6, 7] and presents the methods we used to solve this problem for users of Russian Social Networking Services.

The theoretical significance of the study lies in determining the dependencies between non-speech and speech parameters of behavior on the one hand, and behavior and cognition on the other, which, ultimately, can be used for automatic content tagging and user profiling of social media services.

From the practical standpoint, the distinctive features of the proposed method are low computational cost and the inherent explainability coming from its linguistic nature.

2. Related Work

A review of works on the problem of studying SNS indicates that several main methodological approaches to the study of the personality of social media users are formed in linguo-personology [8]. The following main groups of approaches can be distinguished:

- Building a set of user characteristics based on thematic and psycholinguistic dictionaries (LIWC [9], MRC [10]) [11]. However, such kind of dictionaries in the open access for the Russian language is almost non-existent – there is Russian LIWC spin-off, but it is far from being as complete as the English one.
- Selecting behavioral characteristics as parameters for the profiling models, such as “likes” under images of certain brands, friendship connections, geotags in photos [12]. But such data is usually quite difficult to extract from a social media sources and it usually requires heavy preprocessing.
- Building the parameters of a user profiling model directly from texts using machine learning – for example, using neural networks together with Word2Vec vectors [13]. Here, a serious drawback is the absence of an explanatory component – it’s not possible to understand why the algorithm has made this or that particular decision.

In this paper, we propose our own solution to the profiling problem based on the study of the users’ speech behavior in social media. We hypothesize that the psychological and social characteristics of a person are reflected in the vocabulary and semantics of the texts produced by that person. Based on this hypothesis, we propose a method that is similar in concept to the group of thematic modeling methods.

In order to reuse results of our previous work, we split the task into two closely related parts:

²Here, we understand a *genre* as a type of text that is being distinguished on the basis of an intention embedded in it. For example, gratitude, accusation, advice, request, etc.

³We rely on expert analysis here, but we’re already on our way to develop automated semantic field extraction methods. However, this topic is outside the scope of the paper.

- Building a linguistic portrait of a user by identifying genres and semantic fields in their unlabeled texts
- Determining psychological parameters of the user based on the identified linguistic characteristics

This paper presents the methods used for the second part of the task.

In addition, we compared our method to the deep learning model proposed in [13] as some kind of baseline in order to test the quality of the proposed approach against it.

3. Proposed Solution

3.1. Dataset

The dataset consists of approximately 18,000 comments of 298 Russian social media users from the same SNS who were pre-surveyed to determine their psychological traits according to the Big Five model. All the users gave an informed consent for their data to be used in this research. The BFI characteristics were originally presented as floating point numbers according to the test scale, but for the purpose of our work and due to the relatively small sample size they were reduced to a binary (indicator) form using simple threshold cutoff. This also enables us to facilitate comparison with other studies, as they also tend to use binary form for the Big Five (BFI) traits levels.

The dataset structure is given in the Table 1.

“+” and “-” in the first column mean high and low BFI trait level respectively. Numbers represent the count of users with the specified level of the particular trait. The labels “bfia”, “bfic”, “bfio”, “bfjn” and “bfie” is a codification given for such traits as agreeableness, conscientiousness, openness to experience, neuroticism and extraversion and represents BFI personality traits in the exact same order.

	bfia	bfic	bfio	bfjn	bfie
+	153	129	165	149	133
-	145	169	133	149	165

Table 1. Dataset structure

Text data (user comments) was preprocessed with the state-of-the-art natural language processing pipeline which included the TweeterTokenizer from the NLTK Python package [14] and our own dictionary-based normalizer trained on OpenCorpora.org dataset (<https://opencorpora.org/>).

3.2. Genres and Semantic Field Detection in User Texts

The detection of semantic fields and genres in user comments was performed by experts manually in the “Semograph” system. In total, 40 different genres and about 60 semantic fields (such as “question”, “aggression”, “jargon”, “poetism”, “common language”, “foul language”, etc) were identified in user texts.

3.3. BFI Detection based on Genres and Semantic Fields

At this step, we performed BFI detection for users based on their linguistic behavior.

We started with two matrices. The first one, which we call CF , represents the relation between all comments of all users and their corresponding semantic fields. This matrix was constructed from the data manually labeled by experts in the “Semograph” system. Each element CF_{fc} in it represents the number of occurrences of the specific semantic field f taken from all the fields F in the specific comment c taken from all the comments C . The second matrix, UB , represents each users’ BFI levels calculated according to BFI test. It’s elements UB_{tu} are real-valued numbers that show level of BFI trait t taken from the list of all traits T of the user u from the list of all users U .

First, we converted our real-valued matrix UB into a matrix of indicators I based on the mean value of each parameter:

$$I_{tu} = UB_{tu} > \overline{(UB_{tu})_{\forall u \in U}}, \forall u \in U, \forall t \in T \quad (1)$$

Thus, the matrix I element i_{tu} represents the indicator (0 or 1) for high level of BFI trait $t \in T$ for the user $u \in U$.

Next, user semantic profile S was constructed based on comments-fields matrix CF by averaging number of occurrences of semantic fields between comments of the same user:

$$S_{fu} = \overline{(CU_{fc})_{c \in C_u}}, \forall u \in U, \forall f \in F \quad (2)$$

where C_u denotes a list of the comments from the user u .

These values were normalized among the columns (per-user) to clamp the sum to 1, thus semantic profile matrix S can be viewed as a probability matrix representing the chance of encountering a specific semantic field $f \in F$ in the users’ $u \in U$ comments.

At the last step, we combined S and I to get matrix B which effectively represents the probability of a highly accented BFI trait based on semantic fields’ counts:

$$B_{tf} = \sum_{\forall u \in U} S_{fu} I_{tu}, \forall f \in F, \forall t \in T \quad (3)$$

This matrix B was then used to calculate BFI levels on the test dataset. The process for this follows the same math as above, but as a last step we multiply elements of users’ semantic profile matrix S' by B to get an I' , the matrix that show the users’ BFI trait level:

$$I'_{tu} = \sum_{\forall f \in F} S'_{fu} B_{tf}, \forall u \in U, \forall t \in T \quad (4)$$

We should note here that while an original I matrix built on the train set is a binary indicator matrix, the resulting I' for the test set is real-valued and, in effect, a probability matrix. That makes our classifier fuzzy and allows us to make more flexible evaluation of the results.

Initial testing revealed the need to reduce the number of semantic fields used to determine the level of a specific BFI indicator, in particular to reduce computational costs. For this purpose, the selection of the set of semantic fields F , showing the best results, was carried out using a genetic algorithm. A minimum of the F1 metric among 3 experiments on a random test sample was used as a fitness function. The genes in the chro-

mosomes encoded the presence / absence of a specific semantic field. As a result, each separate psychological trait was matched with its own set of 25-35 language parameters that are relevant for the speech of each user.

Figure 1 displays the experiments' pipeline in the IDEF0 notation.

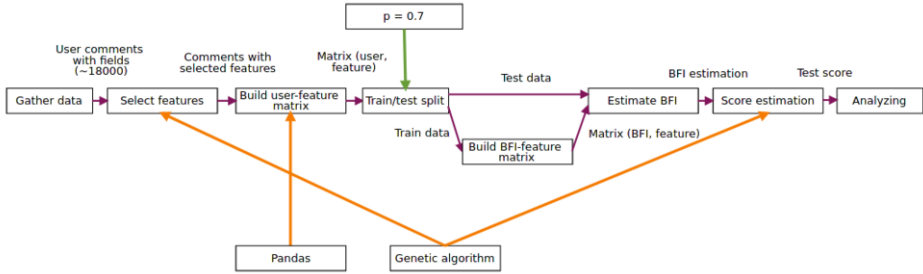


Figure 1. BFI detection pipeline.

The results of this stage of the experiment are shown in the Table 2.

3.4. BFI Detection with Deep Learning

An interesting model based on convolutional neural networks was proposed in [13]. That model solves the problem of user comment-based profiling using word2vec, MRC and LIWC. We decided to compare this model with the one we proposed. However, we were unable to directly use the code provided in our environment, so we implemented the model from scratch according to the described architecture using Keras [15], NumPy [16], Gensim [17], Theano [18] and TensorFlow [19] libraries. The LIWC Russian dictionary was also used.

Figure 2 shows a model of the experiment, also in the IDEF0 notation.

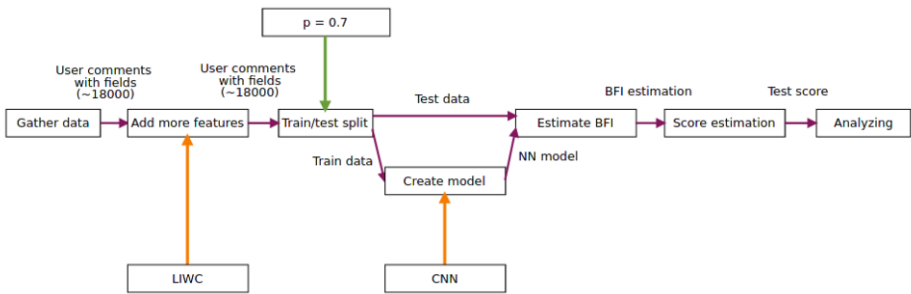


Figure 2. Experiment to identify BFI using a neural network

The results of this experiment are summarised in the Table 2.

3.5. Results

Table 2 shows the results of computational experiments as a F1-scores for each experiment (rows) and BFI traits (columns). CNN (E) – best original work results [13] for

	bfi _a	bfi _c	bfi _o	bfi _n	bfi _e
CNN (E)	0.56	0.57	0.62	0.59	0.58
CNN (R)	0.44	0.45	0.32	0.50	0.50
Our method	0.69	0.65	0.61	0.70	0.59

Table 2. Experiments' results, F1-score

English are taken as a baseline. CNN (R) – our implementation on our Russian dataset. Best results are highlighted.

We can see that in most cases our lingosemantic model scored even higher on Russian than original CNN on English, tailing close in the “bfi_o” case. Original CNN model performs quite low on the Russian language; perhaps some adjustments and tweaks may be of help here.

4. Conclusion

The detection of BFI parameters of social media users, as we have shown, can rely on linguistic analysis of speech behavior. Usage of a genetic algorithm for the selection of significant semantic fields for each psychological trait allowed to eliminate insignificant semantic fields for each psychological trait and significantly improved the profiling model with the BFI detection accuracy reaching 70%. Thus we can say that the presented approach to identifying the psychological parameters of social network users through a preliminary determination of their language behavior gives good results compared to the approaches proposed in the literature.

Overall, it can be concluded that the initial hypothesis about the influence of persons' psychological parameters on his linguistic behavior is proven to be correct, and the method can be used to efficiently build digital representations of SNS users, mark content and calculate optimal patterns of content movement in social media.

5. Future Work

The proposed method offers a wide scope for improvement. The next important step is to move from expert analysis in the data preparation procedure to an automated semantic field annotation methods. In the second stage of the algorithms, instead of using simple probability matrix, it is quite possible to use some more advanced algorithms. It is also possible to expand the list of the fields themselves, as well as apply boosting at the first stage to increase the volume of the training set by the comments of users who did not explicitly pass the psychological survey but gave an informed consent about participation.

Acknowledgments

This study is supported by the Ministry of Science and Higher Education of the Russian Federation, State Assignment No. FSNF-2020-0023 (Research Project of Perm State University, 2020–2022).

The experiment with the CNN was carried out on the computing cluster of the Perm State National Research University (<https://wiki.hpc.psu.ru>).

References

- [1] Buffardi LE, Campbell WK. Narcissism and Social Networking Web Sites. *Personality and Social Psychology Bulletin*. 2008;34(10):1303–1314. PMID: 18599659. Available from: <https://doi.org/10.1177/0146167208320061>.
- [2] Dunbar RIM, Arnaboldi V, Conti M, Passarella A. The structure of online social networks mirrors those in the offline world. *Social Networks*. 2015;43:39–47. Available from: <https://www.sciencedirect.com/science/article/pii/S0378873315000313>.
- [3] Behrens TEJ, Muller TH, Whittington JCR, Mark S, Baram AB, Stachenfeld KL, et al. What is a cognitive map? Organising knowledge for flexible behaviour. *bioRxiv*. 2018. Available from: <https://www.biorxiv.org/content/early/2018/07/10/365593>.
- [4] Wilmer HH, Sherman LE, Chein JM. Smartphones and Cognition: A Review of Research Exploring the Links between Mobile Technology Habits and Cognitive Functioning. *Frontiers in Psychology*. 2017;8:605. Available from: <https://www.frontiersin.org/article/10.3389/fpsyg.2017.00605>.
- [5] Baranov D, Belousov K, Erofeeva E, Leshchenko Y. SEMOGRAPH Information System as a Platform for Network-Based Linguistic Research: A Case Study of Verbal Behavior of Social Network Users. In: Uskov VL, Howlett RJ, Jain LC, editors. *Smart Education and e-Learning 2019*. Singapore: Springer Singapore; 2019. p. 313–324.
- [6] Shchebetenko S. Reflexive characteristic adaptations explain sex differences in the Big Five: But not in neuroticism. *Personality and Individual Differences*. 2017;111:153–156. Available from: <https://www.sciencedirect.com/science/article/pii/S0191886917300806>.
- [7] Belousov K, Erofeeva E, Baranov D, Zelyanskaya N, Shchebetenko S. The Multi-Parameter Analysis of Linguistic Data in the Information System Semograf (On the Example of the Study of Social Network Users' Speech). *Vestnik Tomskogo gosudarstvennogo universiteta Filologiya*. 2020 04:6–29.
- [8] U VG, K S, Shenoy PD, R VK. An Overview on User Profiling in Online Social Networks. *International Journal of Applied Information Systems*. 2017 Jan;11(8):25–42. Available from: <http://www.ijais.org/archives/volume11/number8/960-2017451639>.
- [9] Tausczik YR, Pennebaker JW. The psychological meaning of words: LIWC and computerized text analysis methods. *Journal of Language and Social Psychology*. 2010;0261927–09351676.
- [10] Wilson M, Division I. MRC Psycholinguistic Database: Machine Usable Dictionary, Version 2.00. *Behav Res Methods*. 1997 06;20.
- [11] Tandra T, H, Suhartono D, Wongso R, Lina Prasetyo Y. Personality Prediction System from Facebook Users. *Procedia Computer Science*. 2017 12;116:604–611.
- [12] Kosinski M, Stillwell D, Graepel T. Private traits and attributes are predictable from digital records of human behavior. *Proceedings of the National Academy of Sciences*. 2013;110(15):5802–5805. Available from: <https://www.pnas.org/content/110/15/5802>.
- [13] Majumder N, Poria S, Gelbukh A, Cambria E. Deep Learning-Based Document Modeling for Personality Detection from Text. *IEEE Intelligent Systems*. 2017 Mar;32(2):74–79.
- [14] Loper E, Bird S. NLTK: The Natural Language Toolkit. In: *Proceedings of the ACL Workshop on Effective Tools and Methodologies for Teaching Natural Language Processing and Computational Linguistics*. Philadelphia: Association for Computational Linguistics; 2002. .
- [15] Chollet F, et al.. Keras; 2015. <https://keras.io>.
- [16] Oliphant T. NumPy: A guide to NumPy; 2006.
- [17] Řehůřek R, Sojka P. Software Framework for Topic Modelling with Large Corpora. In: *Proceedings of the LREC 2010 Workshop on New Challenges for NLP Frameworks*. Valletta, Malta: ELRA; 2010. p. 45–50. <http://is.muni.cz/publication/884893/en>.
- [18] Al-Rfou R, Alain G, Almahairi A, Angermueller C, Bahdanau D, Ballas N, et al. Theano: A Python framework for fast computation of mathematical expressions. *arXiv e-prints*. 2016 May;abs/1605.02688. Available from: <http://arxiv.org/abs/1605.02688>.
- [19] Abadi M, Agarwal A, Barham P, Brevdo E, Chen Z, Citro C, et al.. TensorFlow: Large-Scale Machine Learning on Heterogeneous Systems; 2015. Software available from tensorflow.org. Available from: <https://www.tensorflow.org/>.

Ontology-Driven Data Mining Platform for Fuzzy Classification of Mental Maps

Konstantin RYABININ¹, Konstantin BELOUSOV and Roman CHUMAKOV

Perm State University, Perm, Russia

Abstract. Mental maps are valuable material for Digital Humanities research since they represent a summary of humans spatial experience reflected in their minds. Contributing to this research, we developed a high-level Web-based software platform that allows to collect drawings of mental maps and to perform corresponding data mining and fuzzy classification. The novelty of the proposed platform is the ontology-based integration of mental maps drawing engine and data mining engine, wherein all the essential steps of data mining, including data acquisition, transformation, fuzzy classification, and visual analytics are driven by ontologies. The platform consists of a high-level graphical editor to draw maps and a data flow diagram editor to define the data mining pipeline. The operators available to construct this pipeline are described by ontology, which ensures the platform's extensibility on the knowledge base level. Thereby, the platform created can be used not only for Digital Humanities research but also for testing and evaluation of new data mining and fuzzy classification methods. Currently, we have evaluated weighted fuzzy pattern matching for mental maps fuzzy classification and confirmed the reasonable performance of this method.

Keywords. Mental Map, Data Mining, Fuzzy Classification, Ontology Engineering, Data Flow Diagrams

1. Introduction

Mental maps are a representation of spatial experience in the human mind [1]. They have been a research object in different social sciences since the second half of the 20th century, serving a tool able to reflect space perception, cognitive processes, and environmental behavior of individuals [1,2]. Information technologies like data mining (DM) and visual analytics bring new tools to leverage this research, raising the mental maps processing to the next level of automation [3].

Mental maps of particular sites (cities, regions, countries, etc.) can be reconstructed by so-called “sketch maps”. While some authors treat “sketch maps” and “mental maps” as synonyms [4], in this work we denote “sketch map” a particular drawing made by an informant, and “mental map” a meaningful model behind this drawing. Therefore, the DM is performed on mental maps, taking sketch maps as raw input.

It turned out that informants when developing a mental map of their country are highly influenced by their regional identity, reflecting the complex state of the corre-

¹Corresponding Author: Konstantin Ryabinin, Perm State University, Bukireva Str. 15, 614990 Perm, Russia; E-mail: kostya.ryabinin@gmail.com.

sponding region from the residents point of view [5]. This is why regional mental maps are valuable material for Digital Humanities research.

One of the most important tasks of mental maps analysis is classification. It allows discovering the informants attitude to the surrounding spatial environment, which, in turn, helps to justify the public moods in a particular region or social group [2,5], as well as to measure individual differences of informants [6]. Mental maps by their nature contain a lot of variations and uncertainties, so classical methods (including classical set theory) are inappropriate for their comparison/classification. In this regard, fuzzy set theory can be used to tackle the mental maps classification problem.

When it comes to sketch maps, traditionally, informants draw them “by hand on a blank sheet of paper, expressing a subjective reality of space using individual and social memory” [4]. However, this approach hinders a straightforward digital analysis of such maps, because the problem of pattern recognition should involve not only map analysis itself, but also non-trivial preprocessing stage based on computer vision. Therefore, special software sketch map editors are required to digitize the drawing process thus improving the speed and efficiency of mental maps DM.

The goal of our work is to develop a software platform comprising both an informant-friendly sketch map editor to collect the appropriate material and analyst-friendly extensible tools to perform fuzzy classification for the purpose of mental map DM to support Digital Humanities research.

The distinctive feature of the approach proposed is the use of ontology engineering methods and means to unify all the essential steps of DM, including data acquisition, appropriate transformation, fuzzy classification, and subsequent visual analytics within a single Web-based ontology-driven platform. The easiness of extensibility ensured by ontologies allows using this platform not only for DM itself but also for testing and evaluation of new DM and fuzzy classification methods.

2. Related Work

Mental maps are extensively used in social sciences as a material to elicit and analyze socio-spatial representations [4], as well as to study the human skills of understanding the structure and functions of a surrounding space [7]. For example, C. Didelon-Loiseau et al. utilized mental maps to identify the regional perception of the whole world by respondents from different countries [1]. In contrast to this, S. Gül used mental maps as a basis to study the urban perception of students at the city level [8]. K. Hátlová et al. found out that mental maps are most of all influenced by biological, psychological, sociocultural, environmental, and educational factors [6].

One of the algorithms suitable for mental maps classification is weighted fuzzy pattern matching [9]. It is relatively old yet pretty reliable, so we decided to use this algorithm for the first test of our approach. In the future, we plan to consider algorithms based on machine learning in the way suggested by Y. Bodyanskiy et al. (which takes numerical data as input) [10] and by H.-X. Li et al. (which works with linguistic rules) [11].

Regarding the software, F. Aram et al. introduced the system called AMMA that enables quantitative evaluation of mental maps complexity and accuracy based on landmarks and paths [3]. Although this system implements a lot of evaluation methods, it is mainly restricted by urban-scale operation and does not provide tools for drawing men-

tal maps. Instead, it allows comparing scanned hand-drawn mental maps with accurate geographical maps.

The well-known popular software like KNIME, Weka, and RapidMiner [12] incorporate state-of-the-art DM methods, which makes them quite universal standalone desktop tools for analysts. However, when it comes to seamless integration with Web applications or evaluation/testing of new DM techniques, there arise certain limitations. In this regard, high flexibility of customization is required. A promising way to achieve flexibility is an ontology-driven software development approach [13].

According to the elaborate survey of D. Dou et al., ontologies enable so-called semantic DM that bridges “semantic gaps between the data, applications, data mining algorithms, and data mining results”, as well as provide “a formal way for representing the data mining flow” [14]. Y. Li et al. proposed an ontology-based framework for self-service knowledge discovery, utilizing ontology to ensure user-centric DM model management capabilities, including selection and reuse of appropriate models [15]. P. Yan et al. proposed an ontological “model to uncover semantic paths between concepts [...] across documents incorporating Wikipedia knowledge” as a background [16]. This model gains Map-Reduce approach to ensure parallelism and outperforms its analogs in terms of semantic information retrieval and relation discovery [17]. K. Joshi et al. proposed using ontology in a fuzzy classification process to improve semantic information retrieval [18]. K. Okoye suggested to enrich fuzzy models with ontology-based semantic annotations, which allow “to determine [...] the presence of different patterns within the discovered models” [19].

Relying on this positive experience, we have adapted our previously created ontology-driven visual analytics platform SciVi [20] to the tasks of fuzzy classification within the DM process to ensure its configurability and integration capabilities.

3. Proposed Solution

3.1. Background

While working on our previous research, we have created two independent software systems: SciVi ontology-driven client-server platform focused on DM and visual analytics (<https://scivi.tools/>) [20], and Creative Maps Studio focused on creating and editing sketch maps.

The functioning of the SciVi platform is governed by ontologies, which describe available data extraction, transformation, load, and mining mechanisms, whereby forming a SciVi knowledge base (KB). Correspondingly, there are two SciVi user categories: knowledge engineers and analysts. A knowledge engineer acts as a KB administrator, who adapts SciVi to solve the new DM tasks by extending underlying ontologies with necessary functions description or modifying the existing functions descriptions to fine-tune related data processing mechanisms. The ontologies are modified with ONTOLIS visual editor [21] and stored in the lightweight JSON-based format called ONT. An analyst acts as a SciVi end-user, who builds actual DM pipelines using data flow diagrams (DFDs) and performs the data analysis. For this, SciVi provides a high-level graphical DFD editor. DFDs proved their efficiency as a visual language for defining DM pipelines in a variety of real-world case studies in different popular DM software, including KN-

IME, Weka, and RapidMiner. What makes SciVi platform distinctive is that available DFD operators are described by underlying ontologies, so to introduce new operators knowledge engineer just needs to extend the SciVi KB without modifying its source code. Thereby, knowledge engineer can prepare the appropriate operators palette for analyst, without engaging SciVi developers. Technically, each operator is a micro-plugin for the SciVi platform managed by a corresponding fragment of ontology. An ontology-driven approach to managing plugins facilitates the incorporating both self-written and third-party data processing libraries into SciVi platform and documenting them.

Creative Maps Studio (<https://creativemaps.studio/>) is a Web-based editor designed for sketch map drawing. It is implemented using React as a frontend library, FastAPI as a backend framework, and PostgreSQL as a database management system. Unlike traditional maps drawn on paper, digital maps possess full power of automated data processing, including DM, fuzzy set theory, and visual analytics. Moreover, the digital form makes the data collection process much easier, enlarging the geographical coverage of the experiments beyond the borders of particular cities up to nationwide scale.

3.2. *Integrating Creative Maps Studio with SciVi*

To enable in-place mental map DM inside the Creative Maps Studio, we decided to integrate the SciVi platform into it on the basis of loose coupling using ontology-driven REST API.

We have developed a special account type in the Creative Maps Studio, enabling analyst user category along with the regular end-user (informant). In this special account, analyst can see all available sketch maps created by informants and select the arrays of maps for DM. Selected maps can be exported to SciVi. To optimize export process in terms of ergonomics and network traffic, we extended the SciVi server and client with corresponding REST API that enables to request available operators and to order instancing of specified operators with specified settings in the DFD.

Communication between Creative Maps Studio and SciVi platform is as follows. When the analyst logs in to his/her account, Creative Maps Studio requests available data source connectors from the SciVi server, specifying the name of corresponding SciVi DM operators ontology. The SciVi server responds with an ONT-formatted ontology O describing available data extraction operators. This ontology defines the available settings and URI of each operator.

The export menu in the Creative Maps Studio is automatically filled up with available operators, enabling analyst to select maps of interest and give a command to load them to SciVi using particular data extraction operator. Upon this command, the Creative Maps Studio opens up the window with the SciVi client (providing the SciVi DFD editor) and instructs it via WebSocket to instantiate the chosen operator with appropriate settings in DFD editor. WebSocket API call syntax is automatically inferred by Creative Maps Studio from the ontology O . This action can be repeated multiple times when analyst needs to export different maps or map arrays for upcoming DM. After the export of needed maps, analyst specifies the rest of the DM pipeline within the SciVi client DFD editor by instantiating required operators and linking them to define a data flow.

Upon the explicit command of analyst, SciVi executes the created pipeline, wherein the execution of particular operators is being distributed between the SciVi server and

client according to the meta-information stored in the operators ontology. Data flow between server and client is seamless thanks to a direct WebSocket connection. Execution of data extraction operators leads to the specific GET requests to the Creative Maps Studio server that responds with JSON-formatted maps or map arrays. Maps are preprocessed by bringing all the numerical values of objects parameters to the single discrete scale suitable for subsequent classification.

Being ontology-driven, the communication protocol of Creative Maps Studio and SciVi is very flexible: should SciVi platform be extended with new data extraction mechanisms suitable for mental maps, these mechanisms will be automatically available in Creative Maps Studio.

3.3. Fuzzy Classification of Mental Maps in SciVi

In our research, we applied a weighted fuzzy pattern matching algorithm [9] to measure similarity between mental maps created by random informants and mental maps of people living in particular regions. The DM pipeline declared as a DFD within the SciVi platform environment is shown in Figure 1. Each DFD node represents a single operator described in the SciVi ontology.

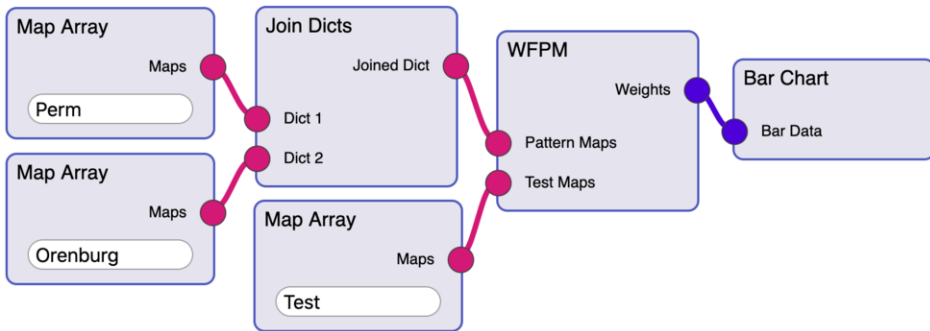


Figure 1. DM pipeline defined in the SciVi platform using DFD graphical notation.

“Map Array” nodes depict the data extraction operators, which are generated automatically according to analyst’s choice as described in Section 3.2. The extracted data are encoded as a key-value dictionary, where the key is the name of map array (“Perm”, “Orenburg”, and “Test”, respectively; these names are assigned by analyst when performing export operation), and the value is the actual array of corresponding maps. The “Join Dicts” node represents the concatenation of dictionaries.

“WFPM” node stands for “Weighted Fuzzy Pattern Matching” operation, which relies on the algorithm presented in [9]. Formally speaking, each map is a set of objects, and each object is a set of properties like coordinates, size, color, etc. Currently, we take into consideration only numerical properties of settlements.

Let us denote the fuzzy classification of maps as F . Then

$$F(P, T, W) = \bigcup_{j=1}^{|T|} \bigcup_{i=1}^{|P|} \max_{k=1, |T_j|} \left(\max_{l=1, |W|} (\min(\mu_{k,l}(P_i, T_{j,k,l}), W_l)) \right), \quad (1)$$

where P is a pattern set (array of maps of known regions; this array is depicted in Figure 1 as “Pattern Maps” slot), T is a test set (array of maps, for which to find fuzzy belonging to the regions from the pattern set; this array is depicted in Figure 1 as “Test Maps” slot), P_i is an individual pattern representing the i -th region, T_j is a j -th test map, $T_{j,k,l}$ is an l -th property of k -th settlement of j -th test map, W_l is a weight denoting the importance of the l -th property, $\mu_{k,l}$ is a function of fuzzy belonging of a j -th test map to the i -th pattern calculated for k -th settlement according to its l -th property. Denoting $T_{j,k,l}$ as x ,

$$\mu_{k,l}(P_i, x) = D_{i,k,l}(g(x)) + \frac{D_{i,k,l}(h(x)) - D_{i,k,l}(g(x))}{h(x) - g(x)} (x - g(x)), \tag{2}$$

where $D_{i,k,l}$ is a frequency distribution of $\{P_{i,m,k,l} \mid m = \overline{1, |P_i|}\}$ set (m denotes particular map in the i -th pattern), $g(x)$ clamps x to the nearest element of $P_{i,k,l}$ range, and $h(x)$ picks the element next to the one given by $g(x)$. The μ function is extended by 0 wherever (2) is undefined.

The ontology fragment describing the “WFPM” operator is shown in Figure 2. It declares that “WFPM” is a “Fuzzy Classification” method with two inputs (“Pattern Maps” and “Test Maps”) of the “MapArrayDict” type and one output (“Weights”) of the “Grid” type. There are also multiple settings defining the weights of different map objects properties used in fuzzy pattern matching (in Figure 2 only “X Weight”, “Y Weight”, and “Size Weight” are shown, however in fact there are more weights; the entire ontology of WFPM operator is available in the SciVi OpenSource repository under <https://github.com/scivi-tools/scivi.web>). An important part of the description is “WFPM Worker” concept representing an actual client-side implementation of the operator that contains a link to the JavaScript source code. The source code is automatically appended to the SciVi Web client when the corresponding operator is requested. This is how the SciVi plugin management works. This way of adding plugins appears to be very fast, easy, and flexible, as we have proved earlier [20].

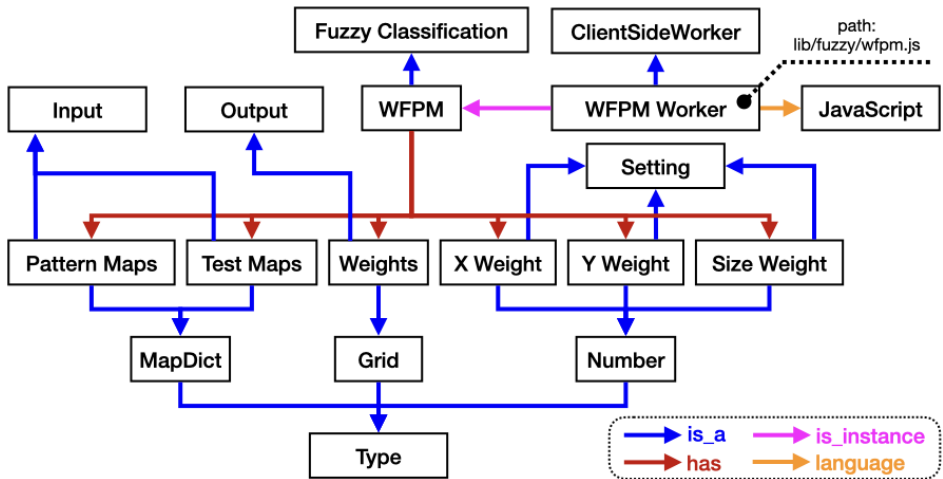


Figure 2. SciVi ontology fragment describing the fuzzy classification operator.

The last step of the DM pipeline is data visualization as a bar chart (“Bar Chart” node), which makes the classification more illustrative. The visualization result is

shown in Figure 3. The interactive visualization is available online at <https://scivi.semograph.com/mmaps?preset=fuzzyMentalMaps.json>. The quantitative analysis and significance test of results obtained is presented in Table 1. WFPM and Reference columns indicate the obtained and ground-truth values in a format (*Perm; Orenburg*). The ground-truth values are known to us since we used maps of the informants with known residence to test the WFPM algorithm. Residual is calculated based on normalized Euclidean distance from WFPM result to the Reference value. The average residual is 0.33, so we consider WFPM as an acceptable fuzzy classification algorithm.

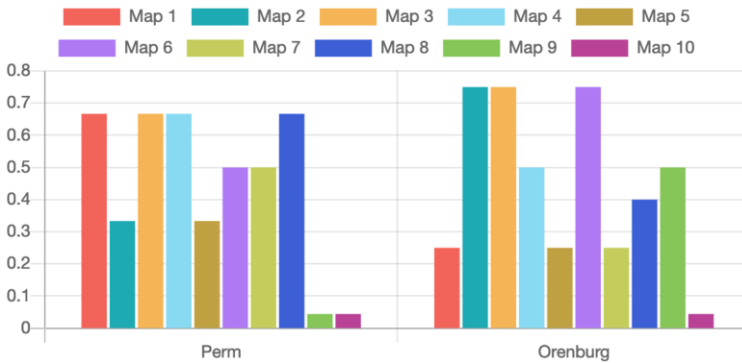


Figure 3. Visualization of mental maps fuzzy classification using a bar chart.

Map	WFPM	Reference	Residual
1	(0.67; 0.25)	(1; 0)	0.29
2	(0.33; 0.75)	(0; 1)	0.29
3	(0.67; 0.75)	(0; 1)	0.51
4	(0.67; 0.5)	(1; 0)	0.42
5	(0.33; 0.25)	(0; 0)	0.29
6	(0.5; 0.75)	(0; 1)	0.4
7	(0.5; 0.25)	(1; 0)	0.4
8	(0.67; 0.4)	(1; 0)	0.37
9	(0; 0.5)	(0; 1)	0.35
10	(0; 0)	(0; 0)	0

Table 1. WFPM quantitative analysis and significance test.

4. Conclusion

We intensively use mental maps drawn by informants to study regional identity within Digital Humanities research. This research requires flexible and extensible DM tools leveraged by fuzzy maths. To suit this need, we integrated Creative Maps Studio map drawing software with SciVi visual analytics system using ontology engineering methods and means. Thereby, the entire research, from the data collecting up to the visualization of the fuzzy classification results, can be conducted within a single software platform. We tested this platform performing weighted fuzzy pattern matching of the mental maps to determine the fuzzy regional identity of particular informants. An ontology-driven approach ensures easy extending of this platform with new DM algorithms, which will help us to evaluate other fuzzy classification methods in the future.

Acknowledgments

This work was supported by Russian Science Foundation (grant number 20-18-00336).

References

- [1] Didelon-Loiseau C, de Ruffray S, Lambert N. Mental Maps of Global Regions: Identifying and Characterizing “Hard” and “Soft” Regions. *Journal of Cultural Geography*. 2018;35(2):210–229.
- [2] Henrikson AK. The Geographical “Mental Maps” of American Foreign Policy Makers. *International Political Science Review / Revue internationale de science politique*. 1980;1(4):495–530.
- [3] Aram F, Solgi E, García EH, Mohammadzadeh D, Mosavi A, Shamshirband S. Design and Validation of a Computational Program for Analysing Mental Maps: Aram Mental Map Analyzer. *Sustainability*. 2019;11(14).
- [4] Derrat S, Johany F, Lardon S. Identifying Choremes in Mental Maps to Better Understand Socio-Spatial Representations. *Cybergeo: European Journal of Geography*. 2016.
- [5] Zelyanskaya N, Belousov K, Ichkineeva D. Naive Geography and Geopolitical Semiotics: The Semiotic Analysis of Geomental Maps of Russians. *Semiotica*. 2017;2017(215):235–253.
- [6] Hátlová K, Hanus M. A Systematic Review into Factors Influencing Sketch Map Quality. *ISPRS International Journal of Geo-Information*. 2020;9(4).
- [7] Castellar SMV, Juliasz PCS. Mental Map and Spatial Thinking. In: *Proceedings of the ICA*. vol. 1; 2018. .
- [8] Gül S. A Case Study on the Urban Perception of Disabled Students in Samsun (Turkey). *Review of International Geographical Education Online*. 2020;10:226–248.
- [9] Dubois D, Prade H, Testemale C. Weighted Fuzzy Pattern Matching. *Fuzzy Sets and Systems*. 1988;28(3):313–331.
- [10] Bodyanskiy Y, Dolotov A, Peleshko D, Rashkevych Y, Vynokurova O. Associative Probabilistic Neuro-Fuzzy System for Data Classification Under Short Training Set Conditions. In: *Contemporary Complex Systems and Their Dependability*; 2019. p. 56–63.
- [11] Li HX, Wang Y, Zhang G. Probabilistic Fuzzy Classification for Stochastic Data. *IEEE Transactions on Fuzzy Systems*. 2017;25(6):1391–1402.
- [12] Naik A, Samant L. Correlation Review of Classification Algorithm Using Data Mining Tool: WEKA, Rapidminer, Tanagra, Orange and Knime. *Procedia Computer Science*. 2016;85:662–668.
- [13] Pan JZ, Staab S, Assmann U, Ebert J, Zhao Y. *Ontology-Driven Software Development*. Springer; 2013.
- [14] Dou D, Wang H, Liu H. Semantic Data Mining: A Survey of Ontology-Based Approaches. In: *Proceedings of the 2015 IEEE 9th International Conference on Semantic Computing (IEEE ICSC 2015)*; 2015. p. 244–251.
- [15] Li Y, Thomas MA, Osei-Bryson KM. Ontology-Based Data Mining Model Management for Self-Service Knowledge Discovery. *Information Systems Frontiers*. 2017;19:925–943.
- [16] Yan P, Jin W. Mining Semantic Relationships between Concepts across Documents Incorporating Wikipedia Knowledge. In: *Advances in Data Mining. Applications and Theoretical Aspects*. vol. 7987; 2013. p. 70–84.
- [17] Yan P, Jin W. Building Semantic Kernels for Cross-Document Knowledge Discovery Using Wikipedia. *Knowledge and Information Systems*. 2017;51:287–310.
- [18] Joshi K, Verma A, Kandpal A, Garg S, Chauhan R, Goudar RH. Ontology Based Fuzzy Classification of Web Documents for Semantic Information Retrieval. In: *2013 Sixth International Conference on Contemporary Computing (IC3)*; 2013. p. 1–5.
- [19] Okoye K. Technique for Annotation of Fuzzy Models: A Semantic Fuzzy Mining Approach. *Frontiers in Artificial Intelligence and Applications*. 2019;320:65–75.
- [20] Ryabinin KV, Belousov KI, Chuprina SI. Novel Circular Graph Capabilities for Comprehensive Visual Analytics of Interconnected Data in Digital Humanities. *Scientific Visualization*. 2020;12(4):56–70.
- [21] Chuprina S, Nasraoui O. Using Ontology-based Adaptable Scientific Visualization and Cognitive Graphics Tools to Transform Traditional Information Systems into Intelligent Systems. *Scientific Visualization*. 2016;8(1):23–44.

R-Calculus for Post Three-Valued Description Logic¹

Cungen CAO^a, Lanxi HU^{a,b,2} and Yuefei SUI^{a,b}

^aKey Laboratory of Intelligent Information Processing,

Institute of Computing Technology Chinese Academy of Sciences, China

^bSchool of Computer Science and Technology University of Chinese Academy of Sciences, China

Abstract. R-calculus is a belief revision operator satisfying AGM postulates, and belief revision in ontology engineering is ontology revision, which based logic is description logics. In Post three-valued description logic, a tableau proof system \mathbf{T}_t will be given such that \mathbf{T}_t is sound and complete for t -satisfiability, and nonmonotonic, that is, a theory Δ is t -satisfiable if and only if Δ is deducible in \mathbf{T}_t . Based on the tableau proof system, an R-calculus \mathbf{R}_t will be given such that a configuration $\Delta|C(a)$ is reducible to $C(a), \Delta$ if and only if $C(a)$ is t -satisfiable with Δ , if and only if reduction $\Delta|C(a) \Rightarrow C(a), \Delta$ is deducible in \mathbf{R}_t .

Keywords. Post three-valued logic, Belief revision, Tableau proof system, R-calculus, Concepts

1. Introduction

Belief revision is a topic of logic, computer science and philosophy. Given a knowledge base Δ and a formula A in a logic, A is enumerated into Δ if and only if A is consistent with Δ . AGM postulates [1] are a set of basic requirements a belief revision operator should satisfy. Belief revision in ontology engineering is ontology revision, which based logic is description logics. Traditional ontology revision is based on binary-valued description logics. We consider the three-valued description logics.

In many-valued logic [2][3], it is important to give an explanation of the truth-values other than the truth t and the falsity f . For example, in a three-valued logic [4], the third value m is interpreted as unknown or indeterminate, and the semantic definition of binary logical connectives are independent of m . Description logics [5] are different from traditional logics, because a concept seems natural to have different counterparts. For example, in three-valued description logics, an interpretation C^I of a concept C is decomposed into three parts: $(\emptyset C)^I$, consisting of these elements taking truth-value t ; $(\sim C)^I$, these taking m , and $(\triangleleft C)^I$, these taking f .

¹Supported by the National Key Research and Development Program of China(2017YFB1002300, 2017YFC1700300), National Natural Science Foundation of China (61702234), Beijing NOVA Program(Cross-discipline, Z191100001119014).

²Corresponding Author: Lanxi Hu, BEIJING, CHINA; E-mail: hulanxi17b@ict.ac.cn

R-calculus [6][7] is a belief revision operator satisfying AGM postulates, and a deduction system for enumerating a formula A into a consistent theory Δ to keep the theory A', Δ consistent (denoted by $\models_{\tau} \Delta | A \Rightarrow A', \Delta$, where $\Delta | A$ is called a configuration; $\Delta | A \Rightarrow A', \Delta$ is called a reduction, and A' is A if A is τ -satisfiable with Δ and otherwise $A' = \lambda$, the empty string). A condition that there is a sound and complete R-calculus is that the based logic is decidable. Hence, there are sound and complete R-calculi for propositional logic [8], propositional modal logic [9], etc., and there is no such R-calculus for first-order logic.

Description logics are fragments of first-order logic, some of which are decidable and some are not. We consider one of many-valued description logics: Post three-valued description logics [10], where the logical language of Post logic contains a unary connective \sim , instead of \neg . For Post logic, there are sound and complete tableau proof systems, Gentzen deduction systems and deduction systems for many-placed sequents [3].

\neg		\sim	
τ	f	τ	f
m	m	m	τ
f	τ	f	m

For decidable description logics, a problem is to define the semantics of quantifier concept constructors. In binary ones, an element a belongs to an interpretation of concept $(\forall R.C)$ if for any element b with $(a, b) \in R^I, b \in C^I$; and an element a belongs to an interpretation of concept $\neg(\forall R.C)$ if for some element b with $(a, b) \in R^I, b \notin C^I$. Correspondingly, in Post three-valued description logic and an interpretation I , we define

- an element a belongs to the interpretation of concept $(\forall R.C)$ if for any element b with $(a, b) \in R^I, b \in C^I$;
- an element a belongs to the interpretation of concept $\sim(\forall R.C)$ if $a \notin (\forall R.C)^I$ and for any element b with $(a, b) \in (\circlearrowright R \cup \sim R)^I, b \in (\circlearrowleft C \cup \sim C)^I$;
- an element a belongs to the interpretation of concept $\triangleleft(\forall R.C)$ if there is an element b such that $(a, b) \in (\circlearrowright R \cup \sim R)^I$ and $b \in (\triangleleft C)^I$.

A theory (a set of statements) Δ is τ -satisfiable if there is an interpretation I such that for any statement $C(a) \in \Delta, (C(a))^I \neq \tau$. We will give a tableau proof system \mathbf{T}_{τ} for τ -satisfiability, which is sound, complete and nonmonotonic.

Based on the tableau proof system \mathbf{T}_{τ} , we construct an R-calculus \mathbf{R}_{τ} for $\Delta | A \Rightarrow A', \Delta$. \mathbf{R}_{τ} is shown to be sound and complete, that is,

$$\models_{\tau} \Delta | A \Rightarrow A, \Delta \text{ iff } \Delta | A \Rightarrow A, \Delta \text{ is provable in } \mathbf{R}_{\tau}.$$

Because $\models_{\tau} \Delta | A \Rightarrow \Delta$ iff $\not\models_{\tau} \Delta | A \Rightarrow A, \Delta$, we have

$$\models_{\tau} \Delta | A \Rightarrow \Delta \text{ iff } \mathbf{R}_{\tau} \not\vdash \Delta | A \Rightarrow \Delta.$$

This paper is organized as follows: The next section defines the logical language and the semantics of Post three-valued description logic; the third section gives a tableau proof system for the description logic and shows soundness and completeness theorems; the fourth section gives an R-calculus for τ -satisfiability, and the last section concludes the whole paper.

2. Post three-valued description logic

Let $\mathbf{L}_3 = (\{t, m, f\}, \emptyset, \sim, \triangleleft, \sqcap, \sqcup)$ be an algebraical structure, where

	\emptyset	\sim	\triangleleft	\sqcap	t	m	f	\sqcup	t	m	f
t	t	f	m	t	t	m	f	t	t	t	t
m	m	t	f	m	m	m	f	m	t	m	m
f	f	m	t	f	f	f	f	f	t	m	f

The logical language of Post three-valued description logic contains the following symbols:

- atomic concepts: A_0, A_1, \dots ;
- roles: R_0, R_1, \dots ;
- concept constructors: $\emptyset, \sim, \triangleleft, \sqcap, \sqcup, \forall$.

Concepts are defined inductively as follows:

$$C ::= A \mid \emptyset C \mid \sim C \mid \triangleleft C \mid C_1 \sqcap C_2 \mid C_1 \sqcup C_2 \mid \forall R.C,$$

where A is an atomic concept, and R is a role.

Statements are defined as follows:

$$\varphi ::= C(a) \mid R(a, b) \mid \emptyset \varphi \mid \sim \varphi \mid \triangleleft \varphi.$$

A model M is a pair (U, I) , where U is a non-empty set, and I is an interpretation such that

- for any atomic concept $A, I(A) : U \rightarrow \mathbf{L}_3$;
- for any role $R, I(R) : U^2 \rightarrow \mathbf{L}_3$.

Given an atomic concept A and a role R , we define concepts $\emptyset A, \sim A, \triangleleft A$ and roles $\emptyset R, \sim R, \triangleleft R$ as follows: for any $x \in U$,

$A(x)$	$\emptyset A(x)$	$\sim A(x)$	$\triangleleft A(x)$	$R(x, y)$	$\emptyset R(x, y)$	$\sim R(x, y)$	$\triangleleft R(x, y)$
t	t	f	m	t	t	f	m
m	m	t	f	m	m	t	f
f	f	m	t	f	f	m	t

The interpretation C^I of a concept C is a function from U to \mathbf{L}_3 such that for any $x \in U$,

$$C^I(x) = \begin{cases} I(A)(x) & \text{if } C = A \\ *(C^I)(x) & \text{if } C = *C_1 \\ C_1^I(x) \sqcap C_2^I(x) & \text{if } C = C_1 \sqcap C_2 \\ C_1^I(x) \sqcup C_2^I(x) & \text{if } C = C_1 \sqcup C_2 \\ \min\{\max\{I(\sim R)(x, y), I(\triangleleft R)(x, y), C_1^I(y)\} : y \in U\} & \text{if } C = \forall R.C_1, \end{cases}$$

where $*$ \in $\{\emptyset, \sim, \triangleleft\}$.

Therefore, $C^I(x) = t^3$ if

³In syntax, we use $\neg, \wedge, \rightarrow, \forall, \exists$ to denote the logical connectives and quantifiers; and in semantics we use $\sim, \&, \Rightarrow, \mathbf{A}, \mathbf{E}$ to denote the corresponding connectives and quantifiers.

$$\left\{ \begin{array}{ll} \mathbf{A}y \in U(I(\odot R)(x, y) = \mathfrak{t} \Rightarrow C_1^I(y) = \mathfrak{t}) & \text{if } C(x) = (\odot \forall R.C_1)(x) \\ \mathbf{A}y \in U(I(\odot R \cup \sim R)(x, y) = \mathfrak{t} \Rightarrow (\odot C_1 \sqcup \sim C_1)^I(y) = \mathfrak{t}) & \\ \mathbf{\&E}y \in U(I(\odot R \cup \sim R)(x, y) = \mathfrak{t} \& (\sim C_1)(y) = \mathfrak{t}) & \text{if } C(x) = (\sim \forall R.C_1)(x) \\ \mathbf{E}y \in U(I(\odot R \cup \sim R)(x, y) = \mathfrak{t} \& (\triangleleft C_1)(y) = \mathfrak{t}) & \text{if } C(x) = (\triangleleft \forall R.C_1)(x). \end{array} \right.$$

A theory Δ is \mathfrak{t} -valid, denoted by $\models^{\mathfrak{t}} \Delta$, if for any interpretation I , there is a statement $\varphi \in \Delta$ such that $(\varphi)^I = \mathfrak{t}$; and Δ is \mathfrak{t} -satisfiable, denoted by $\models_{\mathfrak{t}} \Delta$, if there is an interpretation I such that for each statement $\varphi \in \Delta$, $(\varphi)^I \neq \mathfrak{t}$.

Proposition 2.1. For any concept C and interpretation I , and for any $x \in U$, $C^I(x) \cup (\sim C)^I(x) \cup (\triangleleft C)^I(x) = \mathfrak{t}$.

3. Nonmonotonic tableau proof system

Define

$$\begin{aligned} \text{incon}(\Delta) &\text{ iff } \mathbf{E}p(p, \sim p, \triangleleft p \in \Delta) \\ \text{con}(\Delta) &\text{ iff } \neg \mathbf{E}p(p, \sim p, \triangleleft p \in \Delta) \end{aligned}$$

Proposition 3.1. Let Δ be a set of literals. Δ is \mathfrak{t} -satisfiable iff $\text{con}(\Delta)$.

Nonmonotonic tableau proof system $\mathbf{T}_{\mathfrak{t}}$ contains the following axioms and deduction rules: let a be a constant.

• **Axioms:**

$$\frac{\text{con}(\Delta)}{\Delta} (\mathbf{A}_{\mathfrak{t}})$$

where Δ is a set of literals.

• **Deduction rules for modalities:**

$$\frac{f(*_1, *_2)C_1(a), \Delta}{*_1 *_2 C_1(a), \Delta} (*_1 *_2)$$

where $*_1, *_2 \in \{\lambda, \sim, \triangleleft\}$ and $f(*_1, *_2)$ is defined as follows:

$$\begin{array}{c|c} f(*_1, *_2) & \odot \sim \triangleleft \\ \hline \odot & \odot \sim \triangleleft \\ \sim & \sim \triangleleft \odot \\ \triangleleft & \triangleleft \odot \sim \end{array}$$

• **Deduction rules for logical connectives:**

$$\begin{array}{c}
 \frac{\left\{ \begin{array}{l} \odot C_1(a), \Delta \\ \odot C_2(a), \Delta \end{array} \right.}{\odot(C_1 \sqcap C_2)(a), \Delta} (\odot \sqcap) \quad \frac{\left[\begin{array}{l} \odot C_1(a), \Delta \\ \odot C_2(a), \Delta \end{array} \right.}{\odot(C_1 \sqcup C_2)(a), \Delta} (\odot \sqcup) \quad \frac{\left[\begin{array}{l} \sim R(a, d), \Delta \\ \triangleleft R(a, d), \Delta \\ C_1(d), \Delta \end{array} \right.}{\odot(\forall R.C_1)(a), \Delta} (\odot \forall) \\
 \\
 \frac{\left[\begin{array}{l} \sim C_1(a), \Delta \\ \sim C_2(a), \Delta \\ \odot C_1(a), \Delta \\ \sim C_2(a), \Delta \\ \sim C_1(a), \Delta \\ \odot C_2(a), \Delta \end{array} \right.}{\sim(C_1 \sqcap C_2)(a), \Delta} (\sim \sqcap) \quad \frac{\left[\begin{array}{l} \sim C_1(a), \Delta \\ \sim C_2(a), \Delta \\ \triangleleft C_1(a), \Delta \\ \sim C_2(a), \Delta \\ \sim C_1(a), \Delta \\ \triangleleft C_2(a), \Delta \end{array} \right.}{\sim(C_1 \sqcup C_2)(a), \Delta} (\sim \sqcup) \quad \frac{\left\{ \begin{array}{l} \triangleleft R(a, d), \Delta \\ \odot C_1(d), \Delta \\ \sim C_1(d), \Delta \\ \triangleleft R(a, c), \Delta \\ \sim C_1(c), \Delta \end{array} \right.}{\sim(\forall R.C_1)(a), \Delta} (\sim \forall) \\
 \\
 \frac{\left[\begin{array}{l} \triangleleft C_1(a), \Delta \\ \triangleleft C_2(a), \Delta \end{array} \right.}{\triangleleft(C_1 \sqcap C_2)(a), \Delta} (\triangleleft \sqcap) \quad \frac{\left\{ \begin{array}{l} \triangleleft C_1(a), \Delta \\ \triangleleft C_2(a), \Delta \end{array} \right.}{\triangleleft(C_1 \sqcup C_2)(a), \Delta} (\triangleleft \sqcup) \quad \frac{\left\{ \begin{array}{l} \odot R(a, c), \Delta \\ \sim R(a, c), \Delta \\ \triangleleft C_1(c), \Delta \end{array} \right.}{\triangleleft(\forall R.C_1)(a), \Delta} (\triangleleft \forall)
 \end{array}$$

where d is a constant, c is a new constant, and $\frac{\delta_1}{\delta_2}$ means that δ_1 implies δ and δ_2

implies δ ; and $\frac{\delta_1}{\delta}$ means that δ_1 and δ_2 imply δ .

Definition 3.2. A theory Δ is provable in \mathbf{T}_t , denoted by $\vdash_t \Delta$, if there is a sequence $\{\Delta_1, \dots, \Delta_n\}$ of theories such that $\Delta_n = \Delta$, and for each $1 \leq i \leq n$, Δ_i is either an axiom or deduced from the previous theories by one of the deduction rules in \mathbf{T}_t .

Theorem 3.3. For any theory Δ , $\models_t \Delta$ iff $\vdash_t \Delta$.

Because $\models^t \Delta$ if and only if $\not\models_t \Delta$, we have the following

Corollary 3.4. For any theory Δ , $\models^t \Delta$ iff $\not\vdash_t \Delta$.

4. R-calculus

Intuitively, a statement $\odot(C_1 \sqcap C_2)(a)$ is enumerable into Δ to preserve the t -satisfiability of Δ , if either $\odot C_1(a)$ or $\odot C_2(a)$ is enumerable into Δ ; and $\odot(C_1 \sqcup C_2)(a)$ is enumerable into Δ if $\odot C_1(a)$ is enumerable into Δ and $\odot C_2(a)$ is enumerable into $\Delta \cup \{\odot C_1(a)\}$.

Statement $\sim(C_1 \sqcap C_2)(a)$ is enumerable into Δ , if (1) either $\sim C_1(a)$ or $\sim C_2(a)$ is enumerable into Δ ; (2) either $\odot C_1(a)$ or $\sim C_2(a)$ is enumerable into $\Delta \cup \{\sim C_1 \sqcap \sim C_2(a)\}$, and (3) either $\sim C_1(a)$ or $\odot C_2(a)$ is enumerable into $\Delta \cup \{\sim C_1 \sqcap \sim C_2(a), (\odot C_1 \sqcap \sim C_2)(a)\}$; and statement $\sim(C_1 \sqcup C_2)(a)$ is enumerable into Δ , if (4) either $\sim C_1(a)$ or $\sim C_2(a)$ is enumerable into Δ ; (5) either $\triangleleft C_1(a)$ or $\sim C_2(a)$ is enumerable into $\Delta \cup \{\sim C_1 \sqcap \sim C_2(a)\}$, (6) either $\sim C_1(a)$ or $\triangleleft C_2(a)$ is enumerable into $\Delta \cup \{\sim C_1 \sqcap \sim C_2(a), (\triangleleft C_1 \sqcap \sim C_2)(a)\}$.

Statement $\triangleleft(C_1 \sqcap C_2)(a)$ is enumerable into Δ if $\triangleleft C_1(a)$ is enumerable into Δ , and $\triangleleft C_2(a)$ is enumerable into $\Delta \cup \{\triangleleft C_1(a)\}$; and $\triangleleft(C_1 \sqcup C_2)(a)$ is enumerable into Δ if either $\triangleleft C_1(a)$ or $\triangleleft C_2(a)$ is enumerable into Δ .

A statement $\odot(C_1 \sqcap C_2)(a)$ is not enumerable into Δ , if $\odot C_1(a)$ and $\odot C_2(a)$ are not enumerable into Δ ; and $\odot(C_1 \sqcup C_2)(a)$ is not enumerable into Δ if either $\odot C_1(a)$ is not enumerable into Δ , or $\odot C_2(a)$ is not enumerable into $\Delta \cup \{\odot C_1(a)\}$.

Statement $\sim(C_1 \sqcap C_2)(a)$ is not enumerable into Δ if either (1) $\sim C_1(a)$ and $\sim C_2(a)$ are not enumerable into Δ , or (2) $\odot C_1(a)$ and $\sim C_2(a)$ are not enumerable into $\Delta \cup \{\sim$

$C_1 \sqcap \sim C_2(a)\}$, or (3) $\sim C_1(a)$ and $\odot C_2(a)$ are not enumerable into $\Delta \cup \{(\sim C_1 \sqcap \sim C_2)(a), (\odot C_1 \sqcap \sim C_2)(a)\}$; and statement $\sim (C_1 \sqcup C_2)(a)$ is not enumerable into Δ , if either (4) $\sim C_1(a)$ and $\sim C_2(a)$ are not enumerable into Δ , or (5) $\triangleleft C_1(a)$ and $\sim C_2(a)$ are not enumerable into $\Delta \cup \{(\sim C_1 \sqcap \sim C_2)(a)\}$, or (6) $\sim C_1(a)$ and $\triangleleft C_2(a)$ are not enumerable into $\Delta \cup \{(\sim C_1 \sqcap \sim C_2)(a), (\triangleleft C_1 \sqcap \sim C_2)(a)\}$.

Statement $\triangleleft (C_1 \sqcap C_2)(a)$ is not enumerable into Δ if either $\triangleleft C_1(a)$ is not enumerable into Δ or $\triangleleft C_2(a)$ is not enumerable into $\Delta \cup \{\triangleleft C_1(a)\}$; and $\triangleleft (C_1 \sqcup C_2)(a)$ is not enumerable into Δ if $\triangleleft C_1(a)$ and $\triangleleft C_2(a)$ is not enumerable into Δ .

Given a theory Δ and a statement φ , we use Δ to revise φ and obtain φ' , Δ , denoted by

$$\Delta | \varphi \Rightarrow \varphi', \Delta,$$

if

$$\varphi' = \begin{cases} \varphi & \text{if } \Delta \text{ is } \tau\text{-satisfiable with } \varphi \\ \lambda & \text{otherwise.} \end{cases}$$

R-calculus \mathbf{R}_τ consists of the following axioms and deduction rules:

• **Axioms:**

$$\frac{\vdash_\tau \Delta \Rightarrow \vdash_\tau I, \Delta}{\Delta | I \Rightarrow I, \Delta} (\mathcal{A}_\tau)$$

• **Deduction rules for modalities:**

$$\frac{\Delta | f(*_1, *_2)C_1(a) \Rightarrow f(*_1, *_2)C_1(a), \Delta}{\Delta | *_1 *_2 C_1(a) \Rightarrow *_1 *_2 C_1(a), \Delta} (*_1 *_2)$$

• **Deduction rules for logical connectives:**

$$\frac{\begin{cases} \Delta | \odot C_1(a) \Rightarrow \odot C_1(a), \Delta \\ \Delta | \odot C_2(a) \Rightarrow \odot C_2(a), \Delta \end{cases}}{\Delta | \odot (C_1 \sqcap C_2)(a) \Rightarrow \odot (C_1 \sqcap C_2)(a), \Delta} (\odot \sqcap)$$

$$\frac{\begin{cases} \Delta | \odot C_1(a) \Rightarrow \odot C_1(a), \Delta \\ \Delta, \odot C_1(a) | \odot C_2(a) \Rightarrow \odot C_1(a), \odot C_2(a), \Delta \end{cases}}{\Delta | \odot (C_1 \sqcup C_2)(a) \Rightarrow \odot (C_1 \sqcup C_2)(a), \Delta} (\odot \sqcup)$$

$$\frac{\begin{cases} \Delta | \sim R(a, c) \Rightarrow \sim R(a, c), \Delta \\ \Delta | \triangleleft R(a, c) \Rightarrow \triangleleft R(a, c), \Delta \\ \Delta | \odot C_1(c) \Rightarrow \odot C_1(c), \Delta \end{cases}}{\Delta | \odot (\forall R.C_1)(a) \Rightarrow \odot (\forall R.C_1)(a), \Delta} (\odot \forall)$$

and

$$\begin{array}{c}
\left[\begin{array}{l}
\Delta | \sim C_1(a) \Rightarrow \sim C_1(a), \Delta \\
\Delta | \sim C_2(a) \Rightarrow \sim C_2(a), \Delta \\
\Delta, X | \odot C_1(a) \Rightarrow \odot C_1(a), X, \Delta \\
\Delta, X | \sim C_2(a) \Rightarrow \sim C_2(a), X, \Delta \quad (\sim \sqcap) \\
\Delta, X, Y | \sim C_1(a) \Rightarrow \sim C_1(a), X, Y, \Delta \\
\Delta, X, Y | \odot C_2(a) \Rightarrow \odot C_2(a), X, Y, \Delta
\end{array} \right. \\
\hline
\Delta | \sim (C_1 \sqcap C_2)(a) \Rightarrow \sim (C_1 \sqcap C_2)(a), \Delta \\
\left[\begin{array}{l}
\Delta | \sim C_1(a) \Rightarrow \sim C_1(a), \Delta \\
\Delta | \sim C_2(a) \Rightarrow \sim C_2(a), \Delta \\
\Delta, X | \triangleleft C_1(a) \Rightarrow \triangleleft C_1(a), X, \Delta \\
\Delta, X | \sim C_2(a) \Rightarrow \sim C_2(a), X, \Delta \quad (\sim \sqcup) \\
\Delta, X, Z | \sim C_1(a) \Rightarrow \sim C_1(a), X, Z, \Delta \\
\Delta, X, Z | \triangleleft C_2(a) \Rightarrow \triangleleft C_2(a), X, Z, \Delta
\end{array} \right. \\
\hline
\Delta | \sim (C_1 \sqcup C_2)(a) \Rightarrow \sim (C_1 \sqcup C_2)(a), \Delta \\
\left[\begin{array}{l}
\Delta | \triangleleft R(a, c) \Rightarrow \triangleleft R(a, c), \Delta \\
\Delta, \triangleleft R(a, c) | \odot C_1(c) \Rightarrow \triangleleft R(a, c), \odot C_1(c), \Delta \\
\Delta, \triangleleft R(a, c) | \sim C_1(c) \Rightarrow \sim C_1(c), \triangleleft R(a, c), \odot C_1(c), \Delta \\
\Delta | \odot R(a, d) \Rightarrow \odot R(a, d), \Delta \\
\Delta, \odot R(a, d) | \sim R(a, d) \Rightarrow \sim R(a, d), \odot R(a, d), \Delta \\
\Delta | \sim C_1(d) \Rightarrow \sim C_1(d), \Delta
\end{array} \right. \quad (\sim \forall) \\
\hline
\Delta | \sim (\forall R.C_1)(a) \Rightarrow \sim (\forall R.C_1)(a), \Delta
\end{array}$$

where $X = (\sim C_1 \sqcap \sim C_2)(a)$, $Y = (\odot C_1 \sqcap \sim C_2)(a)$, $Z = (\triangleleft C_1 \sqcap \sim C_2)(a)$, and

$$\begin{array}{c}
\left[\begin{array}{l}
\Delta | \triangleleft C_1(a) \Rightarrow \triangleleft C_1(a), \Delta \\
\Delta, \triangleleft C_1(a) | \triangleleft C_2(a) \Rightarrow \triangleleft C_2(a), \triangleleft C_1(a), \Delta \quad (\triangleleft \sqcap)
\end{array} \right. \\
\hline
\Delta | \triangleleft (C_1 \sqcap C_2)(a) \Rightarrow \triangleleft (C_1 \sqcap C_2)(a), \Delta \\
\left[\begin{array}{l}
\Delta | \triangleleft C_1(a) \Rightarrow \triangleleft C_1(a), \Delta \\
\Delta | \triangleleft C_2(a) \Rightarrow \triangleleft C_2(a), \Delta \quad (\triangleleft \sqcup)
\end{array} \right. \\
\hline
\Delta | \triangleleft (C_1 \sqcup C_2)(a) \Rightarrow \triangleleft (C_1 \sqcup C_2)(a), \Delta \\
\left[\begin{array}{l}
\Delta | \odot R(a, d) \Rightarrow \odot R(a, d), \Delta \\
\Delta, \odot R(a, d) | \sim R(a, d) \Rightarrow \sim R(a, d), \odot R(a, d), \Delta \quad (\triangleleft \forall) \\
\Delta | \triangleleft C_1(d) \Rightarrow \triangleleft C_1(d), \Delta
\end{array} \right. \\
\hline
\Delta | \triangleleft (\forall R.C_1)(a) \Rightarrow \triangleleft (\forall R.C_1)(a), \Delta
\end{array}$$

where d is a constant and c is a new constant.

Definition 4.1. A reduction $\Delta | C(a) \Rightarrow C(a), \Delta$ is provable in \mathbf{R}_t , denoted by $\vdash_t \Delta | C(a) \Rightarrow C(a), \Delta$, if there is a sequence $\{\delta_1, \dots, \delta_n\}$ of reductions such that $\delta_n = \Delta | C(a) \Rightarrow C(a), \Delta$, and for each $1 \leq i \leq n$, δ_i is either an axiom or deduced from the previous theories by one of the deduction rules in \mathbf{R}_t .

Theorem 4.2. For any theory Δ and statement $C(a)$, $\models_t \Delta | C(a) \Rightarrow C(a), \Delta$ iff $\vdash_t \Delta | C(a) \Rightarrow C(a), \Delta$.

Because $\models_t \Delta | C(a) \Rightarrow \Delta$ if and only if $\not\vdash_t \Delta | C(a) \Rightarrow C(a), \Delta$, we have the following

Corollary 4.3. For any theory Δ and statement $C(a)$, $\models_t \Delta | C(a) \Rightarrow \Delta$ iff $\not\vdash_t \Delta | C(a) \Rightarrow C(a), \Delta$.

5. Conclusions

This paper gave an R-calculus \mathbf{R}_t for t-satisfiability in Post three-valued description logic, which is sound and complete. Similarly there are R-calculi \mathbf{R}_m and \mathbf{R}_f for m-satisfiability and f-satisfiability, respectively, and there are transformations between $\mathbf{R}_t, \mathbf{R}_m$ and \mathbf{R}_f , just as transformations between $\mathbf{T}_t, \mathbf{T}_m$ and \mathbf{T}_f .

References

- [1] Alchourrón CE, Gärdenfors P, Makinson D. On the logic of theory change: partial meet contraction and revision functions. *Journal of Symbolic Logic*.1985;50:510-30.
- [2] Urquhart A. Basic many-valued logic. In: D. Gabbay, F. Guentner, editors. *Handbook of Philosophical Logic 2* (2nd edition). Dordrecht: Kluwer.2001:p.249-95.
- [3] Zach R. Proof theory of finite-valued logics, Technical Report TUW-NDARRAY185.2-Z.1-93. Wien: Institut Für Computersprachen, Technische Universität Wien.1993.
- [4] Avron A. Natural 3-valued logics: Characterization and proof theory. *Journal of Symbolic Logic*.1991;56:276-94.
- [5] Baader F, Calvanese D, McGuinness DL, Nardi D, Patel-Schneider PF. *The Description Logic Handbook: Theory, Implementation, Applications*. Cambridge:Cambridge University Press.2003.
- [6] Rademaker A. *A Proof Theory for Description Logics*, SpringerBriefs in Computer Science. London:Springer.2012.
- [7] Li W. R-calculus: an inference system for belief revision. *The Computer Journal*.2007;50:378-90.
- [8] Li W, Sui Y. The Sound and Complete R-Calculi With Respect To Pseudo-Revision and Pre-Revision. *International Journal of Intelligence Science*. 2013;3:110-17.
- [9] Fermé E, Hansson SO. AGM 25 years, twenty-five years of research in belief change. *Journal of Philosophical Logic*. 2011;40:295-331.
- [10] Post EL. Determination of all closed systems of truth tables. *Bulletin American Mathematical Society*. 1920;26:437.

Creation of a Digital Passport for an Electronic Product and Generation of Design Solutions Based on It

Julia V. Donetskaya¹
ITMO University, Russia

Abstract. The work presents the activity analysis of enterprises in the instrumentation industry. This result shown the content of the digital passport is described in the form of a set of models, which makes it possible to use it at the stages of the life cycle of a product for the generation of design solutions. The work lists the variants of design solutions, as well as the tasks of their generation based on the analysis of parameters set by fuzzy variables. The required solution contains the associated components of the digital passport that are a part of the set specified by the values of the variables. The results obtained can be used to create a digital passport on the enterprises in the instrument-making industry.

Keywords. digital passport, generation of design solutions, variants of design solutions, tasks of generation design solutions.

1. Introduction

A modern electronic product is a complex hardware and software system, the development and delivery of which is performed on the basis of customer requests. Its content determines the lists and terms of work, as well as their performers from among the divisions of the enterprise and various organizations. This predesignates the task of organizing their operational interaction - the exchange of relevant data for making design decisions. Its solution is divided into two stages.

At the first stage, enterprises put into operation and integrate such systems as Product Data Management (PDM), Enterprise Resource Planning (ERP), Manufacturing Execution System (MES) and / or Quality Management System (QMS), as well as electronic document management (EDMS), which makes it possible to increase the efficiency of interaction between departments [1,2]. As a result, at each stage of the life cycle, data about the product and the corresponding design and production procedures are formed, which form a digital passport of this product. At the second stage, the tasks of data exchange between different organizations are being solved.

Traditionally, the exchange is associated with correspondence by e-mail or with the transfer of technical documentation in hard copy. This leads to the emergence of human factor problems that affect the efficiency of making design decisions. In order to eliminate them, digital passport technologies are used, which means the introduction and

¹ Corresponding Author: Donetskaya Julia V., ITMO University, Faculty of Secure Information Technology, 191002, Saint-Petersburg, ul. Lomonosova 9, lit.M, Russia; E-mail: donetskaya_julia@mail.ru

synchronization of versions of the same systems, and models of stored data by all participants in the interaction, coordination of the formation rules and structure of a neutral data exchange format in the STEP language.

The defects identified in this case are obvious and more significant in the vector of development of Industry 4.0 [3-7]. This indicates the need to generalize data about the product and design-production procedures at all stages of the life cycle in the instrument-making industry, as well as the implementation of procedures for their analysis for making design decisions by enterprises.

Thus, the creation of a digital passport for an electronic product and the generation of design solutions based on it is a priority task, the results of which are presented in this article. This contains:

1. The activity analysis of enterprises in the instrument-making industry.
2. The variants of design solutions generated on the basis of a digital passport.
3. The tasks of generation of design solutions based on a digital passport.

2. Activity analysis of enterprises in the instrument-making industry

The activity of an instrument-making enterprise is performed at the stages of life cycle of an electronic product, each of which is characterized by different design and production procedures. However, for research, only those that make it possible to form and / or change data about an electronic product, which are represented by the corresponding information objects are determined with their substantive and requisite parts.

The stage of concluding an agreement implies the implementation of such procedures as: consideration and approval of applications for the development or supply of an electronic products; preparation, registration and signing of an agreement with a customer; registration and signing of an agreement with a co-contractor.

As a result, linked documents are created. These include, first of all, an application for the development or supply of products with a corresponding agreement with the customer, and when involving third-party organizations (there may be several of them) – agreements with co-executors. This allows to perform the following development phase procedures:

1. Development, coordination and approval of the work schedules.
2. Management of updating data on standard and other products (purchased component parts – PCP), materials.
3. Development and modification of design data [2].
4. Coordination, approval and submission of documentation to the archive.

Thus, a set of design data about the product is created in the form of the electronic structure of the product in the PDM-system (ESI-PDM), containing documentation, as well as 3D models of parts and assembly units [8]. The results obtained are used in the preparation of production:

1. Development, coordination and approval of the production schedules.
2. Development and modification of manufacturing data.
3. Coordination, approval and submission of documentation to the archive.
4. Recording comments and decisions.
5. Preparation and registration of the agreement for the supply.

6. Recording and registration of the lot entry of supply products.
7. Formation of a production plan for the manufacture of products.

These procedures make it possible to create, on the basis of design data, a set of corresponding manufacturing data about a product, as well as to purchase PCP, materials and products of co-contractors. The information obtained is used at the production stage when performing the following procedures:

1. Verification of purchased products and materials upon delivery from the warehouse.
2. Assignment of identification numbers to parts and assembly units (PAU).
3. Fixing the composition of manufactured assembly units.
4. Fixing the execution of PAU manufacturing operations.
5. Recording comments and decisions during the production of PAU products.

As a result, the structure of a product sample (SPS) is formed, the elements of which are PAU copies, manufactured at the enterprise and purchased under agreements [9]. In the production process, for each of them, the values of quality parameters are monitored and the compliance of the PAU with the developed documentation is being checked.

After the completion of the product production, cycles of its tests are performed, and their successful completion means the possibility of moving to the stages of operation and repair. This means performing the following procedures: registration of shipment of the finished products sample from the warehouse; registration of the complaint report and the result of the refusal study; registration and control of the service request.

At the same time, for a given SPS element, a failure in operation and the result of its study is recorded, for an SPS, the product is shipped to the customer, as well as the serial number of the component parts of the product from the set of spare parts and accessories when processing a service request.

Thus, the stages of the life cycle are set in accordance with design and production procedures $Pr = (pr_1, pr_2, \dots, pr_n)$, during the implementation of which data about an electronic product is created $D = (d_1, d_2, \dots, d_k)$ in the form of information objects of ERP, PDM, MES, QMS systems or EDMS.

The values of each of them allowed to describe the components of the digital passport

$$R(C) = \begin{pmatrix} c_{11} & c_{12} & \dots & c_{1n_1} \\ c_{21} & c_{22} & \dots & c_{2n_2} \\ \dots & \dots & c_{ij} & \dots \\ c_{k1} & c_{k2} & \dots & c_{kn_k} \end{pmatrix} = \begin{pmatrix} C_1 \\ C_2 \\ \dots \\ C_k \end{pmatrix},$$

where $c_{ij} = \langle d_i, pr_j \rangle, i = \overline{1, k}, j = \overline{1, n_k}; n_k \leq n$ – an element of a digital passport.

Moreover $c_{ij} = 1$, if the given object $d_i \in D$ formed as a result of a specific procedure $pr_j \in Pr$ и $c_{ij} = 0$ otherwise.

The results obtained also allowed the creation of many parameters of the components of the digital passport $U = (u_1, u_2, \dots, u_p)$ which are used in a model for describing

components

$$G(C) = \begin{pmatrix} g_{11}(C_1) & g_{12}(C_1) & \dots & g_{1P}(C_1) \\ g_{21}(C_2) & g_{22}(C_2) & \dots & g_{2P}(C_2) \\ \dots & \dots & g_{ij}(C_i) & \dots \\ g_{k1}(C_k) & g_{k2}(C_k) & \dots & g_{kP}(C_k) \end{pmatrix} = \begin{pmatrix} G_1(C_1) \\ G_2(C_2) \\ \dots \\ G_k(C_k) \end{pmatrix}, \quad (1)$$

where each element $g_{ij}(C_i) \in G_i(C_i), i = \overline{1, k}, j = \overline{1, P}$ is described by parameters and formed at a specific stage of the life cycle.

Components are linked

$$X(C) = \begin{pmatrix} 0 & X_{12}(C_1, C_2) & \dots & X_{1k}(C_1, C_k) \\ X_{21}(C_2, C_1) & 0 & \dots & X_{2k}(C_2, C_k) \\ \dots & \dots & X_{ij}(C_i, C_j) & \dots \\ X_{k1}(C_k, C_1) & X_{k2}(C_k, C_2) & \dots & 0 \end{pmatrix}, \quad (2)$$

where

$$X_{ij}(C_i, C_j) = \begin{cases} 0, & out(G_i(C_i)) \neq in(G_j(C_j)) \\ 1, & out(G_i(C_i)) = in(G_j(C_j)) \end{cases}. \quad (3)$$

Then, on the basis of the above, it is logical to assert about the possibility of using the content of a digital passport for the generation of design solutions.

3. Variants of design solutions generated on the basis of a digital passport

So, when considering and approving an application for the development or supply of products, design solutions are formed in the form of lists of products and their component parts to be developed (including products of co-contractors and its suppliers) and lists of documentation for component parts of the product to be adjusted.

The procedures for developing, reconciliation and approving the work schedules use design solutions in the form of lists of developed and changed component parts of the product and products of co-contractors and / or documentation developed or adjusted for component parts of the product, as well as the results of fulfilling the positions of the operational work schedule.

To manage the update of PCP data, a design solution is required that contains a list of approved PCPs, products of co-contractors and materials.

Development and modification of design data requires information to create tabular design documentation and ESI. Similar design solutions are required for the development and modification of software for the device and a set of operational documentation - data for creating tabular and operational documentation, as well as ESI.

When performing the procedure for the development, coordination and approval of the production schedule, information about the component parts of the product to be produced is used; information about PCPs, materials, products of co-contractors and their suppliers; including the results of fulfilling the positions of the application for the start of production.

The development and modification of manufacturing data is performed according to the data for the creation of technological documentation for the manufacture of the product and the electronic structure of the product.

To prepare and register an agreement for the supply, data on the PCP, materials, products of co-contractors and their suppliers are generated.

The formation of a production plan for the manufacture of products requires data on the constituent parts of the product to be produced, the current production load and the results of the production operations.

When registering a complaint act and the result of a failure study, the lists of documentation for the component parts of the product subject to correction, lists of PCPs, materials, products of co-contractors and their suppliers, as well as lists of data on the component parts of the product subject to production are taken into account.

Registration and control of the service request requires the formation of data on the changeable component parts of the product and the corrected documentation, the component parts related to spare parts and the results of fulfilling the plan items for processing the service request.

The listed options for design solutions can be grouped and get the following list of tasks: the task of searching for data about products and their components; the task of finding data about PCPs, materials, products of co-contractors and their suppliers; the task of finding data for the development and correction of documentation; the task of finding data on the documentation for the component parts of the product; the task of monitoring the fulfillment of the positions of the unified task; the task of managing production operations.

4. Tasks of generation of design decisions based on digital passport

The solution to any of these problems is a set of related components of a digital passport, which means the formation of matrix elements (2) that satisfy condition (3) in accordance with the values of the analyzed parameters PR . Moreover, the lists of parameters are defined for each task in the form of fuzzy variables:

$$\langle P, A, \mu(P) \rangle,$$

where P – the name of the parameter from the list below; A – parameter value; $\mu(P)$ – parameter membership function.

For example, for the task of searching for data about a product and their constituent parts are defined: type of product and component, manufacturer of the product and component, sign of a component part of the product, the presence of comments on the documentation, a sign of products of inadequate quality.

For the task of searching for data on documentation for component parts of a product are defined: type of product component; sign of a component part of the product; document sign; the presence of comments on the documentation.

For the task of relating to the control of the execution of the positions of the unified task are defined: type of work; monitored state.

To solve the problem of managing production operations are defined: the presence of comments on the documentation; availability of products in stock; sign of the production process; sign of products of inadequate quality.

Then, the generation of design solutions based on digital passport, it is necessary to solve a number of problems associated with the analysis and selection of descriptions of the components of a digital passport. The first task based on the calculation of the values of the membership functions of fuzzy variables and the second task based on the Takagi-Sugeno-Kanga algorithm.

This will allow developing a similarity criterion given by the least squares method

$$\Delta(\beta) = \sum_{i=1}^K \left(G_i(\bar{C}_i) - G_i^*(\bar{C}_i) \right)^2 = (G - \beta \cdot X)^T \cdot (G - \beta \cdot X) \rightarrow \min, \quad (4)$$

where

- elements $G_i(\bar{C}_i) \in G(C)$ ($i = \bar{1}, \bar{K}; K \leq k$) (1) are calculated using the theory of fuzzy sets and elements of discrete mathematics;
- elements $G_i^*(\bar{C}_i) = a \cdot \sum_{j=1}^P b_j \cdot RP_j \cdot g_{ij}(\bar{C}_i)$ are calculated using the theory of pattern recognition and the theory of decision making;
- $\beta = (a, b_1, b_2, \dots, b_K)$ – column vector;
- $X = RP \cdot G$ – deterministic matrix, dimension $K \times P$.

Consequently, the search for design solutions that satisfy the similarity criterion means calculation the elements of the column vector, according to an expression of the form:

$$\beta = (X^T \cdot X)^{-1} \cdot (X^T \cdot G).$$

The generated design solution is one of the lists in the form of the values of the digital passport components. For the task of searching for data about products and their components: designation of the component part of the product; name of the component part of the product; name of the manufacturer of the product component; sign of referring a component part of the product to spare parts; sign of a component part of the product.

For the task of finding data for the development and correction of documentation: designation of the component parts of the product; designation of documentation; the name of the component parts of the product; title of the documentation; documentation format; version of the documentation; the number of component parts of the product included in the assembly unit.

For the task of searching for data on documentation for component parts of the product: designation of documentation; title of the documentation; version of the documentation; the state of the version of the component parts of the product; state of the documentation version.

For the task of monitoring the fulfillment of the positions of the unified task: number of the unified task; position number of the unified task; name of the position of the unified task; result of execution of the task position and status of the result of the task position execution.

For the task of managing production operations: the number of the production operation; name of the production operation; designation of the manufactured product copy and the result of the production operation.

The set of conditions formed in this way determines the area, falling into which characterizes the desired design solution.

5. Conclusion

Thus, it is shown: the content of the digital passport is determined by the components; the set of components allows you to form the content of the digital passport and use it to generate different design solutions; the tasks of generation design solutions based on digital passport are formulated.

The results obtained can be used to create a digital passport on the enterprises in the instrument-making industry.

References

- [1] Donetskaya J.V., Kuznetsova O.V., Tushkanov E.V., Kuznetsov A.Y. Formation and analysis of engineering alternatives for an integrated electronic product description system. In: Control in Technical Systems (CTS), 2017 IEEE II International Conference on – 2017; 2017. pp. 397-400.
- [2] Donetskaya J.V., Kuznetsova O.V., Tushkanov E.V., Kuznetsov A.Y., Gatchin Yu.A. Mathematical model of a digital passport for an electronic product. In: International Conference on Soft Computing and Measurements – 2018, vol. 1. 2018. pp. 438-441.
- [3] Wagner T., Herrmann Ch., Thiede S. Industry 4.0 impacts on lean production systems. *Procedia CIRP* 63. 2017. pp. 125-131.
- [4] Chen Y. Integrated and intelligent manufacturing: perspectives and enablers. *Engineering* 3. 2017. pp. 588-595.
- [5] Doshi A., Smith R.S., Thomas B.H., Bouras C. Use of projector based augmented reality to improve manual spot-welding precision and accuracy for automotive manufacturing. *The International Journal of Advanced Manufacturing Technology* 89. 2017. pp. 1279-1293.
- [6] Uva A.E., Gattullo M., Manghisi V.M., Spagnulo D., Cascella G.L., Fiorentino M. Evaluating the effectiveness of spatial augmented reality in smart manufacturing a solution for manual working stations. *The International Journal of Advanced Manufacturing Technology* 94. 2018. pp. 509-521.
- [7] Abramovich M., Gobel J. Ch., Savarino Ph., Gebus Ph. Towards smart product lifecycle management with an integrated reconfiguration management. *International Federation for Information Processing*. 2017. pp. 489-498.
- [8] Osepyan A.K. The state and prospects for the development of engineering data management systems in the branch of FSUE TsENKI - Scientific Research Institute of PM named after Academician V.I. Kuznetsov. In: *Proceedings of the XVII conference of young scientists "Navigation and traffic control"*. SPb.: State Scientific Center of the Russian Federation "Concern" TsNII "Elektropribor". 2015. pp. 168-174.
- [9] Shakhovtsev E.V., Balandin A.I., Shvidko A.E. Interaction of automated production preparation systems and product life cycle management: promising options. In: *Proceedings of the conference "Information technologies in management (ITU-2014)"*. 2014. pp. 431-439.

Feature Back-Tracking with Sparse Deep Belief Networks

Chen QIAO^a, Jiajia LI^a, Xuewu ZHANG^b, Cheng ZHANG^b, Wenfeng JING^{a,1} and Danglin YANG^c

^a*School of Mathematics and Statistics, Xi'an Jiaotong University, China*

^b*China Railway First Survey and Design Institute Group Co., Ltd, China*

^c*Suzhou Hanlin Information Technology Development Co., Ltd, China*

Abstract. To find a way of the interpretability of deep learning, in this paper, a features back-tracking (FBT) approach based on a sparse deep learning architecture is proposed. Firstly, for a deep belief network (DBN), both the Kullback-Leibler divergence of the hidden neurons and the L_1 norm penalty on the connection weights are introduced. Thus, the sparse response mechanism as well as the sparse connection of the brain neurons can be simulated directly. That means the DBN can learn a sparse framework and an effective sparse data representation. On this basis, the feature back-tracking technique is put forward. For both the single nucleotide polymorphisms (SNPs) data and MNIST data, FBT has quite well performance on searching for the risk loci on the genes as well as the important sites of the digit data. It reveals that the proposed FBT method can pick out the essential features by deep learning architecture with quite high classification accuracy and data storage ability. Utilizing the sparse layer-wise feature learning to achieve key features from the original data, is an effective attempt to explore the profound mechanism of human brain and interpretability of deep learning.

Keywords. Features back-tracking, Deep belief networks, Sparse learning, Markers selection

1. Introduction

With the quickly growing demand for revealing the intrinsic nature of things under the complex surface phenomena, and with the development of technology methods, high-dimensional data emerge magically every day. To fully explore valuable information contained in such kind of data, models with strong expression ability are needed. As an effective learning approach, deep learning can learn the layer-wise nonlinear expression or features by greedy layer-by-layer training, thus to find out the complex information of the data. In the recent decade, deep learning research has been getting a flourishing development, and setting off a significant booming on various artificial intelligence domains. Its applications have also been extended to more application fields, like audio recognition, social network, automatic control, bioinformatics, etc.

However, for deep learning, there still exist many intrinsic theoretical issues worth to be further clarified. Currently, most of the deep learning methods are used for layer-

¹ Corresponding Author, Wenfeng Jing, School of Mathematics and Statistics, Xi'an Jiaotong University, China; E-mail: wfjing@mail.xjtu.edu.cn.

wise feature extraction and for classification purpose, and one typical issue is the interpretability of the deep learning framework. For interpretability, one of the most commonly used method is feature selection, which can effectively select important features from the original data containing a large number of features and eliminate irrelevant features [1]. With feature selection, the mechanism of recognizing different things by human brains can be explored, and the essential features which help to distinguish different data can be identified. With the direct interpretability of data, feature selection methods are widely applied in text classification, data mining, bioinformatics, computer vision, information retrieval, time series prediction, and so on.

It should be noticed that most of the existing feature selection methods are based on shallow models. They are only performed on the original data directly. Searching for an approach to obtain the essential features of the data from the deep expression with layered structure, will be great helpful to obtain the essential features of the original data in a global and layer-wised way, and what is the most important, to obtain the interpretability of the deep learning framework.

On the other hand, studies of the brain's nervous system have shown that such system employs a highly sparse response mechanism. For each neuron, it has a topology that only some of the other neurons are connected to this neuron. The sparseness of this connection is the sparse structure of the network or sparse topology. It has been shown that there exist connection sparseness properties in the brain's organizational structure [2-4]. The connection sparseness guarantees the high promotion ability of the human neural network system. Sparse connections are more able to provide high-quality storage capabilities and makes the deep network to have better generalization capabilities [2].

How to better simulate the sparseness of the human neuron system and improve the performance of the deep learning algorithm is a hot topic. At present, there are three main approaches to get the topology sparseness of a network, a.k.a., constructive algorithm [5], destructive algorithm [6] and regularization algorithm. For regularization algorithm, it is to solve the problem of constrained optimization problem, remove unnecessary connections and hidden neurons in the training process, and then reduce the complexity of the model (including the structure as well as the parameters). There are two ways of constraining, i.e., constraints on the connection weights of the network, and constraints on the response of hidden neurons or constraints on the relationship between the response of hidden neurons and the target output. The method of weighting constraints includes Gaussian regularizer, Laplace regularizer, weight elimination and soft weight sharing. Among them, the most widely used is the Gaussian regularizer and the Laplace regularizer. They use the L_2 -norm or L_1 -norm of the connection weights as penalty functions, which are embedded in the original training process. These methods aim to achieve the sparse network topology by reducing the value of connective weights [7-9].

Above methods only consider the sparsity of the connection. In this paper, we will consider both the architecture sparsity and the representation sparsity of the neurons in deep learning. This is an effective attempt to simulate the sparse topology structure of the brain networks. We will consider the Deep Belief Network (DBN) as the deep learning model, and introduce the penalty terms on neuronal sparse connections as well as on the response of neurons into the DBN training stage to improve the energy usage and generalization capabilities of the network. By introducing the L_1 -norm penalty on the connection weights and the Kullback-Leibler (KL) divergence of the hidden neurons into each layer of the stacked DBN, the sparse response of the hidden neurons and the sparse connections between different layers can be achieved together in the unsupervised training process. By such methods, the DBN can learn the fundamental weights and the

effective data representation in a sparse way. Above steps thus ensure the sparse architecture of the deep network, and thus improve the compression rate, generalization capacity and discriminative accuracy of the networks.

Based on the sparse DBN network architecture, a novel feature selection method, i.e., the feature back-tracking approach based on sparse deep learning is proposed in this paper. Compared with the shallow feature selection methods, this method can understand the data in a global abstract perspective, thus find out the most crucial features of the data. Further, due to the sparsity and depth of network architecture, the important features of the data can be trace-back easily by the most discriminative abstract feature in the top layer, and an efficient implementation of the feature selection can be assured.

By applying the proposed features back-tracking method based on sparse DBN to two datasets, we can get distinct understanding on them. Mutations in individual nucleotides at the genomic level can lead to DNA sequence diversity, which may lead to human genetic disease. We used the single nucleotide polymorphism data provided by American Mind Clinical Imaging Consortium (MCIC), which had a typical high dimension (12513 SNPs loci) small sample size data (208 samples, including 92 schizophrenia patients and 116 healthy subjects), and there exists a large number of loci that are not associated with the disease. By applied the proposed features back-tracking method, 2973 pathogenic SNPs are selected from the raw SNPs data. Based on these risk loci, the diagnostic accuracy of the test data is 98.56%. In addition, several of these risk loci and their corresponding genes have been shown of great correlation with the schizophrenia in biological explanations. On the other hand, when the method is applied to the MNIST dataset. Experimental results show that with high classification accuracy, the important pixels distinguishing different handwritten digits can be finally picked out. The results show that the features back-tracking approach can identify accurately the risk loci on the genes of the mental disease as well as the key pixels of the handwritten digits, and the proposed method can also deeply improve the storage capacity as well as the search speech.

2. Unsupervised sparse learning of DBN

A DBN is a generative graphical model, composed of multiple layers of hidden units. DBN is composed of several restricted Boltzmann machines (RBMs). An RBM contains two layers, namely, the visible input layer and the hidden layer.

Let $v = (v_1, v_2, \dots, v_{N_v})^T$ be the visible units, $h = (h_1, h_2, \dots, h_{N_h})^T$ be the hidden units, $\alpha = (\alpha_1, \alpha_2, \dots, \alpha_{N_v})^T$ and $\beta = (\beta_1, \beta_2, \dots, \beta_{N_h})^T$ be the bias of the visible units and the hidden units respectively, and $W = \{W_{ij}\}_{N_v \times N_h}$ with each w_{ij} be the connection weight of v_i and h_j . (v, h) is the joint configuration of the visible and hidden units. The energy of it is described in a compact form

$$E_\theta(v, h) := E(v, h) = -\alpha^T v - \beta^T h - v^T W h$$

where $\theta = \{W, \alpha, \beta\}$. The joint probability distribution of state (v, h) is

$$P_\theta(v, h) = \frac{1}{Z_\theta} e^{-E_\theta(v, h)} \quad (1)$$

in which $Z_\theta = \sum_{v,h} e^{-E_\theta(v,h)}$ is the partition function. $P_\theta(v) = \frac{1}{Z_\theta} \sum_h e^{-E_\theta(v,h)}$ is the distribution of the observed data v_θ . The task of training an RBM is to maximizing $P_\theta(v)$, and thus to find a θ^* satisfying

$$\theta^* = \underset{\theta}{\operatorname{argmax}} \mathcal{L}(\theta)$$

with $\mathcal{L}(\theta) = \log P_\theta(v)$. [10] proposed a faster learning using contrastive divergence (CD) to update the parameters:

$$\Delta W_{ij} = \epsilon \cdot (\langle v_i h_j \rangle_{data} - \langle v_i h_j \rangle_{recon})$$

$$\Delta \alpha_i = \epsilon \cdot (\langle v_i \rangle_{data} - \langle v_i \rangle_{recon})$$

$$\Delta \beta_j = \epsilon \cdot (\langle h_j \rangle_{data} - \langle h_j \rangle_{recon})$$

where ϵ is the learning rate, and $\langle \cdot \rangle$ is the operator of expectation with the corresponding distribution denoted by the subscript.

To learn the structured network of each RBM, which helps to improve the interpretability of the network, sparse regularization can be utilized [7-9, 11-13]. Thus, some sparse regularization terms are introduced here obtain the sparsity of connections as well as the response of the neurons. The Kullback-Leibler (KL) divergence on the hidden neurons is used to achieve the response sparsity, and the L_1 -norm is used on the connection weights to obtain the connective sparsity. We also add the L_2 -norm on the connection weights to limit their increasing bounds. The improved objective function of the sparse RBM is given by

$$\max_{\Theta} \mathcal{L}_{new}(\Theta) = \mathcal{L}(\Theta) - \frac{1}{2} \lambda_1 \|W\|_2^2 - \lambda_2 \sum_{j=1}^{N_h} KL(\rho \| p_j) - \lambda_3 \|W\|_1 \quad (2)$$

In which the KL divergence, $KL(\rho \| p_j) = \rho \log \frac{\rho}{p_j} + (1 - \rho) \log \frac{1 - \rho}{1 - p_j}$ is the relative entropy between the two random variables with the mean ρ and the mean p_j . ρ is a sparse parameter. $p_j = \frac{1}{N_s} \sum_{q=1}^{N_s} \frac{1}{1 + e^{-\sum_{i=1}^{N_v} v_i^{(q)} w_{ij} - \beta_j}}$ is the average activation probability of the j -neuron in the hidden layer with N_s samples, N_v is the node numbers of the current visual layer, λ_1 is the parameter to control the bound of W , λ_2 and λ_3 denote the penalty coefficients of the KL divergence and L_1 -norm respectively.

The following is the deviation of the KL divergence.

$$\begin{aligned} \frac{\partial}{\partial W_{ij}} \sum_{j=1}^{N_h} KL(\rho \| p_j) &= \frac{\partial}{\partial W_{ij}} \sum_{j=1}^{N_h} \left(\rho \log \frac{\rho}{p_j} + (1 - \rho) \log \frac{1 - \rho}{1 - p_j} \right) \\ &= \left(-\frac{\rho}{p_j} + \frac{1 - \rho}{1 - p_j} \right) \frac{\partial p_j}{\partial W_{ij}} = \left(-\frac{\rho}{p_j} + \frac{1 - \rho}{1 - p_j} \right) \frac{1}{N_s} \sum_{q=1}^{N_s} \sigma_j^{(q)} (1 - \sigma_j^{(q)}) v_i^{(q)} \end{aligned}$$

$$= \frac{1}{N_s} \left(-\frac{\rho}{p_j} + \frac{1-\rho}{1-p_j} \right) \sum_{q=1}^{N_s} \sigma_j^{(q)} (1 - \sigma_j^{(q)}) v_i^{(q)}$$

$$\text{here } \sigma_j^{(q)} = \sigma(\sum_{i=1}^{N_v} v_i^{(q)} W_{ij} + \beta_j) = \frac{1}{1 + e^{-\sum_{i=1}^{N_v} v_i^{(q)} W_{ij} - \beta_j}}.$$

Thus, the parameters of the unsupervised sparse RBM can be updated by

$$\begin{aligned} \Delta W_{ij} &= \epsilon \cdot (\langle v_i h_j \rangle_{data} - \langle v_i h_j \rangle_{recon}) - \lambda_1 W_{ij} - \lambda_3 \cdot \text{sign}(W_{ij}) \\ &- \lambda_2 \cdot \frac{1}{N_s} \left(-\frac{\rho}{p_j} + \frac{1-\rho}{1-p_j} \right) \cdot \left(\sum_{q=1}^{N_s} \sigma_j^{(q)} (1 - \sigma_j^{(q)}) v_i^{(q)} \right) \end{aligned} \quad (3)$$

$$\Delta \alpha_i = \epsilon \cdot (\langle v_i \rangle_{data} - \langle v_i \rangle_{recon}) \quad (4)$$

$$\Delta \beta_j = \epsilon \cdot (\langle h_j \rangle_{data} - \langle h_j \rangle_{recon}) - \lambda_2 \cdot \frac{1}{N_s} \left(-\frac{\rho}{p_j} + \frac{1-\rho}{1-p_j} \right) \cdot \left(\sum_{q=1}^{N_s} \sigma_j^{(q)} (1 - \sigma_j^{(q)}) \right) \quad (5)$$

According to the above updating formula and combined with the CD sampling process, a sparse RBM and a stacked sparse DBN can be obtained.

3. Features back-tracking approach based on sparse DBN

For deep networks, the connections between two layers are on duty to encode the memories. The larger connection strength can describe the stronger relationship of the corresponding two layers. At the same time, the larger the difference of the response values of neurons between the two kinds of different data, the higher the discriminant ability of the current neurons. The two facts can be combined with the obtained sparse DBN to search for the most contributed features of the data in a back-tracking way.

The following process is the features back-tracking based on sparse DBN. Firstly, a stacked DBN with sparse architecture and sparse representation is trained by Eq. (3)-(5). Then, the learned DBN can be fine-tuned by back-propagation (BP) algorithm. Furthermore, the features back-tracking method is performed top-down to select key features by

$$I = \{i: |w_{ij}| \geq \alpha \ \& \ |h_{j,1} - h_{j,2}| \geq r, \exists j \in \{1, \dots, N_h\}\} \quad (6)$$

Where w_{ij} is the connection between visible unit i and hidden unit j of the current RBM, α and r are given thresholds, $h_{j,k}$ is the mean value of the k -th class on the hidden unit j , and N_h is the unit numbers of the hidden layer. Model (6) is on two aspects. One is the larger the absolute value of w_{ij} , the higher the influence of the i -th visible unit on the j -th hidden unit. The other one is that the larger the difference of the response values between the two classes, the higher the discriminant ability of the current hidden unit. Finally, the very essential features of the data can be obtained in a back-tracking way. Each selected feature has a high probability to cause the output and make the prediction decision. The features back-tracking (FBT) approach on sparse DBN is described in Algorithm 1.

Algorithm 1. The FBT method on sparse DBN

Input: $L, w^{(l)}(l = L - 1, \dots, 1), \alpha^{(l)}(l = L - 1, \dots, 1), I^{(L)}$
 Ensure: $I^{(1)}$
 For $l = L - 1: -1: 1$
 $I^{(l)} = i: |w_{ij}^{(l)}| \geq k^{(l)} \& |h_{j,1}^{(l+1)} - h_{j,2}^{(l+1)}| \geq r^{(l+1)}, \exists j \in I^{(l+1)}$
 $N^{(l)} = \text{length}(I^{(l)})$
 End For
 Return: $I^{(1)}, N^{(l)}(l = L, \dots, 1)$

where L is the layer numbers of the DBN, $w^{(l)}$ is the connecting weight between the $(l + 1)$ -th layer and the l -th layer, $k^{(l)}$ and $r^{(l+1)}$ are thresholds and set $I^{(l)}$ contains the selected positions of the l -th layer. By back-tracking method, finally, $I^{(1)}$ is achieved, which the essential features from the data which contribute most to the final prediction.

4. Results on the SNPs data of Schizophrenia

The rapid development of genomic techniques improves the study of the relationship between mental diseases (such as schizophrenia (SZ)) and genes. Single nucleotide polymorphism (SNP) data of SZ patients is a type of genomic data resulting from genome wide association study. Each SNP is a gene sequence variation occurring commonly within a population, in which a single nucleotide - A, T, C or G - in the genome differs between paired chromosomes. The SNPs data is one typical high-dimensional data. In addition, it is extremely complex, and simple linear models have not yielded the hoped-for benefits. Many studies have investigated the crucial genes associated with SZ [14-17]. In this section, we utilize the features back-tracking method with sparse DBN to find the distinct loci of the SNPs sequence, based on which the potential risk SNPs of SZ from healthy controls can be better sought out.

The data collection was conducted by the Mind Clinical Imaging Consortium. The SNPs data contains 208 subjects including 92 schizophrenia patients and 116 healthy controls. Each SNP was represented by three numbers, 0 for 'BB' (no minor allele), 1 for 'AB' (one minor allele) and 2 for 'AA' (two minor alleles). The dimension for each sample is 12513.

To deal with the SNP data which are coded by 0, 1 or 2, in each RBM, they are transformed into binary sequences first. Here, the visible units $v = (v^{(1)}, v^{(2)}, v^{(3)})$, and $v^{(i)} = (v_1^{(i)}, v_2^{(i)}, \dots, v_{N_v}^{(i)})^T$ ($i = 1, 2, 3$) is an N_v -dim vector with each $v_j^{(i)} \in \{0, 1\}$. For every sample, the SNP sequence is denoted as S with each $S_j \in \{0, 1, 2\}$. $v_j^{(i)}$ ($i = 1, 2, 3, j = 1, 2, \dots, N_v$) is defined as

$$v_j^{(i)} = \begin{cases} 1, & S_j = i - 1 \\ 0, & S_j \neq i - 1 \end{cases}$$

Then by using the unsupervised sparse learning method in Section 2, the DBN with sparse architecture and sparse representation can be achieved with training data. Additionally, based on the features back-tracking algorithm with sparse DBN, the risk SNPs loci of SZ can be selected.

The sparse DBN used here contains 5 layers, including a visible layer, three hidden layers and a decision layer. The sample size of the training data is 168, and the sample

size of the testing data is 40. The number of three hidden layers we used for training the sparse DBN is 1000, 500, 200 respectively. The learning rate is 0.1 and the penalty rate is 0.0002.

The training procedure of sparse DBN and the following features back-tracking process are randomly performed 50 times. Simultaneously, based on the feature back-tracking method with sparse DBN, we use the training data to achieve the risk loci, and from the testing samples with the selected risk loci we get the average classification. The performs for the testing data before and after the feature back-tracking method are shown in Table 1. Where Dim refers to the dimension of the data, ACA is the average classification accuracy, and SCR is the space compression rate.

Table 1. Results before and after back-tracking of SNPs data

	Dim	ACA	SCR
Raw Testing Data	12513*3	0.9867	1.0000
Testing Data with Selected Risk Loci	2973	0.9856	0.0792

From the selected 2973 risk loci, there exist several SNPs that have been shown with great correlations with schizophrenia. Table 2 lists 10 typical SNPs among them.

Table 2. 10 typical selected risk loci by the feature back-tracking method

SNPs	Genes	SNPs	Genes
rs10102965	NRG1	rs1110144	CNTNAP2
rs11607732	GRIK4	rs6586002	GRID1
rs11013103	PIP4K2A	rs2765993	PIP4K2A
rs2098469	GRIN2B	rs220573	GRIN2B
rs111888901	HAAO	rs6433777	CACNB4

By <http://www.genecards.org/>, we can find that some genes in Table 2. have strong correlation with schizophrenia, such as NRG1, GRIK4, GRID1, PIP4K2A. In addition, GRIN2B and CNTNAP2 are related with mental retardation and neuroscience, GRIN2B is related with epileptic encephalopathy and protein-protein interactions at synapses, HAAO is present in the central nervous system, and CACNB4 is related with epilepsy.

Table 1 as well as Table 2 sustain the validation of the feature back-tracking method with sparse DBN when it is applied on the SNPs data. Firstly, the data with the selected loci nearly keep the same high classification accuracy as presented in [18]. Further, the selected risk loci can get a space saving rate about 92% with a classification accuracy around 98%, that means, nearly all of the distinguishable loci of schizophrenia from the raw data have been chosen correctly. What is the most important, several selected loci have been shown owning strong correlation with schizophrenia by biological explanation.

5. Results on MNIST data

The MNIST data contains 60,000 examples as the training set, and 10,000 examples as the test set [19]. It has 10 types handwritten digits, i.e., from 0 to 9. Each one has 784 pixels. We use the proposed FBT method to achieve key pixels of different digits.

The DBN contains 5 layers. Let $\alpha_k^{(l)} = c_k^{(l)} w_{mean}^{(l)}$ ($l = 1, \dots, 4$) be a threshold of key features/sites selection with layer l for digit k , in which $c_k^{(l)}$ is a coefficient and $w_{mean}^{(l)} =$

$\frac{1}{N_v \cdot N_h} \sum_{i=1}^{N_v} \sum_{j=1}^{N_h} |w_{ij}^{(l)}|$, $\alpha_k = (c_k^{(4)} w_{mean}^{(4)}, c_k^{(3)} w_{mean}^{(3)}, c_k^{(2)} w_{mean}^{(2)}, c_k^{(1)} w_{mean}^{(1)})^T$ and $c_k = (c_k^{(4)}, c_k^{(3)}, c_k^{(2)}, c_k^{(1)})^T$. N_o and N_s are the dimension of the original data and that of the selected pixels respectively. AR_o and AR_s are the classification accuracy of the testing data and the selected key pixels of the testing data respectively. SR is the space saving rate, i.e., $SR = 1 - N_s/N_o$. $AVG-AR_o$ and $AVG-AR_s$ denote the average classification accuracy of the testing data and the testing data with selected sites respectively. $AVG-N_s$ denotes the average number of the selected sites, and $AVG-SR$ is the average space saving rate. The performance of the proposed method on all two kinds, all three kinds, and all ten kinds of digits are shown in Table 3.

Table 3. Average performance with FBT

Types of digits	AVG- AR_o	AVG- AR_s	AVG- N_s	AVG- SR
2	0.9976	0.9893	61	0.92
3	0.9975	0.9807	131	0.83
10	0.9607	0.9563	289	0.63

Table 3 shows that by the features back-tacking method combining with sparse DBN, the key pixels identifying different digits can be selected successfully. With only part of the pixels, high recognition accuracy rates can still be well kept. For some cases, the identification accuracy is even improved with the picked pixels. For example, the classification accuracy of digit 1 and digit 2 rises from 96.61% to 100% (see, Table 4 and Figure 1), the classification accuracy of digits 0, 1 and 3 increases to 100% (see Table 5 and Figure 2). The results show that the method can recognize the key positions to distinguish the digits.

Table 4. Results before and after pixel selection of digits 1 and 2

DIGIT	N_o	N_s	AR_o	AR_s	SR
1	784	146	0.9974	0.9522	0.81
2	784	31	0.9961	1	0.96

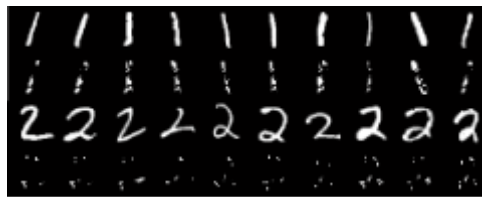


Figure 1. Original images and distinguishable images of digits 1 and 2

Table 5. Results before and after pixel selection of digits 0, 1 and 3

DIGIT	N_o	N_s	AR_o	AR_s	SR
0	784	124	0.9990	0.9801	0.84
1	784	126	0.9982	1	0.84
3	784	122	1	0.9814	0.84

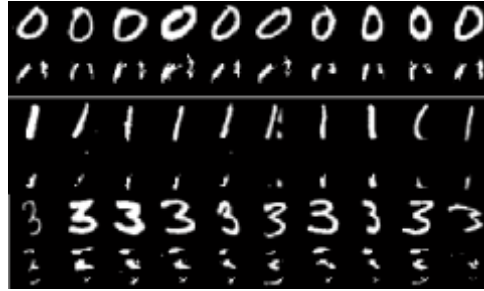


Figure 2. Original images and distinguishable images of digits 0, 1 and 3

Table 3 reveals the average space saving rate for all two kinds of digits is 92%, namely, the number of picked pixels over the data dimension is only 8%. Meanwhile, the average classification accuracy is nearly 99%. The average compression ratio of all three types digits is about 17%, with an average classification accuracy over 98%. For all ten kinds of digits, it also keeps quite high accuracy and spatial storage capacity.

We also tested the performance of one typical feature method, namely, Lasso on two kinds, three kinds, and all ten kinds of digits. Compared with the results obtained by Lasso, the proposed FBT method shows very good performance. For two kinds of digits, the $AVG-N_s$ and $AVG-AR_s$ obtained by Lasso are 82 and 0.9142 respectively. While, those indexes obtained by FBT are 61 and 0.9893 respectively. For three kinds of digits, the $AVG-N_s$ and $AVG-AR_s$ obtained by Lasso are 133 and 0.7620 respectively, and for FBT, the $AVG-N_s$ and $AVG-AR_s$ are 131 and 0.9807. For all ten kinds of digits, the $AVG-N_s$ and $AVG-AR_s$ obtained by Lasso are 213 and 0.6969 respectively, while the $AVG-N_s$ and $AVG-AR_s$ obtained by FBT are 289 and 0.9563. Compared with FBT, we can find that although the $AVG-N_s$ obtained by the two methods are similar, FBT can keep quite higher classification accuracy with the selected pixels.

It usually considers MNIST data as a kind of data owning low dimensional structure. Recently, some dimensionality reduction techniques are applied to explore the lower dimensional subspace of it. While, there is no way to map high-dimensional data into low dimension and preserve all the structures of the raw data, so all the approaches try to make trade-offs, i.e., sacrificing one property to preserve another. It should be noticed that most of them are based on feature abstraction. For example, Principal Component Analysis was utilized in [20] to preserve its linear structure. In [21-24], multi-dimensional scaling and t-Distributed Stochastic Neighbor Embedding were applied to preserve its global geometry or topology structure. Deep learning approach was applied to extract its latent features [11]. Genetic algorithm was carried out to find the feature subsets [25]. Compared with the above methods, the deep learning approach is not a shallow method to find the key features, and it is no longer only a feature abstraction approach. It can directly pick out the distinct pixels of the MNIST digits from a deep layer network with a good performance of the saving ability in storage space, and it improves the classification accuracy of those in [25,26].

6. Conclusion

The interpretability of deep learning framework is quite crucial for further understanding and applying of it. Feature back-tracking method based on sparse DBN architecture

provides a way for solving this issue. By simulating the sparse response of neurons for external stimulus and the sparse connection mechanism in brain system, the corresponding regularization items on the hidden neurons and the connection weights are introduced in the network learning process. Thereby, we can reduce the networks' complexity and enhance the generalization ability. By exploring the correspondence of the connections and response differences of neurons of the sparse DBN, the features back-tracking method is proposed. This method has shown quite well performance of removing irrelevant features and reducing the difficulty and complexity of learning tasks, especially in searching for risk loci of schizophrenia and picking out the intrinsic pixels of different digits.

Acknowledgements

This research was supported by the National Natural Science Foundation of China (Grant No. 11471006, Grant No. 12090020 and No.12090021), the National Key Research and Development Program of China (No. 2020AAA0106302), the Science and Technology Innovation Plan of Xian (No. 2019421315KYPT004JC006) and was partly Supported by HPC Platform, Xi'an Jiaotong University.

References

- [1] Colaco, S., Kumar, S., Tamang, A., Biju, V. G. "A review on feature selection algorithms." In Shetty N.Patnaik L., Nagaraj H., Hamsavath P., Nalini N. (eds) Emerging Research in Computing, Information,Communication and Applications. *Advances in Intelligent Systems and Computing*. **906** (2019) 133–153.
- [2] Morris G, Nevet A, Bergman H, "Anatomical funneling, sparse connectivity and redundancy reduction in the neural networks of the basal ganglia," *Journal of Physiology-Paris*. **97** (2003) 581–589.
- [3] Barlow H B, "Single units and sensation," *Representations of Vision*. 2010.
- [4] Olshausen B A, Field D J, "Sparse coding of sensory inputs," *Current Opinion in Neurobiology*. **14** (2004) 481–487.
- [5] Parekh R, Yang J, Honavar V, "Constructive neural-network learning algorithms for pattern classification," *IEEE Transactions on Neural Netw*. **11** (2000) 436–451.
- [6] Reed R, "Pruning algorithms-a review," *IEEE Transactions on Neural Netw*. **2** (1991) 47–55.
- [7] Chen Qiao, Lan Yang, Vince D. Calhoun, Zong-Ben Xu and Yu-Ping Wang. "Sparse deep dictionary learning identifies differences of time-varying functional connectivity in brain neuro-developmental study," *Neural Networks*. **135**(2021) 91-104.
- [8] Chen Qiao, Yan Shi, Yu-Xian Diao, Vince D. Calhoun and Yu-Ping Wang. "Log-sum enhanced sparse deep neural network," *Neurocomputing*. 2020, 407(24), 206-220.
- [9] Chen Qiao, Bin Gao, Yan Shi. "SRS-DNN: a deep neural network with strengthening response sparsity," *Neural Computing and Applications*. 2020, 32(12), 8127-8142.
- [10] Hinton G, "training products of experts by minimizing contrastive divergence," *Neural Comput*. **14** (2002) 1771–1800.
- [11] Hinton G E, and Salakhutdinov R R, "Reducing the Dimensionality of Data with Neural Networks," *Science*. **313** (2006) 504–507.
- [12] Hinton G E, "A Practical Guide to Training Restricted Boltzmann Machines," *Momentum*. **9** (2010) 599–619.
- [13] Fischer A, and Igel C, "Training restricted Boltzmann machines: An introduction," *Pattern Recognition*. **47** (2014) 25–39.
- [14] Ripke S, O'Dushlaine C, Chambert K, et al., "Genome-wide association analysis identifies 13 new risk loci for schizophrenia," *Nat Genet*. **45** (2013) 1150–1159.
- [15] Luo X J, Mattheisen M, Li M, et al., "Systematic Integration of Brain eQTL and GWAS Identifies ZNF323 as a Novel Schizophrenia Risk Gene and Suggests Recent Positive Selection Based on Compensatory Advantage on Pulmonary Function," *Schizophrenia bulletin*. **41** (2015) 1294–1308.

- [16] Meier L, Geer S and Bühlmann P, “The group lasso for logistic regression,” *J. R. Stat. Soc. Ser. B.* **70** (2008) 53–71.
- [17] Onitsuka T, Shenton M E, Salisbury D F, et al., “Middle and inferior temporal gyrus gray matter volume abnormalities in chronic schizophrenia: an MRI study,” *Am. J. Psychiatry.* **161** (2004) 1603-1611.
- [18] Qiao C, Lin D D, Cao S L, et al., “The effective diagnosis of schizophrenia by using multi-layer RBMs deep networks,” *IEEE International Conference on Bioinformatics and Biomedicine.* 2015, 603–606.
- [19] LeCun, Y., Cortes, C, “MNIST handwritten digit database,” 2010. URL <http://yann.lecun.com/exdb/mnist>.
- [20] Jiang B, Ding C, Luo B, et al, “Graph-Laplacian PCA: Closed-Form Solution and Robustness,” *CVPR.* **9** (2013) 3492–3498.
- [21] Silva V D, Tenenbaum J B, “Sparse Multidimensional Scaling using Landmark Points,” *Technical report.* Stanford University, 2004.
- [22] Dzwiniel W, Wcisło R, “Very Fast Interactive Visualization of Large Sets of High-dimensional Data,” *Procedia Computer Science.* **51** (2015) 572–581.
- [23] Maaten L, Hinton G, “Visualizing data using t-SNE,” *Journal of Machine Learning Research.* **9** (2008) 2579–2605.
- [24] Lee J A, Verleysen M, “Shift-invariant similarities circumvent distance concentration in stochastic neighbor embedding and variants,” *Procedia Computer Science.* **4** (2011) 538–547.
- [25] Stefano C D, Fontanella F, Marrocco C, et al., “A GA-based feature selection approach with an application to handwritten character recognition,” *Pattern Recognition Letters.* **35** (2014) 130–141.
- [26] Wang J, Wonka P, Ye J, “Lasso screening rules via dual polytope projection,” *Journal of Machine Learning Research.* **16** (2015) 1063–1101.

Multi-Step Low-Rank Decomposition of Large PageRank Matrices

Zhao-Li SHEN^a Bruno CARPENTIERI^{b,1}

^aCollege of Science,

Sichuan Agricultural University, Ya'an, Sichuan 625000, P.R. China

^bFaculty of Computer Science, Free University of Bozen-Bolzano, 39100 Bolzano, Italy

Abstract. The PageRank model, initially proposed by Google for search engine rankings, provides a useful network centrality measure to identify the most important nodes within large graphs arising in several applications. However, its computation is often very difficult due to the huge sizes of the networks and the unfavourable spectral properties of the associated matrices. We present a novel multi-step low-rank factorization that can be used to reduce the huge memory cost demanded for realistic PageRank calculations. Finally, we present some directions of future research.

Keywords. PageRank model, network centrality computation, matrix pre-processing algorithms, low-rank factorization.

1. Introduction

The PageRank model proposed by Google in a series of papers [1,2] can quantify the importance of each Web page efficiently from the linking structure of the World Wide Web. In this model, the linking structure is represented by a binary matrix $G \in \mathbb{R}^{n \times n}$ (where n denotes the number of hyperlinked pages) such that $G(i, j)$ is nonzero (being 1) only when there is a hyperlink pointing from the j^{th} to the i^{th} page. Then the stationary distribution of a random walk on this structure represents the importance of each page. An important assumption of the model is the equal probability of each hyperlink to be selected on a given page. Accordingly, the transition matrix P of this random process is defined as

$$P(i, j) = \begin{cases} \frac{1}{\sum_{k=1}^n G(k, j)}, & \text{if } G(i, j) = 1, \\ 0, & \text{otherwise.} \end{cases} \quad (1)$$

To ensure that the process will not stagnate when the surfer visits a node with 0 out-degree, matrix P is usually modified as $\bar{P} = P + vd^T$, where $d \in N^{n \times 1}$ is a binary vector such that $d(i) = 1$ when the i^{th} node has 0 out-degree. Meanwhile the irreducibility of

¹Corresponding Author: Bruno Carpentieri; E-mail: bcarpentieri@gmail.com. This author is a member of the *Gruppo Nazionale per il Calcolo Scientifico* (GNCS) of the Istituto Nazionale di Alta Matematica (INdAM) and this work was partially supported by INdAM-GNCS under Progetti di Ricerca 2020.

the Markov chain is needed for a unique solution, hence \bar{P} is often modified into a matrix \tilde{P} defined as follows

$$\tilde{P} = \alpha \bar{P} + (1 - \alpha)ve^T, \quad (2)$$

where $\alpha \in (0, 1)$ is called the damping factor, $v \in R^{n \times 1}$ is a probability distribution vector, and $e = [1, 1, \dots, 1]^T$. Finally, the PageRank model can be stated as finding the stationary distribution vector x such that

$$\tilde{P}x = x, \quad \|x\|_1 = 1, \quad x > 0. \quad (3)$$

The eigen-problem (3) is mathematically equivalent to the solution of the nonsingular linear system [3]

$$Ax = v, \quad A = (I - \alpha P), \quad x > 0. \quad (4)$$

The PageRank model depends solely on the graph topology of G and on the user-defined damping factor α and distribution vector v . Therefore, it represents a general network centrality measure that can be used to analyze large graphs arising in many computational science and engineering applications [4]. The assumption that the relevance of a node is determined by the number and by the importance of the nodes pointing directly to it is appropriate for many classes of networks arising in applications. Indeed, the model is broadly used far beyond search engine rankings, e.g., in feature selection of intelligent systems [5], in large micro-array experiments of computational biology such as the GeneRank [6] and the ProteinRank [7] problems, in ranking authors from co-citation networks [8], to name only a few examples. Recently, the model has been generalized to analyze multiplex networks as well [9].

In the past decade or so, considerable research attention has been devoted to the efficient solution of problems (3)-(4), especially when n is very large. Nowadays Web page ranking often deals with over billion pages and social networks graphs may consist of more than 100 millions nodes. Solving eigen- or linear systems of such huge sizes is a computational challenge that demands large costs in hardware and time. Direct solvers based on matrix factorizations are clearly not affordable to solve problems of this dimension in linear time and space. Iterative solvers based on sparse matrix-vector products and dense vector operations are thus mandatory to use. In applications where the damping factor α approaches 1, the convergence rate of classical iterative solvers such as the Power method, the Jacobi method and the Gauss-Seidel method will seriously deteriorate, and more robust algorithms need to be used. For example, the Power method initially used by Google for computing PageRank vectors converges about 10 times slower in the case when $\alpha = 0.99$ compared with $\alpha = 0.9$. Because the size of PageRank problems keeps growing, the development of more sophisticated and efficient solvers for this problem class are an active research topic of computational mathematics. In this paper, we present a new multi-step low-rank factorization method that can be used to significantly reduce the memory costs required for realistic PageRank calculations. Throughout the paper, we adopt MATLAB notation and write $A(i, :)$ to denote the i^{th} row of matrix A , while $A(:, j)$ represents the j^{th} column of A , and $A(i_1 : i_2, j_1 : j_2)$ is the block of A from row i_1 to row i_2 and from column j_1 to column j_2 .

2. Multi-step low-rank factorization of PageRank matrices

An iterative method for solving the nonsingular PageRank linear system $Ax = v$ needs to store only the coefficient matrix A and the right-hand side v , plus a few extra temporary vectors. By using sparse storage formats, such as the Compressed Sparse Row (CSR) or the Compressed Sparse Column (CSC) formats, the storage costs mainly depend on the number of nonzeros $nnz(A)$ of A . The algorithmic complexity also depends on $nnz(A)$, since the most expensive operation of an iterative method is the sparse matrix-vector multiplication Au ². Therefore, for very large values of n , significant memory and time efforts could be saved by reducing $nnz(A)$. For this purpose, we recall below two important properties of the transition matrix P that determines the structure of $A = I - \alpha P$.

Property 2.1 (Property 2.1 in [10]) *The nonzero entries in each column of the transition matrix P defined in (1) are positive and have the same value.*

For example, the transition matrix P corresponding to the Web matrix G below has the following form:

$$G = \begin{bmatrix} 1 & 1 & 1 & 1 \\ 0 & 1 & 1 & 0 \\ 0 & 0 & 1 & 1 \\ 1 & 1 & 1 & 1 \end{bmatrix} \rightarrow P = \begin{bmatrix} \frac{1}{2} & \frac{1}{3} & \frac{1}{4} & \frac{1}{3} \\ 0 & \frac{1}{3} & \frac{1}{4} & 0 \\ 0 & 0 & \frac{1}{4} & \frac{1}{3} \\ \frac{1}{2} & \frac{1}{3} & \frac{1}{4} & \frac{1}{3} \end{bmatrix}. \tag{5}$$

Property 2.2 (Property 2.2 in [10]) *Same patterns in the rows of G define identical subrows in P .*

For instance, in the previous example, the last two rows of G have a common pattern in the last two columns. Consequently, the corresponding subrows in P are identical and have values $(\frac{1}{4}, \frac{1}{3})$. Property 2.2 indicates that any two rows of P with similar nonzero pattern contain many identical entries that can be zeroed out by subtracting one row from the other [10], and full blocks of P consisting of rows with same pattern can be suitably compressed by a low-rank matrix representation. For example, in the matrix below

$$P = \begin{bmatrix} 0 & * & * & 0 & * \\ * & * & 0 & * & * \\ * & * & * & * & 0 \\ * & * & * & * & 0 \\ 0 & 0 & * & 0 & * \end{bmatrix}, \tag{6}$$

the 2nd, 3rd and 4th rows of P have nonzero entries in the 1st, 2nd and 4th columns. Therefore, we can compress those nonzero entries by the following low-rank decomposition:

²Hereafter, u means an arbitrary vector with appropriate size.

$$\begin{aligned}
P &= \begin{bmatrix} 0 & * & * & 0 & * \\ 0 & 0 & 0 & 0 & * \\ 0 & 0 & * & 0 & 0 \\ 0 & 0 & * & 0 & 0 \\ 0 & 0 & * & 0 & * \end{bmatrix} + \begin{bmatrix} 0 & 0 & 0 & 0 & 0 \\ * & * & 0 & * & 0 \\ * & * & 0 & * & 0 \\ * & * & 0 & * & 0 \\ 0 & 0 & 0 & 0 & 0 \end{bmatrix} \\
&= \begin{bmatrix} 0 & * & * & 0 & * \\ 0 & 0 & 0 & 0 & * \\ 0 & 0 & * & 0 & 0 \\ 0 & 0 & * & 0 & 0 \\ 0 & 0 & * & 0 & * \end{bmatrix} + \begin{bmatrix} 0 \\ 1 \\ 1 \\ 1 \\ 0 \end{bmatrix} [* , * , 0 , * , 0] = P_R + fh^T. \tag{7}
\end{aligned}$$

The latter form enables to save the storage of three matrix elements. Any submatrix of P consisting of rows with the same nonzero pattern can be compressed. The same operation can be applied to the remaining matrix P_R , recursively, until no more nonzero elements can be further compressed. In practice, such low-rank factorizations will be implemented on the matrix αP to produce a matrix decomposition of the form $\alpha P = \bar{D} + \bar{F}\bar{H}$, where D is the final remaining matrix, F and H are respectively formed by the columns and the rows generated by the low-rank factorizations. Note that since $A = I - \alpha P = (I - \bar{D}) - \bar{F}\bar{H}$, we can also write $A = D + FH$, where $D = I - \bar{D}$ is a nonsingular M -matrix, $F = -\bar{F}$ and $H = \bar{H}$. Therefore, matrix A can be compressed as well and our goal is to maximize the degree of compression of A .

We define a metric, hereafter referred to as the *compression number*, that counts the reduction of nonzero matrix elements to be stored after compression, i.e. $Comp(A) = nnz(A) - nnz(D) - nnz(H) - nnz(F)$. Note that the larger the compression number, the more efficient the algorithm. To start, we select the, say i^{th} , row of P that can maximize the compression number. According to Property 2.2, the largest amount of nonzero matrix elements that can be saved due to compressions on the i^{th} row is given by the sum of number of nonzeros in the columns of P corresponding to the nonzero elements of this row. In the given Example (6), the compression of any block of P that contains the first row, $P(1, :)$, can save at most all the nonzeros in the three columns $P(:, 2)$, $P(:, 3)$ and $P(:, 5)$. Therefore, an upper bound on the compression number obtained by a rank-1 factorization of any block of P that contains $P(1, :)$ is given by $nnz(P(:, 2)) + nnz(P(:, 3)) + nnz(P(:, 5))$, that is equal to 11. For the i^{th} row, we denote such upper bound on its maximum achievable compression number as $maxcom(i)$.

Motivated by these considerations, we adopt the following strategy: initially, we select the row of P with the largest $maxcom$ value. Suppose that it is the i^{th} row $P(i, :)$ of P . Then, we traverse the pattern of P to find other rows that can be merged with $P(i, :)$ to form a suitable block that can be effectively compressed by a rank-1 decomposition. Clearly, $P(i, :)$ should be merged with rows that have the most similar sparsity patterns, as this may potentially lead to a higher compression number. Referring to Example (6), the 3rd and 4th rows $P(3, :)$ and $P(4, :)$ have both the largest $maxcom$ value. We select $P(3, :)$ as a reference row. The row with the highest pattern similarity with $P(3, :)$, that is the largest number of nonzero elements in the same column indices, is $P(4, :)$ followed by $P(2, :)$, $P(1, :)$ and $P(5, :)$. The traverse follows this order. The rank-1 factorization of the block $P(3 : 4, 1 : 4)$ will increase the compression number by 2 since $P(3, :)$ and $P(4, :)$ have nonzero elements in their first four columns. However, it is convenient to merge $P(4, :)$ and $P(3, :)$ also with $P(2, :)$, because the rank-1 factorization of the nonzero

block $P(2 : 4, [1, 2, 4])$ increases the compression number by 3 and therefore a better compression can be achieved. On the other hand, if $P(1, :)$ is merged with $P(2, :)$, $P(3, :)$ and $P(4, :)$, the rank-1 matrix factorization of the block $P(1 : 4, 3)$ can not increase further the compression number, since these four rows are all nonzero only at column 2. Therefore, $P(1, :)$ is not merged with the other three selected rows, the search procedure is stopped, and the rank-1 factorization $P = P_R + fh^T$ is computed as (7). The same process can be repeated on matrix P_R . As mentioned above, such multi-step low-rank factorization in practice is implemented on the matrix αP , yielding the decompositions $\alpha P = \bar{D} + \bar{F}\bar{H}$ and $A = D + FH$.

Two important amendments need to be introduced in the above algorithm, in order to limit the time cost of the compression procedure without sacrificing considerably the number of reduced nonzeros. At first, prior to the multi-step low-rank factorization, the rows of αP are permuted in density increasing order, by moving the most sparse ones to the top and the most dense ones to the bottom of the matrix. For costs reduction, the most sparse rows with a number of nonzero elements equaling to $\theta \cdot nnz(A)$ are excluded from the traverses, where θ is a user-defined ratio. Besides, we set a maximum number of implementations of rank-1 decomposition for the multi-step low-rank factorization. We suggest setting this upper-limit as 1%-15% of the matrix dimension. The reason is twofold: 1) at each step, the algorithm selects and compresses the rank-1 block that may increase most the compression number; as the compression increase is expected to decrease with the number of rank-1 factorizations, a relatively small number of such factorizations should be preferred; 2) the number of rank-1 factorizations is equal to the dimension of the dense capacitance matrix $I + HD^{-1}F$ when preconditioner based on the Woodbury formula are constructed from the decomposition $A = D + FH$ as in [11]. Finally, the whole algorithm of the multi-step low-rank factorization is presented as Algorithm 1, where Matlab functions and their calling methods are used for description.

3. Numerical experiments

We investigate the performance of the multi-step low-rank factorization strategy on several Web adjacency matrices G extracted from the matrix repository of [12] and the Laboratory for Web Algorithmics [13,14,15]. The characteristics of each matrix G are reported in Table 1. The PageRank matrix A is constructed using the damping factor $\alpha = 0.9$. All numerical experiments are carried out in MATLAB R2018b on a 64-bit windows 7 computer equipped with an Intel core i3-8100 processor and 24GB RAM memory.

Table 1. Characteristics of the Web adjacency matrices G , where n is the dimension, and nnz is the number of nonzero elements.

Name	n	nnz	nnz/n^2
uk-2007-100000	100,000	3,050,615	3.1e-4
cnr-2000	325,557	3,216,152	3.0e-5
in-2004	1,382,908	16,917,053	8.8e-6

We set the values of θ as 0.1, 0.2, 0.3, 0.4, and the upper-bound r on the number of rank-1 factorizations divided by n as 0.01, 0.05, 0.1, 0.15, 0.2. For each matrix and

for each pair of parameter setting, we run the multi-step low-rank factorization on the matrix αP and report the time cost *Time* in seconds and the compression ratio $Comr = (nnz(F * H) - nnz(F) - nnz(H)) / nnz(A)$. The results are reported in Table 2.

Table 2. The time cost and the compression ratio of the multi-step low-rank factorization.

Problem:	uk-2007-100000							
$\theta \rightarrow$	0.1		0.2		0.3		0.4	
$r \downarrow$	<i>Time</i>	<i>Comr</i>	<i>Time</i>	<i>Comr</i>	<i>Time</i>	<i>Comr</i>	<i>Time</i>	<i>Comr</i>
0.01	1.64	67.2%	0.95	65.9%	0.80	59.9%	0.70	51.9%
0.05	3.57	72.1%	1.60	67.4%	1.07	60.1%	0.76	51.9%
0.10	5.05	73.1%	2.28	67.4%	1.08	60.1%	0.77	51.9%
0.15	6.28	73.4%	2.47	67.4%	1.09	60.1%	0.76	51.9%
0.20	7.33	73.4%	2.49	67.4%	1.08	60.1%	0.76	51.9%
Problem:	cnr-2000							
$\theta \rightarrow$	0.1		0.2		0.3		0.4	
$r \downarrow$	<i>Time</i>	<i>Comr</i>	<i>Time</i>	<i>Comr</i>	<i>Time</i>	<i>Comr</i>	<i>Time</i>	<i>Comr</i>
0.01	11.4	51.9%	6.65	52.8%	4.02	51.9%	2.68	45.9%
0.05	33.6	59.0%	15.4	58.4%	8.34	53.1%	3.86	45.9%
0.10	58.3	60.4%	24.6	58.2%	8.19	53.1%	3.89	45.9%
0.15	81.8	60.5%	26.7	58.2%	8.22	53.1%	3.90	45.9%
0.20	104.9	60.1%	26.5	58.2%	8.05	53.1%	3.98	45.9%
Problem:	in-2004							
$\theta \rightarrow$	0.1		0.2		0.3		0.4	
$r \downarrow$	<i>Time</i>	<i>Comr</i>	<i>Time</i>	<i>Comr</i>	<i>Time</i>	<i>Comr</i>	<i>Time</i>	<i>Comr</i>
0.01	122	56.4%	45.3	58.6%	16.5	56.6%	9.95	49.7%
0.05	478	66.3%	131	63.2%	30.6	56.9%	10.7	49.7%
0.10	872	67.1%	195	63.1%	30.6	56.9%	10.7	49.7%
0.15	1284	66.8%	196	63.1%	30.9	56.9%	10.7	49.7%
0.20	1632	66.4%	197	63.1%	30.9	56.9%	10.7	49.7%

In our experiments, both the time cost and the compression ratio of the multi-step factorization generally decrease with θ while they increase with r . Consistently with our analysis, a small value of r can guarantee a good compression ratio that tends to raise very slowly with r . In Table 2, the compression ratio is almost constant for each θ and for values of r in the range between 0.05 to 0.20. This observation suggests that a suitable setting for the value of r can be $r \leq 0.05$. Besides, when θ increases, the time cost decreases much faster than the compression ratio, and setting $\theta = 0.3$ or 0.4 is an advisable choice. In such cases, the compression ratio tends to increase little when r increases from 0.01 to 0.05. Thus, it is better to set $r = 0.01$. Seen from this table, the multi-step low-rank factorization can achieve large compression ratio at low to moderate computational cost. Therefore, it can be useful to reduce significantly the storage cost of Web graphes and the PageRank computations. This may be an attractive advantage when solving PageRank problems, especially when the damping factor approaches 1 or several PageRank problems corresponding to the same Web structure need to be solved.

Algorithm 1 Multi-step low-rank factorization for PageRank problems**Input:** $G, \alpha P, \theta, r$

- 1: Compute the number $rownnz$ of nonzero elements for each row of G , set $k = 1$;
- 2: Permute and mark the rows of G and αP in a $rownnz$ increasing order until the amount of nonzero elements in the marked rows reaches $\theta n n z(G)$;
- 3: Suppose the first unmarked row is row_l , generate $PickG = G(l : n, :)$ and $PickA = A(l : n, :)$;
- 4: Compute the number of nonzeros in each column of $PickG$, store it in vector $colsum$;
- 5: Compute the $maxcom$ value of each unmarked row by $maxcom = pickG * colsum'$;
- 6: **for** $i = 1 : r * size(P, 2)$ **do**
- 7: Pick a row row_j from the unmarked rows with the largest $maxcom$ value;
- 8: Set $common_j = row_j$;
- 9: **if** $maxcom(j) == 0$ **then**
- 10: Break;
- 11: **end if**
- 12: Find the column indexes of the nonzero elements of row_j , store them in vector $neighbors$;
- 13: Compute the number of nonzeros of columns $neighbors$ distributed in each row by $repeats = sum(pickG(:, neighbors), 2)$;
- 14: Permute the rows by $[sumrow, order_r] = sort(repeats, 'descend')$;
- 15: Set $compressed_j = 0$, $index_j = 1$, $N(k).group = [j]$;
- 16: **if** $sumrow(2) < 1$ **then**
- 17: Set $maxcom(j) = 0$ and $rownnz(l + j - 1) = 0$;
- 18: Continue;
- 19: **end if**
- 20: **for** $s = 1 : n - l + 1$ **do**
- 21: Compute the common nonzero indexes by $tem_{common} = common_j * pickG(order_r(s), :)$;
- 22: Compute the number of common nonzero indexes by $tem_{common}_{nnz} = nnz(tem_{common})$;
- 23: **if** $tem_{common}_{nnz} * index_j > compressed_j$ **then**
- 24: Set $N(k).group = [N(k).group, order_r(s)]$, $common_j = tem_{common}$;
- 25: Set $compressed_j = tem_{common}_{nnz} * index_j$;
- 26: Set $index_j = index_j + 1$;
- 27: **end if**
- 28: **end for**
- 29: Set $neighbour = find(common_j)$;
- 30: Update $rownnz(N(k).group) = rownnz(N(k).group + l - 1) - nnz(common_j)$;
- 31: Update $maxcom = maxcom - sum(pickG(:, neighbour), 2) * index_j$;
- 32: Set $sumneighbours = sum(pickG(:, neighbour), 2)$;
- 33: Update $maxcom(N(k).group) = maxcom(N(k).group) - sum(sumneighbours) + sumneighbours(N(k).group) * index_j$;
- 34: Compute $common_{neighbour} = find(common_j)$;
- 35: Set $N(k).common = common_j * pickA(j, :)$, $N(k).col = k * ones(1, index_j)$, $k = k + 1$;
- 36: **end for**
- 37: Set $rowf = [N(1 : k - 1).group]$, $colf = [N(1 : rank).col]$, $lenv = length(rowf)$, $vf = ones(1, lenv)$;
- 38: Set $temF = sparse(rowf, colf, vf, size(PickG, 1), k - 1)$;
- 39: Set $F = sparse(n, k - 1)$, $F(i : n, :) = temF$, $H = cat(2, N.common)$, $H = H'$;
- 40: Permute the $rownnz$ back to the original order, and permute the rows of F accordingly;
- 41: **return** F and H .

4. Conclusions and future work

We have presented a novel multi-step low-rank factorization method to reduce the large memory cost demanded for realistic PageRank calculations. Differently from the low-rank factorizations proposed in [11], the proposed method can be implemented to the whole matrix A instead of only the off-diagonal blocks of A , thus leading to higher compression level. The outcome of the algorithm is a low-rank decomposition of the form $A = D + FH$ that is suitable to construct effective preconditioners, e.g. based on the Woodbury formula [11]. Additionally, matrix-vector multiplications that account for the most expensive operation in classical iterative solvers are expected to be cheaper to compute using the low-rank representation $A = D + FH$. The proposed technique can be especially effective when the network has many nodes with similar in-link distributions.

In future work, it will be interesting to investigate the structure characteristics, such as the distributions of the out-degrees and in-degrees and the similarity of in-link (out-link) distributions of large networks from more fields to develop optimal or highly efficient pre-processing techniques for reducing the memory and algorithmic costs of computing large-scale PageRank centralities. An important application of these techniques can be the solution of PageRank problems with multiple damping factors like [16] or with slight modification of the network, that are computationally very demanding.

References

- [1] Sergey Brin and Lawrence Page. The anatomy of a large-scale hypertextual web search engine. 1998.
- [2] Lawrence Page, Sergey Brin, Rajeev Motwani, and Terry Winograd. The pagerank citation ranking: Bringing order to the web. Technical report, Stanford InfoLab, 1999.
- [3] Langville AN, Meyer CD. A reordering for the PageRank problem. *SIAM J. Sci. Comput.* 2006 Feb;27(6):2112-20.
- [4] Gleich DF. PageRank beyond the web. *SIAM Rev.* 2005 Aug;57(3):321-63.
- [5] Henni K, Mezghani N, Gouin-Vallerand C. Unsupervised graph-based feature selection via subspace and pagerank centrality. *Expert Systems with Applications.* 2018;114:46-53.
- [6] Morrison JL, Breitling R, Higham DJ, Gilbert DR. GeneRank: using search engine technology for the analysis of microarray experiments. *BMC bioinformatics.* 2005 Sep;6(1):1-14.
- [7] Wu G, Zhang Y, Wei Y. Accelerating the Arnoldi-type algorithm for the PageRank problem and the ProteinRank problem. *Journal of Scientific Computing.* 2013 Feb;57(1):74-104.
- [8] Ding Y, Yan E, Frazho A, Caverlee J. PageRank for ranking authors in co-citation networks. *Journal of the American Society for Information Science and Technology.* 2009;60(11):2229-43.
- [9] Pedroche F, Romance M, Criado R. A biplex approach to PageRank centrality: From classic to multiplex networks. *Chaos: An Interdisciplinary Journal of Nonlinear Science.* 2017; 26(6): 065301.
- [10] Shen ZL, Huang TZ, Carpentieri B, Gu XM, Wen C. An efficient elimination strategy for solving PageRank problems. *Appl. Math. Comput.* 2017 Apr; 298(1):111-22.
- [11] Shen ZL, Huang TZ, Carpentieri B, Wen C, Gu XM, Tan XY. Off-diagonal low-rank preconditioner for difficult PageRank problems. *J. Comput. Appl. Math.* 2019; 346 (1):456-70.
- [12] Davis TA, Hu Y. The University of Florida sparse matrix collection. *ACM Trans. Math. Softw.* 2011; 38(1): 1:1-1:25. Available at the URL: <http://www.cise.ufl.edu/research/sparse/matrices>.
- [13] Boldi P, Vigna S. The WebGraph Framework I: Compression Techniques. In: Proc. of the 13th international conference on World Wide Web. 2004: 595-602.
- [14] Boldi P, Rosa M, Santini M, Vigna S. Layered label propagation: A multiresolution coordinate-free ordering for compressing social networks. In: Proc. of the 20th international conference on World wide web. 2011: 587-596.
- [15] Boldi P, Codenotti B, Santini M, Vigna S. Ubcrawler: A scalable fully distributed Web crawler. *Software: Practice and Experience.* 2004; 34: 711-726.
- [16] Constantine PG, Gleich DF. Random alpha pagerank. *Internet Mathematics.* 2009; 6: 189-236.

A Novel Possibilistic Variance of Trapezoidal Intuitionistic Fuzzy Number

Qiansheng ZHANG¹

School of Mathematics and Statistics, Guangzhou 510006, P R. China

Abstract. Intuitionistic fuzzy number as the extension of fuzzy number has better capability to model uncertain data in scientific engineering problem. In this paper, we present a novel possibilistic variance for trapezoidal intuitionistic fuzzy number (TIFN) based on possibility theory. We also discuss some notes on possibilistic variance of TIFN and get the important relationships between the possibilistic covariance and possibilistic variance of TIFNs.

Keywords. Intuitionistic fuzzy number, possibilistic mean, possibilistic variance.

1. Introduction

Intuitionistic fuzzy number (IFN) as the special intuitionistic fuzzy set [1] has been widely applied into multi-criteria decision-making [2-6], fault analysis [7,8], programming [9-11] and portfolio selection problems [12,13]. Also, some basic operations and ranking methods of intuitionistic fuzzy number were introduced in literatures [14-16]. Inspired by possibility mean value theory [17-20] of fuzzy number, in this paper we introduce a novel possibilistic variance formula for trapezoidal intuitionistic fuzzy number (TIFN) which is different from the existing ones presented in [21-23]. Then some important properties of the proposed novel possibilistic variance of TIFNs are discussed.

2. Preliminaries

Definition 1[7]. A trapezoidal intuitionistic fuzzy number (TIFN) $\tilde{A} = (e, a, f, b, c, g, d, h)$ is a special kind of intuitionistic fuzzy set on the real number set \mathbb{R} , whose membership function and nonmembership function are respectively defined as the following forms.

$$\mu_{\tilde{A}}(x) = \begin{cases} (x - a) / (b - a), & a \leq x < b, \\ 1, & b \leq x \leq c, \\ (d - x) / (d - c), & c < x \leq d, \\ 0, & \text{otherwise} \end{cases} \quad \nu_{\tilde{A}}(x) = \begin{cases} (f - x) / (f - e), & e \leq x < f, \\ 0, & f \leq x \leq g, \\ (x - g) / (h - g), & g < x \leq h, \\ 1, & \text{otherwise} \end{cases}$$

¹ Corresponding Author, Qiansheng Zhang, School of Mathematics and Statistics, Guangzhou 510006, P R. China; E-mail: zhqiansh01@126.com.

where $e \leq a \leq f \leq b \leq c \leq g \leq d \leq h$, and TIFN $\tilde{A} = (\tilde{A}_*, \tilde{A}^*)$ is viewed as a conjunction of two fuzzy numbers \tilde{A}_*, \tilde{A}^* with low membership $\mu_{\tilde{A}_*}(x) = \mu_{\tilde{A}}(x)$ and high membership $\mu_{\tilde{A}^*}(x) = 1 - \nu_{\tilde{A}}(x)$.

Definition 2. Let $\tilde{A}_i = (e_i, a_i, f_i, b_i, c_i, g_i, d_i, h_i)$, $i = 1, 2$, be two trapezoidal intuitionistic fuzzy numbers, the addition and scale multiplication of TIFNs [15] are defined as follows.

- (1) $\tilde{A}_1 + \tilde{A}_2$
 $= (e_1 + e_2, a_1 + a_2, f_1 + f_2, b_1 + b_2, c_1 + c_2, g_1 + g_2, d_1 + d_2, h_1 + h_2)$.
- (2) $x\tilde{A}_i = (xe_i, xa_i, xf_i, xb_i, xc_i, xg_i, xd_i, xh_i)$, $\forall x \geq 0$.
 $x\tilde{A}_i = (xh_i, xd_i, xg_i, xc_i, xb_i, xf_i, xa_i, xe_i)$, $\forall x < 0$.

Definition 3. Let $\tilde{A} = (e, a, f, b, c, g, d, h)$ be a TIFN, the λ -level cut set of low membership and high membership of TIFN \tilde{A} is defined as, $\forall \lambda \in [0, 1]$,

$$\begin{aligned} \tilde{A}_*^{[\lambda]} &= \{x / \mu_{\tilde{A}_*}(x) = \mu_{\tilde{A}}(x) \geq \lambda\} = [a_*^-(\lambda), a_*^+(\lambda)] \\ &= [a + (b - a)\lambda, d - (d - c)\lambda]; \\ \tilde{A}^{*[\lambda]} &= \{x / \mu_{\tilde{A}^*}(x) = 1 - \nu_{\tilde{A}}(x) \geq \lambda\} = [a^{*-}(\lambda), a^{*+}(\lambda)] \\ &= [e + (f - e)\lambda, h - (h - g)\lambda]; \end{aligned}$$

Definition 4. Let $\tilde{A} = (e, a, f, b, c, g, d, h)$ be a TIFN the lower and upper possibilistic mean value of the low membership function \tilde{A}_* of TIFN \tilde{A} are, respectively, defined as [17, 21]

$$\begin{aligned} M^-(\tilde{A}_*) &= 2 \int_0^1 \lambda a_*^-(\lambda) d\lambda = 2 \int_0^1 \lambda (a + \lambda(b - a)) d\lambda = \frac{1}{3}(a + 2b); \\ M^+(\tilde{A}_*) &= 2 \int_0^1 \lambda a_*^+(\lambda) d\lambda = 2 \int_0^1 \lambda (d - \lambda(d - c)) d\lambda = \frac{1}{3}(d + 2c). \end{aligned}$$

The possibilistic mean of low membership of TIFN \tilde{A} is

$$\begin{aligned} M(\tilde{A}_*) &= [M^-(\tilde{A}_*) + M^+(\tilde{A}_*)] / 2 = \int_0^1 \lambda (a_*^-(\lambda) + a_*^+(\lambda)) d\lambda \\ &= \frac{1}{6}(a + d) + \frac{1}{3}(b + c). \end{aligned}$$

Definition 5. Let $\tilde{A} = (e, a, f, b, c, g, d, h)$ be a TIFN, the lower and upper possibilistic mean value of the high membership function \tilde{A}^* of TIFN \tilde{A} are, respectively, defined as [22]

$$\begin{aligned} M^-(A^*) &= 2 \int_0^1 \lambda a^{*-}(\lambda) d\lambda = \frac{1}{3}(e + 2f); \\ M^+(A^*) &= 2 \int_0^1 \lambda a^{*+}(\lambda) d\lambda = \frac{1}{3}(h + 2g). \end{aligned}$$

The possibilistic mean of high membership of TIFN \tilde{A} is

$$M(\tilde{A}^*) = [M^-(\tilde{A}^*) + M^+(\tilde{A}^*)] / 2 = \frac{1}{6}(e + h) + \frac{1}{3}(f + g).$$

Definition 6. Let $\tilde{A} = (e, a, f, b, c, g, d, h)$ be a TIFN, the possibilistic mean value of TIFN \tilde{A} is defined as

$$M(\tilde{A}) = \frac{1}{2}[M(\tilde{A}_*) + M(\tilde{A}^*)] = \frac{1}{12}(a + d + e + h) + \frac{1}{6}(b + c + f + g).$$

Proposition 1. Let $\tilde{A}_1 = (e_1, a_1, f_1, b_1, c_1, g_1, d_1, h_1)$, $\tilde{A}_2 = (e_2, a_2, f_2, b_2, c_2, g_2, d_2, h_2)$ be two TIFNs, for any $x, x_1, x_2 \in R$, we have

$$M(x_1\tilde{A}_1 + x_2\tilde{A}_2) = x_1M(\tilde{A}_1) + x_2M(\tilde{A}_2).$$

The proof is straightforward from Definitions 4,5, 6. (Omitted)

Definition 7. Let $\tilde{A} = (e, a, f, b, c, g, d, h)$ be a TIFN with λ cut sets $\tilde{A}_*^{[\lambda]} = [a_*^-(\lambda), a_*^+(\lambda)]$, $\tilde{A}^{*[\lambda]} = [a^{*-}(\lambda), a^{*+}(\lambda)]$ of low and high membership function, the possibilistic variance of low membership and high membership of TIFN \tilde{A} are respectively defined as

$$\begin{aligned} \text{var}'(\tilde{A}_*) &= \int_0^1 [(M(\tilde{A}_*) - a_*^-(\lambda))^2 + (M(\tilde{A}_*) - a_*^+(\lambda))^2] \lambda d\lambda; \\ \text{var}'(\tilde{A}^*) &= \int_0^1 [(M(\tilde{A}^*) - a^{*-}(\lambda))^2 + (M(\tilde{A}^*) - a^{*+}(\lambda))^2] \lambda d\lambda. \end{aligned}$$

The possibilistic variance of TIFN \tilde{A} is also defined by

$$\text{var}'(\tilde{A}) = \frac{1}{2}[\text{var}'(\tilde{A}_*) + \text{var}'(\tilde{A}^*)].$$

Definition 8. Let TIFN $\tilde{A}_1 = (e_1, a_1, f_1, b_1, c_1, g_1, d_1, h_1)$ be with λ cut sets $\tilde{A}_{1*}^{[\lambda]} = [a_{1*}^-(\lambda), a_{1*}^+(\lambda)]$, $\tilde{A}_1^{*[\lambda]} = [a_1^{*-}(\lambda), a_1^{*+}(\lambda)]$, and $\tilde{A}_2 = (e_2, a_2, f_2, b_2, c_2, g_2, d_2, h_2)$ with λ cut sets $\tilde{A}_{2*}^{[\lambda]} = [a_{2*}^-(\lambda), a_{2*}^+(\lambda)]$, $\tilde{A}_2^{*[\lambda]} = [a_2^{*-}(\lambda), a_2^{*+}(\lambda)]$, the possibilistic covariance of low membership and high membership of TIFNs \tilde{A}_1, \tilde{A}_2 are respectively defined as

$$\begin{aligned} &\text{cov}'(\tilde{A}_{1*}, \tilde{A}_{2*}) \\ &= \int_0^1 [(M(\tilde{A}_{1*}) - a_{1*}^-(\lambda))(M(\tilde{A}_{2*}) - a_{2*}^-(\lambda)) + (M(\tilde{A}_{1*}) - a_{1*}^+(\lambda))(M(\tilde{A}_{2*}) - a_{2*}^+(\lambda))] \lambda d\lambda \\ &\text{cov}'(\tilde{A}_1^*, \tilde{A}_2^*) \\ &= \int_0^1 [(M(\tilde{A}_1^*) - a_1^{*-}(\lambda))(M(\tilde{A}_2^*) - a_2^{*-}(\lambda)) + (M(\tilde{A}_1^*) - a_1^{*+}(\lambda))(M(\tilde{A}_2^*) - a_2^{*+}(\lambda))] \lambda d\lambda \end{aligned}$$

The possibilistic covariance of TIFNs \tilde{A}_1, \tilde{A}_2 can be computed by

$$\text{cov}'(\tilde{A}_1, \tilde{A}_2) = \frac{1}{2}[\text{cov}'(\tilde{A}_{1*}, \tilde{A}_{2*}) + \text{cov}'(\tilde{A}_1^*, \tilde{A}_2^*)].$$

3. Some properties of the possibilistic variance of TIFNs

Theorem 1. Let $\tilde{A}_1 = (e_1, a_1, f_1, b_1, c_1, g_1, d_1, h_1)$ be a TIFN with λ cut sets $\tilde{A}_{1*}^{[\lambda]} = [a_{1*}^-(\lambda), a_{1*}^+(\lambda)]$, $\tilde{A}_1^{*[\lambda]} = [a_1^{*-}(\lambda), a_1^{*+}(\lambda)]$, $\tilde{A}_2 = (e_2, a_2, f_2, b_2, c_2, g_2, d_2, h_2)$ be a TIFN with λ cut sets $\tilde{A}_{2*}^{[\lambda]} = [a_{2*}^-(\lambda), a_{2*}^+(\lambda)]$, $\tilde{A}_2^{*[\lambda]} = [a_2^{*-}(\lambda), a_2^{*+}(\lambda)]$ of low and high membership, $\forall \theta \in R$, we obtain

- (1) $\text{cov}'(\tilde{A}_1, \tilde{A}_2) = \text{cov}'(\tilde{A}_2, \tilde{A}_1)$; (2) $\text{var}'(\tilde{A}_1) = \text{cov}'(\tilde{A}_1, \tilde{A}_1)$;
- (3) $\text{var}'(\tilde{A}_1 + \theta) = \text{var}'(\tilde{A}_1)$.

Proof. (1), (2) can be directly proved by Definition 8 of $\text{cov}'(\tilde{A}_1, \tilde{A}_2)$ and Definition 7 of $\text{var}'(\tilde{A}_1)$.

(3) Since θ is a constant TIFN, we easily know $\tilde{\theta}_*^{[\lambda]} = [\theta, \theta]$; and $\tilde{\theta}^{*[\lambda]} = [\theta, \theta]$. Thus, $(\tilde{A}_1 + \theta)_*^{[\lambda]} = \tilde{A}_{1*}^{[\lambda]} + \theta = [a_{1*}^-(\lambda) + \theta, a_{1*}^+(\lambda) + \theta]$;

$$(\tilde{A}_1 + \theta)^{*[\lambda]} = \tilde{A}_1^{*[\lambda]} + \theta = [a_1^{*-}(\lambda) + \theta, a_1^{*+}(\lambda) + \theta].$$

$$\begin{aligned} \text{var}'(\tilde{A}_1 + \theta)_* &= \int_0^1 [(M(\tilde{A}_1 + \theta)_* - (a_{1*}^-(\lambda) + \theta))^2 + (M(\tilde{A}_1 + \theta)_* - (a_{1*}^+(\lambda) + \theta))^2] \lambda d\lambda \\ &= \int_0^1 [(M(\tilde{A}_{1*}) + \theta - a_{1*}^-(\lambda) - \theta)^2 + (M(\tilde{A}_{1*}) + \theta - a_{1*}^+(\lambda) - \theta)^2] \lambda d\lambda \\ &= \int_0^1 [(M(\tilde{A}_{1*}) - a_{1*}^-(\lambda))^2 + (M(\tilde{A}_{1*}) - a_{1*}^+(\lambda))^2] \lambda d\lambda = \text{var}'(\tilde{A}_{1*}); \end{aligned}$$

$$\begin{aligned} \text{var}'(\tilde{A}_1 + \theta)^* &= \int_0^1 [(M(\tilde{A}_1 + \theta)^* - (a_1^{*-}(\lambda) + \theta))^2 + (M(\tilde{A}_1 + \theta)^* - (a_1^{*+}(\lambda) + \theta))^2] \lambda d\lambda \\ &= \int_0^1 [(M(\tilde{A}_1^*) + \theta - a_1^{*-}(\lambda) - \theta)^2 + (M(\tilde{A}_1^*) + \theta - a_1^{*+}(\lambda) - \theta)^2] \lambda d\lambda \\ &= \int_0^1 [(M(\tilde{A}_1^*) - a_1^{*-}(\lambda))^2 + (M(\tilde{A}_1^*) - a_1^{*+}(\lambda))^2] \lambda d\lambda = \text{var}'(\tilde{A}_1^*); \end{aligned}$$

Hence, $\text{var}'(\tilde{A}_1 + \theta) = \text{var}'(\tilde{A}_1)$.

Theorem 2. Let $\tilde{A}_1 = (e_1, a_1, f_1, b_1, c_1, g_1, d_1, h_1)$ be a TIFN with λ cut sets $\tilde{A}_{1*}^{[\lambda]} = [a_{1*}^-(\lambda), a_{1*}^+(\lambda)]$, $\tilde{A}_1^{*[\lambda]} = [a_1^{*-}(\lambda), a_1^{*+}(\lambda)]$, $\tilde{A}_2 = (e_2, a_2, f_2, b_2, c_2, g_2, d_2, h_2)$ be a TIFN with λ cut sets $\tilde{A}_{2*}^{[\lambda]} = [a_{2*}^-(\lambda), a_{2*}^+(\lambda)]$, $\tilde{A}_2^{*[\lambda]} = [a_2^{*-}(\lambda), a_2^{*+}(\lambda)]$ of low and high membership, for any $x_1, x_2 \in R$, then $\text{var}'(x_1 \tilde{A}_1 + x_2 \tilde{A}_2) = x_1^2 \text{var}'(\tilde{A}_1) + x_2^2 \text{var}'(\tilde{A}_2) + 2|x_1 x_2| \text{cov}'(\phi(x_1) \tilde{A}_1, \phi(x_2) \tilde{A}_2)$, where $\phi(x)$ is a signal function of $x \in R$.

Proof. (1) If $x_1 > 0$ and $x_2 < 0$, by Zadeh’s fuzzy extension principle one can see that

$$(x_1 \tilde{A}_1 + x_2 \tilde{A}_2)^{[\lambda]}_* = [x_1 a_{1*}^-(\lambda) + x_2 a_{2*}^+(\lambda), x_1 a_{1*}^+(\lambda) + x_2 a_{2*}^-(\lambda)];$$

$$(x_1 \tilde{A}_1 + x_2 \tilde{A}_2)^{*\lambda} = [x_1 a_1^{*-}(\lambda) + x_2 a_2^{*+}(\lambda), x_1 a_1^{*+}(\lambda) + x_2 a_2^{*-}(\lambda)].$$

With Definitions 7,8 and Proposition 1 we easily get

$$\begin{aligned} & \text{var}'(x_1 \tilde{A}_1 + x_2 \tilde{A}_2)_* \\ &= \int_0^1 [M(x_1 \tilde{A}_1 + x_2 \tilde{A}_2)_* - (x_1 a_{1*}^-(\lambda) + x_2 a_{2*}^+(\lambda))]^2 \lambda d\lambda \\ &+ [M(x_1 \tilde{A}_1 + x_2 \tilde{A}_2)_* - (x_1 a_{1*}^+(\lambda) + x_2 a_{2*}^-(\lambda))]^2 \lambda d\lambda \\ &= \int_0^1 \{ [x_1 (M(\tilde{A}_{1*}) - a_{1*}^-(\lambda)) + x_2 (M(\tilde{A}_{2*}) - a_{2*}^+(\lambda))]^2 \\ &+ [x_1 (M(\tilde{A}_{1*}) - a_{1*}^+(\lambda)) + x_2 (M(\tilde{A}_{2*}) - a_{2*}^-(\lambda))]^2 \} \lambda d\lambda \\ &= x_1^2 \text{var}'(\tilde{A}_{1*}) + 2x_1 x_2 \int_0^1 \lambda [(M(\tilde{A}_{1*}) - a_{1*}^-(\lambda))(M(\tilde{A}_{2*}) - a_{2*}^+(\lambda)) + (M(\tilde{A}_{1*}) - a_{1*}^+(\lambda)) \\ &(M(\tilde{A}_{2*}) - a_{2*}^-(\lambda))] d\lambda + x_2^2 \text{var}'(\tilde{A}_{2*}) \\ &= x_1^2 \text{var}'(\tilde{A}_{1*}) - 2x_1 x_2 \text{cov}'(\tilde{A}_{1*}, -\tilde{A}_{2*}) + x_2^2 \text{var}'(\tilde{A}_{2*}) \\ &= x_1^2 \text{var}'(\tilde{A}_{1*}) + 2|x_1 x_2| \text{cov}'(\phi(x_1) \tilde{A}_{1*}, \phi(x_2) \tilde{A}_{2*}) + x_2^2 \text{var}'(\tilde{A}_{2*}); \end{aligned}$$

Similarly, we can prove that

$$\begin{aligned} & \text{var}'(x_1 \tilde{A}_1 + x_2 \tilde{A}_2)^* \\ &= x_1^2 \text{var}'(\tilde{A}_1^*) + 2|x_1 x_2| \text{cov}'(\phi(x_1) \tilde{A}_1^*, \phi(x_2) \tilde{A}_2^*) + x_2^2 \text{var}'(\tilde{A}_2^*); \end{aligned}$$

Hence, we obtain

$$\begin{aligned} \text{var}'(x_1 \tilde{A}_1 + x_2 \tilde{A}_2) &= \frac{1}{2} [\text{var}'(x_1 \tilde{A}_1 + x_2 \tilde{A}_2)_* + \text{var}'(x_1 \tilde{A}_1 + x_2 \tilde{A}_2)^*] \\ &= x_1^2 \text{var}'(\tilde{A}_1) + 2|x_1 x_2| \text{cov}'(\phi(x_1) \tilde{A}_1, \phi(x_2) \tilde{A}_2) + x_2^2 \text{var}'(\tilde{A}_2). \end{aligned}$$

The other cases (2) $x_1 < 0, x_2 > 0$; (3) $x_1 > 0, x_2 > 0$ and (4) $x_1 \leq 0, x_2 \leq 0$ can be similarly proved.

Theorem 3. Let $\tilde{A} = (e, a, f, b, c, g, d, h)$ be a TIFN with λ cut sets $\tilde{A}_*^{[\lambda]} = [a_*^-(\lambda), a_*^+(\lambda)]$, $\tilde{A}^{*\lambda} = [a^{*-}(\lambda), a^{*+}(\lambda)]$ of low and high membership, then we obtain $\text{var}(\tilde{A}) \leq \text{var}'(\tilde{A})$.

Proof.

$$\begin{aligned} \text{var}'(\tilde{A}_*) &= \int_0^1 \{ [M(\tilde{A}_*) - a_*^-(\lambda)]^2 + [M(\tilde{A}_*) - a_*^+(\lambda)]^2 \} \lambda d\lambda \\ &= \int_0^1 [(a_*^+(\lambda))^2 + (a_*^-(\lambda))^2] \lambda d\lambda - \int_0^1 2(M(\tilde{A}_*)) [a_*^-(\lambda) + a_*^+(\lambda)] \lambda d\lambda + 2 \int_0^1 M(\tilde{A}_*)^2 \lambda d\lambda \\ &= \int_0^1 [(a_*^+(\lambda))^2 + (a_*^-(\lambda))^2] \lambda d\lambda - (M(\tilde{A}_*))^2. \end{aligned}$$

Also, by the possibilistic variance definition stated in [17, 21] we know that

$$\begin{aligned}\text{var}(\tilde{A}_*) &= \frac{1}{2} \int_0^1 [a_*^+(\lambda) - a_*^-(\lambda)]^2 \lambda d\lambda \\ &= \frac{1}{2} \int_0^1 [(a_*^+(\lambda))^2 + (a_*^-(\lambda))^2] \lambda d\lambda - \int_0^1 a_*^+(\lambda) a_*^-(\lambda) \lambda d\lambda.\end{aligned}$$

From the Jensen inequality and $\int_0^1 2\lambda d\lambda = 1$, we have

$$\left[\int_0^1 2\lambda (a_*^-(\lambda) + a_*^+(\lambda)) d\lambda \right]^2 \leq \int_0^1 2\lambda (a_*^-(\lambda) + a_*^+(\lambda))^2 d\lambda.$$

That is, $\left[\int_0^1 \lambda (a_*^-(\lambda) + a_*^+(\lambda)) d\lambda \right]^2 \leq \frac{1}{2} \int_0^1 \lambda (a_*^-(\lambda) + a_*^+(\lambda))^2 d\lambda$.

So, $\text{var}(\tilde{A}_*) - \text{var}'(\tilde{A}_*)$

$$\begin{aligned}&= -\frac{1}{2} \int_0^1 [(a_*^+(\lambda))^2 + (a_*^-(\lambda))^2] \lambda d\lambda - \int_0^1 a_*^+(\lambda) a_*^-(\lambda) \lambda d\lambda + (M(\tilde{A}_*))^2 \\ &= -\frac{1}{2} \int_0^1 [(a_*^+(\lambda))^2 + (a_*^-(\lambda))^2] \lambda d\lambda - \int_0^1 a_*^+(\lambda) a_*^-(\lambda) \lambda d\lambda + (M(\tilde{A}_*))^2 \\ &= -\frac{1}{2} \int_0^1 [a_*^+(\lambda) + a_*^-(\lambda)]^2 \lambda d\lambda + \left[\int_0^1 \lambda (a_*^-(\lambda) + a_*^+(\lambda)) d\lambda \right]^2 \leq 0.\end{aligned}$$

Similarly, we can prove $\text{var}(\tilde{A}^*) - \text{var}'(\tilde{A}^*) \leq 0$.

So, $\text{var}(\tilde{A}) = [\text{var}(\tilde{A}_*) + \text{var}(\tilde{A}^*)] / 2 \leq [\text{var}'(\tilde{A}_*) + \text{var}'(\tilde{A}^*)] / 2 = \text{var}'(\tilde{A})$.

4. Conclusion

In this article, we introduce a new definition of possibilistic variance of trapezoidal intuitionistic fuzzy number and discuss some important properties. In the future work, we will study the possibilistic mean and variance of the related uncertain numbers such as fuzzy neutrosophic numbers and dual-connection numbers, which are very important in the uncertain multi-criteria decision and fuzzy portfolio selection problem. Also, we will investigate the intuitionistic fuzzy portfolio decision-making and selection problem by maximizing possibilistic mean and minimizing possibilistic variance of portfolio.

Acknowledgement

This work is supported in part by the Guangdong Basic and Applied Basic Research Foundation under Grant No. 2018A030313996.

References

- [1] Atanassov K.T., Intuitionistic Fuzzy Sets, Fuzzy Sets and Systems, 1986, 20, 87–96.
- [2] Wang J.Q., Zhang Z., Aggregation operators on intuitionistic trapezoidal fuzzy number and its application to multi-criteria decision making problems, Journal of Systems Engineering and Electronics, 2019, 20, 321-326.
- [3] Li D. F., A ratio ranking method of triangular intuitionistic fuzzy numbers and its application to MADM problems, Computers and Mathematics with Applications, 2010, 60(6), 1557-1570.

- [4] Vakkas Ulucay , Irfan Deli, Mehmet Sahin, Trapezoidal fuzzy multi-number and its application to multi-criteria decision-making problems, *Neural Computing & Applications*, 2018,30(5),1469-1478.
- [5] Liu P.D., Liu Y., An approach to multiple attribute group decision making based on intuitionistic Trapezoidal Fuzzy Power Generalized Aggregation Operator, *International Journal of Computational Intelligence Systems*, 2014, 7(2), 291-304.
- [6] Rezvani Salim, Wang X.Z., Pourpanah F., Intuitionistic Fuzzy Twin Support Vector Machines, *IEEE Transactions on Fuzzy Systems*, 2019, 27(11), 2140-2151.
- [7] Kumar M., Applying weakest t-norm based approximate intuitionistic fuzzy arithmetic operations on different types of intuitionistic fuzzy numbers to evaluate reliability of PCBA fault, *Applied Soft Computing*, 2014, 23, 387-406.
- [8] Wang J.Q., Nie R.R, Zhang H.Y., Chen X.H., New operators on triangular intuitionistic fuzzy numbers and their applications in system fault analysis, *Information Sciences*, 2013, 251, 79–95.
- [9] Chen G. H., Liao X. L., Yu X., Multi-objective Portfolio Selection Model Based on Intuitionistic Fuzzy programming, *Fuzzy Systems and Mathematics*, 2012, 26(2),129-135.
- [10] Chakraborty D., Jana D.K., Roy T.K., A new approach to solve intuitionistic fuzzy optimization problem using possibility, necessity and credibility measure, *International Journal of Engineering Mathematics*, 2014, 20, 1-12.
- [11] Garai T., Chakraborty D., Roy T. K., Possibility-necessity-credibility measures on generalized intuitionistic fuzzy numbers and their applications to multi-product manufacturing system, *Granular Computing*, 2018, 3, 285-299.
- [12] Zhou W., Xu Z.S., Score-hesitation trade-off and portfolio selection under intuitionistic fuzzy Environment, *International Journal of Intelligent Systems*, 2019,34(2), 325-341.
- [13] Chen G.H., Luo Z.J., Liao X. L., Yu X., Yang L., Mean-variance-skewness fuzzy portfolio selection Model Based on Intuitionistic Fuzzy optimization, *Procedia Engineering*, 2011,15(2), 2062-2066.
- [14] Rezvani Salim, Ranking method of trapezoidal intuitionistic fuzzy numbers, *Annals of Fuzzy Mathematics and Informatics*,2013, 5(3), 515–523.
- [15] Chakraborty D., Jana D. K, Roy T.K, Arithmetic operations on generalized intuitionistic fuzzy number and its applications to transportation problem, *Opsearch*, 2015,52(3), 431-471.
- [16] Zhou W., Meng S., Chen M. H., Hybrid Atanassov intuitionistic fuzzy Bonferroni means for multi-criteria aggregation, *Journal of Intelligent and fuzzy Systems*, 2014, 27(5), 2679-2690.
- [17] Carlsson C., Fuller R., On possibilistic mean value and variance of fuzzy numbers, *Fuzzy Sets and Systems*, 2001,122, 315-326.
- [18] Carlsson C., Fuller R., Majlender P., A possibilistic approach to selecting portfolios with highest utility score, *Fuzzy Sets and Systems*, 2002,131, 13- 21.
- [19] Zhang W.G., Wang Y.L., Notes on possibilistic variances of fuzzy numbers, *Applied Mathematics Letters*, 2007, 11, 1167-1173.
- [20] Zhang W.G., Xiao W. L., Wu W. J., A possibilistic portfolio adjusting model with new added assets, *Economic Modelling*, 2010, 27, 208-213.
- [21] Wan S. P., Zhang X. L., Li D. F., Possibility mean-variance based method for intuitionistic trapezoidal fuzzy group decision making, *Journal of Systems Engineering*, 2012, 27(6),782-788.
- [22] Wan S.P., Dong J.Y., Possibility method for triangular intuitionistic fuzzy multi-attribute group decision making with incomplete weight information, *International Journal of Computational Intelligence Systems*, 2015, 7(1), 65-79.
- [23] Wan S. P., Multi-attribute decision making method based on possibility variance coefficient of triangular intuitionistic fuzzy numbers, *International Journal of Uncertainty, Fuzziness and Knowledge-Based Systems*, 2013, 21(2), 223–243.

Knowledge Map Reasoning Technology Based on Complex Network

Xiang DAI^{a,1} and Yongchao WEI^b

^aSouthwest China Institute of Electronic Technology, Chengdu 610036, China

^bCivil Aviation Flight University of China, GuangHan, 618307, China

Abstract: In recent years, with the rapid development of artificial intelligence technology, knowledge mapping research based on data mining, machine learning and knowledge engineering has attracted the attention of a large number of researchers. Knowledge mapping has important theoretical value and practical significance for the development of artificial intelligence and machine cognitive intelligence. In recent years, researchers have achieved a lot of excellent research results in the field of knowledge mapping technology, but there are still some problems to be solved. This paper studies the construction technology of knowledge map based on social network, mainly discusses the problems of entity acquisition, entity disambiguation, relationship completion, relationship reasoning and knowledge conflict resolution. The research results of this paper can provide reference for intelligent applications such as intelligent information retrieval, dialogue system and intelligent recommendation.

Keywords: Knowledge Mapping, Complex Network, Entity Disambiguation, Relational Reasoning

1. Introduction

Knowledge mapping is composed of concepts, entities, events of the objective world and their relationships, which are usually represented by a triple. It can provide a large amount of factual knowledge, and structured storage method for unstructured data, which helps to discover the potential association between entities. By establishing the mapping from string description to structured semantic description, it can provide technical support for natural language understanding, machine reading, semantic based information retrieval and other technologies. It has broad application prospects in intelligent search, recommendation system, question answering system, intelligent investment advisory, intelligent marketing, complex network and other scenarios [1].

Knowledge mapping construction is a challenging work, which attracts great attention in academic and industrial fields. Although there are many excellent researches, but still many problems need to be studied. The traditional knowledge comes from domain experts, which has high accuracy but limited quantity, and cannot adapt to the explosive growth of data. Therefore, the research on complex media data has become a hot topic. Aiming at the ubiquitous knowledge defects, PtranSparse is proposed to complete the knowledge graph based on metric space and relational paths, which combines TranSparse model to deal with the heterogeneity and imbalance of

¹ Corresponding Author, Xiang Dai, Southwest China Institute of Electronic Technology, Chengdu, 610036, China; E-mail: 54831015@qq.com.

entities and relationships, and PTransE to make full use of the semantic information of the relationship path, the weight is used to distinguish the relationship type when the entity is projected [2]. The system based on social network knowledge graph includes five modules: the modules of data source, knowledge graph discovery, distributed graph database, and core sub-algorithm are connected to multi-graph network engine module, the distributed graph database module is connected to core sub-algorithm module [3]. The concept graph data developed by Microsoft from web pages and search logs contains 5.4 million core concepts, can provide common sense knowledge and concepts for machine by mapping concepts to vector space, which is used in many regions.

This paper mainly uses machine learning, data mining, relational statistical learning and deep learning to solve the problem of knowledge mapping. Data-driven method and machine learning are used to obtain the entity data; Then, the Markov logic network is proposed to disambiguate double named entities in the knowledge map; thirdly, the entity relationship completion and reasoning of the knowledge map are carried out; finally, the method based on deep learning is proposed to complete the knowledge map, which resolves the knowledge conflict in the process of the change between the two countries.

2. Related Concepts

2.1. Task Association Method Based on Complex Network

The topological structure of nodes is an important feature of complex networks, degree centrality, clustering coefficient and eigenvector centrality are three features of which used to associate people. Degree centrality represents its direct influence on neighbor nodes. The greater the degree centrality is, the greater its influence on neighbor nodes is. We use the normalized node degree to represent the degree centrality DC (i)[4].

$$DC(i) = \frac{k_i}{k_{max}} \quad (1)$$

Clustering coefficient measures the degree of close relationship between neighbors. The value is obtained by dividing the number of edges between its neighbors [5]:

$$C_i = \frac{2n}{k_i(k_i-1)} \quad (2)$$

$$EC(i) = X = \lambda^{-1} \sum_{j=1}^n a_{ij}x_j \quad (3)$$

2.2. Graph Segmentation Based on Spectrum

It is time-consuming to calculate node clustering coefficient and eigenvector centrality; graph segmentation can divide large graph into small subgraphs. Spectral graph partition is a common method. The spectrum is the eigenvalue of a matrix and its eigenvector. G is divided into two disjoint sets U and W, so that the number of edges $\min(\frac{|E(G) \cap (U \times W)|}{|U| \cdot |W|})$ is the least [6].

2.3. Bipartite Graph Matching to Associate Cross Network Tasks

In addition to the user's portrait and complex structure, user's network behavior such as online time, writing style and user interest can also be used to describe the similarity of users. Based on the location trajectory, online time and user generated content, Kong et al. proposed a multi network anchor link method to find related accounts in different platforms, and used a stable matching method to map the matching problem of user pairs. Goga and others use location tags, time information and writing style to solve the task of user identification. Although writing style works well in the long text, it is not suitable for the microblog network with short text [7]. Zafarani used knowledge limitations and typing patterns to model user behavior patterns. Mishari pointed out that the author's online comment writing style can be used as feature to connect the same users. Iofciu used tag to match accounts. Goga used activity information to match accounts.

Existing methods are limited to use certain features, and cannot be extended to large-scale complex networks. In this section, the problem of people linking between complex networks is transformed into a weighted bipartite graph matching problem. Kuhn Munkres (KM) algorithm is used to solve the problem, which use user portraits, online time distribution and interest features to measure the similarity between users [8].

2.4. User Portraits and Complex Structural Features

User profile information, such as nickname, gender, hobbies, educational background, can also be used to identify the same users. Jain designed a system to match Facebook and twitter accounts based on user portraits, user generated content and complex relationships, the disadvantage that it needs to be redesigned for different complex networks. Tan pointed out that 50% of users use the same user name, but some are owned by different users [9]. Malhotra proposed a digital footprint based on name, nickname, location, photo and number of friends to associate a user's information. Jaro Winkler method can measure user ID and account name effectively, but can't associate some people with missing information. Zafarani and Liu proposed Mobius method to find out the relationship between users, based on the user's behavior pattern in complex media. Mobilus uses different content information to correlate user. Vosecky uses user portraits represented by vectors to associate people. Carmagnola used user profile attributes to associate users. Goga constructed a similarity matrix to identify 80% of the character pairs in twitter, Facebook and Google + datasets.

The above research mainly focuses on specific networks, and cannot be applied to academic complex networks. This section uses the complex structure and user portrait characteristics to associate the same users in complex networks [10].

$$sim_{profile}(A, B) = \frac{A_{profile} * B_{profile}}{\|A_{profile}\| * \|B_{profile}\|} = \frac{\sum_{i=1}^n A_i B_i}{\sqrt{\sum_{i=1}^n A_i^2} \sqrt{\sum_{i=1}^n B_i^2}} \quad (4)$$

In order to integrate portrait similarity and network structure similarity, Mapme introduces a balance factor to adjust the weight, as shown in equation 6, where the smoothing factor $\alpha \in [0, 1]$, when α increases, the weight of portrait similarity is larger, and when α decreases, the weight of structure similarity is larger.

$$sim(A, B) = \alpha * sim_{profile}(A, B) + (1 - \alpha) * sim_{structure}(A, B) \quad (5)$$

2.5. Network Entity Disambiguation Based on Markov Logic

In Markov logic network, the weight of rules can be calculated by the prior probability. When the new rule challenges, the weight is greater than that of the old rule, a new relationship is established. It can effectively deal with the problem of relationship conflict in knowledge base, which combines the advantages of probability graph model and first-order logic. Probability graph model can deal with the learning problem, and first-order logic can deal with the reasoning problem. Markov logic network can not only provide a compact description, but also have the ability to integrate modular knowledge flexibly; on the other hand, Markov logic network can provide uncertain reasoning ability for first-order predicate logic, and tolerate the lack and conflict of knowledge.

Eq. (6) gives the probability distribution of a possible benchmark rule X.

$$p = (X = x) = \frac{1}{z} \exp\{\sum_i w_i n_i(x)\} = \frac{1}{z} \prod_i \varphi_i(x_{\{i\}})^{n_i(x)} \quad (6)$$

$n_i(x)$ Indicates the number of corresponding benchmark rules, $x_{\{i\}}$ represents the state of rule X.

Entity disambiguation based on tensor decomposition:

$$H_{\alpha\mu} \leftarrow H_{\alpha\mu} \frac{(w^T v)}{(w^T W H)_{\alpha\mu}}, W_{ia} \leftarrow W_{ia} \frac{(v^T H)_{ia}}{(W H H^T)_{ia}} \quad (7)$$

If W and H are on the fixed distance, the Euclidean distance is invariant in the renewal case. If the initial matrix is nonnegative, all intermediate results are nonnegative.

2.6. Relationship Completion Based on Link Prediction

Lao and Cohen developed a path ranking algorithm (PRA) for knowledge base reasoning. PRA randomly walks on the graph according to the graph structure to find the order (or path) of the relationship, thereby predicts the new relationship between entities. It has stronger expressive ability than other reasoning methods, and can be easily extended to very large graphs for real-time reasoning, but has weak representation ability. So, we use path feature and vector space representation to represent the relationship between entities.

If the relationship path $P=R_1R_2\dots R_T$ not empty, Let $P'=R_1R_2\dots R_{T-1}$, define the path characteristics of node e:

$$h_{s,P}(e) = \sum_{e' \in \text{range}(P)} h_{s,P'}(e') * P(e|e'; R_1) \quad (8)$$

Give path P, the path feature $h_{s,P_I}(e)$, and the nodes can be sorted by linear model $\theta_1 h_{s,P_1}(e) + \theta_2 h_{s,P_2}(e) + \dots + \theta_n h_{s,P_n}(e)$.

The ranking of candidate nodes e related to query node s can be given:

$$\text{score}(e; s) = \sum_{P \in P_I} h_{s,P}(e) \theta_P \quad (9)$$

2.7. Relationship Reasoning Based on Probabilistic Soft Logic

The occurrence times of each relationship can be counted, which represent the support or strength of the relationship. Based on the method proposed by Bhatia, a relational

ranking method is proposed to find out the corresponding target entities and their relationships. We use the following formula to rank the relationships

$$P(r, e_t | e_s) = P(e_t | e_s)P(r | e_t, e_s) = P(r | e_s, e_t) \frac{P(e_t)P(e_s | e_t)}{P(e_s)} \quad (10)$$

Entity class identity thinks that the more and greater the entity relationship between a target and an input, the closer and important the relationship between the two entities is, the higher their entity class identity is. The similarity degree between entities is shown:

$$P(e_s | e_t) = \frac{\sum_{r_i \in R(e_s | e_t)} w(r_i)}{\sum_{r_i \in R(e_t)} w(r_i)} \quad (11)$$

2.8. Uncertain Time Series Knowledge Map

Uncertain time series knowledge graph is the combination of time series and probability graph, which can represent both uncertain knowledge and time characteristics. The semantic temporal relationship based on the joint probability distribution of entity relationship is proposed by Bhatia, finds out the corresponding target entities and their relationships. Given the entity e_s and the relation set Re_s ($Re_s \subseteq R$), Using the following formula to sort these two relations by relevance:

$$P(r, e_t | e_s) = P(e_t | e_s)P(r | e_t, e_s) = P(r | e_t, e_s) \frac{P(e_t)P(e_s | e_t)}{P(e_t)} \quad (12)$$

The relationship probability between an entity with a popular entity is higher than with a rare entity.

$$P(e_t) = relCount(e_t) \quad (13)$$

We mainly consider three constraints types: time disjoint, antecedent and time mutual exclusion. The time disjoint is to limit any two-time intervals with the same relationship. The following template is used to describe it:

$$R_1(e_i, e_j, t_1) \wedge R(e_i, e_k, t_2) \wedge (e_j \neq e_k) \rightarrow disjio\ int(t_1, t_2) \quad (14)$$

Semantic, path and time embedding representation are used to resolve the knowledge conflict, and predict the relationship between entities, so that the knowledge map can change with entities.

3. Experimental Results and Analysis

The platform is Intel i7 2.80GHZ with centos6.4 and C++ program language. The accuracy(P), recall(R) and F1 value were used to evaluate the proposed method. P and R are the proportion of correct node pairs in the found pairs and all correct pairs separately.

Data collected from aminer, sina weibo and science blog from January to June 2015 are the experiment. aminer, sina weibo and science blog contains 17000, 17000 and 16000 user portraits, and 112000, 769000 and 89000 complex relationships separately. The common users are sina weibo 6512, science blog 4096, and aminer 3953.

(1) Result Analysis Using User Portraits and Complex Structural Feature

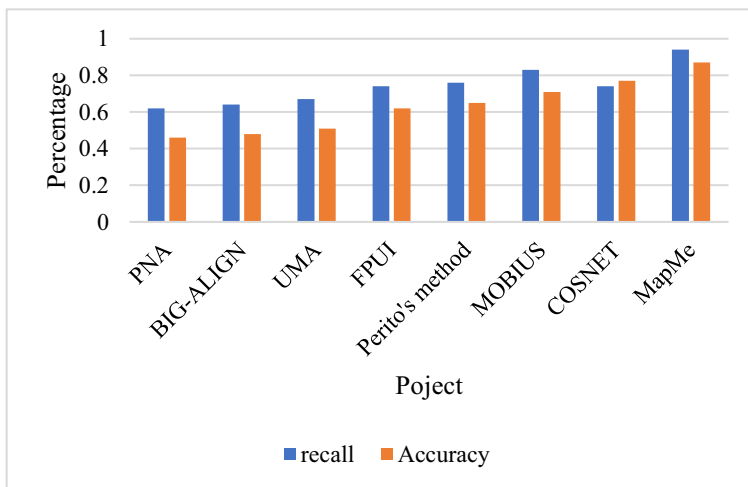


Figure 1. Comparison of recall and accuracy rates

Figure 1 shows the recall and accuracy of mapme and baseline method on Weibo aminer dataset, from which we can see that mapme has achieved the best results. The recall rate of mapme is 10% higher than that of cosnet and 21% higher than that of baseline method, and the accuracy rate of mapme is 10% higher than cosnet and 27% higher than that of baseline method.

(2) Different Sampling Ratio Test

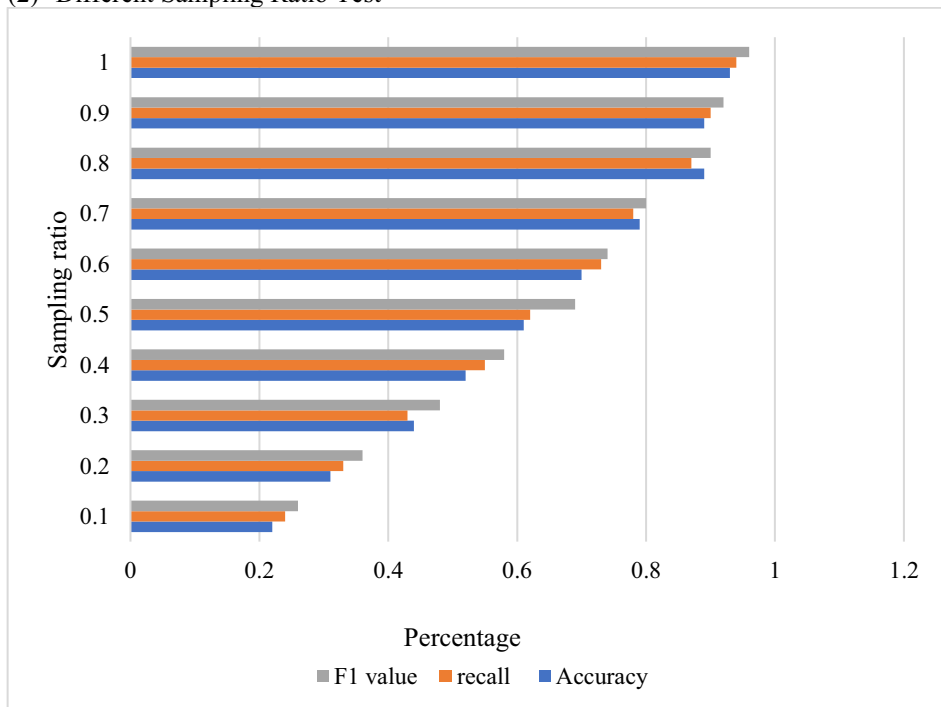


Figure 2. Comparison results of accuracy, recall and F1 values

Figure 2 shows P, R and F1 value of mapme method under different sampling ratios on science dataset. The sampling ratio η is the ratio of the training set to the total data. As can be seen from Figure 2, P of mapme increases with the sampling ratio.

Table 1. Comparison of the accuracy, recall and F1

	PNA	ALIGN	UMA	FRUI	Perito	MOBIUS	COSNET	MapMe
P	0.394	0.443	0.536	0.632	0.703	0.806	0.812	0.937
R	0.401	0.438	0.546	0.641	0.724	0.801	0.823	0.946
F1	0.398	0.439	0.539	0.639	0.716	0.801	0.816	0.941

Table 1 shows the comparison results between mapme and baseline method when the sampling ratio is 0.5 on aminer dataset, and mapme has achieved the best effect.

(3) Bipartite Graph Matching Method

Table 2. Inter-network Matching

OSN	OSN	Matching account pairs
Facebook	Tumblr	392783
Tumblr	Twitter	488667
Twitter	Instagram	413675
Instagram	Facebook	376528
Twitter	Facebook	432846
Tumblr	Instagram	375654

Table 2 shows the statistical information. Instagram is a photo sharing network, includes 1105492 users and 34387876 relationships. Facebook is a complex network with the largest user's number, includes 1101324 users and 27693893 relationships. Twitter is a micro blog network, includes 1260752 users and 46083383 relationships. Tumblr is a light blog based complex network, includes 1007136 users and 29571930 relationships.

On Tumblr & twitter and instagram & Facebook, our method is the best. P, R and F1 value were 90.12%, 73.82% and 81.08% respectively. Compared with NS, Mobius, cosnet and hydra, P, R and F1 are 11%, 17% and 29% average higher respectively.

(4) Entity Disambiguation Experiment Based on Markov Logitech Network

Table 3. Entity disambiguation experiment

Data set	knowledge domain	Method	F1	P	R
Y	YAGO3	Our method	0.711	0.815	0.631
		DoSeR	0.659	0.706	0.617
A	DBpedia	Our method	0.693	0.803	0.609
		DoSeR	0.656	0.729	0.597
	Wikidata	Our method	0.704	0.812	0.621
		DoSeR	0.634	0.737	0.556
D	YAGO3	Our method	0.710	0.821	0.625
		DoSeR	0.646	0.742	0.572
B	DBpedia	Our method	0.712	0.817	0.631
		DoSeR	0.647	0.742	0.573
	Wikidata	Our method	0.706	0.831	0.614
		DoSeR	0.630	0.753	0.542
W	YAGO3	Our method	0.704	0.827	0.613
		DoSeR	0.651	0.749	0.576
	DBpedia	Our method	0.715	0.824	0.631
		DoSeR	0.661	0.759	0.585
	Wikidata	Our method	0.726	0.831	0.645
		DoSeR	0.647	0.742	0.573

The results given in Table 3, show that our method is better than DoSeR. In WD and wikidata, the F1 value is 8% higher; in YA, DB, WD data sets and wikidata knowledge, the F1 value of is 7% higher on average; in wikidata and WD, P is 10% higher, and 5% higher on average. Markov logic network combines the advantages of Markov network

and first-order logic, which makes the statistical relation model based on Markov logic network very suitable for entity disambiguation.

(5) Relationship Completion Based on Link Prediction

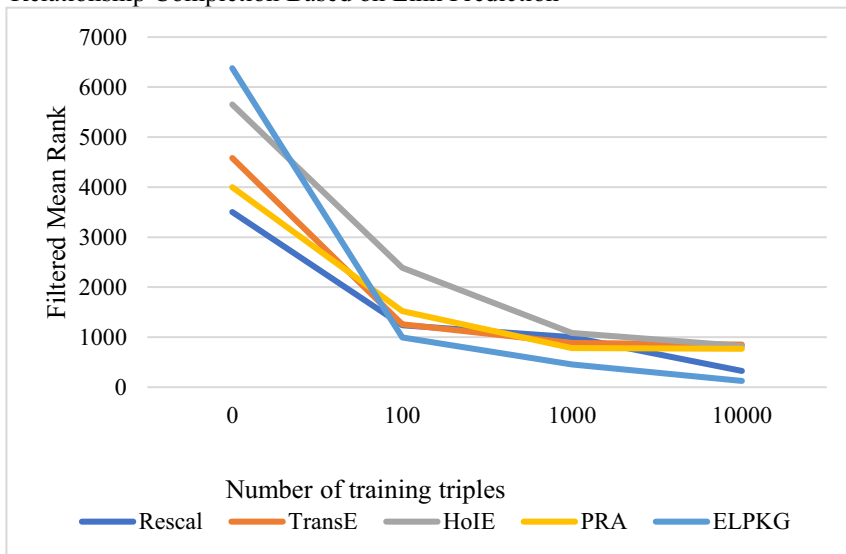


Figure 3. FMR comparison result

Figure 3 shows the comparison results. Elpkg can learn new relationships with fewer samples. When the number of new relational tuples increases from 10 to 100, the learning speed of elpkg is the fastest, and the FMR decreases rapidly from 6378 to 996. The link prediction method elpkg proposed solved missing relationship problem, which can mine the potential relationship between entities more accurately and can be applied to question answering system and precision recommendation system.

(6) Relationship Reasoning Based on Probabilistic Soft Logic

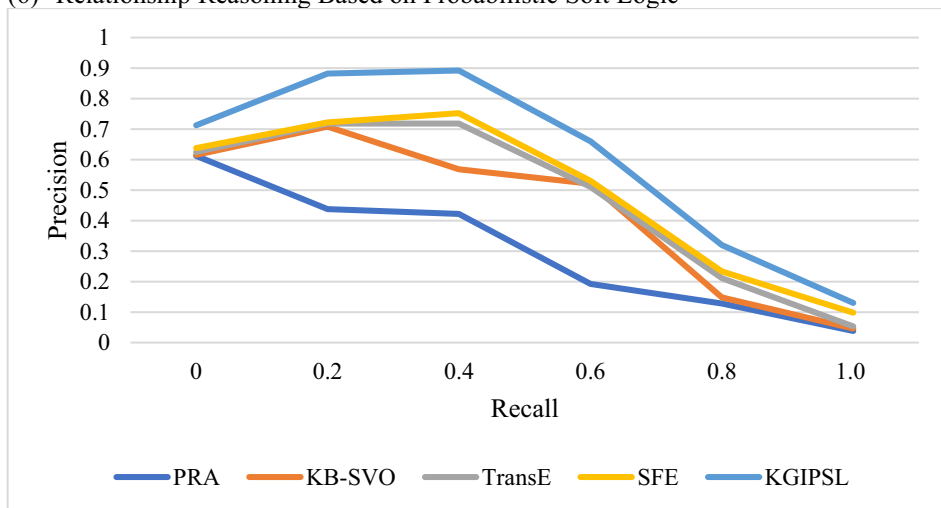


Figure 4. Comparison between the proposed method and the baseline method

Figure 4 shows the P and R curves on the Yago dataset, which shows that the kgipsl method proposed is obviously better than others. When R is 0.4, the maximum P is 0.89, which is higher than SFE and kb-svo respectively. When R is from 0.1 to 1, the average P of kgipsl is 9% higher than others. kgipsl can mine the potential relationship between entities, and improve the knowledge coverage and completeness of the knowledge map.

(7) Knowledge Conflict Resolution Based on Time Constraint

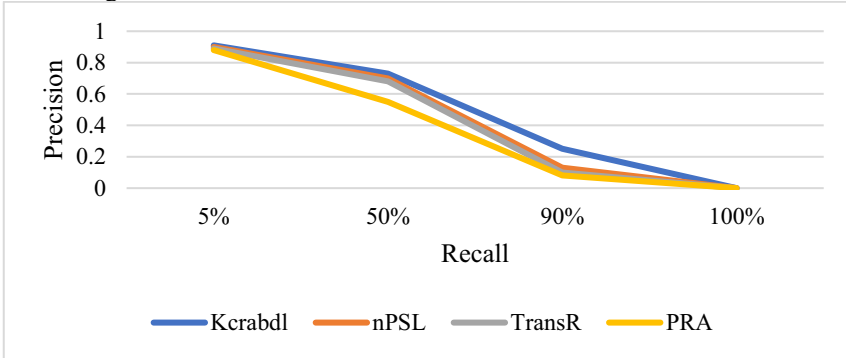


Figure 5. Recall rate of proposed method Kcrabdl and baseline method

Figure 5 shows the comparison results between the proposed kcrabdl method and several other methods on Yago dataset. It can be seen that kcrabdl is superior to other methods. When R is 5%, P of kcrabdl, npsl, TRANSR and PRA is 0.91, 0.9, 0.89 and 0.88 respectively; when R is 50%, P is 0.73, 0.7, 0.68 and 0.55 respectively; when R is 90%, P is 0.25, 0.13, 0.1 and 0.08 respectively. Experiments show that this method is superior to the current mainstream methods.

4. Conclusion

The social network-oriented knowledge mapping technology studied in this paper belongs to the cross domain of knowledge engineering, social network, data mining and machine learning, and has become an important content in the field of artificial intelligence. However, due to the large scale of knowledge mapping, wide range of data sources, complex data types, fast knowledge updating and other characteristics, the research has great challenges. This paper obtains knowledge from social media, knowledge base and other data sources, and studies the key technologies of knowledge mapping construction technology. Different from the traditional method of extracting entities from Wikipedia and knowledge base to build knowledge map, this paper first obtains the person entities from social networks; then proposes an entity disambiguation method based on Markov logic network to solve the entity ambiguity problem in the process of knowledge map fusion; and then proposes a link prediction method combining entity relationship semantic embedding and path embedding to solve the problem of knowledge map fusion, and a method based on probabilistic soft logic is proposed to solve the problem of relational reasoning in knowledge map; finally, a deep learning method based on recurrent neural network is proposed to solve the problem of knowledge conflict in the process of knowledge map changing with time.

Reference

- [1] Niu D, Liu L, Lu S. Augmenting Negation Normal Form with Irrelevant Variables[J]. *IEEE Access*, 2019, PP(99):1-1.
- [2] Gao J, Chen H, Zhang Y, et al. Knowledge-Based Approaches to Accurate Mapping of Mangroves from Satellite Data[J]. *Photogrammetric Engineering and Remote Sensing*, 2015, 70(11):1241-1248.
- [3] Shirahama K, Grzegorzec M. Towards large-scale multimedia retrieval enriched by knowledge about human interpretation[J]. *Multimedia Tools and Applications*, 2016, 75(1):297-331.
- [4] Paulheim H, Cimiano P. Knowledge graph refinement: A survey of approaches and evaluation methods[J]. *Semantic Web*, 2017, 8(3):489-508.
- [5] Uyar A, Aliyu F M. Evaluating search features of Google Knowledge Graph and Bing Satori[J]. *Online Information Review*, 2015, 39(2):197-213.
- [6] Ernst P, Siu A, Weikum G. KnowLife: a versatile approach for constructing a large knowledge graph for biomedical sciences[J]. *Bmc Bioinformatics*, 2015, 16(1):1-13.
- [7] Shengtian S, Zhihao Y, Lei W, et al. SemaTyP: a knowledge graph based literature mining method for drug discovery[J]. *BMC Bioinformatics*, 2018, 19(1):1-11.
- [8] Sun Z, Wang C, Hu W, et al. Knowledge Graph Alignment Network with Gated Multi-Hop Neighborhood Aggregation[J]. *Proceedings of the AAAI Conference on Artificial Intelligence*, 2020, 34(1):222-229.
- [9] Wang T, Shi D, Wang Z, et al. MRP2Rec: Exploring Multiple-Step Relation Path Semantics for Knowledge Graph-Based Recommendations[J]. *IEEE Access*, 2020, PP(99):1-1.
- [10] Wu Y, Liu Q, Chen R, et al. A Group Recommendation System of Network Document Resource Based on Knowledge Graph and LSTM in Edge Computing[J]. *Security and Communication Networks*, 2020, 2020(1):1-11.

Semantic Supervised Training for General Artificial Cognitive Agents

Roman V. DUSHKIN^{a,1} and Vladimir Y. STEPANKOV^b

^aArtificial Intelligence Agency, Volkonsky 1st Lane, 15, 127473 Moscow, Russia

^bNational Research Nuclear University MEPhI, Moscow 115409, Russia

Abstract. The article describes the authors' approach to the construction of general-level artificial cognitive agents based on the so-called «semantic supervised learning». Within this approach in accordance with the hybrid paradigm of artificial intelligence, both machine learning methods and methods of the symbolic approach («good old-fashioned artificial intelligence») are used. A description of current problems with understanding of the general meaning and context of situations in which narrow AI agents are found is presented. The definition of semantic supervised learning is given and its relationship with other machine learning methods is described. In addition, a thought experiment is presented, which shows the essence and meaning of semantic training with a teacher, which makes it possible to «educate» a general-level AI agent. It opens the opportunity to apply not only general-level knowledge about the world around the agent, but also introduce the personal experience, which, according to the authors, will lead to a full understanding of the context and, ultimately, to the construction of general artificial cognitive agents. The article also provides a possible architecture for an artificial cognitive agent that can implement semantic supervised learning. The novelty of the work lies in the authors' approach to combining various methods of artificial intelligence within the hybrid paradigm. The relevance of the work is based on the ever-increasing interest in general-level artificial intelligence methods in science, technology, business and world politics. The article is theoretical. The article will be of interest to specialists in the field of artificial intelligence (especially in the direction of building artificial general intelligence), philosophy of consciousness, and in general to all those who are interested in up-to-date relevant information about the approaches and methods of implementing general artificial cognitive agents.

Keywords. Artificial intelligence, agent, agent-based approach, artificial general intelligence, supervised learning, semantics, context processing, personal experience, ontology, architecture

1. Introduction

The problem of creating general level artificial intelligence (Artificial General Intelligence, AGI) is becoming a technological trend of modern times again [1].

¹Corresponding Author: Roman V. DUSHKIN, Artificial Intelligence Agency, Volkonsky 1st Lane, 15, 127473 Moscow, Russia; E-mail: drv@aiagency.ru.

Successes in the construction of narrow artificial cognitive agents which have already surpassed the human level for some specific tasks [2] give hope that with the proper level of technical elaboration it will be possible to move from narrowly focused artificial intelligence systems to artificial general intelligence. At the same time, there is a lot of skepticism about this trend. Since there are reasonable doubts that the extensive development of narrow artificial intelligence systems will make it possible to make a qualitative transition to AGI [3]. Intensification of research and the renewal of interdisciplinary dialogue are required to search for possible solutions in the field of building artificial general intelligence.

It should be noted that such an intensification of research can take place in several directions simultaneously. The authors see at least the following:

- Development of new types of architecture of artificial cognitive agents which allow them to solve problems inherent for AGI: independent goal-setting and the ability to independently learn new skills.
- Using the achievements of related sciences and organizing a comprehensive interdisciplinary dialogue for a deeper understanding of the nature of human intelligence.
- Application for the design and implementation of the general-level cognitive agent of the new knowledge gained from working with the natural intelligence of humans.

In this work the attempt is made to present the authors' vision and understanding of how one of the processes of «growing» an general-level artificial cognitive agent should be arranged by teaching such an agent general knowledge about its environment (not necessarily coinciding with human reality) for gaining the ability to solve arbitrary cognitive tasks later. An outline of the architecture of such an artificial cognitive agent is given.

2. Recognition and Understanding

All research in the field of artificial intelligence could be divided into several large classes then, in fact, everything can be put into two large paradigms – top-down and bottom-up [4]. This division was proposed back in the days of the first researchers of artificial intelligence at the Computer Science and Artificial Intelligence Laboratory of the Massachusetts Institute of Technology — John McCarthy and Marvin Minsky. The first advocated the methods of the top-down paradigm (the so-called «pure artificial intelligence»), and the second — for the methods of the bottom-up paradigm (respectively, «dirty artificial intelligence»).

The top-down approach in artificial intelligence is focused on methods of working with knowledge — these are knowledge bases and methods of acquiring, representing and processing knowledge, and various kinds of symbolic computation methods. The main feature of the approach is the ability to make decisions and explain the principles and reasons for making exactly such decisions. The disadvantages of this approach include the difficulty of learning for knowledge-based systems [5].

The bottom-up approach, based on training of artificial cognitive agents on data (machine learning, artificial neural networks), allows to effectively teach agents to solve

specific problems. But at the same time, in general terms, such agents remain «black boxes» with the complexity of explaining decision options [6].

Traditionally, bottom-up AI techniques have been used to solve pattern recognition tasks, to find hidden patterns in large data sets, and other similar tasks. In particular, the task of pattern recognition (in a general sense) has become the area where deep learning methods in some special cases have already surpassed the cognitive abilities of the human brain. For these particular cases, the accuracy of neural network solutions in pattern recognition is already higher than that of humans [7]. So there are no fundamental obstacles to increasing the accuracy even higher, as well as to expand the methods to solve new tasks.

At the same time, pattern recognition does not lead to understanding [8]. In general, the problem of understanding is acute today. It stood in the history of the development of artificial intelligence methods, since the understanding of the current cognitive agent's situation, especially taking into account the context and memory of the agent's «life experience», is the key to competent decision making. Without understanding the general meaning, it will only be possible to build narrow artificial intelligence systems for solving insular specific problems [8]. This thesis can be illustrated by the example of insects — their natural neural networks are quite capable of recognizing images, but no understanding arises in them. The bee visually recognizes flowers from which delicious nectar can be extracted, but does not understand exactly (at least in the human sense) what it does, why it does and for what purpose.

However, the methods of the top-down paradigm of artificial intelligence also do not lead to the emergence of understanding in artificial cognitive agents, despite the fact that these methods are initially aimed at working with knowledge and meaning. The processing of the context of the situation in which the artificial cognitive agent could be found is still an unsolved problem. As well as the use of «general common sense» has not yet been implemented. However, the situation is gradually changing — the achievements and successes of the artificial neural network GPT-3 amaze the imagination [9].

Nevertheless, the problem remains open. With all the advances in pattern recognition, the understanding of meaning by artificial cognitive agents leaves much to be desired. This is also because modern solution architectures are initially sharpened for solving a specific applied problem, that is, from their very inception, they are a narrow artificial intelligence. Therefore, new approaches and architectures are required.

3. Semantic Learning

In order for a cognitive agent to understand the meaning of the situation in which it finds itself, its training must be carried out in a way to ensure that it creates a large set of associative connections between units of knowledge [8]. Understanding of the meaning in this case arises after the activation of all relevant units of knowledge by associative connections when the agent focuses on the selected set of stimuli that form a description of the current state of the environment in which the cognitive agent functions.

Therefore, to teach an artificial cognitive agent, which must understand the meaning of the situation in which it finds itself, the new machine learning methods should be used. One of the composite methods that can be proposed for this is based on the simultaneous use of machine learning principles and methods of semantic situation analysis. This

method could be called «semantic learning», and it is based on the same learning principles that are used by a human in the process of its growth and education.

Considering, semantic learning is based on the following principles:

- At the basic level the agent need to use the three classic machine learning methods — supervised, unsupervised and reinforcement learning — all these machine learning methods are used to solve various problems [10], namely:
 - Unsupervised learning — identifying various hidden patterns in a variety of external stimuli, clustering objects and phenomena, simplifying input data.
 - Supervised learning — correlating objects and phenomena identified during unsupervised learning with the specified semantic classes.
 - Reinforcement learning — developing optimal (or at least suboptimal) strategies for working in an agent's environment to achieve particular given goals.
- After obtaining data from the basic level of machine learning, the agent needs to use the methods of top-down artificial intelligence to build semantic relationships and enrich the semantic network. In this process, the agent itself can act from an active position, interacting with the teacher in such a way as to receive more information about those aspects of it's environment that it still knows little about. Thus, semantic learning is carried out, which further leads to the agent's understanding of the meaning of situations in which it functions in accordance with [8].

Further in this work, at the basic level, only the supervised machine learning option will be considered, which, together with the semantic component, leads to the use of supervised semantic learning.

The general scheme of work of supervised semantic learning is as follows:

- Using the methods of supervised machine learning, the agent recognizes the states in which it finds itself in its environment. These recognized situations are placed in its «operative memory» for further use in the process of building semantic relations between a set of concepts, which includes concepts (named or yet unnamed from the point of view of the agent objects and phenomena) from the recognized situation.
- Then, by comparing the recognized information about the current state in which the agent is, with the knowledge available in its knowledge base, it tries to create new associative links between the concepts available in its associative memory and the new ones obtained from the previous stage.
- If gaps remain in the set of connections of new objects and situations at the previous stage, the agent performs some protocol of interaction with the teacher to build the missing associative connections by actively obtaining information in a dialogue with the teacher. An important feature of the described approach is the presence of procedures for identifying such gaps and as a consequence for launching an interaction protocol.

In order to clarify the presented ideas, it is possible to make the following thought experiment. It is based on introspection and observation of preschool children learning in terms of study of new concepts and related objects or phenomena of objective reality.

Imagine a preschooler who studies the world around him with interest. He walks around the garden being on a summer vacation visiting his grandmother and then he sees something on the sorrel garden bed that he has never seen before — some kind of slimy brown lump attached to the stem of the plant. The preschooler asks his grandmother what it is and she answers: «It's a slug». The preschooler finds a few more pieces of slugs and asks if they are slugs. Having received a positive answer, he is satisfied and does not ask anything else. However, for training purposes it would be enough to look at one slug from different angles or even in motion.

After some time, the learning process begins to cycle in his nervous system. The images of several slugs that he saw earlier begin to spin in his head along with the word «slug», which he heard and remembered. It can be assumed that this process is unconscious and is associated with the consolidation of long-term memory during sleep. But it is also possible that the echoes of this process break through to conscious perception in the form of reflexive learning loops at which time the child may even repeat the word «slug» out loud.

After the consolidation of memory which completes the supervising training in the framework of pattern recognition the next stage of training begins — the semantic one. The new concept should be built into the semantic network that the preschooler already has — and it does not matter that this semantic network is encoded in the neural networks of a living cognitive agent by means of sparse coding — the substrate in the current context does not matter. It is only important that there are numerous associative connections of different types between the set of cortical columns, in which the new concept of «slug» is encoded. It should be noted that semantic information should have at least two levels — linguistic and, in fact, semantic.

The linguistic level is usually built implicitly on the basis of those linguistic patterns that already exist in the linguistic space of the preschooler. After some time, he asks: «Slug — who is it?» And they answer him: «Not who, but what. It's a snail». New linguistic information was implicitly received — the word should be declined according to the type of an animate being. And if for the English language this example is a bit artificial, for many other languages the definition of gender is not so trivial. Using the analogy with already learned models and examples of words in tune with the new one does not give an answer. The phonetic consonance of words does not allow to unambiguously determine the gender of the object expressed by it. So, the preschooler continues assuming that the word «slug» is neuter since this can reasonably be assumed on the basis that it is a snail. «Can slug be touched? Will it not bite?» And again, he receives a corrective signal: «The slug can be touched». At this stage most of the linguistic information necessary for the correct use of the word in utterances is recorded in the semantic network.

At the same time, a part of the semantic information has already been formed — the IS-A relation has been received, the «slug» node has been built into the hierarchy of living beings in the «snail» group. Some of the semantic information is obtained from observations — various attributes of an object, such as color, softness, etc., as well as various associative connections, also obtained from observation, such as «creature» (if the slug moved), «lives on sorrel», etc. But then the preschooler can clarify various

additional information in order to extend more and more associative links from the new concept that has so interested him to the existing knowledge.

Thus, the use of a similar approach for training an artificial cognitive agent designed to solve arbitrary problems will create a conceptual field of knowledge for it. This field will consist of two components: universal and individual. The individual conceptual field includes the «personal life experience» of an artificial cognitive agent, while the universal conceptual field is general semantic information on human knowledge [11]. Unlike humans, the general knowledge for an AI agent can be obtained by integrating with such information systems as universal ontologies (for example, CYC [12] or the semantic web [13]).

4. Possible Architecture for an Artificial Cognitive Agent

Having considered the basic principles of semantic supervised learning, it makes sense to start designing a possible architecture of an artificial cognitive agent in which this type of machine learning is possible. This section provides a draft of such an architecture for further discussion in the expert community and testing in practice.

The architecture of an artificial cognitive agent with the possibility of implementing semantic supervised learning is presented in Figure 1.

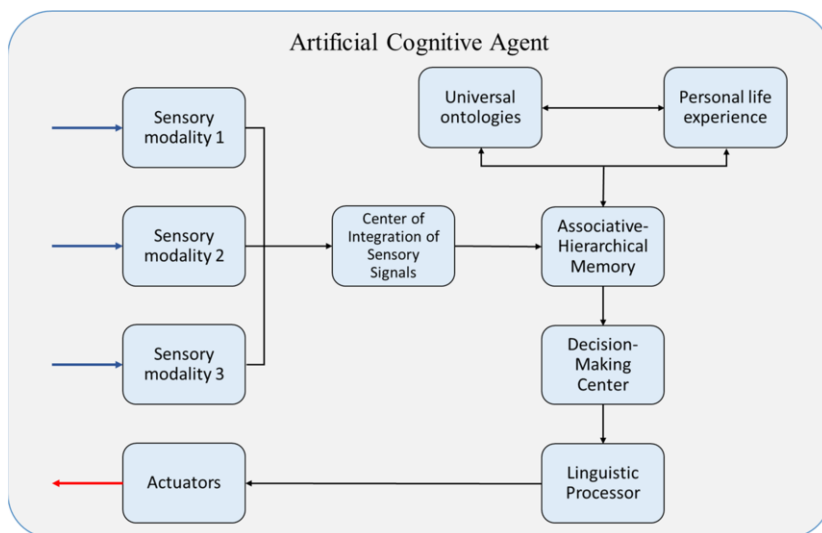


Figure 1. General architecture of artificial cognitive agents for supervised semantic learning.

The presented diagram underlines the high-level structure of an artificial cognitive agent, within which semantic supervised learning could be implemented. The learning cycle in this case is organized as follows:

- The artificial cognitive agent receives signals from the environment through sensors that can be combined with additional elements such as filters and preprocessors. This combination of sensors with additional input signal processing elements is considered together as a separate sensory modality. The

artificial cognitive agent can have more than one sensory modality that receives signals of a different nature from the environment and transforms them into a sequence of data suitable for further processing.

- Further, all data received from different sensory modalities are sent to the Center of Integration of Sensory Signals, where the process of multisensory integration is carried out, which includes a low-level fusion of data and their mutual enrichment to build a holistic description of the current situation perceived in the environment. If an artificial cognitive agent has only one sensory modality, then the Center of Integration may be absent, although there are serious concerns that such an agent will be able to use supervised semantic learning. On the other hand, chatbots, as cognitive agents receiving input signals of only one modality through the messenger console, may well use the described approach. This issue requires additional detailed research and is beyond the scope of this work.
- After the process of sensory integration, a holistic description of the perceived external environment from the Center of Integration is transferred into the Associative-Hierarchical Memory, which also actively interacts with two data banks — general information about the environment and the personal experience of the cognitive agent. Both of these data banks are filled by the process of semantic supervised learning, and this process is carried out constantly and continuously, including the current act of perception and interaction with the environment. The data related to the current perception are recorded to data banks — existing information is updated; new information is added if necessary.
- In the associative-hierarchical memory all the necessary associations and hierarchical concepts associated with the perceived situation in the environment are «excited». This set of excited concepts is passed on to the Decision-Making Center, where a list of possible reactions of the AI-agent to the stimuli received from the environment is formed. Then the optimal response is selected and transmitted to the Linguistic Processor (and other low-level command blocks for actuators, if any exists). The optimal response is selected by the means of symbolic inference within the Decision-Making Center or with any sort of emotional simulation, but this question is still to be investigated.
- The Linguistic Processor receives the formed decision from the Decision-Making Center and forms on its basis the reaction of the cognitive agent and sends it to the actuators (executive devices). The mentioned mechanisms are the output interfaces of the cognitive agent with the environment, transferring to it what they received from the Linguistic Processor in a form understandable to other agents.

By itself, the artificial cognitive agent plays an essential role in organizing supervised semantic learning. It should be the initiator of questions to the teacher, the answers to which will help it to actualize its semantic network. The mechanisms must be implemented in the agent that determine the incompleteness in the semantic network and form the corresponding reactions aimed at filling this incompleteness. These mechanisms must be implemented in the Decision-Making Center.

It should be noted that the presented scheme and its further description are deliberately devoid of indications of any specific technologies or methods for

implementing individual components. The presented architecture is positioned in a generalized way so that when implementing the cognitive AI-agent with the possibility of supervised semantic learning, this scheme could be implemented in specific ways of functional execution. For example, within the framework of the hybrid approach in artificial intelligence [14], professed by the authors, the Center of Integration of Sensory Signals can be implemented in the form of neural networks of suitable architecture, Associative-Hierarchical Memory — in the form of a special semantic maps [15], The Decision-Making Center is in the form of a symbolic inference machine [16], and the Linguistic Processor is again in the form of neural networks [17].

5. Conclusion

The article presents the authors' vision of the opportunities that open up to researchers in the field of building and «growing» general-level artificial cognitive agents. The method of supervised semantic learning is presented, which is aimed not only at the formation of hidden models of pattern recognition or the relationship between stimuli and reactions of an artificial agent, but at the construction of a semantic map of the general description of the surrounding reality and the agent's personal experience of functioning in it. The presented approach probably has the right to exist and be further developed in the framework of interdisciplinary research in the field of building artificial general intelligence.

References

- [1] Williams A. E. (2020). A Model for Artificial General Intelligence // In book: Artificial General Intelligence. — July 2020. — DOI: 10.1007/978-3-030-52152-3_38.
- [2] He K., Zhang X., Ren Sh., Sun J. (2015) Delving Deep into Rectifiers: Surpassing Human-Level Performance on ImageNet Classification / IEEE International Conference on Computer Vision (ICCV 2015). 1502. — DOI: 10.1109/ICCV.2015.123.
- [3] Harnad S. (1990) The Symbol Grounding Problem // *Physica D*. 42 (1-3). — p. 335-346.
- [4] Dushkin R. V. (2018) Obzor podkhodov i metodov iskusstvennogo intellekta [The Review on approaches and methods of artificial intelligence] // *Radioelektronnyye tekhnologii* [Radioelectronic technologies], № 3, 2018. — p. 85-89. — URL: <https://goo.gl/nYczgo>.
- [5] López M. (2015) Four unsolvable problems of symbolic AI // *Revista de Filosofia*. 40. — p. 81-104. — DOI: 10.5209/rev-resF.2015.v40.n1.48441.
- [6] [6] Nikolenko S., Archangelskaya Ye., Kadurin A. (2018) Glubokoye obucheniye. Pogruzheniye v mir neyronnykh setey [Deep Learning. Dive into the world of neural networks]. — SPb: Piter, 2018. — 480 p. — ISBN 978-5-496-02536-2.
- [7] Khanam S., Tanweer S., Khalid S. (2020) Artificial Intelligence Surpassing Human Intelligence: Factual or Hoax // *The Computer Journal*, January 2020. — DOI: 10.1093/comjnl/bxz156.
- [8] Dushkin R. V. (2020) Kritika «Kitayskoy komnaty» J. Searla s pozitsii gibridnoy modeli postroeniya iskusstvennykh kognitivnykh agentov [Criticism of J. Searle's «Chinese Room» from the perspective of a hybrid model for constructing artificial cognitive agents] // *Sibirskiy filosofskiy zhurnal* [Siberian philosophical magazine], № 2, 2020. — p. 30-47.
- [9] Benzon W. (2020) GPT-3: Waterloo or Rubicon? Here be Dragons. — Preprint. — DOI: 10.13140/RG.2.2.18525.03048.
- [10] Shumsky S. A. (2020) Mashinny intellekt. Ocherki po teorii mashinnogo obucheniya i iskusstvennogo intellekta [Machine intelligence. Essays on Machine Learning and Artificial Intelligence Theory]. — Moscow: RIOR, 2020. — 340 p. — ISBN: 978-5-369-01832-3.
- [11] Heck R. G. (2009). Logic, semantics, ontology — PhD Thesis, January 2009. Massachusetts Institute of Technology, Dept. of Linguistics and Philosophy, 2009.

- [12] Witbrock M. et al. (2005) Knowledge Begets Knowledge: Steps towards Assisted Knowledge Acquisition in Cyc // In: Papers from the 2005 AAAI Spring Symposium on Knowledge Collection from Volunteer Contributors (KVCV). — pp. 99-105. Stanford, California, March 2005.
- [13] Yu L. (2014) A Developer's Guide to the Semantic Web. — 2nd ed. Springer. — ISBN 978-3-662-43796-4.
- [14] Dushkin R. V., Andronov M. G. (2020) The Hybrid Design for Artificial Intelligence Systems // In: Arai K., Kapoor S., Bhatia R. (eds) Proceedings of the 2020 Intelligent Systems Conference (IntelliSys), Volume 1 (1250). — Springer, Cham, 2020. — P. 164-170. — ISBN 978-3-030-55179-7. — DOI: https://doi.org/10.1007/978-3-030-55180-3_13.
- [15] Georgakopoulos T. (2019) Semantic Maps // In book: Oxford Bibliographies in Linguistics Publisher: New York: Oxford University Press, January 2019. — DOI: 10.1093/obo/9780199772810-0229.
- [16] Bibel W., Kurfess F., Aspetsberger K., Hintenaus P., Schumann J. (1986) Parallel Inference Machines // In book: Future Parallel Computers, An Advanced Course, Pisa, Italy, June 1986. — Chapter: 5. — Publisher: Springer Verlag, Berlin, Lecture Notes in Computer Science 272. — Editors: P. Treleaven, M. Vanneschi. — DOI: 10.1007/3-540-18203-9_5.
- [17] Liu Zh., Lin Y., Sun M. (2020) Representation Learning and NLP // In book: Representation Learning for Natural Language Processing, July 2020. — DOI: 10.1007/978-981-15-5573-2_1.

A Theorem About the Existence of Minimax Rules for Statistical Decision Problems with Trapezoidal Fuzzy Losses

Alexey S. SHVEDOV¹

Department of Applied Economics, National Research University Higher School of Economics, 20 Myasnitskaya ulitsa, Moscow, 101000, Russia

Abstract. This paper considers the problem of choice of an optimal decision under unknown state of nature when losses are not known exactly for some or all decisions and some or all states of nature. However, it is possible to determine probabilities for all states of nature on the basis of statistical data. So, there are two kinds of uncertainty, randomness and vagueness. That is why both methods of the probability theory and methods of the theory of fuzzy sets are used. There is no a unified approach to choice of an optimal decision even in the classical statistical decision theory. One of existing approaches is to use minimax decision rules when losses are crisp. In this paper, the approach is generalized for problems with trapezoidal fuzzy losses. A theorem about the existence of a minimax decision rule is proved when the set of all possible states of nature is finite.

Keywords. fuzzy set, decision rule, risk function, loss function

1. Introduction

A decision rule, which allocates a decision to statistical data, is the main object of study in the statistical decision theory. It is an important theory since many well-known problems of mathematical statistics are particular cases of problems from this theory. Many of the basic methods of statistical decision theory were developed by Wald [1]. Also, some results connected with minimax decisions were obtained by Von Neumann and Morgenstern [2]. The statistical decision theory proved to be useful in many fields, see, e.g., Berger [3] and Robert [4]. In the classical statistical decision theory, losses are crisp and depend on the decision and the state of nature. But when a decision should be made, the state of nature is not known. However, on the basis of statistical data, which describe the state of nature, it may be possible to make a reasonable decision. The decision rule should satisfy some conditions of optimality. For example, the decision rule may be Bayesian or minimax. In the statistical decision theory, both problems with an infinite set of all possible states of nature Θ and problems with a finite set of all possible states of nature $\Theta = \{\theta_1, \dots, \theta_m\}$ are considered. When Θ is

¹ Corresponding author. Department of Applied Economics, National Research University Higher School of Economics, 20 Myasnitskaya ulitsa, Moscow, 101000, Russia. E-mail: ashvedov@hse.ru

finite, there is a theorem about the existence of minimax decision rules, see, e.g., Berger [3] and Schervish [5].

However, the assumption that losses are known exactly for all decisions and states of nature is not realistic on many occasions. The theory of fuzzy sets can be used to overcome this lack of certainty. The fuzzy statistical decision theory is a relatively new field of research. Some results of the theory were obtained by Gil and Jain [6], Gil and López-Díaz [7], Gil et al. [8], Hryniewicz [9], Viertl and Sunanta [10]. However, these papers do not consider minimax decision rules. To the best of our knowledge, no theorems about the existence of minimax rules for statistical decision problems with fuzzy losses were published before.

This paper develops the fuzzy statistical decision theory. A theorem about the existence of minimax decision rules, which generalizes the result presented by Berger [3] and Schervish [5] for the case of trapezoidal fuzzy losses, is proved. Section 2 contains some definitions. In Section 3, the main theorem is given.

2. Definitions

Let D be a set of all possible decisions. Denote by $\tilde{L}_i(d)$ a loss under the state of nature θ_i and the decision $d \in D$. The membership function of the fuzzy set $\tilde{L}_i(d)$ has the following form. There are real numbers $a_i(d)$ and $b_i(d)$ such that $a_i(d) \leq b_i(d)$, $\mu_{\tilde{L}_i(d)}(\xi) = 1$ for $\xi \leq a_i(d)$, and $\mu_{\tilde{L}_i(d)}(\xi) = 0$ for $\xi > b_i(d)$. When $a_i(d) < b_i(d)$, the membership function is linear on the closed interval $[a_i(d), b_i(d)]$ and continuous on the set of all real numbers. So, the choice of a fuzzy set $\tilde{L}_i(d)$ is equivalent to the choice of a two-dimensional vector $c_i(d) = (a_i(d), b_i(d))$, where $a_i(d) \leq b_i(d)$. It is reasonable to consider semi-infinite trapeziums because we are interested in minimization of maximum losses only.

Suppose \tilde{M}_1 and \tilde{M}_2 are semi-infinite trapezoidal fuzzy sets; \tilde{M}_1 is defined by a two-dimensional vector (α_1, β_1) , where $\alpha_1 \leq \beta_1$; \tilde{M}_2 is defined by a two-dimensional vector (α_2, β_2) , where $\alpha_2 \leq \beta_2$. Let k be a non-negative real number. Then $\tilde{M}_1 + \tilde{M}_2$ is a semi-infinite trapezoidal fuzzy set that is defined by a two-dimensional vector $(\alpha_1 + \alpha_2, \beta_1 + \beta_2)$ and $k\tilde{M}_1$ is a semi-infinite trapezoidal fuzzy set that is defined by a two-dimensional vector $(k\alpha_1, k\beta_1)$.

We say that $\tilde{M}_1 \leq \tilde{M}_2$ if $\alpha_1 \leq \alpha_2$ and $\beta_1 \leq \beta_2$. We say that $\tilde{M}_1 = \tilde{M}_2$ if $\alpha_1 = \alpha_2$ and $\beta_1 = \beta_2$. We say that $\tilde{M}_1 < \tilde{M}_2$ if $\tilde{M}_1 \leq \tilde{M}_2$ and $\tilde{M}_1 \neq \tilde{M}_2$. So, the set of semi-infinite trapezoidal fuzzy sets is a partially ordered set. Similar ranking of fuzzy sets is considered by Ramík and Řimánek [11]. If a semi-infinite trapezoidal fuzzy set \tilde{M}_1 is defined by a two-dimensional vector $c_1 = (\alpha_1, \beta_1)$ and a semi-infinite trapezoidal fuzzy set \tilde{M}_2 is defined by a two-dimensional vector $c_2 = (\alpha_2, \beta_2)$ we say that $c_1 \leq c_2$, $c_1 = c_2$, and $c_1 < c_2$ if and only if $\tilde{M}_1 \leq \tilde{M}_2$, $\tilde{M}_1 = \tilde{M}_2$, and $\tilde{M}_1 < \tilde{M}_2$, respectively.

Denote by $p_i(x)$ a probability of an outcome x under the state of nature θ_i . Assume that x takes values from a set that is at most countable. Obviously,

$$\sum_x p_i(x) = 1$$

for all i . Consider a risk function

$$\tilde{R}_i(\delta) = \sum_x p_i(x) \tilde{L}_i(\delta(x)),$$

where δ is a decision rule.

Denote by $c_i(\delta) = (a_i(\delta), b_i(\delta))$ a two-dimensional vector that corresponds to the semi-infinite trapezoidal fuzzy set $\tilde{R}_i(\delta)$. Suppose that the losses are bounded below. This means that there is a real number K such that $a_i(\delta) > K$ for all i and δ . Without loss of generality, we can assume that $K > 0$. Consider two-dimensional vectors

$$\lambda(\delta) = \left(\max_{1 \leq i \leq m} a_i(\delta), \max_{1 \leq i \leq m} b_i(\delta) \right)$$

for all decision rules δ .

A decision rule δ_0 is said to be *minimax* if there is no decision rule δ such that $\lambda(\delta) < \lambda(\delta_0)$.

Denote by S a set of two-dimensional vectors $c = (a, b)$, where $a \leq b$. Denote by U a set whose elements are (u_1, \dots, u_m) , where $u_i \in S$ for all i . Consider a set

$$V_c = \{ (u_1, \dots, u_m) \in U : u_i \leq c \text{ for all } i \},$$

where $c \in S$. Denote by W a set of elements $(c_1(\delta), \dots, c_m(\delta))$ for all δ . Consider a set

$$T = \{ c \in S : W \cap V_c \neq \emptyset \}.$$

The elements of the set U can be considered as elements of $2m$ -dimensional Euclidean space. By the convergence in the set U we understand the convergence in $2m$ -dimensional Euclidean space. Any subset $Q \subseteq U$ can be considered as a subset of $2m$ -dimensional Euclidean space. When we define the closure and the interior of the subset Q , we take the closure and the interior of the corresponding subset of $2m$ -dimensional Euclidean space, respectively. We denote by \bar{Q} the closure of Q .

We say that an element $(u'_1, \dots, u'_m) \in U$ lies *directly underneath* an element $(u_1, \dots, u_m) \in U$ if $u'_i \leq u_i$ for all i and the inequality is strict at least for one i .

The *lower boundary* of a set $Q \subseteq U$ is the set of elements $(u_1, \dots, u_m) \in \bar{Q}$ such that there are no elements (u'_1, \dots, u'_m) belonging to the interior of Q and lying directly underneath (u_1, \dots, u_m) .

We say that a set Q is *closed from below* if its lower boundary belongs to Q .

3. The main theorem

Theorem. If W is closed from below then a minimax decision rule δ_0 exists.

Proof. By $\|c\|$ denote the Euclidean norm for $c \in S$. Let

$$\rho = \inf_{c \in T} \|c\|$$

and

$$\|e_n\| \downarrow \rho \text{ as } n \rightarrow \infty$$

for elements $e_n \in T$. Since the sequence e_n is bounded, it is possible to choose a convergent subsequence e_q from the sequence. Thus,

$$e_q \rightarrow e_0 \text{ as } q \rightarrow \infty.$$

It is clear that $\|e_0\| = \rho$.

Taking a point from each set $W \cap V_{e_q}$, we obtain a bounded sequence $(c_1(\delta_q), \dots, c_m(\delta_q))$. It is possible to choose a convergent subsequence from this sequence. Let

$$(c_1(\delta_r), \dots, c_m(\delta_r)) \rightarrow (c_1^*, \dots, c_m^*) \text{ as } r \rightarrow \infty,$$

where $c_i^* \in S$ for all i . From the definition of V_{e_r} we get

$$c_1(\delta_r) \leq e_r, \dots, c_m(\delta_r) \leq e_r$$

for all r . Hence, $\lambda(\delta_r) \leq e_r$ for all r . Obviously, $(c_1^*, \dots, c_m^*) \in \overline{W} \cap V_{e_0}$.

It follows from the condition $\|e_0\| = \rho$ that a point from the interior of W can not belong to V_{e_0} . But a point that does not belong to V_{e_0} can not lie directly underneath a point from V_{e_0} . Consequently, the point (c_1^*, \dots, c_m^*) belongs to the lower boundary of the set W . Since W is closed from below, there is a decision rule δ_0 such that

$$(c_1^*, \dots, c_m^*) = (c_1(\delta_0), \dots, c_m(\delta_0)).$$

Clearly, $\lambda(\delta_0) \leq e_0$. It follows from the definition of ρ that there is no decision rule δ for which $\lambda(\delta) < e_0$.

The theorem is proved.

4. Conclusion

When losses are not known exactly, it is reasonable to consider fuzzy-valued losses in statistical decision problems. In this paper, the theorem about the existence of minimax decision rules for the problems with trapezoidal fuzzy losses is proved. Remaining questions concern the existence of minimax decision rules for the problems with non-trapezoidal fuzzy losses.

References

- [1] Wald A. *Statistical Decision Functions*. N.Y.: Wiley, 1950.
- [2] Von Neumann J., Morgenstern O. *Theory of Games and Economic Behavior*. Princeton: Princeton Univ. Press, 1947.
- [3] Berger J.O. *Statistical Decision Theory and Bayesian Analysis*. N.Y.: Springer-Verlag, 1985.
- [4] Robert C.P. *The Bayesian Choice*. N.Y.: Springer-Verlag, 2007.
- [5] Schervish M.J. *Theory of Statistics*. N.Y.: Springer-Verlag, 1995.
- [6] Gil M.A., Jain P. Comparison of Experiments in Statistical Decision Problems with Fuzzy Utilities // *IEEE Trans. Systems Man Cybernet.*, 22 (1992), 662–670.
- [7] Gil M.A., López-Díaz M. Fundamentals and Bayesian Analyses of Decision Problems with Fuzzy-Valued Utilities // *Int. J. of Approximate Reasoning*, 15 (1996), 203–224.
- [8] Gil M.A., López-Díaz M., Rodríguez-Muñiz L.J. An Improvement of Comparison of Experiments in Statistical Decision Problems with Fuzzy Utilities // *IEEE Trans. Systems Man Cybernet. – Part A: Systems and Humans*, 28 (1998), 856–864.
- [9] Hryniewicz O. Bayes Statistical Decisions with Random Fuzzy Data – An Application in Reliability // *Reliability Engineering & System Safety*, 151 (2016), 20–33.
- [10] Viertl R., Sunanta O. On Fuzzy Bayesian Inference // in: Kahraman C., Kabak Ö. (eds.), *Fuzzy Statistical Decision Making*, Switzerland: Springer-Verlag, 2016, 55–64.
- [11] Ramík J., Římánek J. Inequality Relation between Fuzzy Numbers and Its Use in Fuzzy Optimization // *Fuzzy Sets and Systems*, 16 (1985), 123–138.

Chinese Text Event Detection Technology Based on Improved Neural Network

Ying CUI ^{a,1} and Yongchao WEI ^b

^a*Southwest China Institute of Electronic Technology, Chengdu 610036, China*

^b*Civil Aviation Flight University of China, GuangHan, 618307, China*

Abstract. With the development of deep learning, the use of neural network for text detection has been more in-depth research and more widely used. Based on this, this paper studies the Chinese text event detection technology based on improved neural network. In the research, this paper uses the flower pollination algorithm (FPA) to improve the traditional BP neural network algorithm. By optimizing the weights and thresholds of BP neural network, a Chinese text event detection method based on improved neural network is proposed. In order to verify the effect of the Chinese text event detection method based on improved neural network, this paper compares it with the natural scene text detection method, and compares the recall rate, accuracy rate and time-consuming. The results show that the accuracy rate of the natural scene text detection method is 88%, and the recall rate is 73%. The accuracy rate of the text detection method based on the improved neural network is 95% and the recall rate is 86%. The F value of the natural scene text detection method in the Chinese text event detection test is 0.79, which takes 4.56s. The value of F in is 0.90, which takes 0.64s. Therefore, the Chinese text event detection method based on improved neural network has better performance.

Keywords. Improved Neural Network, Text Event Detection, Natural Scene Text Detection, Flower Pollination Algorithm

1. Introduction

BP neural network is an artificial neural network model, since it was proposed, it has been widely used in various detection [1-2]. We know that BP neural network is a kind of multi-level neural network. The topological structure of BP neural network is mainly composed of three parts: input layer, hidden layer and output layer. Among them, the hidden layer has at least one layer. Between layers, neurons are fully connected. Except for the input layer, the input of each layer is closely related to the output of the previous layer [3-4]. Generally speaking, BP neural network is a kind of negative feedback neural network. It adjusts the weight through negative error response to make it closer to the nonlinear function. Therefore, the convergence speed of BP neural network is relatively slow [5-6].

In recent years, text detection has become a research hotspot and a challenging topic in the field of computer vision [7-8]. Tutz proposed the Logit model to estimate weights, rather than using weights that are entirely determined by distance. Automatically select the nearest neighbor by using a selection process such as lasso or

¹ Corresponding Author: Ying CUI, Southwest China Institute of Electronic Technology, Chengdu, 610036, China; E-mail: cuiying.cetc10@foxmail.com

enhancement. Then, based on the concepts of estimation and selection, the predictor space is extended [9]. Nucci proposed an adaptive method named ASCI (Adaptive Selection of Bug Predictive Classifier), which dynamically selects a classifier that can better predict the bug propensity of a class from a set of machine learning classifiers according to the characteristics of the class. An empirical study on 30 software systems shows that ASCI performs better than five classifiers that are used alone and combined with majority voting integration[10].

In the research, this paper improves the traditional BP neural network, uses the flower pollination algorithm (FPA) to optimize the weight and threshold of the network, and proposes a Chinese text event detection method based on the improved neural network. In order to verify the effect of the improved neural network algorithm in Chinese text event detection, this paper introduces the GB2312 format data set for training, and performs fuzzy processing on the Chinese vocabulary to achieve the purpose of analyzing the meaning of the word. In this paper, experiments are conducted on the computer to compare the detection effects of natural scene text detection methods and detection methods based on improved neural networks. Accuracy rate, recall rate, F value and time consumption.

2. Text Detection Algorithm and Improved BP Neural Network Text Detection Algorithm

2.1 Text Detection Algorithm

Traditional text detection algorithms most of the traditional text detection algorithms are based on connected domain analysis. These algorithms first aggregate image pixels into different connected regions according to low-level features (such as light intensity, color, gradient, etc.), and then classify these connected components with classification model to filter the noise area. Traditional text detection algorithms mainly use bottom-up method. These algorithms usually start with character detection or stroke detection, and then apply text detection by filtering text elements, so as to construct text lines and verify text lines. Because of this, the detection results of this method have low accuracy, poor robustness, and the implementation process is too complex. In today's rapid development of society, text detection task is facing greater challenges.

- Any length width ratio, color, font, size and shape of text may appear in the image;
- The image background is more complex and diverse, and there are a lot of texture similar to the text, which is easy to cause confusion, such as fences, vegetation and other objects;
- Image quality is uncertain, and text detection is very sensitive to image quality. The common interferences are illumination condition, motion blur, low resolution and occlusion;
- Image text distribution is dense, different texts have similar features, only in detail strokes are different, the space between multiple texts is small, some tiny details may lead to multiple texts being detected as one text. Facing these more complex and difficult challenges, the traditional multi-step text detection algorithm is easy to generate a large number of non text connected regions, which brings great difficulty to the subsequent text line splicing and text line verification.

2.2 Chinese Text Event Detection Based on Improved Neural Network

The nonlinear system composed of a large number of simple computing units is neural network, which simulates the processing operation of human brain to some extent.

Since the data set of this article is mainly Chinese, it is very difficult to segment words. This article uses the red-black tree method to segment the pre-stored vocabulary in the system. When analyzing the data set, the words in the data set are segmented, and then compared with the words in the system are matched. The FPA neural network in this paper supports the GB2312 data set to achieve the ability to analyze Chinese text.

In the research, we use the error function of BP neural network as the physical state function of FPA, find the minimum value of physical function, and update the state of FPA repeatedly, that is, when the error value is the smallest, we can get the best solution of FPA. It can be used as the initial weight and threshold of BP neural network.

The global pollination process is completed by Levy flight, which is described as follows:

$$x_i^{t+1} = x_i^t + L(x_i^t - g_+) \quad (1)$$

The process of local pollination and the regularity of flowers are described as follows (2):

$$x_i^{t+1} = x_i^t + \varepsilon(x_j^t - x_k^t) \quad (2)$$

Where ε is a random number generated from (0,1) uniform distribution.

x_i^t and x_i^{t+1} in Eqs.(1) and (2) refer to the solutions of generation t and generation t + 1 respectively. It represents the maximum of the current population.

Optimal solution, l is the step parameter of Levy flight, which is calculated according to the following Eq. (3):

$$L \sim \frac{\lambda \Gamma(\lambda) \sin\left(\frac{\pi\lambda}{2}\right)}{\pi} \frac{1}{s^{1+\lambda}} \quad (3)$$

3. Experimental Design

Experimental preparation: This paper selects CEC corpus as the test object. CEC corpus takes the news reports of five kinds of emergencies such as earthquake, fire, road accident, terrorist attack and food poisoning as the materials. Through text preprocessing, text analysis, event marking and consistency checking, the comments are finally stored in the text.

Experimental environment: After the establishment and programming of the text event detection system, we test the system using CEC corpus to comprehensively verify the detection effect of the improved and proposed algorithm.

Programming development environment is as follows: development tools is VS2008; Development language is C++ and STL; Operating system is Windows 7; Test text data set is 2048. The core code of the test is as follows: (Part of the code, as shown in Figure 1):

```

#define NUMBER_OF_SAMPLES (2048)
int main(int argc, char* argv[])
{
    FILE* file;
    char buf[NUMBER_OF_SAMPLES];
    int len;
    uchar_t ud;
    /* Open the detected text file and read a certain number of sample characters */
    file = fopen("gb18030.txt", "rt");
    len = fread(buf, sizeof(char), NUMBER_OF_SAMPLES, file);
    fclose(file);
    /* Analyzing text coding by sample characters */
    ud = uchar_new();
    if(uchar_handle_data(ud, buf, len) != 0) /* If the sample characters are not e
    {
        printf("Failed to parse encoding!\n");
        return -1;
    }
    uchar_data_end(ud);
    printf("What is the encoding of the text%s_\n", uchar_get_charset(ud)); /* Ge
    uchar_delete(ud);
    return 0;
}

```

Figure 1. Text detection algorithm code

4. Analysis and Discussion of Experimental Results

4.1 Data Preprocessing

For text, neural network can not directly identify, so it is necessary to map text data into multidimensional real vector, namely text vectorization. Data preprocessing includes the following three steps.

Particle: There is no obvious boundary between words in Chinese text, so the segmentation of Chinese text is more difficult than that of English text. Whether the text can be accurately segmented has an important impact on the accuracy of text sentiment classification. "Stuttering" Chinese word segmentation is a python Chinese word segmentation library, which supports traditional word segmentation and custom dictionary. Choosing this method can segment sentences more accurately.

Word Vectorization: The distributed representation of words has very strong representation ability, and the similarity between each word can be expressed by space vector. The so-called word vectorization is to process words into the form of word vector. At present, word2vec is the mainstream way to form distributed word vector. Combined with Chinese corpora, the word vector model can be obtained by using the related technology of word2vec, and then the word vector of each word can be obtained by inputting the word after segmentation into the vector model.

Generating word vector matrix: After word segmentation and word vectorization, a $N \times m$ word vector matrix will be formed. Where N is the number of words after word segmentation and m is the dimension of word vector. In order to facilitate the training of the model, it is necessary to standardize the size of the word vector matrix generated by each text, so that the size of the word vector matrix generated by all texts is the same. The processing method is:

$$n = \text{avg}N + 2 \times \text{std}N \quad (4)$$

Among them, n is the number of words in the normalized word vector matrix; $\text{avg}N$ is the average number of words n * after word segmentation in all texts; $\text{std}N$ is the standard deviation of the number of words n * after word segmentation.

Then, the word vector matrix generated by the text is processed. The insufficient word vector matrix is filled with 0, and the super long word vector matrix is pruned. In this way, the $n \times M$ word vector matrix can cover 95% of the samples.

4.2 Selection of Common Chinese Characters

The Chinese character sea contains 85568 Chinese characters. It can be seen that the number of Chinese characters constituting the text is quite large, but most of the Chinese characters are not commonly used. Therefore, if we take the rarely used Chinese characters and some special symbols as forbidden words and remove them from the text in the text preprocessing stage, we can improve the processing speed of the program. Therefore, this paper uses 2500 commonly used Chinese characters in modern Chinese character list to preprocess the text. Establish a common Chinese character code cross reference table, number 2500 common Chinese characters (Chinese characters are marked as *w*) and number them from 1 to 2500. The code of each Chinese character or the corresponding Chinese character of each code can be obtained by looking up the table. Table 1 is a partial example of the Chinese character coding Table.

Table 1. Common word coding table

Chinese characters	One	Yi	Two	Ten	Ding	...	Pot
Number	1	2	3	4	5	...	2500

4.3 Text Event Detection

Whether it is Chinese text or English text, compared with other objects, characters always have their own characteristics, such as stroke width, text structure, color features of characters in images, and edge features of characters. Based on the features of the related text images, the unified induction is carried out, and the relevant decision detection rules are sorted out, so as to achieve the purpose of text event detection. Compared with the image text in the natural scene, it is easy to be affected by complex background conditions. Chinese printed text often has uniform specifications in character size, color, stroke width and texture distribution. Therefore, the printed text is detected based on the above features.

The traditional natural scene text detection algorithm basically takes English text as the detection object. Compared with the image detection of English text, the detection results of Chinese text detection are not ideal because of different styles and complex structure. In this paper, the output region of interest in Chinese printing area is combined with the improved SWT path width algorithm to detect text events. Compared with the traditional process of detecting the whole text image, the fast detection of the text region of the region of interest is undoubtedly faster.

4.4 Analysis of Experimental Results of Chinese Text Event Detection

(1) Analysis of accuracy and recall rate of different detection methods

This paper first analyzes the accuracy and recall rate of the two Chinese text detection methods, and the results are shown in Table 2 and Figure 1.

Table 2. Comparison of accuracy and recall rate of different detection methods

Method	Accuracy	Recall
Text detection algorithm in natural scenes	88%	73%
Text detection algorithm based on Improved Neural Network	95%	86%

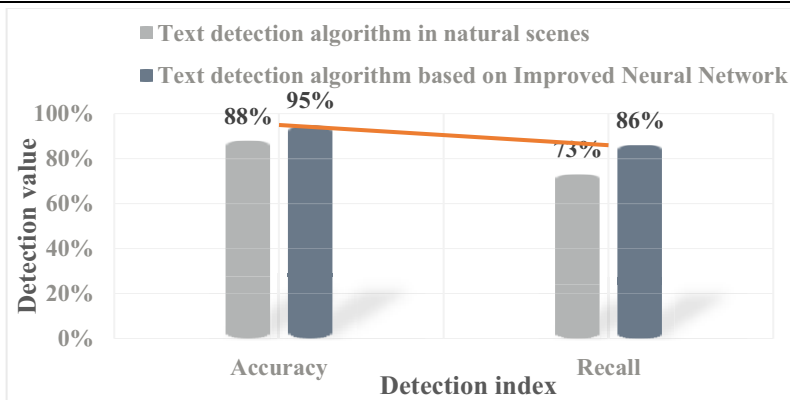


Figure 2. Comparison of accuracy and recall rate of different detection methods

It can be seen from Table 2 and Figure 2, The accuracy rate and recall rate of the two methods are different. The accuracy rate of the natural scene text detection algorithm is 88% and the recall rate is 73%. The accuracy rate of the text detection algorithm based on the improved neural network is 95% and the recall rate is 86%. From the comparison of the two groups of data, it can be seen that the improved neural network text detection algorithm has better performance in Chinese text event detection.

(2) F-value and time-consuming analysis of different detection methods

After analyzing the accuracy and recall rate of the two different detection algorithms, in order to further analyze the practicability of the two algorithms, this paper compares the F value and time consumption of the two different algorithms, and the results are shown in Table 3 and Figure 2.

Table 3. Comparison of F value and time consumption of different detection methods

Method	F value	Time / s
Text detection algorithm in natural scenes	0.79	4.56
Text detection algorithm based on Improved Neural Network	0.90	0.64

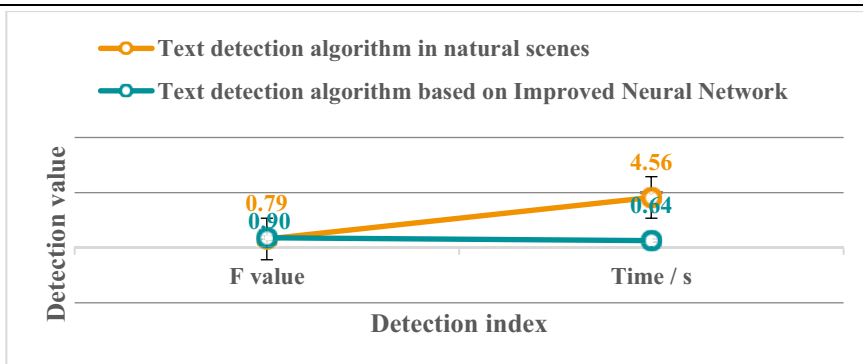


Figure 3. Comparison of F value and time consumption of different detection methods

Table 3 and Figure 3 show that the F value of the natural scene text detection algorithm in the Chinese text event detection test is 0.79, which takes 4.56s. The F value of the text detection algorithm based on the improved neural network in the Chinese text event detection test is 0.90 and takes 0.64s. From the data comparison, it can be seen that the text detection algorithm based on the improved neural network can detect Chinese text events more quickly. It is better in practicability.

5. Conclusions

This paper studies the Chinese text event detection technology and proposes a Chinese text event detection method based on improved neural network. In this study, we use flower pollination algorithm to optimize the weights and thresholds of the neural network. In order to verify the effectiveness of this method, we compared it with the natural scene text detection method, and analyzed the accuracy, recall rate and time consumption. The results show that the accuracy of text detection algorithm based on the improved neural network is 95% and the recall rate is 86%. The F value of the text detection algorithm based on the improved neural network is 0.90, and the time is 0.64s. This method has better performance. Although the text detection algorithm based on the improved neural network proposed in this paper has achieved some results, its performance is not enough to be applied to actual production. This topic will continue to conduct deep learning and optimize the algorithm in the future.

References

- [1] Hu H, Wang H, Wang F, et al. Prediction of influenza-like illness based on the improved artificial tree algorithm and artificial neural network[J]. *entific Reports*, 2018, 8(1):4895.
- [2] Huang Q H, Li B A, Lv X Q, et al. Research on Pipeline Video Defect Detection Based on Improved Convolution Neural Network[J]. *Journal of Physics: Conference Series*, 2020, 1576(1):012028 (6pp).
- [3] Yoganand A V, Kavida A C, Rukmanidevi. Face detection approach from video with the aid of KPCM and improved neural network classifier[J]. *Multimedia Tools & Applications*, 2018, 77(24):1-23.
- [4] Khwaja A S, Zhang X, Anpalagan A, et al. Boosted neural networks for improved short-term electric load forecasting[J]. *Electric Power Systems Research*, 2017, 143(Feb.):431-437.
- [5] Zhang R, Tao J. Data-Driven Modeling Using Improved Multi-Objective Optimization Based Neural Network for Coke Furnace System[J]. *IEEE Transactions on Industrial Electronics*, 2017, 64(4):3147-3155.
- [6] Yang C, Pei W Y, Wu L H, et al. Chinese text-line detection from web videos with fully convolutional networks[J]. *Big Data Analytics*, 2018, 3(1):2.
- [7] Ren X, Zhou Y, He J, et al. A Convolutional Neural Network-Based Chinese Text Detection Algorithm via Text Structure Modeling[J]. *IEEE Transactions on Multimedia*, 2017, PP(3):1-1.
- [8] Zhu W, Lou J, Chen L, et al. Scene text detection via extremal region based double threshold convolutional network classification[J]. *Plos One*, 2017, 12(8):e0182227.
- [9] Tutz G, Koch D. Improved nearest neighbor classifiers by weighting and selection of predictors[J]. *Statistics and Computing*, 2016, 26(5):1039-1057.
- [10] Nucci D D, Palomba F, Oliveto R, et al. Dynamic Selection of Classifiers in Bug Prediction: An Adaptive Method[J]. *IEEE Transactions on Emerging Topics in Computational Intelligence*, 2017, 1(3):202-212.

An Optimized Clustering Algorithm for Contour Data

Yucheng CHU and Lizhen WANG¹

School of Information Science and Engineering, Yunnan University, Kunming 650500, China

Abstract. The initial center's selection of the traditional K-means algorithm is random. It makes the algorithm instability. Traditional clustering methods are hard to apply to the clustering of contour data. The data from the contour data set forms the contour shape, but the cluster center is not on the contour. The final cluster center is in the inner center of the contour. Using K-means algorithm directly is not able to handle this kind of data well. In order to optimize the initial clustering center of the contour data, and in order to solve the problem of contour data clustering. Based on the high density area may be initial clustering centers. And under the thought of the farther apart distance the more likely belonged to different clustering. In this paper, an algorithm of contour data clustering is proposed. This algorithm can obtain better initial central for contour data, so as to improve the clustering effect of contour data. Firstly, the algorithm calculates the distance between the samples. And based on the premise of the two farthest points most probability does not belong to the same class. The algorithm finds out the farthest two points according to the sample distance. With one point as the center, find the point closest to the point to join the point set. Until the data set number greater than or equal to α number (α is the ratio of the number of samples to the number of clusters). Calculate the average of all points as the initial cluster center. Repeat the above steps to get K initial cluster centers. Then the final clustering calculation is carried out according to the K-means algorithm. After the experiment on the experimental data set, the improved algorithm has a strong stability. The initial clustering center is uniformly discrete. And the clustering results have a high accuracy and have a good F1 value. The improved algorithm solves the clustering problem of contour data well.

Keywords. Contour data, Initial cluster center, K-means clustering algorithm.

1. Introduction

Clustering is a kind of unsupervised learning method, which divides data into different data classes according to different data characteristics. Individuals belonging to different data classes have different data characteristics, while individuals belonging to the same data class have same or similar data characteristics. The purpose of clustering is to divide same or similar data individuals into a cluster and assign different categories of individuals to different clusters [1-5]. Traditional clustering algorithms can be divided into partition-based clustering [6], density-based clustering [7], hierarchy-based clustering [8], grid-based clustering [9], etc. K-means algorithm is a

¹ Corresponding Author: Lizhen Wang, School of Information Science and Engineering, Yunnan University, Kunming 650500, China; E-mail: lzhwang2005@126.com.

classically clustering algorithm based on partition. As an indirect clustering method based on the similarity measure between samples, k-means algorithm takes the number of cluster classes as a parameter and divides n data objects in the data set into K clusters according to rules, so that the similarity within the cluster is higher while the similarity between clusters is lower. Although K-means algorithm has the advantages of simple, efficient and easy to understand, it still has many shortcomings. It can only deal with spherical or globular data sets, unstable initial clustering center [10], easy to fall into local optimal solutions, and so on. Aiming at the shortcomings of this algorithm, many scholars have made many improvements. In literature [11], in order to solve the sensitivity problem of the initial clustering center, layered agglomeration clustering algorithm [12] was adopted to select the initial clustering center to ensure the high quality of the central point. Literature [13] proposed an improved initial clustering center selection algorithm for K-means algorithm, which introduced the idea of high-density priority clustering [14], for the sensitivity of initial clustering center and the inability to handle data sets with large density differences. Contour data is a kind of classic data type. Its data form the contour shape, beautiful contour data but not too convenient to handle. But the final clustering center of this kind of data is not on the outline of the data. The final cluster center is usually located on the inner center of the contour. So it's not always good to have a data point as the initial cluster center. Cause the final cluster center is also usually located in the center of the contour. Therefore, the optimization of the initial cluster center is particularly important. Experiments show that the improved algorithm has good ability to deal with contour shape data. The improved algorithm in this paper has strong anti-interference ability due to the operation mechanism. The clustering result is more stable. Compared to the traditional K-means, K-means++, it has good stability and good profile coefficient. This paper fully demonstrated the improved algorithm is feasible, reasonable and effective.

Due to the K-means algorithm is sensitive to the initial clustering center. It can't handle the contour data directly [15]. In order to solve the initial cluster center selection problem of contour data, to improve the feasibility of clustering, enhanced clustering effect, etc. This paper proposes a new simple and effective optimization algorithm. This algorithm can greatly reduce the random selection of the impact of the initial clustering center. We can use the algorithm to select the better initial clustering center. It is very suitable for contour shape clustering analysis of data to find out the initial clustering center which are located in the center of the contour. The algorithm combines the thought that the high density area at the same time may have the clustering center and the thought that the farther away the points are, the more likely they are to belong to different clusters. The algorithm is simple and quick, only need to deal with the distance of all points for the first time. It can speed up the convergence rate of the clustering, enhance the stability of the algorithm, discrete the initial clustering center of the uniform, improves the clustering effect.

2. The basic idea of the improved algorithm

Before describing the basic idea of this algorithm, first we need to know about the basic idea of K-means algorithm [16]. The algorithm proposed in this paper needs to use K-means algorithm. K-means algorithm idea is as follows: first of all, K data objects are selected randomly on the data set as the initial clustering center. And then calculate the Euclidean distance of each data object with the center and division to

the center of the smallest distance. Form K clusters and recalculate the new cluster center. Repeat the above steps until the clustering center are no longer changes or the error sum of squares of the difference of two adjacent clustering results is less than a threshold value.

This article combines the thought that high density regions may have clustering center and the thought that the farther apart the points are, the less likely they are to belong to the same cluster. Firstly, calculate the distance between samples. According to the sample distance form collection, find out the nearest two points. Then according to the calculation formula of collection point to find out all the other point closest to the initial point. Find all relevant data points until the set number greater than or equal to number (ais the ratio of the number of samples to the number of clusters). Calculate the mean of all the collection points to get the first initial cluster center. Repeat the above steps to get K (K is clustering number) collections. Calculate the mean of each set as the initial center. And the final clustering result is obtained by the K-means algorithm. Therefore, the improved algorithm inherits the characteristic that the farthest point is least likely to belong to the same class. And it integrates the characteristic of high-density priority clustering. It discretizes the initial clustering center of contour data uniformly. It increases the ability of the algorithm to resist the interference of outliers. And it can obtain the clustering center that is more consistent with the final clustering result. It can be used to process contour data.

Let's say I have n sample data sets: $D = \{x_1, x_2, \dots, x_n\}$, There are K clusters, $C = \{C_1, C_2, \dots, C_k\}$, m collections: $M = \{M_1, M_2, \dots, M_m\}$.

Definition 1: The Euclidian distance between two data objects is.

$$d(x_i, x_j) = \sqrt{\sum_{l=1}^n (x_{il} - x_{jl})^2} \tag{1}$$

Where, x_i and x_j are data objects, x_{il} is the l attributes of x_i , x_{jl} is the l attributes of x_j .

Definition 2: The cluster center (*Center_k*) of the k th cluster is defined as.

$$center_k = \frac{1}{|C_k|} \sum_{i=1}^{|C_k|} x_i, x_i \in C_k \tag{2}$$

Where, *Center_k* represents the center of the k th cluster, C_k represents the k th cluster, and $x_i \in C_k$ represents the data object x_i belongs to C_k . $|C_k|$ represents the number of points in C_k .

Definition 3: The objective function is the sum of squares of errors

$$E = \sum_{j=1}^k \sum_{i=1}^{|C_k|} d(x_i, Center_k), x_i \in C_k \tag{3}$$

In K-means algorithm, the similarity between data objects is calculated by Euclid distance. The smaller the distance, the higher the similarity between the data objects. On the uneven density data set, the higher the density the more likely it is to

get together. In order to combine the density and distance, find K discrete points respectively. We go through the furthest point to ensure that the clustering centers are discrete. And we go through high density center point set to calculate the mean value. It is not only benefit the objective function of convergence, and is advantageous to the clustering of the accurate and reliable.

According to the above principles, the steps to find discrete and uniformly distributed K points as the initial clustering center on the data space distribution are as follows.

(1) Calculate the Euclidean distance between two data objects $d(x_i, x_j)$, $i, j = 1, 2, \dots, n$, find the two most distant data objects $d1$ and $d2$ and delete them from the total data set D .

(2) Find $\alpha(n/k)$ points closest to $d1$ to form a set $nd1$ and remove them from the total dataset D . According to formula (2), the initial cluster center is calculated and added to the K set of the initial cluster center.

(3) Find $\alpha(n/k)$ points closest to $d2$ to form a set $nd2$ and remove them from the total dataset D . According to formula (2), the initial cluster center is calculated and added to the K set of the initial cluster center.

(4) Repeat (1) ~ (3) until the number of K sets is greater than or equal to $K - 1$.

(5) When the number of initial center points in the K set is equal to $K - 1$, then formula (2) is used to calculate the initial clustering center points of the remaining points and add them to the initial clustering center K set. When the number of initial center points in K set is equal to K , then the process of searching for initial center points of clustering ends.

3. Examples and applications of the improved algorithm

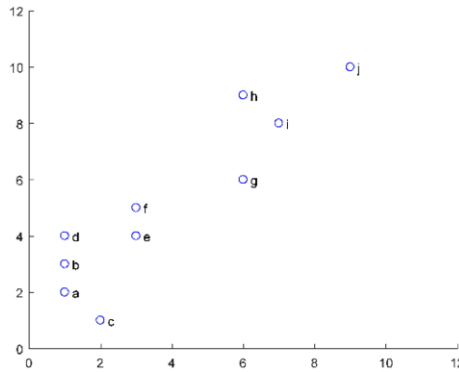


Figure 1. A data distribution diagram.

For example, this is a 2-dimensional dataset W with a data size of 10, and its data distribution is shown in Figure 1.

Now if we need to divide the data set into three categories, we will find the initial clustering center according to the idea of this algorithm. So first of all find out the most remote point, the figure 1 shows that a and j furthest distance, and then respectively from a recent find three data points, the distance is obtained by Formula

(1) a's recent three data points b, c, d, adding them and point a to $N_{\phi d1}$ collection, calculated by Formula (2) as the initial clustering center of K-means clustering center, one of the K concentration and add to the initial clustering center. Then find the three data points closest to J, and get the three data points closest to J through Formula (1), add them and point j to $N_{\phi d2}$ set. Calculate the clustering center through Formula (2) as one of the initial clustering centers of K-means, and add it to the initial clustering center K set. Since the number of initial center points in the K set is equal to $K-1$, then the initial clustering center points of the remaining points are calculated by Formula (2), and added to the initial clustering center K set, and the process of finding the initial clustering center point is completed.

But how can it be used in the contour data. For example, there is a 2-dimensional circular data set G with a data size of 16, and its data distribution is shown in Figure 2. The data constitutes two rings on the left and the right. We can predict that the final clustering center should be the center of the circle.

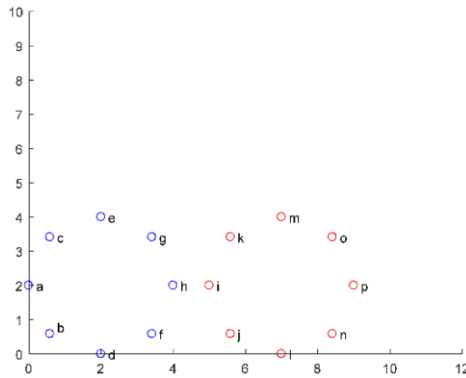


Figure 2. Data distribution diagram2.

Suppose that they need to be divided into two categories, then if the traditional K-means clustering algorithm is adopted, the algorithm has great randomness, and it is difficult to get a good initial clustering center, and the clustering problem of such contour data will not be handled well in the end. According to the improved algorithm proposed in this paper, the initial clustering center is found. It can be seen from Figure 2 that points A and P are the farthest from each other, so the seven data points closest to A are found respectively. According to Formula (1), the data points closest to A are B, C, D, E, F, G and H. Adding them and point a to $N_{\phi d1}$ collection. The clustering center is calculated by formula (2) as one of the initial clustering centers of K-means, and is added to the initial clustering center K set. Then, find the 7 data points closest to P, and get the 7 data points closest to P through Formula (1): I, J, K, L, M, N, O. Adding them and point a to $N_{\phi d2}$ collection. The clustering center is calculated by Formula (2) as one of the initial clustering centers of K-means, and is added to the initial clustering center K set. Therefore, since the number of initial center points in the current K set is equal to K , the process of searching for initial cluster center point's ends. The obtained initial clustering center points are about the center positions of the two rings, so it is easy to carry out subsequent K-means clustering, and the final clustering result is that the left and right two rings belong to two classes, and the clustering effect is very good.

For another example, the data in Figure 2 can be replaced with other contour data, such as square, triangle, polygon, etc. And the size of contour band can be changed, which can be attempted by this algorithm. If the distribution of each contour data volume is uniform, the algorithm will get a good clustering effect.

4. The improved algorithm is described in detail

If the data set $N = \{x_1, x_2, \dots, x_n\}$, contains n data objects, each data object has S dimension. The detailed description of the improved algorithm is as follows (the parameter φ is the ratio of the total number of data set objects to the number of clustering centers, threshold β refers to the difference of the sum of the squares of the two adjacent errors).

Input: Data set $N = \{x_1, x_2, \dots, x_n\}$, Number of cluster classes K , threshold β .

Output: Clustering results.

Methods:

- (1) According to the method proposed in this paper to find initial cluster centers, K cluster centers are selected as the initial centers.
- (2) Calculate the distance between each data object and the center according to Formula (1), divide it into the nearest cluster center, and get K cluster classes.
- (3) Recalculate the center of each cluster class according to Formula (2).
- (4) Reclassify the clusters and update the centers.
- (5) Until the cluster centers no longer change or the difference value of E value for two consecutive times is less than the threshold value β .
- (6) End of algorithm.

5. Experimental results and analysis

5.1 The experimental data

In order to verify the feasibility and effectiveness of the improved algorithm proposed in this paper, the experiment selected the Wine in the UCI database, Hayes Roth, Iris, airport, Ionosphere, Hagerman data set for the experiment and analysis. The dimensions of data sets are from several dimensions to a dozen dimensions. And the size of the data set range from hundreds to thousands of, which reflects the effect of the improved algorithm to cluster the data in different dimensions and size. It makes the results more convincing. The data set details are shown in Table 1.

Table 1. Basic information of the dataset.

The data set name	Data set size	Data dimension	Data categories
Wine	178	13	3
Hayes-Roth	132	5	3
Iris	150	4	3
Tae	151	5	3
Ionosphere	351	34	2
Hagerman	306	3	2

5.2 The experimental results

In order to verify the effectiveness of the improved algorithm, the traditional K-means algorithm and K-Means ++ algorithm are used to compare with the improved algorithm proposed in this paper. In the experiment, precision, recall, F1 and contour coefficient were used to evaluate the clustering results of the algorithm. Accuracy rate refers to the proportion of the correct clustering to be positive in all the clustering results. Its value is generally in the interval of [0, 1]. The larger the value means the more data are correctly clustered. The recall rate refers to the ratio between the correctly clustered positive and all positive samples, which is generally in the interval of [0, 1]. F1 value is the harmonic mean of precision rate and recall rate. F1 value is generally in the interval of [0, 1]. The F1 closer to 1, the better the clustering. Contour coefficient is a way to evaluate the clustering effect. The value of SC is in the interval [-1, 1]. The larger the value is, the better the clustering effect is. The calculation formula of precision rate, recall rate and F1 value is as follows.

$$P = \frac{Tp}{Tp + Fp} ; \quad R = \frac{Tp}{Tp + Fn} ; \quad F1 = \frac{2PR}{P + R} \quad (4)$$

Where, P is the accuracy rate, R is the recall rate. Tp: the sample is positive and the clustering result is positive. Fp: The sample was negative and the clustering result was positive. Tn: The sample is negative and the clustering result is negative. Fn: The sample is positive and the clustering result is negative.

The contour coefficient (SC) of the data object can be obtained by the following formula.

$$S(i) = \frac{b(i) - a(i)}{\max\{a(i), b(i)\}}, (i = 1, 2, \dots, n) \quad (5)$$

Where, $a(i)$ represents the average distance between the number i data object and other points in the cluster to which it belongs, $b(i)$ represents the minimum value of the average distance between the number i data object and all points that are not in its own cluster, and $S(i)$ represents the contour coefficient of any data object. Finally, the contour coefficient SC we need is obtained by averaging the entire $S(i)$.

In order to verify the clustering effect of the improved algorithm, six commonly used data sets of UCI are adopted as experimental data, and the experimental results of the improved algorithm are compared with the traditional K-means algorithm and K-means ++ algorithm, as shown in Table 2~ Table 4.

Table 2. Comparison of accuracy and stability of data results.

Algorithm	Wine		Hayes-Roth		Iris		
	The initial center	accuracy	The initial center	accuracy	The initial center	accuracy	
K-means	1	(74,86,80)	0.478	(122,69,117)	0.273	(69,44,78)	0.240
	2	(118,17,103)	0.169	(6,72,95)	0.386	(18,146,5)	0.473
	3	(42,80,8)	0.702	(29,51,105)	0.280	(107,120,83)	0.320
	4	(139,141,9)	0.112	(115,77,80)	0.424	(26,146,22)	0.500
	5	(175,97,47)	0.354	(130,115,94)	0.295	(30,100,145)	0.440
Ave	—	0.363	—	0.332	—	0.395	
K-means ++	1	(127,17,89)	0.112	(77,131,66)	0.280	(144,149,16)	0.320
	2	(176,177,16)	0.500	(96,131,21)	0.333	(39,149,60)	0.447
	3	(27,177,103)	0.478	(122,131,48)	0.394	(92,149,68)	0.440
	4	(98,177,16)	0.354	(88,131,69)	0.379	(106,149,11)	0.02
	5	(3,177,82)	0.702	(120,131,7)	0.280	(4,149,133)	0.887
Ave	—	0.429	—	0.333	—	0.423	
Improved algorithm	1	—	0.702	—	0.439	—	0.887

Algorithm	Tae		Ionosphere		Hagerman		
	The initial center	accuracy	The initial center	accuracy	The initial center	accuracy	
K-means	1	(102,44,125)	0.318	(269,184)	0.644	(39,120)	0.500
	2	(94,91,102)	0.371	(289,216)	0.291	(18,296)	0.516
	3	(116,29,2)	0.298	(10,239)	0.709	(177,113)	0.242
	4	(48,69,58)	0.358	(44,46)	0.288	(127,43)	0.500
	5	(49,89,116)	0.338	(250,264)	0.712	(10,100)	0.480
Ave	—	0.337	—	0.529	—	0.448	
K-means ++	1	(3,150,92)	0.351	(69,350)	0.709	(39,305)	0.520
	2	(61,150,141)	0.298	(47,350)	0.288	(136,305)	0.520
	3	(47,150,148)	0.298	(152,350)	0.291	(72,305)	0.520
	4	(48,150,41)	0.338	(196,350)	0.288	(192,305)	0.520
	5	(38,150,124)	0.305	(221,350)	0.288	(268,305)	0.520
Ave	—	0.318	—	0.429	—	0.520	
Improved algorithm	1	—	0.351	—	0.709	—	0.520

Note: The "-" means that matching objects cannot be found in the data set.

Table 3. Comparison of SC and F1 results of each algorithm on UCI data sets.

UCI data sets	K-means		K-means++		Improved algorithm	
	SC	F1	SC	F1	SC	F1
Iris	0.524	0.357	0.551	0.295	0.551	0.811
Wine	0.571	0.370	0.563	0.357	0.571	0.710
Hayes-Roth	0.571	0.346	0.571	0.354	0.572	0.436
Ionosphere	0.286	0.457	0.294	0.405	0.296	0.707
Tae	0.316	0.330	0.325	0.312	0.273	0.351
Hagerman	0.387	0.443	0.399	0.547	0.399	0.436

Table 4. Clustering time comparison of all algorithms on UCI data sets.

UCI data sets	K-means(ms)	K-means++(ms)	Improved algorithm(ms)
Iris	0.220	0.245	5.978
Wine	0.312	0.207	7.979
Hayes-Roth	0.193	0.360	6.017
Ionosphere	0.333	0.460	31.959
Tae	0.291	0.358	6.019
Hagerman	0.418	0.527	8.420

5.3 Results analysis

It can be seen in Table 2, in the experimental data set in this paper, the clustering results improved stability obviously than the traditional K-means algorithm and K-means++ algorithm. This is due to the calculation of the improved algorithm is based on the limit range and scope of the distance. That is to say, the result is certain, not volatile, so the stability of calculation is better than K-means algorithm and K-means++. In terms of accuracy, the clustering result accuracy of the improved algorithm in this paper is better than that of the traditional K-means algorithm and K-means++ average. Because the initial clustering center of the improved algorithm is unique and has certain anti-interference ability. Combined with the data information in Table 1, the algorithm is not sensitive to the difference of sample size and density. And it has high adaptability to the difference of sample size and density. The final clustering effect is also good. Compared with the traditional K-means algorithm, the contour coefficients of the algorithm clustering results in this paper are mostly greater than or equal to the contour coefficients of the traditional K-means algorithm and K-Means++ algorithm. And compared with the traditional K-means algorithm and K-Means++ algorithm, the improved algorithm has excellent F1 value.

The convergence rate of the improved algorithm mainly depends on the selection of the initial cluster centers and the number of clusters. For different data sets, the running time comparison of the algorithm is shown in Table 4. From clustering time contrast can be seen in Table 4, compared to the traditional K-means algorithm, the K-means++ algorithm, the improved algorithm requires more execution time. This is because the initial clustering center as the pretreatment.

The complexity analysis of the improved algorithm is mainly composed of two parts. The first part is the center point optimization process of the initial clustering, and then the clustering process is carried out. The total time complexity of the improved algorithm is $O(N(K + N/K - 2) - N^2/k^2 + K \times m \times d \times n)$, which is longer than the time complexity of the traditional K-means algorithm. The space complexity is $O(n/K \times m + m \times n)$, which is greater than that of the traditional K-means algorithm, where N is the number of data objects, K is the number of cluster classes, M is the number of fields of each data object, and d is the number of iterations.

Based on the above analysis, it can be seen that the algorithm presented in this paper has certain effects in processing contour data sets. The improved algorithm presented in this paper is reasonable, feasible and has unique clustering advantages, which can be used for cluster analysis of contour data.

But the improved algorithm time complexity is higher, algorithm running time is longer than the traditional K-means and K-means++ algorithms.

6. Conclusion

Traditional K-means clustering algorithm is widely used in data mining field. With the development of the times and the progress of technology, the arrival of the big data, just by the traditional algorithm is hard to meet the needs of a wide variety of data mining, including the type of a variety of data sets, and the need of algorithm performance, etc. In order to improve the algorithm of clustering effect; ensure the rationality of clustering; enhance the ability of processing contour shape data, this paper proposes a new optimization initial clustering center of the improved clustering algorithm. It provides an entirely new way to think about and process contour data. The farther apart the points are, the more likely they are to belong to different clusters and places with high density may have clustering centers. The experiment shows that the initial clustering center of the improved algorithm is stable. It avoids the problem of poor clustering effect caused by the sensitivity of the initial clustering center. And it has strong anti-outlier interference ability. It can effectively disperse the initial clustering center uniformly, and the improved algorithm has better clustering effect by comparing the value of the clustering evaluation index. Therefore, the improved algorithm is useful to process contour data, which provides a feasible, reasonable and effective method for the processing of discrete distributed data sets.

There are also some shortcomings for the proposed algorithm. Only several commonly used clustering data sets are analyzed, and there are still many places to study and think about the influence of the initial clustering center. The improved algorithm time complexity is higher, algorithm running time is longer, is not conducive to improving the efficiency of the algorithm. Moreover, more contour data are needed to verify potential problems and shortcomings of the algorithm. Based on this research, the next step is to improve the convergence and complexity of the algorithm, explore a better way to improve the efficiency of the algorithm, and improve the application of more kinds of data sets.

References

- [1] Hai Mo. Overview of big data clustering algorithms [J]. Computer science, 2016, 43 (S1): 380-383.
- [2] Wang Qian, Wang Cheng, FengZhenyuan, et al. Overview of K-means Clustering Algorithm Research [J]. Electronic design engineering, 2012, 20 (7): 21-24.
- [3] Liu Wei. A Review of Clustering Algorithms in Data Mining [J]. Jiangsu Business Theory, 2018 (7) : 120-125.
- [4] Ni Ping, Zhang Yuqing, Wen Guanxing, et al. Detection method of social botnet based on Group Characteristics [J]. Journal of the university of Chinese academy of sciences, 2014, 3 (5): 691-700.
- [5] Ma Qian. Overview and Application of Clustering Algorithm [J]. China New Communications, 2012, 20 (14): 225-226.
- [6] Xing Shuning, Liu Fangai, Zhao Xiaohui. An efficient parallel mining algorithm based on clustering [J]. Computer applications, 2016, 36(08): 2202-2206+2212.
- [7] LuoJunfeng, Hong Dandan. A k-means clustering algorithm based on density and distance [J]. Software engineering, 2020, 23(10): 23-25+4.
- [8] Li Qingxu, Chen Tianying, Hu Bo. New hierarchical clustering algorithm based on intersection [J]. Information technology and network security, 2020, 39(10): 18-22.
- [9] Li Xiaoguang, Shao Chao. Density peak clustering algorithm based on grid data center [J]. Computer science, 2019, 46(S1): 457-460+487.
- [10] Wang Yidong. K-means algorithm optimization based on single point density [J]. Fujian computer, 2015, 31(01): 73-74+115
- [11] Feng Jing, Mo Xiuliang, Wang Chundong. A Study of K-means Algorithm based on LDA in this essay clustering [J]. Journal of Tianjin University of Technology, 2008, 34(03): 7-11.

- [12] Yang Bo, Long Pengfei. Application of Condensed hierarchical clustering algorithm in intrusion detection [J]. Journal of Changsha Institute of Electric Power (Natural Science edition), 2005(03): 57-60.
- [13] GuoYongkun, Zhang Xinyou, Liu Liping, Ding Liang, NiuXiaolu. K-means clustering Algorithm for Optimizing initial clustering center [J]. Computer Engineering and Applications, 2020, 56(15): 172-178.
- [14] DuanMingxiu, Tang Chaolin. Journal of jishou university (natural science edition), 2013, 34(01): 26-27.
- [15] Mark Qin, Yang Yanjiao, Qin Hongwu, Geng Lin, Wang Pidong. K-means clustering algorithm combining maximum and minimum distance and weighted density [J]. Computer engineering and applications, 2020, 56(16): 50-54.
- [16] Zhong Xi, Sun Xiang-e. Study on naive Bayesian integrated method based on K-means++ clustering [J]. Computer science, 2019, 46(S1): 439-441+451.

The Employment Senson System of College Students

MinChuan Huang^a, I Ping Chen^{b,1}, ShuYing Chung^b, and AiGuo Wang^a

^aGuangdong University of Petrochemical Technology, China

^bCentral Taiwan University of Science and Technology

Abstract. In the Internet era, we actively promote and broadcast recruitment information to college students, actively help students' employment needs, and provide the latest job market information. The key to the success of wireless sensor systems for job hunting is to actively provide customized requirements and the latest development status of professional titles, and broadcast to students on campus or just leaving school. After strict system requirements analysis, overall model design, coding, system development tool selection, design pattern integration, testing, and completion. The research and design are to store the position information of the recruitment website in MySQL through the crawler technology in the database, and the system selects the position information according to the filing requirements. Through email, APP, and SMS, the employment information can be quickly pushed to the demanders to help teachers, students, and parents quickly screen out their expected employment fields.

Keywords. Job recommendation, Crawler technology, MySQL, Software engineering, Sensing technology

1. Introduction

The school's student psychological counseling center and College Teachers' concern and inquiry. The source of the pressure of college graduates was found in the interview[1]. The results of the survey are as follows: firstly, some students plan to continue their master's degree program with the goal of a doctor's degree. Second, most students hope to get employed as soon as possible, share the source of family income, or choose to enter national enterprises to stabilize their income[2]. Third, to obtain a university diploma, according to the needs of social employment human resources, we can obtain a professional qualification certificate, and then enter the private company and enter the entrepreneurial direction[3,4].

2. System Design

The background of the system design is to actively promote customized recruitment information to college students in the Internet era, actively help students expect to obtain

¹ I Ping Chen, Central Taiwan University of Science and Technology, iping.tc@gmail.com.

employment demand, and provide the latest job market information. With wireless sensor technology, the key to the success of the job search system can accurately provide customized demand, provide the latest development status of expected professional titles, and broadcast rapidly and accurately to students on campus or just leaving school[2,5].

2.1 Software engineering demand analysis

The recruitment sensor has been selected through strict system demand analysis, overall model design, coding, system development tool selection, design mode integration, testing, and completion. The software design and software development tool are to store the position information of recruitment website to MySQL through crawler technology in database. The system selects the position information according to the filing requirements. The software design goal is to quickly push employment information to the demander through email, APP, and SMS contact, and help teachers and students or parents quickly screen out their expected employment fields[6].

2.2 Research object

Second-year students have entered the professional program step by step, and they are not familiar with the characteristics of the course during the four years, so they are not included in the main scope of the job interview. The third and fourth-grade students were selected as the main research objects. In order to do a good job as a tutor[7], all three-year students in the Department of electrical engineering and automatic chemistry were selected as the sample of the job interview. However, there is no questionnaire interview on the four-year students, because most of them have to actively apply for enterprise internships and choose the direction of graduation project production. In view of the convenience of teaching this semester, the interviewee only conducted a general survey on all three-year students in the Department of electrical engineering and automatic chemistry. There were five classes with 246 students in total.

2.3 Survey results

At present, there are 10 people who want to take part in the examination, accounting for 4%, 85 people who want to take the examination of civil servants or state-owned enterprises, accounting for 34.6%, and 151 people, accounting for 61.4%, who have general job demand or follow up family enterprises. From the above, it can be seen that job hunting is one of the most important factors of students' psychological pressure in the past three years. With Internet exploration as the main means, they expect to get information about their expected enterprises or related jobs and positions. This is the demand of the online job agent mechanism. This job-seeking system is to achieve the technology of web crawler and actively push and broadcast the newly updated job search information to Job seeking clients, for reference[8].

The key to the feasibility and success of this automatic job search system is to actively provide the latest daily development of employment-related industries and professional titles, find the job categories and salary orientation of new recruitment work from the professional recruitment website and the company's personnel recruitment and job search line, actively broadcast to the students in school or just leaving school, and actively assist students at all levels to measure their employment intention and plan My own undergraduate course map[9].

2.4 System technology architecture

The function of the system is to explore the web pages, build a large database, and mine the jobs of specific objects. Therefore, the use of crawler technology is based on the Django framework, and the Django framework follows the commonly used MVC (model, view, controller) development model. The system is divided into three parts. The first is the view layer, which is the front-end page display layer. It is mainly used to interact with users. HTML5, CSS3, JavaScript, and other software will be used to achieve this. The second is the controller layer, which belongs to the business logic layer. It mainly deals with the logic operation of the system, which is written in Python language. The third is the model layer, which is the access layer of the database. It is mainly used to add, delete, modify and query the database. The system uses a MySQL database. Figure 1: Conception of system technology architecture[10].

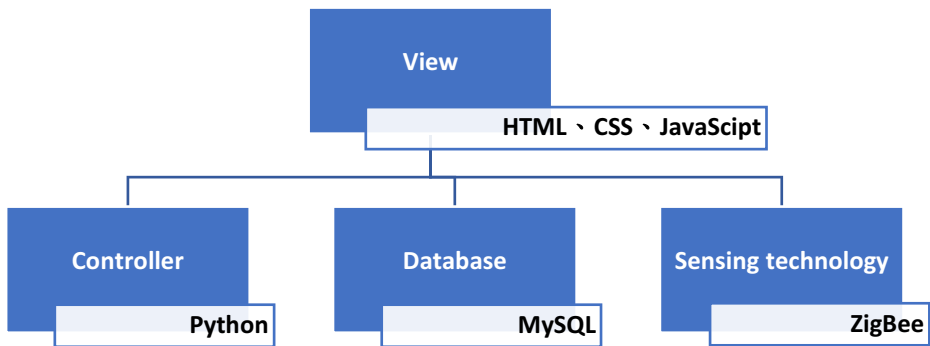


Figure 1. Conception of system technology architecture.

3. Results

According to the demand analysis of the system, firstly, from the two recruitment websites 58 Tongcheng and laguo.com as the experimental objects, we use the web crawler technology to screen the positions or companies according to the needs of customers, in order to successfully and accurately crawl the new information of the required recruitment posts[11].

3.1 Software module design and program flow

The main information can be divided into the job title, salary, company name, company address and company development type, work experience, education background, special nature of the post, etc., and store these data into MySQL database. In addition, in order to prevent large recruitment websites from setting up anti crawler mechanisms, or recruitment websites setting up different anti crawler mechanisms, it will form resistance for the system to obtain data[12].

Therefore, the system also initially wrote a breakthrough program to successfully achieve the work of web crawler data acquisition. The system functional architecture is shown in Figure 2.

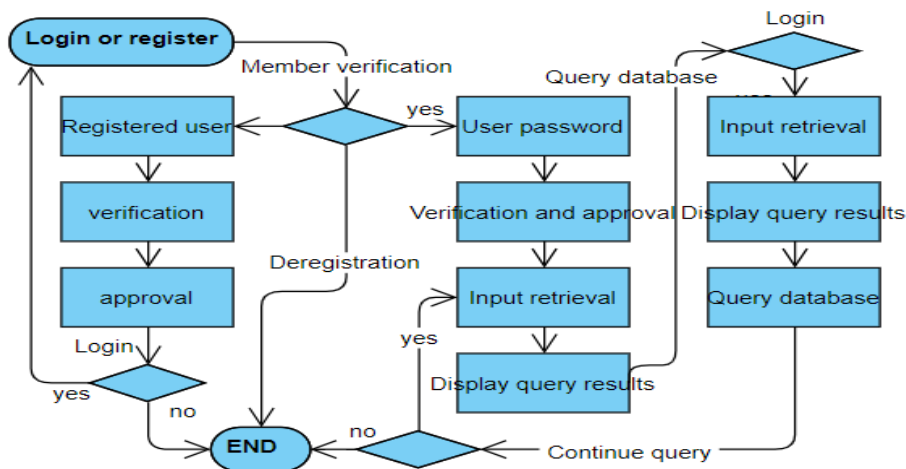


Figure 2. System functional architecture.

3.2 Database Planning

There are four main display interfaces in the system: login and registration page, homepage, personal center page, and position details page. It is convenient for users to take advantage of the opportunity to submit their resume to apply for the job immediately after finding out the satisfactory job. Therefore, the system also provides a jump function to recommend the selected position immediately.

The inquirer can also record the information of the job that has been posted so that they can follow up in the future. In terms of database table design, the system has four tables: registration information table, personal information record form, post information table, and user comment feedback information table. Table 1: Registration table.

Table 1. Registration table

Number	Field name	Paragraph description	Type	Primary key
1	ID	User ID	Int (12)	yes
2	Name	Name	Varchar (160)	
3	Password	Password	Varchar (160)	

Because the division of job market and occupation category is more and more refined, and the demand is more and more huge, there are more and more recruitment websites. The system consists of demand analysis, overall model design, coding, system development tools selection, design pattern integration, testing, and completion.

The main purpose of system testing is to detect whether the system can run normally and find and correct the logic errors in the program as early as possible. System testing is the test of the whole system in the final completion stage. The purpose of the test is to find out whether there are hidden bugs in the system. If it is found that the system program is still wrong, it is necessary to check and modify it in time, to measure whether the system operation quality can reach the ideal standard. Table 2: Job search function table.

Table 2. Job search function table

Module name	Test purpose	Testing procedure	Expected results	Test result
Job search function	Verify the position search function and screening function of the system	1. Enter a position and click search. 2. Give the filter criteria and click search.	1. The system successfully displayed the positions searched by users. 2. Screening succeeded.	Consistent with the expected results

The purpose of adding the jump function is to take the actual needs of users as the starting point. When users find suitable information on the web page and are immediately interested in the job, they can immediately Click to jump to the source website of the post information and post their resume information on the website. Table 3: Jump function.

Table 3. Jump function

Module name	Test purpose	Testing procedure	Expected results	Test result
Jump function	Verify the jump function of the system	Click the apply now button	Jump to source website successfully	Consistent with the expected results

4. Conclusion and discussion

The successful cases of the software engineering experiment project are based on the actual needs of college graduates, effectively reducing the employment pressure of college students, and constructing a simple employment recommendation system. Individual qualitative interviews were carried out on the trial results of the system, and the third and fourth-grade students of the computer college expressed their great affirmation. Most of the graduates think that it is very helpful to inquire about the national civil service examination and search for the ideal job in their mind, and they can effectively use the blank course time to think about their own career positioning.

This system creates a database, uses crawler technology and anti-crawler technology, stores the position information of the recruitment website in MySQL, after the system logs in, according to fill in the registration personal data, according to the application conditions, select the position information and expected salary that meet their own needs.

The job application system will quickly match the latest employment information and push it to students by Email, APP, WeChat, SMS, and other means according to the user's contact information, so as to help teachers, students or family members study and discuss together, screen out the ideal career, give full play to professional knowledge, make contributions to society and serve the people.

Acknowledgment

We would like to thank the assisting units of the School of Nursing, Central Taiwan University of Science and Technology, the nurses of the Taichung Blood Donation Center of the Taiwan Blood Foundation, and all the teachers in the Network Engineering Department of the School of Computer Science and Technology of Guangdong

University of Petrochemical Technology (Project Number: 2019rc076 (702-519186, 702-72100003102)). <https://orcid.org/0000-0003-3218-0643>.

References

- [1] Carl A. Lehnen. 2021. Skills, support networks, and socialization: Needs of dissertating graduate students. *The Journal of Academic Librarianship* 47, 5 (September 2021), 102430. DOI:<https://doi.org/10.1016/j.acalib.2021.102430>
- [2] Fumin Gao, JianChun Fan, Laibin Zhang, Jiankang Jiang, and Shoujie He. 2020. Magnetic crawler climbing detection robot basing on metal magnetic memory testing technology. *Robotics and Autonomous Systems* 125, (March 2020), 103439. DOI:<https://doi.org/10.1016/j.robot.2020.103439>
- [3] Björn Gunnar Hansen and Egil Petter Stræte. 2020. Dairy farmers' job satisfaction and the influence of automatic milking systems. *NJAS: Wageningen Journal of Life Sciences* 92, 1 (December 2020), 1–13. DOI:<https://doi.org/10.1016/j.njas.2020.100328>
- [4] D. Mhamdi, R. Moulouki, M.Y. El Ghomari, M. Azzouazi, and L. Moussaid. 2020. Job Recommendation based on Job Profile Clustering and Job Seeker Behavior. *Procedia Computer Science* 175, (2020), 695–699. DOI:<https://doi.org/10.1016/j.procs.2020.07.102>
- [5] Michael Reusens, Wilfried Lemahieu, Bart Baesens, and Luc Sels. 2017. A note on explicit versus implicit information for job recommendation. *Decision Support Systems* 98, (June 2017), 26–35. DOI:<https://doi.org/10.1016/j.dss.2017.04.002>
- [6] Luis Adrián Cabrera-Diego, Marc El-Bèze, Juan-Manuel Torres-Moreno, and Barthélémy Durette. 2019. Ranking résumés automatically using only résumés: A method free of job offers. *Expert Systems with Applications* 123, (June 2019), 91–107. DOI:<https://doi.org/10.1016/j.eswa.2018.12.054>
- [7] S. Fareri, G. Fantoni, F. Chiarello, E. Coli, and A. Binda. 2020. Estimating Industry 4.0 impact on job profiles and skills using text mining. *Computers in Industry* 118, (June 2020), 103222. DOI:<https://doi.org/10.1016/j.compind.2020.103222>
- [8] Sheng-Yuan Yang. 2009. OntoPortal: An ontology-supported portal architecture with linguistically enhanced and focused crawler technologies. *Expert Systems with Applications* 36, 6 (August 2009), 10148–10157. DOI:<https://doi.org/10.1016/j.eswa.2009.01.004>
- [9] Shivam Bansal, Aman Srivastava, and Anuja Arora. 2017. Topic Modeling Driven Content Based Jobs Recommendation Engine for Recruitment Industry. *Procedia Computer Science* 122, (2017), 865–872. DOI:<https://doi.org/10.1016/j.procs.2017.11.448>
- [10] Shuo Yang, Mohammed Korayem, Khalifeh AlJadda, Trey Grainger, and Siraam Natarajan. 2017. Combining content-based and collaborative filtering for job recommendation system: A cost-sensitive Statistical Relational Learning approach. *Knowledge-Based Systems* 136, (November 2017), 37–45. DOI:<https://doi.org/10.1016/j.knosys.2017.08.017>
- [11] Tian Fang, Tan Han, Cheng Zhang, and Ya Juan Yao. 2020. Research and Construction of the Online Pesticide Information Center and Discovery Platform Based on Web Crawler. *Procedia Computer Science* 166, (2020), 9–14. DOI:<https://doi.org/10.1016/j.procs.2020.02.004>
- [12] Wen-Ren Jong, Han-Ting Chen, Yi-Hsin Lin, Yu-Wei Chen, and Tai-Chih Li. 2020. The multi-layered job-shop automatic scheduling system of mould manufacturing for Industry 3.5. *Computers & Industrial Engineering* 149, (November 2020), 106797. DOI:<https://doi.org/10.1016/j.cie.2020.106797>

Real Time Warning Model of Transmission Tower Tilt Based on Multi-Sensor Data

Xie HU^a, Huikun PEI^a, Bingcai LIU^a, Chen WANG^a, Changjin HAO^{b1}

^aShenzhen Power Supply Bureau Co, Ltd. China Southern Power Grid, Shen Zhen 518001, Guangdong Province, China

^bInstitute of Energy Sensing and Information, Sichuan Energy Internet Research Institute, Tsinghua University, Chengdu 610000, China

Abstract. Transmission line operation environment is complex, prone to tilt collapse accident, so a transmission tower tilt real-time early warning model based on multi-sensor data is established to judge whether the tower is stable operation by detecting the tilt state of the early warning tower. The pressure and inclination sensors are deployed at different positions of the transmission tower to collect the inclination and stress of the tower in real time, and transmit them to the remote monitoring terminal through the wireless network to send out an alarm. The operators can timely adjust according to the alarm situation to maintain the safe operation of the transmission line. The experimental results show that the model can realize the real-time warning of transmission tower tilt, the measurement accuracy can meet the needs of comprehensive detection of tower state, and the application can effectively ensure the safety of staff and reduce the work intensity.

1. Introduction

Power grid transmission tower has the characteristics of large span, long span and large flexibility, which leads to the difficulty and long cycle of staff inspection, and the difficulty of operation and maintenance of some key nodes. It is urgent to carry out real-time on-line detection of tower tilt state through effective technical path, find problems in time and give an alarm, so as to maintain the safe operation of transmission lines, reduce the work intensity of inspection, and improve the management efficiency of power grid.

In reference [1], using geographic information system (GIS) technology and taking the impact energy of slope as the disaster intensity, a landslide probability model which can be used to predict the landslide activity time is proposed, reflecting the quantitative functional relationship of the damage degree of transmission towers in landslide prone areas. The proposed method is feasible and reasonable. However, a lot of preparations need to be done before the method is applied, such as the collection and sorting of historical landslide data, the evaporation and loss properties of rainwater in different soils, the information of landslide geological conditions and the structural parameters of transmission tower. In reference [2], a new all-weather sensing technology is introduced to detect the power tower of the whole scene synthetic aperture radar (SAR) image, so as to realize the rapid assessment of large-scale

¹Corresponding author: Changjin Hao, Institute of Energy Sensing and Information, Sichuan Energy Internet Research Institute, Tsinghua University, Chengdu 610000, China; E-mail: 1527860368@qq.com.

transmission line disaster. However, this method is difficult to implement on site. In reference [3], based on the principle of corrosion electrochemistry, a corrosion monitoring sensor based on "strip groove" structure was proposed, the corrosion mechanism of tower foot was studied, the corrosion monitoring method of tower foot was studied, and a set of data monitoring system was developed. However, this method can only monitor tower faults caused by corrosion. In reference [4], the online monitoring technology of tower foundation deformation of transmission lines is developed based on fiber Bragg grating stress sensor. But the cost of field application of this method is relatively high. According to the previous studies, most of the previous studies are based on a single parameter and cannot fully monitor the state of the tower.

In this paper, a real-time warning model of transmission tower tilt based on multi-sensor data is proposed. The tower tilt data is detected by multiple pressure and tilt sensors. After data fusion processing, it is reflected to the operation and maintenance staff of remote monitoring terminal through wireless communication to remind the staff of tower tilt in real time and effectively, Real time detection and early warning of transmission tower tilt state are realized.

2. Real Time Warning Model of Transmission Tower Tilt Based on Multi-Sensor Data

2.1. Overall structure of real time warning model for transmission tower inclination

Based on the multi-sensor data, a real-time early warning model of transmission tower tilt is established, which is divided into three control levels: field control, centralized control and remote control. Among them, the equipment used to detect the tilt and stress state of transmission tower in real time, such as tension sensor, tilt sensor and detection terminal [5-6], is collectively referred to as the field control layer. By using concentrator, ZigBee technology and GPRS communication module deployed in transmission tower, all tower tilt and tension information are collected from the detection terminal. The equipment of ZigBee and GPRS data frame format conversion is called the centralized control layer. The monitoring terminal with the functions of digital processing and data storage of concentrator tower deployed in the remote monitoring center is called remote control layer. The staff can adjust according to the digital measurement value [7-8]. The structure of the model is shown in Figure 1.

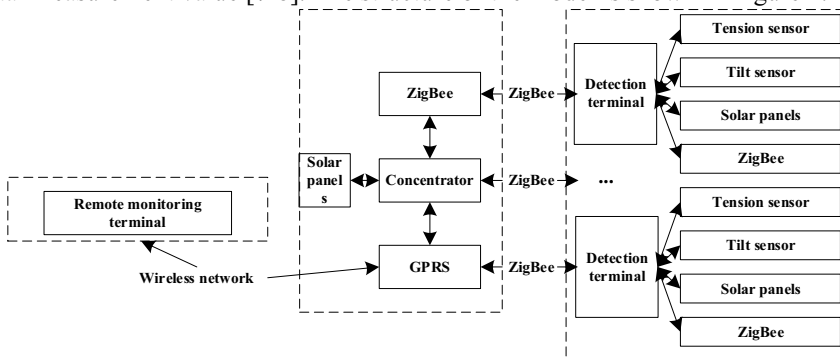


Figure 1. Real time warning structure diagram of transmission tower inclination.

2.2. Multi Sensor Data Fusion Processing

The stability of transmission tower is judged by fusing the data collected by multi-sensor. The treatment process is as follows:

Step1: The sensor data is filtered by discrete wavelet transform, and the continuous wavelet transform of the data $x(t)$ collected by each sensor is defined as:

$$Wx(j, n) = \int_{-\infty}^{\infty} x(t) \psi_{j,n}^*(t) dt \quad (1)$$

The wavelet basis function is as follows:

$$\psi_{j,n}(t) = 2^{-j/2} \psi(2^{-j}t - n) \quad (2)$$

Where, j and n are scale and translation factors respectively. The limitation of wavelet basis function and Fourier transform can be ensured by selecting appropriate mother wavelet $\varphi(t)$, so wavelet analysis adopts time-frequency analysis.

In the process of discrete wavelet transform, it is necessary to discretize the scale factor according to the power series to realize the uniform discretization of the translation factor [9]. The discrete wavelet transform formula of the data collected by each sensor is obtained as follows:

$$Wx(j, n) = \int_{-\infty}^{\infty} x(t) \psi_{j,n}^*(t) dt \quad (3)$$

Step2: Based on the wavelet packet energy spectrum strategy, the pressure and inclination data are decomposed, and the feature vectors are extracted:

$$E_j = \sum_{k=1}^N |x_{jk}|^2 \quad (4)$$

Where E_j is the frequency band component of the j th sensor and X_{jk} is the value of each discrete point, $k=1, 2, 3, \dots, N$. The proportion formula of each frequency band energy in the total energy is calculated as follows:

$$e_i = \frac{E_i}{\sum E_n} \quad (5)$$

Where E_n is the frequency band component of the n th sensor and represents the input characteristic quantity of stability diagnosis.

Step 3: RBF neural network is used to diagnose the stability of transmission tower. RBF neural network mainly includes input-output and hidden three layers, which can realize nonlinear mapping.

$$f_n(e) = \omega_0 + \sum_{i=1}^n \omega_i \phi(\|e - c_i\|) \tag{6}$$

$$\phi(\|e - c_i\|) = \exp\left(-\frac{\|e - c_i\|^2}{\sigma_i^2}\right) \tag{7}$$

Among them, e and ω_j represent the input vector and weight respectively, c_j represents the data center of the basis function, σ_j and n represent its width and number respectively, ϕ and ω_0 represent the radial basis function and deviation respectively.

Step 4: The results are fused by Bayesian reasoning to obtain the final results as follows:

$$u(k) = \begin{cases} \pm 1, a_0(k) > 0 \\ -1, a_0(k) \leq 0 \end{cases} \tag{8}$$

$$a_0(k) = \log \frac{P_k(H_1 / u_1(k), L, u_i(k), L, u_n(k))}{P_k(H_0 / u_1(k), L, u_i(k), L, u_n(k))} \tag{9}$$

Where $u(k)$ and $u_n(k)$ are binary functions, the posterior probability of H_i after the k -th measurement is described by $P_k(H_i / u_1(k), L, u_i(k), L, u_n(k))$, $i=0,1$, and H_0 and H_1 respectively indicate that there is the data in the target.

2.3. On Line Comprehensive Detection Process of Tower State

The gravity acceleration on the X, y and Z axes collected by the sensor is taken as the measurement target to obtain the inclination of the tower in all directions. Firstly, the acceleration of the tower needs to be changed into the inclination. The horizontal direction, the direction perpendicular to the horizontal direction and the direction perpendicular to the horizontal plane are defined as X, Y and Z axes respectively. Based on these axes, a space rectangular coordinate system is constructed to make the included angles of the positive direction of X, Y and Z axes in the case of tower tilt as follows α, β, γ . Figure 2 is the software flow chart of tower inclination detection device.

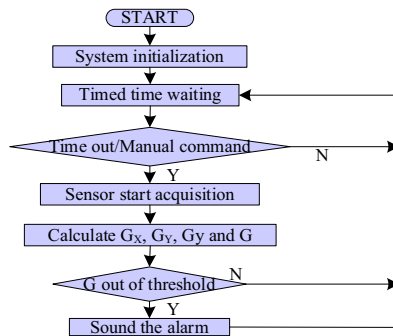


Figure 2. Treatment process of tower inclination monitoring device.

In order to reduce the power loss of transmission tower, the timing data acquisition is selected. When the set threshold is reached, the sensor transmits the inclination data to the equipment control unit and calculates the inclination to determine whether the comprehensive inclination exceeds the threshold and whether the alarm is executed.

The angle between the tower and the positive direction of X, Y and Z axes when the tower is inclined α, β, γ . The calculation formulas are as follows:

$$\alpha = \arctan\left(\frac{G_x}{\sqrt{G_y^2 + G_z^2}}\right) \tag{10}$$

$$\beta = \arctan\left(\frac{G_y}{\sqrt{G_x^2 + G_z^2}}\right) \tag{11}$$

$$\gamma = \arctan\left(\frac{\sqrt{G_x^2 + G_y^2}}{G_z}\right) \tag{12}$$

The gravity acceleration components on X, Y and Z axes are respectively G_x, G_y , and G_z , the value of this component can be positive or negative. When its value is positive, it means that the direction of gravity acceleration is equal to the positive direction of X, y and Z axes. When its value is negative, it is opposite α, β, γ . The value range of is $[-90^\circ, +90^\circ]$. The calculation formula of inclination G is as follows:

$$G = \sqrt{(G_x \cdot G_x + G_y \cdot G_y + G_z \cdot G_z)} \tag{13}$$

According to the comprehensive inclination, the alarm threshold, warning threshold, prompt threshold and normal value of each tower can be set.

3. Experimental Analysis

In order to analyze the performance of the model, the test and analysis are carried out. The analysis results of tower tilt data collected by this model are shown in Table.1.

Table 1. Analysis results.

Serial number	Wind direction	Route direction	$\alpha/^\circ$	$\beta/^\circ$	$\gamma/^\circ$	G	Wind-force
1	Northwest wind	East West	76	68	54	1.2	8
2	West wind	North South	20	35	68	1.1	8
3	Southwest wind	North South	15	45	84	1.1	8
4	Northeast wind	North South	-89	-74	-68	1.2	8
5	Southeast wind	East West	-55	-84	-46	1.8	9
6	East wind	North South	61	75	68	1.9	9
7	North wind	North South	48	36	48	0.6	7
8	North wind	North South	21	48	15	0.8	7
9	North wind	North South	43	81	49	0.9	7
10	North wind	East West	-48	-15	-54	1.2	7

Through the analysis of Table 1, it can be seen that under the condition of 7-level north wind, the route of line 7 is north-south, and the comprehensive inclination degree is the lowest. Under the condition of 9-level southeast wind, the comprehensive inclination degree of line 5 is the highest.

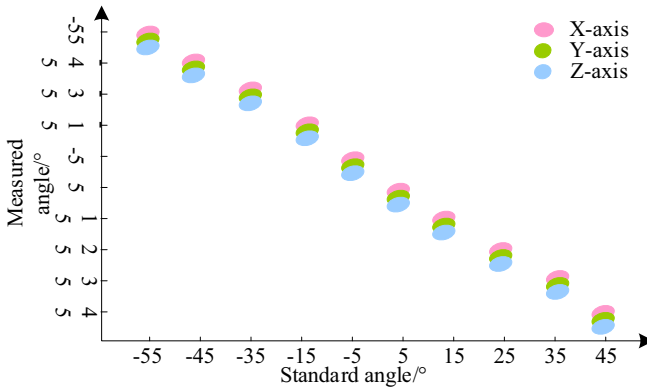


Figure 3. Analysis results of sensor inclination error.

According to the analysis of Figure 3, there are different errors in the angle measured by different axial tower tilt angles, and the average error of x-axis is 0.14° , The maximum error is only 0.19° , The average error of y-axis is 0.21° , The maximum error is 0.24° , The average error of Z axis is 0.19° , The maximum error is 0.23° , Therefore, the measurement accuracy of this model can meet the needs of tower state comprehensive detection.

TE (technical efficiency change index), PTEC (pure technical efficiency change index) and SEC (scale efficiency change index) are used to measure the information utilization rate of the model. When the value of the three indexes is greater than 1, it means that the model has higher information utilization rate. When $TE > 1$, it means that the model has higher technical efficiency, When $PREC > 1$, it means that the model has high technology maturity, and when $SEC > 1$, it means that the model has good scale effect. Test the information utilization rate of this model within one month, as shown in Figure 4.

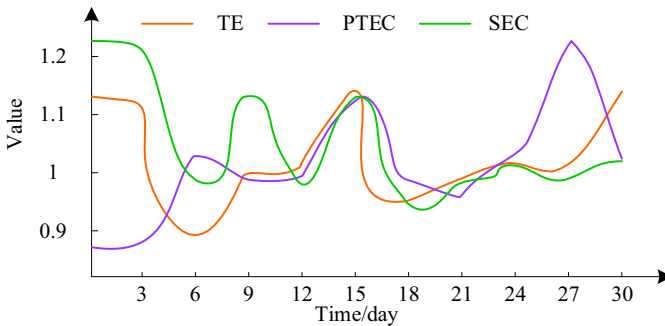


Figure 4. Information utilization test results.

According to the test results in Figure 4, the product of TE, PTEC and SEC of this model is greater than 1, and the average values are 1.049, 1.049 and 1.059, respectively, all large than 1, which indicates that this model has higher information utilization rate,

better technical level and higher scale efficiency, which can enrich the detailed information of sensor data collection and improve the safety early warning effect.

The missing alarm rate and false alarm rate represent the proportion of positive and negative samples in negative and positive samples respectively. According to the statistics, this paper uses the model to detect the missing alarm rate and false alarm rate of different types of indicators of transmission tower tilt real-time warning, and analyzes whether it can achieve the expected goal. The test results are shown in Figure 5.

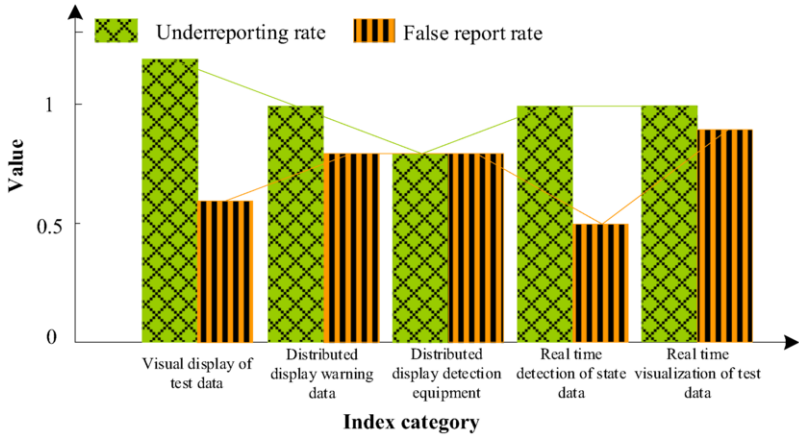


Figure 5. Comparison of missed alarm rate and false alarm rate of different types of indicators.

According to the test results of the model in Figure 5, the leakage rate and false alarm rate of different types of indicators are obviously lower by using this model to detect the tilt of transmission towers, which is not more than 1.5%. It shows that the model can correctly display the specific modules of the real-time warning of transmission tower tilt in practical application. The accuracy of the model detection samples is high and meets the expected target, The tower status can be visualized at the remote monitoring terminal for the staff.

The early warning accuracy performance of this model is analyzed on KDD-99 and CICIDS2017 data sets, and the results are shown in Figure 6.

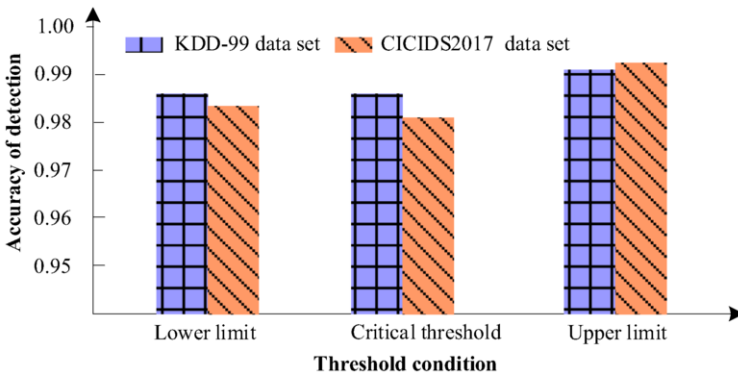


Figure 6. Early warning accuracy under correlation threshold.

It can be seen from Figure 6 that the model has high detection accuracy under the conditions of lower threshold and critical threshold, both of which are higher than 97%, and the detection accuracy near the upper threshold is higher than 99%. It shows that the real-time warning model of transmission tower tilt based on multi-sensor data has good practical application effect.

The comparison of the actual application effect is shown in Figure 7. It can be seen from Figure 7 that the real-time early warning model of transmission tower inclination based on multi-sensor data proposed in this paper has good practical application effect. By comparing the effects before and after application, it is found that the model can effectively ensure the personal safety of workers, reduce their work intensity and improve the maintenance quality.

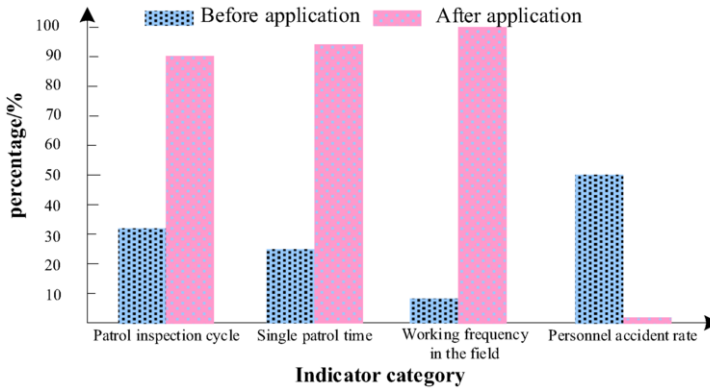


Figure 7. Comparison of practical application effect.

4. Conclusions

A real-time early-warning model of transmission tower tilt detection based on multi-sensor data fusion method is proposed. Through the data collected by sensors, the force distribution of the tower can be analyzed, and the stability of the tower can be judged. At the same time, the tilt angle can be analyzed to judge whether the tower is in a safe state, so as to realize accurate alarm. The effects before and after the application of the model show that the model can effectively ensure the personal safety of staff, improve work efficiency and reduce work intensity. The application of the results of this paper can effectively solve the problem that it is difficult to find the inclination of transmission tower in time by manual monitoring.

References

- [1] Tang Yi, Xu Xiangxiang, Chen Bin, Yi Tao. Space-Time-Intensity online early-warning of transmission tower faults by caused rainfall-induced landslides. *Electric Power*, 2020, 53(1): 56-65.
- [2] Yang Zhi, Ou Wenhao, Fei Xiangze, Li Chaung, Ma Xiao, Zhao Binbin. Smart identification of transmission tower based on high-resolution SAR image and deep learning. *Electrical Measurement & Instrumentation*, 2020, 57(4): 71-77.
- [3] Chen Wencan, Meng Xiaobo, Zhang Haipeng, Yang Daiming, Mei Hongwei, Wang Liming. Development of on-site real-time monitoring system for corrosion of power transmission tower feet. *High Voltage Apparatus*, 2020, 56(12): 196.

- [4] Huang Xinbo , Zhao Long , Chen Ziliang , Liu Cheng. An online monitoring technology of tower foundation deformation of transmission lines. *Structural health monitoring*, 2019, 18(3):949-962.
- [5] Hou Hui , Yu Shiwen , Wang Hongbin , Huang Yong, Wu Hao, Xu Yan, Li Xianqiang, Geng Hao. Risk assessment and its visualization of power tower under typhoon disaster based on machine learning algorithms. *Energies*, 2019, 12(2).
- [6] Chen Qiang, Wang Jian, Xiong Xiaofu, Feng Changyou, Ma Chao. Monitoring and early warning method for transmission tower under rainfall-induced landslide disaster. *Power System Protection and Control*, 2020, 48(3).
- [7] An Liqiang, Guan Yongyu, Zhu Zhijian, Zhang Ronglun. Research on windage yaw flashovers of transmission lines under wind and rain conditions. *Energies*, 2019, 12.
- [8] Zhang Anan, Deng Fangming. Low Delay Technology of Transmission Line Tower Monitoring Network Integrating Wireless Sensor Network and Radio Frequency Identification. *Science Technology and Engineering*, 2020, 20(4).
- [9] Du Hao, Huang Huan , Mao Xianyin, Lv Qianyong, Zhou Zhenhua, Huang Li. Distributed monitoring of wind deflection angle of insulator on transmission line. *Telecom Power Technology*, 2017, 34(6).

A New Indeterminacy Decision Making Approach Considering Partial Environmental State Knowledge

Bo FENG^{a,b}, Zhipeng HUI^a, Junwen FENG^{a,b,1}

^aNanjing University of Science and Technology, 210094, China

^bNanjing Audit University Jinshen College, 210023, China

Abstract. The types of decisions people make depend on how much knowledge or information they have about the decision environmental situation or called state. There are three decision-making environments: decision making under certainty, decision making under uncertainty and decision making under risk. Based on possibility theory and evidence theory, a new indeterminacy decision making approach with the decision-maker's environmental knowledge information about the state of nature is proposed. This approach provides a general framework for three types of decision problems, that is, deterministic, risky and uncertain problems.

Keywords. Decision analysis, Possibility theory, Evidence theory, Fuzzy analysis

1. Introduction

Decision analysis can be used to develop an optimal strategy when a decision maker is faced with several decision alternatives and an uncertain or risk-filled pattern of future environmental state events. Even when a careful decision analysis has been conducted, the uncertain future events make the final consequence uncertain [1]. In some cases, the selected decision alternative may provide good or excellent results. In other cases, a relative unlikely future event may occur, causing the selected decision alternative to provide only fair or even poor results [2]. We begin the study of decision analysis by considering problems that involve reasonably few decision alternatives and reasonably few possible future environmental state events [3]. The payoff tables are introduced to provide a structure for the decision problem and to illustrate the fundamentals of decision analysis [4].

Consider the decision making problem expressed by Table 1:

Table 1 Decision making problem

Alternatives	S_1	S_2	\dots	S_n
A_1	Q_{11}	Q_{12}	\dots	Q_{1n}
A_2	Q_{21}	Q_{22}	\dots	Q_{2n}
\vdots	\vdots	\vdots	\dots	\vdots
A_m	Q_{m1}	Q_{m2}	\dots	Q_{mn}

¹ Corresponding Author, Nanjing University of Science and Technology, Nanjing, China; E-mail: 313472714@qq.com

Among the table, $A = \{A_1, A_2, \dots, A_m\}$ is the unit of decision makings, they are independent and can not be substituted each other. $S = \{S_1, S_2, \dots, S_n\}$ is a collection of various decision-making uncertain environmental situation which may called the state of nature. Q_i means that the loss value of A_i when decision-makers encounter the natural state S_j (we suppose it is better for decision-makers when the loss value is larger in this paper). The question is which option is best for decision-maker?

If decision-makers know the state {for example S_k } will happen, the question turns to a determined decision-making problem. The best option A^* satisfies:

$$E(A_i / S) = Q_{ik} \quad E(A^* / S) = \max_i E(A_i / S)$$

If decision-makers know probability distribution of natural state $P = \{P_1, P_2, \dots, P_m\}$, where P_j is the probability of occurrence of the natural state S_j the problem turns to a risk-based decision making problem. At this time, decision-making choose the optimal option through the principle of the maximum expected loss value. The best option A^* should satisfies:

$$E(A_i / S) = \sum_{j=1}^n Q_{ij} P_j \quad E(A^* / S) = \max_i E(A_i / S)$$

If the decision-makers do not know the occurring of natural state, the question turns to a uncertain decision-making problem. Decision-makers must resort to certain criteria to make the appropriate decisions. There are five common decision criteria, they are, maximin criteria, maximax criteria, minimal regret criteria, Hurwicz criteria and equal opportunity criteria [1]. The reference [5] gives an optimism factor making-decision criteria through the five criterion above. We suppose the level of one decision-maker's optimism factor is $\alpha = (\alpha_1, \alpha_2, \dots, \alpha_n)$, the best option A^* based on optimism factor making-decision criteria should satisfies:

$$E(A_i / S) = \alpha^T \text{Maxorder} \{Q_{ij}\} \quad E(A^* / S) = \max_i E(A_i / S)$$

Among it, $\text{Maxorder} \{Q_{ij}\}$ is the descending ordered vector of $Q_{i1}, Q_{i2}, \dots, Q_{in}$, $\alpha^T \beta$ is the vector product. Here α reflects the attitude of decision-makers. The determination of α can request Reference 3.

In all the cases above, we call $E(A_i / S)$ is the evaluation value of decision A_i . Actually, the three cases above are all the extreme cases of such decision-making problems. The criteria to distinguish them is decision-maker's evaluation of the state (or the state knowledge of decision-makers). There are various ways to express the state knowledge of decision makers actually [6]. The decision-makers should collect a lot of useful information when they evaluate the state and gradually reduce the scope of the estimates. Under normal circumstances, the evaluation of state is to figure out the probability of a state in the range of one space or the other. We can express this kind of state knowledge by possibility distribution or the structural reliability of evidence. We make the decision-makers' state knowledge as an evidence, that is to say, it's the proof which the state evaluation should be trusted. The decision-makers can form the confident degree of the state evaluation in the state space by these evidences. The degree is the reflection of the role of the state space, and it makes the estimation no longer blindness.

In our paper, we will use Dempster-Shafer granule [7] to express the state knowledge of a decision-maker., and put the three decisions (determine type, risky type and uncertain type) in a unified framework.

2. The expression of the state knowledge

At first, we consider the following question. Suppose θ is a variable in a collection X, C is a subset of X. If the decision-maker only knows θ is an element of C, we can use the possibility distribution function to express the knowledge of the decision-maker –“ θ is an element of C”, that is to say: $\pi_{\theta}(x) = \begin{cases} 1, & \text{if } x \in C \\ 0, & \text{if } x \notin C \end{cases}$

Here, $\pi_{\theta}(x)$ is the possibility when θ equals to x. Further, if C is a fuzzy set of X, we can give the following equation: $\pi_{\theta}(x) = C(x)$

Among the C(x), we call X is the degree of membership in the fuzzy set C. We call C(x) is the membership function of C. The sense of C(x) is the possibility when θ equals to x. We also suppose m is the map from the fuzzy set x to unit interval, that is to say, $m : I^X \rightarrow [0,1]$

Among it, I^X is the collection of all the fuzzy set of X. Suppose that $A_i, i = 1, 2, \dots, p$ is a fuzzy subset of X, $m(A_i) = a_i \neq 0$. Simultaneously, we call A_1, A_2, \dots, A_p are the central elements of m if it satisfies the following condition:

$$(1) \sum_{i=1}^p m(A_i) = 1 \quad (2) \quad m(\phi) = 0$$

We call m is a function of supportive level. If θ is a variable in X and m is a function of supportive level, we call “ θ is m” is a rule of D-S.

Now, let’s consider θ is a variable expressed the state of decision-making, that is, θ is a variable which is defined in $S = \{S_1, S_2, \dots, S_n\}$. We can use the D-S regulation to express the three types of decision-making statement.

- Determined type, θ is m if $m(\{S_k\}) = 1, S_k \in S$
- Risky type, θ is m if $m(\{S_j\}) = P_j, j = 1, 2, \dots, n$
- Uncertain type, θ is m if $m\{S\} = 1$

Suppose B is a subset of S, if the possibility of the decision-makers’ knowledge is θ at least α , we can express the knowledge to “ θ is m”, which $m(B) = \alpha, m(S) = 1 - \alpha$.

At this time, we can use the supportive function to express the common state knowledge.

3. The decision-making based on D-S rule

Suppose θ is a variable which is defined in the state space $S = \{S_1, S_2, \dots, S_n\}$. We can use the supportive function to express the knowledge of state space. Now let $E(A^*/m)$ be the evaluation when “ θ is m ”, at this time, A^* is the optimal choice under the state knowledge “ θ is m ”. We can express it by, $E(A^*/m) = \max_i E(A_i/m)$

The question is how to estimate $E(A^*/m)$. Let’s discuss under the three circumstances below.

Case 1. Suppose B is the nonempty subset of S, m is as follows: $m(B) = 1, m(\phi) = 0$

We use $\theta_i(B)$ to express the subset of possible loss under the Program A_i , that is $Q_i(B) = \{Q_{ij} : S_j \in B\}$. We can believe the evaluation function $E(A^*/m)$ is based on $\theta_i(B)$. If B is a collection many elements, the decision-makers should choose a rule to pick up programs. Suppose the makers choose the decision by levels of optimism factor criteria.

The evaluation function can be expressed to:

$$E(A^*/m) = \alpha^T \text{Maxorder} Q_i(B)$$

In the equation, $\text{Maxorder} Q_i(B)$ is the descending order of $Q_i(B)$, the dimension is same with B. α is the level of optimism factor.

Case 2. Suppose that B is a fuzzy set of S, m is as follows:

$$m(B) = 1, m(\phi) = 0$$

The possible loss under the decision A_i becomes the fuzzy set of loss,

$$Q_i(B) = \bigcup_{j=1}^n (B(S_j)/Q_{ij}) = \{B(S_1)/Q_{i1}, B(S_2)/Q_{i2}, \dots, B(S_n)/Q_{in}\}$$

Among that, $B(S_j)$ is the membership function of B under the S_j . In this case, we should decide an order by preparing the elements of $Q_i(B)$ when determine the $E(A^*/m)$. Then make the decision by rule of level optimism factors. One possible way is to order by the membership, the other is ordering by the results of membership multiply loss value. Now, we decide the evaluation function by the level of fuzzy sets.

The definition β of fuzzy set $Q_i^{(\beta)}$ is: $Q_i^{(\beta)}(B) = \{Q_{ij} : B(S_j) \geq \beta\}$

$Q_i^{(\beta)}(B)$ may contains different elements for different $\beta \in [0,1]$, so the dimension of $Q_i^{(\beta)}(B)$ may be different, but none of them may be larger than the dimension of state space n.

Others, we suppose the same element of $Q_i^{(\beta)}(B)$ may be different, the “same” means the numerically equal.

Suppose the optimism factor of decision-makers is $\alpha = (\alpha_1, \alpha_2, \dots, \alpha_n)$, we may

define the evaluation function of A_i , $E(A_i^* / m)$ is :

$$E(A_i^* / m) = \int_0^1 [\alpha]^T \text{Maxorder} Q_i^{(\beta)}(B) d\beta$$

The $[\alpha]$ here is the dimension of $\alpha = (\alpha_1, \alpha_2, \dots, \alpha_n)$, $\text{Maxorder} Q_i^{(\beta)}$ is the descending ordered vector. If $n=4$, the dimension of $Q_i^{(\beta)}(B)$ is 3, $[\alpha] = [\frac{\alpha_1}{\alpha_1 + \alpha_2 + \alpha_3}, \frac{\alpha_2}{\alpha_1 + \alpha_2 + \alpha_3}, \frac{\alpha_3}{\alpha_1 + \alpha_2 + \alpha_3}]$; if the dimension is 2, $[\alpha] = [\frac{\alpha_1}{\alpha_1 + \alpha_2}, \frac{\alpha_2}{\alpha_1 + \alpha_2}]$; if the dimension is n , $[\alpha] = \alpha$. So the $[\alpha]$ is changing by β . The evaluation function can be determined if the level optimism of factor α can be decided. Then we will give the application examples.

Case 3 (common case) $B_k, K = 1, 2, \dots, p$ is the fuzzy set of S , m is as follows:

$$\begin{cases} m(B_K) = \alpha_K \neq 0, K = 1, 2, \dots, p \\ m(\phi) = 0 \\ \sum_{K=1}^p m(B_K) = \sum_{K=1}^p \alpha_K = 1 \end{cases}$$

Here, we define the evaluation of A_i is:

$$E(A_i / m) = \sum_{K=1}^p E(A_i / m_K) \cdot \alpha_K \text{ Where } m_K(B_K) = 1, m_K(\phi) = 0$$

Notes: Case 1 and Case 2 are the special situation of Case 3. Further, if $B = \{S_K\}$, the case 1 becomes a determined type; if $B=S$, the case 1 becomes a certain type; if $B_K = \{S_K\}, K = 1, 2, \dots, n, m(B_K) = P_K$, the case 3 becomes a risky type. So the case 3 is the unified structure of this paper. If contains a serious of expression of the state space knowledge.

4. Numerical Examples

Example 1. Consider a decision-making problem in Table 2

Table 2. Decision making example 1

Alternatives	S_1	S_2	S_3	S_4
A_1	10	-15	5	20
A_2	5	5	10	10
A_3	0	10	15	0

Suppose the level optimism factor $\alpha = \{\alpha_1, \alpha_2, \alpha_3, \alpha_4\} = \{0.25, 0.20, 0.30, 0.25\}$, the actual definition is, to every program, the weight of the decision-makers is 0.25, 0.20, 0.30 and 0.25. If the decision-maker only decide among the three programs, the corresponding optimism factor becomes

$$[\alpha] = \left[\frac{\alpha_1}{\alpha_1 + \alpha_2 + \alpha_3}, \frac{\alpha_2}{\alpha_1 + \alpha_2 + \alpha_3}, \frac{\alpha_3}{\alpha_1 + \alpha_2 + \alpha_3} \right] = (0.33, 0.27, 0.40);$$

if the decision-maker only decide among the two programs, the corresponding optimism factor becomes

$$[\alpha] = \left[\frac{\alpha_1}{\alpha_1 + \alpha_2}, \frac{\alpha_2}{\alpha_1 + \alpha_2} \right] = (0.56, 0.44).$$

In addition, the knowledge of decision-maker is “ θ is m”, $m(B) = 1, m(\phi) = 0$, B is the fuzzy set of S, $B = \left\{ \frac{1}{S_1}, \frac{1}{S_2}, \frac{0.5}{S_3}, \frac{0.2}{S_4} \right\}$, now give the decision analysis.

Solutions:

At the moment,

$$Q_1(B) = \left\{ \frac{1}{10}, \frac{1}{-15}, \frac{0.5}{5}, \frac{0.2}{20} \right\}$$

$$Q_2(B) = \left\{ \frac{1}{5}, \frac{1}{5}, \frac{0.5}{10}, \frac{0.2}{10} \right\}$$

$$Q_3(B) = \left\{ \frac{1}{0}, \frac{1}{10}, \frac{0.5}{15}, \frac{0.2}{0} \right\}$$

The corresponding sets are as follows in Table 3:

Table 3. Decision making Maxorder values

β	Maxorder $Q_1^{(\beta)}(B)$	Maxorder $Q_2^{(\beta)}(B)$	Maxorder $Q_3^{(\beta)}(B)$
[0,0.2]	{20,10,5,-15}	{10,10,5,5}	{15,10,0,0}
[0.2,0.5]	{10,5,-15}	{10,5,5}	{15,10,0}
[0.5,1.0]	{10,-15}	{5,5}	{10,0}

$$\begin{aligned} \text{So, } E(A_1 / m) &= \int_0^1 [\alpha]^T \text{Maxorder} Q_1^\beta(B) d\beta \\ &= \int_0^{0.2} \{ 0.25 \times 20 + 0.20 \times 10 + 0.30 \times 5 + 0.25 \times (-15) \} d\beta \\ &\quad + \int_{0.2}^{0.5} \{ 0.33 \times 10 + 0.27 \times 5 + 0.40 \times (-15) \} d\beta \\ &\quad + \int_{0.5}^1 \{ (0.56 \times 10 + 0.44 \times (-15)) \} d\beta \\ &= 4.75 \times 0.2 + (-1.35) \times 0.3 + (-1) \times 0.5 = 0.045 \end{aligned}$$

$$E(A_2 / m) = \int_0^1 [\alpha]^T \text{Maxorder} Q_2^\beta(B) d\beta$$

$$\begin{aligned}
 &= \int_0^{0.2} \{ 0.25 \times 10 + 0.20 \times 10 + 0.30 \times 5 + 0.25 \times 5 \} d\beta \\
 &+ \int_{0.2}^{0.5} \{ 0.33 \times 10 + 0.27 \times 5 + 0.40 \times 5 \} d\beta \\
 &+ \int_{0.5}^1 \{ 0.56 \times 5 + 0.44 \times 5 \} d\beta \\
 &= 7.25 \times 0.2 + 6.65 \times 0.3 + 5 \times 0.5 = 5.945
 \end{aligned}$$

$$\begin{aligned}
 E(A_3 / m) &= \int_0^1 [\alpha]^T \text{Maxorder} Q_3^\beta(B) d\beta \\
 &= \int_0^{0.2} \{ 0.25 \times 15 + 0.20 \times 10 + 0.30 \times 0 + 0.25 \times 0 \} d\beta \\
 &+ \int_{0.2}^{0.5} \{ 0.33 \times 15 + 0.27 \times 10 + 0.40 \times 0 \} d\beta \\
 &+ \int_{0.5}^1 \{ (0.56 \times 10 + 0.44 \times 0) \} d\beta \\
 &= 5.75 \times 0.2 + 7.65 \times 0.3 + 5.6 \times 0.5 = 6.245
 \end{aligned}$$

Finally, the decision-maker should choose A_3 .

Note: if $\alpha_1=1$, the other $\alpha_n=0$, at this point it corresponds to the optimistic decision; if $\alpha_1=0$, the other $\alpha_n=1$, Maxorder turns to be the increasing order and Minorder corresponds to the pessimistic decision. If $\alpha_1 = \alpha'$, $\alpha_2 = 1 - \alpha'$, Maxorder turns to be the composition of binary group with the maximum and minimum, and it corresponds to the optimistic decision; if turning the decision matrix to the regret matrix, and let $\alpha_1 = 1$, the other $\alpha_n = 0$, increasing ordering, it corresponds to the regretted decision. If let $\alpha_i = \frac{1}{n}$ ($n=4$, in this example), $i = 1, 2, \dots, n$, it corresponds to the equal possibility decision.

Example 2. The decision table is same as in example 1, but the knowledge of the decision-makers is following: Q is m , $m(B_1) = 0.7$, $m(B_2) = 0.3$, $B_1 = \{S_1, S_2\}$, $B_2 = \{S_1, S_2, S_3, S_4\}$, the possibility when the evaluation of state by decision-makers is $B_1 = \{S_1, S_2\}$ at least 0.7. Others are all the same to example 1.

Now, $Q_1(B_1) = \{0, -15\}$, $Q_2(B_1) = \{5, 5\}$, $Q_3(B_1) = \{0, 10\}$

So we has the equation:

$$\begin{aligned}
 E(A_1 / m_1) &= 0.56 \times 10 + 0.44 \times (-15) = -1 \\
 E(A_2 / m_1) &= 0.56 \times 5 + 0.44 \times 5 = 5 \\
 E(A_3 / m_1) &= 0.56 \times 10 + 0.44 \times 0 = 5.6
 \end{aligned}$$

Among the above equations: $m_1(B_1) = 1, m_1(\phi) = 0$

Similarly,

$$\begin{aligned}
 Q_1(B_2) &= \{10, -15, 5, 20\}, Q_2(B_2) = \{5, 5, 10, 10\}, Q_3(B_2) = \{0, 10, 15, 0\} \\
 \text{So, } E(A_1 / m_2) &= 0.25 \times 20 + 0.20 \times 10 + 0.30 \times 5 + 0.25 \times (-15) = 4.75 \\
 E(A_2 / m_2) &= 0.25 \times 10 + 0.20 \times 10 + 0.30 \times 5 + 0.25 \times 5 = 7.25 \\
 E(A_3 / m_2) &= 0.25 \times 15 + 0.20 \times 10 + 0.30 \times 0 + 0.25 \times 0 = 5.75
 \end{aligned}$$

Among the above equations: $m_2(B_2) = 1, m_2(\phi) = 0$. So,

$$E(A_1 / m) = 0.7 \times (-1) + 0.3 \times 4.75 = 0.725$$

$$E(A_2 / m) = 0.7 \times 5 + 0.3 \times 7.25 = 5.675$$

$$E(A_3 / m) = 0.7 \times 0.56 + 0.3 \times 5.75 = 5.645$$

The decision-maker should choose the program A_1 .

5. Conclusion

The paper is based on the decision analysis method by Possibility and Evidence theory. The method puts the common three decision type under a framework. And it used the knowledge which the decision-makers easily express. This approach is the generalization of the existed methods and has the decision-making supporting function.

The paper discussed the problem with discrete states and finite alternatives, which also can solve the infinite decision solutions through appropriate extension. Further, it is useful to extent the situation involving the multiple object decision-makings.

References

- [1] David R. Anderson, Dennis J. Sweeney, Thomas A. Williams, Jeffrey D. Camm, James J. Cochran, Michael J. Fry, Jeffrey W. Ohlmann. *An Introduction to Management Science: Quantitative Approaches to Decision Making*, Fifteenth Edition, Cengage Learning, Inc. 2016.
- [2] Kirkwood, C. W. An Overview of Methods for Applied Decision Analysis, *Interfaces* 22, 6 (November–December 1992): 28–39.
- [3] Maxwell, Daniel T. Improving Hard Decisions, *OR/MS Today* 33, 6(December 2006): 51–61.
- [4] Patchak, William M. “Software Survey: Decision Analysis.” *OR/MS Today* 39, 5 (October 2012).
- [5] Feng Junwen. Hierarchical Optimistic Approach for Uncertain Decision Making. *Systems Engineering and Electronics*, No.3, 1992
- [6] Shafter G. A. *Mathematical Theory of Evidence*. Princeton University Press, Princeton, New Jersey, 1976
- [7] Yager R. R. *A General Approach to Decision Making with Evidential Knowledge in Uncertainty in Artificial Intelligence*. Elsevier Science Publishers B. V. (North-Holland), 1986

Subject Index

advertising	115	decision analysis	469
agent	422	decision rule	431
agent-based approach	422	deep belief networks	386
analytic hierarchy process	220	deep learning	23, 250
ant colony algorithm	339	deep residual network	86
anthropometric measurements	175	Delphi analysis	220
AODV	285	Dempster-Shafer evidence theory	183
architecture	422	determination of weights	220
artificial general intelligence	422	diagonal stabilization	236
artificial intelligence	1, 250, 422	differential privacy	8
attention mechanism	86	digital passport	379
axiomatic method	162	digital platform	190
bearing fault diagnosis	94	divergence	183
behavioural analysis	356	drought	348
belief revision	371	ECC	285
Bi-LSTM	140, 200	edge AI	94
big data	1	edge computing	94
bilevel programming	264	enhanced AODV	285
bolt defect recognition	86	entity disambiguation	412
cardiovascular disease	23	estate marketing	30
category of fuzzy sets	226	evidence theory	469
centroid processing	296	facial expression recognition	63
Chaozhou Chinese paper cutting	130	factor space	226
Chinese text matching	140	fat body percentage	175
classification	152	fault diagnosis	94
climate change	348	features back-tracking	386
cloud computing	348	flower pollination algorithm	436
CNN	63	fragile watermarking	277
co-attention	200	function recovery	77
compatibility	122	fuzzy analysis	469
complex network	412	fuzzy classification	356, 363
concepts	371	fuzzy co-location pattern	314
context processing	422	fuzzy Delphi analytic hierarchy process	220
contour data	443	fuzzy evaluation	220
convolutional neural network	94	fuzzy goal programming	264
crawler technology	454	fuzzy multi-information GCM	162
cross entropy	183	fuzzy relation equation	210
data augment	86	fuzzy set	431
data flow diagrams	363	fuzzy subtractive clustering	329
data hiding	277	generalized-multiquadric	77
data mining	363	generation of design solutions	379
data perturbation	8	Google Earth Engine	348
Davies-Bouldin index	329		

granular computing	162	multiple features	54
H_∞ performance	257	multiprocessing	70
hierarchical level	70	MV*-algebras	305
human activity recognition	250	MySQL	454
ideals	305	natural language processing	30
image authentication	277	natural scene text detection	436
image description	63	network centrality computation	397
image recovery	277	neural networks	54
imbalanced data	23	NSTEMI	23
imbalanced problem	152	ontology	422
improved neural network	436	ontology engineering	363
improved score function	41	oversampling	152
indefinite quadratic transportation	264	PageRank model	397
inertial measurement unit	250	partial-order relationship	162
information extraction	356	partition coefficient	329
initial cluster center	443	personal experience	422
integrated loading and unloading	339	personalized information	
intelligent learning platform	200	recommendation	130
international trade	122	PLMFs	257
intuitionistic fuzzy number	405	plot extractor	296
intuitionistic fuzzy programming	264	point state delay	236
job recommendation	454	positive systems	236
K-means clustering algorithm	443	positive T-S fuzzy systems	257
knowledge graph	130	possibilistic mean	405
knowledge mapping	412	possibilistic variance	405
large-scale data mining	348	possibility theory	469
linear matrix inequalities	236	post three-valued logic	371
linked data	190	prime ideals	305
loss function	431	pruning	314
low-rank factorization	397	Pythagorean fuzzy sets	183
LSTM	63	QMV*-algebras	305
machine learning	1	quadratic stability	236
major adverse cardiovascular event	23	Quasi-MV algebras	305
markers selection	386	R-AODV	285
marketing	115	R-calculus	371
mass ratio variance score	152	radar measurement	296
matrix pre-processing algorithms	397	Radial Basis Function Neural	
max-Dubois-Prade composition	210	Networks (RBFNs)	77
maximum power tracking	104	ranking	41
Mekong River basin	190	rattan over Y	226
mental map	363	recommendation system	8
Metzler-Takagi-Sugeno systems	236	recommender systems	54
minimal solution	210	recursive procedure	70
modular	122	relational reasoning	412
Monte Carlo cross validation	175	residual encoding	140
motion capture	250	review text	54
multi-fuzzy information		reviews	30
granularity	162	risk function	431
multi-granularity	140	Rényi differential privacy	8

scheduling platform development	339	text mining	356
semantic repeatability	200	thesaurus	190
semantics	422	TikTok	115
semi-Markov process	70	time interval	70
sensing technology	454	time series analysis	296
sentence semantic matching	140	tracking control	257
sentence vector	200	trapezoidal bipolar fuzzy number	41
sentiment analysis	30	triangular bipolar fuzzy number	41
ship microgrid	104	Type-2 fuzzy set	314
social media	115, 356	UAV distribution path	339
soft alignment attention	140	uncertainty	264
software engineering	454	uncertainty measure	183
solar power	104	undersampling	152
solution set	210	unemployment	1
sorting	220	user profiling	356
sparse learning	386	variable shape parameters	77
spatial data mining	314	variants of design solutions	379
stability	122	VGG16	63
supervised learning	422	vibration diagnostics	94
support vector machine	175	virtual experiment platform	122
SVD recommendation model	8	Von Neumann controller	70
tableau proof system	371	weak topos	226
tamper localization	277	web service	190
tasks of generation design		wind power	104
solutions	379	Word2vec	30
text event detection	436	YOLOv5	63

This page intentionally left blank

Author Index

Alekseevna, A.T.	70	Jaén-Vargas, M.	250
Anatolievich, G.K.	70	Jeevaraj S	41
Arora, R.	264	Jiang, Q.	86
Arora, S.	264	Jiang, Y.	305
Belousov, K.	356, 363	Jing, W.	386
Buranarach, M.	190	Kaennakham, S.	77
Cai, J.	8	Kalita, J.	63
Cao, C.	371	Khan, K.U.R.	285
Carpentieri, B.	397	Korzun, D.	94
Chansanam, W.	190	Krokavec, D.	236
Chen, H.	140	Kwiecien, K.	190
Chen, S.	8	La Cruz, A.	175
Chen, W.	305	Labutin, I.	356
Chen, X.	339	Lam, H.K.	257
Chu, Y.	443	Lam, K.N.	63
Chumakov, R.	363	Lee, J.Y.	23
Chung, S.	454	Lei, J.S.	54
Cui, Y.	436	Li, G.	348
Dai, X.	412	Li, J.	386
Deng, Y.	183	Li, P.	348
Donetskaya, J.V.	379	Li, T.	30
Dushkin, R.V.	422	Liang, C.	122
Eliyanto, J.	329	Liang, G.M.	54
Ermakov, V.	94	Liang, Y.	86
Feng, B.	220, 469	Liao, X.	130
Feng, J.	220, 469	Lin, Z.	86
Fernandes, F.	250	Liu, B.	460
Filasová, A.	236	Liu, F.	257
Fu, L.	257	Liu, J.	200
Gao, X.	183	Liu, W.	162
Gonçalves, S.B.	250	Liu, X.	210
Guo, J.	314	Lopes, D.S.	250
Hao, C.	460	Luo, N.	122
Haryati, A.E.	329	Meng, A.	257
Hayat, K.	210	Neena Raj N.R.	277
Hu, C.	54	Nguy, L.H.	63
Hu, L.	371	Nguyen, K.-N.T.	63
Hu, X.	460	Paewpolsong, P.	77
Huang, M.	454	Pan, L.	183
Huang, W.	130	Paz López, M.E.	1
Huang, X.	226	Pei, H.	460
Huerta, M.	175	Perminov, V.	94
Hui, Z.	220, 469	Ping Chen, I.	454

Polvimoltham, P.	152	Van Truong, T.	296
Qiao, C.	386	Vasilevich, L.E.	70
Quoc Tuan, T.	296	Virgilio, G.P.M.	1
Rach, M.	115	Vu Hop, T.	296
Reyes Leiva, K.	250	Wang, A.	454
Ryabinin, K.	363	Wang, C.	460
Serrano Olmedo, J.	250	Wang, L.	314, 443
Severeyn, E.	175	Wang, Q.	162
Shang, D.	30	Wei, M.	339
Shen, Z.-L.	397	Wei, Y.	412, 436
Sherazi, S.W.A.	23	Wong, S.	175
Shi, Y.	200	Wu, L.	339
Shreelekshmi R.	277	Wu, T.	30
Shvedov, A.S.	431	Xie, B.	130, 200
Sinapiromsaran, K.	152	Xu, J.	257
Singh, A.	264	Yan, W.	30
Son, S.H.	23	Yang, D.	386
Song, W.	54	Yang, S.-J.	226
Sriapai, N.	77	Yang, S.Y.	54
Stepankov, V.Y.	422	Yang, X.	210
Sui, Y.	371	Yin, M.	122
Sun, L.	8	Yu, G.	30
Surono, S.	329	Yuan, Z.	104
Tallón-Ballesteros, A.J.	v	Zhang, C.	386
Taranum, F.	285	Zhang, L.	104, 140
Tavaen, S.	77	Zhang, Q.	405
Tavares Silva, M.	250	Zhang, X.	386
Trung Kien, T.	296	Zheng, H.	23
Tuamsuk, K.	190	Zhu, C.S.C.	54
Van Loi, N.	296		